The Institution of Engineering and Technology

Power Distribution System State Estimation

Edited by
Elizete Maria Lourenço and João Bosco Augusto London Junior

IET ENERGY ENGINEERING SERIES 183

Power Distribution System State Estimation

Other volumes in this series:

Volume 1 **Power Circuit Breaker Theory and Design** C.H. Flurscheim (Editor)
Volume 4 **Industrial Microwave Heating** A.C. Metaxas and R.J. Meredith
Volume 7 **Insulators for High Voltages** J.S.T. Looms
Volume 8 **Variable Frequency AC Motor Drive Systems** D. Finney
Volume 10 **SF6 Switchgear** H.M. Ryan and G.R. Jones
Volume 11 **Conduction and Induction Heating** E.J. Davies
Volume 13 **Statistical Techniques for High Voltage Engineering** W. Hauschild and W. Mosch
Volume 14 **Uninterruptible Power Supplies** J. Platts and J.D. St Aubyn (Editors)
Volume 15 **Digital Protection for Power Systems** A.T. Johns and S.K. Salman
Volume 16 **Electricity Economics and Planning** T.W. Berrie
Volume 18 **Vacuum Switchgear** A. Greenwood
Volume 19 **Electrical Safety: a guide to causes and prevention of hazards** J. Maxwell Adams
Volume 21 **Electricity Distribution Network Design, 2nd Edition** E. Lakervi and E.J. Holmes
Volume 22 **Artificial Intelligence Techniques in Power Systems** K. Warwick, A.O. Ekwue and R. Aggarwal (Editors)
Volume 24 **Power System Commissioning and Maintenance Practice** K. Harker
Volume 25 **Engineers' Handbook of Industrial Microwave Heating** R.J. Meredith
Volume 26 **Small Electric Motors** H. Moczala et al.
Volume 27 **AC-DC Power System Analysis** J. Arrillaga and B.C. Smith
Volume 29 **High Voltage Direct Current Transmission, 2nd Edition** J. Arrillaga
Volume 30 **Flexible AC Transmission Systems (FACTS)** Y-H. Song (Editor)
Volume 31 **Embedded generation** N. Jenkins et al.
Volume 32 **High Voltage Engineering and Testing, 2nd Edition** H.M. Ryan (Editor)
Volume 33 **Overvoltage Protection of Low-Voltage Systems, Revised Edition** P. Hasse
Volume 36 **Voltage Quality in Electrical Power Systems** J. Schlabbach et al.
Volume 37 **Electrical Steels for Rotating Machines** P. Beckley
Volume 38 **The Electric Car: Development and future of battery, hybrid and fuel-cell cars** M. Westbrook
Volume 39 **Power Systems Electromagnetic Transients Simulation** J. Arrillaga and N. Watson
Volume 40 **Advances in High Voltage Engineering** M. Haddad and D. Warne
Volume 41 **Electrical Operation of Electrostatic Precipitators** K. Parker
Volume 43 **Thermal Power Plant Simulation and Control** D. Flynn
Volume 44 **Economic Evaluation of Projects in the Electricity Supply Industry** H. Khatib
Volume 45 **Propulsion Systems for Hybrid Vehicles** J. Miller
Volume 46 **Distribution Switchgear** S. Stewart
Volume 47 **Protection of Electricity Distribution Networks, 2nd Edition** J. Gers and E. Holmes
Volume 48 **Wood Pole Overhead Lines** B. Wareing
Volume 49 **Electric Fuses, 3rd Edition** A. Wright and G. Newbery
Volume 50 **Wind Power Integration: Connection and system operational aspects** B. Fox et al.
Volume 51 **Short Circuit Currents** J. Schlabbach
Volume 52 **Nuclear Power** J. Wood
Volume 53 **Condition Assessment of High Voltage Insulation in Power System Equipment** R.E. James and Q. Su
Volume 55 **Local Energy: Distributed generation of heat and power** J. Wood
Volume 56 **Condition Monitoring of Rotating Electrical Machines** P. Tavner, L. Ran, J. Penman and H. Sedding
Volume 57 **The Control Techniques Drives and Controls Handbook, 2nd Edition** B. Drury
Volume 58 **Lightning Protection** V. Cooray (Editor)
Volume 59 **Ultracapacitor Applications** J.M. Miller
Volume 62 **Lightning Electromagnetics** V. Cooray
Volume 63 **Energy Storage for Power Systems, 2nd Edition** A. Ter-Gazarian
Volume 65 **Protection of Electricity Distribution Networks, 3rd Edition** J. Gers
Volume 66 **High Voltage Engineering Testing, 3rd Edition** H. Ryan (Editor)
Volume 67 **Multicore Simulation of Power System Transients** F.M. Uriate
Volume 68 **Distribution System Analysis and Automation** J. Gers
Volume 69 **The Lightening Flash, 2nd Edition** V. Cooray (Editor)
Volume 70 **Economic Evaluation of Projects in the Electricity Supply Industry, 3rd Edition** H. Khatib
Volume 72 **Control Circuits in Power Electronics: Practical issues in design and implementation** M. Castilla (Editor)
Volume 73 **Wide Area Monitoring, Protection and Control Systems: The enabler for Smarter Grids** A. Vaccaro and A. Zobaa (Editors)
Volume 74 **Power Electronic Converters and Systems: Frontiers and applications** A. M. Trzynadlowski (Editor)
Volume 75 **Power Distribution Automation** B. Das (Editor)
Volume 76 **Power System Stability: Modelling, analysis and control** A.A. Sallam and B. Om P. Malik
Volume 78 **Numerical Analysis of Power System Transients and Dynamics** A. Ametani (Editor)
Volume 79 **Vehicle-to-Grid: Linking electric vehicles to the smart grid** J. Lu and J. Hossain (Editors)
Volume 81 **Cyber-Physical-Social Systems and Constructs in Electric Power Engineering** S. Suryanarayanan, R. Roche and T.M. Hansen (Editors)
Volume 82 P**eriodic Control of Power Electronic Converters** F. Blaabjerg, K.Zhou, D. Wang and Y. Yang
Volume 86 **Advances in Power System Modelling, Control and Stability Analysis** F. Milano (Editor)

Volume 87 **Cogeneration: Technologies, Optimisation and Implentation** C. A. Frangopoulos (Editor)
Volume 88 **Smarter Energy: from Smart Metering to the Smart Grid** H. Sun, N. Hatziargyriou, H. V. Poor, L. Carpanini and M. A. Sánchez Fornié (Editors)
Volume 89 **Hydrogen Production, Separation and Purification for Energy** A. Basile, F. Dalena, J. Tong and T.N.Veziroğlu (Editors)
Volume 90 **Clean Energy Microgrids** S. Obara and J. Morel (Editors)
Volume 91 **Fuzzy Logic Control in Energy Systems with Design Applications in Matlab/Simulink®** i. H. AltaŞ
Volume 92 **Power Quality in Future Electrical Power Systems** A. F. Zobaa and S. H. E. A. Aleem (Editors)
Volume 93 **Cogeneration and District Energy Systems: Modelling, Analysis and Optimization** M. A. Rosen and S. Koohi-Fayegh
Volume 94 **Introduction to the Smart Grid: Concepts, technologies and evolution** S.K. Salman
Volume 95 **Communication, Control and Security Challenges for the Smart Grid** S.M. Muyeen and S. Rahman (Editors)
Volume 96 **Industrial Power Systems with Distributed and Embedded Generation** R Belu
Volume 97 **Synchronized Phasor Measurements for Smart Grids** M.J.B. Reddy and D.K. Mohanta (Editors)
Volume 98 **Large Scale Grid Integration of Renewable Energy Sources** A. Moreno-Munoz (Editor)
Volume 100 **Modeling and Dynamic Behaviour of Hydropower Plants** N. Kishor and J. Fraile-Ardanuy (Editors)
Volume 101 **Methane and Hydrogen for Energy Storage** R. Carriveau and D. S-K. Ting
Volume 104 **Power Transformer Condition Monitoring and Diagnosis** A. Abu-Siada (Editor)
Volume 106 **Surface Passivation of Industrial Crystalline Silicon Solar Cells** J. John (Editor)
Volume 107 **Bifacial Photovoltaics: Technology, applications and economics** J. Libal and R. Kopecek (Editors)
Volume 108 **Fault Diagnosis of Induction Motors** J. Faiz, V. Ghorbanian and G. Joksimović
Volume 109 **Cooling of Rotating Electrical Machines: Fundamentals, modelling, testing and design** D. Staton, E. Chong, S. Pickering and A. Boglietti
Volume 110 **High Voltage Power Network Construction** K. Harker
Volume 111 **Energy Storage at Different Voltage Levels: Technology, integration, and market aspects** A.F. Zobaa, P.F. Ribeiro, S.H.A. Aleem and S.N. Afifi (Editors)
Volume 112 **Wireless Power Transfer: Theory, Technology and Application** N.Shinohara
Volume 114 **Lightning-Induced Effects in Electrical and Telecommunication Systems** Y. Baba and V. A. Rakov
Volume 115 **DC Distribution Systems and Microgrids** T. Dragičević, F.Blaabjerg and P. Wheeler
Volume 116 **Modelling and Simulation of HVDC Transmission** M. Han (Editor)
Volume 117 **Structural Control and Fault Detection of Wind Turbine Systems** H.R. Karimi
Volume 119 **Thermal Power Plant Control and Instrumentation: The control of boilers and HRSGs, 2nd Edition** D. Lindsley, J. Grist and D. Parker
Volume 120 **Fault Diagnosis for Robust Inverter Power Drives** A. Ginart (Editor)
Volume 121 **Monitoring and Control using Synchrophasors in Power Systems with Renewables** I. Kamwa and C. Lu (Editors)
Volume 123 **Power Systems Electromagnetic Transients Simulation, 2nd Edition** N. Watson and J. Arrillaga
Volume 124 **Power Market Transformation** B. Murray
Volume 125 **Wind Energy Modeling and Simulation Volume 1: Atmosphere and plant** P.Veers (Editor)
Volume 126 **Diagnosis and Fault Tolerance of Electrical Machines, Power Electronics and Drives** A.J. M. Cardoso
Volume 128 **Characterization of Wide Bandgap Power Semiconductor Devices** F. Wang, Z. Zhang and E.A. Jones
Volume 129 **Renewable Energy from the Oceans: From wave, tidal and gradient systems to offshore wind and solar** D. Coiro and T. Sant (Editors)
Volume 130 **Wind and Solar Based Energy Systems for Communities** R. Carriveau and D. S-K. Ting (Editors)
Volume 131 **Metaheuristic Optimization in Power Engineering** J. Radosavljević
Volume 132 **Power Line Communication Systems for Smart Grids** I.R.S Casella and A. Anpalagan
Volume 134 **Hydrogen Passivation and Laser Doping for Silicon Solar Cells** B. Hallam and C. Chan (Editors)
Volume 139 **Variability, Scalability and Stability of Microgrids** S. M. Muyeen, S. M. Islam and F. Blaabjerg (Editors)
Volume 143 **Medium Voltage DC System Architectures** B. Grainger and R. D. Doncker (Editors)
Volume 145 **Condition Monitoring of Rotating Electrical Machines** P. Tavner, L. Ran, C. Crabtree
Volume 146 **Energy Storage for Power Systems, 3rd Edition** A.G. Ter-Gazarian
Volume 147 **Distribution Systems Analysis and Automation 2nd Edition** J. Gers
Volume 151 **SiC Power Module Design: Performance, robustness and reliability** A. Castellazzi and A. Irace (Editors)
Volume 152 **Power Electronic Devices: Applications, failure mechanisms and reliability** F Iannuzzo (Editor)
Volume 153 **Signal Processing for Fault Detection and Diagnosis in Electric Machines and Systems** M. Benbouzid (Editor)
Volume 155 **Energy Generation and Efficiency Technologies for Green Residential Buildings** D. Ting and R. Carriveau (Editors)
Volume 156 **Lithium-ion Batteries Enabled by Silicon Anodes** C. Ban and K. Xu (Editors)
Volume 157 **Electrical Steels, 2 Volumes** A. Moses, K. Jenkins, Philip Anderson and H. Stanbury
Volume 158 **Advanced Dielectric Materials for Electrostatic Capacitors** Q Li (Editor)
Volume 159 **Transforming the Grid Towards Fully Renewable Energy** O. Probst, S. Castellanos and R. Palacios (Editors)
Volume 160 **Microgrids for Rural Areas: Research and case studies** R.K. Chauhan, K. Chauhan and S.N. Singh (Editors)
Volume 161 **Artificial Intelligence for Smarter Power Systems: Fuzzy Logic and Neural Networks** M. G. Simoes
Volume 166 **Advanced Characterization of Thin Film Solar Cells** N. Haegel and M Al-Jassim (Editors)
Volume 167 **Power Grids with Renewable Energy Storage, integration and digitalization** A. A. Sallam and B. OM P. Malik
Volume 169 **Small Wind and Hydrokinetic Turbines** P. Clausen, J. Whale and D. Wood (Editors)

Volume 170 **Reliability of Power Electronics Converters for Solar Photovoltaic Applications** F. Blaabjerg, A.l Haque, H. Wang, Z. Abdin Jaffery and Y. Yang (Editors)
Volume 171 **Utility-scale Wind Turbines and Wind Farms** A. Vasel-Be-Hagh and D. S.-K. Ting
Volume 172 **Lighting interaction with Power Systems, 2 volumes** A. Piantini (Editor)
Volume 174 **Silicon Solar Cell Metallization and Module Technology** T. Dullweber (Editor)
Volume 180 **Protection of Electricity Distribution Networks, 4th Edition** J. Gers and E. Holmes
Volume 811 **Modelling and Simulation of Complex Power Systems** A. Monti and A. Benigni
Volume 182 **Surge Protection for Low Voltage Systems** A. Rousseau (Editor)
Volume 184 C**ompressed Air Energy Storage: Types, systems and applications** D. Ting and J. Stagner
Volume 186 S**ynchronous Reluctance Machines: Analysis, optimization and applications** N. Bianchi, C. Babetto and G. Bacco
Volume 191 **Electric Fuses: Fundamentals and new applications 4th Edition** N. Nurse, A. Wright and P. G. Newbery
Volume 193 **Overhead Electric Power Lines: Theory and practice** S. Chattopadhyay and A. Das
Volume 194 **Offshore Wind Power Reliability, availability and maintenance, 2nd edition** P. Tavner
Volume 198 **Battery Management Systems and Inductive Balancing** A. Van den Bossche and A. Farzan Moghaddam
Volume 199 **Model Predictive Control for Microgrids: From power electronic converters to energy management** J. Hu, J. M. Guerrero and S. Islam
Volume 204 **Electromagnetic Transients in Large HV Cable Networks: Modeling and calculations** Ametani, Xue, Ohno and Khalilnezhad
Volume 208 **Nanogrids and Picogrids and their Integration with Electric Vehicles** S. Chattopadhyay
Volume 212 **Battery State Estimation: Methods and Models** S. Wang
Volume 215 **Industrial Demand Response: Methods, best practices, case studies, and applications** H. H. Alhelou, A. Moreno-Muñoz and P. Siano (Editors)
Volume 225 **Fusion-Fission Hybrid Nuclear Reactors: For enhanced nuclear fuel utilization and radioactive waste reduction** W. M. Stacey
Volume 905 **Power system protection, 4 volumes**

Power Distribution System State Estimation

Edited by
Elizete Maria Lourenço and João Bosco
Augusto London Junior

The Institution of Engineering and Technology

Published by The Institution of Engineering and Technology, London, United Kingdom

The Institution of Engineering and Technology is registered as a Charity in England & Wales (no. 211014) and Scotland (no. SC038698).

First published 2022

The Institution of Engineering and Technology
Futures Place
Kings Way, Stevenage
Hertfordshire, SG1 2UA.

www.theiet.org

British Library Cataloguing in Publication Data
A catalogue record for this product is available from the British Library

ISBN 978-1-83953-201-6 (Hardback)
ISBN 978-1-83953-202-3 (PDF)

Typeset in India by Exeter Premedia Services Private Limited
Printed in the UK by CPI Group (UK) Ltd, Croydon

To my husband and to our beloved sons Erico and Plinio.
To my father (*in memoriam*), mother, brothers and sisters.
Elizete

To my wife and to our beloved daughters Mariana and Clara.
To my father (*in memoriam*), mother and sisters.
João Bosco

This page intentionally left blank

Contents

About the Editors **xv**
Preface **xvii**

1 Introduction **1**
Elizete Maria Lourenço and João Bosco Augusto London Junior

2 Real-time monitoring of distribution systems brazilian experience **5**
João Bosco Augusto London Junior, Julio Augusto Druzina Massignan, José Paulo Ramos Fernandes, Vitor Henrique Pereira de Melo, Marcos Henrique Marçal Camillo, Rodrigo Zempulski Fanucchi, and Elizete Maria Lourenço

2.1 Introduction 5
2.2 Brazilian distribution system monitoring 6
2.3 Description of the RTMT implemented in COPEL 6
2.3.1 Step 1: Data preprocessing 7
2.3.2 Step 2: Real-time load modeling 9
2.4 Application results 14
2.4.1 In-field verification 14
2.4.2 Application in service restoration 17
2.4.3 Application in distribution system state estimation 20
2.4.4 Application for real-time load forecasting 22
2.5 Concluding remarks 25
References 26

3 Practical experiences of distribution state estimation in real life **29**
Goran Švenda

3.1 Introduction 29
3.2 Problem settings 31
3.2.1 Background 31
3.2.2 Sources of the problems 32
3.3 Industrial-grade product 43
3.3.1 Requests for practical implementation in real life 44
3.3.2 Problems of practical application and how to solve them 45
3.4 Where are we today? 56
3.5 Where are we going, and what awaits us? 57
3.6 Conclusion 59
3.6.1 Achieved to date 59

3.6.2 In front of us 60
Appendix – Schneider Electric DMS Novi Sad LLC 61
References 62

4 Three-phase network model for steady-state analysis of distribution systems 67
Julio Augusto Druzina Massignan, João Bosco Augusto London Junior, Gustavo Miranda Hebling, Elizete Maria Lourenço, Renan Kovalczuk Portelinha, and Odilon Luis Tortelli

4.1 Introduction 67
4.1.1 Distribution system state estimation 67
4.1.2 The unbalanced and asymmetrical nature of distribution systems 69
4.2 Three-phase two-port models 72
4.2.1 Three-phase two-port admittance model 73
4.2.2 Polar coordinates 74
4.2.3 Rectangular coordinates 76
4.3 Models of the physical components of a distribution system 77
4.3.1 Distribution lines 77
4.3.2 Power transformers 81
4.3.3 Voltage regulators 84
4.3.4 Loads 89
4.3.5 Shunt capacitors and reactors 92
4.3.6 Distributed generation 93
4.3.7 Energy storage 97
4.3.8 Electric vehicles 99
4.3.9 Static compensators (D-FACTS) 100
4.4 Concluding remarks 102
References 104

5 Current-based power flow calculation methods for distribution systems 109
Madson C. de Almeida, Antônio P. Feltrin, and Luís H. T. Bandória

5.1 Introduction 109
5.2 Basics of the current-based three-phase power flow 110
5.2.1 State variables 111
5.2.2 Specified quantities and bus types 111
5.2.3 Load modelling 112
5.3 Branch current–based and admittance matrix–based load flows 112
5.3.1 State variables 113
5.3.2 Bus types and equivalent specified quantities 114
5.3.3 General modelling 116
5.3.4 Computational aspects and discussion 118
5.4 Backward/forward sweep load flow 119
5.4.1 Basic aspects 120

5.4.2 General modelling 120
5.4.3 Computational aspects and discussion 121
5.5 Case studies 123
5.5.1 Data preparation 124
5.5.2 Execution of the AMBLF 124
5.5.3 Execution of the BCBLF 126
5.5.4 Execution of the BFSLF 130
5.6 Conclusions and special remarks 132
References 132

6 Classical methods applied to distribution system state estimation 135
Eduardo N. Asada, Madson C. de Almeida, and Luis F. Ugarte

6.1 Introduction 135
6.2 Historical notes 137
6.3 Basics of BCB and AMB state estimators 138
6.3.1 State variables 140
6.3.2 Equivalent measurements 140
6.3.3 Variances of the equivalent measurements 142
6.3.4 Reference bus 143
6.3.5 WLS solution via normal equation 145
6.4 Jacobian matrix of the AMBSE 146
6.4.1 Derivatives of the complex current injections 146
6.4.2 Derivatives of the complex current flows 147
6.4.3 Derivatives of the equivalent voltages 147
6.4.4 Derivatives of the complex voltages of the reference bus 148
6.5 Jacobian matrix of the BCBSE 148
6.5.1 Derivative of the magnitude of the current flows 149
6.5.2 Derivative of the complex current injections 149
6.5.3 Derivative of the complex current flows 149
6.5.4 Derivative of the equivalent voltages 150
6.5.5 Derivatives of the complex voltages of the reference bus 151
6.6 Computational aspects 151
6.6.1 AMBSE algorithm 151
6.6.2 BCBSE algorithm 152
6.7 Case studies 152
6.7.1 Solving the AMBSE 154
6.7.2 Solving the BCBSE 156
6.8 Conclusion 158
References 159

7 Fast-decoupled power flow method for active distribution systems 163
Odilon Luis Tortelli, Elizete Maria Lourenço, Bikash Chandra Pal, Ariovaldo Verandio Garcia, and Renan Kovalczuk Portelinha

7.1 Introduction 163
7.1.1 Power flow analysis for active DS 164

7.2 Basics of Newton–Raphson-based power flow 164
7.2.1 Fundamentals of the power flow analysis 164
7.2.2 NRPF formulation 165
7.2.3 Fast-decoupled approach 167
7.3 *cpu*-based fast-decoupled power flow for distribution systems 169
7.3.1 Fundamentals of the complex per unit normalization 169
7.3.2 *cpu*-based power flow algorithm 172
7.4 Multilevel voltage analyses 172
7.5 Case studies and performance evaluation 174
7.5.1 Two-bus test system—convergence example 174
7.5.2 141-bus distribution feeder 176
7.6 Final remarks 181
References 182

8 Fast-decoupled distribution system state estimation 185
Elizete Maria Lourenço, Odilon Luis Tortelli, Bikash Chandra Pal, Ellen Mara Medeiros Nogueira, and Andressa Lorayne Monteiro

8.1 Introduction 185
8.2 Fast-decoupled weighted least-squares state estimation 186
8.2.1 Conventional weighted least-squares state estimation 186
8.2.2 Decoupled formulation 189
8.2.3 Model-decoupled state estimator 191
8.2.4 Algorithm-decoupled state estimator 192
8.3 Bus-section level modeling in state estimation 193
8.3.1 Generalized decoupled formulation 194
8.4 *cpu*-based fast-decoupled DSSE 198
8.4.1 Data and measurement under cpu normalization 198
8.4.2 Conventional measurement data in cpu system 198
8.5 Measurement simulator 200
8.6 *cpu*-based real-time distribution system network modeling algorithm 201
8.7 Case studies and performance evaluation 203
8.8 Final remarks 205
References 205

9 Bayesian approach for distribution system state estimation 209
Marco Pau, Paolo Attilio Pegoraro, Ferdinanda Ponci, and Sara Sulis

9.1 Introduction 209
9.2 Power statistics and pseudo-measurements 212
9.3 Bayesian approach for state estimation in distribution systems 218
9.3.1 Measurement model 218
9.3.2 A Bayes framework for DSSE 220
9.3.3 Measurement handling 223
9.3.4 Prior description 224
9.3.5 Numerical computation of the Bayesian DSSE 225

9.4 Examples of Bayesian distribution system state estimation 227
9.5 Concluding remarks 234
References 235

10 Multiarea state estimation for distribution systems 239
Julio Augusto Druzina Massignan, João Bosco Augusto London Junior, Marco Pau, and Paolo Attilio Pegoraro

10.1 Introduction 239
10.1.1 Large-scale distribution systems and motivations for MASE 239
10.2 Multiarea State Estimation 242
10.2.1 Terminology, definitions, and classifications of multiarea state estimators 242
10.2.2 Hierarchical architecture 245
10.2.3 Distributed architecture 247
10.3 MASE for distribution systems 247
10.3.1 Two-step method with branch current estimator 247
10.3.2 Bayesian inference method with nodal voltage estimator 256
10.4 Application examples of MASE for distribution systems 261
10.4.1 Example I: Two-step multiarea DSSE 261
10.4.2 Example II: Bayesian inference multiarea DSSE 268
10.5 Concluding remarks 275
References 276

11 Including synchronized and non-synchronized measurements with different sample rates in distribution system state estimation 279
Mohammed Ansar Mohammed Manaz, Yu-Jen Lin, Shao-Jie Wang, João Bosco Augusto London Junior, Julio Augusto Druzina Massignan, and Chan-Nan Lu

11.1 Introduction 279
11.2 Data sources for DSSE 280
11.2.1 Measurement data used in DSSE 281
11.3 Temporal aspects of DSSE 283
11.3.1 Dynamic state estimation concepts and introduction to Kalman filters 285
11.3.2 Dynamic, forecasting-aided and tracking state estimation 287
11.4 Multistages state estimators based on quasi-dynamic techniques 288
11.4.1 Limitations of Kalman filter-based methods 292
11.4.2 Consensus DSSE method 292
11.4.3 Matrix completion-based system state update with granular measurements 296
11.4.4 Implementations of matrix completion-based DSSE 298
11.4.5 Numerical results 300
11.5 Bayesian information fusion approach for multistage DSSE 302
11.5.1 Bayesian inference concepts and application in DSSE 303
11.5.2 Posterior inference via orthogonal methods 305

11.5.3 Bayesian credibility test 306
11.5.4 Numerical results 306
11.6 Applications of DSSE and challenges 311
11.7 Concluding remarks 312
References 313

12 State estimation for low voltage distribution grids 319
Andreas Kotsonias, Markos Asprou, Lenos Hadjidemetriou, and Christos Panayiotou

12.1 The need for DSSE in LVDGs 319
12.2 Classical DSSE approach 323
12.2.1 WLS DSSE 323
12.2.2 State variables and measurement functions 325
12.2.3 Kron's reduction: four wires to three wires 327
12.3 Challenges for DSSE in LVDGs 329
12.3.1 Limited sensing 329
12.3.2 Limited system knowledge 331
12.3.3 Slow reporting rate – asynchronous measurements 332
12.3.4 Nonzero neutral voltage 334
12.4 Enhancing DSSE 338
12.4.1 Addressing asynchronous measurements using historical data 339
12.4.2 Addressing the nonzero neutral voltage 342
12.5 Future directions 349
12.5.1 State estimation for the whole distribution grid 349
12.5.2 Leveraging information from PV and EV inverters 350
12.5.3 Validation in a real-time hardware-in-the-loop framework 350
12.6 Concluding remarks 351
References 352

13 Conclusions 355
Elizete Maria Lourenço and João Bosco Augusto London Junior

13.1 Historical context 355
13.2 Alternative modeling and approaches for DSSE 357
13.3 Future perspectives for the evolution of the DSSE process 358
13.4 Final remarks 359

Index 361

About the Editors

Elizete Maria Lourenço is a professor at the Electrical Engineering Department of the Federal University of Paraná, Brazil. Her research interests are in the area of computational methods for the analysis and operation of transmission and distribution systems, with emphasis on power system state estimation. She serves on the editorial boards or as reviewer for numerous key journals, including IEEE Transactions on Sustainable Energy, *IEEE Transactions on Power Systems*, *IEEE Transactions on Smart Grid*, *IET Generation*, *Transmission & Distribution and Journal of Modern Power Systems and Clean Energy*.

Joao Bosco Augusto London Junior is a professor at the Electrical and Computer Engineering Department of the EESC-University of São Paulo, Brazil. His research interests are primarily concerned with real-time modelling and analysis of transmission and distribution systems, focusing on state estimation and service restoration problems. He serves as reviewer for numerous key journals, including *IEEE Transactions on power System*, *IEEE Transactions on Smart Grids*, *Electric Power Systems Research and IET Generation*, *Transmission & Distribution*.

This page intentionally left blank

Preface

Electrical power systems are experiencing huge transformations in present time. New renewable energy sources with intermittent behavior and connected to the system by inverters, both centralized or distributed, are assuming a predominant role in the generation expansion, creating new challenges for the optimal dispatch and control of the interconnected systems. The process of digitalization introduced by the deployment of sophisticated information processing and communication systems, associated with new instrumentation and telemetry devices, has been offering new possibilities for supervision and control. Also, new characteristics of the load introduced by demand response and transports electrification have opened up new opportunities to better match production and consumption. State estimation has been accompanying the evolution of power systems since it was introduced in the early 1970s. Its importance has long been recognized as a fundamental component of the energy management systems. As the power system evolutes, it also must be improved to accommodate the systems transformations.

The role of state estimation was initially aimed to track the evolution of the slow time varying "static state" resulting from the variations in load followed by the corresponding adjustments in generation. It was initially totally dedicated to the transmission system, particularly oriented to avoid catastrophic events in the power system, like the 1965 blackout occurred in the northeastern region of the USA. It was based on information obtained alongside the transmission system by the socalled SCADA system, a high latency system formed by remote units and dedicated telecommunication channels, supervised from a control center running dedicated and specialized hardware. Since its early days up to the beginning of this century, little has changed in its basic concepts except for a natural evolution on computation and telecommunication hardware as well as algorithmic improvements.

New developments in state estimation methods have been reported in the literature in relation to the modern power system features. A main development has been in the application of state estimation to the distribution system. This power system segment was the most impacted by the new developments as it is the area where most to the modern technologies has been implemented. The main deployment of the Smart Grid technology, as well of Distributed Energy Resources, has been concentrated in the distribution segment, creating the conditions and the necessity of a more accurate tracking of the operating conditions of this part of the grid. The information gathered by Smart Meters and other sensors installed in the distribution level has opened up opportunities to improve the existing distribution state estimation algorithms and the development of completely new ones. Some of these

developments deal with particular requirements of the distribution systems like the need for three-phase modeling, the different nature of the high, medium, and low voltage grids, and most importantly, the lack of redundancy in the real time information. In the transmission system, the spread use of Phasor Measurement Units (PMU) has proportioned the establishment of the wide area monitoring, protection, and control system, with a much accurate condition for the system situational awareness but introducing the challenge of mixing measurements with significant difference in sampling rates. Also, the high sampling rate available in PMUs offers the opportunity to development of highly effective state estimation algorithms able to incorporate the temporal evolution of the states, leading to the possibility of estimation of the power system dynamic behavior. Also, developments of artificial intelligence, particularly machine leaning methods, have been introducing Data Driven Methods to state estimation, initially applied to the pre-filtering process, but with potential to be extended to other phases of the state estimation process. Last, but not least, developments in high-performance computing have induced the research in Multiarea State Estimation to take advantage of the distributed and parallel computing environment.

This book represents an important contribution to this new era of power system state estimation. It presents a thorough review of several new developments in the state estimation theory and practice and proposes new developments, some of them still in the research stages. The main emphasis of the book is in modeling and alternative solution methods for distribution system state estimation. Both conventional and newly proposed approaches to three-phase modeling and solution algorithms, as well as the treatment of new kind of information, like PMU and Smart Meter data, are extensively described. The authors are a dedicated research team who has been working in the power system state estimation field for quite a long time, including consulting and new developments for electrical utilities in the implementation of actual applications. The book contains a solid presentation of the basic power system state estimation theory, alongside with the introduction of new concepts and methods, and the report of actual applications.

Djalma Mosqueira Falcão
Federal University of Rio de Janeiro, Rio de Janeiro, Brazil

Chapter 1

Introduction

Elizete Maria Lourenço[1] and João Bosco Augusto London Junior[2]

Recent developments in new electrical equipment and devices, associated with so-called smart grids, are changing the paradigms of operation and control of electrical power systems. If, on the one hand, smart grids concepts and technologies have brought innumerous advantages and opportunities, creating new data sources at unprecedented volume (e.g., phasor measurement units, intelligent electronic devices, and smart meters), on the other hand, it has increased the complexity of the power system in all voltage levels (due to intermittent dispersed energy resources, sensitive loads, new storage technologies, and growing electric vehicles fleet). The distribution system is clearly the segment of the electrical system most affected by the evolution of smart grids, driving the search for new tools and methodologies capable of meeting the needs of the sector.

The combination of the operational complexity and the increasing volume of data at distribution systems resulted in the need and, at the same time, the possibility of new developments in distribution system state estimation. As a result, the interest of researchers, public agents, and industry in developing and implementing the state estimation process in distribution systems has grown considerably in recent years.

In the context of transmission systems, there is a vast literature (scientific papers and books) providing comprehensive anatomy of the state estimation process theory and practice. However, despite several scientific efforts, there is a lack of references that systematically addresses all the steps involved in the state estimation process when applied to the distribution system, the main motivator for compiling this book.

Written by international authors from the academy and industry, the book approaches the process of distribution system state estimation both theoretically (on developing models that can be applied in real distribution networks) and practically (on the realization of distribution system state estimation projects). It brings together (i) practical experiences in real-time monitoring of distribution systems, (ii) network modeling (considering the unbalance and typical characteristics of the distribution

[1]Department of Electrical Engineering, Federal University of Paraná, Paraná, Brazil
[2]Department of Electrical and Computing Engineering, School of Engineering of São Carlos, University of São Paulo, São Paulo, Brazil

system), (iii) classical methods for distribution system power flow and state estimation, and (iv) alternative modeling and approaches to meet the needs of the emerging active distribution system.

The book's contents are organized into 13 chapters, including this introductory one. The chapters were elaborated following a logical sequence. However, readers may also find the book's chapters useful as self-contained references on specific issues of interest.

The first part of the book (Chapters 2 and 3) shares valuable experiences of electric utilities by providing new insights and challenges faced by real-time monitoring projects focused on determining the operational state of distribution systems.

Chapter 2 reports field results for a real-time monitoring tool that was implemented at COPEL, a Brazilian electricity utility. The tool has the objective of providing better quality real-time state load values to characterize the pre-fault steady-state condition for the execution of service restoration software. Its development was motivated by the fact that the effectiveness of such software was endangered by the low quality of the load values generated by the typical load profiles and load aggregation process available in COPEL at that time. The chapter presents the implemented real-time monitoring tool in detail together with in-field verification in a single distribution feeder of Londrina City, in Brazil, to evaluate the accuracy of the estimated load. This feeder is responsible for the energy supply of 7,305 consumers, with 560 buses (192 with distribution transformers) and 559 branches. Its nominal voltage is 13.8 kV.

Chapter 3 starts from the characteristics of distribution systems that directly affect the application and quality of distribution state estimation results in real networks. Then, a gap related to the conflict of interests in the relation of theory and practice, i.e., different wishes, interests, and practical possibilities of researchers, writers, manufacturers of industrial-grade products, and finally users of these systems, is presented and analyzed. The problem of integrating distribution state estimation into an industrial-grade product is briefly discussed, and the key system components for its practical application are highlighted. Finally, the results of distribution state estimation implementation in real life achieved to date and expectations on the topic in the near future are presented. It is worth noting that Chapter 3 is based on material previously published by the author and on his experiences gained working on Advanced Distribution Management System Schneider Electric projects.

The second part of the book (Chapters 4–6) reviews network modeling (in view of the unbalance and typical characteristics of the distribution system) and classical methods for distribution system power flow and state estimation.

Chapter 4 introduces the basic concepts regarding three-phase network models for distribution systems steady-state analysis, emphasizing a state estimation perspective. A general two-port branch model is conceived for each component of distribution systems. Different types of equipment are exemplified along with the respective particularities of their admittance matrix models, from the classical distribution system components to the novels of modern power grids, such as distributed generation, energy storage devices, electric vehicles, and flexible power electronics converters.

Chapter 5 presents three specialized methods for load flow calculation in distribution systems based on branch currents, namely, the classical Backward/Forward-Sweep, the Branch Current-Based, and the Admittance Matrix-Based load flows. Following the description of each method, the results of simulations performed in a didactic 4-bus distribution network are presented and discussed. The chapter ends with a qualitative comparison between the methods where aspects regarding convergence, computational implementation, and performance are analyzed.

Chapter 6 focuses on two classical state estimation approaches devoted to distribution systems, namely the Branch Current-Based State Estimator and the Admittance Matrix-Based State Estimator. After a detailed description of each method, the results of simulations performed using both approaches are presented and discussed.

The third and final part of the book (Chapters 7–12) is dedicated to presenting alternative approaches developed to meet the needs of emerging active distribution systems.

Chapter 7 presents the complex per unit (*cpu*) normalization technique applied to the fast decoupled power flow formulation to extend its computational efficiency to active distribution system analysis. The fundamentals of power flow calculation and *cpu* technique are fully described. Simulation results considering active distribution systems under distinct operational conditions are presented to illustrate the applicability of the *cpu*-based fast decoupled power flow approach.

Chapter 8 initially reviews the classical weighted least-squares state estimation, with special attention given to the main versions of the decoupled formulation, usually referred to as fast-decoupled state estimation. The explicit representation of switches and circuit breakers in the decoupled approach and its benefits against the traditional bus-branch model are presented and discussed in the sequel. A detailed description of the application of the *cpu* concept described in Chapter 7 to enable effective use of the fast-decoupled state estimation in the distribution system is presented. Finally, the particularities and versatility of the *cpu*-based distribution system state estimation are discussed through numerical results involving a case study.

In Chapter 9, a Bayesian approach integrates all the available information concerning the real-time measurements and the uncertainty of pseudo-measured quantities by exploring distinct density distributions for absorbed and generated energy, as well as available instrument specifications. The resulting Bayesian distribution system state estimation is theoretically presented, and its features and capabilities are illustrated through real-field-based simulation results.

Chapter 10 initially presents decomposition methods to perform state estimation in large-scale distribution networks, employing the concepts of Multiarea State Estimation. A brief context of scalability and decentralization is presented to locate the necessity of such architectures. Then, the main ideas of Multiarea State Estimation are discussed. Two methods specialized for distribution systems are detailed, a branch-current-based and a complex nodal voltage-based, as suitable algorithms for multiarea state estimator in distribution networks. Finally, numerical examples with both estimators illustrate the accuracy and computational aspects.

Chapter 11 focuses on the effective integration of different sources of information commonly available in modern distribution systems for state estimation. Such sources of information consist of load profiles and forecasts (referred to as pseudo measurements), passive buses with no generation or load (virtual measurements), and different kinds of sensors, such as smart meters, supervisory control and data acquisition measurements and phasor measurement units. It presents theoretical arguments for tackling the synergy among a large amount of heterogeneous data with various formats, sources, unsynchronized polling cycles, and communication delays. Approaches based on Kalman filter theory are presented and demonstrated through computer simulation results. Also, an approach based on Bayesian inference to manage different sampling rates of typical sources of information in the distribution system for state estimation is presented. Theoretical arguments and simulation results are provided to support the interesting features of this approach when dealing with multiscale instrumentation devices separately in different sampling layers.

Chapter 12 discusses the subject of estimating the state of the distribution system in low-voltage networks. The particularities and limiting factors of low-voltage networks are presented and discussed, while a weighted four-wire least squares approach is described. The extent needed to improve the state estimation performance under the effects of asynchronous measurements and the typical characteristics of low-voltage networks are presented, within a close look at the role played by smart grid technologies and their impact on the modern energy system.

Chapter 13 brings the concluding remarks to the book content, presenting a historical context of the challenges encountered and solutions proposed by the pioneers in the area of distribution system state estimation in their quest to meet the needs of the emerging active distribution systems; and, finally, the future research directions for the area.

Chapter 2

Real-time monitoring of distribution systems: Brazilian experience

João Bosco Augusto London Junior[1], Julio Augusto Druzina Massignan[1], José Paulo Ramos Fernandes[1], Vitor Henrique Pereira de Melo[1], Marcos Henrique Marçal Camillo[2], Rodrigo Zempulski Fanucchi[2], and Elizete Maria Lourenço[3]

2.1 Introduction

The objective of this chapter is to share the valuable experiences of COPEL, a Brazilian electricity utility, by providing new insights and the challenges faced during the development of the Project of Research and Development (R&D) of Brazilian Electricity Regulatory Agency number 2866-0271/2013.

This R&D project resulted in the development and implementation of a (i) service restoration software (SRS) and (ii) real-time monitoring tool (RTMT) to provide better quality load values to characterize the pre-fault steady-state condition for the execution of that SRS.

The focus of this chapter is the RTMT which will be presented in detail together with in-field verification in a single distribution feeder of Londrina City, in Brazil, to evaluate the accuracy of the estimated load. This feeder is responsible for the energy supply of 7,305 consumers, with 560 buses (192 with distribution transformers) and 559 branches. Its nominal voltage is 13.8 kV. Also, the application of the developed RTMT in providing the load values for the solution of the service restoration problem in a real large distribution system (DS) is presented. For this application, the processing time required by each step of the RTMT will be presented to show that it satisfies the performance requirements on practically sized DSs. Finally, initial

[1]Department of Electrical and Computing Engineering, School of Engineering of São Carlos, University of São Paulo, São Paulo, Brazil

[2]Companhia Paranaense de Energia - COPEL, Paraná, Brazil

[3]Department of Electrical Engineering, Federal University of Paraná, Paraná, Brazil

results of two further applications of the RTMT are presented, the first into the DS state estimation problem and the second along with a load nowcasting method.

2.2 Brazilian distribution system monitoring

Historically, one of the main challenges for real-time determination of the DS operating state is the lack of real-time measurements in distribution feeders. Therefore, to have some basic information about the operating conditions of distribution feeders, a load estimation procedure is usually proposed, which is generally referred to as a load estimator or load allocator [1].

In recent years, smart grid initiatives have been developed creating new sources of data at unprecedented volumes in distribution systems (e.g., micro phasor measurement units, intelligent electronic devices, smart meters). These initiatives have motivated the proposition of DS state estimators. However, the deployment of these new sources of data in Brazilian utilities is still focused on pilot projects [2–7]. Therefore, the operating condition of distribution feeders is usually determined through statistical characterization of their loads performed by a process called load aggregation [8], which is based on:

- Customer monthly energy consumption (kWh);
- Customer classification, e.g., residential, commercial, and industrial
- Typical load profiles for each customer class.

According to Brazilian regulatory issues, load profiles are generally updated every year [9]. As such profiles are only a rough approximation to given load demand, the quality of the feeder operating state obtained is poor and does not have similar precision for DS monitoring when compared to measured values along the feeder. This motivated the development and implementation of an RTMT in COPEL, which allows the treatment of load estimation as a real-time application, very similar to state estimation, but with the aim of adjusting load profiles according to the available real-time measurements, rather than determining the state variables (complex nodal voltages or complex branch currents).

2.3 Description of the RTMT implemented in COPEL

Figure 2.1 presents the flowchart of the RTMT implemented in COPEL [10]. It was designed to provide load values for an SRS* used in the DSs of COPEL, a Brazilian electricity utility. Moreover, other automated features of distribution operation centers (DOCs) can use the load values provided by the RTMT.

*This software is based on the methodology proposed in Ref. [11].

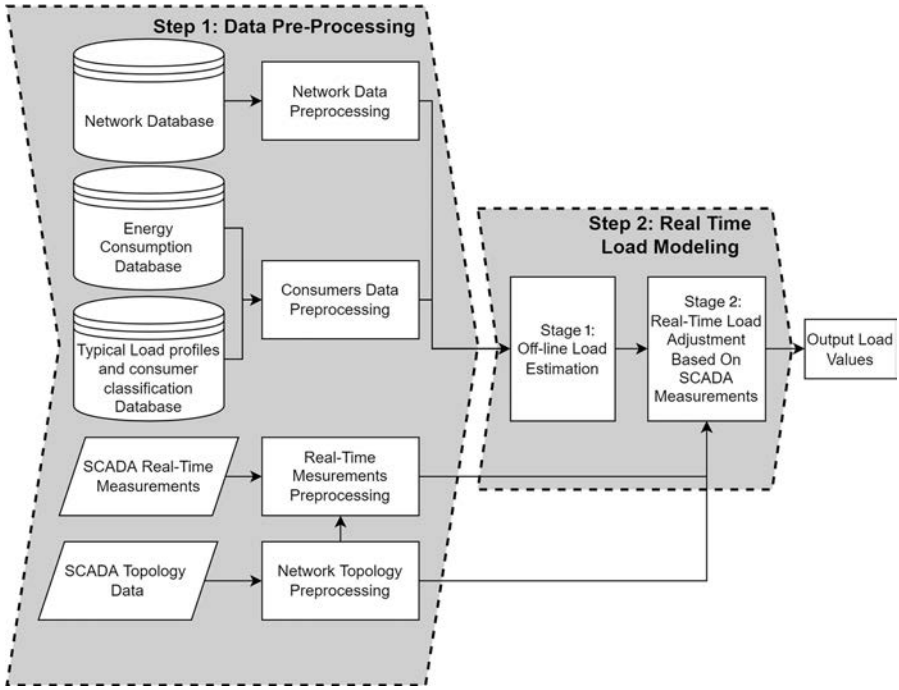

Figure 2.1 Flowchart of the RTMT implemented in COPEL

The RTMT implemented in COPEL uses information usually available in Brazilian utilities and consists of two steps (see Figure 2.1):

Step 1—Data preprocessing to provide the required information for the second step;

Step 2—Real-time load modeling.

Step 2 is performed by the real-time load estimator proposed in [12]. This estimator can handle multiple and different kinds of real-time measurements, treating all measurements present on the feeder and not only on its head. However, it cannot deal with "obviously" Bad Data since it treats the available real-time measurements as entirely accurate. To surpass this limitation, Step 1 performs the preprocessing routines proposed in [10], which is able to eliminate "obviously" Bad Data in the real-time measurements, reducing the overall quantity of Bad Data. Therefore, this elimination process enables the RTMT algorithm to satisfy the performance requirements on practically sized DSs.

2.3.1 Step 1: Data preprocessing

The distribution circuits are usually very extensive, and as a consequence, automated applications designed for these networks have to process a large amount of data. Therefore, the computational efficiency of these applications relies upon preprocessing techniques to reduce the amount of data to be analyzed. This subsection

details the preprocessing routines (Step 1) used to provide the necessary information for the real-time load modeling (Step 2).

As the consumer data (energy consumption, classification, and typical load profiles) and the network data (line and equipment parameters) do not change significantly along with the SCADA sampling, their preprocessing procedure can be performed off-line. The energy consumption is updated monthly, and the network data only changes when new equipment or cables are added to the system. Basically, these two preprocessing routines filter the necessary data in a more extensive database for the feeders monitored by the RTMT.

The network topology preprocessing updates the feeder topology according to the switch statuses in real time. The network topology preprocessing and real-time updating of the DS network are based on the use of the graph tree encoding named node-depth encoding (NDE), which ensures a high computational efficiency [13]. Each graph tree stored in NDEs represents a DS feeder, where the graph nodes represent the DS buses (substation, zero injection buses, or load buses) or sectors,[†] and the graph branches symbolize switches or conductors. If a topology change is detected, i.e., changes in switch status, NDE operators are responsible for the efficient updating of the network topology stored in NDEs. The topology changes are detected via changes on switch status telemetered by the Supervisory Control and Data Acquisition (SCADA) system and database updates for manual switches. NDE details and their computational efficiency for the treatment of DS problems are demonstrated in Refs. [11, 13, 14].

The preprocessing of real-time measurements treats the electrical quantities provided by the SCADA system. Initially, the DS is divided into subnetworks named measurement areas (MAs) using the current topology of the feeder and the location of the available real-time measurements. In sequence occurs the processing of the value of these measurements, according to the sampling rate that they arrive, generally one per minute, for each telemetered device (this is the case in COPEL). It is essential to divide the feeders in MAs, as the real-time load estimator proposed in [12] uses this concept to take into account the possibility of multiple real-time measurements in feeders (power flow and/or current magnitude), like other real-time load estimator in the literature [15–17]. The next subsection presents more details about the MAs.

In sequence, the method processes the measured values with the sampling method aiming to characterize them with the periodicity of the aggregated load curves (e.g., 15 minutes). At a specific instant t, which triggers the RTMT, all the real-time measurements inside a time frame $t - \Delta t$ are used to define a conservative estimate of the measured value using the sampling method. This application assumes that the sampling time frame Δt is sufficiently small, and so it is possible to model the measured values as stationary processes, as considered in the typical load profiles, i.e., the expected value and variance do not change within the time frame. Moreover, the measurement preprocessing provides a conservative estimate

[†]A sector is a group of buses and conductors separated by switches.

by using the maximum measured value inside a confidence interval of the samples as shown in (2.1):

$$z_{\text{est}}(t) = \max\{z_i \mid \bar{z} - 2.\sigma_z \leq z_i \leq \bar{z} + 2.\sigma_z\} \tag{2.1}$$

where z_i are the measured values acquired into the sampling time frame; $t - \Delta t$ is the standard deviation of z_i; $\bar{z}$ is the mean value of z_i; and z_{est} is the conservative estimated value of the measurement at t for the RTMT.

The choice of sampling strategy depends on the final application requirements. In other cases, other ones such as integrating the measured values along the time frame to represent the same amount of energy, using the mean value from the sampled values, or even other time frames smaller than 15 minutes may be required depending on the application. Another important aspect is that in service restoration, it is interesting to give a conservative estimate because of the uncertainty associated with typical load profiles.

It is essential to point out that if a topology change occurs during the sampling time frame, the procedure must consider only the values sampled after this event, maintaining the sampling method as a stationary process. Figure 2.2 exemplifies the sampling process.

Although the measured values are generally precise, gross errors (Bad Data) still may occur, and as [12] exposes, detecting Bad Data in DS monitoring is challenging since there is a lack of measurement redundancy. In this regard, there are some propositions to detect Obviously Bad Data for DS monitoring, usually based on significant inconsistencies between measured values and other prior knowledge about the system (e.g., topology, typical load profiles, parameters) [15]. The RTMT implemented in COPEL aims to detect Obviously Bad Data based on the following inconsistency tests:

- A measured value became zero without any topology changes (possible loss of communication).
- A measured value is larger than two times the expected value given by the typical load profiles.
- A measured value is greater than an upstream measured value (a case-specific rule defined by COPEL).

If any of these tests indicate the presence of Obviously Bad Data, the measurement is discarded.

2.3.2 Step 2: Real-time load modeling

The real-time load estimator in [12] is composed of two stages, executed in distinguished time frames. The first one is named off-line load estimation and, in its procedure, there is no need for information updated in real time. On the other hand, the second stage, called real-time load adjustment, based on estimated values of SCADA measurements, needs to be updated in real time.

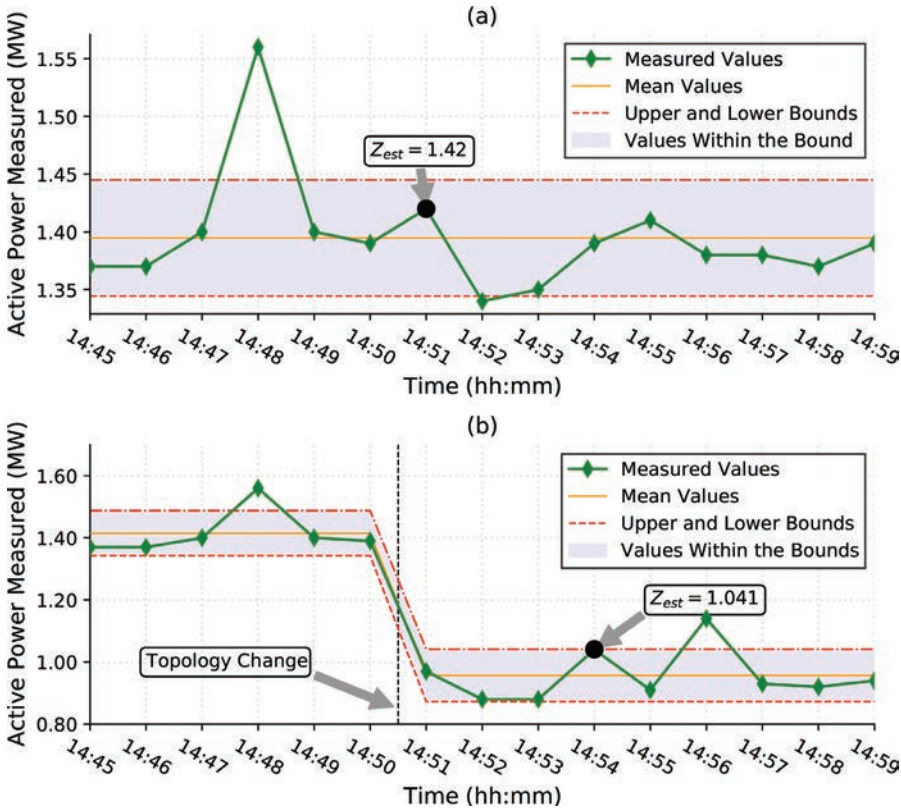

Figure 2.2 *Example of measurements sampling by the real-time measurement preprocessing. The final processed measured values are highlighted: (a) without topology change within the sampling time frame and (b) with topology change within the sampling time frame.*

2.3.2.1 Stage 1: Off-line load estimation

The first stage is accountable for the initial load estimation, and it uses prior knowledge regarding the energy consumers. The loads are assigned as active and reactive power injections to buses with distribution transformers and their values are derived from the load aggregation process [8]. This procedure assumes that each consumer (cons) load is an independent random variable, with a probabilistic model given by its respective class and typical load profile.

Therefore, to obtain the load aggregation, the process must neglect the losses in the secondary circuit. Hence, the total load of each Medium-Voltage/Low-Voltage transformer j is also a random variable given by the sum of all loads connected to its secondary circuit. The load aggregation process provides a probabilistic load model to describe each distribution transformer by using consumer profile data and their

energy consumption, which are represented by an expected value and a standard deviation at each instant t of one day as defined in (2.2) and (2.3).

Moreover, as the previous section states, the typical load profiles are obtained according to a predefined periodicity (e.g., at each 15 minutes). Any instant t within this periodicity has the same expected value and standard deviation (stationary process). Also, it is possible to use different typical load profiles according to the type of day (e.g., weekday or weekend) and the season of the year.

$$m_j(t) = \sum_{\text{cons}\in j} m_{\text{class\_cons}}(t) \cdot P_{\text{base\_cons.}} \tag{2.2}$$

$$\sigma_j(t) = \sqrt{\sum_{\text{cons}\in j} \left(\sigma_{\text{class\_cons.}}(t) \cdot P_{\text{base\_cons.}}\right)^2} \tag{2.3}$$

where $m_j(t)$ is the expected value for the active power of the load and $\sigma_j(t)$ is the standard deviation of the aggregated loads at the bus j (or transformer j) at each instant t; $m_{\text{class\_cons}}(t)$ and $\sigma_{\text{class\_cons.}}(t)$ are, respectively, the expected value of the active power and the standard deviation of the typical load profiles of the consumers at bus j at each instant t; and $P_{\text{base\_cons.}}$ is the consumer base load given by its monthly energy consumption. Equation (2.2) provides the off-line estimation of the active load (power injection) at bus j. The off-line estimation of the reactive power injection at bus j can be calculated similarly if analog information is available, or by using a typical power factor for each transformer (0.92 in this application).

2.3.2.2 Stage 2: Real-time load adjustment based on SCADA measurements

In this stage, the main goal is to adjust the load values that are the product of the first stage. The inputs for this process are the estimated values of the real-time measurements that the preprocessing routines provide in an instant t and a load flow calculation performed in the DS considering the concept of MAs.

An MA is a connected subnetwork that includes only branches with no real-time measurements and whose connections to other MAs are made through branches with real-time measurements. Figure 2.3 illustrates a DS feeder divided into three MAs.

The real-time load estimator presented in [12] makes use of an efficient backward/forward sweep load flow algorithm, which is based on the NDEs obtained by the preprocessing routines [11, 13, 14]. It is essential to notice that to perform this load flow calculation it is necessary to model the network, i.e., to obtain the mathematical representation of the circuit including all its components such as switches, voltage regulators, capacitor banks, transformers, and so on. Nevertheless, as the RTMT focuses on the service restoration application, it only considers the positive sequence.

After finishing the load flow calculation, it is necessary to evaluate, at the boundary of the MAs, the difference between the estimated measurement values (obtained by the sampling method in Step 1) and the calculated ones (determined by the load flow). If this difference is smaller than two standard deviations of the corresponding measurements, convergence has been achieved. Otherwise, the load

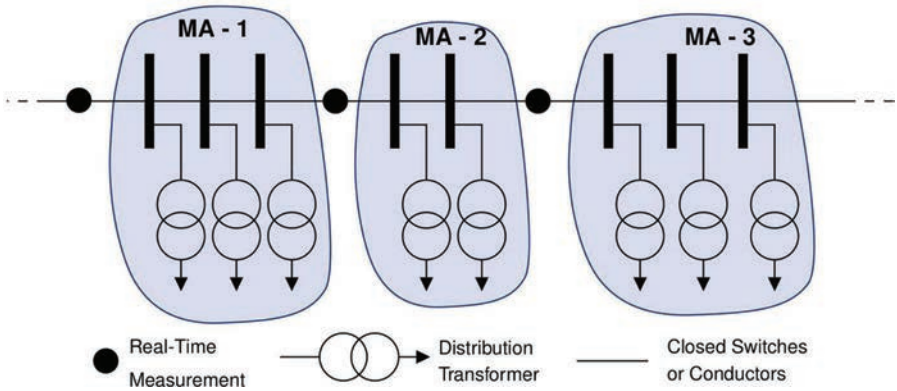

Figure 2.3 Example of distribution feeder divided into MAs

values estimated in Stage 1 are adjusted using these mismatches, and the process returns to the load flow calculation. This convergence test is defined in (2.4) and (2.5):

$$\left|z_{\text{est}}(t) - z_{\text{calc}}(t)\right| \leq \left|2.\sigma_{\text{meas}}\right| \tag{2.4}$$

$$\sigma_{\text{meas}} = \frac{pr \cdot \left|z_{\text{est}}(t)\right|}{3} \tag{2.5}$$

where $z_{\text{est}}(t)$ and $z_{\text{calc}}(t)$ are, respectively, the estimated value obtained from the preprocessing at instant t and the corresponding value determined by the load flow calculated from the load estimates. The σ_{meas} is the standard deviation of the measurement device, and pr is the precision of the measurement device (in this work 0.6% for current magnitude measurements and 2% for active and reactive power flow measurements). Only MAs with distribution transformers need load adjustment, so that the convergence does not consider those without transformers.

It is fundamental to notice that, as the real-time load estimator does not deal with measurement redundancy, one of the two MAs created when there is a measurement at each end of a branch will not be considered by the real-time load estimator, because the upstream MA will have no load. Although this redundancy type is rare in Brazilian DSs (COPEL cases do not exhibit it), the real-time load estimator implemented in COPEL could deal with it by applying the method presented in [18].

The process to perform load adjustment uses the mismatches in the active and reactive power (ΔP_{MA}, ΔQ_{MA}) of each MA. They are calculated separately for each MA by subtracting the values of downstream MAs, as shown, respectively, in (2.6) and (2.7):

$$\Delta P_{\text{MA}_i}(t) = \left(P^{\text{ups}}_{\text{est}_i}(t) - \Sigma P^{\text{downs}}_{\text{est}_i}(t)\right) - \left(P^{\text{ups}}_{\text{calc}_i}(t) - \Sigma P^{\text{downs}}_{\text{calc}_i}(t)\right) \tag{2.6}$$

$$\Delta Q_{\text{MA}_i}(t) = \left(Q^{\text{ups}}_{\text{est}_i}(t) - \Sigma Q^{\text{downs}}_{\text{est}_i}(t)\right) - \left(Q^{\text{ups}}_{\text{calc}_i}(t) - \Sigma Q^{\text{downs}}_{\text{calc}_i}(t)\right) \tag{2.7}$$

where $P^{ups}_{esp_i}(t)$ and $P^{downs}_{esp_i}(t)$ ($Q^{downs}_{esp_i}(t)$ and ($Q^{ups}_{esp_i}(t)$) are the estimated active (reactive) power flow measurements at the upstream and downstream boundary branches of the MA i. The $P^{ups}_{calc_i}(t)$ and $P^{downs}_{calc_i}(t)$ ($Q^{ups}_{calc_i}(t)$), ($Q^{downs}_{calc_i}(t)$) are, respectively, the active (reactive) power flows of the branch upstream and downstream of the MA i calculated by Stage 2.

In addition, with the calculated information, the current magnitude measurements are converted to equivalent active and reactive power. In this way, it is possible to use them to define MAs and calculate their power mismatches with (2.6) and (2.7). Furthermore, Ref. [12] shows how to perform this procedure more closely. This reference also exhibits that it is possible to deal with voltage measurements along the feeder similarly, except for those in the substations that are the reference voltage for each feeder.

Furthermore, the process to adjust the load, estimated in Stage 1, distributes the mismatches of each MA regarding the value expected for the aggregated loads estimated in each MA. Equation (2.8) summarizes this procedure:

$$m_{j_{\text{adjusted}}}(t) = m_j(t) + \frac{\Delta P_{MAi} \cdot m_j(t)}{\sum_{i \in MA} m_i(t)} \tag{2.8}$$

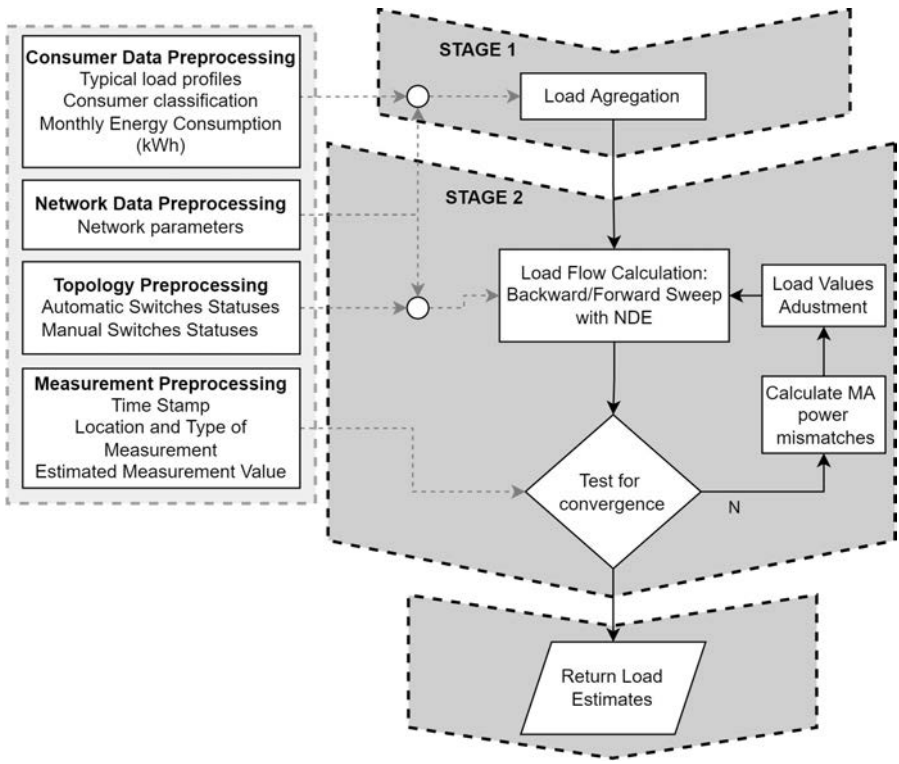

Figure 2.4 Flowchart of the real-time load estimator (Step 2 of the RTMT implemented in COPEL)

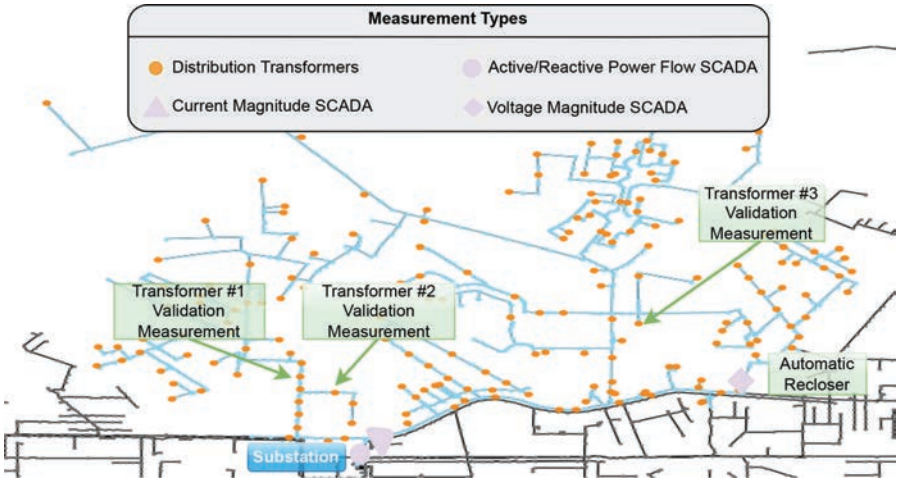

Figure 2.5 Real distribution feeder used in in-filed verification

where $m_j(t)$ is the off-line estimation of the active load at bus j, at instant t, calculated using (2.2) and $m_{j_{\text{adjusted}}}(t)$ is its new adjusted value. The procedure for the mismatch of the reactive loads is similar, this time considering the off-line estimation of the reactive load at bus j at instant t. Therefore, the process returns to the load flow calculation considering the adjusted load values. The flowchart in Figure 2.4 summarizes the real-time load estimator executed in Step 2 of the RTMT, including Stages 1 and 2, and the input data from the preprocessing routines.

It is fundamental to highlight that there are other strategies for load adjustment. However, different approaches can result in different solutions because the load estimation is, in essence, a rescaling process of the initial load values provided, considering a finite number of typical load profiles.

2.4 Application results

2.4.1 In-field verification

In order to perform in-field verification, a real distribution primary feeder responsible for supplying 7,305 consumers with 560 buses, 559 branches, and 192 transformers from the city of Londrina, Brazil, was chosen. This feeder operates at 13.8 kV, and its single-line diagram is presented in Figure 2.5. Load profiles are characterized based on the utility company's database, which contains 33 typical load profiles that are addressed to consumers in accordance with their classification and serve as a reference for the load aggregation stage. This is the first stage of the RTMT that was developed using the C language.

Monitoring devices were installed in three distribution transformers to validate the RTMT estimates. Note that measurements from these devices are not considered

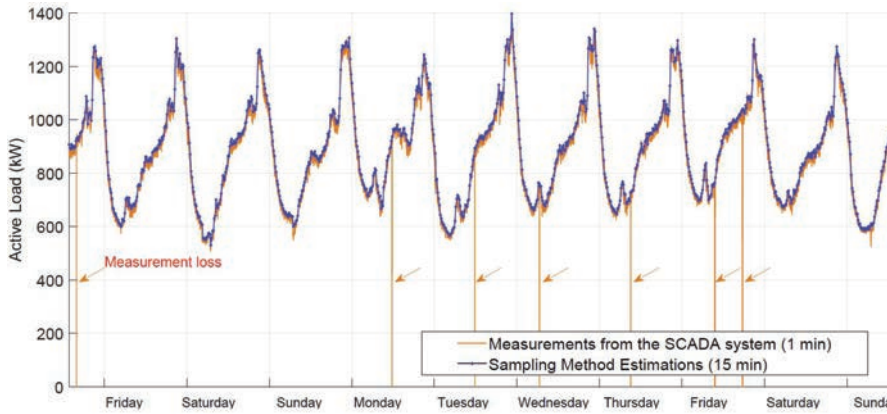

Figure 2.6 Active power flow sampled values measured from SCADA and the estimated measurement values determined by the sampling method used in Step 1 of the RTMT

by the RTMT, serving only as reference values. In this validation process, RTMT performs the load estimation at the DOC every 15 minutes. Then, the initial and the final load estimates values are compared to the reference ones. The measurements used for validation were obtained by monitoring 15-minute intervals for a week in January 2016.

The chosen distribution transformers are divided as follows:

- Transformer 1: Mainly residential consumers;
- Transformer 2: Mainly commercial consumers;
- Transformer 3: Mix of commercial and residential consumers;

The feeder in analysis has current magnitude and power flows (active and reactive) real-time measurements, as illustrated in Figure 2.5. The power flow measurements are obtained from the substation, while the current is from an automatic recloser along the feeder. To highlight the importance of the measurement preprocessing (Step 1 of the RTMT), Figure 2.6 presents the measured values from the SCADA system for the feeder active power flow measurement (z_i at each minute). It also shows the conservative estimation of the measurement value $z_{est}(t)$ obtained by (2.1) (output of Step 1 of the RTMT).

The possibility of obviously bad data occurrence must be evaluated since null measurement values are identified (communication problems in the monitoring system may be the cause), as highlighted in Figure 2.6. The sampling method of the RTMT implemented in COPEL overcomes such kind of problem by using descriptive statistics to characterize each time frame of measurements rather than the individual measured values that are subjected to those failures. As it can be seen in Figure 2.6 this sampling method does not have a meaningful impact on the measurements quality, as for some applications, such as service restoration, the interval

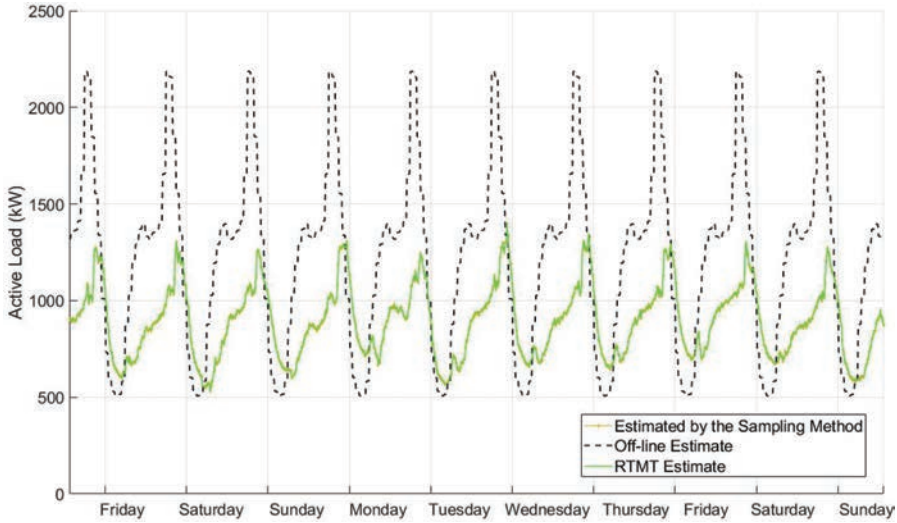

Figure 2.7 *Estimate for active power flow by the sampling method and the calculated values in Stages 1 (off-line estimate) and 2 (RTMT estimate) at the substation*

is small enough so that it can be considered a stationary process. Furthermore, the accuracy impact caused by using time frame approximations rather than actual measurements is minor compared to other uncertainties. The reason is that the load estimation process uses typical load profiles. For other applications, such as state estimation, improvements in the sampling method of the RTMT implemented in COPEL may be required, as will be further discussed.

From the measurement values estimated by the sampling method executed in Step 1, the real-time load adjustment stage of Step 2 of the RTMT adjusts the load values estimated in the off-line load estimation stage. Figure 2.7 shows both the active power flow values estimated by the sampling method (Step 1) at the substation and the respective calculated values using the off-line load estimates, and the final RTME estimates (obtained after the load adjustment—the output of Step 2) . The curve that represents RTMT estimates is over the curve that corresponds to the sampler estimated values, which is expected by the RTMT algorithm. It is possible to note that using prior knowledge of typical load profiles alone, without real-time refinement, can lead to poor estimations.

The sampler also estimates current magnitudes, which are shown in Figure 2.8. Again, it is possible to see results similar to the previous one when comparing Stages 1 and 2 estimations.

The transformers loading for the in-field validation process are shown in Figure 2.9. Measured values used as reference are shown in black, while estimated values for Stages 1 and 2 of the RTMT are shown in green and orange, respectively.

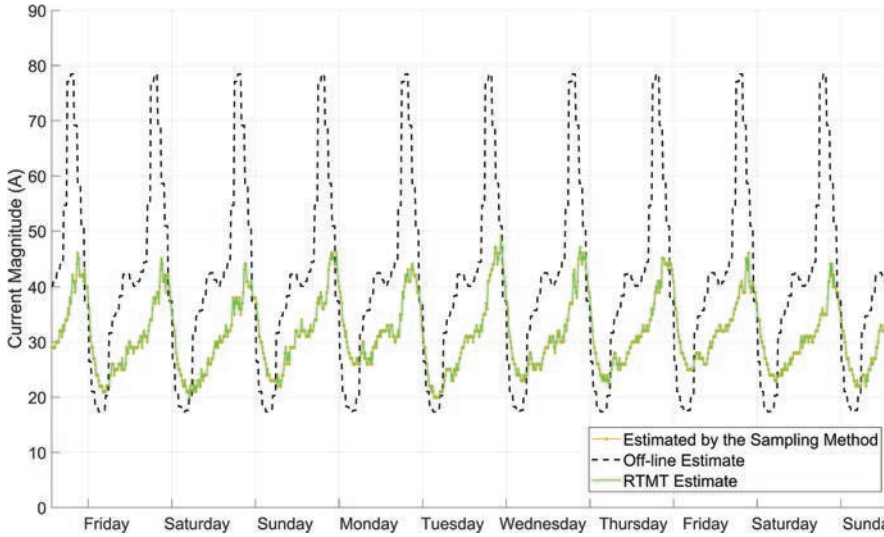

Figure 2.8 *Estimate for current magnitude by the sampling method and the calculated in Stages 1 (off-line estimate) and 2 (RTMT estimate) at the automatic recloser*

In all three transformers, Stage 2 of the RTMT was able to adjust the values obtained in Stage 1. This statement is valid for both active and reactive load estimations.

Estimations performed using the RTMT have attained better accuracy for Transformer 1 when compared to measurements for all days considered. A similar result is obtained for Transformer 2, with the exception of Sundays values. Meanwhile, Transformer 3 showed the least precision, even though the adjustment between Stages 1 and 2 has been significant. These differences in accuracy are most likely related to the quality of the data used in Stage 1, as typical load profiles available did not consider the differences between weekdays and weekends, which is specially concerning when evaluating commercial consumers. This problem is clear for Transformer 2, but more can be taken into account for Transformer 3, which had poor accuracy for every day. This lack of accuracy may be an indication that load profiles have been modeled badly. The inclusion of seasonal updates, improved probabilistic models, and smart meters data [19, 20] could enhance its performance.

Most RTMTs in literature are subject to such issues, as most rely on prior knowledge of typical load profiles. Still, this issue is rarely debated and the majority of works consider only ideal and controlled situations where prior profiles are good enough for the load aggregation process. Some cases even ignore load data, focusing the results on voltage magnitude and angle estimations [16, 17, 19–21].

2.4.2 Application in service restoration

This section discusses the utilization of the RTMT implemented in COPEL for supplying SRS with load values in the real large-scale DS of the city of Londrina,

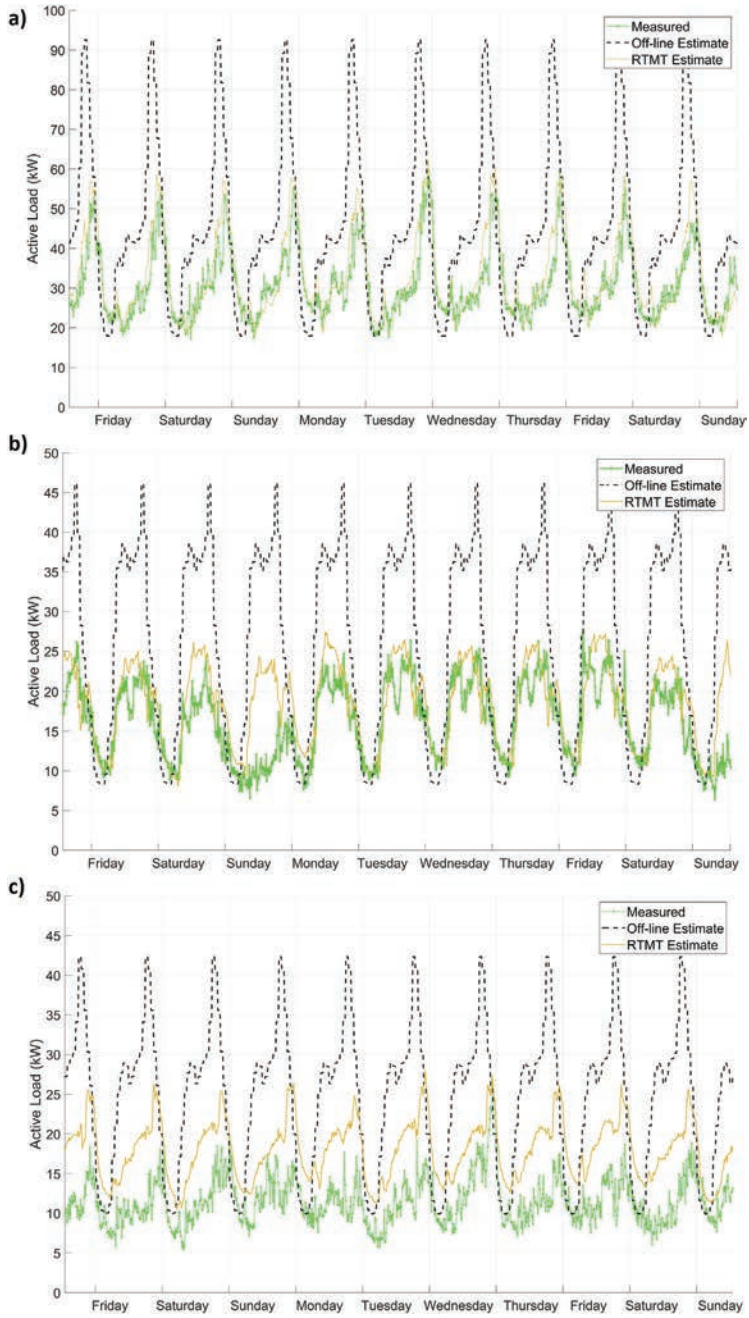

Figure 2.9 *Estimates for active load obtained in Stages 1 and 2 of the RTMT and measured values on the in-field verification: (a) Transformer 1; (b) Transformer 2; and (c) Transformer 3*

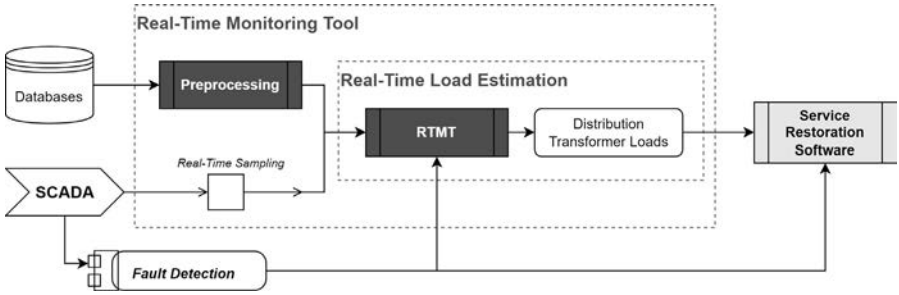

Figure 2.10 Flowchart of the interaction between the RTMT and the SRS. This feature provides the distribution transformer loads across the network in a pre-fault situation to support the optimized service restoration and fast inspection/repair planning.

Brazil. This SRS provides service restoration plans through network reconfiguration based on the pre-fault characteristics as given by the load estimations provided by the RTMT. The DS considered has 3,289 normally closed (NC) switches, 391 normally open switches, 36,851 buses, 7 substations, and 73 feeders and supplies more than 235,000 customers, with a nominal voltage of 13.8 kV. The monitoring system consists of 73 active and reactive power measurements located at each substation feeder and 41 current magnitude measurements along the feeders. The algorithm's computational performance is also discussed in this section.

In order to evaluate the RTMT usage in service restoration, a single fault situation in the studied DS was simulated. Both RTMT and the SRS are executed once protection devices detect the problem. The RTMT is responsible for preprocessing the data gathered by the SCADA devices. As stated in the previous section, the preprocessing uses time frames instead of actual measurements, in this test case a 15-minute time frame is assumed. Load values are sent to the SRS after the RTMT concludes its load modeling process. Figure 2.10 presents an overview of the RTMT integration with the SRS.

Whenever a fault occurs, SRS must isolate it by opening the necessary NC switches. This maneuver implies that systems operating in radial configuration can have healthy areas disconnected in the process if the NC switches being open are downstream the faulty one. Healthy areas that are disconnected should be restored [11] by the service restoration plan. The SRS is responsible for obtaining restoration plans that perform the least switching operations and restore the most healthy out-of-service areas in a radial configuration while respecting operational constraints, such as voltage limits, network loading, and substations loading. To verify that the constraints are not violated, the SRS performs a load flow considering the pre-fault condition as characterized by the RTMT estimations.

The computational efficiency of the RTMT is closely related to the preprocessing routines, which are responsible for reducing the data volume and the number of files to be read by each routine. Its effect is highlighted in Table 2.1, which presents

Table 2.1 Data volume and processing time of the preprocessing routines.

Processing routine	Number of files	Data volume (MB)	Processing time (s)
Network data*	7	104.0	*
Consumers data*	3	369.0	*
Network topology data	17	0.021	∼ 2.00
Real-time measurement data	14	8.0	∼ 3.00
Stage 1—Off-line load estimation*	4	21.8	3.92*
Stage 2—Real-time load adjustment	16	4.2	0.24

*Off-line routines.

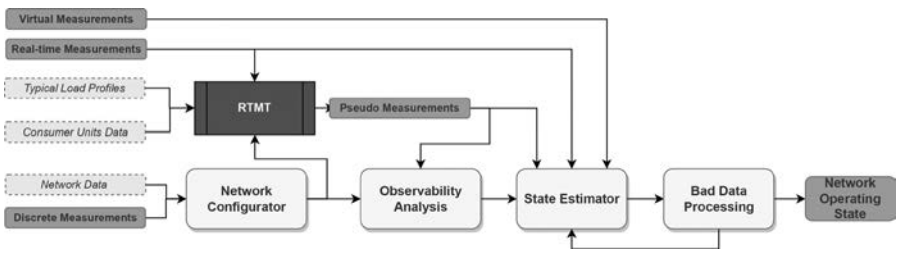

Figure 2.11 Flowchart of the interaction between the RTMT and a distribution system state estimator. This feature provides the distribution transformer loads across as the necessary pseudo-measurement to ensure observability of the state estimation process.

the data volume in Megabytes and the number of files read by routine. Off-line preprocessing leads to a reduced execution time for the real-time routines.

The only routines performed in real-time are the network topology data preprocessing, the real-time measurements data preprocessing, and the second stage of Step 2 (real-time load adjustment). This also highlights the scalability of the RTMT, since it was able to perform load estimation for a large-scale DS such as Londrina's system in less than 6 seconds, which is a reasonable execution time [12, 15].

2.4.3 Application in distribution system state estimation

Another possible application of the estimated load values is in a DS state estimator, providing better quality pseudo-measurements obtained directly from the RTMT results. This section illustrates the application of the RTMT load profiles, on the same feeder illustrated in Figure 2.2, with a state estimator based on information fusion [22]. Like most distribution feeders, this one is monitored by SCADA devices at the substation and at a recloser that provides one measurement per minute, along with pseudo-measurements based on typical load profiles sampled at every 15 minutes.

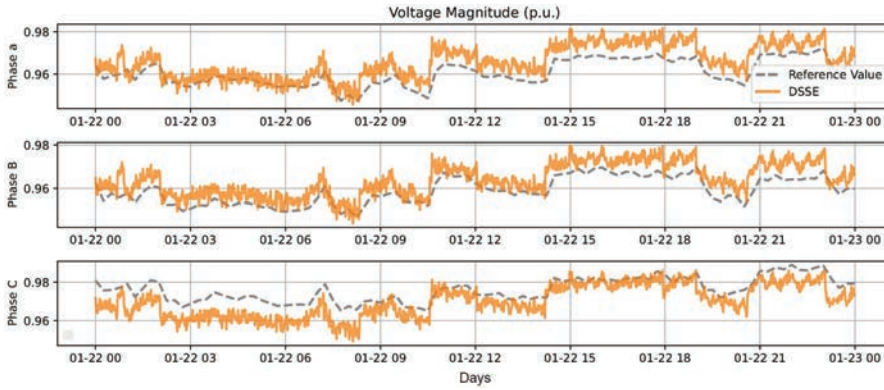

Figure 2.12 *Example of estimated voltage magnitude (one of the state variables in the state estimator) in the real feeder and its validation measurement*

Pseudo-measurements quality is one of the biggest setbacks for state estimators. This is because the lack of actual measurements implies the usage of a large amount of typical load profiles and other sources of complementary information to ensure observability. The strategy to use the RTMT results (the output refined load values) is an important application of the RTMT, improving the input information for the state estimator. Such types of applications are referred to as pseudo-measurement modeling and play a crucial role in the overall accuracy of the state estimator. Figure 2.11 presents an overview of the RTMT integration with a state estimator as a pseudo-measurement modeling technique.

To illustrate the results of this interaction between the RTMT and a state estimator, a comparison of estimated and measured voltage magnitude values for Transformer 1 phase *A*, phase *B*, and phase *C* along an entire day is presented in Figure 2.12. Note that the measured voltages are used for comparison purposes only and were not considered as input to the state estimator. From the initially obtained load values of the RTMT, initial loadings for the transformers are obtained, which are then processed according to the SCADA measurements, resulting in the final real-time state vector of the distribution feeder. The sampling rate of the SCADA measurement (1 measurement per minute) is also an interesting feature illustrated in the figure, where a corresponding estimated state is obtained for each SCADA sample, resulting in an apparently spiked voltage profile but following fast transitions occurring on the system. This is most notable in voltage transitions related to tap operations (indicated by fast and subtle voltage values transitions). These tap changes consist of tap operations at the on-load tap changer of the substation (a sudden increase of the substation voltage) and captured by the measured voltage values at the feeder's bay and reflect on the most abrupt spikes of the estimated voltages.

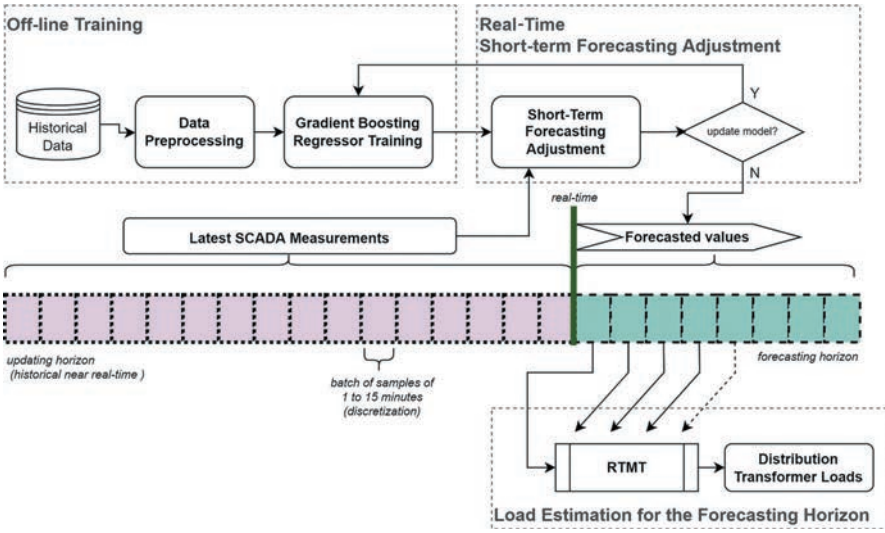

Figure 2.13 Flowchart of the load nowcasting concept, joining together the RTMT and a real-time short-term forecasting algorithm

2.4.4 Application for real-time load forecasting

As presented in Section 2.4.2, the RTMT implemented in COPEL supplies the SRS with the load values across the network to characterize the pre-fault steady-state condition. However, as the DS is a time-variant system, the load varies during the period of failure recovery. Therefore, to ensure a feasible recovery plan by the SRS in COPEL, it is necessary to use load values across the time intervals in a future forecasting horizon instead of just the pre-fault load values. In this way, it is possible to improve the RTMT implemented in COPEL with the inclusion of the nowcasting method proposed in [23] in its preprocessing step.

The term "nowcasting" describes a forecasting process that will obtain values for very short horizons and with real-time adaptation. In this case, forecasted values are adjusted to fit the ongoing load profiles, according to the available measurements. Another essential aspect of nowcasting is providing high-granularity forecasts, which are adequate for real-time system monitoring and operation.

Figure 2.13 presents a flowchart of the load nowcasting concept, joining together the RTMT implemented in COPEL and a real-time short-term forecasting algorithm (based on the gradient boosting technique). This feature provides the distribution transformer loads across time intervals of a future forecasting horizon, supporting predictive network analysis by the distribution system operators. Observe that the forecasting models can be obtained off-line. In contrast, only an adjustment stage of such a model is performed in real time with a reduced set of information, meaning the impact on computational efficiency should be minimal. In order to get good

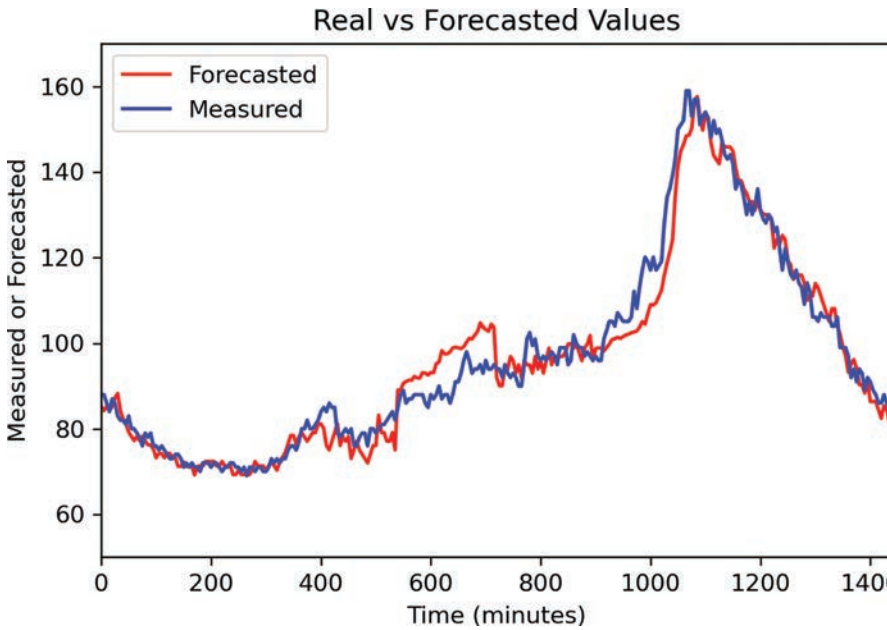

Figure 2.14 *Comparison between forecasted and measured values using the nowcasting method presented in [23]*

forecasting models, the data availability is crucial. Therefore, it is necessary to have historical data from the systems it will operate.

Initial results using the forecasting method proposed in [23] with COPEL systems presented accuracy compatible with the requirements of the DS real-time operation. The predictor accuracy is especially promising when considering 1-hour and smaller forecasting horizons. It comprises an exciting feature to enhance the quality of the load profiles or serve as complementary information for state estimation in case of missing values. To demonstrate the forecasting precision of the nowcasting method, the forecasted load curve from one of the feeders (at the circuit breaker in the feeder's bay) is compared to the actual measurements, as illustrated in Figure 2.14. The results are based on 3 hours of the nowcasting method forecasting period.

The performance is strongly related to the forecasting horizon since smaller intervals imply the algorithm can use more recent data, adjusting itself to possible changes in the load profiles. This can be clearly observed when comparing the estimated distribution density of absolute percentage errors (APE) and the mean absolute percentage errors (MAPE) distribution from 1-hour and 6-hour forecasting intervals, as shown in Figure 2.15. This figure refers to the results obtained by the traditional persistence technique, the nonadjustable forecasting method gradient boosting regressor, and by the nowcasting method presented in [23]. These results

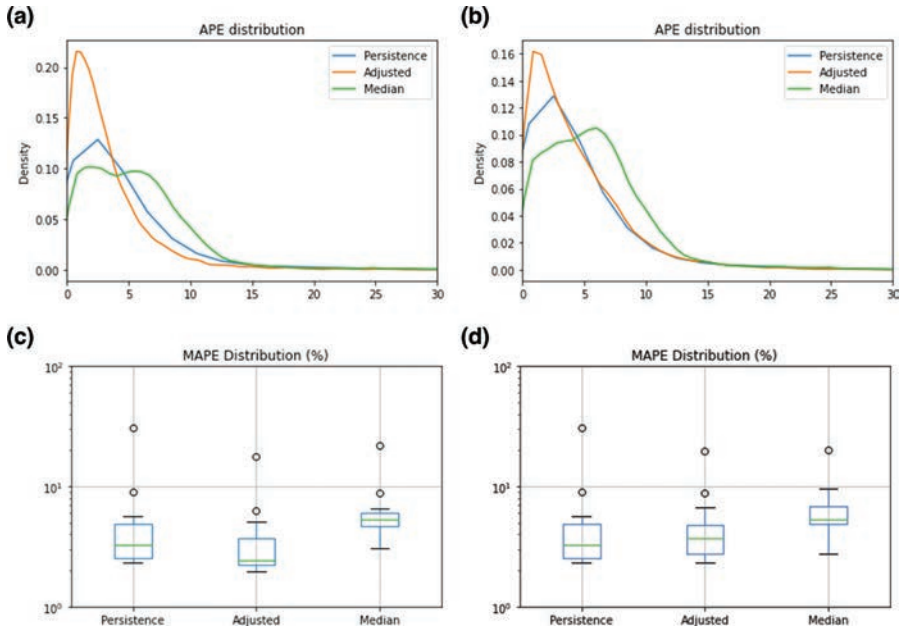

Figure 2.15 *Error distributions for each tested methodology considering different forecasting horizons: (a) Estimated distribution density of APE considering 1-hour forecasting horizons; (b) Estimated distribution density of APE considering 6-hour forecasting horizons; (c) MAPE distribution considering 1-hour forecasting horizons; (d) MAPE distribution considering 6-hour forecasting horizons*

are related to a total of 40 measuring devices, considering the same day presented in Figure 2.14.

Figure 2.15 also highlights the accuracy of the nowcasting method presented in [23] when compared to traditional persistence techniques or nonadjustable forecasting methods (in this example a gradient boosting regressor). It is noteworthy that persistence performance is generally poor when used to predict holidays or special event days loads, since it relies on previous day data. Although the focus of this section is not an in-depth discussion of such particularities, those must be considered when analyzing this brief results presentation.

Furthermore, the nowcasting technique presented in [23] offers enough computational performance to keep up with real-time operating requirements. These aspects make it a good choice for pairing with algorithms such as the RTMT, as it is adjusted in real time according to recent past measurements. In essence, nowcasting can offer more accurate data to the operator and a predictive perspective, thus potentially improving load estimation within a short-time horizon.

2.5 Concluding remarks

Real-time monitoring of DSs is a practical engineering exercise. The operator's expertise has a crucial role in ensuring that appropriate information is being provided for network analysis and control center applications. The low number of real-time measurements on the SCADA systems is a well-known and old challenge for proper grid assessment. The control center is embedded with diverse information with different levels of confidence. The operator is given the task to process such information adequately and extracts substantial knowledge about the power distribution networks, thus ensuring a whole stack of quality of service.

Within such an uncertain environment, load estimation at medium voltage level comprises a vital feature for many applications. It can be seen as a preprocessing stage that provides pseudo-measurements for state estimation and is sometimes employed directly as a grid assessment tool. The load estimaiton at the medium voltage level also provides the majority of information on nowadays state estimators, supplies the loading characteristics for asset management, ensures technical constraints are met during switching operations and, finally, may be incorporated into a predictive analysis of the distribution networks. Thus, load estimation accuracy, computational performance, and availability are crucial for advanced distribution management systems.

Brazil's practical experience demonstrates a significant dependence on typical load profiles and customer classification. Employing real-time measurements to refine such initial profiles is beneficial. It tends to provide increased accuracy on both active and reactive power loading of unmonitored (without sensors) distribution transformers. This must be supported by highly efficient computational tools to ensure real-time technical requirements at operation centers. The results of load estimation are naturally integrated with databases, instrumentation and automation systems, as well as real-time decision-making and network assessment tools. They increase operators' flexibility since they can operate the system on tighter margins while ensuring security and quality.

The deployment of smart meters at the low-voltage circuits is drastically changing the load estimation procedures and purposes, sometimes even repurposing load estimation. However, this transition is not direct, and load estimators will not be obsolete tools. Although such new meters increase the accuracy for real-time operation, the smart meters alone will not provide the grid assessment for the entire network. The technical challenge due to the increased scale of incorporating low-voltage circuits into network models imposes numerical and computational challenges for state estimators. Besides, the lack of synchronization among SCADA measurements and smart meters, updated asynchronously throughout the day, also motivates the use of special aggregation techniques to provide loading information at medium voltage levels. Moreover, the increase in dispersed renewable resources at DSs, such as rooftop photovoltaics and energy storage, adds more uncertainty for proper load estimation, which also must incorporate distributed generation estimation.

In this perspective, data analytics is prominent in processing diverse information from smart meters, customer classifications, weather conditions, and large customer behavior databases. The state estimator can then process accurate load information along SCADA measurements (and phasor measurement units) to provide operators with real-time monitoring and operation capability, harmonically processing data and detailed network models together.

References

[1] Feng X., Yang F., Peterson W. 'A practical multi-phase distribution state estimation solution incorporating smart meter and sensor data'. *IEEE Power and Energy Society General Meeting*; San Diego - California - United States, july 22-26; 2012. pp. 1–6.

[2] Gonzaga R.M., Massignan J.A.D., Maciel C.D., Augusto London J.B Jr., Almeida R.M.A., Camillo M. 'An embedded state estimator for reducing data volume and processing in smart grids monitoring'. *Workshop on Communication Networks and Power Systems*; Brasília-Brazil, from November 7th to November 9th; 2018. pp. 1–5.

[3] Pereira de Melo V.H., Massignan J.A.D., London Junior J.B.A., Fanucchi R.Z. 'Estimation of voltage unbalance at the reference bus in distribution system state estimation'. *IEEE Madrid PowerTech*; Madrid-Spain, from june 22th to july 2nd; 2021. pp. 1–6.

[4] Hebling G.M., Massignan J.A.D., London Junior J.B.A., Camillo M.H.M. 'Sparse and numerically stable implementation of a distribution system state estimation based on Multifrontal QR factorization'. *Electric Power Systems Research*. 2020, vol. 189(5), p. 106734.

[5] Manassero G., Yoshida E.S., Senger E.C., Pellini E.L., Koehler M. 'Automated digital fault recording analysis system'. *22nd International Conference on Electricity Distribution*; Stockholm - Sweden, June10-13; 2013.

[6] Primadianto A., Lu C.-N. 'A review on distribution system state estimation'. *IEEE Transactions on Power Systems*. 2017, vol. 32(5), pp. 3875–83.

[7] Majdoub M., Boukherouaa J., Cheddadi B., Belfqih A., Sabri O., Haidi T. 'A review on distribution system state estimation techniques'. *6th International Renewable and Sustainable Energy Conference (IRSEC)*; Rabat-Morocco, 05-08 December; 2018. pp. 1–6.

[8] Jardini J.A., Tahan C.M.V., Gouvea M.R., Ahn S.U., Figueiredo F.M. 'Daily load profiles for residential, commercial and industrial low voltage consumers'. *IEEE Transactions on Power Delivery*. 2000, vol. 15(1), pp. 375–80.

[9] RODIST - Module 6 – Required information and obligations - ANEEL [online]. Available from http://www.aneel.gov.br/modulo-6 [Accessed 19 Dec 2021].

[10] Massignan J.A.D., London J.B.A., Bessani M., *et al.* 'In-field validation of a real-time monitoring tool for distribution feeders'. *IEEE Transactions on Power Delivery*. 2018, vol. 33(4), pp. 1798–808.

[11] Camillo M.H.M., Fanucchi R.Z., Romero M.E.V., *et al.* 'Combining exhaustive search and multi-objective evolutionary algorithm for service restoration in large-scale distribution systems'. *Electric Power Systems Research*. 2016, vol. 134(3), pp. 1–8.

[12] Massignan J.A.D., Fantin C.A., London J.B.A., Camillo M.H.M. 'Real-time load estimation for distribution feeders'. *IEEE Eindhoven PowerTech*; Eindhoven - Netherlands, 29 June 2015 - 02 July; 2015. pp. 1–6.

[13] Delbem A.C., de Carvalho A., Policastro C.A., Pinto A.K.O. 'Node-depth encoding for evolutionary algorithms applied to network design'. *Genetic and Evolutionary Computation Conference*. Springer; 2004–678–87.

[14] Santos A., Nanni M., Mansour M., Delbem A.C.B. 'A power flow method computationally efficient for large-scale distribution systems'. *IEEE/PES Transmission and Distribution Conference and Exposition*; Bogota - Colombia, 13-15 August; 2008. pp. 1–6.

[15] Džafić I., Gilles M., Jabr R.A., Pal B.C., Henselmeyer S. 'Real time estimation of loads in radial and unsymmetrical three-phase distribution networks'. *IEEE Transactions on Power Systems*. 2013, vol. 28(4), pp. 4839–48.

[16] Nguyen D.T. 'Modeling load uncertainty in distribution network monitoring'. *IEEE Transactions on Power Systems*. 2014, vol. 30(5), pp. 2321–8.

[17] Manitsas E., Singh R., Pal B.C., Strbac G. 'Distribution system state estimation using an artificial neural network approach for pseudo measurement modeling'. *IEEE Transactions on Power Systems*. 2012, vol. 27(4), pp. 1888–96.

[18] Deng Y., He Y., Zhang B. 'A branch-estimation-based state estimation method for radial distribution systems'. *IEEE Transactions on Power Delivery*. 2002, vol. 17(4), pp. 1057–62.

[19] Alimardani A., Therrien F., Atanackovic D., Jatskevich J., Vaahedi E. 'Distribution system state estimation based on nonsynchronized smart meters'. *IEEE Transactions on Smart Grid*. 2015, vol. 6(6), pp. 2919–28.

[20] Simendic Z.J., Vladimir C., Svenda G.S. 'In-field verification of the real-time distribution state estimation'. *CIRED 2005-18th International Conference and Exhibition on Electricity Distribution. IET*; Turin - Italy, 06-09 June; 2005. pp. 1–4.

[21] Rousseaux P., Toubeau J.F., De Greve Z., Vallee F., Glavic M., Cutsem T.V. 'A new formulation of state estimation in distribution systems including demand and generation states'. *2015 IEEE Eindhoven PowerTech. IEEE*; Eindhoven - Netherlands, 29 June 2015 - 02 July; 2015. pp. 1–6.

[22] Massignan J.A.D., London J.B.A., Bessani M., Maciel C.D., Fannucchi R.Z., Miranda V. 'Bayesian inference approach for information fusion in distribution system state estimation'. *IEEE Transactions on Smart Grid*. 2022, vol. 13(1), pp. 526–40.

[23] Fernandes J.P.R., Massignan J.A.D., London J.B.A., Fanucchi R.Z. 'Very short-term current and load forecasting for distribution systems in data constrained situations'. *IEEE Madrid PowerTech*; Madrid-Spain, 28 June 2021 - 02 July; 2021. pp. 1–6.

This page intentionally left blank

Chapter 3

Practical experiences of distribution state estimation in real life

Goran Švenda[1]

Distribution and transmission networks are fundamentally different (their purpose, concept, amount of real-time data, security, dimensions, and degree of automation). Accordingly, it is natural that an efficient distribution state estimation (DSE) model and procedure for its solution follow the characteristics of the distribution network (DN). Only such specialized model and procedure for its solution, integrated into the industrial-grade product, can be robust, fast, and their results are accurate enough for application in various distribution power utilities (DPUs) worldwide.

This chapter presents the experiences of real-life applications of the specialized DSE firmly integrated into the advanced distribution management system (ADMS). These experiences have been gathered over the years by realizing a large number of Schneider Electric projects worldwide.

3.1 Introduction

The imperative of today's DPU is to increase the DN's reliability, efficiency, and resiliency while reducing and/or at least delaying unnecessary investments and growing profits. To achieve these goals, DPUs are increasingly investing in advanced metering infrastructure, smart meters, smart appliances, automation, telecommunication infrastructure, and, of course, industrial-grade softwares. In this way, DNs are increasingly changing their traditional concept and becoming smart grid networks. Thus, DNs get not only new opportunities but also new obligations. Just to mention some of them, to:

[1]Schneider Electric DMS NS and University of Novi Sad, Faculty of Technical Sciences, Novi Sad, Serbia

- manage in real time all devices, consumers, and producers of electricity, and remotely controlled automation; this can be realized through a unique system with a unique database, mathematical modeling and data processing, and uniform calculations at the level of the entire DN;
- raise machine-to-machine and human-to-machine communication to a much higher level;
- realize fully integrated, self-awareness, self-regulating, and self-healing DN;
- optimize the consumption, supply, and production of electricity;
- ensure optimal use of the existing human resources and other resources that are managed;
- provide reliable monitoring, control, analysis, communication of the field crews, and so on.

All this will enable better real-time monitoring, management, and control of DN, reduce technical and commercial losses, improve reliability indices and, above all, increase end-user satisfaction. For this to happen, it is necessary to provide a minimum of the following, to:

- take full advantage of new DN opportunities, smart equipment, and technologies;
- fully cover DN with a reliable, redundant two-way communication system;
- apply advanced information technologies and operational technologies (IT/OT);
- achieve complete and reliable integration of all internal and external systems.

Complete and reliable integration of all internal and external systems (supervisory, control, and data acquisition (SCADA), geographic information system (GIS), billing, customer information system (CIS), etc.) is a crucial moment, the foundation for realizing smart grid DN. This integration is realized through a unique advanced distribution management system (ADMS) with numerous real-time and simulation functions. The DSE results are the primary source of information for almost all these functions. Therefore, the capabilities and quality of results of all other DMS functions (primarily real-time functions), and the capabilities and quality of the entire smart grid DN, depend on the reliability, speed, and quality of DSE results.

Since the last decade of the previous century, DSE models and procedures for their solution have attracted significant research interest and led to the publishing of quite a few scientific papers. These research studies and papers are predominantly directed toward the mathematical improvement of models and procedures for their solution but not toward their practical application and verification in real DN, in real life. Therefore, this chapter presents and analyses the conditions under which DSE, in real life, can be practically applied in today's DNs. The analyses are based on the author's experiences in many projects implemented worldwide in diverse distribution environments [1].

In this sense, the setting of the problem of state estimation in DN is given in Section 3.2. The need, expectations, and practical issues of integrating DSE into

industrial-grade products are discussed in Section 3.3. The achieved results in the field of DSE are presented in Section 3.4. Expected directions of DSE development, as new challenges and new expectations, for researchers, writers, development companies (and product vendors), and users of ADMS software, are discussed in Section 3.5. Conclusions and used literature are presented in Sections 3.6 and 3.7, respectively. A brief overview of Schneider Electric DMS Novi Sad is given in Appendix.

3.2 Problem settings

As the essential energy function of modern ADMS and one of the critical factors for realizing smart grid DNs, DSE has been one of the biggest research challenges in DN calculations for years. Numerous papers focus on it, providing diverse ideas, mathematically high-quality models, and procedures for their solutions. Some of them are presented in other chapters of this book. Unfortunately, published models and procedures are rarely practically integrated into the ADMS and smart grid concept. Thus, the list of papers proving practical experiences of long-term application and verification of DSE in real, multi-voltage active DN, with large dimensions, in real time, is short. Despite many published papers, the lack of a long-term application of DSE in various DPUs in real life is the main reason why the standard DSE model and procedure for its solution have not been established yet. For the same reason, to date, the standards of its practical application have not been defined in terms of the rules of its full integration into modern industrial-grade products, i.e., into the overall smart grid concept.

For that to happen, it is necessary to look at the state estimation problem from its importance for the entire distribution engineering, primarily in real time. At the same time, it is essential to consider the characteristics of DNs and the possibilities of today's DPUs. The distribution companies' wishes, interests, and practical possibilities must also be considered and compared with the requirements that must be met for the published DSE models to be practically applicable. Unfortunately, there is a big, silent gap between theory and practice today. First of all, to understand this gap and then narrow it, it is necessary to start from the experiences gained in the application of DSE in real DNs, in real life.

At the same time, the essential question is "What have we learned from the implementation of DSE in the field, and how can we use these experiences in the future?"

3.2.1 Background

The intensive development of the smart grid concept and its establishment in the DN is growing interest in DSE development [2–28]. Numerous papers have been published on this topic in the past 30 years. In these papers, various DSE models can be recognized, and to list some of them: models in which the traditional transmission network state estimation (TSE) [6, 7] is adapted for application in the DN environment [3, 8–10]; models for simultaneous state estimation of transmission and DNs [11, 12]; highly specialized models for DN [4, 13–18]; models based on heuristic

rules [13, 15], or probabilistic rules [9, 10, 14, 15, 18]; models in which the state vector consists of buses voltages [3, 5, 8, 9, 14], or the branch currents [18–21]; models in which measurements of active and reactive powers, currents, and voltages are processed simultaneously [9, 13], models in which voltage measurements are neglected [19, 20], i.e., models that take into account synchronous measurements of voltages and currents phasors [5, 10]. Also, very different procedures are used to solve the previously presented models. Only some of them are weighted least squares (WLS) [8, 9, 11, 19, 20], decomposition of WLS problem of entire DN into a set of separate WLS problems [18], fuzzy logic [22, 23], artificial intelligence [24], and so on.

Unfortunately, there are very few papers in which models and procedures are integrated into the industrial-grade product, and fewer are papers in which the results of the practical application of the entire solution are presented. If low-voltage networks are considered, real demonstrations of this technique are even fewer.

Finally, based on a literature review, it can be concluded that the standard DSE model and a procedure for its solution have not been determined yet despite a wide range of very high-quality papers and decades-long research. This issue and the gaps between wishes and practical possibilities and challenges and experiences were discussed at the IEEE General Meetings in 2013 [25, 26] and 2014 [27, 28], respectively. Unfortunately, that discussion is still relevant.

Of course, many questions arise. Some of them are why this is the case, what the problems related to DSE are, what the practical application is, and how progress in this area can be made toward high-quality and practically applicable solutions. Finally, why, unlike transmission networks, an industrial-grade DSE product has not been established yet? Key issues, practical application experiences, and answers to the most raised questions are considered below.

3.2.2 Sources of the problems

Based on the experience of DSE practical application on numerous real-life projects worldwide [1], the primary sources of problems of practical implementation of industrial-grade DSE products can be divided into the following four groups:

1. characteristics and possibilities of today's DNs;
2. different wishes, interests, and practical possibilities of the users, researchers, and development company of DSE systems;
3. attempts to apply the models and procedures, which were developed for the needs of transmission networks, into DNs;
4. DSE is not a stand-alone application.

3.2.2.1 Characteristics and possibilities of today's DNs

In this section, the characteristics of DNs are considered. These characteristics make essential differences related to transmission networks, and as such, directly impose the need to differentiate their models and procedures for their solutions. At the same

time, these differences affect the possibilities of their practical application and the quality of their results in real transmission and distribution networks.

Unlike transmission networks, DNs and their characteristics can be very different. To see this, it is necessary to compare concepts of the DNs in America, Europe, and Australia. The consequence is that DNs can be balanced or unbalanced systems with symmetrical and asymmetrical states and entirely radial or weakly mashed schemes, with a dominant medium-voltage or low-voltage part of the network, and so on. At the same time, the distribution of electricity can be realized with four, three, two, or even with one conductor (single wire earth return DN).

In the following text, the basic characteristics of distribution and transmission networks are individually considered and compared: their purposes, dimensions, parameters, topology, redundancy of telemetry measurement values, consumption and production, degree of automation, and telecommunication infrastructure. All in order to better understand the state estimation problem of DNs.

3.2.2.1.1 Concept change

Today's DNs are planned and built as if they will forever be exclusively passive networks. They implied that the transmission of electricity (active power flows) is exclusively from the root of the DN to the end consumers. Its consumers are of low power, and their values are individually challenging to predict. With the introduction of distributed generators, electric cars, and energy storages, traditionally passive DNs become more and more active, with active and reactive powers having both directions (bidirectional power flow).

The four quadratic power flow direction of the DN with the distributed generator is given in Figure 3.1 [29]. Active and reactive powers injected into DN, power factor, and current phase angle for possible DN states are shown (voltage phasor is a reference with respect to phase angle). In passive DN, active power flows are one-way, from the root of the DN to its consumers, in this case quadrants I and IV are possible. That is vertically oriented DN. Unlike passive DN, in an active DN, active power flows can be bidirectional and all four quadrants I, II, III, and IV are possible. That is horizontally oriented DN.

DPUs and their management systems cannot quickly adapt to the new situation and promptly transform DNs, their technologies, and principles, from the concept of passive DN to the concept of active DN. Real-time operation planning and flexibility services will be the basis of real-time management in the transition period. Quality DSE is the basic DMS function in such management, and the quality of the entire real-time smart grid management depends on its results.

3.2.2.1.2 Dimension

The dimensions of DN are incomparably larger than the dimensions of transmission networks. Due to such huge dimensions (they can be larger than a million nodes), it is simply unthinkable to form and solve a model of the entire network

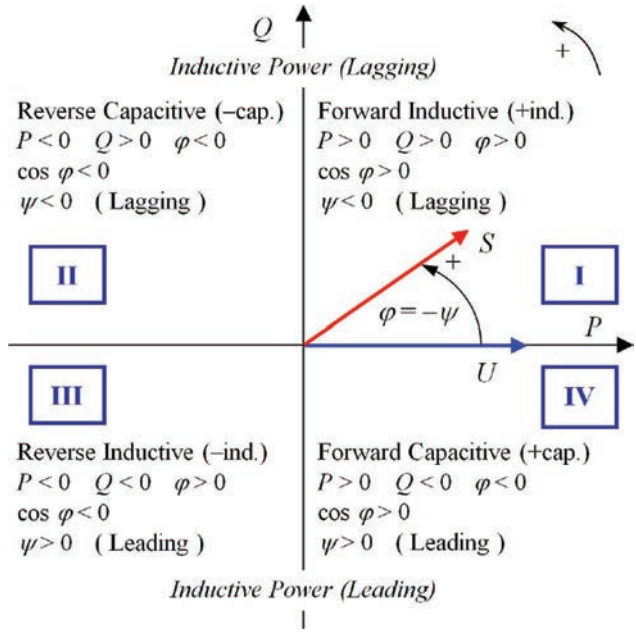

Figure 3.1 Four quadratic flow directions of a DN with distributed generators [29]

simultaneously. In fact, it is not even necessary because, in most calculation*, each DN root can be treated individually. In that way, the problem of model dimensions is reduced to the problem of model dimensions of the largest root. Note, the root of the DN is the exchange node between the distribution and transmission network, which is usually the busbar at the primary side of the supply transformer.

Regardless of the size of the model it is necessary to automatically form, correct, and solve the DSE model after each change in DN. This procedure must not be limited to the number of network buses and/or locations and the number of measurements. Drawing on experience, it is recommended to implement these procedures based on incidence matrices (buses to branches, and branches and shunts to areas). The observable areas and voltage regulation zones can be automatically formed based on these matrices. Processing of the power/current measurements and voltage measurements are enabled based on observable areas, and voltage regulation zones, respectively, Section 3.3.2.1.

The observable area of the DN is considered to be the part of the DN connected to the rest of the network exclusively via branches with power/current telemetered measurements. The voltage regulation zone consists of the root of the voltage

*The exception is, somewise, optimal network reconfiguration, but this DMS function is not the subject of this text.

regulation zone (a node on which the voltage value is controlled, e.g., bus on the secondary side of the under load tap changing transformer), and all nodes below that node, up to the first next node in which the voltage control is performed too.

3.2.2.1.3 Network parameters

The section lengths in DNs are significantly shorter than in transmission networks. In DNs, they can be from a few meters to several kilometers. Therefore, there is a wide range of values of their parameters, which directly affect the stability of calculations based on the matrix model of the network – the so-called problem of the ill-conditioned Newton–Raphson-based load flow equations. The ratio of the imaginary and the real parts of the conductor's impedances have significantly lower values in the DNs than in transmission networks. So, traditionally used fast- and high-quality procedures in transmission networks, such as Fast-decoupled load flow [30], cannot be used in DNs.

In transmission networks, the imbalance of the elements is minimal. So, by their presence, these elements cannot significantly disrupt the symmetry of electrical quantities of the transmission network. It can be considered that the equality of modules and mutual phase shift of three-phase voltages and currents and three-phase quantities of the active and three-phase quantities of the reactive powers is preserved. Also, it is considered that the consumption, i.e., production in each three-phase node, is evenly distributed in phases. In accordance with that, it is considered that all elements, its production, consumption, and thus the entire transmission network are balanced, i.e., that the regime of that network is symmetrical. Based on that, calculations in transmission networks can be realized on the model of only one phase, that is, only on the direct sequence of domains of symmetric components.

In contrast to transmission networks, in DNs, elements, sections, consumers, generators, and so on are predominantly unbalanced elements, especially at the low voltage level (these are single- and two-phase elements; note: even when they are three-phase elements, they are commonly unbalanced elements). As such, these elements disrupt the symmetry of the DN electrical values by their presence. Therefore, the models of DN elements and their influence by phases cannot be decoupled. Modeling DNs as unbalanced networks significantly increases:

- the level of complexity of the formulation of the state estimation problem; this primarily refers to specialized models of sections, transformers [31], and consumers, which can include the effects of unbalanced elements (e.g., their parameters, geometry, and phasing);
- dimensions of the entire DN model; it must not be forgotten that the model's dimensions are growing not only due to the increase in the number of phases that must be modeled at the same time but also due to the significantly larger number of nodes that DN has.

As a result, the time required to prepare the model and the number of iterations to solve it increase. That is, the speed of the entire calculation decries.

3.2.2.1.4 Topology

The structure of DN is dominantly radial, rarely, or only occasionally, with a small number of loops (so-called weakly meshed network). Topology changes in the DN happen every day, and they are incomparably more frequent than changes in the topology of transmission networks. The entire DN of one DPU is divided into galvanically separated roots. These roots occasionally exchange parts of their network. Consequently, not only the topology of the network parts has been changed over time but also the structure and dimensions of the DSE model. Therefore, every real-time system must be aware of changes in the DN topology, and, based on these changes, it must automatically form or correct the network model (topology matrix). Commonly, this automation is realized by network inspection (graph theory).

Thereby, topological data include all fast and slow status changes of the switching equipment, tap changer positions of control transformers, equipment for changing the capacity of resources for reactive power compensation, and so on. These data are collected by SCADA, substation automation, and manually.

3.2.2.1.5 Redundancy

The minimum amount of data required for an unambiguous calculation of power flows (to determine the network state vector) represents redundancy 1 (100% observability). In general, the data are redundant if its removal will not impair the observability of the network. Two redundant measurements are measurements whose simultaneous removal will make the system unobservable [7]. In transmission networks, the redundancy value is from 1.5 to 2 and even greater than 2, while the number of virtual and fictitious measurements is relatively small. In DN, the redundancy of the measured data is far smaller. Based on the literature, its value is 0.2–0.3 [32], but based on practical experience, for a large number of projects, it is far smaller, on average even below 0.05. Such a significant lack of data makes it impossible to unambiguously calculate the power flows in the DN, let alone to estimate the state, with its classic step of "bad data detection". Under such circumstances, the estimation of the topology and parameters of real DN elements, in real time, is at the level of initial ideas, far from any practical application and verification in real DNs.

Data redundancy values recorded on ADMS projects done in Europe, Asia, and North and South America are shown in Figure 3.2 (redundancy values for 43 DPUs are indicated in different colors). Redundancy was calculated as follows: the total number of telemetry measurement values was divided by two and divided by the number of DN nodes. The average redundancy value is 0.02, and the maximum is 0.12, in any case far less than 1 and far below the standard values in transmission networks. So far, only the medium voltage (MV) network has been considered. If the low voltage (LV) network is added, the value of redundancy decreases further.

In the state estimation, zero active and reactive power injection values for all nodes, without consumption and/or production, can be used as virtual measurements. If virtual measurements are treated as additional telemetry values, the information needed for unambiguous calculation of power flows, and thus for state estimation, is

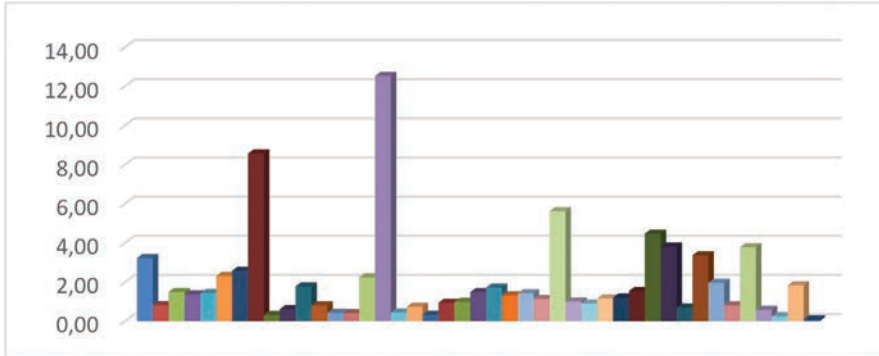

Figure 3.2 Redundancy in DNs [1]

significantly increased. But the value of redundancy is still far from 1, which is not enough for an unambiguous calculation of power flows.

In any case, DN is a dominantly unobservable network. This is one of the reasons why the application of the classical state estimation model (which is created for transmission systems with a high degree of redundancy) in DN often does not converge. However, if it does converge, its results are usually of low reliability (primarily due to high fluctuations, uncertainties of injection of consumers and generators).

3.2.2.1.6 Consumption and production

Consumption and production in transmission networks are usually large, stable, and relatively easy to forecast. Therefore, the quality application of a large number of real-time functions and functionalities (state estimation, voltage and reactive power regulation, economic dispatching, unit commitment, etc.) has long been possible in transmission networks.

Individual consumption and production in DN are minimal, usually from a few kilowatts to a few tens of kilowatts. In practice, for completely unpredictable reasons, these values can radically change or fluctuate in a very short period of time. Therefore, production and consumption in DN are and must be treated as difficult to predict. Load forecasting tools for a large number of MV and LV consumers are still being developed [33, 34]. The consequence of the great uncertainty of the injection into DN nodes is the great uncertainty of the quality of application of all resident, real-time functions (state estimation, Volt Control, Var Control, Volt-Var Control, etc.).

In such circumstances, the lack of real-time data must be artificially compensated. Based on historical data, a historical consumption model is formed. It consists of qualitative and quantitative indicators of the burden on all consumers. In order to form quantitative consumption indicators, it is necessary to group all consumers according to the similarity of their diagrams. Unique normalized consumption diagrams (diagrams of active and reactive powers and/or currents and power factors) are formed for each group of similar consumers for all characteristic days and

characteristic periods [35]. Quantitative indicators are defined for each consumer. They can be the energy taken by the consumer, the average power consumption, or the maximum current. Based on the historical consumption indicators, the first assessment of the regime of the considered DN at the considered moment is performed. This approach has significant advantages overload models based on all consumers' individual daily load diagrams. The advantages consist of the following:

- significant reduction in the amount of data that needs to be collected, processed, and maintained;
- great memory savings;
- increase the speed of all real-time calculations.

All this without a visible reduction in the quality of the state estimation results. Example:

If DN has millions of consumers, and if the measurements of active and reactive powers are obtained from smart meters with a resolution of each minute, and recorded as floats (4 bytes), then it is necessary to store 3.8 TB values in a year. At best, 65 GB is required if hourly values are recorded. The additional problem is that it is most efficient for real-time calculations (the fastest access is provided) if data are stored in memory (RAM) and not in the data warehouse. If the same consumers present themselves with, e.g., 1,000 characteristic consumers, each with two 24-hour diagrams (active and reactive power diagrams), for three characteristic days, and four characteristic periods, then the total required amount of data (2 106 + 103 576) is $\times 4$ bytes $\approx$10 MB. That's 99.985% less than 65 GB! The basic problem of this approach comes down to determining the best group of similar consumers, especially when the number and dimensionality of time series are huge [33].

3.2.2.1.7 Automation and remote control

Today, the level of automation, and thus the possibilities of remote control in DNs, is very modest. Compared to transmission networks, even at a very low level. The reason for that is the fact that for decades, significantly less was invested in the equipment and infrastructure of DNs, especially in their telecommunications. In addition to being modest, automation and remote control in DNs are based on very different devices, software, and heuristic solutions. Some of them are automatic voltage regulators which have a preset characteristic of the voltage control law, supply transformers and feeder voltage regulators with set-point values, capacitors and controllable distributed energy resources (individual distributed generators and energy storage devices), Yukon feeder automation, substation automation, peer-to-peer communication, and so on. Such a situation further complicates the formation of a quality DSE model and procedures for its solving.

In addition to various solutions, which are the product of different manufacturers, the regulation is conditioned by various systemic and technical rules and limitations. Some of them are the maximum number of changes in the status of the capacitor bank in one day; the minimum time allowed since the last change;

load change position speed; system constraints related to the maximum allowable change of reactive power in DN, and so forth. These and similar rules and limitations directly affect the formation of the DN regime and, as such, cannot be ignored. They cannot be modeled within DSE, but their effects can be considered well within specialized algorithms for power flow calculations, volt var control, and so on. This is certainly a sufficient reason why both power flow and DSE must be integrated into the industrial-grade product. In this way, power flow can be used within the DSE as one of its basic subfunctions.

3.2.2.1.8 Telecommunications infrastructure

The development of the smart grid concept and the application of IT/OT solutions directly depend on the data exchange's accuracy and speed. This exchange is limited by the capabilities of the communication system (with its redundancy, availability, bandwidth, network capacity, and latency). So, in order to establish a robust and fast real-time ADMS system, it is necessary to provide a quality telecommunications infrastructure. This quality is defined by the following requirements: a dedicated redundant telecommunications connection with a pre-defined minimum capacity, the availability of communication links, and latency.

When meeting the previously set requirements in the DN, the following problems are encountered: insufficient speed, limited flow, and/or incomplete redundancy of connections, both between facilities and toward real-time centers (data centers and dispatch centers). An additional problem is the fact that very different systems and technologies are used to transfer data. Some of them are local area network – Ethernet, neighborhood area network, wide area network, Home area network, general packet radio services (GPRS), asymmetric digital subscriber line (ADSL), radio frequency, optical ground wire, all-dielectric self-supporting, IP/Ethernet comm, power line communication, network, broadcast over power line, worldwide interoperability for microwave access, point-to-point (TR-45), synchronous digital hierarchy, wireless local area network, ZigBee, and others. Different systems are used at different voltage levels. If it is known that these systems and technologies have very different values of reliability, speed, and bandwidth, it is clear that the synchronization of their data is one of the biggest problems in the application of real-time systems. Very interesting research on the impact of data transmission systems on the quality of state estimation results in transmission networks is presented in [36]. This research should be extended to much more complicated DNs.

The redundancy problem has to be considered on two bases: redundancy of telemetry measurement values and redundancy of transmission paths. As already emphasized, the redundancy of the measured real-time data is minor. The additional problem is that the redundancy of transmission pathways in DNs is also minimal. Finally, if the redundancy of data exchange (signal) exists, it is realized by combining several different systems. Note: the radial structure of DNs has undoubtedly made its total contribution to making redundancy of transmission paths challenging to achieve.

3.2.2.2 Wishes, interests, and practical possibilities

There are obvious problems, from diverse wishes to mutual misunderstandings and conflicts of interest, between researchers and writers on the one hand, and manufacturers of industrial-grade solutions and users of these solutions, on the other hand. From a theoretical point of view, researchers and writers mathematically offer better and better DSE models and procedures for their solutions (if they were not, they would not be able to publish them). Typically, the practical application of such complex models and procedures requires radical changes and significant investments in DNs. Therefore, they are practically difficult to apply in most of today's DNs, and as such, they are not interesting (cost-effective) for development companies of industrial-grade products.

At the same time, the interests of software producers and users are not the same. The user expects that the delivered solution is fully applicable in their DN and that it solves all their requests. Incomplete solutions, additional possibilities of an advanced solution, and a solution that requires bigger system changes and more significant investments are not of interest to users, both in technical and in material terms. On the other hand, the manufacturer must deliver the same solution (or at least the most similar) in as many places as possible to do business positively. The reasons for this are straightforward, the delivery of the same/similar solution drastically reduces problems and investments related to the development, practical implementation, and then maintenance of the delivered solution. Under such conditions, the manufacturer does not have to hire many experts with different domain knowledge for a long time to take care of numerous projects with different solutions. Conversely, any deviation from a unique, basic solution raises the price of the offer and usually makes it economically unacceptable to the user.

In accordance with the above, it is a great challenge for everyone to solve the problem of DSE in terms of fulfilling the wishes and interests of users and manufacturers of DSE systems. This solution must undoubtedly be in accordance with the capabilities of today's models and procedures for their solution and the quality of telecommunications infrastructure, equipment, and IT/OT technology. Experiences from successfully implemented projects can greatly help to set the problem and solve it.

Finally, the consequence of significant differences between transmission and DNs is that conventional models, developed and applied in transmission networks and procedures for their solution, are unusable at the level of DN [16, 37, 38].

3.2.2.3 TSE vs DSE

The idea of TSE is well known. Its standard model was established in the 1970s [39–41], and the industrial-grade product was realized and verified 40 years ago. Due to a large amount of real-time data, estimation of state vectors, topologies, and even network parameters is enabled.

The idea of distribution network state estimation (DSE) was launched in the 90s. References [8–10, 13, 19] are the first publications on this topic. Practical implementation and verification of the DSE models and procedures for their solution in real DN are underway. Despite the numerous papers published on this topic

so far, it is practically possible to verify the estimation of measurement values (state vectors) and a very modestly rough estimation of network topology. The estimation of network parameters is still far, far from practical application. The first industrial-grade products intended for the overall needs of DPUs were realized and modestly verified at the end of the last century. Today, they have made significant progress and are called the ADMS. Information about Schneider Electric's fully integrated smart control system for power utilities can be found in Ref. [1].

The significant difference in the characteristics of transmission and DNs (primarily in the value of redundancy of telemetry measurement values) means that both their state estimation models and the procedures for their solution are different.

3.2.2.3.1 TSE

In transmission networks, primarily due to the high redundancy of telemetric measurement values, it is possible to directly estimate the values of voltage phasors – values with which the regime of DN best matches with telemetry measurement values. The concept of TSE, known as the classical WLS state estimation, was initially created for transmission networks and has long been established as the standard for transmission networks [6, 7]. It has been verified both in theory and in practice. Good characteristics of its application in transmission networks are the simplicity of model formation for a large number of measurements, high estimation accuracy, and fast convergence.

Problems with TSE application can occur due to its high sensitivity to gross measurement errors (the data seriously deviate from the actual) and failures in signal transmission systems and instruments. Problems of convergence and quality of results are common in networks with dominant measurements of current modules (especially with small values), low redundancy, and short sections. In general, the estimation of light-loaded DNs is a typical problem for TSE application, especially in DN with current measurements. Current measurement module treatment problems and their application in state estimation are well known [7]. In doing so, when the data do not follow the normal distribution, the least square method loses the original good characteristics.

In fact, TSE is sensitive to many common occurrences in DN.

3.2.2.3.2 DSE

The idea of state estimation in a DN is based on (1) observable areas defined by topology and incidence matrices (created based on power and current measurements locations); (2) voltage regulation zones; (3) fictitious measurements (provided by pre-estimation); (4) equations of a balance of P and Q of the area; (5) classic constrained optimization problem; and (6) load flow calculation. Due to the lack of data, very low redundancy, and the high sensitivity of the results to changes in voltage, state estimation is divided into two essential steps. The first step starts with estimating the total injections of each observable area. Load calibration of the total area injection to all area buses enables the power flow calculation of the considered DN. In the second step, the voltage values of the roots of the voltage regulation zones are

harmonized with the measurements of the voltage modulus and the previously calculated voltage profiles within the zones. If necessary, these two steps are repeated until the desired accuracy is achieved – the last power flow results are best match the current topology and telemetry values of currents, voltages, and active and reactive powers. In doing so, power flows specialized for DN are used, e.g., back/forward sweep-based load flow calculation. Finally, the harmonized state gives the estimated state vector of considered DN. The DSE procedure's basic steps for solving the DSE model are shown in Section 3.3.2.1.

Specialized DSE, developed in accordance with the common characteristics of the DN, has the following advantages, it can be practically applied in DN with: (1) light- or hard-loaded regimes; (2) only or dominantly current module measurements; and (3) long and short lines, even those with zero value parameters (this is a classic problem for procedures based on node equations, nodal admittance matrix). Additionally, the DSE convergence is faster than the convergence of TSE when both are applied in the distribution environment, at least as the convergence of BFS-based load flow is faster than the convergence of NR-based load flow.

3.2.2.3.3 Comparison

Finally, the differences between distribution and transmission networks and problems of estimation of their states are apparent. Therefore, two utterly different load flow and state estimation concepts should be applied in transmission and distribution environments. For example, suppose the state estimation concept, developed and intended for application in one system, is applied in another. In that case, some of or all of the following consequences can be expected: convergence problem, low process reliability, low robustness, unacceptably poor assessment results, unnecessarily slow calculation, and so on. These concepts can only be applicable and give good results on a few well-chosen test networks. The large gap between theory and practice was highlighted and analyzed in detail at the IEEE GMs held in 2013 and 2014 in Vancouver [25, 26] and Washington [27, 28], respectively, and in the journals [16, 42].

Theoretical and numerical comparisons between the application of a transmission and distribution power flow and transmission and DSEs are presented in Ref. [16, 42], respectively. In terms of speed, it has been shown that DSE applied in DN is even 50–60% faster than TSE (CPU times), depending on the initial solution. Apart from the state estimation concept change, the load flows specialized for DN certainly contribute to that. Specialized load flow calculation (e.g., branch-oriented, back/forward sweeping procedures – BFC) does not have the problem of short lines, even those with zero value parameters (a classic problem for procedures based on node equations). Furthermore, BFC procedures are significantly faster and more efficient than traditional Implicit ZBUS Gauss and bus-oriented (current injection and Newton-Raphson derivatives) procedures. According to research in Ref. [43], the application of BFC in DNs is as much as 2.50 times faster, at the time of calculation, than the application procedures developed for transmission networks.

The additional problem is that by applying Newton-Raphson-based TSE into the distribution environment, all shortcomings of Newton-Raphson-based load flow would be transferred into the estimation of DN state. Some of them are higher CPU time, ill-conditioned Newton-Raphson-based load flow equations for DNs, frequent topology change of DNs, and low X/R ratios that disable the application of Fast decoupled load flow in DSE calculation [16, 30].

Note: In the case of redundancy of 100%, both TSE and DSE reduce to the corresponding load flow models and calculation procedures. TSE reduces to transmission Newton-Raphson-based load flow and DSE to the distribution back/forward sweep-based load flow. These models and calculation procedures are conceptually different. In cases of measurement redundancy higher than 100%, TSE and DSE more or less represent extensions of the corresponding load flow procedures.

3.3 Industrial-grade product

Considering all the above, the great interest of users, and numerous quality papers published on this topic, the fundamental question "Why has not industrial-grade DSE product been established yet, as it was established for transmission networks a long time ago?" is still open. To answer this question, one must start with the following subquestions:

- Are the developed models practically applicable? Or, must a new specialized model be developed that is much closer to the characteristics of distribution systems? Or have we just not found a way to adapt and practically apply the existing models?
- Are DPUs ready for advanced applications integrated into an industrial-grade product? Or maybe, the benefits these systems bring are insufficient to encourage DPUs to invest in them?
- What is a theory, and what is an industrial-grade product?

Based on the stated characteristics of DN and their differences concerning transmission networks, there is an obvious need to implement specialized, conceptually different models and procedures for solving the state estimation problem in DN. These models and procedures need to be adapted to both the characteristics of the DN and the capabilities of users and manufacturers of ADMS systems.

In general, the problems to be solved can be divided into two groups:

1. problems of formation of the DSE model and procedure for its solution;
2. problems of practical realization of DSE in real life.

To solve these problems, multiple significant compromises are needed. First of all:

- a compromise between very complex methods proposed in the literature and characteristics and practical possibilities of distribution utilities; and

- a compromise between wishes and expectations of the industrial-grade product researchers, manufacturers, and users.

The result of these compromises should be the best practical solution, one industrial-grade product that can be applied in real time in all DPUs (or at least the vast majority of them). In short, the essential characteristics of such a product should be:

- very robust;
- sufficient quality results;
- fast enough calculation;
- for practical application possible and reliable product.

These problems are discussed in detail below, and most of them are answered.

3.3.1 Requests for practical implementation in real life

One of the key questions related to DSE and the entire ADMS, as an industrial-grade product, is what do DPUs want, and what do manufacturers offer to them? Unfortunately, on this issue, customer requirements and expectations and system vendor capabilities are often on opposite sides.

The user expects the offered solution will fully satisfy all requirements, give sufficient quality results, and be a robust solution covering the entire DN. But, of course, 24/7/365 reliability is a mandatory request. At the same time, apart from the technical ones, the time and economic moments of contracting and realization of the system are also significant. Of course, the economical moment is often crucial, so the total price must be reasonable and justified with cost/benefit analysis. It is this moment that crucially influences the attitude of the manufacturer.

To be competitively affordable, the manufacturer must create a unique system, which has to be applicable in any distribution utilities with minimal corrections (minimum additional investments). In doing so, it must consider the significantly different characteristics of DNs and clients' requirements worldwide. The requirements set ahead of system manufacturers are certainly aggravated by the fact that different standards, rules, work order procedures, and so forth, are applied in different DPUs. At the same time, utterly different control devices with different local logics (from different manufacturers), different signal transmission systems, different IT/OT technologies, and so on, can be found in DN.

To meet expectations, a compromise is needed. A compromise based on which a practically applicable specialized DSE model and a procedure for its solution can be formed. Model and procedure must consider all equipment and technologies and all available real-time and historical data and effects, such as local logic, load-to-voltage dependences, and so forth. At the same time, they must not depend on the dimensions of the network, network state, and the number of voltage levels. To achieve this, DSE must be incorporated into an industrial-grade product, and that product must be applicable in different DPUs, which DNs are (1) entirely or partially covered by SCADA systems, (2) small or very huge, (3) passive or active, (4)

multi-voltage level, (5) radial or weakly mashed, and (6) (un)balance system with (un)symmetric state. Finally, in order for DSE to be a resident function, it is necessary to ensure that DSE automatically adapts itself to changes in the system (after all changes in DN topology, a new system of equations and new optimization problems are automatically formed) and is executed automatically.

3.3.2 Problems of practical application and how to solve them

This section discusses the following problems of practical implementation:

- Basic steps of the procedure for solving the DSE model;
- Automatic sustainability, changes in the DSE model;
- Effects of local automation and network self-regulation, due to load-to-voltage dependences;
- DSE is not a stand-alone function;
- Integration of DSE into industrial-grade product;
- System architecture;
- Verification of application.

3.3.2.1 Basic steps of the procedure for solving the DSE model

State estimation is a classic optimization problem, with its objective function and many technical and electrical constraints (limitations). Its goal is to determine the state of DN that is optimally harmonized with the original telemetered values of power/current and voltage measurements; historical data; laws of regulation of under-load tap-changing transformers; values obtained based on TSE, representing injections in DN; effects of different devices for regulation of active and reactive power, load-to-voltage dependences, and so on. It is based on previously prepared network data, historical data, and telemetered measurement values. The DSE optimization procedure is iterative; voltage and power/current measurements are processed sequentially in each DSE iteration. It fully follows the idea on which specialized power flow calculation in DN is based, e.g., the BFS procedure for power flow calculations [43–45].

Considering all the above and the very low redundancy of telemetric measurement values, fast and sufficiently accurate estimation of injection into all nodes of one observable area is impossible. However, a fast and accurate estimation of the total injection of that area is possible. Based on that fact, a specialized DSE method and procedure for its solution have been developed.

The basic steps of a specialized procedure for solving the state estimation problem in DNs are shown in Figure 3.3. This procedure can be divided into two basic steps [16]: data preparation and the optimization procedure.

Within the first step, data preparation is realized through the following four substeps:

1. Basic load flow calculation – This is the first state assessment. It is realized based on the voltage at the DN root and predicted values injected into all DN nodes.

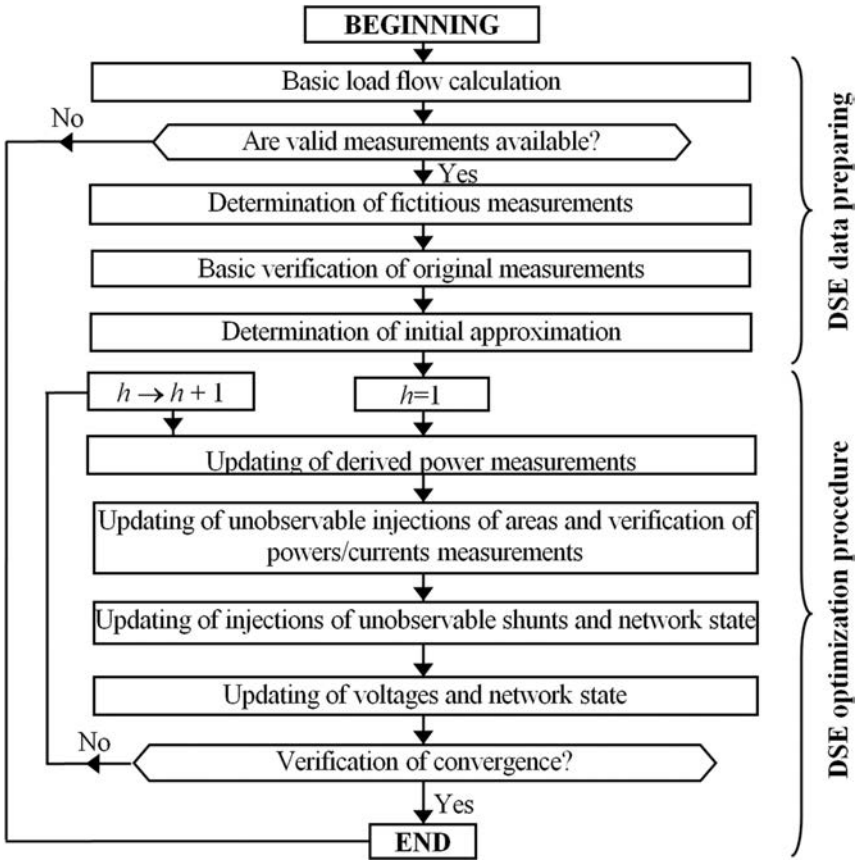

Figure 3.3 Procedure for solving the state estimation problem in DN [16]

The first predicted injections were obtained based on historical and weather data. At the same time, the load flow calculation considers all effects, control lows, and rules of local logic;

2. Determination of fictitious measurements – To increase the degree of redundancy, two types of fictitious measurements are introduced. First type: fictitious measurements of active and reactive power (values calculated in the basic load flow calculation) are assigned to each branch. Second type: fictitious measurements of total active and reactive power (sum of injections of all buses of area, based on historical data) are assigned to each observable area. Certainties of fictitious measurements are equal to the certainties of their historical data;
3. Basic verification of original measurements – Verification is realized by comparing the telemetry values of measurements and the basic load flow calculation results. Additionally, heuristic analysis is performed only on measurements with uncertain quality;

4. Determination of initial approximation – This consists of the first assessment of the DN state and the quality of the original measurements.

Within the second step, the optimization procedure is solved through the following five substeps:

1. Updating of derived power measurements – Each measurement of the current module is assigned two derived, fictitious measurements of active and reactive power. In the first iteration, these values are defined based on the basic load flow calculation. In the successive iterations, these values are defined based on the results of the last power flows;
2. Updating of unobservable injections of areas and verification of power/current measurements (first two WLS optimization problems) – In each iteration, non-observable injections of all areas and original power/current measurements are updated simultaneously. Lagrange equations are used to solve these two optimization problems, one for real and one for imaginary parts. These verifications also include bad data detection of power/current measurements with gross errors (measured data seriously deviates from the calculated). The results are new power/current approximations with the original measurements at all points;
3. Updating injections of unobservable shunts and network state, so-called load calibration – represents updating previous approximations of injected active and reactive powers into DN nodes. Areas realize this according to the mismatches of active and reactive powers injected into the considered area. These mismatches are consequences of the differences between the most recent and previous approximations of injections in the area;
4. Updating voltages and network state (the third WLS optimization problem) aims to harmonize the last calculated DN voltage profiles with voltage measurements, control low, and rules of local logic. The following load flow calculation is performed based on all regulation zones' last updated root voltage values;
5. Verification of convergence – the iterative procedure is completed if the estimated voltage values in the last two iterations do not exceed the allowable values (convergence criteria). If this is not the case, the iterative procedure continues by returning to the update of derived power measurements step.

3.3.2.2 Automatic model generation

The problem of large dimensions of the entire DPU network is overcome by dividing the network into its galvanically separated parts. Each of these parts consists of the DN root and all the nodes supplied through that node. The DN root is usually the node of energy exchange between the distribution and transmission network – the primary side of the supply transformer. There are no electromagnetic connections between the galvanically separated parts of the DN, so for these parts, DSE models can be independently formed, and procedures for solving them can be independently performed.

Due to the low redundancy, all galvanically separated parts are predominantly non-observable. A small number of observable areas are defined by branches with measurements of power and currents. By removing non-observable network parts, a high-dimensional model of highly non-observable galvanically separated parts of the DN is reduced to fully observable small-dimensional models of the same part of the DN. These areas consist of electrically connected elements without telemetry measurement values. They are connected to the rest of the network exclusively galvanically via branches with current and power measurements telemetry values. Areas are not observable in detail, but their total consumption is. In this way, solving the state estimation problem of predominantly non-observable large-dimensional DN comes down to solving the state estimation problem of an equivalent, fully observable network of small dimensions.

The idea of dividing DN into observable areas defined with power and current measurements is not new; it dates from the first to today's papers related to DSE [13, 18, 46]. However, the formalism for automatically defining observable areas and voltage regulation zones, based on which the DSE model and procedure for its solution are automatically generated, has only recently been presented in [16] for balanced and in [17] for unbalanced DNs. Almost the same idea used to determine the areas defined with power/current measurements is also used to define the incidence matrix related to voltage regulation zones. In both cases, the starting point is the topology and incidence matrix. The concepts of observable areas and voltage regulation zones allow power/current and voltage measurement processing, respectively. Frequent changes in topology, within one DN root or between a few of them, require equally frequent changes in the DN model. At the same time, these changes are triggers for a set of resident functions. Accordingly, the DSE model and procedure for its solving must be automatically adapted to any change in the DN.

Finally, in order for DSE to be practically applied in real DN, in real time, it is necessary to provide automatic, fast enough data preparation and model formation (system of optimization problem equations), performing optimization procedures, displaying results, and forwarding them to other interested functions. Triggers of the set of resident functions, including DSE, can be a change in topology, a change in measurement above the allowable value, or an expiration of the allowable time.

3.3.2.3 Local automation

Very different types of control laws and rules of local automation of control resources can be found in DPUs. For example, depending on the type of capacitor bank controller, its control may depend on changes in local values, e.g., voltage, active power, reactive power, current modulus, temperature, and time. But also, control can be conditioned by changes at the system level, e.g., due to transmission system operator requirements, high total harmonic distortion values, and so forth.

Depending on the type of local automation, its settings and the applied rules, various effects and their impact on the DN state must be considered. These are, first of all unplanned operation of the device, the so-called device hunting; automatic "restart" of the controller – switch to failsafe mode; violation of boundaries for

the implementation of commands – boundary conditions; unsuccessfully executed commands – command failed, with a re-attempt to execute a failed command – remediation, and finally removing the problematic device from the list of remotely controlled devices – exclusion list; time delay; a "watch dog" that monitors whether the setpoint value has been changed/confirmed, within the allotted time, if not the controller returns to the default value; and so forth.

3.3.2.4 Consumption self-regulation

There are two types of consumption self-regulation in power systems due to changes in voltage and frequency. In DN, only the first type is of interest.

Load-to-voltage dependences have been described in different ways. A simple ZIP model is most often used to describe consumption. Based on it, consumption is modeled as a combination of basic load types: constant power (does not depend on voltage change), constant current modulus and power factor (linearly depends on voltage change), and impedance/admittance constant (depends on the square of voltage change). Other models are used as needed, such as static exponential models and very complex advanced load models, such as models for constant energy and constant time consumption. One or more of the listed models are used depending on the final calculation goal, which of the advanced DMS functions are used, and what the desired accuracy is. For example, if the project goal is distribution system demand response, or energy conversation in closed-loop, then DSE must give very accurate results, and for that, it must use consumption models with the most quality response to voltage changes. Otherwise, for example, if only DN monitoring is of interest, then the simplest consumption models are good enough.

Here, we should add other effects that directly affect the quality of consumption value estimation, and thus the quality of the state estimation, such as coincidence factor, cold load pick up, decay effect, and load inertia after a temperature change. For the correct operation of DSE and all functions that rely on DSE results, local automation and the effects of self-regulation of consumer load due to voltage change must be taken into account. Direct modeling of these effects into a state estimation model is complicated and even impossible. Even to create a state estimation model that encompasses all these effects, that model would be highly complex for automatic generation, practical application, and maintenance.

Based on everything shown so far and practical experiences, it is obvious that the DSE model and procedure for its solution alone are not enough to provide a quality estimation of the DN state. Based on experience, the fundamental problem is how to turn a good idea into a tool that can be practically applied in the whole DPU. Its components must provide monitoring, control, outage, and hazard management, planned work management, storm management, network conditions analysis, network optimization, operation planning, network development planning, what-if analysis, and so on. Thereby, this tool must be a fully integrated smart control system for the entire DPU. So, different components are integrated into a single platform to achieve the desired functionality and accuracy of the results (Section 3.3.2.6).

3.3.2.5 DSE is not a stand-alone application

First of all, real-time state estimation is not and practically cannot be a stand-alone software application that is not bundled with other software (self-sufficient for launch and implementation). The considerations that follow are in line with that.

Every industrial-grade product, which is intended for application in the entire DPU, from the dispatch center, through smart grid engineers, all the way to the company management, must have the following features:

- primarily real-time-oriented product, which can perform various simulations (so-called "what-if" analysis);
- solving all user requests quickly and accurately enough, in all possible situations;
- no redundant data entry, i.e. it is not possible to enter any data in two or more places;
- exchanging data with various internal and external parts of the DPU;
- warranty and long-term maintenance;
- price and time of practical implementation are mutually acceptable for both the user and the manufacturer.

To implement such a product (tool), DSE must be fully integrated into the real environment. In that environment, the exchange of historical and real-time data and data with all other functions and functionalities must be enabled. A rough picture of the functions and functionalities necessary for the operation of DSE and their data exchange is shown in Figure 3.4. Each block and each connection between blocks are problems for the practical implementation of DSE in a real environment and in real time. A detailed overview of all the challenges facing the realization of a practically applicable DSE is beyond the scope of this book. Therefore, these challenges are divided into critical parts and, as such, are only listed in the next paragraph.

Based on experience, the problems of practical implementation of DSE integrated into the ADMS system can be divided into the following types of problems: data collection and preparation; formation of mathematical models and architecture of the system; system configuration and administration; integrations (adapters and integration platform); different services, standards, and protocols; customer environment; real-time triggering; communications; different local logic and automation; closed-loop (if applicable); synchronization (from different vendors, different control devices, different command execution, different data collection); time and money (the project is a very consuming process); long-term system maintenance; subsequent addition and installation of new resources and technologies; verification system; and so forth. The list of challenges is certainly not final.

Each of the listed items is a problem for itself and the entire system. If only one of them is not well-made, the entire system will not be practically applicable.

It can be noticed that for the practical implementation of DSE, the problem of forming the DSE model and procedure for its solution is only one, a small problem in relation to the problems of creating and applying the entire industrial-grade product in real life.

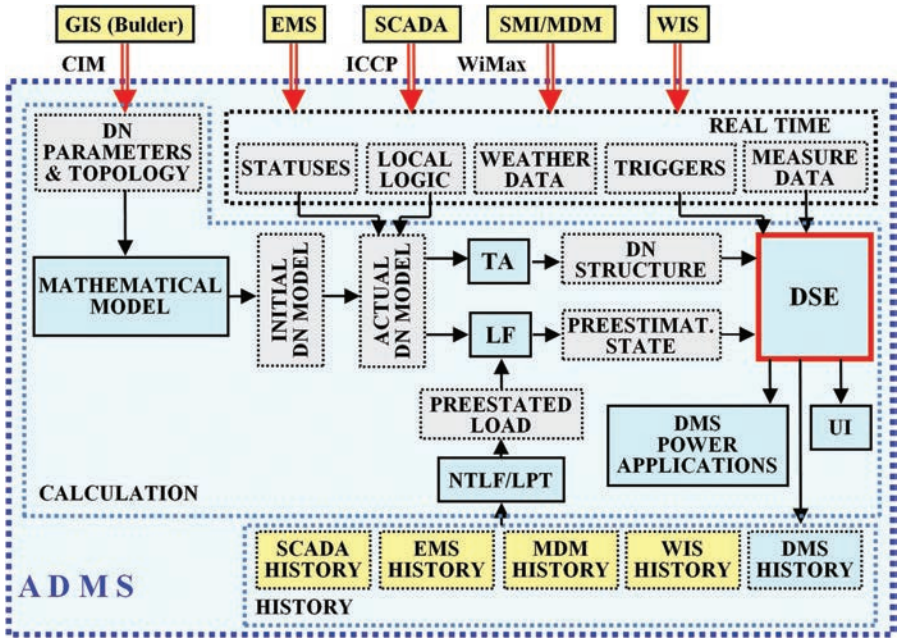

Figure 3.4 DSE is not a stand-alone function [28]

In order to meet the previously set requirements and solve the problems, the industrial-grade product must be implemented on a single software platform. Its speed and robustness are ensured by applying a unique mathematical network model and a unique database available to all functions and functionalities and all users. Unique preparation and data processing, and the use of specialized models and procedures for DN, guarantee the quality of the results. Finally, the product must have a unique user interface for all real-time and all simulation activities to be easy to use.

This is achieved by integrating DSE into ADMS systems and integrating ADMS systems with various internal and external data sources, for example with: GIS, customer databases, billing, smart meter concentrators, advanced metering infrastructure (AMI) head-end system, and so on. In this way, all ADMS functions and functionalities and all ADMS users have easy access to the state estimation results. Finally, a single integrated system reduces the costs and effort incurred during the collection, processing, exchange, use, and maintenance of the database and significantly simplifies the administration of the entire system.

Keeping in mind all the above, from the characteristics of DN, the wishes, and capabilities of users and manufacturers of solutions, all the way to the features that must have an industrial-grade product, it is obvious that the model and procedure are one of the minor problems. The dominant problems are primarily related to the following:

- development of model, procedure, and tool based on which DSE can be integrated into the industrial-grade product;
- development of a common platform and adapter for data exchange – full integration of DSE and all other system components;
- tools for coordinated actions of different program units;
- practical implementation, with several critical steps, primarily the following: design of documents, adapting the product to specific client requirements, implementation of factory acceptance test, deployment on-site and site acceptance test, preliminary acceptance – GoLive, system commissioning and putting into operation, until the warranty and maintenance of the system after the expiration of the warranty period;
- verification of the realized solution, as one of the most challenging moments; the difficulty of its implementation depends on the final goal and requirements of the project (e.g., whether only DN monitoring or some of the automatic closed-loop functionality are expected); in addition, practical experiments are very demanding, both in preparation and in the implementation itself, and later in data processing; the additional problem is that experiments have to be repeated several times, so they are expensive and often critical for the user.

Finally, the DSE integrated into an industrial-grade product is not just a mathematical model of DSE and a procedure for solving it; it is a very expensive, complicated, robust system within which state estimation can be performed reliably and quickly enough while providing sufficiently accurate estimates of DN.

The development and application of DSE integrated into the industrial-grade product are discussed below.

3.3.2.6 Integration of DSE into industrial-grade product

During the procedure for solving the DSE model, various data and calculations are used (the basic steps of the procedure are shown in Section 3.3.2.1). Due to the circumstances, DPUs store their data in different systems: GIS, AutoCade, CIS, billing system (BS), outage management software, various excel documents and text files, meter data management (MDM), advanced meter management (AMM) and automatic meter reading (AMR) data collection systems from intelligent meters, enterprise resource planning, fixed assets database, meteorological data archiving system, asset management, and so on. In addition to the previously mentioned internal systems, the operation of the ADMS system also requires data from external IT/OT systems (e.g., weather information system (WIS), energy market, e-mail services).

Typically, files with geo-referenced data (GIS files containing feeder data, or a portion of network data), as well as files from other systems (CIS, BS, equipment data, etc.) are exchanged with the ADMS system via file transfer protocol (FTP) or secure FTP. At the same time, GIS is the primary system for building a network but not for real-time data. Depending on the type and capabilities of the intelligent meters available in the network, to exchange data with MDM and AMI (head-end) systems, it is necessary to implement (1) various integration messages,

which comply with IEC 61968-9 and IEC 61968-100; or (2) direct communication with devices via standard IEC 60870-5-104 and/or DNP3 protocols. It is necessary to enable the ADMS system to receive information registered on intelligent meters via the MDM system, e.g. warning before voltage interruption ("last gasp power down"), voltage re-establishment ("power up"), voltage too low ("under-voltage"), too high voltage ("over-voltage"), and establishment of normal status ("return to normal"). At the same time, the ADMS system must receive, process, and respond to messages with changes in voltage, active power, or reactive power – messages sent on its initiative by specially tuned smart meters ("bellwether meters") every 15 or 30 minutes "unsolicited inbound meter readings"). At the same time, it should be possible for the ADMS system to send query messages and receive a response on the status of the smart meter ("meter ping request") and the current-voltage value ("meter poll request"), either individually per meter or for a group of selected intelligent meters.

Such a complex exchange of data, and the coordinated operation of different program units, requires the full integration of all system components. This integration must have a single place for data exchange, with all the necessary internal and external IT/OT systems. Reducing the number of integration points directly increases the reliability of the entire system. For this purpose, data downloaded from various data sources (automatically, through integrations, or manually) are converted to CIM XML files. In doing so, the network data model and data exchange should be defined in accordance with the IEC 61970 and IEC 61968 series of standards, known as CIM standards. Messages exchanged via a standard software environment must comply with IEC 61968-100 while retaining the standard semantics for integrations between different systems.

Integration with AMI is realized through Web Service. For file sharing via the Web Service, it is recommended to use a secure socket layer and hypertext transfer protocol secure.

Real-time data are collected from the SCADA system and transmitted to the ADMS system via the standard Inter-Control Center Communications Protocol (ICCP or TASE.2). If necessary, in the same way, the switching order list from the ADMS system is automatically returned to the SCADA system for execution (e.g., if one of the automatic closed-loop functions is implemented).

All these data, the speed, and the quality of their processing affect the quality of DSE results, and thus the quality of results of all other ADMS functions.

Static and dynamic data exchange requires a single platform for data exchange, the so-called integration busbar (e.g., enterprise message bus). Data exchange between external and internal IT/OT systems is realized through integration adapters. By applying a single integration busbar and adapter, information and data are routed following the active process (instead of being exchanged individually between the concerned systems). For example, as soon as a change occurs in one of the integrated systems, it is forwarded to the platform via the adapter and is thus immediately available to all components of the ADMS system. In this way, it is incomparably simpler to ensure the administration and security of the entire system's data. At the same time, the speed and reliability of real-time procedures are increased.

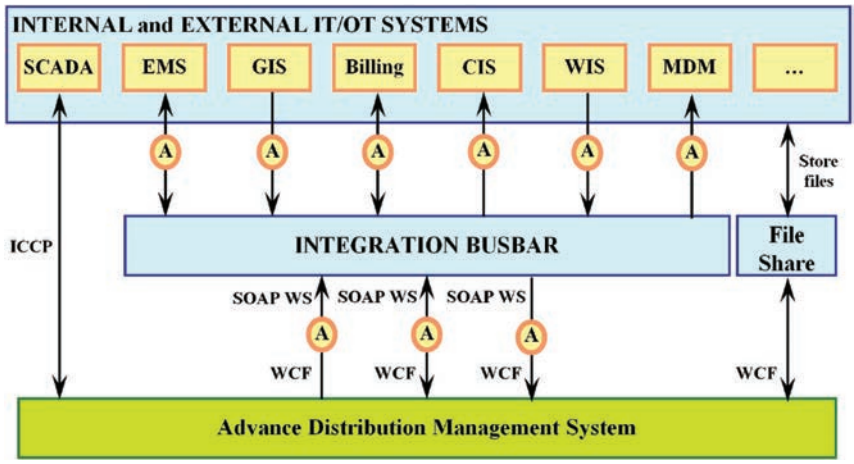

Figure 3.5 ADMS system integration with internal and external IT/OT systems

A classic example of ADMS system integration with internal and external IT/OT systems is shown in Figure 3.5. The figure shows integration adapters (A), Windows Communication Foundation (WCF), and Simple Object Access Protocol Web Service (SOAP WS).

Implementation and verification of integration adapters and data exchange platforms are just some of the problems of integrating internal and external IT/OT systems with the ADMS system.

Finally, only an integrated ADMS system is a "state-of-the-art" technological solution for modern DPUs. As such, it represents the central integration of all DPU components and a basic prerequisite for the practical application of state estimation in DN.

3.3.2.7 The architecture of the system in which DSE is located

In order for DSE to be realized as a resident function, it must be integrated into an industrial-grade product – the ADMS system. The complexity of such a system is briefly illustrated through its global architecture. This architecture consists of the main data center (MDC) and backup data center (BDC), both with ADMS systems and a substantial number of control centers. MDC and BDC are implemented at the two remote locations.

In regular operation, the ADMS system in the MDC is active, and the passive ADMS system in the BDC is ready to take an active role. Workstations in control rooms and remote user access environments are connected to the active data center. Data from active services are automatically replicated to passive services. In doing so, all critical services in both data centers are redundant and configured execution in high-availability clusters. In this way, wide solution accessibility is provided. If the ADMS system from the MDC becomes inaccessible for some reason, the ADMS client takes control of the DN by automatically switching to the ADMS in the BDC.

3.3.2.7.1 MDC

MDC contains production and test environments. The production environment consists of core (real time) ADMS, access services ADMS, and staging ADMS. Core or real-time ADMS is the essential part of the solution used for monitoring and managing the network in real time ("dispatching"). Therefore, this is part of a system in which DSE is executed automatically in real time. Access services are in the demilitarized zone (DMZ). It is an access point for corporate users – for simulations and different analyses of the energy network and integrations with business applications (e.g., with GIS). In this zone, DSE is used for "what-if" analysis. The staging system is used to modify data models (system configuration, data import, network modeling, etc.) and their testing (validation and verification) before the new data models are implemented in core and access services ADMS.

A test environment is an additional environment, separate from the production environment, and it is used to test modifications of system and application software in ADMS, including software patches before being implemented in the production environment. A new version of the DSE model and procedures for solving it can be tested in this environment. After successful tests, the old model and/or procedure can be replaced with a new version. The management environment uses IT employees to operate the physical and virtual machines of the entire ADMS solution in one location. In addition, this environment allows to back up ADMS data and manage antivirus protection. The operator training system is used for different types of training where the instructor creates scenarios to be carried out by the students.

Each of these environments and ADMS can be configured as a separate IT security zone. The zones are separated by firewalls, which are configured to allow only the traffic necessary for the system to function. For this purpose, the ADMS must have its Domain controller.

3.3.2.7.2 BDC

BDC has only the core system within its production environment. It allows critical business processes to run continuously in situations where MDC is disabled. The BDC contains only critical ADMS functionalities (core ADMS only) related to operator monitoring and management of DN. Access services (DMZ), staging systems, training systems, and test environment are not critical parts of the ADMS; so there is no need to form them in BDC.

Operational workstations from control centers connect directly to MDC and BDC, using VPN. Remote operational workstations are connected using a remote control service.

3.3.2.8 Verification of EDS models and procedures for their solution

Unfortunately, DSE solutions that can be found in the literature are either not practically verified at all or have been tested and verified only in laboratory conditions (on a computer, on simple test networks, e.g., on IEEE test networks).

The only way to gain trust in any solution, and therefore in DSE models and procedures for their solution, is their verification in real DN, in real time, in real life.

The DSE solution can be verified only based on its long-term practical application in different distribution environments. These environments should be multi-voltage, balanced and unbalanced DN, with small and extremely large dimensions, with a low and high degree of telemetry. Finally, the speed and quality of their results must be such that they can be successfully used in other DMS functions.

A such DSE solution, DSE integrated into ADMS and established as an industrial-grade product, is presented in [16, 27, 46–48]. Its practical possibilities, harmonized with the wishes and possibilities of both customers and system manufacturers, are presented in [26, 28].

3.4 Where are we today?

Today's specialized models and procedures for their solution, which are based on the characteristics of DN and integrated into industrial-grade products, enable the development and practical application of robust, fast, and sufficiently accurate state estimation of DNs.

An example of such a solution is shown in Refs. [16, 17]. The robustness of this solution is reflected in the fact that it has been repeatedly verified on real-life projects worldwide [1]. These projects include complex and very different DNs:

- with several voltage levels;
- with renewable energy sources and different regulation resources (load-tap-changers, step voltage regulators, switched shunt capacitors, and energy storages);
- with balanced and unbalanced elements;
- with symmetrical and asymmetrical states;
- with all types of measurements (with individual or a combination of P, Q, V, I, $\cos\varphi$), without limitation on their number and location;
- without telemetry, with a low and high level of telemetry (note: the quality of DSE results is directly proportional to the level of telemetry and the quality of historical DN data), and so on.

All these are without limitation on DNs' dimensions.

The speed of this solution is based on the characteristics of DN, artificially achieved observability, and automatic formalism definition of the observable areas, voltage regulation zones, DSE model, and procedure for its solution. This formalism is essentially based on the concept of the incidence matrix and is practically performed by network inspection. The automatic formation of the DSE model not only provides the necessary speed in the practical realization but, above all, enables its practical application without limitation to the number of network buses and the location and number of measurements. The speed of the procedure for solving the DSE model is based on the integration of DSE into the industrial-grade product – ADMS. In such an environment, state estimation can be realized as needed (e.g., in accordance with changes in DN): individually – for only one DN root, in parallel

for several DN roots, or even for all roots simultaneously. Accordingly, the time required to calculate the DSE for all DN roots of the considered DPU can be reduced to the time required to estimate its largest DN root. This feature is crucial for the implementation of real-time functions and especially for automatically implemented closed-loop functions [27].

3.5 Where are we going, and what awaits us?

More and more new measurement units (sensors) and electrical equipment, which did not exist until yesterday, are being applied in the DPUs. Some of them are phasor measurement unit (PMU), micro-PMU, power quality monitor devices, digital fault recorders, smart meters, smart houses, electric vehicles, energy storage, distributed generators, smart grid substation automation, and so forth. They are accompanied by new IT/OT technologies, new participants in the electricity market, and new legal, economic, and technical regulations and processes. The fact is that these changes require fundamental changes not only in long-established procedures but also in the overall concept of traditional DNs. New innovative solutions lead DPU toward a new, intelligent, and substantially more expensive structure, requiring more and more knowledge, innovation, information, and operational technologies. It makes the energy transition of DN, from entirely passive to fully active DN, very temporally and materially demanding. The transition has already started a long time ago and will continue for a long time. It brings with it major changes and even more significant challenges, both technical (regulation, management, operation planning) and economic (trade, investment, network planning). In parallel, new electric business models are being established in distribution during the transition. In this new model, passive customers (electricity buyers) become active participants in the electricity market (prosumers on the demand side, and independent power producers, on the supply side).

The three pillars of this transition are certainly (1) decentralization – the highest possible production of electricity from small geographically distributed renewable energy sources; (2) decarbonization – the transition to renewable energy sources and changes in consumer behavior, primarily related to heating and transport; and (3) digitalization – the introduction of IT/OTs (ADMS, IoT, SaaS, and Claud) and smart infrastructure that provides fast and reliable two-way transmission of the extremely large amounts of data.

Changes in DN and their effects on DSE development are discussed below. Some of them are large-scale data, real-time data synchronization, model dimensions, interval reduction between two state estimations, and LV network.

Even today's smart meters can register a large amount of information. Their large-scale deployment has intensively transformed DN from systems with no information to systems with a huge amount of quality data. This, the new incoming PMU and wide area measurement system, which are hesitantly entering the DN for now, should definitely be added. A large amount of new data will soon result in various additional problems. One of the largest is the so-called "data tsunami" problem. As

the number of data increases, the load on data exchange systems will increase, and their processing will be significantly more difficult. The consequence is that the number of variables will increase as well, and thus the dimensions of future DSE models will be far larger than today's and far, far larger than the dimensions of the largest TSE.

By including the information coming from the PMU, the requirements for the speed of data processing and the state estimation calculation will increase enormously. In such calculations, the signal delay will have to be considered. The choice of optimal latency, related to the synchronization of all data and the final calculation quality, is a problem that has yet to be set and solved. By choosing the correct number, types, and classes of the accuracy of measuring instruments, the quality of DSE results can be significantly raised. This new situation requires more than the optimal sensor placement function, which has yet to be practically verified in active DNs. Note: Based on previous experience, increasing the number of measurements does not mean a proportional increase in the quality of DSE results.

The consequence of increasing investment, both in equipment and IT/OT and in the telecommunications infrastructure of DN, enables the development and application of new technologies, procedures, and concepts. Some of them are direct load control, full automation – automatic closed-loop, self-learning, model self-correction, self-awareness, self-healing distribution systems, smart house, smart city smart grids, Internet of Everything or Network of Everything, and high-performance computing (cluster computing, multi-core computing, grid, SaaS and cloud computing). At the same time, the DPU imposes new rules and new systems for coordinated control of electricity quality, voltage regulation, and balance of production and consumption, which should fully harmonize and integrate the DPU with the rules of the transmission network. If increasing penetration distributed generation is added to this, it is clear that traditional long-established and verified procedures for management, regulation, and operational planning of passive DNs will be less and less efficient and useful.

The most significant increase in new devices and information occurred in the LV network, so the growing interest in state estimation in the LV network is understandable. Unfortunately, the problem of DSE in LV networks is far less addressed than DSE in MV networks. In this area, the following problems are obvious: LV network is predominantly unbalanced, with asymmetric regimes, so the neutral conductor cannot be neglected, and the volatility of LV-level demand and production dominantly affects the quality of estimated values. Research, implementation, and verification of DSE specialized for LV networks are yet to come.

Cyber-security is becoming an integral part of every IT/OT solution. Therefore, it is an integral part of management and control in the active DN. The whole system should be aligned with the security requirements defined for the software and systems in the ISA/IEC 62443 suite of standards and the relevant privacy (general data protection regulation) and data protection requirements. In this area, there are many problems, primarily related to data transmission, e.g., it is difficult to provide 100% broadband coverage, and it has to work with third parties' companies.

The trends of DN development are apparent: the share of distributed renewable energy sources, energy storage systems, and e-mobility is increasing, and the number of prosumers (network members who are both consumers and producers) is on the market. These elements are predominantly unbalanced, and changes in production and consumption are extremely random and volatile. All this additionally increases the asymmetry of the network state, prevents them from being modeled as one-phase networks, and additionally spoils the already modest accuracy and reliability of DSE. The consequences are that classic everyday activities are becoming more complicated, and the application of traditional models and procedures are becoming less reliable.

Finally, the state estimation of the large-scale active DN needs to meet increasing expectations in terms of the requirement to increase the quality of its results and be executed in shorter and shorter time intervals. Theoretically, the accuracy of its results can be significantly improved by using information from smart measuring instruments in real time. In practice, for that to happen, not only today's models and procedures for their solutions must be significantly improved but also infrastructure and telecommunication routes. As far as models and procedures are concerned, this primarily refers to the development and verification of specialized models that would include the effects of new elements and new technologies and overcome the problems of transmission speed and quality of processing large amounts of data. If it is known that most of these information are at low voltage, it is clear that the development, implementation, and verification of these models and procedures, together with the necessary infrastructure and telecommunications, have only just begun.

Experts from various fields must be involved in solving the problem of the future DSE, its modeling, integration into the industrial-grade product, practical application, and verification. Some of them are experts in the following fields: power engineering, telecommunication, data mining, big data processing, artificial intelligence, and forecasting production and consumption at the low voltage level.

For this purpose, the energy system (subtransmission, MV, and LV DN) and telecommunication system must be integrated and simultaneously modeled and processed as much as possible.

3.6 Conclusion

3.6.1 Achieved to date

To date, it has been confirmed that DSE is not just an idea on the paper and a research subject. DSE can be practically implemented and has been implemented in real life on many projects in very different DNs worldwide [1]. Today's DSE is very robust and reliable. According to the available data, its application provides good-quality estimation results. It is practically speedy because it can be performed in parallel for all supply substations. Due to this, the time required for the state estimation of the whole DPU network of any total dimension can be reduced to the time required to calculate its largest DN root.

As such, today's DSE has been developed and practically applied based on the following facts:

- Many mathematically high-quality DSE models and procedures for their solution can be found in the literature. Unfortunately, the list of papers in which their application is presented and practically verified, in distribution control centers, in the large-scale DN, with several voltage levels, high penetration of renewable energy sources, and voltage and reactive power control, in real time, is more than modest;
- The characteristics of the distribution and transmission networks are very different. Consequently, DSE needed to develop specialized models and procedures for their solution, conceptually different from TSE;
- For a practically applicable DSE, two compromises are needed, between very complex methods proposed in the literature and characteristics and possibilities of DPU, and between the wishes, interests, and expectations of researchers, producers, and users of the industrial-grade product;
- Practically and mathematically, it has been confirmed that specialized DSE is much more efficient than the traditional TSE for state estimation in the distribution environment;
- DSE is not and practically cannot be a stand-alone application. Therefore, in order for DSE to be applied as one of the automatic, real-time functions, its full integration into the industrial-grade product is required – it must be integrated with all important internal and external DPU systems. Such a system cannot be realized on one computer (server). According to user requirements, this system requires different zones, in which several dozen computers are applied, and according to the user requirements, sometimes even more than a hundred servers. A small group of engineers cannot do its realization. This work requires the participation of many well-organized various experts. Thus, the DSE model and procedure for its solution represent minimal problems.

Although today's DSE has been practically verified in many DPUs and extensive experience has been gained from the ADMS projects, a standard DSE solution has not yet been established (as it has long been established for transmission networks). However, much remains to be done on this topic. The aggravating circumstances along this way are certainly (1) very modest verification of published models and procedures and practical implementation of DSE in DNs; (2) researchers do not have a test environment and therefore a lot of practice; (3) DPUs are not ready to conduct real-life experiments in order to verify DSE (they are beware of any risk).

In addition, it should be borne in mind that the practical implementation of DSE integrated into an industrial-grade product is very expensive (requires significant investments in telecommunication, metering, IT/OT infrastructure, and experts) and a time-consuming process (from planning to commissioning the system requires more years).

3.6.2 In front of us

In future large-scale active DNs, huge amounts of real-time data will be continuously generated. DN will become 100% and even more observable with the increase of

telemetered measurement values. Due to the number of data increases, the number of variables and thus the DSE problem's dimensions will also increase. Consequently, it will be required not only to improve the quality of real-time DSE results but also to speed up the procedure for resolving it significantly. To enable this, an extremely large amount of real-time data must be transmitted and prepared (synchronized and filtered). With all this in mind, future research in this area will focus on developing, implementing, and verifying new DSE models and procedures for their solution, which are fully specialized in DN and firmly integrated into the industrial-grade product. The DSE model will primarily be a three-phase unbalanced model designed for active large-scale networks. Procedures for solving them will go to parallel and distributed solutions. Combining the telecommunication and power network models into one model will be one of the most important future challenges.

The development and practical application of such systems will enable the accelerated modernization of active DNs, and will be the basis for future smart grid systems.

Appendix – Schneider Electric DMS Novi Sad LLC

Schneider Electric DMS NS LLC is a unique research and development company for smart grid solutions. It is especially devoted to developing and delivering its main product, the advanced distribution management system (ADMS). ADMS is the most advanced software system in the world for performing all technical tasks in DPUs efficiently and optimally, which fulfills modern power industry development requirements worldwide. It is a modern and comprehensive solution for power network management, including but not limited to monitoring, control, outage and hazard management, planned work management, storm management, network conditions analysis, network optimization, operation planning, network development planning, what-if analysis, operators training, applicable on all voltage levels – from low voltage up to transmission.

ADMS is a fully integrated smart control system for utilities, integrating six components into a single platform for a seamless operation of power systems:

1. SCADA – New generation of supervisory control and data acquisition
2. DMS – Distribution management system to monitor, analyze and optimize DN with more than 50 specialized power applications
3. EMS – Transmission management system to monitor, analyze, and optimize subtransmission and transmission networks
4. NetOps – Network operations to manage all unplanned outages with embedded FLISR, hazards, planned work, major storms, including damage assessment
5. PCS – Power control system to manage the operation of islanded and connected microgrids
6. DERMS – Distribution energy resource management system to manage and optimize the impact of DERs on the DN

https://www.schneider-electric-dms.com/
Schneider Electric DMS LLC Novi Sad
Narodnog fronta 25 a,b,c,d
21000 Novi Sad; Vojvodina, Serbia

References

[1] Schneider Electric DMS NS [Homepage on the Internet]. Vojvodina, Serbia: Schneider Electric DMS NS, Inc. 2022. Available from https://www.schneider-electric-dms.com [Accessed 15 Feb 2022].
[2] Ranković A., Maksimović B.M., Sarić A.T. 'A three-phase state estimation in active distribution networks'. *International Journal of Electrical Power & Energy Systems*. 2014, vol. 54, pp. 154–62.
[3] Nusrat N., Lopatka P., Irving M.R., Taylor G.A., Salvini S., Wallom D.C.H. 'An overlapping zone-based state estimation method for distribution systems'. *IEEE Transactions on Smart Grid*. 2015, vol. 6(4), pp. 2126–33.
[4] Leite J.B., Mantovani J.R.S. 'Distribution system state estimation using the Hamiltonian cycle theory'. *IEEE Transactions on Smart Grid*. 2015, vol. 7(1), pp. 366–75.
[5] Sharma A., Srivastava S.C., Chakrabarti S. 'Multi-agent-based dynamic state estimator for multi-area power system'. *IET Generation, Transmission & Distribution*. 2016, vol. 10(1), pp. 131–41.
[6] Monticelli A. *State Estimation in Electric Power Systems: A Generalized Approach*. Springer Science & Business Media; 1999.
[7] Abur A., Expósito A.G. *Power System State Estimation: Theory and Implementation*. New York: CRC Press; 2004.
[8] Baran M.E., Kelley A.W. 'State estimation for real-time monitoring of distribution systems'. *IEEE Transactions on Power Systems*. 1994, vol. 9(3), pp. 1601–9.
[9] Li K. 'State estimation for power distribution system and measurement impacts'. *IEEE Transactions on Power Systems*. 1996, vol. 11(2), pp. 911–16.
[10] Meliopoulos A.S., Zhang F. 'Multiphase power flow and state estimation for power distribution systems'. *IEEE Transactions on Power Systems*. 1996, vol. 11(2), pp. 939–46.
[11] Sun H.B., Zhang B.M. 'Global state estimation for whole transmission and distribution networks'. *Electric Power Systems Research*. 2005, vol. 74(2), pp. 187–95.
[12] Gomez-Exposito A., Abur A., de la Villa Jaen A., Gomez-Quiles C. 'A multilevel state estimation paradigm for smart grids'. *Proceedings of the IEEE*. 2011, vol. 99(6), pp. 952–76.
[13] Roytelman I., Shahidehpour S.M. 'State estimation for electric power distribution systems in quasi real-time conditions'. *IEEE Transactions on Power Delivery*. 1993, vol. 8(4), pp. 2009–15.

[14] Ghosh A.K., Lubkeman D.L., Jones R.H. 'Load modeling for distribution circuit state estimation'. *IEEE Transactions on Power Delivery*. 1997, vol. 12(2), pp. 999–1005.

[15] Lubkeman D.L., Jianzhong Zhang., Ghosh A.K., Jones R.H. 'Field results for a distribution circuit state estimator implementation'. *IEEE Transactions on Power Delivery*. 2000, vol. 15(1), pp. 399–406.

[16] Venda G., Strezoski V., Kanjuh S. 'Real-life distribution state estimation integrated in the distribution management system'. *International Transactions on Electrical Energy Systems*. 2017, vol. 27(5), e2296.

[17] Švenda G., Kanjuh S. 'Automatically generated three-phase state estimation for unbalanced distribution power drids'. *IEEE Power & Energy Society General Meeting (PESGM)*; 2021. pp. 1–5.

[18] Deng Y., He Y., Zhang B. 'A branch-estimation-based state estimation method for radial distribution systems'. *IEEE Transactions on Power Delivery*. 2002, vol. 17(4), pp. 1057–62.

[19] Baran M.E., Kelley A.W. 'A branch-current-based state estimation method for distribution systems'. *IEEE Transactions on Power Systems*. 1995, vol. 10(1), pp. 483–91.

[20] Lin W.M., Teng J.H., Chen S.J. 'A highly efficient algorithm in treating current measurements for the branch-current-based distribution state estimation'. *IEEE Transactions on Power Delivery*. 2001, vol. 16(3), pp. 433–9.

[21] Wang H., Schulz N.N. 'A revised branch current-based distribution system state estimation algorithm and meter placement impact'. *IEEE Transactions on Power Systems*. 2004, vol. 19(1), pp. 207–13.

[22] Miranda V., Pereira J., Saraiva J.T. 'Load allocation in DMS with a fuzzy state estimator'. *IEEE Transactions on Power Systems*. 2000, vol. 15(2), pp. 529–34.

[23] Sarić A.T., Ćirić R.M. 'Integrated fuzzy state estimation and load flow analysis in distribution networks'. *IEEE Transactions on Power Delivery*. 2003, vol. 18(2), pp. 571–8.

[24] Manitsas E., Singh R., Pal B.C., Strbac G. 'Distribution system state estimation using an artificial neural network approach for pseudo measurement modeling'. *IEEE Transactions on Power Systems*. 2012, vol. 27(4), pp. 1888–96.

[25] Atanacković D., Dabić V. 'Deployment of real-time state estimator and load flow in BC hydro DMS-challenges and opportunities'. *IEEE Power & Energy Society General Meeting IEEE*; Vancouver, BC, Canada, 2013. pp. 1–5.

[26] Švenda G., Strezoski V. 'Distribution state estimation: Wishes and practical possibilities' *2013 IEEE PES GM - Shaping the Future Energy Industry. July; Panel Session: State Estimation for Distribution Operations: Sharing the Experiences of Implementation, Usage, and Complexities*, No. GM2515 – Lecture invited by IEEE PES Committees. Available from http://www1.ece.neu.edu/~abur/ieee/PES2013/Paper4.pdf

[27] Johnson M. 'Application of distribution state estimation in Duke energy's DSDR Carolinas Project'. *2014 IEEE PES GM. Panel Session: State Estimation for Distribution System Monitoring and Control–Implementation*

Challenges, No. 14PESGM–2760 – Lecture invited by IEEE PES Committees, 2014 July. Washington, National Harbor, MD, USA..

[28] Švenda G., Strezoski V. 'Distribution State Estimation in Real-Life: Challenges and Experiences. 2014 IEEE Power & Energy Society General Meeting – IEEE PESGM'. *Panel Session: State Estimation for Distribution System Monitoring and Control-Implementation Challenges, No. 14PESGM2761 – Lecture Iinvited by IEEE PES Committees. Washington, National Harbor, MD, USA.*. 2014.

[29] Švenda G., Simendić Z. 'Adaptive on-load tap-changing voltage control for active distribution networks'. *Electrical Engineering*. 2022, vol. 104(April), pp. 1041–56.

[30] Stott B., Alsac O. 'Fast decoupled load flow'. *IEEE Transactions on Power Apparatus and Systems*. 1974, vol. PAS-93(3), pp. 859–69.

[31] Švenda G., Nahman J.M. 'Transformer phase coordinate models extended for grounding system analysis'. *IEEE Transactions on Power Delivery*. 2002, vol. 17(4), pp. 1023–9.

[32] Celik M.K., Liu W.H., IEEEIEEE. 'A practical distribution state calculation algorithm'. *IEEE Power Engineering Society. Winter Meeting*. 1999, vol. 1, pp. 442–7.

[33] Manojlović I., Švenda G., Erdeljan A., Gavrić M. 'Time series grouping algorithm for load pattern recognition'. *Computers in Industry*. 2019, vol. 111(1), pp. 140–7.

[34] Manojlović I., Švenda G., Erdeljan A., Gavrić M., Čapko D. 'Hierarchical multiresolution representation of streaming time series'. *Big Data Research*. 2021, vol. 26,100256.

[35] Kuzmanović S., Švenda G., Ovcin Z. Practical statistical methods in distribution load estimation. *CIRED 2009-20th International Conference and Exhibition on Electricity Distribution-Part 1*. Prague: IET; 2009. pp. 1–4.

[36] Vanja S. *State Estimation for Cyber-Physical Systems with Communication Irregularities*. PhD thesis, Medford, MA: Tufts University; 2020.

[37] Wu F.F. 'Power system state estimation: survey'. *International Journal of Electrical Power & Energy Systems*. 1990, vol. 12(2), pp. 80–7.

[38] Dehghanpour K., Wang Z., Wang J., Yuan Y., Bu F. '*A survey on state estimation techniques and challenges in smart distribution systems*'. *IEEE Transactions on Smart Grid*. 2018, vol. 10(2), pp. 2312–22.

[39] Schweppe F., Wildes J. 'Power system static-state estimation, part I: Exact model'. *IEEE Transactions on Power Apparatus and Systems*. 1970, vol. PAS-89(1), pp. 120–5.

[40] Schweppe F., Rom D. 'Power system static-state estimation, part II: Approximate model'. *IEEE Transactions on Power Apparatus and Systems*. 1970, vol. PAS-89(1), pp. 125–30.

[41] Schweppe F. 'Power system static-state estimation, part III: Implementation'. *IEEE Transactions on Power Apparatus and Systems*. 1970, vol. PAS-89(1), pp. 130–5.

[42] Táczi I., Sinkovics B., Vokony I., Hartmann B. 'The challenges of low voltage distribution system state estimation - An application oriented review'. *Energies*. 2021, vol. 14(17) 5363.

[43] Strezoski V.C., Vidović P.M. 'Power flow for general mixed distribution networks'. *International Transactions on Electrical Energy Systems*. 2015, vol. 25(10), pp. 2455–71.

[44] Shirmohammadi D., Hong H.W., Semlyen A., Luo G.X. 'A compensation-based power flow method for weakly meshed distribution and transmission networks'. *IEEE Transactions on Power Systems*. 1988, vol. 3(2), pp. 753–62.

[45] Luo G.X., Semlyen A. 'Efficient load flow for large weakly meshed networks'. *IEEE Transactions on Power Systems*. 1990, vol. 5(4), pp. 1309–16.

[46] Simendić Z.J., Vladimir C., Švenda G. 'In-field verification of the real-time distribution state estimation'. *CIRED 2005 - 18th International Conference and Exhibition on Electricity Distribution*; Session No. 3, 547,Turin, Italy, 6-9 June; 2005. pp. 1–4 pp..

[47] Katić N., Fei L., Švenda G., Yongji Z. 'Distribution state estimation field testing'. *China International Conference on Electricity Distribution*; Shanghai, China; 2012. pp. 1–4.

[48] Katić N., Fei L., Švenda G., *et al.*. 'Field testing of distribution state estimator'. *22nd International Conference and Exhibition on Electricity Distribution (CIRED 2013)*; Stockholm; 2013. pp. 1–4.

This page intentionally left blank

Chapter 4

Three-phase network model for steady-state analysis of distribution systems

Julio Augusto Druzina Massignan[1], João Bosco Augusto London Junior[1], Gustavo Miranda Hebling[1], Elizete Maria Lourenço[2], Renan Kovalczuk Portelinha[2], and Odilon Luis Tortelli[2]

4.1 Introduction

The electrical network model is the core of any computational analysis of power systems. It captures the physical phenomena through mathematical relations among different electrical quantities of the power system. The level of details of such models is a fundamental step to ensure adequate accuracy in the analysis of different matters by power systems engineers.

This chapter introduces the basic concepts regarding three-phase network models for distribution system steady-state analysis, emphasizing a state estimation perspective. A general two-port branch model is conceived for each component of the distribution system. Also, general equations to calculate currents and power flows in the network as well as their derivatives are presented. Different types of equipment are exemplified along with the respective particularities of their admittance matrix models, from the classical distribution system components to the novels of modern power grids, such as distributed generation (DG), energy storage devices, electric vehicles, and flexible power electronic converters.

4.1.1 Distribution system state estimation

The context of real-time monitoring is related to most of the operation and automation processes of power distribution systems. The goal is to obtain a proper evaluation of power quality, network reliability, risk assessment, and more efficient use of the components of distribution networks. Thereby, to improve energy management

[1]Department of Electrical and Computing Engineering, School of Engineering of São Carlos, University of São Paulo, São Carlos, Brazil

[2]Department of Electrical Engineering, Federal University of Paraná, Curitiba, Brazil

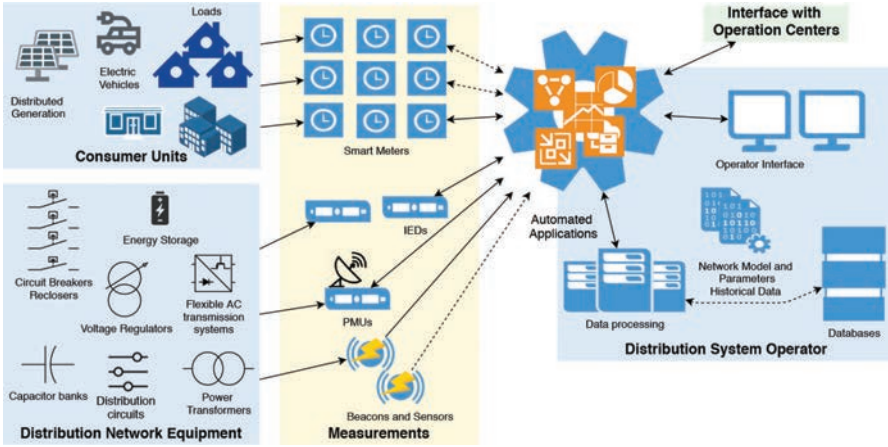

Figure 4.1 *Overview of the distribution system components, measurement devices, and state estimation framework*

capabilities, distribution operators rely on the accuracy of network modeling to assess distribution network features.

The level of resolution for the network models may be the first challenge to decide when assessing distribution systems. The balance between precision and promptitude is a matter of long debates among power engineers and typically is discussed under particular application frameworks [1–5].

Network operators must be able to evaluate the condition of the grid taking into account the simultaneous interaction among multiple components and the data gathered from measurement devices [1–3, 6].

The state estimation problem emerges from this scenario to capture the relations among measured electrical quantities and the network state. It is traditionally formulated as static analysis, that is, intending to obtain steady-state features of the network. It has a strong relation with power flow analysis. Although both problems frequently share similar network models, they have some conceptual differences. The main one regards the input data. In state estimation, the steady state is evaluated from measured values, assumed with some degree of uncertainty, and able to deal with redundancy. Whereas in power flow analysis, a specified loading/generation condition is evaluated, without any redundancy. Figure 4.1 provides an overview of distinct components of the distribution systems concerning the states estimation problem. A diverse set of equipment is responsible to provide electricity infrastructure for the final consumer units. Associated with this infrastructure, different types of sensors are installed across the network to measure electrical quantities. The distribution system operators gather this information from the sensors and extract tangible knowledge about the system's condition, for instance, through the state variables. The network model consists of the bridge between the measurements and the state variables, a detailed mathematical representation of the physical behavior of different equipment in the distribution system.

The static state estimation problem for a distribution network with m measurements and n state variables consists of a nonlinear measurement model that can be formulated as [7–10]:

$$z = h(x, p) + e \tag{4.1}$$

where z is the $(m \times 1)$ measurement vector composed of the measured values, virtual measurements, and pseudo-measurements; x is the $(n \times 1)$ vector of state variables (see Box 4.1); $h(x)$ is the $(m \times 1)$ set of nonlinear equations that relate the measurements with the state variables; e is the $(m \times 1)$ noise vector associated with the inherent uncertainty of the measurement process, typically assumed as independent normally distributed random variables, with zero mean and known covariance matrix $(R \times m)$; and p is the set of parameters of the different components that comprise the distribution network, as distribution circuits, power transformers, voltage regulators, switching devices, DG, controllers, and others.

The main motivation for three-phase network models in state estimation applications is the fact that the input data enable a detailed overview of the latest condition of the network, in real time. They help to evaluate if the system operates in one of the following conditions: (1) *Normal and secure state;* (2) *Alert state*; or (3*) Emergency state*. This characterization of the system is provided both as a holistic overview of the network, as well as a local analysis of each component of the network, given by the model resolution level. It provides detailed results for distinct automated applications in real time. Regarding distribution systems specifically, particular characteristics of these networks motivate a detailed mathematical representation of the electrical network and its components. That is, with greater level of details when compared to the transmission system, where the model is often represented only by its positive sequence circuit.

The major effort for proper modeling in distribution system state estimation is to capture the unbalanced and asymmetrical nature of such networks. A three-phase representation of the network enables evaluating power quality issues, and also performing inferences about the system condition in each phase and at different parts of the power grid.

4.1.2 The unbalanced and asymmetrical nature of distribution systems

The distribution systems represent the connections of the power grid that delivers electricity to the final consumers, such as households, commercial businesses, and industrial plants. The diversity of components, connections, load behavior (and spatial arrangements), make distribution systems peculiar when compared to the transmission and generation systems. Some of these peculiarities are well-known challenges for distribution system state estimation, such as [1, 8, 11–16]:

- diversity of circuit connections, with single-, two-, and three-phase circuits, and transformer connections;
- unbalanced loads;
- short distance and untransposed lines with a high resistance/reactance ratio;

Box 4.1 The state variables in the distribution system state estimation

Among the particularities of the steady-state models for distribution systems, another relevant aspect related to the state estimation problem is the choice of the state variables. In order to face the particularities of the estimation problem in distribution networks, distinct alternatives for choosing state variables are presented below.

The traditional set of state variables is the complex nodal voltage in polar coordinates:

$$x = \{V_k^i, \theta_k^i\} \qquad i \in \{a, b, c, ...\} \qquad k \in \{1, 2, ..., N_{nodes}\} \tag{4.2}$$

in which V denotes the voltage magnitude, θ is the voltage phase angle, the superscript i indicates the phase, and the subscript k is the node identification. In the example, N_{nodes} is the number of nodes in the system, and the superscripts a, b, and c describe the three phases a, b, and c. Additionally, neutral to ground voltages may also be introduced as complementary state variables.

The complex nodal voltages may also be written in their rectangular coordinates form, described in (4.3). In this case, V_{re} is the real part of the complex nodal voltage and V_{im} is the imaginary part of the complex nodal voltage.

$$x = \{V_{re,k}^i, V_{im,k}^i\} \qquad i \in \{a, b, c, ...\} \qquad k \in \{1, 2, ..., N_{nodes}\} \tag{4.3}$$

For radial networks, it is also common to consider the branch currents of the system as state variables. Typically, the current phasor through each branch connecting nodes k and m is represented in polar coordinates. If I_{km} is the branch current magnitude and δ_{km} its respective current phase angle, in each phase for all $N_{branches}$ branches of the network, the state variables are defined as:

$$x = \{I_{km}^i, \delta_{km}^i\} \qquad i \in \{a, b, c, ...\} \qquad km \in \{1, 2, ..., N_{branches}\} \tag{4.4}$$

It can also be represented in rectangular coordinates, with I_{re} and I_{im}, the real and imaginary parts of the current phasor, respectively, as the state variables, that is:

$$x = \{I_{re,km}^i, I_{im,km}^i\} \qquad i \in \{a, b, c, ...\} \qquad km \in \{1, 2, ..., N_{branches}\} \tag{4.5}$$

Furthermore, active and reactive power injections may also be defined as the state vector. This approach is generally referred to as load estimation, load allocation, or pseudo-measurement generation. In this case, the active and reactive power injection, P and Q, respectively, in each phase for all nodes of the distribution network composes of the state vector:

$$x = \{P_k^i, Q_k^i\} \qquad i \in \{a, b, c, ...\} \qquad k \in \{1, 2, ..., N_{nodes}\} \tag{4.6}$$

(Continues)

The state vector is often extended to discrete and continuous controller variables, such as voltage regulator taps, capacitor bank switching, or firing angle in power electronics devices. The alternative formulation may also accommodate the status of switching elements (circuit breakers and sectionalizers) or inner variables of detailed dynamic models, such as generator parameters and internal voltages, state of charge in storage devices, and detailed machine models for loads.

- typically, very large-scale radial networks;
- presence of discrete variables, such as switching devices statuses and voltage regulators not directly monitored;
- reduced number of real-time measurements, usually located at the substation and some particular components along the feeders;
- presence of current magnitude measurements instead of active and reactive power measurements;
- as a consequence of the above, the distribution system state estimation often is numerically ill-conditioned.

Besides, different parts of the distribution systems also present their own particularities regarding steady-state analysis and state estimation that can be devised in the following [2, 17]:

- **High-voltage substation:** comprises the power transformer with both high-voltage and medium-voltage nodes, as well as feeder's bays. Typically contains a high number of measurements from the supervisory control and data acquisition (SCADA) systems, and phasor measurement units (PMUs) with a small number of state variables;
- **Medium-voltage primary feeders:** comprise the medium-voltage circuits and components typically spread across a large area including urban and rural feeders. Contain a very small number of measurements, typically from the SCADA system at specific equipment, such as automatic reclosers, voltage regulators, and shunt capacitors, or at special consumers directly connected at the medium-voltage level. Moreover, it requires a large number of state variables to be properly represented. Observability of such networks may be obtained through typical load curves in the form of load pseudo-measurements, or through new procedures capable to incorporate and to process new measurement technologies, such as intelligent electronic devices;
- **Low-voltage secondary circuits:** comprise the final connection with consumers at the low-voltage level, with a diverse set of connections, grounding systems, and neutral conductors. The loading is usually characterized by typical load profiles as pseudo-measurements. It is expected that the advanced metering infrastructure (AMI) provides smart meters instalation on individual loads as well as at the local controller of the power transformers. A large number of state variables is expected.

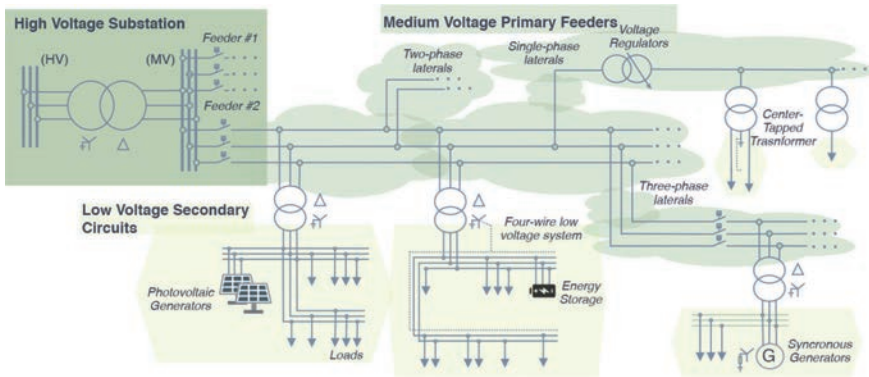

Figure 4.2 Three-phase diagram of a generic distribution system comprising a high-voltage substation, medium-voltage primary feeders, and low-voltage secondary circuits

Figure 4.2 illustrates a general configuration of a distribution network along with some characteristics and different components installed in each part. The unbalanced nature of the distribution system is a consequence of load unbalance, since different phases in the same node may present a diverse set of connected equipment and nominal loading, as well as the presence of asymmetrical connections, such as single- and two-phase laterals, distinct transformer connections and untransposed circuits, for instance.

In this sense, the definitions of appropriate models should not only comprise different phases of the system but also be able to incorporate the diverse set of possible information about the distribution system at the distinct parts of the network. This unbalanced nature of the distribution system demands more detailed models to capture the asymmetrical characteristics and diverse types of connections present in distribution system components [1, 8, 12]. The success in this task can provide valuable information regarding power quality, voltage unbalance, neutral and grounding conditions, detect anomalies in specific phases, accurately assess asset conditions, and enable fine-tuning of controllers and others to aid real-time management and decision-making from distribution system operators [18].

4.2 Three-phase two-port models

This section introduces the formulation of a generic three-phase unbalanced model able to capture the main electrical quantities for steady-state analysis. Power flow equations are initially derived. A generic two-port model based on admittance matrices is formulated to simplify the equations of a diverse set of possible connections, number of phases, grounding conductors, and asymmetries from different equipment.

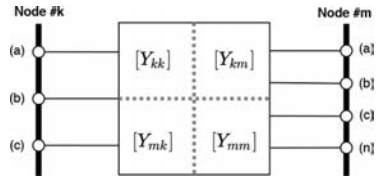

Figure 4.3 *Generic component model based on a two-port admittance matrix. Four submatrices relate the voltage and current phasors between both terminals, according to the type of component.*

4.2.1 Three-phase two-port admittance model

The three-phase network model may be derived by representing each network component by its two-port admittance matrix, using direct concepts from the classic linear circuit theory, as illustrated in Figure 4.3. Different types of equipment and connections can be incorporated into the network model by properly defining their contribution to the respective admittance matrix, which represents an advantage when complex distribution networks with several distinct components are considered [8, 15, 19].

Each element is modeled by the following two-port admittance system:

$$\begin{pmatrix} \dot{I}_k \\ \dot{I}_m \end{pmatrix} = \begin{pmatrix} Y_{kk} & Y_{km} \\ Y_{mk} & Y_{mm} \end{pmatrix} \begin{pmatrix} \dot{V}_k \\ \dot{V}_m \end{pmatrix} \tag{4.7}$$

where k and m denote the terminals of the branch element, $\dot{I}_k$ and $\dot{I}_m$ are the current phasor injected in each terminal of the branch element, $\dot{V}_k$ and $\dot{V}_m$ the voltage phasor of each terminal, and Y_{kk}, Y_{km}, Y_{mk}, and Y_{mm} are the admittance submatrices that represent each physical component and the respective parameters.

The power flow equations can be written for the respective branch as the following matrix expression for the terminal k:

$$S_{km} = P_{km} + jQ_{km} = \dot{V}_k \odot (\dot{I}_k)^* = \dot{V}_k \odot (Y_{kk}\dot{V}_k + Y_{km}\dot{V}_m)^* \tag{4.8}$$

where S_{km} is a vector with the per-phase complex power at terminal k (active and reactive power flows, P_{km} and Q_{km}), $\odot$ denotes the Hadamard product (element-wise), and $*$ denotes the complex conjugate. As an example, for a three-phase terminal k with phases abc, the following equation can be written through the matrix notation of the two-port model and the above product:

$$S_{km} = \dot{V}_k \odot (\dot{I}_k)^* = \begin{pmatrix} \dot{V}_k^a (\dot{I}_k^a)^* \\ \dot{V}_k^b (\dot{I}_k^b)^* \\ \dot{V}_k^c (\dot{I}_k^c)^* \end{pmatrix} = diag(\dot{V})(\dot{I}_k)^* = \begin{pmatrix} \dot{V}_k^a & 0 & 0 \\ 0 & \dot{V}_k^b & 0 \\ 0 & 0 & \dot{V}_k^c \end{pmatrix} \begin{pmatrix} (\dot{I}_k^a)^* \\ (\dot{I}_k^b)^* \\ (\dot{I}_k^c)^* \end{pmatrix} \tag{4.9}$$

Besides, the voltage and current phasors can also be written with the following notation to split magnitude and phase angle, for instance:

$$\dot{V}_k = V_k \odot \theta_k = diag(V_k)\theta_k = [V_k]\theta_k = \begin{pmatrix} V_k^a & 0 & 0 \\ 0 & V_k^b & 0 \\ 0 & 0 & V_k^c \end{pmatrix} \begin{pmatrix} e^{j\theta_k^a} \\ e^{j\theta_k^b} \\ e^{j\theta_k^c} \end{pmatrix} \tag{4.10}$$

where [.] denotes only in this section, for the sake of simplification, the diagonal matrix operator *diag*(), which forms a diagonal matrix with the vector elements, V_k denotes the voltage magnitude vector in each phase of the node k of the two-port model, and θ_k is the vector composed of the complex exponentials of the voltage phase angle in each phase of the node k of the two-port model.

Expanding the power flow matrix expression, it is possible to obtain the classical active and reactive power flow equations for a three-phase component [20]:

$$\begin{aligned} P_{km}^i = V_k^i \sum_{j\in\Phi_{km}} \Big(& V_k^j \left(g_{kk}^{ij} \cos(\theta_k^i - \theta_k^j) + b_{kk}^{ij} \sin(\theta_k^i - \theta_k^j) \right) \\ & - V_m^j \left(g_{km}^{ij} \cos(\theta_k^i - \theta_m^j) + b_{km}^{ij} \sin(\theta_k^i - \theta_m^j) \right) \Big) \end{aligned} \tag{4.11}$$

$$Q_{km}^i = V_k^i \sum_{j\in\Phi_{km}} \left(V_k^j \left(g_{kk}^{ij} \sin(\theta_k^i - \theta_k^j) - b_{kk}^{ij} \cos(\theta_k^i - \theta_k^j) \right) \right. \tag{4.12}$$

$$\left. - V_m^j \left(g_{km}^{ij} \sin(\theta_k^i - \theta_m^j) - b_{km}^{ij} \cos(\theta_k^i - \theta_m^j) \right) \right) \tag{4.13}$$

where i and j denote different phases of the component; g_{kk}^{ij} and b_{kk}^{ij} are the real and imaginary parts of the ij element from the two-port model submatrix; Y_{kk} and b_{km}^{ij} are the real and imaginary parts of the ij element from the two-port model submatrix Y_{km} is the set of existing phases at branch k-m.

Regarding voltage phasors as state variables, they are typically represented in polar coordinates. However, representing the state variables in rectangular coordinates may benefit estimators designed to deal with phasor measurement units.

The next subsections describe in detail the matrix equations for active and reactive power flows and their respective derivatives for each two-port model. Distinct measurements for a diverse set of components may be described using such equations, only by changing the respective two-port admittance matrices according to the type of component and connections.

4.2.2 Polar coordinates

The voltage phasor in its exponential representation is:

$$\dot{V}_k = V_k \odot \theta_k = diag(V_k)\theta_k = [V_k]\theta_k \tag{4.14}$$

where V_k is a vector composed of the voltage magnitude in the ith phase of the system ($V_k^i = |\dot{V}_k^i|$), and θ_k is a vector composed of the complex exponential part of the angle of the phasor ($\theta_k^i = e^{j\theta_k^i}$). And the expression for the power flow:

$$S_{km} = [V_k][\theta_k]Y_{kk}^*[V_k]\theta_k^* + [V_k][\theta_k]Y_{km}^*[V_m]\theta_m^* \tag{4.15}$$

The derivatives of such equation regarding the state variables (complex nodal voltages in polar coordinates) are:

$$\frac{\partial S_{km}}{\partial V_k^i} = J^{ii}[\theta_k]Y_{kk}^*[V_k]\theta_k^* + [V_k][\theta_k]Y_{kk}^*J^{ii}\theta_k^* + J^{ii}[\theta_k]Y_{km}^*[V_m]\theta_m^* \tag{4.16}$$

$$\frac{\partial S_{km}}{\partial V_k^i} = [V_k][\theta_k]Y_{km}^*J^{ii}\theta_m^* \tag{4.17}$$

$$\frac{\partial S_{km}}{\partial \theta_k^i} = je^{\theta_k^i}[V_k]J^{ii}Y_{kk}^*[V_k]\theta_k^* - j[V_k][\theta_k]Y_{kk}^*[V_k]J^{ii}\theta_k^* + je^{\theta_k^i}[V_k]J^{ii}Y_{km}^*[V_m]\theta_m^* \tag{4.18}$$

$$\frac{\partial S_{km}}{\partial \theta_m^i} = -j[V_k][\theta_k]Y_{km}^*[V_m]J^{ii}\theta_m^* \tag{4.19}$$

where J^{ii} is a matrix with the same size as the number of phases and only the *ii* element equals one and the others equal zero. The above equation yields derivatives for all phases of the active and reactive power flow at once.

They represent general equations for multiple phase systems and different types of components. They also are in full vector and matrix format, which facilitates the implementation of generic models in a plug-and-play manner for different types of components.

Similarly, the power flow equations in the opposite terminal *m* of the two-port model:

$$S_{mk} = [V_m][\theta_m]Y_{mk}^*[V_k]\theta_k^* + [V_m][\theta_m]Y_{mm}^*[V_m]\theta_m^* \tag{4.20}$$

And also its derivatives:

$$\frac{\partial S_{mk}}{\partial V_k^i} = [V_m][\theta_m]Y_{mk}^*J^{ii}\theta_k^* \tag{4.21}$$

$$\frac{\partial S_{mk}}{\partial V_m^i} = J^{ii}[\theta_m]Y_{mk}^*[V_k]\theta_k^* + J^{ii}[\theta_m]Y_{mm}^*[V_m]\theta_m^* + [V_m][\theta_m]Y_m^*J^{ii}\theta_m^* \tag{4.22}$$

$$\frac{\partial S_{mk}}{\partial \theta_k^i} = -j[V_m][\theta_m]Y_{mk}^*[V_k]J^{ii}\theta_k^* \tag{4.23}$$

$$\frac{\partial S_{mk}}{\partial \theta_m^i} = je^{\theta_m^i}[V_m]J^{ii}Y_{mk}^*[V_k]\theta_k^* + je^{\theta_m^i}[V_m]J^{ii}Y_{mm}^*[V_m]\theta_m^* - j[V_m][\theta_m]Y_{mm}^*[V_m]J^{ii}\theta_m^* \tag{4.24}$$

Typically, distribution feeders present current magnitude measurements that are often neglected in transmission system state estimation to avoid numerical issues. However, in distribution systems, such practice reduces the already compromised observability and is often modeled to increase real-time information about the feeders. Current magnitudes and phase angles can be modeled as:

$$I_{km}^i = \frac{\sqrt{P_{km}^{i\,2} + Q_{km}^{i\,2}}}{V_k^i} \tag{4.25}$$

$$\delta_{km}^i = \theta_k^i - \arctan\left(\frac{Q_{km}^i}{P_{km}^i}\right) \tag{4.26}$$

The derivatives can be refereed to in Refs. [21, 22]. It is noteworthy that, in polar coordinates, the derivative of current equations may present some numerical issues, especially for lightly loaded circuits.

4.2.3 Rectangular coordinates

Based on the voltage phasor in rectangular coordinates, the following expression for the power flow equations is obtained:

$$\begin{aligned} S_{km} = {} & [V_{re,k}]Y^*_{kk}V_{re,k} + [V_{re,k}]Y^*_{km}V_{re,m} + [V_{im,k}]Y^*_{kk}V_{im,k} + [V_{im,k}]Y^*_{km}V_{im,m} \\ & -j[V_{re,k}]Y^*_{kk}V_{im,k} - j[V_{re,k}]Y^*_{km}V_{im,m} + j[V_{im,k}]Y^*_{kk}V_{re,k} + j[V_{im,k}]Y^*_{km}V_{re,m} \end{aligned} \tag{4.27}$$

where $V_{re,k}$ is a vector composed of the real part of the voltage phasor in each ith phase of the system ($V^i_{re,k} = \Re\{\dot{V}^i_k\}$), and $V_{im,k}$ is a vector composed of the imaginary part of the voltage phasor in each ith phase of the system ($V^i_{im,k} = \Im\{\dot{V}^i_k\}$). The above equation is used to build an active and reactive power flow model for steady-state analysis. The derivatives of such an equation regarding the state variables (complex nodal voltages in rectangular coordinates) in the same matrix representation are:

$$\begin{aligned} \frac{\partial S_{km}}{\partial V^i_{re,k}} = {} & [J^i](Y^*_{kk}V_{re,k} + Y^*_{km}V_{re,m} - jY^*_{kk}V_{im,k} - jY^*_{km}V_{im,m}) + ([V_{re,k}]Y^*_{kk} \\ & +j[V_{im,k}]Y^*_{kk})J^i \end{aligned} \tag{4.28}$$

$$\frac{\partial S_{km}}{\partial V^i_{re,m}} = [V_{re,k}]Y^*_{km}J^i + j[V_{im,k}]Y^*_{km}J^i \tag{4.29}$$

$$\begin{aligned} \frac{\partial S_{km}}{\partial V^i_{im,k}} = {} & [J^i](jY^*_{kk}V_{re,k} + Y^*_{kk}V_{im,k} + jY^*_{km}V_{re,m} + Y^*_{km}V_{im,m}) + ([V_{im,k}]Y^*_{kk} \\ & -j[V_{re,k}]Y^*_{kk})J^i \end{aligned} \tag{4.30}$$

$$\frac{\partial S_{km}}{\partial V^i_{im,k}} = -j[V_{re,k}]Y^*_{km}J^i + [V_{im,k}]Y^*_{km}J^i \tag{4.29}$$

where J^i is a vector with the same size as the number of phases and only the ith element equals one and the others equal zero.

Similarly, the power flow equations in the opposite terminal m of the two-port model:

$$\begin{aligned} S_{mk} = {} & [V_{re,m}]Y^*_{mk}V_{re,k} + [V_{re,m}]Y^*_{mm}V_{re,m} + [V_{im,m}]Y^*_{mk}V_{im,k} + [V_{im,m}]Y^*_{mm}V_{im,m} \\ & +j[V_{im,m}]Y^*_{mk}V_{re,k} - j[V_{re,m}]Y^*_{mk}V_{im,k} + j[V_{im,m}]Y^*_{mm}V_{re,m} - j[V_{re,m}]Y^*_{mm}V_{im,m} \end{aligned} \tag{4.32}$$

And also its derivatives:

$$\frac{\partial S_{mk}}{\partial V^i_{re,k}} = [V_{re,m}]Y^*_{mk}J^i + j[V_{im,m}]Y^*_{mk}J^i \tag{4.33}$$

$$\begin{aligned} \frac{\partial S_{mk}}{\partial V^i_{re,m}} = {} & [J^i](Y^*_{mk}V_{re,k} - jY^*_{mk}V_{im,k} + Y^*_{mm}V_{re,m} - jY^*_{mm}V_{im,m}) + ([V_{re,m}]Y^*_{mm} \\ & +j[V_{im,m}]Y^*_{mm})J^i \end{aligned} \tag{4.34}$$

$$\frac{\partial S_{mk}}{\partial V^{i}_{im,k}} = [V_{im,m}]Y^{*}_{mk}J^{i} - j[V_{re,m}]Y^{*}_{mk}J^{i} \tag{4.35}$$

$$\frac{\partial S_{mk}}{\partial V^{i}_{im,k}} = [J^{i}](jY^{*}_{mk}V_{re,k} + Y^{*}_{mk}V_{im,k} + jY^{*}_{mm}V_{re,m} + Y^{*}_{mm}V_{im,m}) + ([V_{im,m}]Y^{*}_{mm} - j[V_{re,m}]Y^{*}_{mm})J^{i} \tag{4.36}$$

The current real and imaginary parts may also be modeled with this formulation. By dealing both with the current phasor as well as the state variables in rectangular coordinates is possible to build a linear model.

$$I_{re,km} = \Re\{Y_{kk}\}V_{re,k} - \Im\{Y_{kk}\}V_{im,k} + \Re\{Y_{km}\}V_{re,m} - \Im\{Y_{km}\}V_{im,m} \tag{4.37}$$

$$I_{im,km} = \Im\{Y_{kk}\}V_{re,k} + \Re\{Y_{kk}\}V_{im,k} + \Im\{Y_{km}\}V_{re,m} + \Re\{Y_{km}\}V_{im,m} \tag{4.38}$$

$$I_{re,mk} = \Re\{Y_{mk}\}V_{re,k} - \Im\{Y_{mk}\}V_{im,k} + \Re\{Y_{mm}\}V_{re,m} - \Im\{Y_{mm}\}V_{im,m} \tag{4.39}$$

$$I_{im,mk} = \Im\{Y_{mk}\}V_{re,k} + \Re\{Y_{mk}\}V_{im,k} + \Im\{Y_{mm}\}V_{re,m} + \Re\{Y_{mm}\}V_{im,m} \tag{4.40}$$

The derivatives can be easily obtained from the real and imaginary parts of the two-port model admittance submatrices. This is an important aspect of distribution systems, since it motivated the pursuit of current-based state estimation formulations [8, 14, 23]. This approach is also often employed when dealing with PMUs, in order to simplify the representation and take computational advantage without losing accuracy [14, 23].

4.3 Models of the physical components of a distribution system

There is a variety of different components installed in the distribution systems, with different characteristics, connections, and functionalities. Despite the intrinsic differences, they can be individually described by their effects on the electrical quantities of the power system. This section presents the main components of distribution networks. The model parameters are described and discussed and the respective two-port model is derived.

4.3.1 Distribution lines

The electric cables installed as overhead or underground lines represent the majority of the distribution network. The distribution line model comprises a series impedance, to accommodate thermal losses and the effect of the magnetic fields surrounding the conductors, and a shunt admittance, to represent the electrical field effect between the conductors and the ground [2, 17, 24, 25]. Figure 4.4 illustrates a typical geometric disposition for a three-wire overhead medium-voltage distribution circuit and the respective electrical model.

The series impedance (z) comprises a resistance (r) and an inductive reactance (x), from the circuit inductance (l) and system frequency (f), for each phase (i) of the circuit. Also, the model comprises mutual coupling among phases. The series parameter may be expressed by the general form described in (4.41) for the

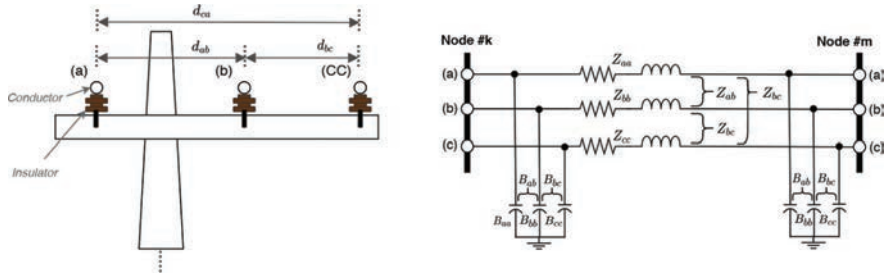

Figure 4.4 Example of distribution circuit with an overhead configuration for a three-phase medium-voltage circuit and its respective electrical model

self-impedance of each phase i, and in (4.42) for the mutual impedance among different phases i and j.

$$z^{ii} = r^{ii} + j2\pi f l^{ii} = r^{ii} + jx^{ii} \tag{4.41}$$

$$z^{ij} = r^{ij} + j2\pi f l^{ij} = r^{ij} + jx^{ij} \tag{4.42}$$

The series self-resistance r^{ii} reflects the thermal losses in the circuit according to the Joule effect. The resistance of the cable is related to the type of material, cross-sectional area, and length. Typically, manufacturers provide cable resistance values for direct current conditions. For alternating current, the existence of a varying magnetic field inside the conductor results in a nonuniform distribution of current, thickening the current density near the surface of the cables, known as the *skin effect* [24]. The effect of the magnetic field of adjacent conductors, for instance, different phases near the conductor, also increases such effect, known as the *proximity effect*. In practice, both effects increase the effective resistance of the cable and can be compensated by correction factors when calculating the cable resistance. Another important factor is temperature, which tends to increase the electrical resistivity of the conductor, also compensated by a thermal coefficient related to the type of material.

Besides the series resistance, the series inductance comprises the magnetic field effects among the conductors, resulting in a self l^{ii} and a mutual l^{ij} inductance, respectively. Such magnetic fields are a direct result of the alternated electric current flowing through the conductors, derived from *Faraday's law of electromagnetic induction*. The geometric disposition of the cables is essential to the proper calculation of the distribution line inductance and magnetic coupling among phases [2]. The inner geometric radius of the conductors is provided by manufacturers, and the distance among different conductors depends on the geometric disposition of the cables in the structures of the poles and cross arms, as illustrated in Figure 4.5, with the respective distances among the phase conductors (d_{ab}, d_{bc}, and d_{ca}).

The effect of the return path of the current through the ground resistance can also be taken into account by performing a correction in the impedance values, known as *Carson's equations* [2, 24, 26]. The Carson method consists basically of reflecting the conductors in the soil and considering a uniform ground resistance

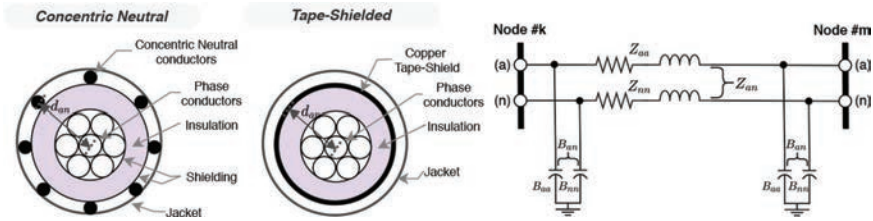

Figure 4.5 Example of distribution circuit with an underground cable configuration, with concentric or with tape-shielded neutral, for a single-phase medium-voltage circuit and its respective electrical model

and infinite extension. The method comprises introducing correction factors for the self and mutual series impedance to take into account the effect of grounding resistance. Indeed, the mutual resistance r^{ij} term in (4.42) appears after this correction. For practical purposes, a simplified version known as Modified Carson equations is typically used, by considering a few terms for the correction factors.

The distribution line model may also comprise a shunt admittance (y_{shunt}) from the circuit shunt capacitance (c) and system frequency (f), for each phase of the circuit. Shunt parameter may be expressed by the general form described in (4.43) for the self-admittance of each phase i and in (4.44) for the mutual admittance among different phases i and j. This shunt admittance captures the electric field among the conductors and the soil, also resulting in a self c^{ii} and a mutual c^{ij} capacitance. The electric field arises from the charged conductors and can be derived from *Coulomb's law* using the reflected image of the geometric disposition of the cables in the soil [2]. Besides the electric permittivity physical constants, the geometric disposition of the cables is essential to the proper calculation of the distribution circuit capacitance among phases. The calculation comprises the electric potentials difference among conductors, from which a capacitance matrix can be derived, as the inverse of the potential coefficient matrix. Shunt conductances (employed, for instance, to capture ionizing effects of the conductors due to the *Corona effect* or to insulator leakage) are usually neglected since they are very small [2, 27].

$$y_{shunt}^{ii} = j2\pi f c^{ii} = jb^{ii} \tag{4.43}$$

$$y_{shunt}^{ij} = j2\pi f c^{ij} = jb^{ij} \tag{4.44}$$

In the case of underground cables, the same Carson method can be applied to model the series and shunt parameters, according to the geometric disposition of the cables and manufacturer parameters. There are, however, some additional considerations to be taken into account regarding different underground configurations and cables with concentric neutral conductors or with tape-shielded conductors. In this case, each phase will present a particular neutral conductor and associated variables and parameters for each phase. This will increase the dimension of the model to capture each neutral conductor for each cable of each phase, yielding in a (6×6) impedance

matrix with three dimensions for the phase conductors and the other three dimensions for each neutral conductor, all with its respective coupling terms.

Once distribution circuits consist of single-, two-, or three-phase untransposed lines, the Carson method provides an accurate model to represent them in any steady-state analysis for distribution systems. There are some cases where sequence components (positive, negative, and zero sequence impedances and admittances) are employed to model three-phase circuits. Such an approach, however, is only accurate for dealing with transposed circuits, where the mutual coupling terms of the model are equal (off-diagonal elements of the impedance and admittance matrices). It is not the case in distribution systems, where the majority of circuits are untransposed and asymmetrical, the main reason for using phase domain rather than symmetrical components in distribution systems analysis [2]. Details of the calculation of the resistance, inductance, and capacitance parameters for a distribution circuit, through Carson's method, can be found in [2].

The respective two-port admittance model can be described previously by the following equations. Single-phase or two-phase circuits can also be represented by such a model, by only considering the elements of the respectively connected phases.

$$\begin{aligned} Y_{kk} &= Y_{mm} = Z_{serie}^{-1} + Y_{shunt} \\ Y_{km} &= Y_{mk} = -Z_{serie}^{-1} \end{aligned} \tag{4.45}$$

where Z_{serie} is the primitive series impedance matrix of the circuit composed of the self z^{ii} and mutual z^{ij} series impedances, and Y_{shunt} is the shunt admittance matrix of the circuit composed of the self y_{shunt}^{ii} and mutual z_{shunt}^{ij} shunt admittances. As an example, for a three-wire distribution line, those matrices would be:

$$Z_{serie} = \begin{pmatrix} r^{aa} + jx^{aa} & r^{ab} + jx^{ab} & r^{ac} + jx^{ac} \\ r^{ab} + jx^{ab} & r^{bb} + jx^{bb} & r^{bc} + jx^{bc} \\ r^{ac} + jx^{ac} & r^{bc} + jx^{bc} & r^{cc} + jx^{cc} \end{pmatrix} \tag{4.46}$$

$$Y_{shunt} = \begin{pmatrix} jb^{aa} & jb^{ab} & jb^{ac} \\ jb^{ab} & jb^{bb} & jb^{bc} \\ jb^{ac} & jb^{bc} & jb^{cc} \end{pmatrix} \tag{4.47}$$

The model can also be extended to represent the neutral conductors if available, which is the case of four-wire distribution circuits or underground cables with concentric neutral [6, 25]. In this case, an additional dimension is incorporated into the model to capture the neutral conductor condition, and the associated neutral-ground voltages and neutral conductor current are considered in the two-port model as well, by the following matrices:

$$Z_{serie} = \begin{pmatrix} r^{aa} + jx^{aa} & r^{ab} + jx^{ab} & r^{ac} + jx^{ac} & r^{an} + jx^{an} \\ r^{ab} + jx^{ab} & r^{bb} + jx^{bb} & r^{bc} + jx^{bc} & r^{bn} + jx^{bn} \\ r^{ac} + jx^{ac} & r^{bc} + jx^{bc} & r^{cc} + jx^{cc} & r^{cn} + jx^{cn} \\ r^{an} + jx^{an} & r^{bn} + jx^{bn} & r^{cn} + jx^{cn} & r^{nn} + jx^{nn} \end{pmatrix} \tag{4.48}$$

$$Y_{shunt} = \begin{pmatrix} jb^{aa} & jb^{ab} & jb^{ac} & jb^{an} \\ jb^{ab} & jb^{bb} & jb^{bc} & jb^{bn} \\ jb^{ac} & jb^{bc} & jb^{cc} & jb^{cn} \\ jb^{an} & jb^{bn} & jb^{cn} & jb^{nn} \end{pmatrix} \tag{4.49}$$

A common practice for distribution circuits is to simplify the model by discarding the dimensions and variables associated with the neutral conductors through a technique known as *Kron reduction* [2, 28]. The Kron reduction is based on the assumption of multi-grounded systems as if each node of the distribution circuit has the neutral terminals solidly grounded. Consequently, the neutral-to-ground voltage equals zero in all nodes of the distribution circuit, which enables discarding the associated variables and reducing the dimensionality of the distribution circuit only to the phase conductors. The Kron reduction technique then consists of a matrix elimination process applied to the series impedance and shunt admittance matrices obtained by the Carson method, which is described in (4.50) for the series impedance as an example.

$$Z^{abc} = Z^{ij} - Z^{in}(Z^{nn})^{-1}Z^{jn} \tag{4.50}$$

where the elements of the equation are the submatrices of the original full series impedance matrix: Z^{ij} is associated with all the phase conductors i and j; Z^{jn} are associated with coupling elements between i and j phases and n neutral conductors; and Z^{nn} is associated with the n neutral conductors. With this reduction, the final matrix Z^{abc} has the same size of phase conductors, for instance, a (3×3) for three-phase *abc* circuits.

4.3.2 Power transformers

Power transformers are equipment responsible for connecting different voltage levels of the distribution network, for instance, high-voltage with medium-voltage and medium-voltage with low-voltage circuits. They are mainly inductive elements

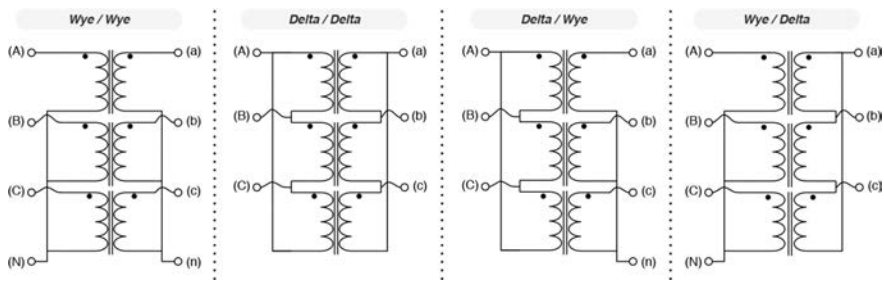

Figure 4.6 *Three-phase transformer connections of the primary and secondary windings. The wye connection may present a solidly grounded connection (wye grounded). Detailed grounding models may incorporate a reactor as well.*

Table 4.1 Submatrices for step-down three-phase transformers according to their most common primary and secondary connections

Connection		**Self-admittance**		**Mutual admittance**	
Primary	**Secondary**	Y_{kk}	Y_{mm}	Y_{km}	Y_{mk}
Grounded wye	Grounded wye	Y_I	Y_I	$-Y_I$	$-Y_I$
Grounded wye	Wye	Y_{II}	Y_{II}	$-Y_{II}$	$-Y_{II}$
Grounded wye	Delta	Y_I	Y_{II}	Y_{III}	Y_{III}^T
Wye	Grounded wye	Y_{II}	Y_{II}	$-Y_{II}$	$-Y_{II}$
Wye	Wye	Y_{II}	Y_{II}	$-Y_{II}$	$-Y_{II}$
Wye	Delta	Y_{II}	Y_{II}	Y_{III}	Y_{III}^T
Delta	Grounded wye	Y_{II}	Y_I	Y_{III}^T	Y_{III}
Delta	Wye	Y_{II}	Y_{II}	Y_{III}^T	Y_{III}
Delta	Delta	Y_{II}	Y_{II}	$-Y_{II}$	$-Y_{II}$

Source: [20].

constructed with magnetic coils in two separate windings, the primary side and the secondary side. Figure 4.6 illustrates the most common three-phase transformer connections delta, wye, and grounded wye.

The transformers may also be represented by 4.7, in which the submatrices Y_{kk}, Y_{km}, Y_{mk}, and Y_{mm} assume distinct values according to the connection of the three-phase transformer. The most common connections are presented in Table 4.1 for the step-down transformers. For a step-up transformer, columns regarding the mutual admittance have to be swapped [29, 30]. Also, the submatrices Y_I, Y_{II}, and Y_{III} in Table 4.1 are given as follows, in which y_t is the *per-unit* transformer admittance [20].

$$Y_I = \begin{pmatrix} y_t & 0 & 0 \\ 0 & y_t & 0 \\ 0 & 0 & y_t \end{pmatrix}; \qquad Y_{II} = \frac{1}{3}\begin{pmatrix} 2y_t & -y_t & -y_t \\ -y_t & 2y_t & -y_t \\ -y_t & -y_t & 2y_t \end{pmatrix}; \qquad Y_{III} = \frac{1}{\sqrt{3}}\begin{pmatrix} -y_t & y_t & 0 \\ 0 & -y_t & y_t \\ y_t & 0 & -y_t \end{pmatrix} \tag{4.51}$$

If the transformer has an off-nominal tap, namely α for the primary and β for the secondary tap ratio, the self- and mutual-admittance matrices have the following adjustment [20]:

- divide the primary self-admittance matrix by α^2
- divide the secondary self-admittance matrix by β^2
- divide the mutual-admittance matrices by $\alpha\beta$

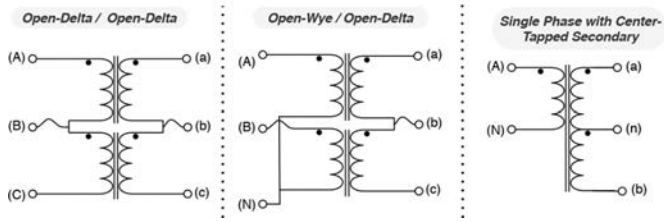

Figure 4.7 Three-phase transformer open connections and single-phase with the center-tapped secondary connection.

Furthermore, all of the above models comprise three-wire or solidly grounded connections. For open grounded or grounding systems, the above models can be extended to incorporate neutral-to-earth voltages as complementary state variables. Similar to the four-wire distribution circuits, another variable is included in the two-port model to represent the effect of transformer grounding.

Also, the open-wye and open-delta connections may be employed in distribution systems, as illustrated in Figure 4.7. In this case, the two-port model must be adequate to represent the specific connections of each transformer, that is the proper input voltages and currents according to the connected phases of the transformer, as presented by [31]. Equation (4.52) presents the two-port model for an open-delta/open-delta (OD/OD) transformer, and (4.53), for an open-wye/open-delta (OY/OD) transformer.

$$
\begin{aligned}
&Y_{kk} = \frac{y_t}{\alpha^2}\begin{pmatrix} 1 & -1 & 0 \\ -1 & 2 & -1 \\ 0 & -1 & 1 \end{pmatrix} \qquad Y_{km} = Y_{mk} = \frac{y_t}{\alpha\beta}\begin{pmatrix} 1 & -1 & 0 \\ -1 & 2 & -1 \\ 0 & -1 & 1 \end{pmatrix} \\
&Y_{mm} = \frac{y_t}{\beta^2}\begin{pmatrix} 1 & -1 & 0 \\ -1 & 2 & -1 \\ 0 & -1 & 1 \end{pmatrix}
\end{aligned} \tag{4.52}
$$

$$
\begin{aligned}
&Y_{kk} = \frac{y_t}{\alpha^2}.\begin{pmatrix} 1 & 0 \\ 0 & 1 \end{pmatrix} \qquad Y_{km} = Y^t_{mk} = \frac{y_t}{\alpha\beta}.\begin{pmatrix} -\frac{1}{\sqrt{3}} & \frac{1}{\sqrt{3}} & 0 \\ 0 & -\frac{1}{\sqrt{3}} & \frac{1}{\sqrt{3}} \end{pmatrix} \\
&Y_{mm} = \frac{y_t}{\beta^2}.\begin{pmatrix} \frac{1}{3} & -\frac{1}{3} & 0 \\ -\frac{1}{3} & \frac{2}{3} & -\frac{1}{3} \\ 0 & -\frac{1}{3} & \frac{1}{3} \end{pmatrix}
\end{aligned} \tag{4.53}
$$

Another possibility, for single-phase transformers, is the center-tapped secondary winding. Such a type of connection is common for distribution transformers in the United States, interfacing medium- and low-voltage networks. The center tap is typically grounded, which enables phase to neutral and phase to phase loads. The winding individual impedance values may be difficult to find in practice, and often empirical equations provide individual parameters for each winding and also their

coupling [2, 32]. With such parameters, the transformer can be described by the following two-port admittance matrices:

$$Y_{kk} = \frac{y_{AN}}{\alpha^2} \qquad Y_{km} = Y_{mk}^{t} = \frac{1}{\alpha\beta}\cdot\begin{pmatrix} -y_{Aa} & -y_{Ab} \end{pmatrix}$$
$$Y_{mm} = \frac{1}{\beta^2}\cdot\begin{pmatrix} y_{an} & -y_{ab} \\ -y_{ab} & y_{bn} \end{pmatrix} \tag{4.54}$$

where y_{AN} denotes the self-admittance of the primary winding; y_{Aa} and y_{Ab} indicate the coupling admittance between the primary winding and each half of the secondary winding; y_{an} and y_{bn} are the self-admittance of the two halves of the secondary winding; and y_{ab} their mutual coupling admittance.

Three-winding three-phase transformers are typical at large distribution substations with a medium-voltage supply. Another important application of this transformer is interfacing power electronic converters that may benefit from the phase displacement between the secondary and tertiary windings, with grounded wye and delta connections, respectively. Three individual three-phase transformers represent the three-winding transformer according to the windings' connections and manufacturer impedance data from the different terminals: from primary to secondary; from primary to tertiary; and from tertiary to secondary. Typically, the secondary presents a wye connection and the tertiary a delta connection.

Some analyses may even consider core losses and magnetizing reactances [29, 31]. These parameters, omitted in the above models, can be incorporated as shunt elements. A shunt resistance for the core loss and a shunt inductance for the magnetizing reactance are both represented at the primary terminal of the transformers. Such models may be necessary for assessing transient responses, evaluating harmonic content, or even for a more detailed loss calculation on distribution networks. Box 4.2 presents an example of a small distribution feeder to illustrate the distribution circuit and power transformer models.

4.3.3 Voltage regulators

Voltage regulators are a special kind of transformer that controls the voltage at specific nodes of the network by changing the transformation relation according to discrete tap switching operations. They perform an essential control task to keep voltage levels within operational limits. Typically, they are built as a particular type of auto-transformers with a tap switching mechanism through on-load tap changers. The tap switching can be performed on the primary or the secondary side of the voltage regulator, referred to as "Type A" and "Type B" voltage regulators [2]. In distribution systems, it is often employed 16 taps that correspond to an increase/decrease of 10% of the voltage on the secondary side (16 taps to increase, 16 taps to decrease, and a nominal position). Figure 4.8 illustrates the main components of the voltage regulator and the associated instrumentation and control equipment.

Regarding the voltage regulator mathematical model, a similar approach to the power transformer is employed to represent their different connections. In practice, due to constructive characteristics, their resistance and reactance are very small and

Box 4.2 Example of the IEEE 4 nodes test feeder

The IEEE 4 nodes test feeder contains distribution circuits as well as a transformer between nodes 2 and 3. In order to build the three-phase two-port model of its circuits, it is necessary to know the conductor parameters as well as the pole configuration. The conductor parameters are used in the so-called modified Carson's equations to compute the primitive series impedance matrix [28]. This primitive series impedance matrix can be partitioned as:

$$Z_{serie} = \begin{pmatrix} Z^{ij} & Z^{in} \\ Z^{nj} & Z^{nn} \end{pmatrix} \tag{4.55}$$

This partition is useful in order to apply the Kron reduction technique, which then produces the phase impedance matrix as shown in [28]:

$$Z^{abc} = Z^{ij} - Z^{in} Z^{nn-1} Z^{nj} \tag{4.56}$$

The matrix Z^{abc} is equivalent to the Z_{serie} matrix in (4.45). There are no shunt elements in the test feeder, and therefore, the two-port model is fully represented by the series impedance matrix. In order to build the power transformer model, it is necessary to obtain the primary and secondary connections as well as the three-phase parameters.

The transformer has a delta–wye connection and its impedance are $R = 1.0\%$ and $X = 6.0\%$.

As a consequence, the transformer admittance, used to build the submatrices Y_I, Y_{II}, Y_{III}, is $y_t = 2.702 - j16.216 p.u.$ For a delta–wye connection, only Y_{II}, Y_{III} are needed. The resulting matrices of the two-port model for the circuits are:

$$\begin{aligned} Y_{kk} &= Y_{mm} = (Z^{abc})^{-1} \\ Y_{km} &= Y_{mk} = (Z^{abc})^{-1} \end{aligned} \tag{4.57}$$

$$(Z^{abc})^{-1} = \begin{pmatrix} 0.783 - j1.624 & -0.380 + j0.557 & -0.137 + j0.362 \\ -0.380 + j0.557 & 0.876 - j1.683 & -0.233 + j0.442 \\ -0.137 + j0.362 & -0.233 + j0.442 & 0.703 - j1.568 \end{pmatrix} \tag{4.58}$$

The resulting matrices for the two-port model of the delta-wye transformer are $Y_{kk} = Y_{mm} = Y_{II}$, $Y_{km} = Y_{III}^T$ and $Y_{mk} = Y_{III}$ which are:

$$Y_{II} = \begin{pmatrix} 1.801 - j10.806 & -0.900 + j5.403 & -0.900 + j5.403 \\ -0.900 + j5.403 & 1.801 - j10.806 & -0.900 + j5.403 \\ -0.900 + j5.403 & -0.900 + j5.403 & 1.801 - j10.806 \end{pmatrix} \tag{4.59}$$

(Continues)

$$Y_{III} = \begin{pmatrix} -1.560 + j9.358 & 1.560 - j9.358 & 0 \\ 0 & -1.560 + j9.358 & 1.560 - j9.358 \\ 1.560 - j9.358 & 0 & -1.560 + j9.358 \end{pmatrix} \tag{4.60}$$

the voltage regulators are often represented as ideal transformers. However, this approach may severely aggravate numerical ill-conditioning [33]. To overcome this effect, the voltage regulator model may be associated with adjacent components, or by employing more stable numerical methods [19]. Alike the power transformer, the type of connection of the voltage regulator (wye grounded, wye, delta, open wye, open delta, or single-phase) defines the two-port model according to the equations of admittance submatrices in (4.51). The difference relies on the off-nominal tap parameters that now comprise an individual transformer relation for each phase i, denoted as α^i. Typically, only one side will present off-nominal tap relations. As an example, the wye-grounded voltage regulator, with tap switching represented on the secondary, two-port model is presented below in (4.61).

$$\begin{pmatrix} Y_{kk} & Y_{km} \\ Y_{mk} & Y_{mm} \end{pmatrix} = \begin{pmatrix} \begin{pmatrix} y_t & 0 & 0 \\ 0 & y_t & 0 \\ 0 & 0 & y_t \end{pmatrix} & \begin{pmatrix} -\frac{1}{\alpha^a} y_t & 0 & 0 \\ 0 & -\frac{1}{\alpha^b} y_t & 0 \\ 0 & 0 & -\frac{1}{\alpha^c} y_t \end{pmatrix} \\ \begin{pmatrix} -\frac{1}{\alpha^a} y_t & 0 & 0 \\ 0 & -\frac{1}{\alpha^b} y_t & 0 \\ 0 & 0 & -\frac{1}{\alpha^c} y_t \end{pmatrix} & \begin{pmatrix} \frac{1}{\alpha^{a2}} y_t & 0 & 0 \\ 0 & \frac{1}{\alpha^{b2}} y_t & 0 \\ 0 & 0 & \frac{1}{\alpha^{c2}} y_t \end{pmatrix} \end{pmatrix} \tag{4.61}$$

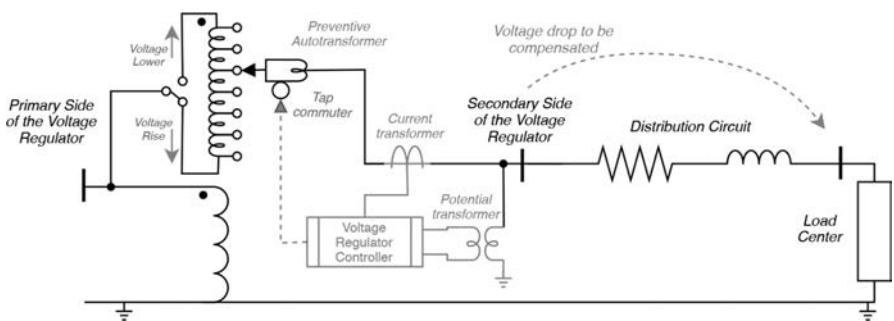

Figure 4.8 Single-phase schematic of a "Type A" voltage regulator, its main components, and voltage control strategy illustration

where α^a, α^b, and α^c are the off-nominal voltage regulator transformation relation according to the tap position for the respective phase a, b, and c.

The main difference from a conventional power transformer is the automated voltage control through a tap switching mechanism. Different control techniques and philosophies may be employed for tap control, such as centralized Volt/VAr control or local automated line drop compensation (LDC). The first is based on the communication of tap values from a central processor at the operation center, according to optimization or network-based strategy. The latter, more usual, is based on measured information and a local controller. The terminal voltages and currents are measured in all phases, and a control strategy to compensate for voltage drop is employed. Through the parameter of the LDC, the voltage regulator can be tuned to control the voltage at a far away node or its own secondary winding [2, 33, 34]. Typically, such parameters are the following, given in terms of the voltage regulator parametrization and voltage levels:

- *Current transformer and voltage transformer relations:* correspond to the transformation relation for the instrumentation transformers that transduces the voltage and current of the voltage regulator to reduced levels according to the nominal inputs of the controller (typically, around 120 secondary volts for the voltage transformer, and five secondary Amperes for the current transformer).
- *Voltage setpoint:* the controlled voltage value for each phase that will be set as the target voltage for the controller, through the LDC parameters.
- *Line drop resistance and reactance:* a resistance R^i_{LDC} and a reactance X^i_{LDC} parameters for each phase i, which correspond to the voltage drop downstream the controlled voltage regulator. For instance, if both values are set equal to zero, then the regulator controls the voltage at its secondary terminal; otherwise, those parameters may reflect the line voltage drop downstream the regulator until the load center.
- *Voltage bandwidth:* the acceptable voltage deviation from the controlled voltage setpoint,typically set to two volts. If the calculated voltage value by the LDC falls outside the range of the voltage setpoint, with a tolerance range given by the bandwidth, a tap switching operation is performed.
- *Time delay:* length of time before the tap changing operation happens, necessary to reduce unwanted tap switching during transitory responses of the systems, typically set within a few tens of seconds.
- *Maximum number of taps:* the maximum number of discrete tap positions available in the voltage regulator (e.g. 16 taps).

The control strategy is based on the calculation of the mismatch between the setpoint voltage and the measured ones while considering the voltage drop on the LDC parameters. This voltage drop calculation uses the LDC resistance and reactance controller parameters to compensate for voltage drop on distribution circuits, hence remotely regulating the voltage near the load center. The criterion for this mismatch V^i_{diff} is given by the following equation:

$$V_{diff}^{i} = V_{set}^{i} - \left| \frac{\dot{V}_{m}^{i}}{RPT} - (R_{LDC}^{i} + jX_{LDC}^{i}) \frac{-\dot{I}_{mk}^{i}}{RCT} \right| \tag{4.62}$$

where $\dot{V}_{m}^{i}$ and $\dot{I}_{mk}^{i}$ are the voltage and current phasors measured at the secondary terminal of the voltage regulator at phase i and RCT are the instrumentation voltage transformer and current transformer transformation relations, respectively; V_{set}^{i} is the controller voltage setpoint and R_{LDC}^{i} and X_{LDC}^{i} are the LDC parameters. If the absolute value of the above difference becomes less than the voltage regulator bandwidth ($|V_{diff}^{i}| < \Delta V$), a tap switching operation is performed. The new tap that compensates for the deviation from the setpoint can be calculated by (4.63). The sign of the equation depends if there is a need to increase or decrease the voltage. The *round*() function will approximate the function to the nearest larger or smaller integer, depending on the sign [34].

$$tap^{i,new} = tap^{i} \pm round(V_{diff}^{i} - \Delta V/2) \Big/ \frac{Regulation}{N_{taps}} \tag{4.63}$$

where $tap^{i,new}$ is the new tap position to be switched into, tap^{i} is the current tap position, *Regulation* is the total voltage regulation in percentage for the voltage regulator, and N_{taps} is the total number of taps. As an example, a voltage regulator with 10% with 16 taps for voltage regulation yields an increase/decrease of voltage transformation relation of 0.625% for each tap. The transformation relation parameter α^{i} for each phase is then calculated for the specific tap position according to (4.64).

$$\alpha^{i} = 1 + \frac{Regulation}{N_{taps}} tap^{i} \tag{4.64}$$

Besides the LDC configuration, distinct control strategies may be employed in modern voltage regulator digital controllers based on the upstream and downstream variables of the network. Such voltage regulators are typically highly monitored, with current and voltage sensors that also provide the active and reactive power through the regulator in both terminals (primary and secondary) in real time. The control strategies are defined upon these different measured values and mainly defined based on the direction of the power flow through the regulator [34, 35], as follows:

- **Forward control:** the traditional approach where the voltage regulator controls a downstream voltage, using the secondary side electrical quantities in the LDC control settings, independently of the direction of the power flowing through the regulator.
- **Locked forward control:** the voltage regulator controls a downstream voltage, using the secondary side electrical quantities in the LDC control settings if the power flow direction is from the primary toward the secondary (the forward direction); otherwise, the regulator keeps a pre-specified fixed tap value (the reverse direction).
- **Locked reverse control:** the voltage regulator controls an upstream voltage, using the primary side electrical quantities in the LDC control settings if the

power flow direction is from the secondary toward the primary (the reverse direction); otherwise, the regulator keeps a pre-specified fixed tap value (the forward direction).

- **Co-generation control:** the voltage regulator presents two separate settings for the LDC depending on the power flow direction, but always controlling a downstream voltage, using the secondary side electrical quantities in the LDC control settings: with the first set of control configurations (voltage setpoints and LDC parameters) if the power flow direction is from the primary toward the secondary (the forward direction); and the second set of configurations otherwise if power flow direction is from the secondary toward the primary (the reverse direction).
- **Bidirectional control:** the voltage regulator presents two separate settings for the LDC depending on the power flow direction: the first if the power flow direction is from the primary toward the secondary (the forward direction), controlling a downstream voltage, using the secondary side electrical quantities in the LDC control settings; the second, otherwise if the power flow direction is from the secondary toward the primary (the reverse direction), controlling an upstream voltage, using the primary side electrical quantities in the LDC control settings.

Although an important detail for steady-state analysis of distribution networks, in the context of distribution system state estimation, the tap values are typically assumed as monitored parameters, without incorporating detailed controller models. This assumption is not always valid, and besides, the response time of such controllers may be faster than the updates on the measurement set. It motivates some approaches that incorporate the tap positions as complementary variables to be estimated as in Ref. [36].

4.3.4 Loads

In steady-state analysis, loads are often considered independent of the voltage, leading to a constant power load representation. However, in distribution system analysis, a more accurate representation of the loads may be required, which leads to distinct models. One of the most traditional approaches is the exponential model [37, 38]:

$$\begin{aligned} P_k^i &= P_k^{inom} \cdot \bar{V}_k^{\,a} \\ Q_k^i &= Q_k^{inom} \cdot \bar{V}_k^{\,b} \end{aligned} \tag{4.65}$$

In which the superscript i denotes the phase, the subscript k is the node, *nom* denotes the nominal load (at the beginning of the iterative process), and $\bar{V}_k^i$ corresponds to the relation between the updated voltage and its nominal value ($\bar{V}_k = V_k / V_k^{nom}$). The exponents a and b are used to represent a constant power, constant current, or constant impedance load characteristics, assuming the values of 0, 1, and 2, respectively. However, for composite loads, these values usually range from 0.5 to 0.8 for a, and from 1.5 to 6 for b [37].

Another model is the polynomial one, which is also known as the *ZIP* model [37, 38]:

$$\begin{aligned} P_k^i &= P_k^{i-nom} \cdot \left(p_1 \bar{V}_k^{i\,2} + p_2 \bar{V}_k^i + p_3 \right) \\ Q_k^i &= Q_k^{i-nom} \cdot \left(q_1 \bar{V}_k^{i\,2} + q_2 \bar{V}_k^i + q_3 \right) \end{aligned} \tag{4.66}$$

This model is composed of three distinct parts, constant impedance (Z), constant current (I), and constant power (P) portion (hence known as ZIP). Each one is multiplied by a coefficient that defines the proportion of each component in the load (p_1 to p_3 for the active load, and q_1 to q_3 for the reactive load). For example, a constant power load would have $p_3 = q_3 = 1$ while the other coefficients are set to zero. Any composite load may be represented as long as the sum of the distinct coefficients of the active or reactive load equals one [37].

While the previous models efficiently represent most wye-connected loads, delta-connected loads need a few adjustments. Since most three-phase power system analyses are conducted using phase power and voltage, the consumed power of the delta-connected load needs to be converted to its phase equivalent. To do so, it is assumed that the complex power and voltage of the delta-connected load are given by:

$$\dot{S}_k^{ab} = P_k^{ab} + jQ_k^{ab}; \quad \dot{S}_k^{bc} = P_k^{bc} + jQ_k^{bc}; \quad \dot{S}_k^{ca} = P_k^{ca} + jQ_k^{ca} \tag{4.67}$$

$$\dot{V}_k^{ab} = V_k^{ab} \angle \theta_k^{ab}; \quad \dot{V}_k^{bc} = V_k^{bc} \angle \theta_k^{bc}; \quad \dot{V}_k^{ca} = V_k^{ca} \angle \theta_k^{ca} \tag{4.68}$$

Therefore, the delta active and reactive power is obtained using (4.67) or (4.68), according to the load model. The line currents in the load are:

$$\dot{I}_k^{ab} = \left(\dot{S}_k^{ab} / \dot{V}_k^{ab} \right)^*; \quad \dot{I}_k^{bc} = \left(\dot{S}_k^{bc} / \dot{V}_k^{bc} \right)^*; \quad \dot{I}_k^{ca} = \left(\dot{S}_k^{ca} / \dot{V}_k^{ca} \right)^* \tag{4.69}$$

Furthermore, the wye equivalent complex phase load at bus k is obtained by:

$$\begin{aligned} \dot{S}_k^a &= \left(\dot{I}_k^{ab} - \dot{I}_k^{ca} \right)^* \dot{V}_k^a \\ \dot{S}_k^b &= \left(\dot{I}_k^{bc} - \dot{I}_k^{ab} \right)^* \dot{V}_k^b \\ \dot{S}_k^c &= \left(\dot{I}_k^{ca} - \dot{I}_k^{bc} \right)^* \dot{V}_k^c \end{aligned} \tag{4.70}$$

Consequently, the active and reactive powers (P_k^i and Q_k^i) of the specified wye equivalent complex phase load are obtained with the real and imaginary parts of the wye equivalent phase load, respectively. The same set of equations may also be applied to bi-phase loads.

The loads in distribution systems can also be associated with sensors, typically called smart meters, under an AMI concept [13]. If the load values are effectively measured, they can be included in the state estimation measurement model, with some practical considerations that will be dealt with in future chapters. If such loads are not measured, typically the load model comprises the use of typical load profiles [8, 39]. Such load profiles are adopted as an approximate estimative of the load values and are based mainly on consumer stratification and electricity monthly energy consumption. Although such profiles provide only a rough approximation of the real load values, in the absence of smart meters they are the only source of information

regarding the load values for the steady-state analysis. In the state estimation topic, such a technique is named load pseudo-measurement modeling.

Each consumer unit is associated with a typical load profile based on the consumer classification (e.g., residential, commercial, or industrial), the monthly energy consumption in kWh, the number of phases of the consumer, and a respective typical load profile [16, 39, 40]. The load profiles are associated with the consumer's stratification and consist of daily curves with each point being associated with a normalized mean active load value and the respective standard deviation throughout the instants of a day and can be given for every 10 minutes up to each hour or more, often separated between a day of the week or weekends. The energy consumption is measured each month for billing purposes, or may be used previous day smart meter information, and is the typical choice as the scale factor for the typical load profile. With such information, each phase of the consumer can be associated with an active load curve with (4.71). The reactive power can be estimated using typical power factors or similar information, if available.

$$p_c^i(t) = \frac{kWh_c^i}{\Delta t_k} p_\omega(t), c \in \omega \tag{4.71}$$

where $p_c^i(t)$ is the active load for each consumer c in the ith phase at each instant t, kWh_c^i and Δt_k are the respective energy consumption and measured time interval to be used as scaling factor, and $p_\omega(t)$ is the typical normalized load profile for the respective classification ω of the consumer unit among all possible classifications Ω (e.g., residential, commercial, or industrial).

Typically, such pseudo-measurements provide information for achieving observability at the medium-voltage primary feeders, that is, they provide enough information to reach the minimum in order to perform the state estimation process in the primary feeder, in a complementary manner. Although they are associated with the consumer units at low-voltage secondary systems, they are often represented in the primary feeders, for medium-voltage system analysis. The loads within a secondary low-voltage system are aggregated at the respective power transformer that supplies energy from the primary feeder. The pseudo-measurement load consists of the expected value for the active load in each transformer k that connects the primary feeder to the secondary circuits ($E[P_k^i(t)]$), and the respective variance ($Var[P_k^i(t)]$), obtained by the aggregation process [16, 39]. It can be calculated by (4.72) and (4.73).

$$E[P_k^i(t)] = E\left[\sum_{c \in \mathfrak{S}_k} p_c^i(t)\right] = \sum_{\omega \in \Omega}\left(\sum_{\substack{c \in \mathfrak{S}_k \\ c \in \omega}} \frac{kWh_c^i}{\Delta t_c}\right) E[p_\omega(t)] \tag{4.72}$$

$$Var[P_k^i(t)] = Var\left[\sum_{c \in \mathfrak{S}_k} p_c^i(t)\right] = \sum_{\omega \in \Omega}\left(\sum_{\substack{c \in \mathfrak{S}_k \\ c \in \omega}} \frac{kWh_c^i}{\Delta t_c}\right)^2 Var[p_\omega(t)] \tag{4.73}$$

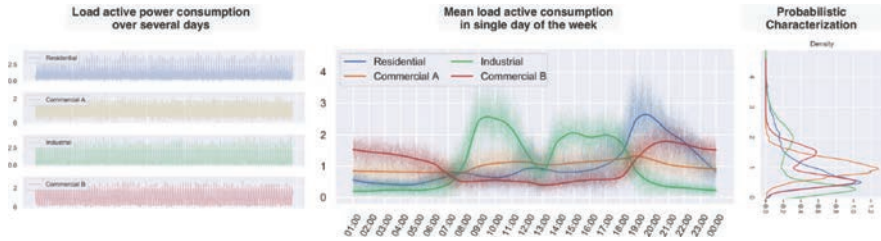

Figure 4.9 Example of typical load curves and stratification of consumers to characterize distribution system loads

where $\mathfrak{S}_k$ is the set of consumer units c connected to the secondary circuits of transformer k, in each ith phase. The expected value and variance, $E[p_\omega(t)]$ and $Var[p_\omega(t)]$, for each class of consumers are obtained by the typical load profiles associated with the respective class. Figure 4.9 illustrates the idea of typical load profiles and how they represent the normalized mean value of different consumers pertaining to the same class. The pseudo-measurement model tries to capture this typical behavior of the load over a day. By performing the load aggregation, multiple consumers have their loads aggregated at the transformer that feeds their respective secondary circuits. The probabilistic interpretation associated with the typical load profiles can also provide additional information for more detailed methods [16, 40, 41].

4.3.5 Shunt capacitors and reactors

A shunt capacitor is a type of equipment that offers reactive support for the grid, improving voltage quality aspects. It can be installed as a fixed or as a variable capacitor bank. The variable capacitor bank which consists of a group of capacitors and a local controller is able to modify the total capacitance of the group by turning *on* or *off* capacitor unities [2, 33]. Since the shunt capacitor is directly connected to one node, it can be modeled as a single port:

$$\dot{I}_k = Y_{kk}\dot{V}_k \tag{4.74}$$

The admittance matrix depends upon the type of connection of the shunt capacitor, which may be a wye, a wye-grounded, a delta, or even a single-phase connection. For three-phase modeling, the structure of the admittance matrix is given in (4.75), considering the matrix Y_I for wye-grounded connection, Y_{II} for wye connection, and Y_{III} for delta connection, respectively. For single-phase capacitors, they are modeled directly on the respective connected phase.

$$Y_I = jb_c^{sh}\begin{pmatrix}1&0&0\\0&1&0\\0&0&1\end{pmatrix};\quad Y_{II} = j\frac{b_c^{sh}}{3}\begin{pmatrix}2&-1&-1\\-1&2&-1\\-1&-1&2\end{pmatrix};\ Y_{III} = j\frac{b_c^{sh}}{\sqrt{3}}\begin{pmatrix}-1&1&0\\0&-1&1\\1&0&-1\end{pmatrix} \tag{4.75}$$

The capacitor's susceptance b_c^{sh} is obtained from the nominal parameters, following:

$$b_c^{sh} = \frac{MVAr_{nom}}{kV_{nom}^2} \tag{4.76}$$

where $MVAr_{nom}$ is the nominal reactive power of the capacitor in *MVAr* and kV_{nom} is the capacitor nominal voltage in kV.

The control strategy of capacitor banks comprises one of the following aspects/approaches:

- **Voltage control:** This approach uses bandwidth to control the voltage level to a setpoint value by switching *on* or *off* capacitors to increase or decrease the nodal voltage.
- **Power factor control:** this approach measures the power factor of a specific point in the network and is able to turn *on* or *off* capacitors according to the pre-specified power factor setpoint.
- **Time control:** the simplest control strategy, in which the capacitor bank is switched *on* or *off* according to specified instants of the day, for example, turn capacitors *on* during peak load periods.

Other types of shunt equipment are reactors and grounding resistances, often used in grounding systems of distribution networks. Equation (4.77) expresses the relation between the voltage and current phasor of the neutral-to-ground variables:

$$\dot{I}_k^n = Y_k^{nn} \dot{V}_k^n \tag{4.77}$$

where the superscript n denotes the neutral-to-ground variables and parameters at node k. For a shunt reactor, the parameter Y_k^{nn} is equal to $1/jX_{grounding}$, and it is equal to $1/R_{grounding}$ for resistance. Box 4.3 presents an example of a radial distribution feeder to illustrate the shunt capacitors and voltage regulators models.

4.3.6 Distributed generation

The nature of distribution systems is being modified from a passive to an active network due to the growth of DG. Some positive impacts may include reduced power flow and, therefore, decreased losses and voltage drop; however, some negative impacts such as voltage fluctuation, voltage rise, reverse power flows, and power factor alterations may occur if DG operation is not properly oriented [42]. Consequently, several studies have emerged, aiming to properly represent the DG presence in power system analysis to support expansion and operation planning.

The energy injected into the distribution system may be generated through distinct technologies [43]:

- *Electric machine directly connected to the grid*: the electric machine is usually a synchronous one, and the generated energy is connected to the grid directly. This technology is usually related to internal combustion engines and gas turbines.
- *Electric machine with a power electronics interface*: the electric energy produced by the electric machines needs to be converted to grid compatible

Box 4.3 Example of the IEEE123 nodes test feeder

The 123 nodes test feeder contains voltage regulators and single- and three-phase shunt capacitors. Since the three-phase shunt capacitor, $b_c^{sh} = \frac{0.2}{4.16^2}$, is connected via a wye-grounded connection, the matrix Y_I is used. The resulting Y_{kk} is:

$$Y_{kk} = j\begin{pmatrix} 0.0115 & 0 & 0 \\ 0 & 0.0115 & 0 \\ 0 & 0 & 0.0115 \end{pmatrix} \tag{4.78}$$

In turn, the voltage regulator can be modeled similarly to the transformers with the addition of *taps* for each phase. These taps are either known from the system's model or calculated by the LDC technique.

The LDC technique can be applied in the 123 nodes test feeder since there are single-, two-, and three-phase regulators. Specifically for the three-phase regulator, its current transformer and voltage transformer ratios are 300 and 20, respectively. The voltage setpoint is 124 V for each phase and the voltage bandwidth is 2 V. Resistance and reactance values are different for each phase; therefore, the parameters α^a, α^b, and α^c must be calculated separately.

With the three tap positioned at step 7, the transformer relation parameter α^i is:

$$\alpha^i = 1 + 7 * 0.1/16 = 1.0437 \quad i \in \{a, b, c, \dots\} \tag{4.79}$$

It is common to represent the voltage regulator as an ideal transformer, disregarding its series resistance and considering a very small reactance value, such as 0.0001 p.u. With these considerations, the two-port model is:

$$Y_{km}, Y_{mk} = -\begin{pmatrix} j9548.362 & 0 & 0 \\ 0 & j9548.362 & 0 \\ 0 & 0 & j9548.362 \end{pmatrix} \tag{4.80}$$

$$Y_{mm} = \begin{pmatrix} j9180.125 & 0 & 0 \\ 0 & j9180.125 & 0 \\ 0 & 0 & j9180.125 \end{pmatrix} \tag{4.81}$$

A single increase in the tap position would yield a transformer relation parameter of $\alpha^i = 1.05$, changing the matrices Y_{km}, Y_{mk}, and Y_{mm}. Since Y_{kk} does not vary with the transformer relation, it is the same for all tap positions and it is equal to:

(Continues)

$$Y_{kk} = \begin{pmatrix} j10000 & 0 & 0 \\ 0 & j10000 & 0 \\ 0 & 0 & j10000 \end{pmatrix} \tag{4.82}$$

The 123 nodes test feeder presents a unique model for steady-state analysis of distribution systems since it contains, in addition to the voltage regulators and shunt capacitors, two-phase and single-phase branches. The resulting Z^{abc} matrix has zeros on the missing phases and this reflects in different parameters in the two-port model when compared to full three-phase branches.

energy via power electronic converters. It is the case for wind turbines and micro-turbines.

- *Power electronics*: this is the case for fuel cells and photovoltaic (PV) systems. Fuel cells convert stored chemical energy directly into electric and thermal energy, while PV systems convert solar energy into electric and thermal energy. The DC energy output of these generators has to be converted to AC grid compatible energy via power electronics.

It is a common practice in steady-state studies to define DG as a constant injected complex power or as a constant injected active power with controlled voltage [43]. Hung *et al*. [44] propose four distinct classifications/types for the DG operation based on its active and reactive power generation characteristics: (i) DG capable of injecting active power only; (ii) DG capable of injecting reactive power only; (iii) DG capable of injecting active and reactive power; and (iv) DG injects active but consumes reactive power. However, some power system analyses may require a more detailed representation of the generation unit; therefore, while the simplistic approach is generally suitable for balanced electrical systems, it may lead to errors when dealing with electrical machines in unbalanced systems due to their electromechanical behavior.

When dealing with intermittent energy sources, such as wind and solar energy, the power electronics interface between the generation unit and the power grid plays a pivotal role in the generation unit's effectiveness. It is responsible for controlling the generated power while attending to the power systems requirements.

In the PV generation, the power electronics interface is responsible for converting the DC-generated power to a suitable AC power for the power grid. The distinct inverter topologies used for PV conversion may be classified by distinct characteristics, such as standalone or on-grid operation, the presence of galvanic isolation, the number of power processing stages, the presence or absence of transformer, the employed electronic topology of the power inverter(s), and the control strategy [45].

The stand-alone unit operates off the power grid and is used to supply power to small areas. It is usually composed of the PV modules, DC/DC and DC/AC inverters, controllers, and a storage system, which is often used to store the excess

generated power during the peak hours of production to be dispatched later. On the other hand, on-grid PV units do not require a storage system while maintaining all other components [45].

When a single-stage inverter is applied, it is directly responsible for the DC/AC conversion and injection of the generated power in the system; therefore, it is also in charge of the control of the injected currents, voltage amplification, and the maximum power point tracking (MPPT); whereas in a multi-stage inverter two or more inverters are present, in which the last one is responsible for the last AC conversion, while the first and intermediate ones usually amplify the generated voltage and sometimes create galvanic isolation [45]. As pointed out in [46], multi-stage inverters are mostly used, mainly two-stage power conversion topologies, in which the first inverter is a DC/AC/DC or DC/DC stage, used to amplify the generated voltage, and the second one is DC/AC conversion for power injection in the network.

When it comes to the electronic topology of the inverters and their controls, several strategies have been developed over the years. Some are the half-bridge diode-clamped inverters, full-bridge single-leg-clamped inverters, and cascaded inverters. These may also be classified according to their soft or hard switching inverters, while the soft switching ones have been preferred to achieve better performance [45].

The inverter helps to control the power factor and to ensure that the sinusoidal injected current attends safety requirements of the grid; therefore, it is a critical component in a PV generation unit. This control system is usually divided into two groups: (i) maximum power point control module, which searches for the PV operational point with maximum power output; and (ii) inverter control modules, which provide enough quality of the injected power by guaranteeing proper synchronization with the power grid, controlling the injected active and reactive power into the grid and the voltage of the DC-link [45]. Several methodologies have been proposed to offer efficient control of PV inverters, which goes from the classical control approaches, such as linear controllers with proportional/integral/derivative schemes, to nonlinear, robust, adaptive, predictive, and intelligent ones [45].

Like load models, it is often common to represent the temporal behavior of the DG for steady-state analysis and state estimation applications, especially in the case of renewable resources like wind and solar. This temporal behavior is much the same as the load profiles and has a strong relation to environmental characteristics such as temperature, solar irradiance, and wind speed. This complementary information provides the available input energy for the distributed generator models. It will define the maximum output of active and reactive power to be injected into the grid at each instant. Figure 4.10 illustrates a typical monthly temporal behavior of active power injection from a PV and from a wind turbine distributed generator. The dependency on environmental characteristics is the main source of variability of such types of resources.

This large variability consists of the intermittent characteristic of renewable DG, which translates itself into fast and abrupt variations in the output power due to these environmental changes. Typically, a stochastic random component is added to the generation profile to assess the effects of steady-state analysis [47]. It typically

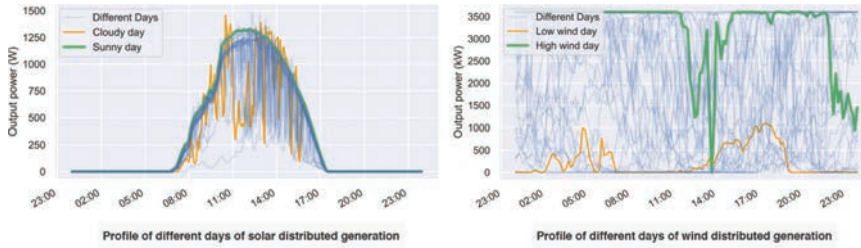

Figure 4.10 Active power injection profiles of one month of generation from renewable resources (solar and wind)

induces a larger variability in the power injection of the distribution system nodes to capture the intermittent behavior of renewable resources.

4.3.7 Energy storage

The advent of DG with high intermittency levels, especially from renewable resources, has driven a parallel effort for the inclusion of energy storage equipment in the distribution networks. Different energy storage technologies may be included in the power grid to provide such flexibility and ancillary systems. They can be classified as follows: (1) *electrical* (such as supercapacitors and superconducting magnetic storage); (2) *mechanical* (such as pumped hydroelectric, compressed air, and flywheel storage); (3) *electrochemical* (such as different types of batteries); (4) *chemical* (such as hydrogen and synthetic natural gas); and (5) *thermal* (such as water tanks and molten salts) [48].

The BESSs are often based on lithium-ion batteries connected to the grid with power electronic converters [49]. Other prospective technologies comprise advanced lead-acid, sodium-sulfur, and vanadium flow batteries. Regarding the batteries, the main characteristics for developing their models are total capacity, charge/discharge rates, internal voltage, open circuit resistance, and the number of associated batteries (in series, to increase voltage, or on parallel to increase current). The power electronic converters are also crucial components of the storage systems, which may include a DC/DC converter, DC/AC converter, and also sometimes another step of an AC/AC converter. They provide a high level of flexibility, and control for the charging and discharging process, and also enable advanced features like voltage support, harmonic compensation, and frequency regulation [48]. Figure 4.11 illustrates the main components of a typical BESS, where an array of batteries is associated with a two-level of interfacing converters. Detailed models for the BESS may even include the transitory polarization resistance and capacitance in parallel for the batteries.

The main characteristic to evaluate the operating point of a BESS is to accurately calculate the state of charge (SOC), defined as the ratio between the available amount of charge and the maximum charge of the batteries. This fundamental definition is often not practical and motivated distinct SOC estimation methods, ranging among lookup tables, dynamic parametric models, recursive filters, and, more

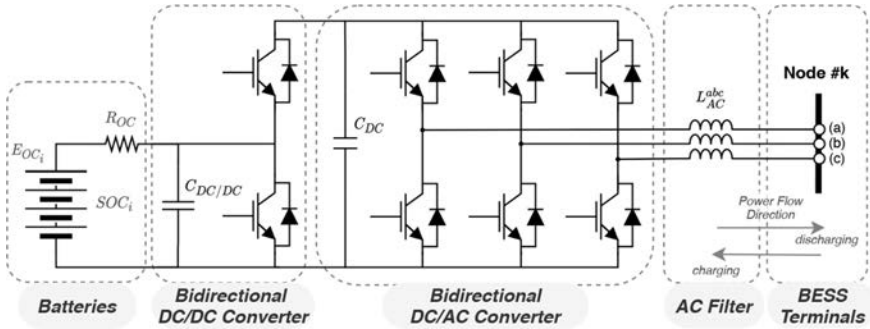

Figure 4.11 Detailed diagram of a battery energy storage system (BESS) and main components: battery association, DC/DC converter, DC/AC converter, AC filter, and AC terminals

recently, data-driven methods based on artificial intelligence [50, 51]. One approach relies on the *Coulomb Counting method*, which is based on the continuous monitoring of the BESS current and estimating the SOC from known initial conditions.

$$SOC(t) = SOC_0(t_0) - \frac{\eta}{C_n}\int_{t_0}^{t} I(t)dt \tag{4.83}$$

where $SOC_0(t_0)$ is the initial condition for the SOC, C_n is the total capacity, η is the Coulombic efficiency, and $I(t)$ is the instantaneous discharge current. Another method employs a detailed model of the BESS in order to estimate the internal voltage of the batteries accurately, and hence estimate the SOC through nonlinear functions depending on the type of batteries and parameters [50, 51].

$$SOC(t) = f(E_{OC}, R_{OC}, R_p, C_p) \tag{4.84}$$

where E_{OC} is the internal open-circuit voltage of the battery, R_{OC} is the open circuit resistance, and R_p and C_p are the polarization resistance and capacitance. Such methods provide an accurate assessment of the total energy available in the storage systems, thus enabling the evaluation of possible increments of power injected into the grid. Otherwise, if in a low SOC condition, it provides an estimate of the necessity of charging them, an increment on the load of the distribution system.

From a distribution network perspective, the BESS can operate in steady state as loads when charging, or injecting active (and reactive) power as a DG when discharging. The total amount of power is constrained by the SOC, the total capacity of the BESS, and the maximum charge/discharge rates. The control strategy of the BESS is also an influential factor since it can be optimized according to different strategies, based on market behavior, operation requirements, or specific strategies to aid power quality. Depending upon the level of analysis, these advanced controllers may be included or even use high-resolution models of distribution networks. For instance, Ref. [52], presents an optimized operation of BESS with other different energy resources to compensate for power quality issues on the grid while minimizing costs. Typically, at this level of control strategy, the response time falls within

steady-state methods and it is very common to associate this type of control strategy with high-resolution steady-state models of the distribution network.

4.3.8 Electric vehicles

The trend for seeking more renewable distributed energy resources is entangled within a larger social movement, going away from fossil-fuel dependency and toward more electrified systems in general. It culminated in a new thrust for the electric transportation systems, especially with electric vehicles, and that has significant impacts on the distribution systems as new kinds of special loads. It has only been possible due to the recent advances in energy storage technologies, especially lithium-ion batteries, that enabled the commercial manufacturing of plug-in electric vehicles (PEV). The adoption of such PEVs will increase the diversity of electrical loads and the total amount of power required from distribution networks. In this sense, the introduction of charging technologies as new equipment in the distribution system can change the load profiles dramatically.

Detailed models include the same level of resolution as previously presented for BESS. Thus, the SOC plays a key role in the model and acts as the primary constraint to be considered [50]. Different PEVs manufacturers may also present particularities regarding the battery technology employed that should be included in the model [53]. From a distribution system perspective, the interface with the PEVs is done by the charging stations. The charging station is in essence a power electronic converter, based on different levels of AC/DC and DC/DC converters. The converters can either be connected to low-voltage systems (for domestic cases) or also with medium-voltage connections (for multi-level converters). They can be installed on-board, that is, inside the PEVs, or off-board, as outside infrastructure reducing the weight of the PEV. Regarding charging rates, the stations can be separated into Level 1 (slow charge in the order of several hours), Level 2 (semi-fast chargers with a few hours), and Level 3 (fast chargers within minutes) [54].

Another important aspect comprises the control strategies of multiple charging stations, which may be separate in uncoordinated and coordinated [53]. For the uncoordinated strategy, PEVs charge independently with fixed charging rates defined by standards for domestic and commercial charging stations. For coordinated charging, they can be divided into optimized charging and the vehicle-to-grid (V2G) strategies. In optimized charging, the time and power of charging stations are defined by optimizing an objective function (typically costs) and considering the technical constraints of the distribution systems. In V2G charging strategies, besides the scheduling of charging stations, it also comprises optimization of discharging the batteries from the vehicles in order to provide grid support.

Regarding the model of these new loads, different approaches can be applied in order to perform a steady-state analysis of the distribution networks. They can be separated into deterministic, probabilistic, artificial intelligence, and dynamic [53, 55, 56]. Deterministic approaches consider the charging station loads as known values and are often derived in scenario-based analysis. Probabilistic approaches capture the stochastic nature of the charging process, often including exogenous

variables to capture features of the traveling times. Artificial intelligence is based on exploiting large data sets and building associative models to mimic past learned behavior. Finally, dynamic models include temporal relations in order to track changes in the PEVs' behavior along with exogenous variables. Besides their conceptual differences, such methods often incorporate similar new features to increment PEV model resolution and to properly assess their impacts on the grid, which often comprise:

- departure, arrival, and traveling times from a typical PEV. These type of variables are included in the model to relate the usage of the PEVs and their respective SOC, indicating if charging is needed, or even inducing injecting power in the grid in a controlled manner.
- the total capacity of the PEV according to manufacturer specifications, like battery technology, rated capacity, efficiency, and mechanical conversion relations.
- the charging station features, especially the rate of charge, efficiency, control strategies, and the possibility to inject power into the grid.
- the total fleet of electric vehicles and the location of off-board charging stations in the distribution system.

In this sense, PEVs change the traditional load models sensibly, and due to particular aspects of such equipment, they have a large effect on the operation of distribution systems, especially in the context of modern active low-voltage distribution networks.

4.3.9 Static compensators (D-FACTS)

Static compensators have been used in power systems to supplement controllability and power transfer in the network. They are based on power electronics to control power system variables, such as power flows and voltages magnitudes.

The static compensators were referred to as flexible alternation current transmission systems (FACTS) since their application occurred in transmission systems. However, due to the increasing complexity of the distribution system, these technologies started to be applied in distribution networks as well to support stability, control, and security [57]. The distributed FACTS (D-FACTS) aim to minimize the cost of regular FACTS devices by distributing small power electronics components in the distribution system [58].

To represent these devices in power system analysis, several models have been proposed. According to the working principle of the controller, it may have distinct state variables and, therefore, distinct equivalent representations, which may be summarized as [58, 59]:

- Variable reactance static compensators: often referred to as the first generation of static controllers, these are based on the application of thyristors connected to capacitor and reactor banks. Through this connection, the static compensator may electronically change its equivalent reactance to capacitive or inductive

values, and, therefore, it absorbs or generates reactive power. In steady-state power flow analysis, these compensators are often represented as a variable reactance connected in series or shunt to the system. Some of these compensators are the static VAR compensator (SVC) and the thyristor-controlled series compensator (TCSC).

- Solid-state voltage generator static compensators: commonly referred to as the second generation of static controllers, these emerged with the usage of gate turn-off thyristors, which enabled the application of solid-state voltage sources in the power systems. Therefore, in steady-state analysis, these components are often represented as a voltage source with its intrinsic impedance connected in series or shunt to the power system. Some of these controllers are the static synchronous compensator (STATCOM), synchronous series compensator (SSSC), and the universal power flow controller (UPFC).

The process for modeling the SVC, TCSC, STATCOM, and UPFC controllers in the steady-state analysis may be found in [59], as summarized in the following.

For the static VAR compensator, Ref. [59], presents a model in which the SVC is represented through an equivalent reactor bank connected in delta to the connection point of the system. Each equivalent susceptance may have its individual value adjusted according to the stipulated power restrictions of the operation. Also, when including this equipment in the power system model, it is possible to choose as state variables the controllable susceptances or the firing angles of the thyristors. It is also presented the power injection contribution of this equipment as a function of the controlled susceptances, and the controlled power system parameter is the nodal voltage magnitude of the bus to which the equipment is connected to.

The three-phase TCSC model presented in Ref. [59] comprises three independent variable susceptances connected in series to the controlled line that have no mutual coupling between themselves. Just like for the SVC, the authors present two distinct modeling possibilities, one considering the controllable susceptances as state variables and another with the firing angles of the thyristors as state variables. Just like for the SVCs, the authors present the power injection contributions of the TCSC as a function of the controlled susceptances, and, for the TCSC, the controlled power system parameter is the active power flow in the line.

Furthermore, the three-phase STATCOM is represented through three independent voltage sources, each with its own impedance and without the presence of mutual coupling, shunt-connected to each phase of the controlled bus. The state variables are defined as the voltage magnitude and angle for each voltage source. Also, the power injection contribution of the STATCOM is presented as a function of its state variables, and the equipment controls the voltage magnitude at its connection point [59].

Moreover, the three-phase UPFC is two three-phase voltage sources: a shunt- and a series-connected voltage sources, each with its intrinsic impedance and without mutual coupling. The state variables are the voltage magnitude and angle of both voltage sources. They control the voltage magnitude of the bus connected to the shunt-voltage source and the active and reactive power flow of the line connected

with the series-voltage source. The model comprises also an active power constraint for shunt and series voltage sources, representing a zero exchanged net active power for such devices. As with the other devices, it is also presented the influence of the controlled state variables on the active and reactive power injections of the buses connected to the UPFC [59].

Finally, Box 4.4 presents the description of the typical distribution systems available in the literature, widely adopted for testing new methods and equipment, and assessing distribution feeder conditions.

4.4 Concluding remarks

Power system computational analysis is essential for operating and planning electrical distribution networks. In their essence, distribution systems are unbalanced and asymmetrical electrical networks, spread across large areas connecting a diverse set of components with final consumers. The challenges associated with suitable distribution systems modeling, add complexity to any analysis performed. It includes the increase of variables that three-phase representation carries and also encompasses detailed component representation. From the perspective of distribution system state estimation, the challenges rely on accurate network models capable of dealing with measurements and information from all different elements of the distribution systems to translate into adherent models that capture the reality of such systems.

This chapter presented the fundamental equations to perform steady-state analysis in distribution networks based on the power flow of the network. The model comprises a three-phase generic representation of different components and the main electrical quantities of such models, as active and reactive power flows and voltage and current phasors. A two-port admittance model facilitates the implementation of the steady-state models of the distribution system components, under a matrix implementation.

The traditional components, as well as the modern technologies from the smart grid concept, are briefly discussed under a steady-state distribution system analysis perspective. The main components of substations, primary feeders, and secondary low-voltage circuits are also presented, such as power transformers, distribution circuits, shunt capacitors, and loads. Moreover, this chapter addresses the key features of modern distribution systems associated with distributed energy, energy storage, electric vehicles, and flexible power converters. Details of both the two-port models are shown, and important aspects regarding controllers and probabilistic behavior were also discussed.

All these aspects, if adequately addressed within the network models, can increase awareness of the system, providing accurate information for all components in distribution systems. It is a crucial feature for state estimators to act more actively in the operation of the modern distribution systems. It enables moving toward identifying abnormal behavior in each component at a per-phase level. It can also lead to extrapolations of controller conditions and advanced equipment in the network, assessing flexibility to accommodate unexpected risks.

Box 4.4 The IEEE test feeders

Different test feeders provide different analytic challenges for researchers. These feeders model different equipment, network topology while feeder was designed with a specific challenge to be studied and their descriptions are:

- **IEEE 4 nodes:** small feeder for testing the representation of different three-phase transformers connections, three-phase-coupled circuits as well as unbalanced loads.
- **IEEE 13 nodes:** aims to test the convergence for a very unbalanced feeder, it contains a single-voltage regulator and shunt capacitors. The feeder operates at 4.16 kV.
- **IEEE 34 nodes:** based on an actual feeder operating at 24.9 kV, it requires the modeling of voltage regulators, shunt capacitors, and unbalanced loads.
- **IEEE 37 nodes:** contains three-wire delta underground electrical lines operating at 4.16 kV. This test feeder is based on an actual feeder and it represents a common configuration for distribution networks.
- **IEEE 123 nodes:** these feeders operate at 4.16 kV and, because of voltage drop problems, it requires the modeling of voltage regulators and shunt capacitors. This feeder is supposed to present minimal convergence problems.
- **IEEE US low voltage:** although it is not an actual feeder, it represents low-voltage networks in urban centers. This system presents a different topology from common radial feeders since it contains multiple feeders, a highly meshed network, and parallel lines as well as transformers.
- **IEEE European low voltage:** this feeder represents a European network with radial and meshed low-voltage systems. It contains unbalanced low-voltage feeders and the dataset also contains time-series simulations.
- **IEEE neutral-earth-voltage:** requires a more detailed model of equipment since it requires the modeling of connections to earth. It is based on an actual feeder.
- **IEEE 8500 nodes:** large-scale system, unbalanced. Represents a full-scale distribution system and requires the modeling of a center-tap transformer.

These feeders have been developed by the Test Feeder Working Group, a part of the IEEE Distribution System Analysis Subcommittee, and are openly available at https://site.ieee.org/pes-testfeeders/resources/. Other models are also

(Continues)

available, such as the EPRI test circuits which contain small, medium, and large systems and the UKGDS test system, which represents a generic distribution system network in the UK grid.

The next chapters present the main methods to perform steady-state analysis and real-time state estimation in distribution systems. All these methods will essentially rely on the presented distribution network electrical models, in the form of the measurement model or to represent power flow equations. More details may be included in all the presented models, and the reader is referred to the specific literature on each type of equipment.

References

[1] Hansen C.W., Debs A.S. 'Power system state estimation using three-phase models'. *IEEE Transactions on Power Systems*. 1995, vol. 10(2), pp. 818–24.
[2] Kersting W.H. *Distribution System Modeling and Analysis*. 3rd edition. Boca Raton, FL: CRC Press; 2002.
[3] Spitsa V., Salcedo R., Xuanchang R., Juan F.M. 'Three–phase time–domain simulation of very large distribution networks'. *IEEE Transactions on Power Delivery*. 2012, vol. 27, pp. 677–87.
[4] Marques L.T., Delbem A.C.B., London J.B.A. 'Service restoration with prioritization of customers and switches and determination of switching sequence'. *IEEE Transactions on Smart Grid*. 2018, vol. 9(3), pp. 2359–70.
[5] Vahidinasab V., Tabarzadi M., Arasteh H., *et al.* 'Overview of electric energy distribution networks expansion planning'. *IEEE Access*. 2020, vol. 8, pp. 34750–69.
[6] De Oliveira-De Jesus P.M., Henggeler Antunes C. 'A detailed network model for distribution systems with high penetration of renewable generation sources'. *Electric Power Systems Research*. 2018, vol. 161(3), pp. 152–66.
[7] Abur A., Expósito A.G. *Power System State Estimation: Theory and Implementation*. New York: CRC Press; 2004.
[8] Primadianto A., Lu C.-N. 'A review on distribution system state estimation'. *IEEE Transactions on Power Systems*. 2017, vol. 32(5), pp. 3875–83.
[9] Zhao J., Qi J., Huang Z., Gomez-Exposito A. 'Power system dynamic state estimation: Motivations, definitions, methodologies, and future work'. *IEEE Transactions on Power Systems*. 2019, vol. 34(4), pp. 3188–98.
[10] Monticelli A. *State Estimation in Electric Power Systems: A Generalized Approach*. Massachussets-USA: Springer Science & Business Media; 1999.

[11] Ahmad F., Rasool A., Ozsoy E., Elitas M., Rajasekar S., Sabanovic A. 'Distribution system state estimation: a step towards smart grid'. *Renewable and Sustainable Energy Reviews*. 2017, vol. 81(Part 2), pp. 2659–71.

[12] venda G., Strezoski V., Kanjuh S. 'Real-Life distribution state estimation integrated in the distribution management system'. *International Transactions on Electrical Energy Systems*. 2017, vol. 27(5), pp. 1–16.

[13] Huang S.-C., Lu C.-N., Lo Y.-L. 'Evaluation of AMI and SCADA data synergy for distribution feeder modeling'. *IEEE Transactions on Smart Grid*. 2015, vol. 6(4), pp. 1639–47.

[14] Pau M., Pegoraro P.A., Sulis S. 'Efficient branch-current-based distribution system state estimation including synchronized measurements'. *IEEE Transactions on Instrumentation and Measurement*. 2013, vol. 62(9), pp. 2419–29.

[15] Lefebvre S., Prévost J., Lenoir L. 'Distribution state estimation: A necessary requirement for the smart grid'. *2014 IEEE PES General Meeting—Conference Exposition*; 2014. pp. 1–5.

[16] Massignan J.A.D., London J.B.A., Bessani M., *et al.* 'In-field validation of a real-time monitoring tool for distribution feeders'. *IEEE Transactions on Power Delivery*. 2018, vol. 33(4), pp. 1798–808.

[17] Sallam A.A., Malik O.P.. ' 'IEEE press series on power engineering''. *Electric Distribution Systems*. Hoboken - New Jersey - U.S.: Wiley-IEEE Press; 2018.

[18] Zhao J., Netto M., Huang Z. 'Roles of dynamic state estimation in power system modeling, monitoring and operation'. *IEEE Transactions on Power Systems*. 2020, vol. 36, pp. 2462–72.

[19] Hebling G.M., Massignan J.A.D., London Junior J.B.A., Camillo M.H.M. 'Sparse and numerically stable implementation of a distribution system state estimation based on multifrontal QR factorization'. *Electric Power Systems Research*. 2020, vol. 189(5), p. 106734.

[20] Arrillaga J., Harker B.J. 'Fast-decoupled three-phase load flow'. *Proceedings of the Institution of Electrical Engineers*. 1978, vol. 125(8), pp. 734–40.

[21] Zhu J., Abur A. 'Effect of phasor measurements on the choice of reference bus for state estimation'. *IEEE Power Engineering Society General Meeting*; Tampa - Florida - US, 24 - 28 june; 2007. pp. 1–5 pp..

[22] Korres G.N., Manousakis N.M. 'State estimation and observability analysis for phasor measurement unit measured systems'. *IET Generation, Transmission & Distribution*. 2012, vol. 6(9), pp. 902–13.

[23] De Almeida M.C., Ochoa L.F. 'An improved three-phase AMB distribution system state estimator'. *IEEE Transactions on Power Systems*. 2017, vol. 32(2), pp. 1463–73.

[24] Kagan N. *Introdução aos sistemas de distribuição de energia elétrica*. São Paulo - Brazil: Editora Edgard Blücher; 2008.

[25] Kersting W. 'A three-phase unbalanced line model with grounded neutrals through a resistance'. *IEEE Power and Energy Society General Meeting*; Pittsburgh - PA - US, 20 - 24 July; 2008. pp. 1–2.

[26] Carson J.R. 'Wave propagation in overhead wires with ground return'. *Bell System Technical Journal*. 1926, vol. 5(4–539–554.

[27] Glover J.D., Sarma M.S., Overbye T. *Power System Analysis & Design, SI Version*. Boston - MA - US: Cengage Learning Engineering; 2011.

[28] Kron G. 'Tensorial analysis of integrated transmission systems Part I. The six basic reference frames'. *Transactions of the American Institute of Electrical Engineers*. 1951, vol. 70(2–1239–1248.

[29] Chen T.-H., Chen M.-S., Inoue T., Kotas P., Chebli E.A. 'Three-phase co-generator and transformer models for distribution system analysis'. *IEEE Transactions on Power Delivery*. 1991, vol. 6(4), pp. 1671–81.

[30] Xiao P., Yu D.C., Yan W. 'A unified three-phase transformer model for distribution load flow calculations'. *IEEE Transactions on Power Systems*. 2006, vol. 21(1), pp. 153–9.

[31] Chen T.-H., Chang J.-D. 'Open wye-open delta and open delta-open delta transformer models for rigorous distribution system analysis'. *IEE Proceedings C Generation, Transmission and Distribution*. 1992, vol. 139(3), pp. 227–34.

[32] Kersting W.H. 'Center-tapped transformer and 120-/240-V secondary models'. *IEEE Transactions on Industry Applications*. 2009, vol. 45(2), pp. 575–81.

[33] Cheng C.S., Shirmohammadi D. 'A three-phase power flow method for real-time distribution system analysis'. *IEEE Transactions on Power Systems*. 1995, vol. 10(2), pp. 671–9.

[34] Massignan J.A.D., Pereira B.R., London J.B.A. 'Load flow calculation with voltage regulators bidirectional mode and distributed generation'. *IEEE Transactions on Power Systems*. 2016, vol. 32(2), pp. 1576–7.

[35] Agalgaonkar Y.P., Pal B.C., Jabr R.A. 'Distribution voltage control considering the impact of PV generation on TAP Changers and autonomous regulators'. *IEEE Transactions on Power Systems*. 2014, vol. 29(1), pp. 182–92.

[36] Nanchian S., Majumdar A., Pal B.C. 'Three-phase state estimation using hybrid particle Swarm optimization'. *IEEE Transactions on Smart Grid*. 2015, vol. 8(3), pp. 1035–45.

[37] Kundur P. *Power system stability and control*. McGraw Hill; 1994. pp. 272–4.

[38] Milanovic J.V., Yamashita K., Martínez Villanueva S., Djokic S.Z., Korunovic L.M. 'International industry practice on power system load modeling'. *IEEE Transactions on Power Systems*. 2013, vol. 28(3), pp. 3038–46.

[39] Jardini J.A., Tahan C.M.V., Gouvea M.R., Ahn S.U., Figueiredo F.M. 'Daily load profiles for residential, commercial and industrial low voltage consumers'. *IEEE Transactions on Power Delivery*. 2000, vol. 15(1), pp. 375–80.

[40] Ghosh A.K., Lubkeman D.L., Jones R.H. 'Load modeling for distribution circuit state estimation'. *IEEE Transactions on Power Delivery*. 1997, vol. 12(2), pp. 999–1005.

[41] Singh R., Pal B.C., Jabr R.A. 'Statistical representation of distribution system loads using Gaussian mixture model'. *IEEE Transactions on Power Systems*. 2010, vol. 25(1), pp. 29–37.

[42] Passey R., Spooner T., MacGill I., Watt M., Syngellakis K. 'The potential impacts of grid-connected distributed generation and how to address them: A review of technical and non-technical factors'. *Energy Policy*. 2011, vol. 39(10), pp. 6280–90.

[43] Moghaddas-Tafreshi S.M., Mashhour E. 'Distributed generation modeling for power flow studies and a three-phase unbalanced power flow solution for radial distribution systems considering distributed generation'. *Electric Power Systems Research*. 2009, vol. 79(4), pp. 680–6.

[44] Hung D.Q., Mithulananthan N., Bansal R.C. 'Analytical expressions for dG allocation in primary distribution networks'. *IEEE Transactions on Energy Conversion*. 2010, vol. 25(3), pp. 814–20.

[45] Zeb K., Uddin W., Khan M. A., *et al.* 'A comprehensive review on inverter topologies and control strategies for grid connected photovoltaic system'. *Renewable and Sustainable Energy Reviews*. 2018, vol. 94(1), pp. 1120–41.

[46] Scarabelot L.T., Rambo C.R., Rampinelli G.A. 'A relative power-based adaptive hybrid model for DC/AC average inverter efficiency of photovoltaics systems'. *Renewable and Sustainable Energy Reviews*. 2018, vol. 92(6), pp. 470–7.

[47] Soroudi A., Aien M., Ehsan M. 'A probabilistic modeling of photo voltaic modules and wind power generation impact on distribution networks'. *IEEE Systems Journal*. 2012, vol. 6(2), pp. 254–9.

[48] Chang L., Zhang W., Xu S., Spence K. 'Review on distributed energy storage systems for utility applications'. *CPSS Transactions on Power Electronics and Applications*. 2017, vol. 2(4), pp. 267–76.

[49] Stecca M., Ramirez Elizondo L., Batista Soeiro T., Bauer P., Palensky P. 'A comprehensive review of the integration of battery energy storage systems into distribution networks'. *IEEE Open Journal of the Industrial Electronics Society*. 2020, vol. 1, pp. 46–65.

[50] Xiong R., Cao J., Yu Q., He H., Sun F. 'Critical review on the battery state of charge estimation methods for electric vehicles'. *IEEE Access*. 2018, vol. 6, pp. 1832–43.

[51] How D.N.T., Hannan M.A., Hossain Lipu M.S., Ker P.J. 'State of charge estimation for Lithium-Ion batteries using model-based and data-driven methods: A review'. *IEEE Access*. 2019, vol. 7, pp. 136116–36.

[52] Agnoletto E.J., Silva de Castro D., Neves R.V.A., Quadros Machado R., Oliveira V.A. 'An optimal energy eanagement technique using the ε-constraint method for grid-tied and stand-alone battery-based microgrids'. *IEEE Access*. 2019, vol. 7, pp. 165928–42.

[53] Ahmadian A., Mohammadi-Ivatloo B., Elkamel A. 'A review on plug-in electric vehicles: Introduction, current status, and load modeling techniques'. *Journal of Modern Power Systems and Clean Energy*. 2020, vol. 8(3), pp. 412–25.

[54] Rubino L., Capasso C., Veneri O. 'Review on plug-in electric vehicle charging architectures integrated with distributed energy sources for sustainable mobility'. *Applied Energy*. 2017, vol. 207(1), ppTransformative Innovations for a Sustainable Future – Part II. 438–64. Transformative Innovations for a Sustainable Future – Part II.

[55] Fahmy S., Gupta R., Paolone M. 'Grid-aware distributed control of electric vehicle charging stations in active distribution grids'. *Electric Power Systems Research*. 2020, vol. 189(3), p. 106697.

[56] Rossetto B.M., LourenÃ M.E. 'Analysis of the impacts of the electrification of the vehicle fleet in the electric power system in Curitiba'. *Brazilian Archives of Biology and Technology*. 2018, vol. 00, p. 61.

[57] Bloemink J.M., Green T.C. 'Benefits of distribution-level power electronics for supporting distributed generation growth'. *IEEE Transactions on Power Delivery*. 2013, vol. 28(2), pp. 911–19.

[58] Gandoman F.H., Ahmadi A., Sharaf A.M., *et al.* 'Review of facts technologies and applications for power quality in smart grids with renewable energy systems'. *Renewable and Sustainable Energy Reviews*. 2018, vol. 82(10), pp. 502–14.

[59] Acha E., Fuerte-Esquivel C.R., Ambriz-Perez H., Angeles-Camacho C. *FACTS: Modelling and Simulation in Power Networks*. John Wiley & Sons; 2004.

Chapter 5

Current-based power flow calculation methods for distribution systems

Madson C. de Almeida[1], Antônio P. Feltrin[2], and Luís H. T. Bandória[1]

This chapter presents three current-based power flow calculation methods devoted to distribution systems, namely, the branch current-based load flow (BCBLF), the admittance matrix-based load flow (AMBLF) and the classical BFSLF. Due to similarities, the BCBLF and the AMBLF are presented simultaneously. The formulations presented are devoted to three-phase radial distribution systems; however, the AMBLF can be successfully applied to meshed distribution systems exactly as it is presented. After describing the basic theoretical aspects of the methods, detailed results based on small size distribution networks are presented and discussed.

5.1 Introduction

The load flow calculation in a power system consists in determining the state of the system. From that, quantities such as power flows, current flows, and power losses can be obtained. The values of the state variables describe the state of the system. These values change according to the operating conditions of the power system.

In the classical and well-established load flow calculation approach solved by the Newton–Raphson method (NRLF), the state variables are the system bus voltage magnitudes and angles [1–3]. Given that the specified quantities are power injections and voltage magnitudes, the equations relating state variables and specified quantities are nonlinear. As a result, the Jacobian matrix required by the NRLF needs to be updated at every iteration of the solution process [1–3]. Due to its robustness, this method is widely accepted and can be successfully applied to transmission and distribution systems [1, 2].

[1]University of Campinas, Campinas, São Paulo, Brazil
[2]Unesp, Ilha Solteira, São Paulo, Brazil

Despite all the good features of the classical NRLF, alternative load flow techniques can be found in the literature, not necessarily based on the Newton–Raphson iterative scheme, mainly to overcome the need of updating the Jacobian matrix of the NRLF at every iteration [3–7]. This is especially desired in the context of distribution systems, where the three-phase modelling of the networks is usually adopted [3, 8]. Compared to the single-phase modelling commonly adopted in transmission systems, the three-phase model increases the number of state variables by three and, consequently, increases the computational times.

The literature presents many load flow approaches using complex voltages and currents in rectangular form as state variables, while the specified quantities, i.e., power injections and voltage magnitudes, are converted, for instance, into complex currents and voltages. These alternative approaches aim to obtain linear equations relating the state variables and the converted specified quantities to yield a constant Jacobian matrix. Once the Jacobian matrix is constant, it needs to be built and factorised just once. In this case, the number of iterations required for the load flow convergence can slightly increase; however, the time spent in each iteration can significantly decrease, speeding up the load flow computational performance [2].

One of these current-based load flows was proposed by Dommel, Tinney and Powell [9]. It consists in modelling the specified active and reactive power injections of the load buses as current injections, while the active power injection and the voltage magnitudes from the generation buses are modelled in terms of active power mismatches and angle deviations. This modelling for the generation buses is often considered unsatisfactory [10]. Although many approaches available in the literature can be successfully applied to modelling generation buses in current-based power flows, none results in a constant Jacobian matrix when applied to distribution systems. Therefore, the well-known BFSLF [11] becomes very attractive once it does not require building a Jacobian matrix and can successfully cope with load and generation buses.

In this context, this chapter presents three current-based power flow calculation methods devoted to distribution systems: the BCBLF, the AMBLF, and the classical BFSLF. Due to their similarities, the BCBLF and AMBLF are presented simultaneously. Although these formulations are devoted to three-phase radial distribution systems, the AMBLF can be successfully applied to meshed distribution systems. When presenting the AMBLF and BCBLF, only the reference and load buses will be considered, resulting in constant Jacobian matrices. This makes both load flows very attractive from the computational point of view, despite limiting their applications.

5.2 Basics of the current-based three-phase power flow

The power flow solution in electric power networks refers to the calculation of the state variables from the network topology, system parameters and specified quantities. The typical solutions are based on the NRLF, where the specified quantities are written in terms of the state variables [1]. All state variables are simultaneously calculated, and a Jacobian matrix is required. As stated above, the AMBLF and BCBLF

can result in constant Jacobian matrices, whereas the Jacobian matrix of the NRLF needs to be updated every iteration.

In the BFSLF, the state variables are iteratively updated one at a time. For that, the branches of the network are considered one at a time. As a result, a Jacobian matrix is not required, speeding up the computational times. The main drawback of the BFSLF is related to the presence of meshes in the network [12]. Beyond that, this power flow requires the ordering of the buses and nodes of the distribution system from the substation to the terminal buses.

5.2.1 State variables

The state variables can be defined as a minimum set of variables that completely describes a system [13]. Thus, given the values of the state variables for a certain operating condition of a power system, all electrical quantities related to the system in that operating condition can be calculated from the equations that describe the system. In the NRLF and BFSLF methods, the state variables are the system bus voltage magnitudes and angles [1, 11]. The complex bus voltages are adopted in the AMBLF as state variables; however, they are used in rectangular coordinates, i.e., the real and imaginary parts of the complex bus voltages. In the BCBLF, the state variables are the complex currents flowing in the branches in rectangular coordinates, i.e., the real and imaginary parts of the branch currents. Furthermore, the phasor voltage at the substation, represented in rectangular coordinates, is also included as a state variable in the BCBLF.

Despite the set of state variables adopted, the number of state variables is the same. Considering a fully three-phase distribution system, the number of state variables is $6N_{buses}$, where N_{buses} is the number of three-phase buses on the systems.

5.2.2 Specified quantities and bus types

In power systems, the variables associated with every bus are voltage magnitudes, voltage angles, active power injections and reactive power injections. In power flow calculation, these variables are classified as specified quantities and quantities to be calculated. Based on the specified quantities, the buses of the system are, then, referred to as reference bus, load buses and generation buses.

To make the problem solvable, the number of specified quantities must be equal to the number of the quantities to be calculated. In three-phase systems, given that the three phases are present, each bus has 12 variables. According to the type of the buses, six variables are known (specified), and six variables need to be calculated. In the reference bus, the complex voltages for the three phases are specified. In load buses, the active and reactive power injections are specified for the three phases. In generation buses, the active power injections and the voltage magnitudes are specified for the three phases. Only one reference bus is required.

Depending on the adoption of control strategies, other types of buses can be considered; however, this is out of the scope of this chapter and only the three basic types will be considered.

5.2.3 Load modelling

The loads connected to the distribution systems mainly represent residential, commercial and industrial consumers. The loads are represented by the specified active powers, $P_k^{i,spe}$, and reactive powers, $Q_k^{i,spe}$. These powers can be constant or vary according to the bus voltages. The loads are usually represented by the exponential or polynomial (ZIP) models [14]. For the sake of simplicity, only the exponential model is presented here. The exponential model is described in (5.1) and (5.2). These load models can be used with all the load flow methods discussed in this chapter.

$$P_k^{i,spe} = P_k^{i,nom}\left(\frac{V_k^{i,\eta}}{V_k^{i,nom}}\right)^{\alpha_k^i} \quad i \in \{a,b,c\} \tag{5.1}$$

$$Q_k^{i,spe} = Q_k^{i,nom}\left(\frac{V_k^{i,\eta}}{V_k^{i,nom}}\right)^{\beta_k^i} \quad i \in \{a,b,c\} \tag{5.2}$$

In (5.1) and (5.2), $P_k^{i,nom}$ and $Q_k^{i,nom}$ are, respectively, the nominal values of the active and reactive powers of the loads on phase i of the bus k, $V_k^{i,nom}$ is the nominal voltage magnitude on phase i of the bus k and $V_k^{i,\eta}$ is the magnitude of the voltage on phase i of the bus k. As this voltage is unknown before the load flow calculation, it is updated every iteration η during the load flow process.

The constants α_k^i and β_k^i can assume values 0, 1 or 2 to represent, respectively, a constant power, a constant current or a constant impedance. However, in practice, loads are a combination of these behaviours, and these constants can assume different values [15]. For instance, Table 5.1 shows the typical values for these constants.

5.3 Branch current-based and admittance matrix-based load flows

Figure 5.1 shows an overview of the AMBLF and BCBLF. In these approaches, the specified quantities are converted into equivalent specified quantities and compose the vector $z(x^\eta)$. For that, the current values of the state variables, x^η, are required. Equations representing the equivalent specified quantities are derived and used to

Table 5.1 Representative parameters of typical consumers of distribution networks [15]

Consumer type	α	β
Residential	1.04	4.19
Commercial	1.50	3.15
Industrial	0.18	6.00

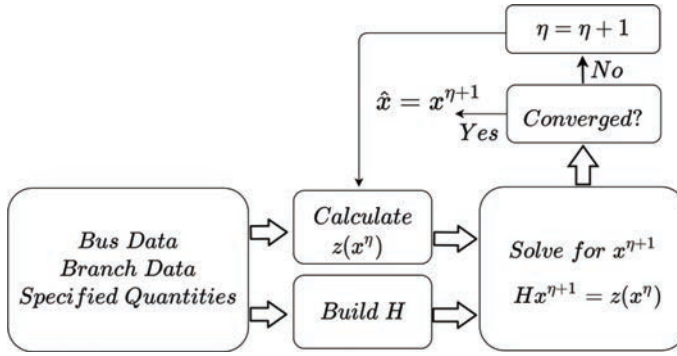

Figure 5.1 Overview of the AMBLF and BCBLF

build the Jacobian matrix H. The resulting Jacobian matrix is constant, therefore, it is built and factorised just once. This is possible due to the conversion of the specified quantities into equivalent specified quantities and the choice of the state variables. From H and $z(x^{\eta})$, the vector containing the state variables is calculated, giving rise to $x^{\eta+1}$. Then, the convergence is checked. If the convergence condition is met, the load flow solution is $\hat{x} = x^{\eta+1}$, otherwise, the iteration counter η is incremented, and a new iteration is run.

5.3.1 State variables

The AMBLF adopts the real and imaginary parts of the complex bus voltages as state variables [7, 16]. Therefore, the state vector for the AMBLF is given in (5.3). The variables $V^{i}_{re,k}$ and $V^{i}_{im,k}$ stand, respectively, for the real and imaginary parts of the complex voltages on three phases i of each bus of the distribution system. Assuming that the system has N_{buses} three-phase buses, the vector x has $6N_{buses}$ elements. The superscript T stands for transpose.

$$x = \left(V^{i}_{re,k} \quad V^{i}_{im,k}\right)^{T} \quad i \in \{a, b, c\} \quad k \in \{1, 2, ..., N_{buses}\} \tag{5.3}$$

The state variables adopted in the BCBLF are the real and imaginary parts of the complex voltages at the reference bus and the real and imaginary parts of the complex currents in the branches [17], as presented in (5.4). The variables $V^{i}_{re,r}$ and $V^{i}_{im,r}$ stand, respectively, for the real and imaginary parts of the complex voltages at three phases i of the reference bus r. The variables $I^{i}_{re,km}$ and $I^{i}_{im,km}$ stand, respectively, for the real and imaginary parts of the complex currents at three phases i of the branches of the distribution system. For the sake of simplicity, it is assumed that the distribution system is radial and, therefore, it has $N_{branches} = N_{busues} - 1$ three-phase branches. If the distribution system contains meshes, a set of $N_{branches} - 1$ branches forming a spanning three needs to be selected and their currents will be used as state variables [18]. Given that there is only one three-phase reference bus, the vector x has $6N_{buses}$ elements.

$$x = \left(V_{re,r}^{i} \quad I_{re,km}^{i} \quad V_{im,r}^{i} \quad I_{im,km}^{i} \right)^{T} \quad i \in \{a,b,c\} \quad km \in \{1,2,...,N_{branches}\} \tag{5.4}$$

Regardless if the state variables are the ones shown in (5.3) or (5.4), the number of state variables is six per bus, given that each bus or branch has three phases and two state variables per phase. In cases where there are single- and two-phase buses and branches, the concept of dummy lines and dummy nodes can be applied and, therefore, all buses can be treated as three-phase buses [19].

5.3.2 Bus types and equivalent specified quantities

As stated above, the specified quantities are given according to the bus types. In the AMBLF and BCBLF, the specified quantities are converted into equivalent specified quantities. As it is shown in this section, depending on the type of the bus, the resulting equivalent quantities need to be updated at every iteration of the solution process.

5.3.2.1 Load buses

Given the bus k is a load bus, the active power injections $P_k^{i,spe}$ and the reactive power injections $Q_k^{i,spe}$ are specified quantities for the three phases i of the N_{loads} load buses. In both load flow approaches, the AMBLF and BCBLF, these specified power injections need to be converted into current injections. In the AMBLF, this is done according to (5.5). Note that the equivalent specified quantities, $I_{re,k}^{i}$ and $I_{im,k}^{i}$, need to be updated at every iteration of the iterative process once they depend on the complex bus voltage, $\dot{V}_k^{i,\eta}$, which is updated at every iteration η [16, 17]. The superscript $*$ stands for complex conjugate and the superscript *spe* stands for specified quantities.

$$I_{re,k}^{i} + jI_{im,k}^{i} = \left(\frac{P_k^{i,spe} + jQ_k^{i,spe}}{\dot{V}_k^{i,\eta}} \right)^{*} \quad i \in \{a,b,c\} \quad k \in \{1,2,...,N_{loads}\} \tag{5.5}$$

In distribution systems, the line shunt capacitances are usually negligible. However, the presence of shunt admittances on buses is common for voltage control purposes. In the AMBLF, these admittances are added to the system admittance matrix and, consequently, their effect is taken into account in the Jacobian matrix. On the other hand, in the BCBLF, the Jacobian matrix does not contain elements of the system admittance matrix. Therefore, to take into account the shunt admittances of the lines, Y_{km}^{sh}, and the shunt admittances of the buses, Y_k^{sh}, (5.5) needs to be rewritten as (5.6), where Y_k is a matrix containing the association of all shunt admittances connected to the bus k. Given that Y_k is a matrix and $\dot{V}_k$ is a vector, the product $Y_k\dot{V}_k$ is a vector containing the currents injected by the shunt elements in the bus k.

$$I_{re,k}^{i} + jI_{im,k}^{i} = \left(\frac{P_k^{i,spe} + jQ_k^{i,spe}}{\dot{V}_k^{i}} \right)^{*} - \left(Y_k\dot{V}_k \right)^{i} \quad i \in \{a,b,c\} \quad k \in \{1,2,...,N_{loads}\} \tag{5.6}$$

5.3.2.2 Reference bus

In power flow analysis, an angular reference is required to make the problem solvable. This angular reference is set on the reference bus, r, which is usually the substation bus. For three-phase systems, the voltage angles need to be phase shifted by 120°. For simplicity, the angles $\theta_r^{i,spe}$ are normally set to 0°, −120° and +120°, for phases $i \in \{a, b, c\}$, respectively. The voltage magnitudes, $V_r^{i,spe}$, are specified with the same values for the three phases i, for instance, 1 pu [20]. As the voltage magnitudes and the voltage angles at substation bus are specified for the three phases, the real and imaginary parts of these complex voltages can be written according to (5.7) and (5.8), and included in the load flow as equivalent specified quantities. Once the magnitudes and angles are specified for the three phases of the reference bus, the equivalent specified quantities, $V_{re,r}^i$ and $V_{im,r}^i$, for the three phases are constant during the solution process.

$$V_{re,r}^i = V_r^{i,spe} \cos \theta_r^{i,spe} \quad i \in \{a, b, c\} \tag{5.7}$$

$$V_{im,r}^i = V_r^{i,spe} \sin \theta_r^{i,spe} \quad i \in \{a, b, c\} \tag{5.8}$$

Alternatively, the reference bus can be modelled as a balanced three-phase voltage source behind an equivalent impedance that represents the network backward (i.e. upstream) the distribution main substation [20].

5.3.2.3 Generation buses

For a generation bus k, the active power injection $P_k^{i,spe}$ and the voltage magnitude $V_k^{i,spe}$ are the specified quantities for the three phases i of the bus k. The literature presents several approaches for modelling generation buses given the state variables are complex currents and voltages in rectangular form [7, 21–23]. However, none of them, unlike the reference bus and the load buses, results in a constant Jacobian matrix.

Table 5.2 summarises the approaches available to model generation buses in both the AMBLF and BCBLF. Given that these buses are not common in distribution

Table 5.2 Summary of load and generation bus models

Bus type	References	State variables	Dependent variables
PQ	[7]	$V_{re,k}^i, V_{im,k}^i$	$I_{re,k}^i, I_{im,k}^i$
PV	[7]	$V_{im,k}^i, \Delta Q_k^i$	$I_{ire,k}^i, I_{im,k}^i$
PQ	[21]	$V_{re,k}^i, V_{im,k}^i$	$I_{re,k}^i, I_{im,k}^i$
PV	[21]	δ_k^i	ΔP_k^i
PQ	[22]	$V_{re,k}^i, V_{im,k}^i$	$I_{re,k}^i, I_{im,k}^i$
PV	[22]	$V_{re,k}^i, V_{im,k}^i$	$\Delta P_k^i, \Delta \lvert V_k^i \rvert^2$
PQ	[23]	$V_{re,k}^i, V_{im,k}^i$	$I_{re,k}^i, I_{im,k}^i$
PV	[23]	$V_{re,k}^i, V_{im,k}^i, \Delta Q_k^i$	$I_{re,k}^i, I_{im,k}^i, \Delta V_k^i$

systems, and these approaches require updating the Jacobian matrix during the load flow solution process, increasing the computational times, for the sake of simplicity, generation buses will not be considered in this chapter.

In summary, for the AMBLF and BCBLF, the specified quantities are used to obtain the equivalent specified quantities, which are, in fact, used in the load flow. Table 5.3 summarises the equations required to obtain the equivalent specified quantities from the specified quantities according to the bus type. These equations apply to the three phases of the corresponding buses. Recall that generation buses will not be considered, as they result in a variable Jacobian matrix.

5.3.3 General modelling

The classical nonlinear and well-established load flow problem is usually solved by the NRLF, which is described by the iterative process in (5.9) and (5.10), where $h(x)$ contains the equations relating the specified quantities to the state variables x, z contains the values of the specified quantities, and η is the iteration counter [1].

$$\Delta x^{\eta} = H(x^{\eta})^{-1}\left[z - h(x^{\eta})\right] \tag{5.9}$$

$$x^{\eta+1} = x^{\eta} + \Delta x^{\eta} \tag{5.10}$$

The Jacobian matrix $H(x^{\eta})$ contains the derivatives of the equations $h(x)$ with respect to the state variables x. These derivatives need to be updated at every iteration η. As stated above, for the AMBLF and BCBLF, the specified quantities are converted into real and imaginary parts of voltages and currents, according to (5.5)–(5.8). As the converted quantities for the load buses need to be updated at every iteration η, the vector containing the specified quantities will be represented by $z(x^{\eta})$. In the BCBLF, in order to update the vector $z(x^{\eta})$, it is required to obtain the bus voltages from the branch currents, which are the state variables. This can be done, for instance, applying the forward sweep step of the BFSLF described in this chapter [24].

Given the state variables are the real and imaginary parts of complex voltages and currents, as shown in (5.3) and (5.4), the converted specified quantities and the state variables relate from linear equations and, therefore, $h(x^{\eta}) = Hx^{\eta}$. Note that the Jacobian matrix H is constant and does not need to be updated at every iteration. As a result, (5.9) and (5.10) can be rewritten as (5.11).

$$\Delta x^{\eta} = H^{-1}\left[z(x^{\eta}) - Hx^{\eta}\right] = H^{-1}z(x^{\eta}) - H^{-1}Hx^{\eta} = H^{-1}z(x^{\eta}) - x^{\eta} \tag{5.11}$$

Table 5.3 Bus types and equivalent specified quantities

Bus type	Specified quantities	Equivalent specified quantities	Equations
Load bus (PQ)	$P_k^{i,spe}, Q_k^{i,spe}$	$I_{re,k}^{i}, I_{im,k}^{i}$	(5.5) or (5.6)
Reference bus (Vθ)	$\theta_k^{i,spe}, V_k^{i,spe}$	$V_{re,k}^{i}, V_{im,k}^{i}$	(5.7) and (5.8)

From (5.10) and (5.11), the values of the state variables in the next iteration $\eta + 1$ are directly obtained in,

$$x^{\eta+1} = x^{\eta} + \Delta x^{\eta} = H^{-1} z(x^{\eta}) \tag{5.12}$$

From the computational point of view, solving (5.12) is much more attractive than solving (5.9) and (5.10), given the Jacobian matrix is built and factorised just once.

5.3.3.1 Jacobian matrices

A distribution system containing N_{loads} load buses and one reference bus, the total number of buses is $N_{buses} = N_{loads} + 1$. Assuming that every bus has the three phases, the total number of state variables is $6N_{buses}$. In order to make the problem solvable, $6N_{buses}$ quantities must be specified and converted into $6N_{buses}$ equivalent specified quantities. For simplicity, assuming that the distribution system is radial, then, $N_{branches} = N_{buses} - 1$.

The vector containing the equivalent specified quantifies, $z(x^{\eta})$, is as shown in (5.13). The variables $V^{i}_{re,r}$ and $V^{i}_{im,r}$ stand for the real and imaginary parts of the complex voltages at the three phases i of the reference bus, r. As there is one reference bus, these vectors have three elements. The variables $I^{i}_{re,k}(x^{\eta})$ and $I^{i}_{im,k}(x^{\eta})$ contain, respectively, the real and imaginary parts of the complex currents injected at the three phases i of the N_{loads} load buses. Therefore, the vector $z(x^{\eta})$ has $6N_{buses}$ elements.

$$z(x^{\eta}) = \begin{pmatrix} V^{i}_{re,r} \\ I^{i}_{re,k}(x^{\eta}) \\ V^{i}_{im,r} \\ I^{i}_{im,k}(x^{\eta}) \end{pmatrix} \quad i \in \{a, b, c\} \quad k \in \{1, 2, ..., N_{loads}\} \tag{5.13}$$

Given the vectors x and $z(x^{\eta})$ contain $6N_{buses}$ elements, the Jacobian matrix is $6N_{buses} \times 6N_{buses}$ and has full rank, i.e., the inverse of the Jacobian matrix can be obtained. Indeed, instead of inverting this matrix, it is recommended to adopt well-consolidated sparse matrix factorisation methods [25].

For the sake of simplicity, considering that the reference is at the bus 1 and the state variables are those shown in (5.3), the Jacobian matrix of the AMBLF can be partitioned as in (5.14), where $[L \;\; O]$ contains the derivatives of $V^{i}_{re,r}$ regarding the state variables, $[O \;\; L]$ contains the derivatives of $V^{i}_{im,r}$ regarding the state variables, $[G \;\; -B]$ contains the derivatives of $I^{i}_{re,k}(x^{\eta})$ regarding the state variables and $[G \;\; B]$ contains the derivatives of $I^{i}_{im,k}(x^{\eta})$ regarding the state variables. Furthermore, $L = [I_{3\times3} \;\; 0_{3\times3N_{loads}}]$ and $O = [0_{3\times3N_{buses}}]$. In (5.14), G and B stand for the real and imaginary parts of the system admittance matrix. As bus 1 is not a load bus, the lines of G and B referring to bus 1 are removed from (5.14).

$$H_{AMB} = \begin{pmatrix} L & O \\ G & -B \\ O & L \\ B & G \end{pmatrix}_{6N_{buses} \times 6N_{buses}} \tag{5.14}$$

For the sake of simplicity, considering that the reference is at bus 1 and the vector of state variables is (5.4), the Jacobian matrix of the BCBLF can be partitioned as in (5.15), where matrices L and O are the same as in (5.14), $M = [0_{3N_{loads} \times 3} \ A]$, $N = [0_{3N_{loads} \times 3N_{buses}}]$ and A is the node to branch incidence matrix of the distribution system [8]. Therefore, A contains the derivatives of $I^i_{re,k}(x^\eta)$ and $I^i_{im,k}(x^\eta)$ with respect to the branch currents.

$$H_{BCB} = \begin{pmatrix} L & O \\ M & N \\ O & L \\ N & M \end{pmatrix}_{6N_{buses} \times 6N_{buses}} \tag{5.15}$$

5.3.4 Computational aspects and discussion

In both load flow approaches, the AMBLF and BCBLF, given that there are no generation buses, the resulting Jacobian matrices, H_{AMB} and H_{BCB}, will be constant. These matrices will change only if the system topology changes. As a result, these matrices are built and factorised just once, significantly speeding up the load flow computational performance [2, 10].

As stated in Section 5.3.2.3, generation buses can be modelled in both load flows; however, based on the more promising available approaches, the resulting Jacobian matrices will not remain constant during the load flow solution process, deteriorating the computational performance. Even though, it is expected the AMBLF and BCBLF to perform better than the classical NRLF.

5.3.4.1 AMBLF and BCBLF algorithms

For the AMBLF and BCBLF, the solution is obtained by solving (5.12). Thus, despite the difference between the AMBLF and BCBLF, both approaches can be accomplished by iteratively running the following steps.

AMBLF / BCBLF Algorithm

1. Data Preparation;
2. Set the iteration counter to zero, i.e., $\eta = 0$;
3. Set the first guess to the complex bus voltages;
4. Build and factorise the Jacobian matrix;
5. Calculate the vector $z(x^{\eta})$;
6. Calculate $x^{\eta+1}$ according to (5.12);
7. Check for convergence;
   (a) If convergence is reached then $\hat{x} = x^{\eta+1}$;
   (b) Otherwise, do $\eta = \eta + 1$ and go back to step 5;

The data preparation consists in the conversion of the quantities to the per unit system and the formation of the system admittance matrix and the node to branch incidence matrix [8], when required. After the data preparation, in the second step, the iteration counter is initialised and, in step 3, the first guess to the bus voltages needs to be provided. Usually, the three-phase flat start is adopted; however, this first guess can be obtained, for instance, from a previous load flow calculation. In step 4, the Jacobian matrix H can be built and factorised. In step 5, the vector containing the equivalent specified quantities, $z(x^{\eta})$, is updated. In step 6, the state vector is updated solving (5.12) and, then, in the seventh step, convergence is checked. The convergence criterion can be, for example, the one shown in (5.16). Typical values for *tolerance* are in between a range from 10^{-3} to 10^{-6}. If the convergence criterion is satisfied, the process is done, and the final state $\hat{x}$ is obtained. If the criterion is not satisfied, the process returns to step 5 and is repeated until the convergence criterion is satisfied.

$$max|x^{\eta+1} - x^{\eta}| \leq tolerance \tag{5.16}$$

For the BCBLF, after the first iteration, in order to update the vector containing the equivalent specified quantities, $z(x^{\eta})$, it is required to obtain the bus voltages from the branch currents, which are the state variables. This can be done applying (5.21), to be presented in Section 5.4.3.1, from the reference bus to the terminal buses.

5.4 Backward/forward sweep load flow

In the BFSLF, the state variables are iteratively updated one bus at a time. For that, the branches of the network are handled individually. For that, the buses and nodes of the distribution system need to be ordered from the substation to the terminal buses. As a result, a Jacobian matrix is not required.

Beyond that, this power flow requires the ordering of the buses and nodes of the distribution system from the substation to the terminal buses.

Similar to the load flow approaches discussed above, in the BFSLF, an initial guess to the bus complex voltages is required. Usually, the voltages at the reference bus are used as the first guess. Given the bus voltages, the current injections are obtained from the specified quantities, allowing to obtain the complex current flowing in the branches, in the so-called backward step. Once the current flows are known, in the forward step, the complex voltages are updated from the substation towards the terminal buses. These steps are repeated until the convergence criterion is reached.

5.4.1 Basic aspects

The BFSLF adopts the magnitude and the angles of the complex bus voltages as state variables. Therefore, the state vector for the BFSLF is given in (5.17). The variables V_k^i and θ_k^i stand, respectively, for the magnitudes and angles of the complex voltages at the three phases i of each bus of the distribution system. Assuming that the system has N_{buses} three-phase buses, the vector x has $6N_{buses}$ elements. Considering the concept of dummy lines and dummy nodes, all buses can be treated as three-phase buses [19]. The superscript T stands for transpose.

$$x = \begin{pmatrix} V_k^i & \theta_k^i \end{pmatrix}^T \quad i \in \{a, b, c\} \quad k \in \{1, 2, ..., N_{buses}\} \tag{5.17}$$

Similar to the AMBLF and BCBLF, the buses are classified as reference bus, load bus and generation bus, according to the specified quantities. The most important feature of BFSLF is that it does not require a Jacobian matrix, while its main drawbacks are associated with the presence of meshes in the networks and the need of ordering the branches. Therefore, this method is especially attractive for radial and weakly meshed networks [26].

As usually done, only the three phases of the distribution systems are being considered in the load flow calculation. Despite that the neutral wire and the ground are not explicitly represented, their effects are merged into the phases [11]. In cases, where the neutral and ground currents and voltages are required, a complete model can be adopted. For instance, a BFSLF considering the three phases, the neutral wire and the ground is presented in [11].

5.4.2 General modelling

In the BFSLF, the branches of the network are handled one at a time. Therefore, consider the three-phase branch shown in Figure 5.2. The shunt admittances and loads are connected to the terminal buses. As the lines are short, their shunt capacitances are usually neglected [12]. It is assumed that bus k is the bus upstream of bus m. This figure also shows the current flowing in branch km, namely, $\dot{I}_{km}^a$, $\dot{I}_{km}^b$ and $\dot{I}_{km}^c$.

The series self and mutual impedances of the branch are represented by the diagonal and off-diagonal elements of the primitive impedance matrix (5.18). They can be calculated from Carson equations [24].

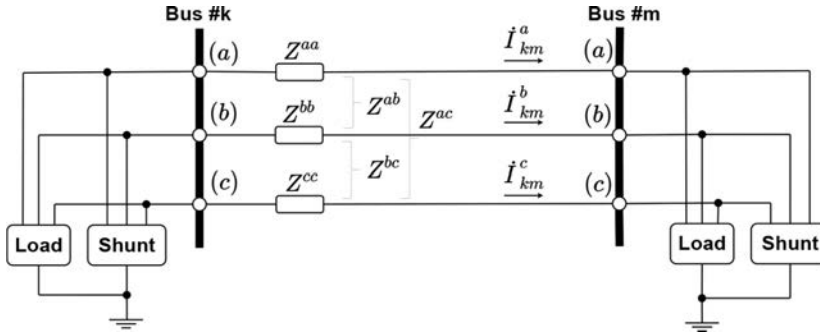

Figure 5.2 General model of a distribution branch [11]

$$Z_{km} = \begin{pmatrix} Z_{aa}\ Z_{ab}\ Z_{ac} \\ Z_{ab}\ Z_{bb}\ Z_{bc} \\ Z_{ac}\ Z_{bc}\ Z_{cc} \end{pmatrix} \tag{5.18}$$

5.4.3 Computational aspects and discussion

In the BFSLF, a Jacobian matrix is not required, making this approach very attractive from the computational point of view. For that, the branches are taken one at a time. The solution is obtained by updating all the current injections and, then, all the buses voltages at each iteration. The main drawbacks of this approach are regarded to the presence of meshes in the distribution system and the need of ordering the branches. In the following, the algorithm of the BFSLF is presented and discussed.

5.4.3.1 Backward/forward power flow algorithm

The computation of the power flow by the BFSLF requires the ordering of the buses and nodes of the distribution system. In the first step of the proposed algorithm, the branches and nodes are ordered by layers from the substation to the terminal buses. Here, the approach shown in [26],11], was adopted. The data preparation is also realised in the first step. It consists in the conversion of the quantities to the per unit system. The BFSLF calculation is accomplished by iteratively running the following steps.

BFSLF Algorithm

1. Data Preparation and ordering branches and nodes;
2. Set the the iteration counter to zero, i.e., $\eta = 0$;
3. Set the first guess to the complex bus voltages;
4. Obtain the current injections at every bus according to (5.19)
5. The Backward step:
   (a) Calculate the currents starting from the extreme buses and proceeding towards the substation bus;
6. The Forward step:
   (a) Update the voltages starting from the reference bus and proceeding towards the extreme buses;
   (b) Do $\eta = \eta + 1$;
7. Check for convergence;
   (a) If convergence is reached then $\hat{x} = x^{\eta+1}$;
   (b) Otherwise go back to step 4;

In the second step, the iteration counter is initialised and, in step 3, the first guess to the bus voltages needs to be provided. Usually, the voltage of the substation is adopted as the first guess for all buses. These voltages have the same magnitude and are 120° displaced [20]. In the fourth step, the current injections at every bus k are obtained from (5.19), where Y_k is a 3×3 matrix containing the association of all shunt admittances (of the bus and the branches) connected to the bus k.

$$\begin{pmatrix} \dot{I}_k^a \\ \dot{I}_k^b \\ \dot{I}_k^c \end{pmatrix}^{\eta+1} = \begin{pmatrix} \left(\frac{P_k^{a,spe}+jQ_k^{a,spe}}{\dot{V}_k^a}\right)^* \\ \left(\frac{P_k^{b,spe}+jQ_k^{b,spe}}{\dot{V}_k^b}\right)^* \\ \left(\frac{P_k^{c,spe}+jQ_k^{c,spe}}{\dot{V}_k^c}\right)^* \end{pmatrix}^{\eta} - Y_k \begin{pmatrix} \dot{V}_k^a \\ \dot{V}_k^b \\ \dot{V}_k^c \end{pmatrix}^{\eta} \tag{5.19}$$

In step 5, after the current injections in all buses have been calculated, in order to run the backward step, the current flows in the branches are obtained from (5.20), where Ω_m is the set of branches connected downstream to the bus m.

$$\begin{pmatrix} \dot{I}_{km}^a \\ \dot{I}_{km}^b \\ \dot{I}_{km}^c \end{pmatrix}^{\eta+1} = -\begin{pmatrix} \dot{I}_m^a \\ \dot{I}_m^b \\ \dot{I}_m^c \end{pmatrix}^{\eta+1} + \sum_{l \in \Omega_m} \begin{pmatrix} \dot{I}_{ml}^a \\ \dot{I}_{ml}^b \\ \dot{I}_{ml}^c \end{pmatrix}^{\eta+1} \tag{5.20}$$

In step 6, the forward step, the voltages on all buses are updated according to (5.21). If the powers depend on the voltages, they also need to be updated in this step.

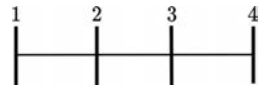

Figure 5.3 4-Bus test feeder

$$\begin{pmatrix} \dot{V}_m^a \\ \dot{V}_m^b \\ \dot{V}_m^c \end{pmatrix}^{\eta+1} = \begin{pmatrix} \dot{V}_k^a \\ \dot{V}_k^b \\ \dot{V}_k^c \end{pmatrix}^{\eta+1} - \begin{pmatrix} Z_{aa} & Z_{ab} & Z_{ac} \\ Z_{ab} & Z_{bb} & Z_{bc} \\ Z_{ac} & Z_{bc} & Z_{cc} \end{pmatrix} \begin{pmatrix} \dot{I}_{km}^a \\ \dot{I}_{km}^b \\ \dot{I}_{km}^c \end{pmatrix}^{\eta+1} \tag{5.21}$$

In step 7, convergence is checked. The convergence criterion can be, for instance, as shown in (5.16). Typical values for tolerance are in between a range from 10^{-3} to 10^{-6}. This procedure is repeated until the convergence criterion is satisfied.

5.5 Case studies

In this section, detailed case studies are presented. The main aspects of the presented power flows are reinforced and discussed. Based on these studies, it is possible to better understand the approaches and compare them. For the sake of didactic, the tests are performed on a 4-bus test feeder with a rated nominal voltage of 12.47 kV, whose single-line diagram is shown in Figure 5.3. This system is a simplified version of the IEEE 4-bus test system [27].

All three line segments are 2 000-ft long and have the same series impedance and shunt admittances. The primitive series impedance matrix, given by Z_{km}, and the primitive shunt admittance matrix, given by B_{km}^{sh}, are shown below.

$$Z_{km} = \begin{pmatrix} 0.4576 + j1.0780 & 0.1559 + j0.5017 & 0.1535 + j0.3849 \\ 0.1559 + j0.5017 & 0.4666 + j1.0482 & 0.1580 + j0.4236 \\ 0.1535 + j0.3849 & 0.1580 + j0.4236 & 0.4615 + j1.0651 \end{pmatrix} \Omega/\text{mile}$$

$$B_{km}^{sh} = \text{j} \begin{pmatrix} 6.29980 & -1.9958 & -1.2595 \\ -1.9958 & 5.95970 & -0.7417 \\ -1.2595 & -0.7417 & 5.63860 \end{pmatrix} \Omega/\text{mile} \tag{5.22}$$

The system supplies a wye-grounded, unbalanced, three-phase constant power load connected at the bus 4. The power of the loads connected to the three phases is:

- S_4^a = 1275kW at 0.85 lagging power factor;
- S_4^b = 1800kW at 0.90 lagging power factor;
- S_4^c = 2375kW at 0.95 lagging power factor.

For voltage control purposes, the system also has a wye-grounded capacitor bank with 300 kVAr at each phase, connected at the bus 4.

5.5.1 Data preparation

Before applying the methods, the data must be converted to the per unit system. For this, a base power of 100 MVA and a base voltage equal to the system nominal voltage are adopted. Once this conversion is done, the primitive admittance matrices are built. Since all the branches are identical, their primitive admittance matrices, given by Y_{12}, Y_{23} and Y_{34}, are the same and equal to Y_{km}, as shown below. The corresponding primitive shunt admittance matrices, given by Y_{12}^{sh}, Y_{23}^{sh} and Y_{34}^{sh}, are also the same and equal to Y_{km}^{sh}, as shown below. The primitive bus shunt admittance matrix is given by Y_{k}^{sh}.

$$Y_{km} = \begin{pmatrix} 0.6659 - j1.3806 & -0.3235 + j0.4738 & -0.1167 + j0.3079 \\ -0.3235 + j0.4738 & 0.7446 - j1.4306 & -0.1981 + j0.3758 \\ -0.1167 + j0.3079 & -0.1981 + j0.3758 & 0.5982 - j1.3325 \end{pmatrix} \text{pu}$$

$$Y_{km}^{sh} = \text{j} \begin{pmatrix} 1.2369 & -0.3919 & -j0.2473 \\ -0.3919 & 1.1701 & -0.1456 \\ -0.2473 & -0.1456 & 1.1071 \end{pmatrix} \times 10^{-6}\text{pu} \tag{5.23}$$

$$Y_{k}^{sh} = \text{j} \begin{pmatrix} 0.003 & 0 & 0 \\ 0 & 0.003 & 0 \\ 0 & 0 & 0.003 \end{pmatrix} \text{pu}$$

Bus 1 is the reference bus. Its voltage magnitude is set to 1 pu, and its voltage angle is set to 0°. In order to initialise the methods, it is necessary to set an initial guess for the bus voltages and angles. As it is usually done, a flat start initialisation is adopted [1]. The convergence for the interactive solution is achieved when the largest voltage mismatch between consecutive iterations is lower than the specified tolerance. The specified tolerance for all methods is chosen to be 10^{-5}, and the iteration number was limited to 20 iterations.

5.5.2 Execution of the AMBLF

5.5.2.1 State variables

The AMBLF adopts the real and imaginary parts of the complex bus voltages as state variables, as shown in (5.3). As the studied system has four buses, this vector has 24 elements, being the first 12 positions composed of the real part of the voltages, and the subsequent 12 positions composed of the imaginary part of the voltages, as presented below.

$$x = \begin{pmatrix} V_{re,1}^{i} & V_{re,2}^{i} & V_{re,3}^{i} & V_{re,4}^{i} & V_{im,1}^{i} & V_{im,2}^{i} & V_{im,3}^{i} & V_{im,4}^{i} \end{pmatrix}^{T} \quad i \in \{a, b, c\} \tag{5.24}$$

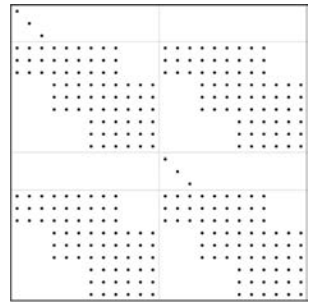

Figure 5.4 Sparsity of the AMBLF's Jacobian Matrix – 4-bus test feeder

5.5.2.2 Formation of the Jacobian matrix

The Jacobian matrix of the AMBLF is presented in (5.14). It contains conductances and susceptances extracted from the system admittance matrix Y. Moreover, it contains zeros and ones corresponding to derivatives of the real and imaginary parts of the voltages of the reference bus regarding the state variables.

The system admittance matrix is built directly from the primitive admittance matrices Y_{km}, Y_{km}^{sh} and Y_{k}^{sh}. It is worth mentioning that the primitive shunt admittance matrices Y_{km}^{sh} must be divided by two, and each half is assumed to be connected to the terminal buses k and m. The system admittance matrix is sized 12×12 since it is composed of four three-phase buses. The Y matrix can be separated in its real and imaginary parts, resulting in the conductance matrix G and the susceptance matrix B, both being sized 12×12 and having the same sparsity of the system admittance matrix.

$$Y = \begin{pmatrix} Y_{12} + \frac{Y_{12}^{sh}}{2} & -Y_{12} & 0 & 0 \\ -Y_{12} & Y_{12} + Y_{23} + \frac{Y_{12}^{sh}}{2} + \frac{Y_{23}^{sh}}{2} & -Y_{23} & 0 \\ 0 & -Y_{23} & Y_{23} + Y_{34} + \frac{Y_{23}^{sh}}{2} + \frac{Y_{34}^{sh}}{2} & -Y_{34} \\ 0 & 0 & -Y_{34} & Y_{34} + \frac{Y_{34}^{sh}}{2} + Y_{4}^{sh} \end{pmatrix} \tag{5.25}$$

The sparsity pattern of the Jacobian matrix can be observed in Figure 5.4. The eight submatrices shown in (5.14) can also be identified in the figure. The dimension of the Jacobian matrix is 24×24 since there are 24 state variables and 24 specified quantities. Recall that there are four three-phase buses and each phase has two state variables and two specified quantities.

5.5.2.3 Converting specified into equivalent specified quantities

The specified quantities for the reference bus (bus 1) and load buses (buses 2, 3 and 4) are converted into the equivalent quantities, according to (5.5), (5.7) and (5.8). The equivalent quantities obtained from the flat start just before the first iteration ($\eta = 0$) are given in Table 5.4.

Table 5.4 Equivalent specified quantities ($\eta = 0$)

Phase	Bus 1	Bus 2	Bus 3	Bus 4
a	1.0000 + *j*0.0000	0.0000 + *j*0.0000	0.0000 + *j*0.0000	−0.0127 + *j*0.0079
b	−0.5000 − *j*0.8660	0.0000 + *j*0.0000	0.0000 + *j*0.0000	0.0165 + *j*0.0112
c	−0.5000 + *j*0.8660	0.0000 + *j*0.0000	0.0000 + *j*0.0000	0.0051 − *j*0.0245

5.5.2.4 Solving the AMB power flow

Once the equivalent specified quantities and the Jacobian matrix are available, equation (5.12) is then used to calculate the state variables for $\eta = 1$, as given in Table 5.5. Recall that the values for the state variables before the first iteration ($\eta = 0$) are given by the flat start.

At the end of the first iteration, the maximum voltage mismatch is equal to 0.0464, which is greater than the tolerance. So, in order to continue the iterative process, the iteration counter must be incremented and the equivalent specified quantities must be updated. After four iterations, the process achieves convergence with a maximum voltage mismatch equal to 8.8824×10^{-6}. The equivalent specified quantities and the state variables for the remaining iterations are shown in Tables 5.6 and 5.7, respectively.

Note that during this solution process, the state variables were updated four times and, therefore, the load flow has converged with four iterations.

5.5.3 Execution of the BCBLF

State variables vector

The BCBLF adopts the real and imaginary parts of the complex bus voltages of the reference bus, and the real and imaginary parts of the complex branch currents as state variables, as shown in (5.4). As the studied system has three branches, this vector has 24 elements, as presented below.

$$x = \left(V^i_{re,1} \quad I^i_{re,12} \quad I^i_{re,23} \quad I^i_{re,34} \quad V^i_{im,1} \quad I^i_{im,12} \quad I^i_{im,23} \quad I^i_{im,34} \right)^T \quad i \in \{a, b, c\} \tag{5.26}$$

Table 5.5 State variables ($\eta = 1$)

Phase	Bus 1	Bus 2	Bus 3	Bus 4
a	1.0000 + j0.0000	0.9961 − j0.0022	0.9923 − j0.0045	0.9884 − j0.0067
b	−0.5000 − j0.8660	−0.5001 − j0.8553	−0.5004 − j0.8446	−0.5005 − j0.8339
c	−0.5000 + j0.8660	−0.4845 + j0.8670	−0.4691 + j0.8680	−0.4536 + j0.8690

Table 5.6 Equivalent specified quantities

η	Phase	Bus 1	Bus 2	Bus 3	Bus 4
	a	1.0000 + j0.0000	0.0000 + j0.0000	0.0000 + j0.0000	−0.0128 + j0.0081
2	b	−0.5000 − j0.8660	0.0000 + j0.0000	0.0000 + j0.0000	0.0172 + j0.0112
	c	−0.5000 + j0.8660	0.0000 + j0.0000	0.0000 + j0.0000	0.0041 − j0.0252
	a	1.0000 + j0.0000	0.0000 + j0.0000	0.0000 + j0.0000	−0.0128 + j0.0081
3	b	−0.5000 − j0.8660	0.0000 + j0.0000	0.0000 + j0.0000	0.0172 + j0.0112
	c	−0.5000 + j0.8660	0.0000 + j0.0000	0.0000 + j0.0000	0.0042 − j0.0252
	a	1.0000 + j0.0000	0.0000 + j0.0000	0.0000 + j0.0000	−0.0128 + j0.0081
4	b	−0.5000 − j0.8660	0.0000 + j0.0000	0.0000 + j0.0000	0.0172 + j0.0113
	c	−0.5000 + j0.8660	0.0000 + j0.0000	0.0000 + j0.0000	0.0042 − j0.0252

Table 5.7 State variables

η	Phase	Bus 1	Bus 2	Bus 3	Bus 4
	a	1.0000 + j0.0000	0.9961 − j0.0024	0.9922 − j0.0047	0.9883 − j0.0071
2	b	−0.5000 − j0.8660	−0.4999 − j0.8551	−0.4998 − j0.8443	−0.4998 − j0.8336
	c	−0.5000 + j0.8660	−0.4842 + j0.8662	−0.4687 + j0.8664	−0.4529 + j0.8666
	a	1.0000 + j0.0000	0.9961 − j0.0023	0.9922 − j0.0047	0.9884 − j0.0070
3	b	−0.5000 − j0.8660	−0.4999 − j0.8552	−0.4998 − j0.8443	−0.4998 − j0.8335
	c	−0.5000 + j0.8660	−0.4843 + j0.8662	−0.4685 + j0.8664	−0.4529 + j0.8666
	a	1.0000 + j0.0000	0.9961 − j0.0023	0.9923 − j0.0047	0.9884 − j0.0070
4	b	−0.5000 − j0.8660	−0.4999 − j0.8552	−0.4999 − j0.8444	−0.4998 − j0.8335
	c	−0.5000 + j0.8660	−0.4843 + j0.8662	−0.4686 + j0.8664	−0.4528 + j0.8667

Formation of the Jacobian matrix

The Jacobian matrix of the BCBLF is presented in (5.15). It contains the node to branch incidence matrix A. Moreover, it contains zeros and ones corresponding to derivatives of the real and imaginary parts of the voltages of the reference bus with respect to the state variables.

In the node to branch incidence matrix, each row corresponds to a bus and each column corresponds to a branch. For each branch km, the position corresponding to the bus k is set to 1, while the position corresponding to the bus m is set to −1. All the other elements are set to zero. This process is done for each phase of the three branches connecting the four buses, resulting, therefore, on a 12×9 matrix.

The sparsity pattern of the Jacobian matrix can be observed in Figure 5.5. The eight submatrices shown in (5.15) can also be identified in the figure. Both L and O submatrices are 3×12, and A is 9×12 since the system has four buses and three branches. The dimension of the Jacobian matrix is 24×24 since there are 24 state variables and 24 specified quantities.

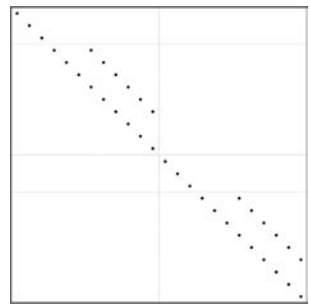

Figure 5.5 Sparsity of the BCBLF's Jacobian Matrix – 4-bus test feeder

Table 5.8 Equivalent specified quantities ($\eta = 0$)

Phase	Bus 1	Bus 2	Bus 3	Bus 4
a	1.0000 + j0.0000	0.0000 + j0.0000	0.0000 + j0.0000	−0.0127 + j0.0049
b	−0.5000 − j0.8660	0.0000 + j0.0000	0.0000 + j0.0000	0.0140 + j0.0127
c	−0.5000 + j0.8660	0.0000 + j0.0000	0.0000 + j0.0000	0.0077 − j0.0230

Converting specified into equivalent specified quantities

The specified quantities for the reference bus (bus 1) and load buses (buses 2, 3 and 4) are converted into the equivalent quantities, according to (5.6), (5.7) and (5.8). The equivalent quantities obtained with the flat start just before the first iteration ($\eta = 0$) are given in Table 5.8.

Solving the BCBPF

Once the equivalent specified quantities and the Jacobian matrix are available, (5.12) is then used to calculate the state variables for the first iteration ($\eta = 1$), given in Table 5.9. Once the current flows in all branches are obtained, (5.21) is used to update the bus voltages, and the values are given in Table 5.10. Recall that the values for the bus voltages before the first iteration ($\eta = 0$) are given by the flat start.

At the end of the first iteration, the maximum voltage mismatch is equal to 0.2662, which is greater than the tolerance. So, in order to continue the iterative process, the iteration counter must be incremented and the equivalent specified

Table 5.9 State variables ($\eta = 1$)

Phase	Bus 1	Branches 1–2	Branches 2–3	Branches 3–4
a	1.0000 + j0.0000	0.0127 − j0.0048	0.0127 − j0.0048	0.0127 − j0.0049
b	−0.5000 − j0.8660	−0.0139 − j0.0127	−0.0139 − j0.0127	−0.0140 − j0.0127
c	−0.5000 + j0.8660	−0.0077 + j0.0229	−0.0077 + j0.0229	−0.0077 + j0.0229

Table 5.10 Bus voltages ($\eta = 1$)

Phase	Bus 1	Bus 2	Bus 3	Bus 4
a	1.0000 + j0.0000	0.9961 − j0.0022	0.9922 − j0.0044	0.9883 − j0.0067
b	−0.5000 − j0.8660	−0.5002 − j0.8553	−0.5004 − j0.8447	−0.5007 − j0.8340
c	−0.5000 + j0.8660	−0.4846 + j0.8670	−0.4693 + j0.8680	−0.4539 + j0.8690

Table 5.11 Equivalent specified quantities

η	Phase	Bus 1	Bus 2	Bus 3	Bus 4
	a	1.0000 + j0.0000	0.0000 + j0.0000	0.0000 + j0.0000	−0.0129 + j0.0051
2	b	−0.5000 − j0.8660	0.0000 + j0.0000	0.0000 + j0.0000	0.0147 + j0.0127
	c	−0.5000 + j0.8660	0.0000 + j0.0000	0.0000 + j0.0000	0.0068 − j0.0239
	a	1.0000 + j0.0000	0.0000 + j0.0000	0.0000 + j0.0000	−0.0129 + j0.0051
3	b	−0.5000 − j0.8660	0.0000 + j0.0000	0.0000 + j0.0000	0.0147 + j0.0127
	c	−0.5000 + j0.8660	0.0000 + j0.0000	0.0000 + j0.0000	0.0068 − j0.0239
	a	1.0000 + j0.0000	0.0000 + j0.0000	0.0000 + j0.0000	−0.0129 + j0.0051
4	b	−0.5000 − j0.8660	0.0000 + j0.0000	0.0000 + j0.0000	0.0147 + j0.0128
	c	−0.5000 + j0.8660	0.0000 + j0.0000	0.0000 + j0.0000	0.0068 − j0.0239

quantities must be updated. After four iterations, the process achieves the convergence with a maximum mismatch of 9.0352×10^{-6}. The equivalent specified quantities and the state variables at each iteration are shown in Tables 5.11 and 5.12, respectively.

Note that during this solution process, the state variables were updated four times and, therefore, the load flow converged with four iterations.

Table 5.12 State variables

η	Phase	Bus 1	Branches 1–2	Branches 2–3	Branches 3–4
	a	1.0000 + j0.0000	0.0128 − j0.0051	0.0128 − j0.0051	0.0128 − j0.0051
2	b	−0.5000 − j0.8660	−0.0146 − j0.0127	−0.0147 − j0.0127	−0.0147 − j0.0127
	c	−0.5000 + j0.8660	−0.0067 + j0.0237	−0.0067 + j0.0237	−0.0067 + j0.0237
	a	1.0000 + j0.0000	0.0128 − j0.0051	0.9922 − j0.0047	0.0128 − j0.0051
3	b	−0.5000 − j0.8660	−0.0147 − j0.0127	−0.0147 − j0.0127	−0.0147 − j0.0127
	c	−0.5000 + j0.8660	−0.0067 + j0.0238	−0.0067 + j0.0238	−0.0067 + j0.0238
	a	1.0000 + j0.0000	0.0129 − j0.0051	0.0129 − j0.0051	0.0129 − j0.0051
4	b	−0.5000 − j0.8660	−0.0147 − j0.0127	−0.0147 − j0.0127	−0.0147 − j0.0127
	c	−0.5000 + j0.8660	−0.0068 + j0.0238	−0.0068 + j0.0238	−0.0068 + j0.0238

Table 5.13 Nodal current injections (η = 0)

Phase	Bus 1	Bus 2	Bus 3	Bus 4
a	0.0000 + j0.0000	0.0000 + j0.0000	0.0000 + j0.0000	−0.0127 + j0.0049
b	0.0000 + j0.0000	0.0000 + j0.0000	0.0000 + j0.0000	0.0140 + j0.0127
c	0.0000 + j0.0000	0.0000 + j0.0000	0.0000 + j0.0000	0.0077 − j0.0230

Table 5.14 Branch current flow (η = 0)

Phase	Branches 1–2	Branches 2–3	Branches 3–4
a	0.0127 − j0.0049	0.0127 − j0.0049	0.0127 − j0.0049
b	−0.0139 − j0.0127	−0.0139 − j0.0127	−0.0139 − j0.0127
c	−0.0077 + j0.0230	−0.0077 + j0.0230	−0.0077 + j0.0230

5.5.4 Execution of the BFSLF

State variables vector

The BFSLF adopts the magnitude and the angles of the complex bus voltages as state variables, as shown in (5.17). As the studied system has four buses, this vector has 24 elements, being the first 12 positions composed of the magnitude of the complex voltages and the subsequent 12 positions composed of the angles of the complex voltages, as presented below.

$$x = \left(V_1^i \quad V_2^i \quad V_3^i \quad V_4^i \quad \theta_1^i \quad \theta_2^i \quad \theta_3^i \quad \theta_4^i\right)^T \qquad i \in \{a, b, c\} \tag{5.27}$$

Nodal current injection

To calculate the nodal current injections, (5.19) is used. The nodal current injections obtained from the flat start are given in Table 5.13.

Backward sweep

After the current injections are calculated, in order to run the backward step, the current flows are obtained from (5.20), and the values are given in Table 5.14.

Table 5.15 State variables (η = 1)

Phase	Bus 1	Bus 2	Bus 3	Bus 4
a	1.0000 + j0.0000	0.9961 − j0.0022	0.9922 − j0.0044	0.9883 − j0.0067
b	−0.5000 − j0.8660	−0.5002 − j0.8553	−0.5004 − j0.8447	−0.5007 − j0.8340
c	−0.5000 + j0.8660	−0.4846 +j0.8670	−0.4693 + j0.8680	−0.4539 + j0.8690

Table 5.16 Nodal current injections

η	Phase	Bus 1	Bus 2	Bus 3	Bus 4
	a	1.0000 + j0.0000	0.0000 + j0.0000	0.0000 + j0.0000	−0.0129 + j0.0051
2	b	−0.5000 − j0.8660	0.0000 + j0.0000	0.0000 + j0.0000	0.0147 + j0.0127
	c	−0.5000 + j0.8660	0.0000 + j0.0000	0.0000 + j0.0000	0.0068 − j0.0239
	a	1.0000 + j0.0000	0.0000 + j0.0000	0.0000 + j0.0000	−0.0129 + j0.0051
3	b	−0.5000 − j0.8660	0.0000 + j0.0000	0.0000 + j0.0000	0.0147 + j0.0127
	c	−0.5000 + j0.8660	0.0000 + j0.0000	0.0000 + j0.0000	0.0068 − j0.0239
	a	1.0000 + j0.0000	0.0000 + j0.0000	0.0000 + j0.0000	−0.0129 + j0.0051
4	b	−0.5000 − j0.8660	0.0000 + j0.0000	0.0000 + j0.0000	0.0147 + j0.0128
	c	−0.5000 + j0.8660	0.0000 + j0.0000	0.0000 + j0.0000	0.0068 − j0.0239
	a	1.0000 + j0.0000	0.0000 + j0.0000	0.0000 + j0.0000	−0.0129 + j0.0051
5	b	−0.5000 − j0.8660	0.0000 + j0.0000	0.0000 + j0.0000	0.0147 + j0.0128
	c	−0.5000 + j0.8660	0.0000 + j0.0000	0.0000 + j0.0000	0.0068 − j0.0239

Table 5.17 Branch current flow

η	Phase	Branches 1–2	Branches 2–3	Branches 3–4
	a	0.0128 − j0.0051	0.0128 − j0.0051	0.0128 − j0.0051
2	b	−0.0146 − j0.0127	−0.0147 − j0.0127	−0.0147 − j0.0127
	c	−0.0067 + j0.0237	−0.0067 + j0.0237	−0.0067 + j0.0237
	a	0.0128 − j0.0051	0.9922 − j0.0047	0.0128 − j0.0051
3	b	−0.0147 − j0.0127	−0.0147 − j0.0127	−0.0147 − j0.0127
	c	−0.0067 + j0.0238	−0.0067 + j0.0238	−0.0067 + j0.0238
	a	0.0129 − j0.0051	0.0129 − j0.0051	0.0129 − j0.0051
4	b	−0.0147 − j0.0127	−0.0147 − j0.0127	−0.0147 − j0.0127
	c	−0.0068 + j0.0238	−0.0068 + j0.0238	−0.0068 + j0.0238
	a	0.0129 − j0.0051	0.0129 − j0.0051	0.0129 − j0.0051
5	b	−0.0147 − j0.0128	−0.0147 − j0.0128	−0.0147 − j0.0128
	c	−0.0068 + j0.0239	−0.0068 + j0.0239	−0.0068 + j0.0239

Forward sweep

After the current flows in all branches are calculated, in the forward step, the voltages in all buses are updated from (5.21). The bus voltages, that is, the state variables converted to rectangular coordinates are given in Table 5.15. The conversion was made in order to allow the comparison with remaining loaf flows.

At the end of the first iteration, the maximum mismatch is equal to 0.0422, which is greater than the tolerance. So, in order to achieve the convergence, the iterative process is repeated as described above. After five iterations, the process achieves the convergence with a maximum mismatch of 5.3355×10^{-7}. The equivalent nodal current injections, the branch current flows and the state variables at each iteration are in shown in Tables 5.16–5.18, respectively.

Table 5.18 State variables

η	Phase	Bus 1	Bus 2	Bus 3	Bus 4
	a	1.0000 + j0.0000	0.9961 − j0.0023	0.9922 − j0.0047	0.9883 − j0.0070
2	b	−0.5000 − j0.8660	−0.4999 − j0.8552	−0.4999 − j0.8443	−0.4998 − j0.8335
	c	−0.5000 + j0.8660	−0.4843 + j0.8662	−0.4687 + j0.8664	−0.4529 + j0.8667
	a	1.0000 + j0.0000	0.9961 − j0.0023	0.9922 − j0.0047	0.9884 − j0.0070
3	b	−0.5000 − j0.8660	−0.4999 − j0.8552	−0.4998 − j0.8443	−0.4998 − j0.8335
	c	−0.5000 + j0.8660	−0.4843 + j0.8662	−0.4685 + j0.8664	−0.4528 + j0.8667
	a	1.0000 + j0.0000	0.9961 − j0.0023	0.9923 − j0.0047	0.9884 − j0.0070
4	b	−0.5000 − j0.8660	−0.4999 − j0.8553	−0.4999 − j0.8444	−0.4998 − j0.8335
	c	−0.5000 + j0.8660	−0.4843 + j0.8662	−0.4686 + j0.8664	−0.4528 + j0.8666
	a	1.0000 + j0.0000	0.9961 − j0.0023	0.9923 − j0.0047	0.9884 − j0.0070
5	b	−0.5000 − j0.8660	−0.4999 − j0.8552	−0.4999 − j0.8444	−0.4998 − j0.8335
	c	−0.5000 + j0.8660	−0.4843 + j0.8662	−0.4686 + j0.8664	−0.4528 + j0.8667

5.6 Conclusions and special remarks

This chapter presented three current-based power flow calculation methods devoted to distribution systems. Due to their similarities, the BCBLF and the AMBLF were presented simultaneously. In these load flows, the specified quantities are converted into complex voltages and currents. As the state variables are the complex voltages or currents, the resulting Jacobian matrix is constant, speeding up the computations. Furthermore, building the Jacobian matrices is much simpler in comparison to the classical NRLF method. To maintain the Jacobian matrix constant, the generation buses were not considered. To the best of the author's knowledge, the literature does not present approaches to model generation buses in the AMBLF and BCBLF able to maintain the Jacobian matrices constant without approximations or simplifications. Generally, these approaches are attractive and provide many advantages.

This chapter also presented the well-known BFSLF. In this approach, a Jacobian matrix is not required. For that, the branches are considered one at a time, and, consequently, the state variables are updated one at a time. This approach accommodates generation buses; however, the literature points out convergence issues when it is applied to meshed distribution networks. In general, this approach is powerful, robust and easy to implement.

References

[1] Price W., Casper S., Nwankpa C., *et al*. 'Bibliography on load models for power flow and dynamic performance simulation'. *IEEE Transactions on Power Systems*. 1995, vol. 10(1), pp. 523–38.

[2] da Costa V.M., Martins N., Pereira J.L.R. 'Developments in the Newton Raphson power flow formulation based on current injections'. *IEEE Transactions on Power Systems*. 1999, vol. 14(9), pp. 1320–6.

[3] Kamel S., Abdel-Akher M., El-Nemr M.K. A new technique to improve voltage controlled nodes (PV nodes) in the current injection Newton-Raphson power-flow analysis. In 45th International Universities Power Engineering Conference; Cardiff - UK, 31 August - 03 September; 2010. pp. 1–4.

[4] Whei-Min L., Zhan T.S., Tsay M.T. ' 'Multiple-frequency three-phase load flow for harmonic analysis''. *IEEE Transactions on Power Systems*. 2004, vol. 19(2), pp. 897–904.

[5] Garcia P.A.N., Pereira J.L.R., Carneiro S., Vinagre M.P., Gomes F.V. 'Improvements in the representation of pv buses on three-phase distribution power flow'. *IEEE Transactions on Power Delivery*. 2004, vol. 19(2), pp. 894–6.

[6] Cespedes R.G. 'New method for the analysis of distribution networks'. *IEEE Transactions on Power Delivery*. 1990, vol. 5(1), pp. 391–6.

[7] da Costa V.M., Martins N., Pereira J.L.R. 'Developments in the Newton Raphson power flow formulation based on current injections'. *IEEE Transactions on Power Systems*. 1999, vol. 14(4), pp. 1320–6.

[8] Stagg E.-A. *Computer methods in power system analysis*. New York City - US: McGraw-Hill Book Company; 1968.

[9] Dommel H.W., Tinney W.F., Powell W.L. *Further Developments in Newton's Method for Power System Applications*. 161-PWR. New York: IEEE Winter Power Meeting; 1970. pp. 1–6.

[10] TinneyW. 'A presentation to the workshop in engineering mathematics and computer sciences'. *Proceedings of the Workshop on Advanced Mathematics and Computer Science for Power Systems Analysis*. 1991, pp. 1–1.

[11] Ciric R.M., Feltrin A.P., Ochoa L.F. 'Power flow in four-wire distribution networks-general approach'. *IEEE Transactions on Power Systems*. 2003, vol. 18(4), pp. 1283–90.

[12] Cheng C.S., Shirmohammadi D. 'A three-phase power flow method for real-time distribution system analysis'. *IEEE Transactions on Power Systems*. 1995, vol. 10(2), pp. 671–9.

[13] Monticelli A. *State estimation in electric power systems: A generalized approach*. Norwell - Massachusetts - US: Kluwer Academic Publishers; 1999.

[14] Martí J.R., Ahmadi H., Bashualdo L. 'Linear power-flow formulation based on a voltage-dependent load model'. *IEEE Transactions on Power Delivery*. 2013, vol. 28(3), pp. 1682–90.

[15] Price W., Casper S., Nwankpa C., *et al.* 'Bibliography on load models for power flow and dynamic performance simulation'. *IEEE Power Engineering Review*. 1995, vol. 15(2), p. 70.

[16] de Almeida M.C., Ochoa L.F. 'An improved three-phase AMB distribution system state estimator'. *IEEE Transactions on Power Systems*. 2016, vol. 32(2), pp. 1–1473.

[17] Baran M.E., Kelley A.W. 'A branch-current-based state estimation method for distribution systems'. *IEEE Transactions on Power Systems*. 1995, vol. 10(1), pp. 483–91.

[18] Silva R.S. *Contributions to distribution systems state estimation* [online]. University of Campinas. 2017. Available from http://repositorio.unicamp.br/jspui/handle/REPOSIP/332805.
[19] Abdel-Akher M., Nor K.M., Single-Phase R. 'Two-Phase lines with dummy lines and dummy nodes' in Hassan M.Y. (ed.). *Recent Developments in Three Phase Load Flow Analysis*. Malaysian Book Publishers Association; 2008. pp. 107–12.
[20] Schincariol da Silva R., Fernandes T.R., Almeida M.C. 'Specifying angular reference for three-phase distribution system state estimators'. *IET Generation, Transmission & Distribution*. 2018, vol. 12(7), pp. 1655–63.
[21] Kamel S., Abdel-Akher M., El-Nemr M.K. 'A new technique to improve voltage controlled nodes (PV nodes) in the current injection Newton-Raphson power-flow analysis'. *45th International Universities Power Engineering Conference UPEC2010*; 2010. pp. 1–4.
[22] Lin W.-M., Zhan T.-S., Tsay M.-T. 'Multiple-frequency three-phase load flow for harmonic analysis'. *IEEE Transactions on Power Systems*. 2004, vol. 19(2), pp. 897–904.
[23] Garcia P.A.N., Pereira J.L.R., Carneiro S., Vinagre M.P., Gomes F.V. 'Improvements in the representation of PV buses on three-phase distribution power flow'. *IEEE Transactions on Power Delivery*. 2004, vol. 19(2), pp. 894–6.
[24] Kersting W.H. *Distribution system modeling and analysis*. 4. Boca Raton, FL: CRC Press; 2017.
[25] Tinney W., Brandwajn V., Chan S., 'Sparse vector methods'. '*IEEE transactions on power apparatus and systems*Ieee Transactions on Power Apparatus and Systems'. . 1985, vol. 2, pp. 295–301.
[26] Shirmohammadi D., Hong H.W., Semlyen A., Luo G.X. 'A compensation-based power flow method for weakly meshed distribution and transmission networks'. *IEEE Transactions on Power Systems*. 1988, vol. 3(2), pp. 753–62.
[27] Kersting W.H. 'Radial distribution test feeders'. *IEEE Transactions on Power Systems*. 1991, vol. 6(3), pp. 975–85.

Chapter 6

Classical methods applied to distribution system state estimation

Eduardo N. Asada[1], Madson C. de Almeida[2], and Luis F. Ugarte[2]

This chapter presents two-state estimation approaches devoted to distribution systems, namely, the Branch Current-Based State Estimator (BCBSE) and the Admittance MatrixBased State Estimator (AMBSE). The formulation presented is devoted to distribution networks and, therefore, three-phase network modelling is adopted. After a detailed description of the methods, the results of simulations performed in both approaches are presented and discussed.

6.1 Introduction

Several methods to determine the most accurate state of distribution systems have been proposed over the years, especially with the modernisation of monitoring and automation infrastructure. Recently, artificial intelligence (AI)-based methods have also been applied to help diagnosing the system, and its application has focused on identifying situations that may affect the correct operation of the system. Usually, the current method used for comparison or to generate reference solutions is based on classical distribution state estimation.

The classical state estimation methods are those derived from the concept of determining the most probable state of the system based on current system information. The information is gathered from analog and digital measurements, as well as system parameters and topology. Since the information processing is affected by the quantity of data and also by the meter quality or due to other expected or unexpected events, mathematical approaches based on statistical models have been adopted.

In order to obtain the state of the system, the model of information flow used for applying the state estimator can be observed in the following figure.

[1]University of São Paulo, São Paulo, Brazil
[2]University of Campinas, São Paulo, Brazil

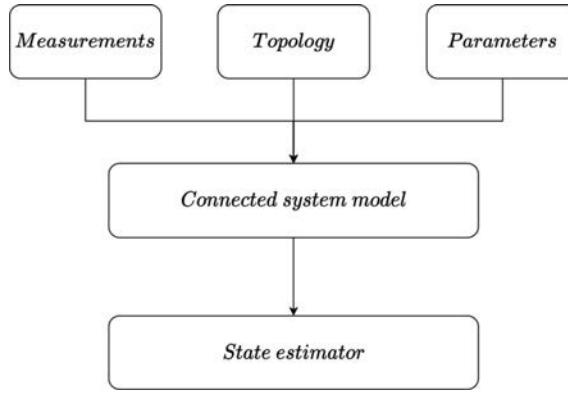

Figure 6.1 Simplified data flow model

The model presented in Figure 6.1 has been adopted for state estimator development in transmission systems, and it served as a reference for earlier distribution system state estimator models.

In general, after gathering information from the available data and control infrastructure (usually, the Supervisory Control and Data Acquisition - SCADA system), a verification is carried out to relate the analog or digital measurements to the corresponding monitored component, and the identification of gross errors and missing data is carried out (observability analysis [1]). After processing and building cohesive system information, the estimation is performed. At this point, different techniques can be applied and procedures for post-processing the estimation to identify bad data [1] or even to identify model inconsistencies.

In the literature, it is also possible to find other methods that deal with the difficulties of having enough measurements to estimate the state of distribution systems. Usually in distribution systems, the monitoring is focused at the substation and at important load points. Although smart meters may be available for collecting measurements in low voltage networks, they may not be fully integrated into the SCADA system. For those situations with scarce measurements, it becomes a challenge to determine the state of the system considering the uncertainty regarding many aspects of distribution systems (topology, parameters and specially load behaviour). This fact is explored in distribution load flow problems or probabilistic load flow algorithms. For those algorithms, basically, the objective is to determine the state that best fits with actual operation considering the limitations regarding the measurement and communication infrastructure. In Ref. [2], the practical characteristics and a classification of these methods as probabilistic or heuristic methods are proposed, and the Gauss–Seidel-based power flow algorithm for distribution state estimation is presented. Earlier, Ghosh *et al.* [3] have dealt with the state estimation as an extension of probabilistic load flow applied to radial distribution systems, where the telemetered values were treated as constraints to be satisfied and the state variables are modelled as random variables. In that proposal, the load modelling

(or load estimation) becomes critical and affects the results. In [4], the use of the loads as pseudo-measurements through the Gaussian mixture model is proposed to improve the weighted least squares (WLS) state estimation under the scarce measurement scenario.

The classical state estimator provides the real-time state of the system taking into account measurements, system topology, the power flow equations and Kirchhoff's Laws. For this, different solution methods have been devised taking into account the system modelling. Usually, it is solved by applying the optimisation of a function considering the maximum likelihood criterion. Due to differences between transmission and distribution systems regarding parameters and topology, specialised algorithms applied to transmission systems such as decoupled power flow methods that cannot be directly applied to distribution systems without adaptations. The same situation applies to the state estimator algorithms; therefore, this chapter presents two classical estimators. The BCBSE algorithm has been proposed observing the radial topology of the system and considers the branch current as the state variable, in opposition to classical transmission system state estimators (SEs), which normally consider the voltage magnitude and angles as the state variables. Also proposed in the same period, the AMBSE is a more general method that uses the admittance matrix representation as the core system model for state estimation formulation, and their basics will be presented in the next sections.

6.2 Historical notes

The state estimation for distribution systems has been evolving to improve automation and supervisory controls with the aim to increase reliability, power quality, security and control of distributed energy resources. Although the maturity of its application and several methods have been reached for transmission systems since the seminal propositions of [5, 6], the concurrent application to distribution systems has not been observed [7]. One issue regarding this point is the low availability of real-time measurements and the low priority to monitor the state of the three-phase system with a high R/X ratio, unbalanced loads and asymmetric parameters. Despite of the limitations, earlier propositions of SEs for distribution systems have been made in Refs. [8–11]. For those propositions, the main criticism has been the lack of measurements to support its application.

The BCBSE proposed by Baran and Kelley [8, 9] explored the characteristics of the distribution systems; nevertheless, the voltage measurements in the earlier propositions were disregarded. In Ref. [12], its potential application was shown with the introduction of the decoupled method in which the distribution system state estimator can be solved by dividing the problem into six different independent equations considering the real and imaginary parts for each of the phases. Although being solved very efficiently, the voltage measurements have been dealt only in Ref. [13] where the BCBSE has been modelled using only constant coefficient matrices. In Ref. [14], the updation of the Jacobian and the Gain matrices during the iterative process is required due to the nonlinear model of these measurements. In the BCBSE,

usually, the state variables are the real and imaginary parts of the branch currents, and the conventional measurements, such as voltage magnitudes and powers flows, are translated into equivalent current measurements in rectangular coordinates [10, 15], resulting in a constant Jacobian matrix composed of system impedances, zeros and unitary elements considering the Newton–Raphson method.

The AMBSE initially proposed in Ref. [10] considered the normal equations resulting in a constant coefficient Jacobian matrix, which is state independent. In Ref. [16], a fast-decoupled AMBSE was proposed to reduce the computational time by simplifying the constant-coefficient Jacobian matrix. In order to improve the convergence features, in Ref. [17], the zero injections were adopted in the AMBSE considering the normal equation with constraints. In Ref. [15], the AMBSE adopting the concept of phasor rotation to obtain the three-phase equivalent voltage measurements is proposed, improving the convergence features and keeping the constant coefficient matrices. The common state variables of the AMBSE are the real and imaginary parts of the bus voltages in rectangular coordinates. The linear relationship between the state variables and equivalent measurements results in a constant Jacobian matrix composed of system admittances, zeros and unitary elements [10, 15]. The AMBSE can also be designed considering the theory of symmetrical components. The equivalent measurements are transformed into their counterparts in sequence components, and the sequence Jacobian matrices are constant. In order to solve the sequence distribution system, single-phase AMBSE is applied, greatly simplifying the implementation complexity [18]. The AMBSE can be applied in both radial and meshed topologies, since the state variables are the real and imaginary parts of the bus voltages.

The resolution of the nonlinear overdetermined system of equations is the main issue for both BCBSE and AMBSE. This is related to two characteristics associated with the modelling of the problem. One is regarding the observability (solvability of the problem based on available measurements) and another one is related to the numerical conditioning of the problem that affects the numerical algorithms.

6.3 Basics of BCB and AMB state estimators

The BCBSE, proposed initially in Refs. [8, 9], considered the following conditions: three-phase model, few measurements (most of the current measurements) and the line modelling based on distribution feeder characteristics. As the name suggests, the branch current is chosen as the state variables to provide a better computational performance of the algorithm by simplifying the Jacobian matrix of the measurement model and also by taking into account the radial topology of the system. Another advantage is the possibility to run the estimation in phase decoupled mode (with appropriate modelling) and also independently by the feeder. The estimator problem is formulated as the minimisation of residual estimate and involves the iterative resolution of normal equations. Its original method [8] did not consider the voltage measurements.

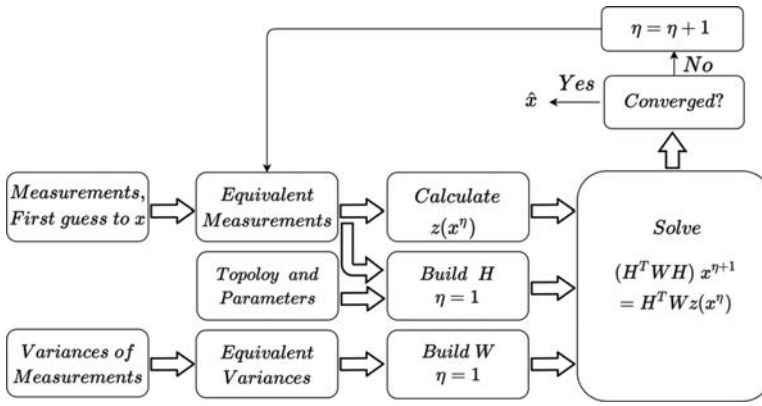

Figure 6.2 Overview of the AMB and BCB SEs

The AMBSE, proposed in Ref. [10], considered the complex nodal voltages in rectangular form as state variables. This method is general and it is not based on specific system features, and all measurements are converted to fit the admittance matrix formulation. The problem is put into $I = YV$ form with redundant measurements by converting the measurements into equivalent current and voltage measurements. This approach results in a constant Jacobian matrix that provides better computational performance. Similar to the branch current state estimator, the normal equations are also used for the iterative process.

The AMBSE and the BCBSE share many aspects in common. Indeed, the main difference between these methods lies in the choice of state variables. Figure 6.2 shows an overview of these SEs. Initially, the measured quantities (actual, virtual and pseudo-measurements) are converted into equivalent measurements. For that, the current values for the state variables, x^η, are required and, therefore, the equivalent measurements are updated at every iteration. These equivalent measurements will compose the vector $z(x^\eta)$. The derivative of the equations representing the equivalent measurements is used to build the Jacobian matrix H and, consequently, the Gain matrix $H^T WH$. The variances of the measurements are used to calculate the variances and covariances of the equivalent measurements, which can be used to build the weighting matrix W for the equivalent measurements. However, this is not mandatory, given the weights for the equivalent measurements can be defined according to the purpose the state estimator is being applied.

Despite the vector containing the equivalent measurements, $z(x^\eta)$ is updated at every iteration η, and the Jacobian and Gain matrices are constant during the iterative process [15]. This significantly reduces the computational times. Beyond that, as it will be shown, the Jacobian matrix for the AMBSE and the BCBSE is much easier to build when compared to the classical Newton–Raphson state estimator. This is especially true and attractive in the context of three-phase systems.

According to the Figure 6.2, from the Gain matrix $H^T WH$ and $z(x^\eta)$, the vector containing the state variables is updated, given rise to $x^{\eta+1}$. Then, the convergence is

verified. If the convergence condition is met, the estimated state $\hat{x} = x^{\eta+1}$; otherwise, the iteration counter η is incremented and a new iteration is run. In this section, the basic aspects of both SEs are presented.

6.3.1 State variables

The AMBSE adopts the real and imaginary parts of the complex bus voltages as state variables. The state vector for the AMBSE is given in (6.1). The superscript T stands for transpose. The variables $V^i_{re,k}$ and $V^i_{im,k}$ stand, respectively, for the real and imaginary parts of the complex voltages at three phases i of the N_{buses} buses in the distribution system. Assuming that the system has N_{buses} three-phase buses, the state vector x has $6N_{\text{buses}}$ elements:

$$\boldsymbol{x} = \left(V^i_{re,k} \quad V^i_{im,k}\right)^T, \qquad i \in \{a, b, c\}, \qquad k \in \{1, 2, ..., N_{\text{buses}}\} \tag{6.1}$$

The BCBSE adopts the real and imaginary parts of some complex currents flowing on the branches of the distribution system and the bus voltages at the reference bus as state variables. The state vector for the BCBSE is given in (6.2). The variables $V^i_{re,r}$ and $V^i_{im,r}$ stand, respectively, for the real and imaginary parts of the complex voltages at three phases i of the reference bus r. The variables $I^i_{re,km}$ and $I^i_{im,km}$ stand, respectively, for the real and imaginary parts of some complex currents flowing on branches of the distribution system. For a radial system, there are $N_{\text{branches}} = N_{\text{buses}} - 1$ branches and the currents in all branches will be in the set of state variables. For meshed systems, a set of $N_{\text{buses}} - 1$ branches forming a spanning tree needs to be selected and their currents are used in the set of state variables. In both cases, the vector $\mathbf{x}$ has $6N_{\text{buses}}$ elements:

$$\mathbf{x} = \left(I^i_{re,km} \quad I^i_{im,km} \quad V^i_{re,r} \quad V^i_{im,r}\right)^T, \quad i \in \{a, b, c\}, \; km \in \{1, 2, ..., N_{\text{buses}} - 1\} \tag{6.2}$$

In cases where there are single- and two-phase buses and branches, the concept of dummy lines and dummy nodes can be applied and, therefore, all buses and branches can be treated as three-phase elements [19].

6.3.2 Equivalent measurements

The typical measurements available for the state estimation are the root mean square (RMS) values of the active and the reactive powers injections and flows and voltage magnitude measurements. Eventually, synchronised phasors of currents and voltages provided by micro-phasor measurements units (μ-PMU) can be available.

For both, the AMBSE and the BCBSE, it is required to convert these measurements into equivalent measurements [9, 10, 12, 15]. According to that, power measurements are converted into complex currents, while voltage magnitudes can be directly used or converted into complex voltages. Three main approaches are available in the literature to cope with voltage magnitude measurements [20].

6.3.2.1 Converting power measurements

The calculation of equivalent current measurements from the active and reactive power injections and flows is shown, respectively, in (6.3) and (6.4).

According to (6.3), the active and reactive power injections measured in phases i of the bus k, $P_k^{i,\text{mea}}$ and $Q_k^{i,\text{mea}}$, respectively, are converted into equivalent complex injection currents. The real and imaginary parts of the equivalent current injection, $I_{re,k}^i$ and $I_{im,k}^i$, respectively, are used as known quantities:

$$I_{re,k}^i + jI_{im,k}^i = \left(\frac{P_k^{i,\text{mea}} + jQ_k^{i,\text{mea}}}{\dot{V}_k^{i,\eta}} \right)^* \tag{6.3}$$

where the superscript '*' stands for complex conjugate.

Similar to (6.3), in (6.4), the active and reactive power flows measured in phases i of the branch km, $P_{km}^{i,\text{mea}}$ and $Q_{km}^{i,\text{mea}}$ are converted into equivalent flow measurements. The real and imaginary parts of the equivalent current injection, $I_{re,k}^i$ and $I_{im,k}^i$, respectively, are used as known quantities:

$$I_{re,km}^i + jI_{im,km}^i = \left(\frac{P_{km}^{i,\text{mea}} + jQ_{km}^{i,\text{mea}}}{\dot{V}_k^{i,\eta}} \right)^* \tag{6.4}$$

The equivalent current measurements (injections and flows) are updated every iteration, η, of the state estimation solution, due to their dependency on the complex bus voltages $\dot{V}_k^{i,\eta}$.

In distribution systems, as the branches are typically short, the shunt admittance of the branches is usually disregarded [21]. For the sake of simplicity, this assumption will be considered in this chapter. On the other hand, the presence of shunt admittances at buses is common and will be considered.

In AMBSE, the shunt admittances are added to the system admittance matrix and, consequently, their effect is taken into account in the Jacobian matrix. In the BCBSE, the Jacobian matrix does not contain elements of the system admittance matrix. Therefore, to model the shunt admittances, equation (6.3) needs to be rewritten as (6.5), where Y_k is a matrix containing the association of all shunt admittances connected to the bus k. Given that Y_k is a matrix and $\dot{V}_k$ is a vector, the product $Y_k\dot{V}_k$ is a vector containing the currents injected by the shunt elements in the bus k:

$$I_{re,k}^i + jI_{im,k}^i = \left(\frac{P_k^{i,\text{mea}} + jQ_k^{i,\text{mea}}}{\dot{V}_k^i} \right)^* - (Y_k\dot{V}_k)^{i,\eta} \tag{6.5}$$

It is worth noting that if μ-PMUs are available, the real and imaginary parts of the equivalent complex currents are directly measured and, therefore, the conversion of powers in currents is not necessary.

6.3.2.2 Modelling voltage measurements

The literature presents three main approaches to model voltage magnitude measurements in AMBSE and BCBSE [20]. In Ref. [13], the voltage angles estimated during the solution process are used to convert the voltage magnitude measurements into complex voltages. The real and imaginary parts of these complex voltages are used as equivalent measurements. This approach leads to a constant Jacobian matrix; however, it is prone to present convergence issues [20]. In Refs. [22, 23], the voltage magnitude measurements are directly included in the state estimator, and

the resulting Jacobian matrix needs to be updated during the solution process. In Ref. [15], the voltage magnitude measurements are converted into rotated complex voltages and their real parts are used as equivalent voltage. This approach results in a constant Jacobian matrix and presents good convergence features.

The approach presented in Ref. [15] will be adopted in this chapter; however, it is strongly recommended to the reader to investigate the method proposed in Refs. [13, 22], once they present some important features that may result more fitted to the corresponding application.

In Ref. [15], the voltage magnitude measurement $V_k^{i,\text{mea}}$ is converted into equivalent voltage $V_{re,k}^{i,\text{equ}}$, according to (6.6). The angles ϕ_k^i are set to 0°, −120° and +120° for phases *a*, *b* and *c*, respectively. As it can be seen in (6.6), this equivalent measurement depends $\theta_k^{i,\eta}$ and, therefore, it needs to be updated during the solution process:

$$V_{re,k}^{i,\text{equ}} = \text{Real}\left\{V_k^{i,\text{mea}} e^{-j\theta_k^{i,\eta}} e^{-j\phi_k^i}\right\} \tag{6.6}$$

Using basic mathematical operations, equation (6.6) can be rewritten as (6.7), given that $V_{re,k}^{i,\eta} = V_k^{i,\text{mea}} \cos\theta_k^{i,\eta}$ and $V_{im,k}^{i,\eta} = V_k^{i,\text{mea}} \sin\theta_k^{i,\eta}$. Indeed, note that these are the real and imaginary parts of the complex bus voltages:

$$V_{re,k}^{i,\text{equ}} = V_{re,k}^{i,\eta} \cos\phi_k^i - V_{im,k}^{i,\eta} \sin\phi_k^i \tag{6.7}$$

In AMBSE, as the state variables are the real and imaginary parts of the complex bus voltages, the nonzero derivatives of (6.7) regarding the state variables are $\cos\phi_k^i$ and $\sin\phi_k^i$, which are constant values. In BCBSE, as the state variables are the real and imaginary parts of the branch currents, the voltage magnitude measurements are modelled as voltage drops from the reference bus *r* to the bus *k* [9]. Therefore, the nonzero derivatives of these voltage drops regarding the state variables contain the resistances and the susceptances of the branches in the path between the bus *k* and the reference bus *r* [24].

If the voltage measurements are obtained from μ-PMUs, the real and imaginary parts of the complex voltages are directly measured. In this case, it is recommended to use the real and imaginary parts of the given complex voltages as measurements and represent them directly in the AMBSE and the BCBSE, avoiding the usage of the equivalent voltage measurement $V_{re,k}^{i,\text{equ}}$. In this case, the real and imaginary parts of the complex voltage measurements are not updated during the state estimation solution process. Finally, note that if all the measurements are provided by μ-PMUs, both the AMBSE and the BCBSE will be linear and an iterative solution process will no longer be required.

6.3.3 Variances of the equivalent measurements

Given the measurements are converted into equivalent measurements, the variances of these equivalent measurements need to be obtained. These variances can be calculated from the error propagation theory [15, 25]. The inverse of the variances can be used as weights in the state estimation process. However, depending on the application, different values for the weights can be adopted [1, 26].

The variances and covariances of the real and imaginary parts of the equivalent current injections are obtained, according to (6.8). The constants a_k^i and b_k^i are calculated only once according to (6.9) and (6.10), respectively, before the estate estimation. The real and imaginary parts of the complex voltages required to obtain these constants are obtained from a previous state estimation or a load flow run [15]:

$$\begin{pmatrix} \sigma^2_{I^i_{re,k}} & \sigma_{I^i_{re,k},I^i_{im,k}} \\ \sigma_{I^i_{re,k},I^i_{im,k}} & \sigma^2_{I^i_{im,k}} \end{pmatrix} = \begin{pmatrix} a_k^{i\,2}\sigma^2_{P_k^{i,\mathrm{mea}}} + b_k^{i\,2}\sigma^2_{Q_k^{i,\mathrm{mea}}} & a_k^i b_k^i(\sigma^2_{P_k^{i,\mathrm{mea}}} - \sigma^2_{Q_k^{i,\mathrm{mea}}}) \\ a_k^i b_k^i(\sigma^2_{P_k^{i,\mathrm{mea}}} - \sigma^2_{Q_k^{i,\mathrm{mea}}}) & b_k^{i\,2}\sigma^2_{P_k^{i,\mathrm{mea}}} + a_k^{i\,2}\sigma^2_{Q_k^{i,\mathrm{mea}}} \end{pmatrix} \tag{6.8}$$

$$a_k^i = \frac{V^i_{re,k}}{V^{i\,2}_{re,k} + V^{i\,2}_{im,k}} \tag{6.9}$$

$$b_k^i = \frac{V^i_{im,k}}{V^{i\,2}_{re,k} + V^{i\,2}_{im,k}} \tag{6.10}$$

Similar equations apply to the variances of the equivalent current flows by just considering the variances of the power flows instead of the variances of the power injections.

According to (6.7) and considering the error propagation theory, the variance for the equivalent voltage measurements is obtained from (6.11). The constants c_k^i and d_k^i are calculated only once according to (6.12) and (6.13), respectively, before the estate estimation. The real and imaginary parts of the complex voltages required to obtain these constants are obtained from a previous state estimation or a load flow run [15]:

$$\sigma^2_{V^{i,\mathrm{equ}}_{re,k}} = c_k^i \cos\phi_k^i + d_k^i \sin\phi_k^i \sigma^2_{V_k^{i,\mathrm{mea}}} \tag{6.11}$$

$$c_k^i = \frac{V^i_{re,k}}{\sqrt{V^{i\,2}_{re,k} + V^{i\,2}_{im,k}}} \tag{6.12}$$

$$d_k^i = \frac{V^i_{im,k}}{\sqrt{V^{i\,2}_{re,k} + V^{i\,2}_{im,k}}} \tag{6.13}$$

6.3.4 Reference bus

In power system state estimation, a reference bus is required to make the problem solvable. In three-phase distribution systems, the common practice is to adopt the substation bus as the reference bus. For that, the angles of the complex voltages on the substation bus are 120° displaced, while the voltage magnitudes are the same for the three phases. For the sake of simplicity, these angles are usually set to 0°, −120° and +120° [27]. This is equivalent to consider that the substation bus is a balanced bus. Despite this approach is simple, it cannot be adequate for unbalanced feeders [28].

For unbalanced feeders, as recommended in Ref. [28], the reference bus can be placed in the internal balanced bus of the Thévenin equivalent circuit representing the system upstream the substation. The impedance matrix of this Thévenin equivalent circuit is obtained from the single-phase and the three-phase short-circuit levels,

as shown in Ref. [28]. As the internal bus of the Thévenin equivalent circuit is, by definition, a balanced bus, the voltage magnitudes are the same at the three phases and the voltage angles are displaced from 120° as in (6.14):

$$\begin{cases} \dot{V}_r^a = V_r^a \cos(\theta_r^a) + jV_r^a \sin(\theta_r^a) \\ \dot{V}_r^b = V_r^a \cos(\theta_r^a - 120°) + jV_r^a \sin(\theta_r^a - 120°) \\ \dot{V}_r^c = V_r^a \cos(\theta_r^a + 120°) + jV_r^a \sin(\theta_r^a + 120°) \end{cases} \tag{6.14}$$

Beyond that, as the angle θ_r^a must be set, for instance, to 0°, equation (6.14) can be rewritten as (6.15). These equations must be used as perfect measurements (also referred in the literature as virtual measurements or constraints) and, therefore, associated with high weights in the normal equation or treated as equality constraints in the Sparse Tableau.

$$\begin{cases} V_{re,r}^a = V_r^a \\ V_{im,r}^a = 0 \\ V_{re,r}^b = V_r^a \cos(-120°) \\ V_{im,r}^b = V_r^a \sin(-120°) \\ V_{re,r}^c = V_r^a \cos(+120°) \\ V_{im,r}^c = V_r^a \sin(+120°) \end{cases} \tag{6.15}$$

Considering that the reference bus r is the internal bus of the Thévenin equivalent circuit representing the system upstream the substation, the state vector for the AMBSE and BCBSE can be rewritten, respectively, as (6.16) and (6.17). Note that a fictitious bus and a fictitious branch representing the Thévenin equivalent circuit were added to the distribution system. Therefore, equation (6.17) applies to all $N_{\text{buses}} - 1$ branches, given the system is radial, plus the branch of the Thévenin equivalent circuit*:

$$\boldsymbol{x} = \begin{pmatrix} V_{re,r}^i & V_{re,k}^i & V_{im,r}^i & V_{im,k}^i \end{pmatrix}^T, \quad i \in \{a,b,c\}, \quad k \in \{1,2,...,N_{\text{buses}}+1\} \tag{6.16}$$

$$\boldsymbol{x} = \begin{pmatrix} I_{re,km}^i & I_{im,km}^i & V_{re,r}^i & V_{im,r}^i \end{pmatrix}^T, \quad i \in \{a,b,c\}, \quad km \in \{1,2,...,N_{\text{buses}}\} \tag{6.17}$$

In (6.16) and (6.17), $V_{re,r}^i$ and $V_{im,r}^i$ stand, respectively, for the real and imaginary parts of the complex voltages at phases $i \in \{a,b,c\}$ of the reference bus r.

Given that six new state variables are added to the problem due to the reference bus, the real and imaginary parts of the null current injections on the three phases of the substation bus can be included as perfect measurements. Therefore, the real and imaginary parts of these injections must be associated with high weights in the normal equation or treated as equality constraints in the Sparse Tableau.

*In meshed systems a set of N_{buses}-1 branches forming a spanning tree needs to be selected [29].

According to (6.15), given the reference bus is a balanced bus, indeed, only one unknown variable, V_r^a, is added to the problem. Therefore, instead of including six new state variables, $V_{re,r}^i$ and $V_{im,r}^i$, it is possible to reduce of the number the state variables as proposed in Ref. [28]. For the sake of simplicity, the six state variables will be considered in this chapter.

6.3.5 WLS solution via normal equation

The measurements model for the AMBSE and the BCBSE is shown in (6.18), where vector $z(x)$ contains the equivalent measurements, and Hx is the set of linear equations relating the equivalent measurements to the state variables x. The vector e contains the errors inherent to the equivalent measurements [15]:

$$z(x) = Hx + e \tag{6.18}$$

The WLS solution is obtained by minimising the objective function (6.19), where W is the weighting matrix and $z(x) - Hx$ contains the residuals of the measurement. W is usually a diagonal matrix where the inverse of the variances is used as weights. The inverse of the covariance matrix of the equivalent measurements can also be used as W. Beyond that, the weight can be set according to the application. Details regarding W for the AMBSE and the BCBSE can be found, for instance, in Refs. [15, 28]:

$$J(x) = \tfrac{1}{2}(z(x) - Hx)^T W(z(x) - Hx) \tag{6.19}$$

By applying the Gauss–Newton method, the vector x that minimises (6.19) is obtained by solving iteratively the equations in (6.20). This is the so-called normal equation and it is characterised by the presence of the Gain matrix G obtained by squaring the Jacobian matrix H, i.e. $G = H^T WH$.

$$\begin{aligned} G\Delta x^\eta &= H^T W[z(x^\eta) - Hx^\eta] \\ x^{\eta+1} &= x^\eta + \Delta x^\eta \end{aligned} \tag{6.20}$$

The equations in (6.20) can be reduced to (6.21). As the Gain matrix G can be maintained constant, it is build and factorised just once. This simplifies the calculations and significantly reduces the computational times [15]:

$$x^{\eta+1} = G^{-1} H^T W z(x^\eta) \tag{6.21}$$

The normal equation is a fair, reliable and widely accepted way to find the WLS solution for distribution systems SEs. However, under particular conditions, it can experience numerical instabilities [1, 26]. In these cases, the Sparse Tableau is a strongly recommended alternative. In the Sparse Tableau, the Gain matrix (the square of the Jacobian matrix) does not appear, reducing the condition number of the coefficient matrix (the Tableau) and, consequently, increasing the numerical stability of the solution process [1, 26]. The Sparse Tableau for the AMBSE and the BCBSE is shown in (6.22):

$$\begin{pmatrix} R & H & 0 \\ H^T & 0 & C^T \\ 0 & C & 0 \end{pmatrix} \begin{pmatrix} \mu \\ x^{\eta+1} \\ \lambda \end{pmatrix} = \begin{pmatrix} z(x^{\eta}) \\ 0 \\ -c(x^{\eta}) \end{pmatrix} \tag{6.22}$$

In the Sparse Tableau, the equivalent measurements obtained from the perfect measurements (also known as virtual measurements or constraints), i.e. the zero injections and the voltages (6.15), are represented in vector $c(x^{\eta})$. The remaining equivalent measurements are maintained in $z(x^{\eta})$. Thus, the Jacobian matrix C refers to the perfect measurements and the Jacobian matrix H refers to the equivalent measurements (actual and pseudo). R contains the variances and covariances of the measurements placed in H and μ that are the vectors containing the Lagrange multipliers. Similar to the normal equation, in the Sparse Tableau for the AMBSE and BCBSE, $x^{\eta+1}$ can be directly obtained from x^{η}.

6.4 Jacobian matrix of the AMBSE

In both AMBSE and BCBSE, the size of the Jacobian matrix is $N_{\text{mea}} \times 6N_{\text{buses}} + 6$, where N_{mea} is the number of equivalent measurements, and $6N_{\text{buses}} + 6$ is the number of state variables. Recall that there are 6 state variables per bus and 6 additional state variables due to the reference bus. As a result, the Gain matrix $G = H^T WH$ is a square matrix sized $6N_{\text{buses}} + 6$.

In both SEs, the available measurements (perfect, actual and pseudo) need to be written (or converted when required) as complex currents or complex voltages to be included in the Jacobian Matrix. Given that, every row of the Jacobian matrix will contain the derivatives of the equations representing the real or the imaginary parts of these complex currents and voltages regarding the state variables. In the following, the derivatives that form the Jacobian matrix of the AMBSE are presented.

6.4.1 Derivatives of the complex current injections

By applying Kirchhoff's current law (KCL) to a power system, it is possible to write the complex currents injected into the buses as a product of the nodal system admittance matrix, $Y = G + jB$ and the complex bus voltages as (6.23), where G is the nodal system conductance matrix, and B is the nodal system susceptance matrix [30, 31]:

$$\begin{pmatrix} I^i_{re,k} \\ I^i_{im,k} \end{pmatrix} = \begin{pmatrix} G & -B \\ B & G \end{pmatrix} \begin{pmatrix} V^i_{re,k} \\ V^i_{im,k} \end{pmatrix}, \quad i \in \{a, b, c\}, \quad k \in \{1, 2, ..., N_{\text{buses}} + 1\} \tag{6.23}$$

From (6.23), the nonzero derivatives of the real and imaginary parts of the currents injected on bus k regarding the state variables of the AMBSE are shown from (6.24a) to (6.24d), where the phases i and $j \in \{a, b, c\}$ and the bus $m \in \{1, 2, ..., N_{\text{buses}} + 1\}$. Observe that the internal bus of the Thévenin equivalent representing the system upstream the substation, used as reference bus, is included in the nodal admittance matrix:

$$\frac{\partial I^{i}_{re,k}}{\partial V^{j}_{re,m}} = G^{i,j}_{km} \tag{6.24a}$$

$$\frac{\partial I^{i}_{re,k}}{\partial V^{j}_{im,m}} = -B^{i,j}_{km} \tag{6.24b}$$

$$\frac{\partial I^{i}_{im,k}}{\partial V^{j}_{re,m}} = B^{i,j}_{km} \tag{6.24c}$$

$$\frac{\partial I^{i}_{im,k}}{\partial V^{j}_{im,m}} = G^{i,j}_{km}. \tag{6.24d}$$

6.4.2 Derivatives of the complex current flows

Consider a branch connecting two buses, k and m. Recall that in this chapter the shunt admittances of the branches are disregarded [21]. Therefore, the real and imaginary parts of the currents flowing in this branch can be written as (6.25) and (6.26), respectively, where the phases i and $j \in \{a, b, c\}$, and g and b refer to the series conductances and series susceptances of the branch km [30, 31]:

$$I^{i}_{re,km} = \sum_{j} \left(g^{i,j}_{km}(V^{j}_{re,k} - V^{j}_{re,m}) - b^{i,j}_{km}(V^{j}_{im,k} - V^{j}_{im,m}) \right) \tag{6.25}$$

$$I^{i}_{im,km} = \sum_{j} \left(b^{i,j}_{km}(V^{j}_{re,k} - V^{j}_{re,m}) + g^{i,j}_{km}(V^{j}_{im,k} - V^{j}_{im,m}) \right) \tag{6.26}$$

From (6.25) and (6.26), the nonzero derivatives of the real and imaginary parts of the currents flowing in the branch km regarding the state variables of the AMBSE are shown from (6.27a) to (6.27d), where the phases i and $j \in \{a, b, c\}$:

$$\frac{\partial I^{i}_{re,km}}{\partial V^{j}_{re,n}} = \begin{cases} g^{i,j}_{km}, & \text{if } n = k \\ -g^{i,j}_{km}, & \text{if } n = m \end{cases} \tag{6.27a}$$

$$\frac{\partial I^{i}_{re,km}}{\partial V^{j}_{im,n}} = \begin{cases} -b^{i,j}_{km}, & \text{if } n = k \\ b^{i,j}_{km}, & \text{if } n = m \end{cases} \tag{6.27b}$$

$$\frac{\partial I^{i}_{im,km}}{\partial V^{j}_{re,n}} = \begin{cases} b^{i,j}_{km}, & \text{if } n = k \\ -b^{i,j}_{km}, & \text{if } n = m \end{cases} \tag{6.27c}$$

$$\frac{\partial I^{i}_{im,km}}{\partial V^{j}_{im,n}} = \begin{cases} g^{i,j}_{km}, & \text{if } n = k \\ -g^{i,j}_{km}, & \text{if } n = m \end{cases} \tag{6.27d}$$

6.4.3 Derivatives of the equivalent voltages

As stated in Section 6.3.2.2, the voltage magnitude measurements $V^{i,\text{mea}}_{k}$ are written as $V^{i,\text{equ}}_{re,k}$ according to (6.6) and (6.7) resulting into (6.28), with the angles ϕ^{i}_{k} set to 0°, −120° and +120° for phases a, b and c, respectively:

$$V^{i,\text{equ}}_{re,k} = V^{i}_{re,k} \cos \phi^{i}_{k} - V^{i}_{im,k} \sin \phi^{i}_{k} \tag{6.28}$$

From (6.28), the nonzero derivatives of the equivalent voltage magnitude $V_{re,k}^{i,\text{equ}}$ regarding the state variables of the AMBSE are, respectively, (6.29a) and (6.29b), where the phases $i \in \{a, b, c\}$:

$$\frac{\partial V_{re,k}^{j,\text{equ}}}{\partial V_{re,k}^{i}} = \cos \phi_k^i \tag{6.29a}$$

$$\frac{\partial V_{re,k}^{j,\text{equ}}}{\partial V_{im,k}^{i}} = -\sin \phi_k^i \tag{6.29b}$$

If the voltage measurements are obtained from μ-PMUs, the real and imaginary parts of the complex voltages, $V_{re,k}^{i}$ and $V_{im,k}^{i}$, are directly measured. In this case, the derivatives of the real and imaginary parts of the complex voltages measured in bus k regarding, respectively, the real and imaginary parts of the voltages on bus k are unitary. The remaining derivatives of $V_{re,k}^{i}$ and $V_{im,k}^{i}$ are zero.

6.4.4 Derivatives of the complex voltages of the reference bus

As recommended in Ref. [28], the reference bus r is placed in the internal bus of the Thévenin equivalent circuit representing the system upstream of the substation. As this internal bus is, by definition, a balanced bus, the constraints (6.15) must be used as perfect measurements and, therefore, associated with high weights in the normal equation or treated as equality constraints in the Sparse Tableau. Recall that in (6.15) θ_r^a was set to 0°.

From (6.15), the nonzero derivatives of the real and imaginary parts of the voltages on the reference bus r regarding the state variables of the AMBSE are, respectively, (6.30a) and (6.30b), where the phases $i \in \{a, b, c\}$:

$$\frac{\partial V_{re,r}^{i}}{\partial V_{re,r}^{i}} = 1 \tag{6.30a}$$

$$\frac{\partial V_{im,r}^{i}}{\partial V_{im,r}^{i}} = 1 \tag{6.30b}$$

6.5 Jacobian matrix of the BCBSE

In BCBSE algorithms, similar to AMBSE algorithms, the measurements are converted to rectangular complex variables. If all measurements were only current type measurements the corresponding function would be linear and as a consequence, it simplifies the Jacobian matrix construction. Therefore, based on this, Baran and Kelley [9] proposed the conversion of the power flow and power injections to equivalent current measurements as seen in (6.4). The following measurements are normally observed in BCBSE papers: power flow, power injection, current magnitude, voltage magnitude, voltage phasor, current phasor, substation voltage magnitude and substation voltage phasor.

6.5.1 Derivative of the magnitude of the current flows

The three-phase complex currents flowing in a branch connecting buses k and m are given in (6.31):

$$\dot{I}^i_{km} = I^i_{re,km} + jI^i_{im,km} \tag{6.31}$$

The magnitude of these currents can be written as (6.32):

$$I^i_{km} = \sqrt{(I^i_{re,km})^2 + (I^i_{im,km})^2} \tag{6.32}$$

In this case, the nonzero derivatives of the magnitude of the current flowing on the branch km regarding the state variables of the BCBSE are given in (6.33a) and (6.33b), where the phases $i \in \{a, b, c\}$:

$$\frac{\partial I^i_{km}}{\partial I^i_{re,km}} = \frac{I^i_{re,km}}{\sqrt{(I^i_{re,km})^2 + (I^i_{im,km})^2}} \tag{6.33a}$$

$$\frac{\partial I^i_{km}}{\partial I^i_{im,km}} = \frac{I^i_{im,km}}{\sqrt{(I^i_{re,km})^2 + (I^i_{im,km})^2}} \tag{6.33b}$$

6.5.2 Derivative of the complex current injections

As discussed earlier, the power injections need to be converted into equivalent current measurements. Based on KCL, a complex current injection on bus k can be written as the summation of the currents flowing on the branches connected to the bus, as shown in (6.34), where Ω_k is the set of branches connected to bus k:

$$\dot{I}^i_k = \sum_{km \in \Omega_k} I^i_{re,km} + jI^i_{im,km} \tag{6.34}$$

From (6.34), the nonzero derivatives of the real and imaginary parts of the equivalent complex current injection on bus k regarding the state variables of the BCBSE are given in (6.35a) and (6.35b), where l and $n \in \Omega_k$ and the phases $i \in \{a, b, c\}$:

$$\frac{\partial I^i_{re,k}}{\partial I^i_{re,ln}} = \begin{cases} 1, & \text{if } l = k \\ -1, & \text{if } n = k \end{cases} \tag{6.35a}$$

$$\frac{\partial I^i_{im,k}}{\partial I^i_{im,ln}} = \begin{cases} 1, & \text{if } l = k \\ -1, & \text{if } n = k \end{cases} \tag{6.35b}$$

6.5.3 Derivative of the complex current flows

Similar to the power injections, the power flow needs to be converted into equivalent current measurements. The nonzero derivatives of the real and imaginary parts of the equivalent complex currents flowing on branch km regarding the state variables of the BCBSE are given in (6.36a) and (6.36b), where the phases $i \in \{a, b, c\}$:

$$\frac{\partial I^{i}_{re,km}}{\partial I^{i}_{re,km}} = 1 \tag{6.36a}$$

$$\frac{\partial I^{i}_{im,km}}{\partial I^{i}_{im,km}} = 1 \tag{6.36b}$$

6.5.4 Derivative of the equivalent voltages

Similar to the AMBSE, initially the voltage magnitude measurements $V^{i,\text{mea}}_{k}$ are written as $V^{i,\text{equ}}_{re,k}$, according to (6.6) and (6.7) resulting into (6.37). The angles ϕ^{i}_{k} are set to 0°, −120° and +120° for phases a, b and c, respectively:

$$V^{i,\text{equ}}_{re,k} = V^{i}_{re,k}\cos\phi^{i}_{k} - V^{i}_{im,k}\sin\phi^{i}_{k} \tag{6.37}$$

From Ref. [22], the real and the imaginary parts of the complex bus voltages in (6.37) can be written as voltage drops in terms of branch currents, as shown in (6.38a) and (6.38b), where V^{i}_{r} refers to the voltage magnitude on the phases i of the reference bus r, and Ω_{kr} is the set of branches connecting the bus k and the reference bus r. The second parcel on the right side of these equations represents the voltage drops in the branches of the set Ω_{kr}. Note that $Z_{ln} = R_{ln} + jX_{ln}$ is the series impedance matrix of the branch ln and, $I_{re,ln}$ and $I_{im,ln}$ are the vectors containing the real and imaginary parts of the currents on the branches:

$$V^{i}_{re,k} = V^{i}_{r}\cos\theta^{i}_{r} - \left(\sum_{ln\in\Omega_{kr}} R_{ln}I_{re,ln} - X_{ln}I_{im,ln}\right)^{i} \tag{6.38a}$$

$$V^{i}_{im,k} = V^{i}_{r}\sin\theta^{i}_{r} - \left(\sum_{ln\in\Omega_{kr}} X_{ln}I_{re,ln} - R_{ln}I_{im,ln}\right)^{i} \tag{6.38b}$$

From (6.38a) and (6.38b), the nonzero derivatives of the equivalent voltages regarding the state variables of the BCBSE are given in (6.39a) and (6.39d), respectively, where $ln \in \Omega_{kr}$ and the phases i and $j \in \{a, b, c\}$. Note that the angles on the reference bus θ^{i}_{r} are known and, therefore, these derivatives are constant:

$$\frac{\partial V^{i,\text{equ}}_{re,k}}{\partial I^{j}_{re,ln}} = -R^{i,j}_{ln}\cos\phi_{k}{}^{i} - X^{i,j}_{ln}\sin\phi_{k}{}^{i} \tag{6.39a}$$

$$\frac{\partial V^{i,\text{equ}}_{re,k}}{\partial I^{j}_{im,ln}} = X^{i,j}_{ln}\cos\phi_{k}{}^{i} - R^{i,j}_{ln}\sin\phi_{k}{}^{i} \tag{6.39b}$$

$$\frac{\partial V^{i,\text{equ}}_{re,k}}{\partial V^{i}_{re,r}} = \cos\theta^{i}_{r}\cos\phi_{k}{}^{i} + \sin\theta^{i}_{r}\sin\phi_{k}{}^{i} \tag{6.39c}$$

$$\frac{\partial V^{i,\text{equ}}_{re,k}}{\partial V^{i}_{im,r}} = \cos\theta^{i}_{r}\sin\phi_{k}{}^{i} - \sin\theta^{i}_{r}\cos\phi_{k}{}^{i} \tag{6.39d}$$

6.5.5 Derivatives of the complex voltages of the reference bus

As recommended in Ref. [28], the constraints (6.15) must be used as perfect measurements in the SEs in order to guarantee the reference bus remain balanced. In (6.15) θ_r^a was set to 0°. Therefore, the nonzero derivatives of the real and imaginary parts of the voltages (6.15) on the reference bus r regarding the state variables of the BCBSE are, respectively, (6.40a) and (6.40b), where the phases $i \in \{a, b, c\}$:

$$\frac{\partial V_{re,r}^i}{\partial V_{re,r}^i} = 1 \tag{6.40a}$$

$$\frac{\partial V_{im,r}^i}{\partial V_{im,r}^i} = 1 \tag{6.40b}$$

6.6 Computational aspects

In both SEs, AMBSE and BCBSE, depending on the way voltage magnitude measurements are modelled, the resulting Jacobian matrices will be constant [20]. Beyond that, as stated in Ref. [15], the weighting matrix can be made constant, resulting in the Gain matrix, as well as the Sparse Tableau, constant. These matrices will change only if the system topology or the set of measurements is changed. As a result, these matrices are build and factorised just once during the state estimation process, which significantly speeds up the computational performance.

For AMBSE and BCBSE, the state vector is estimated by solving the normal equation (6.21) or the Sparse Tableau (6.22). For the sake of simplicity, the solution via the normal equation is being considered. Based on that, the algorithms for AMBSE and BCBSE are presented in this section.

6.6.1 AMBSE algorithm

For AMBSE, the estimated state can be found by iteratively running the following steps:

AMBSE Algorithm

1. Set the the iteration counter to one, i.e., $\eta = 1$;
2. Build and factorise the Gain matrix;
3. Set the first guess to the complex bus voltages;
4. Calculate the vector $z(x^{\eta})$;
5. Calculate $x^{\eta+1}$ according to 6.21;
6. Check for convergence;
   (a) If convergence is reached $\hat{x} = x^{\eta+1}$;
   (b) Otherwise, do $\eta = \eta + 1$ and go back to step 4;

After setting the iteration counter to one, the Gain matrix G can be built and factorised. For that, the Jacobian and the weighting matrices, H and W, respectively, are required. In the third step, the first guess to the bus voltages is required. Usually, the three-phase flat start is adopted[†]; however, the bus voltages can be obtained from recent estimates. In the fourth step, the vector containing the equivalent measurements, $z(x^{\eta})$, is updated. In the fifth step, the state vector is updated solving (6.21) and, then, in sixth step, convergence is verified. The convergence criterion can be, for instance, the one shown in (6.41). Typical values for tolerance are from 10^{-3} to 10^{-6}. This procedure is repeated until the convergence criterion is reached.

$$\max|x^{\eta+1} - x^{\eta}| \leq \text{tolerance} \tag{6.41}$$

6.6.2 BCBSE algorithm

The basic steps for the BCBSE algorithm are the same for the AMBSE. However, as in the BCBSE, the state variables are the branch currents, after the first iteration it is necessary to calculate the bus voltages from the branch currents before updating $z(x^{\eta})$. This can be done by using a forward sweep procedure similar to one adopted in the Backward/Forward load flow [21][‡].

In the first iteration, the voltages required to obtain the equivalent measurements placed in $z(x^{\eta})$ are usually the three-phase flat start.

6.7 Case studies

This section presents case studies for the AMBSE and BCBSE. The cases have been performed on the IEEE 13-Bus Test Feeder [32]. This test feeder has several key distribution system components such as overhead and underground lines, spot and distributed loads, capacitors, transformers and voltage regulators. All the details of this feeder can be found in Ref. [32]. In this case section, a modified version of the IEEE 13-bus test feeder is adopted, where for the sake of simplicity, the following modifications are considered:

- The buses are renumbered.
- The voltage regulator at the substation has been excluded.
- The switch located between buses 4 and 9 is replaced by a distribution line with a resistance of 1×10^{-4}.
- The distributed load located in lines 2–4 is concentrated at bus 3.
- The reference bus (r) placed in the internal balanced bus of the Thévenin equivalent representing the system upstream the substation is considered.

The modified IEEE 13-bus test feeder is shown in Figure 6.3. In order to estimate the system state, a set of measurements was generated from a load flow calculation run on EPRI's open-source Distribution System Simulator and OpenDSS software [33].

[†]Voltage magnitudes set at 1 p.u. and angles 120° displaced.
[‡]See the forward step of the Backward/Forward Load Flow in Chapter 5 of this book.

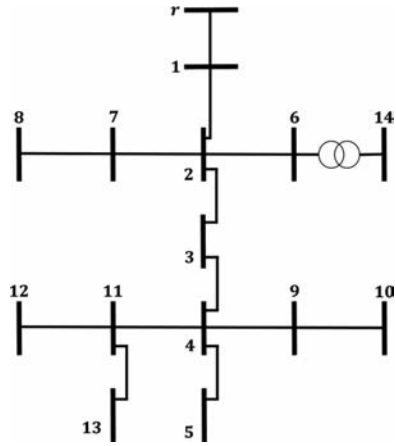

Figure 6.3 Modified IEEE 13-bus test feeder

Table 6.1 Power measurements in p.u.(1×10^{-3})

Bus	Phase a		Phase b		Phase c	
	P	***Q***	***P***	***Q***	***P***	***Q***
3	−0.143	−0.934	−0.532	−0.353	−0.942	−0.613
4	−2.669	−1.597	−3.185	−2.354	−2.511	−1.639
7	0	0	−1.471	−1.277	−0.264	−0.331
8	0	0	−1.354	−0.125	−0.552	−1.198
9	−0.283	−1.121	−3.495	−1.162	−1.092	−0.392
10	−4.239	−2.058	−0.656	−0.735	−2.489	−2.249
12	0	0	0	0	−1.445	−0.873
13	−1.034	−0.780	0	0	0	0
14	−1.546	−1.063	−1.199	−0.892	−1.154	−0.864

The power and voltage magnitude measurements are shown in Tables 6.1 and 6.2, respectively. The base power is 100 MVA and the base voltages are the nominal rated voltages of the system (4.16 or 0.48 kV).

Table 6.2 Voltage magnitude measurements in p.u.

Bus	Phase a	Phase b	Phase c
1	0.999	0.999	0.999
10	0.918	1.001	0.914
14	0.934	0.968	0.932

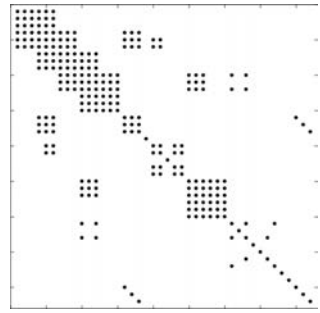

Figure 6.4 Sparsity of the admittance matrix

6.7.1 Solving the AMBSE

According to Section 6.3, the AMBSE was implemented in the MATLAB®. The estimated state was obtained by iteratively running the algorithm of the Section 6.6.1. The normal equation is used. The convergence tolerance was set to 1×10^{-3}, and the maximum iteration number was set to 20.

6.7.1.1 Data preparation and building matrix *Y*

In the AMBSE, the admittance matrix Y is required to build the Jacobian matrix H and, consequently, the Gain matrix G. Before building Y, all system data are transformed into the per-unit system (p.u.). Here, the base power is 100 MVA, and the base voltages are the nominal rated voltages of the system (4.16 or 0.48 kV). The single-phase branches and buses were modelled as three-phase by using the concept of dummy lines and buses [19]. As a result, the system admittance matrix size is 42×42 with 249 nonzero elements, as shown in Figure 6.4.

6.7.1.2 Building matrices *H*, *G* and *W*

The dimension of the Jacobian matrix is $(N_{mea}) \times (6N_{buses} + 6)$, where N_{mea} (85 measurements) is the number of equivalent measurements, and $6N_{buses} + 6 = (70 + 6)$ is the number of state variables, where the last six state variables corresponding to the reference bus placed in the internal balanced bus of the Thévenin equivalent representing the system upstream the substation (please see (6.16)). As a result, the size of the Jacobian matrix is 85×76.

For the sake of simplicity, the variances of the equivalent measurements were directly set to 1×10^{-7} and 1×10^{-5} for the equivalent current measurements and the equivalent voltage measurements, respectively. Recall that these variances can be calculated as stated on Section 6.3.3. For that, the variances of the measurements and a previous estimate of the bus voltage are required [15]. For virtual measurements, a low value is chosen for the variances, 1×10^{-8}. The inverse of these variances is used as weights to build the corresponding weighting matrix W. As a result, W has dimension of $(N_{mea} \times N_{mea})$, i.e., 85×85. With matrices H and W, the Gain matrix, $G = H^T WH$, can be built and factorised. The G matrix has dimension of

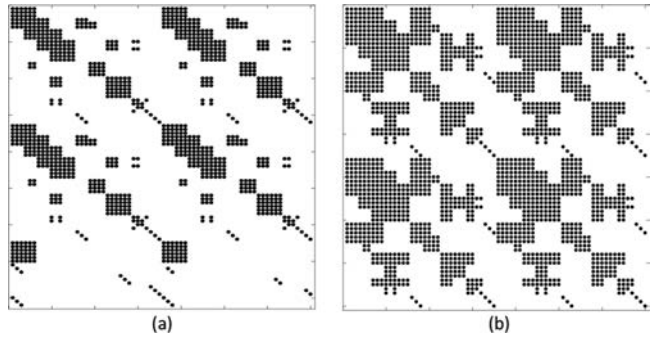

Figure 6.5 Sparsity of the (a) Jacobian and (b) Gain matrices for the AMBSE

$(6N_{\text{buses}} + 6) \times (6N_{\text{buses}} + 6)$, i.e. 76×76. Figure 6.5 shows the structure of the (*a*) Jacobian and the (*b*) Gain matrices for the AMBSE with 1017 and 2092 nonzero elements, respectively.

6.7.1.3 Initialising the system state

The system state is initialised at flat start with the voltage magnitudes set at 1 p.u. and angles for phases *a*, *b* and *c* at 0°, −120° and 120°. The iteration counter is set to $\eta = 1$.

6.7.1.4 Converting measurements into equivalent measurements

The measurement set comprises virtual measurements (at buses 1, 2, 5, 6 and 11), power injection measurements (see Table 6.1) and voltage magnitude measurements (see Table 6.2). Given that the six new state variables are added to the problem due to the reference bus, the real and imaginary parts of the null current injections of the substation bus (bus 1) were included as virtual measurements. The equivalent measurements are updated every iteration, η, once they depend on the complex bus voltages $\dot{V}_k^{i,\eta}$, as stated in Section 6.3.2. These equivalent measurements will compose the vector $z(x^{\eta})$.

6.7.1.5 Obtaining the system state for $\eta = 1$

Once the equivalent measurements $z(x^{\eta})$ and the matrices H, G and W are available, equation (6.21) is then used to calculate the state variables for the first iteration $\left(x^1\right)$.

6.7.1.6 Checking for convergence

At the end of the first iteration, the maximum mismatch is equal to 0.111, which is greater than the specified tolerance ($tol = 1 \times 10^{-3}$). Therefore, the convergence has not been reached yet and a new iteration is required. So, in order to continue the iterative process, the iteration counter must be increased and the equivalent measurements must be recalculated after every iteration. Following the execution process,

the solution is obtained in four iterations. Table 6.3 shows the system state during the solution the AMBSE.

6.7.2 Solving the BCBSE

According to Section 6.3, the BCBSE was implemented in MATLAB®. The estimated state was obtained by iteratively running the algorithm of the Section 6.6.2. The normal equation is used. The convergence tolerance was set to 1×10^{-3} and the maximum iteration number was set to 20.

6.7.2.1 Building matrices H, G and W

The dimension of the Jacobian matrix is $(N_{\text{mea}}) \times (6N_{\text{buses}} + 6)$, where N_{mea} (85 measurements) is the number of equivalent measurements and $6N_{\text{buses}} + 6 = 70 + 6$ is the number of state variables, where the last six state variables corresponding to the reference bus. Therefore, the size of the Jacobian matrix is 85×76.

Similar to the AMBSE, the variances of the equivalent measurements were directly set to 1×10^{-7} and 1×10^{-5} for the equivalent current measurements and the equivalent voltage measurements, respectively. Again, for virtual measurements, the variances were set to 1×10^{-8}. The inverse of these variances is used as weights to build the corresponding weighting matrix W. As a result, W has dimension of $(N_{\text{mea}}) \times (N_{\text{mea}})$, i.e. 85×85. With matrices H and W, the Gain matrix, $G = H^T WH$, can be built and factorised. The G matrix has dimension of $(6N_{\text{buses}} + 6) \times (6N_{\text{buses}} + 6)$, i.e. 76×76.

Figure 6.6 shows the structures of the (*a*) Jacobian and the (b) Gain matrices for the BCBSE with 282 and 1754 nonzero elements, respectively. The Jacobian and the Gain matrices of the BCBSE are sparser than the matrices for the AMBSE. However, it should be noticed that the sparsity of the H and G matrices for the BCBSE is significantly deteriorated as the number of voltage measurements increase.

6.7.2.2 Initialising the system states

The system state is initialised at a flat start with the voltage magnitudes set at 1 p.u. and angles set for phases *a*, *b* and *c* at 0°, −120° and 120°. Besides, the iteration counter is set at $\eta = 1$.

6.7.2.3 Converting conventional into equivalent measurements

The measurement set is the same adopted for the AMBSE, including the virtual measurements.

6.7.2.4 Obtaining the system state $\eta = 1$

Once the equivalent measurements $z(x^{\eta})$ and the matrices H, G and W are available, equation (6.21) is then used to calculate the state variables for the first iteration $\left(x^{1}\right)$. Then, it is necessary to calculate the bus voltages from the branch currents before updating $z(x^{\eta})$.

Table 6.3 System state during the iterative process of the AMBSE

		$\eta = 2$		$\eta = 3$		$\eta = 4$	
Bus	**Phase**	V **(p.u.)**	Ang. (°)	V **(p.u.)**	Ang. (°)	V **(p.u.)**	Ang. (°)
1	1	0.999	−0.011	0.999	−0.011	0.999	−0.011
1	2	0.999	−120.010	0.999	−120.010	0.999	−120.010
1	3	0.999	119.987	0.999	119.987	0.999	119.987
2	1	0.962	−2.137	0.962	−2.137	0.962	−2.137
2	2	0.989	−121.547	0.989	−121.547	0.989	−121.547
2	3	0.954	118.111	0.954	118.111	0.954	118.111
3	1	0.954	−2.907	0.953	−2.927	0.952	−2.934
3	2	0.990	−121.746	0.991	−121.749	0.991	−121.747
3	3	0.942	117.521	0.941	117.558	0.941	117.555
4	1	0.938	−4.491	0.933	−4.556	0.933	−4.577
4	2	0.995	−122.134	0.997	−122.152	0.997	−122.147
4	3	0.924	116.532	0.919	116.641	0.919	116.631
5	1	0.938	−4.491	0.932	−4.556	0.933	−4.577
5	2	0.995	−122.134	0.997	−122.152	0.998	−122.146
5	3	0.924	116.532	0.919	116.641	0.919	116.631
6	1	0.957	−2.164	0.959	−2.186	0.959	−2.183
6	2	0.987	−121.561	0.988	−121.581	0.988	−121.582
6	3	0.949	118.186	0.951	118.115	0.952	118.117
7	2	0.980	−121.692	0.981	−121.678	0.981	−121.678
7	3	0.952	118.141	0.952	118.148	0.952	118.148
8	2	0.979	−121.757	0.979	−121.741	0.979	−121.741
8	3	0.950	118.189	0.951	118.201	0.951	118.201
9	1	0.931	−4.693	0.925	−4.723	0.925	−4.745
9	2	0.997	−122.298	0.999	−122.328	0.999	−122.323
9	3	0.921	116.512	0.916	116.643	0.916	116.633
10	1	0.926	−4.939	0.919	−4.942	0.918	−4.965
10	2	0.999	−122.460	1.001	−122.503	1.001	−122.499
10	3	0.919	116.529	0.913	116.683	0.914	116.673
11	1	0.936	−4.508	0.931	−4.569	0.931	−4.589
11	3	0.922	116.432	0.917	116.552	0.917	116.542
12	3	0.920	116.297	0.915	116.426	0.914	116.414
13	1	0.9245	−4.4714	0.9257	−4.4996	0.9257	−4.4995
14	1	0.934	−2.924	0.934	−2.924	0.934	−2.921
14	2	0.969	−122.091	0.968	−122.087	0.968	−122.089
14	3	0.931	117.651	0.932	117.587	0.932	117.591

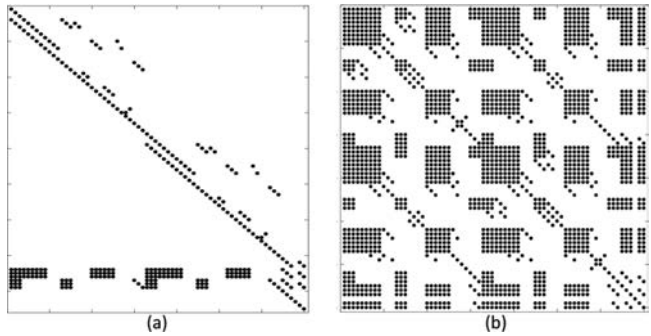

Figure 6.6 Sparsity of the (a) Jacobian and (b) Gain matrices for the BCBSE

6.7.2.5 Checking for convergence

At the end of the first iteration, the maximum mismatch is equal to 0.0159, which is greater than the specified tolerance (10^{-3}). Therefore, the convergence is not reached and a new iteration is run. So, in order to continue the iterative process, the iteration counter must be increased, and the equivalent measurements must be recalculated after every iteration. Following the execution process, the solution is obtained in 4 iterations. Table 6.4 shows the system voltages during the solution the BCBSE.

6.8 Conclusion

In this chapter, a review of classical SEs developed to distribution systems has been presented. Amongthose, two SEs have been thoroughly analysed, where the measurement modelling, mathematical formulation, algorithm and tests have been presented with a reference IEEE Test feeder. The AMBSE and BCBSE have been presented concurrently due to their similarities. The AMBSE and the BCBSE are viable and interesting alternative to classical Newton–Raphson SE due to the usage of constant Jacobian matrix and consequently a constant Gain matrix can be obtained. The main idea of AMBSE and BCBSE is the adoption of the complex nodal voltage and complex branch current in rectangular coordinates as state variables, respectively. Some comparisons between the two methods have shown that BCBSE presents higher sparsity in its Jacobian matrix when compared with the classical Newton–Raphson SE and AMBSE, which can benefit even more from sparse matrix techniques. However, this sparse feature is affected when voltage measurements are included in the measurement model. Another practical issue presented is how the angular references must be specified for these three-phase SEs. One option is to place balanced angular reference at the substation bus, which corresponds to balanced voltages at this bus. However, this assumption adds errors to the estimated state. In order to overcome this problem for unbalanced feeders, in this chapter, the angular reference is placed in the internal balanced bus of the Thévenin equivalent circuit representing the system upstream the substation.

Table 6.4 Bus voltages during the iterative process of the BCBSE

		$\eta = 2$		$\eta = 3$		$\eta = 4$	
Bus	**Phase**	***V* (p.u.)**	**Ang. (°)**	***V* (p.u.)**	**Ang. (°)**	***V* (p.u.)**	**Ang. (°)**
1	1	0.9923	0.0021	1.0000	0.0184	0.9998	−0.0109
1	2	1.0019	−120.0497	0.9996	−120.0239	0.9999	−120.0108
1	3	0.9940	120.1236	1.0002	120.0013	0.9998	119.9878
2	1	0.9545	−2.1405	0.9620	−2.1340	0.9620	−2.1374
2	2	0.9916	−121.5836	0.9895	−121.5485	0.9895	−121.5472
2	3	0.9481	118.2423	0.9540	118.1118	0.9540	118.1111
3	1	0.9468	−2.9164	0.9524	−2.9316	0.9524	−2.9338
3	2	0.9928	−121.7828	0.9913	−121.7478	0.9913	−121.7472
3	3	0.9370	117.6532	0.9410	117.5548	0.9410	117.5548
4	1	0.9309	−4.5150	0.9325	−4.5773	0.9325	−4.5772
4	2	0.9974	−122.1720	0.9973	−122.1468	0.9973	−122.1468
4	3	0.9181	116.6652	0.9186	116.6314	0.9186	116.6314
5	1	0.9309	−4.5150	0.9325	−4.5773	0.9325	−4.5772
5	2	0.9974	−122.1720	0.9973	−122.1468	0.9973	−122.1468
5	3	0.9181	116.6652	0.9186	116.6314	0.9186	116.6314
6	1	0.9499	−2.1673	0.9590	−2.1841	0.9591	−2.1830
6	2	0.9899	−121.5969	0.9876	−121.5814	0.9876	−121.5816
6	3	0.9436	118.3154	0.9515	118.1138	0.9516	118.1162
7	2	0.9829	−121.7280	0.9806	−121.6776	0.9806	−121.6777
7	3	0.9466	118.2730	0.9523	118.1486	0.9523	118.1480
8	2	0.9814	−121.7934	0.9790	−121.7401	0.9790	−121.7407
8	3	0.9449	118.3210	0.9506	118.2019	0.9506	118.2013
9	1	0.9240	−4.7185	0.9248	−4.7450	0.9248	−4.7450
9	2	0.9994	−122.3364	0.9994	−122.3234	0.9994	−122.3234
9	3	0.9152	116.6465	0.9154	116.6339	0.9154	116.6339
10	1	0.9183	−4.9648	0.9183	−4.9647	0.9183	−4.9647
10	2	1.0014	−122.4992	1.0014	−122.4992	1.0014	−122.4992
10	3	0.9135	116.6651	0.9135	116.6734	0.9135	116.6734
11	1	0.9293	−4.5323	0.9308	−4.5900	0.9308	−4.5899
11	3	0.9163	116.5662	0.9165	116.5424	0.9165	116.5424
12	3	0.9145	116.4311	0.9144	116.4146	0.9144	116.4147
13	1	0.9245	−4.4714	0.9257	−4.4996	0.9257	−4.4995
14	1	0.9275	−2.9335	0.9342	−2.9275	0.9344	−2.9210
14	2	0.9715	−122.1264	0.9683	−122.0858	0.9682	−122.0885
14	3	0.9259	117.7793	0.9320	117.5805	0.9322	117.5907

References

[1] Monticelli A. *State estimation in electric power systems: a generalized approach*. New York: Springer Science & Business Media; 1999, vol. 507.

[2] Celik M.K., WHE L. 'A practical distribution state calculation algorithm'. *IEEE Power Engineering Society. 1999 Winter Meeting (Cat. No.99CH36233)*; 1999. pp. 442–7.

[3] Ghosh A.K., Lubkeman D.L., Downey M.J., Jones R.H. 'Distribution circuit state estimation using a probabilistic approach'. *IEEE Transactions on Power Systems*. 1997, vol. 12(1), pp. 45–51.

[4] Singh R., Pal B.C., Jabr R.A. 'Distribution system state estimation through Gaussian mixture model of the load as pseudo-measurement'. *IET Generation, Transmission & Distribution*. 2010, vol. 4(1), pp. 50–9.

[5] Schweppe F., Wildes J., Rom D.B. 'Power system static-state estimation, part I: Exact model'. *IEEE Transactions on Power Apparatus and Systems*. 1970, vol. PAS-89(1), pp. 120–5.

[6] Schweppe F., Rom D. 'Power system static-state estimation, part II: Approximate model'. *IEEE Transactions on Power Apparatus and Systems*. 1970, vol. PAS-89(1), pp. 125–30.

[7] Pau M., Pegoraro P.A., Sulis S. 'Performance of three-phase WLS distribution system state estimation approaches'. *Applied Measurements for Power Systems (AMPS), 2015 IEEE International Workshop on. IEEE*; 2015. pp. 138–43.

[8] Baran M.E., Kelley A.W. 'State estimation for real-time monitoring of distribution systems'. *IEEE Transactions on Power Systems*. 1994, vol. 9(3), pp. 1601–9.

[9] Baran M.E., Kelley A.W. 'A branch-current-based state estimation method for distribution systems'. *IEEE Transactions on Power Systems*. 1995, vol. 10(1), pp. 483–91.

[10] Lu C.N., Teng J.H., Liu W.-H.E. 'Distribution system state estimation'. *IEEE Transactions on Power Systems*. 1995, vol. 10(1), pp. 229–40.

[11] Roytelman I., Shahidehpour S.M. 'State estimation for electric power distribution systems in quasi real-time conditions'. *IEEE Transactions on Power Delivery*. 1993, vol. 8(4), pp. 2009–15.

[12] Lin W.M., Teng J.H., Chen S.J. 'A highly efficient algorithm in treating current measurements for the branch-current-based distribution state estimation'. *IEEE Transactions on Power Delivery*. 2001, vol. 16(3), pp. 433–9.

[13] Teng J.-H. 'Using voltage measurements to improve the results of branch-current-based state estimators for distribution systems'. *IEE Proceedings - Generation, Transmission and Distribution*. 2002, vol. 149(6), pp. 667–72.

[14] Baran M.E., Jung J., McDermott T.E. 'Including voltage measurements in branch current state estimation for distribution systems'. *IEEE Power Energy Society General Meeting*; Calgary, Alberta, Canada, 26–30 July; 2009. pp. 1–5.

[15] de Almeida M.C., Ochoa L.F. 'An improved three-phase AMB distribution system state estimator'. *IEEE Transactions on Power Systems*. 2016, vol. 32(2), pp. 1–1473.

[16] Lin W.-M., Teng J.-H. 'Distribution fast decoupled state estimation by measurement pairing'. *IEE Proceedings - Generation, Transmission and Distribution*. 1996, vol. 143(1), pp. 43–8.

[17] Guo Y., Wu W., Zhang B., Sun H. 'An efficient state estimation algorithm considering zero injection constraints'. *IEEE Transactions on Power Systems*. 2013 Aug, vol. 28(3), pp. 2651–9.

[18] Fernandes T.R., Venkatesh B., de Almeida M.C. 'Symmetrical components based state estimator for power distribution systems'. *IEEE Transactions on Power Systems*. 2021, vol. 36(3), pp. 2035–45.

[19] Abdel-Akher M., Nor K.M. 'Representing single-phase and two-phase lines with dummy lines and dummy nodes' in Hassan M.Y. (ed.). *Recent Developments in Three Phase Load Flow Analysis*. Malaysian Book Publishers Association; 2008. pp. 107–12.

[20] Ugarte L.F., Tuo J., de Almeida M.C. 'Assessing approaches to modeling voltage magnitude measurements in state estimators devoted to active distribution networks'. *Electric Power Systems Research*. 2021, vol. 200(1), pp. 107440–10.

[21] Kersting W.H (ed.):. *Distribution System Modeling and Analysis*. 4th ed. Boca Raton, FL: CRC Press; 2017.

[22] Baran M.E., Jung J., McDermott T.E. Topology error identification using branch current state estimation for distribution systems. *IEEE Transmission & Distribution Conference & Exposition: Asia and Pacific*; Seoul, Korea, 26 - 30 Oct; 2009. pp. 1–4.

[23] Pau M., Pegoraro P.A., Sulis S. 'Efficient branch-current-Based distribution system state estimation including synchronized measurements'. *IEEE Transactions on Instrumentation and Measurement*. 2013 Sept, vol. 62(9), pp. 2419–29.

[24] Silva R.S., Almeida M.C. Voltage measurements and the sparsity of coefficient matrices in distribution systems state estimation. *IEEE Power Energy Society General Meeting*; Chicago, Illinois, US, 16 - 20 Jul; 2017. pp. 1–5.

[25] Haughton D.A., Heydt G.T. 'A linear state estimation formulation for smart distribution systems'. *IEEE Transactions on Power Systems*. 2013, vol. 28(2), pp. 1187–95.

[26] Abur A., Exposito A.G. *Power System State Estimation: Theory and Implementation*. Boca Raton, FL: CRC Press; 2004.

[27] de Almeida M.C., Asada E.N., Garcia A.V. 'A new method for redundancy analysis of measurements applied to three-phase state estimation'. *Electric Power Systems Research*. 2009, vol. 79(1), pp. 234–8.

[28] Schincariol da Silva R., Fernandes T.R., Almeida M.C. 'Specifying angular reference for three-phase distribution system state estimators'. *IET Generation, Transmission & Distribution*. 2018, vol. 12(7), pp. 1655–63.

[29] Almeida M.C., Asada E.N., Garcia A.V. A numerical method for finding spanning trees in power system state estimation. *International Conference on Power System Technology*; Chongqing, China, 22 - 26 Oct; 2006. pp. 1–6.

[30] Arrillaga J., Arnold C.P. *Computer Analysis of Power Systems*. 1st ed. Chichester, UK: John Wiley & Sons; 1990.

[31] Das J.C. *Short-Circuit Load Flow and Harmonics*. 2nd ed. 1092. Boca Raton, FL: CRC Press; 2017.

[32] Kersting W.H. 'Radial distribution test feeders'. *IEEE Transactions on Power Systems*. 1991, vol. 6(3), pp. 975–85.
[33] Dugan R.C., McDermott T.E. 'An open source platform for collaborating on smart grid research'. *IEEE Power and Energy Society General Meeting*; Detroit - Michigan - US, 24–28 Jul; 2011. pp. 1–7.

Chapter 7

Fast-decoupled power flow method for active distribution systems

Odilon Luis Tortelli[1], Elizete Maria Lourenço[1], Bikash Chandra Pal[2], Ariovaldo Verandio Garcia[3], and Renan Kovalczuk Portelinha[1]

7.1 Introduction

Distributed generation (DG) brought significant changes to the planning and operation of distribution systems (DS). The presence of DG, allied with advanced technologies of measurement and control related to Smart Grid concepts, converts the DS into active networks, subject to bidirectional power flows. As a consequence, aiming to improve the efficiency and reliability of the power supply, active networks begin to operate more often as closed-loop circuits or even as fully meshed topologies.

This context points to the need to update traditional computational methods related to DS analysis to incorporate the consequences of technological advances. At the same time, such updated methods must still consider intrinsic invariable characteristics of the distribution networks, like the low-voltage levels and the low X/R ratio of DS lines.

This chapter presents a fast-decoupled power flow (FDPF) formulation combined with the complex per unit (*cpu*) normalization technique that extends the well-known efficiency of FDPF algorithm to active distribution system analysis. The formulation bases of power flow calculation and *cpu* technique are fully described. Simulation results with DS under distinct operational conditions are presented to demonstrate the effectiveness and versatility of the *cpu*-based FDPF approach.

[1]Department of Electrical Engineering, Federal University of Parana, Curitiba, Brazil
[2]Department of Electrical and Electronic Engineering, Imperial College London, London, UK
[3]Retired from Electrical and Computing Engineering, Universidade Estadual de Campinas (UNICAMP), Campinas, SP, Brazil

7.1.1 Power flow analysis for active DS

The power flow calculation is one of the basic studies for different stages of power systems planning and operation. One of the most widespread power flow approaches is the Newton–Raphson power flow (NRPF) method [1]. This traditional method, distinguished by its quadratic convergence characteristic, is usually able to solve the power flow problem with adequate precision in a few iterations, regardless of the size of the system. Nevertheless, this attractive qualities come with high computational costs.

To alleviate the computational burden of the NRPF, the FDPF method incorporates simplifications to the linearized NRPF system of equations related to typical characteristics of transmission lines. The application of such simplifications allows dividing the linearized NRPF system of equations into two independent subsets, one active and one reactive, and also making the Jacobian matrices constant. The significant reduction in computational cost achieved with the fast-decoupled approach has made FDPF the standard method for transmission systems power flow analysis [2].

However, the FDPF method presents convergence problems when applied to power networks with low X/R ratio lines, which is typical in DS [3]. Several proposals were presented to circumvent the limitations of the fast-decoupled approach to deal with distribution system analysis [3–10].

From a distinct perspective of the power flow problem and based on characteristics, such as radial topology and unidirectional power flows, backward-forward sweep (BFS) methods [11] were proposed and became the standard approach for power flow analysis of conventional passive DS. Further developments to enhance convergence properties and to provide ability to handle weakly meshed networks and presence of DG to BFS methods are presented in [12, 13].

7.2 Basics of Newton–Raphson-based power flow

7.2.1 Fundamentals of the power flow analysis

The fundamental equations that define the power flow problem are the active and reactive power injection equations [14] defined at each system bus as:

$$P_k = V_k \sum_{m \in \kappa} V_m \left(G_{km} \cos \theta_{km} + B_{km} \sin \theta_{km}\right) \tag{7.1}$$

$$Q_k = V_k \sum_{m \in \kappa} V_m \left(G_{km} \sin \theta_{km} - B_{km} \cos \theta_{km}\right) \tag{7.2}$$

where k and m represent the bus indexes, and κ indicates the set of buses connected to bus k, plus bus k itself.

These two equations are composed of the parameters conductance (G) and susceptance (B), which contain all the information relating the physical structure of the power network, and four electrical variables, defined as:

- bus voltage magnitude, V
- bus voltage angle, θ

- bus active power injection, P
- bus reactive power injection, Q

To be solvable, only two of the bus variables can remain unknown. The other two must have values assigned relating to the operating condition of the power system. Based on this, all system buses are classified into three main categories:

1. PQ: buses where the values of the active and reactive power injection are known;
2. PV: buses where the values of the active power injection and the voltage magnitude are known;
3. $V\theta$: bus where the voltage angle is known, to provide the angular reference to the system (hence known as *reference bus*), and where the active power injection must remain unknown, to enable the systems active power balance (hence also known as *slack* or *swing bus*).

Thus, considering the nonlinear nature of the equations, the solution to the power flow problem consists of two stages:

1. Iterative stage: From the loads (and, eventually, power sources) reported as power injections, the magnitudes and angles of the unknown bus voltages, which are the problem state variables, are determined.
2. Noniterative stage: The voltages at all buses being known, the unknown injections can be calculated, as well as the power flows and losses in any element of the power network.

7.2.2 NRPF formulation

The Newton–Raphson method consists of applying successive linear approximations around the state variables of the problem's set of equations, until the solution is reached within a required precision margin. From the Taylor Series expansion, a linear system approximation, to be solved at each iteration, is given by:

$$\mathbf{g}(\mathbf{x}^{(v)}) = -\mathbf{J}(\mathbf{x}^{(v)})\Delta\mathbf{x}^{(v)} \tag{7.3}$$

where:

- $\mathbf{x}^{(v)}$: state variables vector evaluated at iteration (v)
- $\mathbf{g}(\mathbf{x}^{(v)})$: vector of the nonlinear functions of the problem (v)
- $\mathbf{J}(\mathbf{x}^{(v)})$: Jacobian matrix, formed by the partial derivatives of the nonlinear equations in relation to the state variables, evaluated at iteration (v)
- $\Delta\mathbf{x}^{(v)}$: state variable increments vector at iteration (v)

By applying the Newton–Raphson method to solve the iterative stage of the power flow problem, the general formulation of the linearized system of equations takes the following form [1]:

$$\begin{pmatrix} \Delta\mathbf{P} \\ \Delta\mathbf{Q} \end{pmatrix}^{(v)} = \begin{pmatrix} \mathbf{H} & \mathbf{N} \\ \mathbf{M} & \mathbf{L} \end{pmatrix}^{(v)} \begin{pmatrix} \Delta\theta \\ \Delta\mathbf{V} \end{pmatrix}^{(v)} \tag{7.4}$$

where $\Delta\mathbf{P}$ and $\Delta\mathbf{Q}$ are, respectively, the active and reactive power mismatches vectors, defined by the differences, at iteration v, between specified (spec) and calculated (calc) power injections, as:

$$\begin{cases} \Delta\mathbf{P}^{(v)} = \mathbf{P}^{\text{spec}} - \mathbf{P}^{\text{calc}}(\mathbf{V}^{(v)}, \theta^{(v)}) \\ \Delta\mathbf{Q}^{(v)} = \mathbf{Q}^{\text{spec}} - \mathbf{Q}^{\text{calc}}(\mathbf{V}^{(v)}, \theta^{(v)}) \end{cases} \tag{7.5}$$

Also, **H**, **N**, **M**, and **L** are the Jacobian submatrices of partial derivatives of power injections with respect to the state variables, which are evaluated at each iteration and whose main diagonal (kk) and off-diagonal (km, with $m \neq k$) elements are defined as:

$$\mathrm{H}\begin{cases} H_{km} = \partial P_k/\partial\theta_m = V_k V_m(G_{km}\sin\theta_{km} - B_{km}\cos\theta_{km}) \\ \\ H_{kk} = \partial P_k/\partial\theta_k = -Q_k^{calc} - V_k^2 B_{kk} \end{cases} \tag{7.6}$$

$$\mathrm{N}\begin{cases} N_{km} = \partial P_k/\partial V_m = V_k(G_{km}\cos\theta_{km} + B_{km}\sin\theta_{km}) \\ \\ N_{kk} = \partial P_k/\partial V_k = V_k^{-1}(P_k^{calc} + V_k^2 G_{kk}) \end{cases} \tag{7.7}$$

$$\mathrm{M}\begin{cases} M_{km} = \partial Q_k/\partial\theta_m = -V_k V_m(G_{km}\cos\theta_{km} + B_{km}\sin\theta_{km}) \\ \\ M_{kk} = \partial Q_k/\partial\theta_k = P_k^{calc} - V_k^2 G_{kk} \end{cases} \tag{7.8}$$

$$\mathrm{L}\begin{cases} L_{km} = \partial Q_k/\partial V_m = V_k(G_{km}\sin\theta_{km} - B_{km}\cos\theta_{km}) \\ \\ L_{kk} = \partial Q_k/\partial V_k = V_k^{-1}(Q_k^{calc} - V_k^2 B_{kk}) \end{cases} \tag{7.9}$$

The algorithm for the NRPF method can be summarized by the following steps:

1. Initialize the iteration counter ($v = 0$) and determine the initial values of the state variables;
2. Calculate the active power injection for PQ and PV buses and the reactive power injection for PQ buses. Evaluate the power mismatches vectors $\Delta\mathbf{P}$ and $\Delta\mathbf{Q}$;
3. Check convergence: if the highest power mismatch is less than a given tolerance, the convergence is reached at iteration v and the iterative process is terminated; otherwise, proceed to the next step.

4. Calculate the Jacobian matrix:

$$\mathrm{J}(\mathrm{V}^{(v)}, \theta^{(v)}) = \begin{pmatrix} \mathbf{H} & \mathbf{N} \\ \mathbf{M} & \mathbf{L} \end{pmatrix}^{(v)}$$

5. Solve (7.4) to obtain the state variables increments $\Delta\theta$ and $\Delta\mathbf{V}$ and update the state variables:
   $\theta^{(v+1)} = \theta^{(v)} + \Delta\theta^{(v)}$ and $\mathbf{V}^{(v+1)} = \mathbf{V}^{(v)} + \Delta\mathbf{V}^{(v)}$
6. Increment the counter v and return to step 2.

7.2.3 Fast-decoupled approach

The FDPF method is an extension of the NRPF method based on the $P\theta - QV$ decoupling, a noticeable characteristic in high voltage transmission networks, as a consequence of the typically high X/R ratio of its conductors [15].

Such decoupling implies that the elements of submatrices N and M, in (7.4), assume relatively low values, in view of the weak sensitivity between active power and voltage magnitude $(\partial P/\partial V)$ and between reactive power and voltage angle $(\partial Q/\partial\theta)$. From this inference, the FDPF method neglects submatrices **N** and **M**, and the system of equations is divided into two independent sets: one active and one reactive.

In addition to the decoupling procedure, approximations to make constant the Jacobian submatrices **H** and **L** are introduced based on the following assumptions [2]:

1. High X/R ratio power lines $\Rightarrow G_{km} \ll B_{km}$ and $G_{kk} \ll B_{kk}$
2. Small voltage angular deviation $\Rightarrow \cos\theta_{km} \approx 1$ and $\sin\theta_{km} \approx 0$
3. Bus voltage magnitudes around their nominal values $\Rightarrow V_k = V_m \approx 1\ pu$

From these considerations, the elements of the submatrices **H** and **L** are simplified to:

$$\begin{cases} H'_{km} = H_{km}/V_k = -B_{km} \\ \\ H'_{kk} = H_{kk}/V_k = -B_{kk} \end{cases} \tag{7.10}$$

$$\begin{cases} L'_{km} = L_{km}/V_k = -B_{km} \\ \\ L'_{kk} = L_{kk}/V_k = -B_{kk} \end{cases} \tag{7.11}$$

From (7.10) and (7.11), and renaming the constant submatrices as $\mathbf{B}'$ and $\mathbf{B}''$, the final form of the two subsystems that defines the FDPF method is reached:

$$\Delta\mathbf{P}/\mathbf{V} = \mathbf{B}'\Delta\theta \tag{7.12}$$

$$\Delta\mathbf{Q}/\mathbf{V} = \mathbf{B}''\Delta\mathbf{V} \tag{7.13}$$

Equation (7.12) represents the active subproblem that has a dimension equal to the number of *PQ* plus *PV* buses. In turn, the size of the reactive subproblem, represented by (7.13), is equal to the number of *PQ* buses.

As can be seen from (7.10) and (7.11) the elements of the simplified Jacobian submatrices $\mathbf{B}'$ and $\mathbf{B}''$ are related to those of the bus susceptance matrix.

Furthermore, it was observed that if the line resistances are ignored in the formation of such submatrices, it can significantly alter the convergence of the fast-decoupled method.

When line resistances are ignored in the elements of submatrice $\mathbf{B}'$, the so-called *XB* version of the fast-decoupled method is derived. On the other hand, when line resistances are ignored only in the elements of $\mathbf{B}''$, this procedure defines the *BX* version. Such modifications provide significant gains in the performance of the fast-decoupled method. For this reason, the *XB* and *BX* versions are the standard approaches for the fast-decoupled method. It should be noted that, if line resistances are ignored in both submatrices (*XX* version), as well as in the original formulation (*BB* version, where the resistances are not neglected), the decoupled method presents a much lower performance [9].

Regarding shunt elements, while in Reference 2 it is recommended to eliminate the shunt elements in the formation of $\mathbf{B}'$ and double their values in $\mathbf{B}''$, [9] indicates disregard this recommendation but still neglect the shunt elements in $\mathbf{B}'$.

While active and reactive subproblems are independent but interrelated, distinct schemes of interaction between them can be devised. In the original arrangement proposed in [2], the sequential solution is maintained until one of the subsystems reach convergence. After that, the iterative process continues only with the subproblem that has not converged yet. In turn, in [9], it is proposed that a strict sequential solution where the first subsystem that reaches convergence continues in the iterative scheme. This arrangement tends to facilitate the whole iterative process.

It is possible to summarize the FDPF method, based on a strict sequential scheme, in the following algorithm:

1. Initialize the active and reactive iteration counters ($v_p = 0$ and $v_q = 0$, respectively) and determine the initial values of the state variables
2. Form the simplified Jacobian submatrices $\mathbf{B}'$ and $\mathbf{B}''$ according to the chosen version (XB or BX)
3. Calculate the active power injection for *PQ* and *PV* buses, and the reactive power injection for *PQ* buses. Evaluate the power mismatch vectors $\Delta\mathbf{P}$ and $\Delta\mathbf{Q}$
4. Check convergence: if the highest power mismatch of active and reactive subproblems is less than a given tolerance, the convergence is reached at iterations $v_p = v_q$ and the iterative process is terminated; otherwise, proceed to the next step
5. Solve the active subproblem (7.12) to obtain the voltage angles increments $\Delta\theta$ and update the voltage angles: $\theta^{(v_p+1)} = \theta^{(v_p)} + \Delta\theta^{(v_p)}$
6. Increment the counter v_p
7. Calculate the active power injection for *PQ* and *PV* buses, and the reactive power injection for *PQ* buses. Evaluate the power mismatch vectors $\Delta\mathbf{P}$ and $\Delta\mathbf{Q}$

8. Check convergence: if the highest power mismatch of active and reactive subproblems is less than a given tolerance, the convergence is reached at iterations v_p and v_q, and the iterative process is terminated; otherwise, proceed to the next step
9. Solve the reactive subproblem (7.13) to obtain the voltage magnitudes increments $\Delta\mathbf{V}$ and update the voltage magnitudes: $\mathbf{V}^{(vq+1)} = \mathbf{V}^{(vq)} + \Delta\mathbf{V}^{(vq)}$
10. Increment the counter v_q and return to step 3

7.3 *cpu*-based fast-decoupled power flow for distribution systems

7.3.1 Fundamentals of the complex per unit normalization

The concept of *per unit* normalization basically consists of dividing a quantity by a base value of the same unit, as shown in (7.14).

$$\text{Quantity}_{pu} = \frac{\text{Quantity [unit]}}{\text{Base [unit]}} \tag{7.14}$$

To apply the *per unit* normalization procedure to power system analysis, two independent bases need to be defined. Usually the independent bases are the three-phase power (S_{base}), in volt-ampere (VA), whose value is considered for the entire system, and the line voltage magnitude (V_{base}), in volts (V), which, as a general rule, assumes the values of each of the nominal voltages of the power grid. Bases for other electrical quantities of interest, like the impedance base (Z_{base}) and current base (I_{base}), are calculated from the independent bases, as:

$$Z_{\text{base}} = \frac{V_{\text{base}}^2}{S_{\text{base}}} \tag{7.15}$$

$$I_{\text{base}} = \frac{S_{\text{base}}}{V_{\text{base}}} \tag{7.16}$$

The most notable advantage of using *per unit* normalization in power system analysis is that it allows excluding the representation of transformers with nominal tap position. This is possible because the impedance assumes the same value, in *pu*, for both the high voltage and the low voltage side. It is noteworthy that this benefit is achieved as long as voltage bases are adopted in correspondence with the transformation ratio of the transformers present in the system.

The same principles, which oriented the *pu* normalization, are applied to the *cpu* normalization. However, in *cpu* normalization, a complex value is defined for the system's power base. Therefore, the power base of the system is composed by a magnitude base (S_{base}) and a phase angle base (ϕ_{base}):

$$\dot{S}_{\text{base}} = S_{\text{base}} e^{-j\phi_{\text{base}}} \tag{7.17}$$

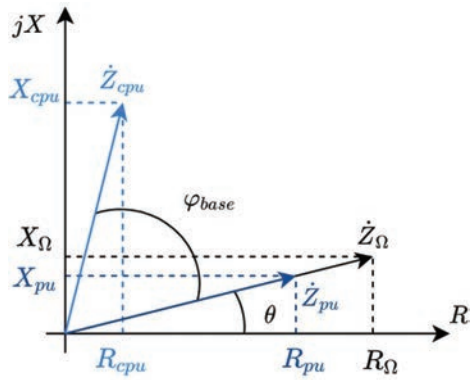

Figure 7.1 Impedance normalization

In turn, the voltage bases are kept as real values. Therefore, conventional *per unit* normalization can be seen as a particular case of the *cpu* normalization, where the base angle is equal to zero.

Accordingly, the base impedance $(\dot{Z}_{\text{base}})$, in *cpu*, is also a complex value:

$$\dot{Z}_{\text{base}} = \frac{V_{\text{base}}^2}{\dot{S}_{\text{base}}^*} = \frac{V_{\text{base}}^2}{S_{\text{base}} e^{j\phi_{\text{base}}}} = Z_{\text{base}} e^{-j\phi_{\text{base}}} \tag{7.18}$$

Thus, a *cpu* normalized impedance, where the subscript Ω represents the quantity in ohms, and θ is the original impedance angle, is given by:

$$\dot{Z}_{cpu} = \frac{\dot{Z}_\Omega}{\dot{Z}_{\text{base}}} = \frac{Z_\Omega e^{j\theta}}{Z_{\text{base}} e^{-j\phi_{\text{base}}}} = Z_{pu} e^{j(\theta+\phi_{\text{base}})} \tag{7.19}$$

The resistance and reactance, in *cpu*, can be defined, respectively, as:

$$R_{cpu} = Z_{pu} \cos\left(\theta + \phi_{\text{base}}\right) \tag{7.20}$$

$$X_{cpu} = Z_{pu} \sin\left(\theta + \phi_{\text{base}}\right) \tag{7.21}$$

And the *X*/*R* ratio of the impedance becomes a function of the power base angle (ϕ_{base}):

$$\frac{X_{cpu}}{R_{cpu}} = \tan\left(\theta + \phi_{\text{base}}\right) \tag{7.22}$$

Figure 7.1 presents the effect of a positive ϕ_{base} over resistance and reactance values, increasing the X/R ratio of the impedance in *cpu* bases.

It is also possible to convert resistance and reactance directly from their values in *pu* to *cpu* using the following equations:

$$R_{cpu} = R_{pu} \cos\phi_{\text{base}} - X_{pu} \sin\phi_{\text{base}} \tag{7.23}$$

$$X_{cpu} = R_{pu} \sin\phi_{\text{base}} + X_{pu} \cos\phi_{\text{base}} \tag{7.24}$$

Power quantities are also affected by *cpu* normalization, that is:

$$\dot{S}_{cpu} = \frac{\dot{S}_{VA}}{\dot{S}_{\text{base}}} = \frac{S_{VA} e^{j\delta}}{S_{\text{base}} e^{-j\phi_{\text{base}}}} = S_{pu} e^{j(\delta+\phi_{\text{base}})} \tag{7.25}$$

Accordingly, the active and reactive power are normalized in the *cpu* system by:

$$P_{cpu} = S_{pu} \cos\left(\delta + \phi_{\text{base}}\right) \tag{7.26}$$

$$Q_{cpu} = S_{pu} \sin\left(\delta + \phi_{\text{base}}\right) \tag{7.27}$$

which may also be given through their *pu* values, that is:

$$P_{cpu} = P_{pu} \cos\phi_{\text{base}} - Q_{pu} \sin\phi_{\text{base}} \tag{7.28}$$

$$Q_{cpu} = P_{pu} \sin\phi_{\text{base}} + Q_{pu} \cos\phi_{\text{base}} \tag{7.29}$$

Also, the current base, in *cpu*, is given by:

$$\dot{I}_{\text{base}} = \frac{\dot{S}^{*}_{\text{base}}}{V_{\text{base}}} = \frac{S_{\text{base}} e^{j\phi_{\text{base}}}}{V_{\text{base}}} = I_{\text{base}} e^{j\phi_{\text{base}}} \tag{7.30}$$

Therefore, the *cpu* normalization of a current with I_{A} magnitude, in amperes, and angle β, results in:

$$\dot{I}_{cpu} = \frac{I_{\text{A}} e^{j\beta}}{I_{\text{base}} e^{j\phi_{\text{base}}}} = I_{pu} e^{j(\beta - \phi_{\text{base}})} \tag{7.31}$$

The *cpu* normalization does not modify the complex voltage values. As demonstrated by (7.32), the values of the state variables of a power flow solution remain the same regardless the ϕ_{base} value adopted:

$$\dot{V}_{cpu} = \frac{S_{pu} e^{j(\delta + \phi_{\text{base}})}}{I_{pu} e^{-j(\beta - \phi_{\text{base}})}} = V_{pu} e^{j(\delta - \beta)} = \dot{V}_{pu} \tag{7.32}$$

Since the X/R ratio of impedances can be numerically increased by adopting a positive ϕ_{base}, the use of the *cpu* normalization allows to improve the performance of the FDPF method for power networks with low X/R ratio lines, commonly found in DS [16].

7.3.1.1 Power base angle definition

A useful formulation to help the definition of a suitable power base angle (ϕ_{base}) to boost the effectiveness of FDPF method, proposed in [17], is presented here.

The central idea is guided by raising the angle of the line impedances to close to 90°, that is, to make them eminently inductive, providing the best decoupling between the active and reactive problems. To this end, the following relationships can be considered:

- The average line impedance angle of the network, α_{avg} calculated as (7.33), where l is the number of system's lines.

$$\alpha_{\text{avg}} = \frac{\sum_{i=1}^{l} \tan^{-1}\left(X_i/R_i\right)}{l} \tag{7.33}$$

- For power networks that include lines with highly different impedance characteristics, the mean between maximum and minimum angles of the line impedances γ_{avg} can also be considered:

$$\gamma_{\text{avg}} = \frac{\tan^{-1}\left(X/R\right)_{MAX} + \tan^{-1}\left(X/R\right)_{MIN}}{2} \tag{7.34}$$

- The influence of the power factor of the loads can also be accounted for using (7.35), in which n is the number of system's nodes.

$$\varepsilon = 1 - \frac{\sum_{i=1}^{n} \cos\left(\tan^{-1}\left(Q_i/P_i\right)\right)}{n} \tag{7.35}$$

Therefore, a suitable base angle may be calculated using the following expression:

$$\phi_{\text{base}} = \frac{\pi}{2} - \left(\frac{\alpha_{\text{avg}} + \gamma_{\text{avg}}}{2}\right)\left(1 + \varepsilon\right) \tag{7.36}$$

For power systems where small variation in the X/R characteristic of their lines is observed (i.e. $\alpha_{\text{avg}} \approx \gamma_{\text{avg}}$) and also where the power factor of their loads are all close to one (i.e. $\epsilon \approx 0$), the following simplified equation may be enough to the determine an adequate power base angle:

$$\phi_{\text{base}} = \frac{\pi}{2} - \alpha_{\text{avg}} \tag{7.37}$$

7.3.2 cpu-*based power flow algorithm*

The *cpu* normalization can be easily incorporated into power flow routines. It only modifies the preprocessing stage of any power flow algorithm. Just like the regular *pu* normalization process, the *cpu* normalization keeps the core of the power flow method intact.

Figure 7.2 emphasizes this procedure. First, the original line and bus data are normalized by *cpu*. Then, the normalized parameters feed the preferred power flow method. Although *cpu* normalization primarily benefits the FDPF methods, it can also be applied to any other power flow method. The solutions provided by the power flow method, that is, the system's nodal voltages are then considered along with the original system data to determine the active and reactive power flows in the network components.

7.4 Multilevel voltage analyses

To analyze a network composed of distinct subsystems with different voltage levels, the FD-PF method may have convergence problems due to the differences in the X/R characteristics of the lines of each subsystem. In these situations, distinct power bases for each subsystem can be applied.

Figure 7.3 illustrates some possibilities for applying the *cpu* normalization for a distribution system composed of two primary feeders (PF) and three secondary feeders (SF). Closed-loop arrangements are also feasible through the switching of normally open (N.O.) circuit breakers.

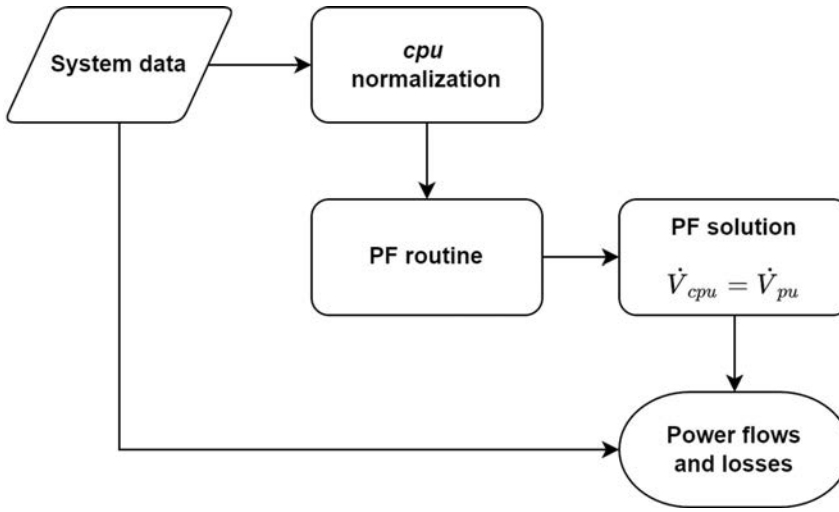

Figure 7.2 cpu-based power flow algorithm

To generalize the multi *cpu* normalization procedure, consider a power system composed of *n*s subsystems, namely SD_1, SD_2, …, and SD_n, which are connected through *nc* branches. Different power bases ($\dot{S}_{\text{base},n} = S_{\text{base},n}\angle\phi_{\text{base},n}$) are adopted to each subsystem SD_n. In thes circumstances, the power injections at each bus k are normalized according to the power bases of the subsystem it belongs to [18].

Considering that bus k belongs to subsystem S_K, which is under cpu_k normalization bases, the bus power injections are written as:

$$P_k^{cpu_k} = V_k \sum_{m \in K} V_m \left(G_{km}^{cpu_k} \cos\theta_{km} + B_{km}^{cpu_k} \sin\theta_{km}\right) \tag{7.38}$$

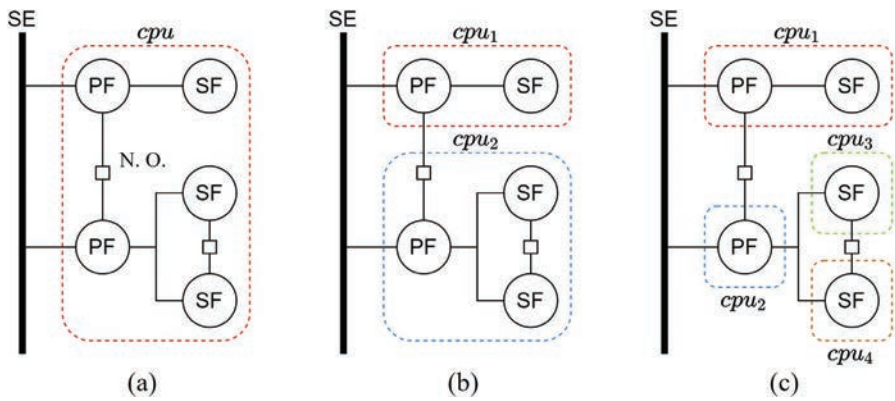

Figure 7.3 Distinct cpu *normalization settings: (a) whole network under a single normalization, (b) two areas with two distinct normalization bases and (c) four distinct normalization bases*

$$Q_k^{cpu_k} = V_k \sum_{m \in K} V_m \left(G_{km}^{cpu_k} \sin\theta_{km} - B_{km}^{cpu_k} \cos\theta_{km} \right) \tag{7.39}$$

The values of the bus admittance matrix $\left(\mathbf{Y}_{\text{bus}}\right)$ are also modified. As indicated in (7.40), each row of the admittance matrix is normalized according to the *cpu* bases of the correspondent subsystem: the admittance of the branch connecting SD_K and SD_L is normalized by cpu_K when viewed from buses belonging to SD_K, and by cpu_L when viewed from buses belonging to SD_L:

$$\mathbf{Y}_{bus} = \begin{pmatrix} \mathbf{Y}_{\text{bus},SD_1}^{cpu_1} \\ \mathbf{Y}_{\text{bus},SD_2}^{cpu_2} \\ \vdots \\ \mathbf{Y}_{\text{bus},SD_n}^{cpu_n} \end{pmatrix} = \begin{pmatrix} \mathbf{G}_{\text{bus},SD_1}^{cpu_1} \\ \mathbf{G}_{\text{bus},SD_2}^{cpu_2} \\ \vdots \\ \mathbf{G}_{\text{bus},SD_n}^{cpu_n} \end{pmatrix} + j \begin{pmatrix} \mathbf{B}_{\text{bus},SD_1}^{cpu_1} \\ \mathbf{B}_{\text{bus},SD_2}^{cpu_2} \\ \vdots \\ \mathbf{B}_{\text{bus},SD_n}^{cpu_n} \end{pmatrix} \tag{7.40}$$

Thereafter, the bus admittance matrix is no longer symmetrical, since the elements related to the connection branches differ in value due to the distinct normalization bases. This asymmetry also occurs in the constant submatrices of the FD-PF algorithm [18]:

$$\begin{pmatrix} \vdots \\ \Delta P_{SD_K}^{cpu_K} \\ \vdots \\ \Delta P_{SD_L}^{cpu_L} \\ \vdots \end{pmatrix} = \begin{pmatrix} \vdots & & \vdots & \\ \cdots & (B')_{SD_K SD_K}^{cpu_K} & \cdots & (B')_{SD_K SD_L}^{cpu_K} & \cdots \\ \vdots & & \vdots & \\ \cdots & (B')_{SD_L SD_K}^{cpu_L} & \cdots & (B')_{SD_L SD_L}^{cpu_L} & \cdots \\ \vdots & & \vdots & \end{pmatrix} \begin{pmatrix} \vdots \\ \Delta\theta_{SD_K} \\ \vdots \\ \Delta\theta_{SD_L} \\ \vdots \end{pmatrix} \tag{7.41}$$

$$\begin{pmatrix} \vdots \\ \Delta Q_{SD_K}^{cpu_K} \\ \vdots \\ \Delta Q_{SD_L}^{cpu_L} \\ \vdots \end{pmatrix} = \begin{pmatrix} \vdots & & \vdots & \\ \cdots & (B'')_{SD_K SD_K}^{cpu_K} & \cdots & (B'')_{SD_K SD_L}^{cpu_K} & \cdots \\ \vdots & & \vdots & \\ \cdots & (B'')_{SD_L SD_K}^{cpu_L} & \cdots & (B'')_{SD_L SD_L}^{cpu_L} & \cdots \\ \vdots & & \vdots & \end{pmatrix} \begin{pmatrix} \vdots \\ \Delta V_{SD_K} \\ \vdots \\ \Delta V_{SD_L} \\ \vdots \end{pmatrix} \tag{7.42}$$

7.5 Case studies and performance evaluation

7.5.1 Two-bus test system—convergence example

To illustrate the influence of the line *X/R* ratio and the load power factor in the performance of the FD-PF, a two-bus test system, presented in Figure 7.4, is considered in this section. The FD-PF convergence is evaluated for a wide range of line impedance angles and load power factor values: the angle impedance spans from 0° to 90°, and the inductive load power factors from 0.75 to 1. Considering the conventional *pu* normalization, the convergence, for both BX and XB versions of the FD-PF, is

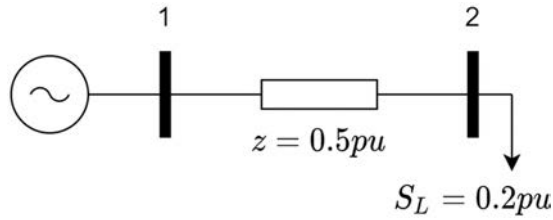

Figure 7.4 Two-bus test system

presented in Figures 7.5 and 7.6, respectively, based on a tolerance of 10^{-6}. The displayed convergence surfaces are limited to 10 full FD-PF iterations.

It is observed that, for both XB and BX versions, the closer the impedance angle is to 90^o, that is, the higher the *X/R* ratios, the fewer iterations are needed for convergence. Regarding load power factor, the values between 0.95 and 1.0 provide the best results.

However, when *cpu* normalization is applied, with power base angles defined according to (7.37), the convergence performance changes substantially, as shown in Figure 7.7. The convergence pattern for both FD-PF versions is exactly the same, indicating <6 iterations for convergence under all conditions, even where the line is purely resistive (*X*/*R* = 0).

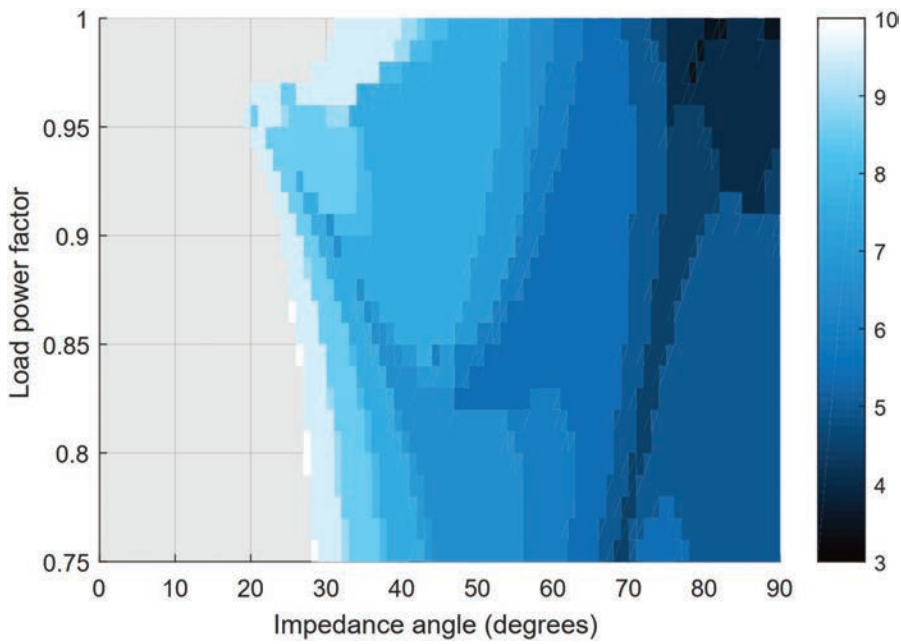

Figure 7.5 Two-bus test system convergence pattern for FD-PF BX version

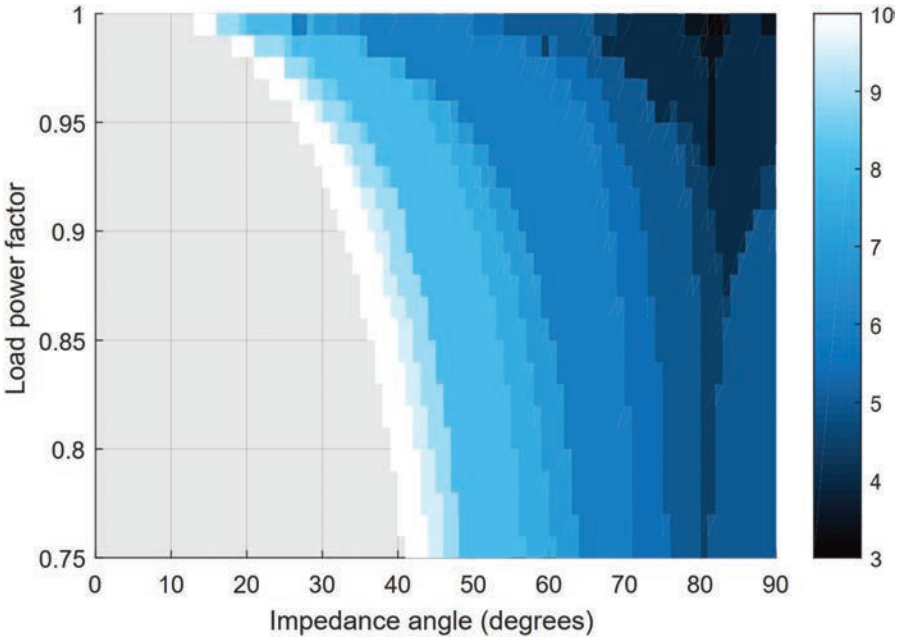

Figure 7.6 Two-bus test system convergence pattern for FD-PF XB version

Another evaluation of the *cpu* performance over FD-PF convergence for the two-bus test system, is summarized in Table 7.1. The system's line impedance and load are set to $z = 0.5\angle 30^{o} pu$ and $S_L = 0.2\angle 10^{o} pu$, respectively.

Table 7.1 presents the values of the line impedance and load, in *cpu*, for distinct power base angles (ϕ_{base}). Assuming a flat start condition, all cases converge to the same solution, that is, to $V_2 = 0.8942\angle -2.19^{o} pu$. The number of iterations to convergence for the BX and XB versions of the FD-PF, presented in the last two columns of Table 7.1, confirms that the best performance is obtained with a pure reactive line characteristic.

7.5.2 141-bus distribution feeder

This section presents the impact on the performance of the *cpu*-based FD-PF over the 141-bus distribution test feeder [19], whose online diagram is shown in Figure 7.8. Dotted lines are included in the original network to represent switchable branches that enable closed-loop operational arrangements. All simulations are carried out for both FD-PF versions and consider a convergence tolerance of $10^{-6} pu$.

Figures 7.9 and 7.10 present a graphic evaluation of the number of iterations of *cpu*-based FD-PF BX and XB versions for different power base angles and *X*/*R* ratios. The system's original data are considered the base case. Also, two constant multiplication factors are applied to the line resistances to decrease the *X*/*R* ratio

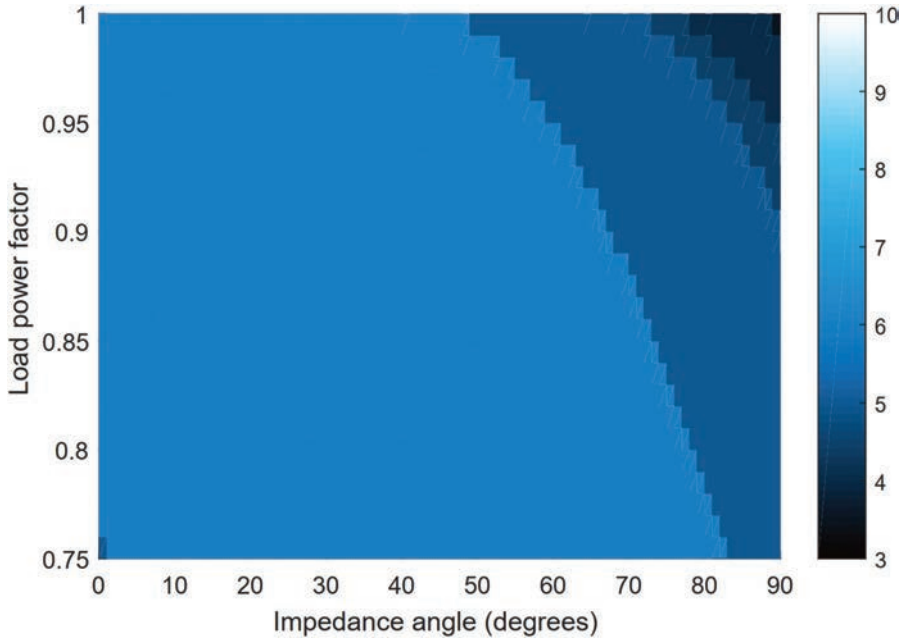

Figure 7.7 *Two-bus test system convergence pattern for FD-PF BX and XB version with* cpu

Table 7.1 *Two-bus test system—FD-PF convergence performance with* cpu

ϕ_{base}	r (*cpu*)	x (*cpu*)	P_L (*cpu*)	Q_L (*cpu*)	BX	XB
0º	0.4330	0.2500	0.1970	0.0347	9.5	8
30º	0.2500	0.4330	0.1532	0.1286	6	7
60º	0.0000	0.5000	0.0684	0.1879	6	6
90º	−0.2500	0.4330	−0.0347	0.1970	7	8
120º	−0.4330	0.2500	−0.1286	0.1532	9.5	13

of the network. The *cpu* is able to significantly improve the performance of the FD-PF methods in all evaluated scenarios, when compared to the *pu* normalization ($\phi_{base} = 0$).

Furthermore, the performance of the *cpu*-based FD-PF algorithms are evaluated for three different loading conditions.

Figures 7.11 and 7.12 present the number of iterations over power base angle for the BX and XB versions, respectively. Along with the base case, two additional loading conditions are considered, by applying multiplier factors to all system loads.

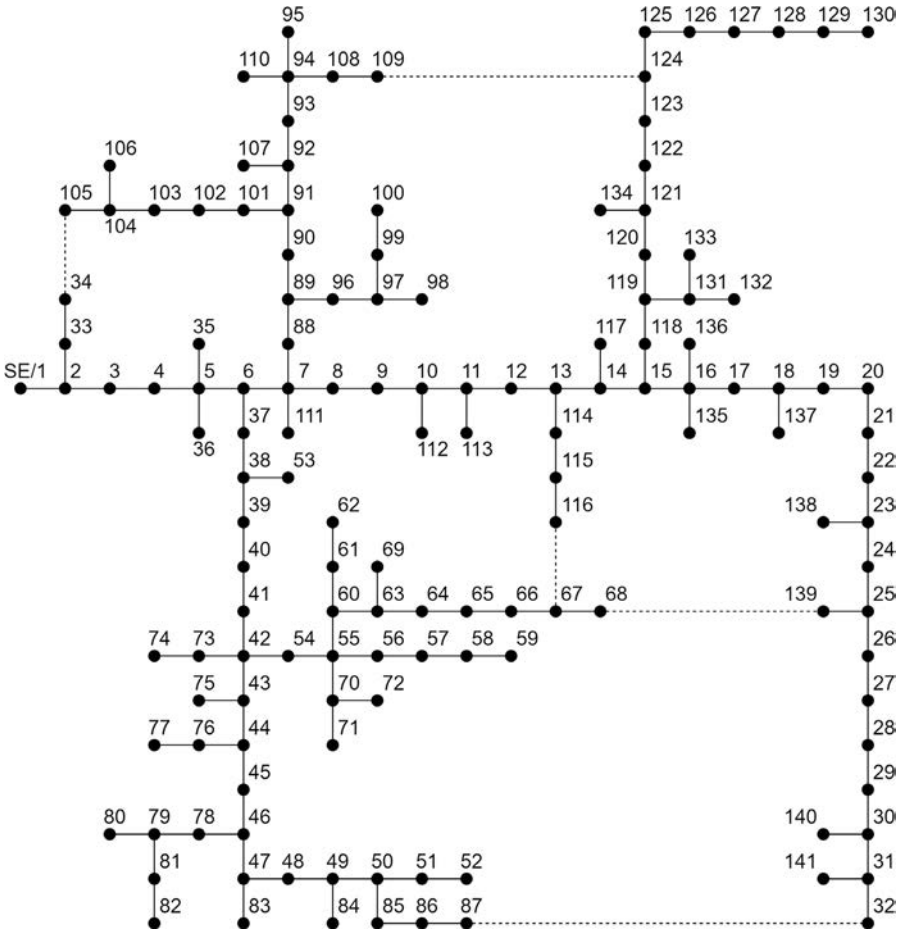

Figure 7.8 141-bus feeder

Again, for all scenarios, the *cpu* normalization enhances the convergence performance of the FD-PF method.

7.5.2.1 Power base angle considerations

Table 7.2 presents an evaluation of the power base angle determined by the formulation presented in Section 7.3.1.1 in relation to the observed results presented in Figures 7.9 and 7.10.

In all situations, (7.36) provides a power base angle within the range of the ϕ_{base} values which results in the best performance of the *cpu*-based FD-PF algorithms. Even the simplest formula, represented by (7.37), indicates power base angles within or very close to the best range of values, and it can also be considered to determine an adequate power base angle.

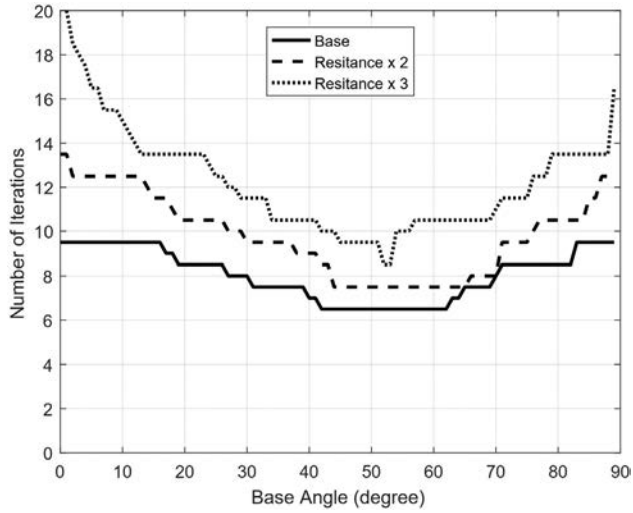

Figure 7.9 141-bus feeder: convergence performance for different R/X *ratios—FD-PF BX version*

7.5.2.2 Network topology considerations

The performance of the FD-PF algorithms is evaluated considering the 141-bus test feeder under distinct operational conditions. A 0.3 MW distributed generation unit is added to all even buses. Closed-loop operation is also considered by closing the

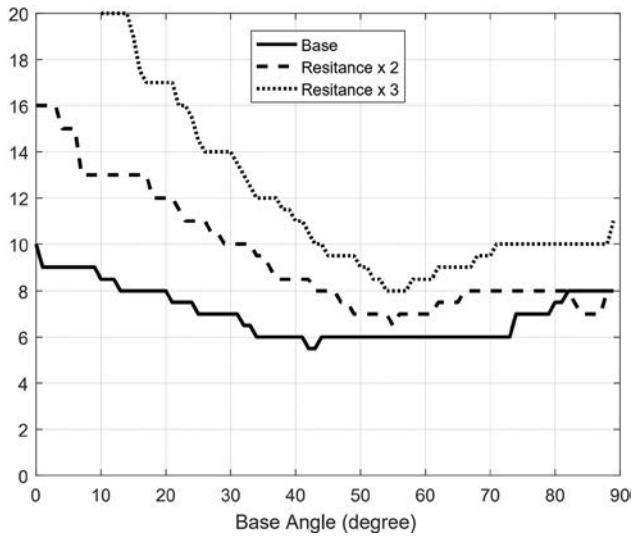

Figure 7.10 141-bus feeder: convergence performance for different R/X *ratios—FD-PF XB version*

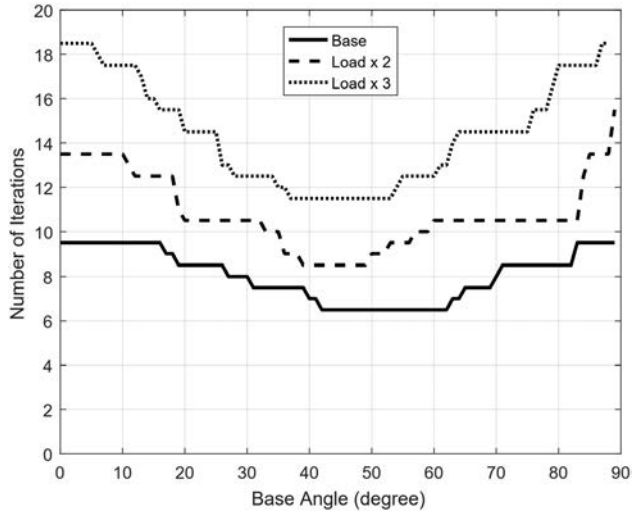

Figure 7.11 141-bus feeder: convergence performance for different load conditions—FD-PF BX version

switching branches represented by the dotted lines displayed in Figure 7.8. In addition to the nominal loading, simulations were also carried out with an increased load, twice as high as the nominal one.

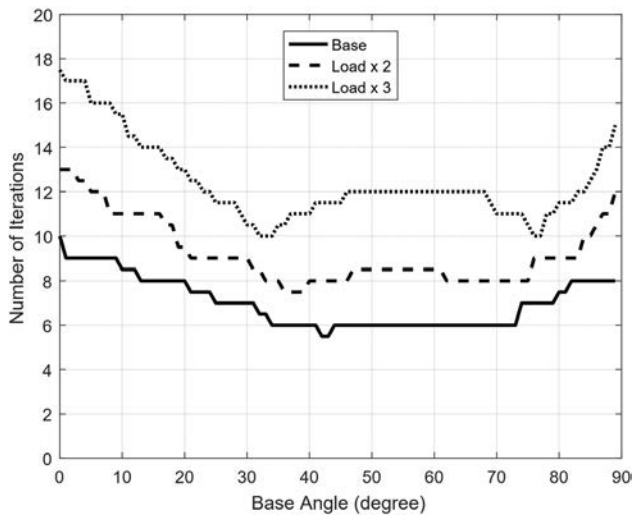

Figure 7.12 141-bus feeder: convergence performance for different load conditions—FD-PF XB version

Table 7.2 Evaluation of power base angle choice

	Base	**Resistance x2**	**Resistance x3**
α_{avg}	33.70°	18.97°	13.02°
γ_{avg}	32.44°	23.42°	17.71°
ϵ	0.4936	0.4936	0.4936
Best ϕ_{base} range (BX)	40° to 60°	45° to 65°	40° to 70°
Best ϕ_{base}range (XB)	35° to 75°	45° to 65°	50° to 70°
ϕ_{base} via (7.36)	40.60°	58.34°	67.05°
ϕ_{base} via (7.37)	56.30°	71.03°	76.98°

The results presented in Table 7.3 demonstrate the efficiency and robustness of the *cpu* normalization that improves the convergence performance of the FD-PF algorithms under distinct operational arrangements and stressed loading conditions.

7.6 Final remarks

This chapter presented the fundamentals of the decoupled approach of the NRPF algorithms, along with the *cpu* normalization technique. The *cpu* normalization technique, proposed as an extension of the conventional *per unit* normalization, enables the effective application on the traditional FDPF method to distribution system analysis.

At the core of the *cpu* normalization is the power base angle that is responsible to artificially adjust the *X*/*R* ratio of the network lines. A formulation to determine a suitable power base angle is presented based on the characteristics of the conductors impedance angle and load power factor.

The implementation of the *cpu* technique in power flow algorithm is straightforward and does not require any changes in the iterative routine, since it alters only the procedure for normalizing the input data.

Comprehensive simulation results demonstrated that *cpu* technique is able to significantly improve the convergence performance of the FDPF algorithms when compared to the usual *pu* normalization.

Table 7.3 Convergence performance with distinct operational scenarios

Topology	**Load**	**pu**($\phi_{base} = 0^o$)		***cpu***($\phi_{base} = 57^o$)	
		BX	XB	BX	XB
Radial	Nominal	8.5	8	4.5	5
	Increased	10.5	12	7	6
Meshed	Nominal	12	11.5	6.5	6
	Increased	12	12	7.5	7

By extending the well-known efficiency of the traditional fast-decoupled Newton–Raphson algorithm to networks with low X/R ratio lines, and combining it with the method's inherent versatility to deal with any topological arrangement, the *cpu*-based FD-PF algorithm proves to be a very effective computational tool to support the planning and operation of modern active DS.

References

[1] Tinney W.F., Hart C.E. 'Power flow solution by Newton's method'. *IEEE Transactions on Power Apparatus and systems*. 1967, vol. 11, pp. 1449–60.

[2] Stott B., Alsac O. 'Fast decoupled load flow'. *IEEE Transactions on Power Apparatus and Systems*. 1974, vol. PAS-93(3), pp. 859–69.

[3] Wu F.F. 'Theoretical study of the convergence of the fast decoupled load flow'. *IEEE Transactions on Power Apparatus and Systems*. 1977, vol. 96(1), pp. 268–75.

[4] Deckmann S., Pizzolante A., Monticelli A., Stott B., Alsac O. 'Numerical testing of power system load flow equivalents'. *IEEE Transactions on Power Apparatus and Systems*. 1980, vol. PAS-99(6), pp. 2292–300.

[5] Haley P.H., Ayres M. 'Super decoupled loadflow with distributed Slack bus'. *IEEE transactions on Power Apparatus and Systems*. 1985, vol. 1, pp. 104–13.

[6] Rajicic D., Bose A. 'A modification to the fast decoupled power flow for networks with high R/X ratios'. *IEEE Transactions on Power Systems*. 1988, vol. 3(2), pp. 743–6.

[7] Wang L., Xiang N., Wang S., Zhang B., Huang M. 'Novel decoupled power flow'. *IEE Proceedings C Generation, Transmission and Distribution*. 1990, vol. 137(1), pp. 1–7.

[8] Nanda J., Kothari D.P., Srivastava S.C. 'Some important observations on fast decoupled load flow algorithm'. *Proceedings of the IEEE*. 1987, vol. 75(5), pp. 732–3.

[9] van Amerongen R.A.M. 'A general-purpose version of the fast decoupled load flow'. *IEEE Transactions on Power Systems*. 1989, vol. 4(2), pp. 760–70.

[10] Singh S., Raju G., Rao V.S. 'A technique to improve the convergence of FDLF for systems with high R/X lines'. *TENCON'91. Region 10 International Conference on EC3-Energy, Computer, Communication and Control Systems*; 1991. pp. 204–7.

[11] Berg R., Hawkins E., Pleines W. 'Mechanized calculation of unbalanced load flow on radial distribution circuits'. *IEEE Transactions on Power Apparatus and Systems*. 1967, vol. PAS-86(4), pp. 415–21.

[12] Eminoglu U., Hocaoglu M.H. 'Distribution systems forward/backward sweep-based power flow algorithms: A review and comparison study'. *Electric Power Components and Systems*. 2008, vol. 37(1), pp. 91–110.

[13] Shirmohammadi D., Hong H.W., Semlyen A., Luo G.X. 'A compensation-based power flow method for weakly meshed distribution and transmission networks'. *IEEE Transactions on Power Systems*. 1988, vol. 3(2), pp. 753–62.
[14] Monticelli A. *State Estimation in Electric Power Systems: A Generalized Approach*. New York, NY: Springer Science & Business Media; 2012.
[15] Monticelli A.J. *Fluxo de carga em redes de energia elétrica*. São Paulo, Brazil: Edgard Blücher; 1983.
[16] Durce C.C., Lourenço E.M., Tortelli O.L. 'Power flow analysis for interconnected T&D networks with meshed topology'. *2nd IEEE PES International Conference and Exhibition on Innovative Smart Grid Technologies*; Manchester, UK; 2011. pp. 1–7 pp..
[17] Tortelli O.L., Lourenço E.M., Garcia A.V., Pal B.C. 'Fast decoupled power flow to emerging distribution systems via complex Pu normalization'. *IEEE Transactions on Power Systems*. 2014, vol. 30(3), pp. 1351–8.
[18] Portelinha R.K., Durce C.C., Tortelli O.L., Lourenço E.M. 'Fast-decoupled power flow method for integrated analysis of transmission and distribution systems'. *Electric Power Systems Research*. 2021, vol. 196(6), p. 107215.
[19] Khodr H.M., Olsina F.G., Jesus P.M.D.O.-D., Yusta J.M. 'Maximum savings approach for location and sizing of capacitors in distribution systems'. *Electric Power Systems Research*. 2008, vol. 78(7), pp. 1192–203.

This page intentionally left blank

Chapter 8

Fast-decoupled distribution system state estimation

Elizete Maria Lourenço[1], Odilon Luis Tortelli[1], Bikash Chandra Pal[2], Ellen Mara Medeiros Nogueira[1], and Andressa Lorayne Monteiro[1]

8.1 Introduction

As discussed in the previous chapters, the advances in measurement infrastructure, smart grid technologies, and uptake of distributed generation have reinforced the use of state estimation, previously focused on high- and extra-high voltage systems, spreading its relevance to all voltage levels of the electric power system. Thereby, initial efforts for distribution system state estimation (DSSE) were revisited and a new series of advances and alternative methods are being proposed to meet the needs of the emerging distribution system (DS) monitoring tools while taking its particularities and characteristics into account [1–6].

The DSSE's new methodologies and computational packages address the different challenges that present themselves for the current and future scenarios of distribution networks. The current low redundancy of measures associated with the need for adequate weighting of the still essential pseudo-measures (see Chapter 9) and the adequate treatment of different samples associated with the range of measures available for treatment by the DSSE (see Chapter 12) are some of the challenges faced by the alternative approaches presented in other chapters.

This chapter, specifically, presents an alternative DSSE method that seeks to meet the following challenges and required features, also evident in this new scenario:

- active nature of distribution networks
- transition from radial/weakly meshed to composed radial-meshed networks
- numerical robustness and low computational cost tools to overcome the large dimensions of DSs

[1]Department of Electrical Engineering, Federal University of Parana, Curitiba, Brazil
[2]Department of Electrical and Electronic Engineering, Imperial College London, London, UK

- transmission lines with low X/R ratios
- proper use of consolidated and traditionally applied methodologies for TS following the characteristics of active DSs
- adequate appropriation of the benefits and guarantees of consolidated and traditionally applied methodologies for TS while meeting the characteristics of active DSs.

The main idea of this approach consists of the combined application of the traditional $P\theta$-QV decoupling techniques, to meet the required robustness and computational efficiency, with the recent developments associated and the complex per unit (*cpu*) normalization [7], to circumvent low X/R ratios of distribution lines. Additionally, the representation of switches and circuit breakers presented in the generalized state estimation (GSE) is brought to the context of distribution networks, allowing the increase in redundancy from the use of possible internal measurements of the substations and making room for more efficient bad data and topology error processing.

The resulting tool is presented in this chapter as an alternative to real-time solutions involving future scenarios, for which the level of monitoring of distribution networks is more optimistic. It can also be applied in combination with other alternative tools discussed in this book or available in the literature in general, where transition and diversification scenarios of the measurement infrastructure are considered.

8.2 Fast-decoupled weighted least-squares state estimation

The monitoring of the electrical power system provides a set of redundant measurements used to estimate the current state of the network. In order to maintain the operational conditions in a normal and safe state, those measurements are continuously monitored [8]. These measures are inexact as a result of the nature of the transducers, communications failures, incomplete metering or mathematical models, and others [9]. The state estimation is the result of the statistical process of these redundant and imperfect set of measurements that estimates the true value of the system node complex voltages. This section presents the state estimation formulation based on the commonly used statistical criterion, which consists of minimizing the sum of the squares of the differences between the estimated and the measured values: the well-known weighted least-squares state estimation (WLS-SE). Special attention is given to the decoupled approach of the WLS-SE and its main versions, usually referred to as fast-decoupled state estimation.

8.2.1 Conventional weighted least-squares state estimation

The conventional state estimator is used to build a real-time model for the observable part of the network. Performed on the same bus-branch model used in power flow studies, the data set is processed in two steps. First, the logical data are processed to transform bus-section/switching-device/physical level into the bus-branch model of the network: the topology processor. Then, observability analysis and state

estimation itself are performed, in which network topology is considered as correct and analog data are processed [10].

The measured value can be represented by the true value of the quantities modified by an unknown error that models the measurement uncertainty, that is:

$$z = z_{\text{true}} + \eta \tag{8.1}$$

where z_{true} is the vector containing the true values of the measured quantities and η is the noise vector associated with the inherent uncertainty of the measurement process.

A normal distribution with zero mean is commonly used for modeling η, since many factors contribute to the overall measurement error, such that:

$$\begin{aligned} E(\eta) &= 0 \\ E(\eta\eta^T) &= R \end{aligned} \tag{8.2}$$

where $E(.)$ is the expected value and R is the diagonal covariance matrix of the measurement errors.

Applying Kirchhoff's laws and Ohm's law over the bus-branch model of the network, z_{true} values can be expressed by the nonlinear functions that relate the measured quantities to the state variable, so that the measurement model used in the state estimation process can be expressed by:

$$z = h(x) + \eta\,, \tag{8.3}$$

where $h(x)$ is the vector of nonlinear measurement functions; and x is the true state vector, composed by the magnitudes and phases of the bus complex voltages.

The classical formulation of the WLS-SE consists in minimizing the sum of the squares of the measurement residuals, weighted by the inverse of the covariance matrix, so that higher precision measurements have greater influence on the estimated states and vice versa. The WLS-SE can be expressed by the following minimizing problem [8, 10]:

$$J(x) = \frac{1}{2}[z - h(x)]^T R^{-1}[z - h(x)] \tag{8.4}$$

The first-order optimal condition of the performance index $J(x)$ is given by:

$$g(x) = \nabla J(x) = \frac{\partial J(x)}{\partial x} = 0 \tag{8.5}$$

or

$$g(x) = \frac{\partial J(x)}{\partial x} = -H^T(x)R^{-1}[z - h(x)] = 0 \tag{8.6}$$

where $H(x)$ is the Jacobian matrix of $h(x)$, that is:

$$H(x) = \frac{\partial h(x)}{\partial x} \tag{8.7}$$

Finally, solving the nonlinear system in (8.6) by Newton–Raphson method, the WLS-SE solution can be expressed by:

$$G(x)\Delta x = T(x) \tag{8.8}$$

where $G(x)$ is the Jacobian matrix of $g(x)$, or the Hessian matrix of $J(x)$, known as the Gain matrix:

$$G(x) = \frac{\partial g(x)}{\partial x} = H^T(x)R^{-1}H(x) \tag{8.9}$$

and, the right-hand side vector of the linear system (8.8), given by:

$$T(x) = H^T(x)R^{-1}[z - h(x)] \tag{8.10}$$

The equation in (8.9) can be iteratively solved, with the update of the state vector at each iteration, k, given by:

$$x^{k+1} = x^k + \Delta x^k \tag{8.11}$$

It is worth to emphasize that, in the conventional WLS-SE problem, the state vector is composed by:

$$x = \begin{bmatrix} \theta \\ V \end{bmatrix} \tag{8.12}$$

where θ and V correspond to the angles and magnitudes of the complex voltages in the buses, respectively.

The measurement vector, in turn, is commonly composed of power flow, power injection, and voltage magnitudes measurements, represented by:

$$z = \begin{bmatrix} z_{P_{\text{flow}}} \\ z_{Q_{\text{flow}}} \\ z_{P_{\text{inj}}} \\ z_{Q_{\text{inj}}} \\ z_{V_{\text{mag}}} \end{bmatrix} \tag{8.13}$$

where $z_{P_{\text{flow}}}$ ($z_{Q_{\text{flow}}}$) is the vector of active (reactive) power flow measurements, $z_{P_{\text{inj}}}$ ($z_{Q_{\text{inj}}}$) is the vector of active (reactive) power injection measurements, and $z_{V_{\text{mag}}}$ is the vector of voltage magnitude measurements.

The corresponding vector of nonlinear equations is given by:

$$h(x) = \begin{bmatrix} P_{\text{flow}} \\ Q_{\text{flow}} \\ P_{\text{inj}} \\ Q_{\text{inj}} \\ V_{\text{mag}} \end{bmatrix} \tag{8.14}$$

where P_{flow} (Q_{flow}) is the vector of active (reactive) power flow equations and P_{inj} (Q_{inj}) is the vector of active (reactive) power injection equations, both derived from power flow studies. V_{mag} is the vector of voltage magnitude of monitored buses.

The iterative process to obtain the WLS-SE solution can be summarized by the following steps [8]:

1. Start of iterations ($k = 0$)
2. Initialize state vector x^k (usually flat start)
3. Calculate the Gain matrix $G(x^k)$ and right-hand side vector $T(x^k)$, given by (8.9) and (8.10)
4. Solve (8.8) to obtain Δx^k
5. Apply the convergence test:$\max(\Delta x^k) \leq$ tolerance
6. If the criteria is met, x^k is the solution. Otherwise, update x^k by (8.11) and go back to step 3.

From the classical state estimation, other formulations emerged to circumvent the major computational burden of the state estimation solution in (8.8), that is, the calculation and triangular factorization of the Gain matrix. The $P\theta - QV$ decoupling can be applied in a similar fashion as done to power flow studies [11, 12], to derive lower time execution approaches, as discussed next.

8.2.2 Decoupled formulation

In the usual range of power systems operations, relatively small power angle* is found. When added to the high levels of X/R ratios of transmission lines, a low sensitivity of the active (reactive) quantities with respect to the bus voltage magnitudes (phase angles) is found. The low sensitivities of PV and $Q\theta$ can be applied to simplify the state estimation Jacobian matrix, as discussed next.

To comply with the $P\theta - QV$ decoupling, the state vector and the measurement vector z, as well as its corresponding equation vector $h(x)$, are partitioned into two parts, following the active and reactive nature of the quantity, that is [11]:

$$x_A = \theta \tag{8.15}$$

$$x_R = V \tag{8.16}$$

$$z_A = \begin{bmatrix} z_{P_{flow}} \\ z_{P_{inj}} \end{bmatrix} \qquad h_A(x) = \begin{bmatrix} P_{flow} \\ P_{inj} \end{bmatrix} \tag{8.17}$$

$$z_R = \begin{bmatrix} z_{Q_{flow}} \\ z_{Q_{inj}} \\ z_{V_{mag}} \end{bmatrix} \qquad h_R(x) = \begin{bmatrix} Q_{flow} \\ Q_{inj} \\ V_{mag} \end{bmatrix} \tag{8.18}$$

where the indexes A and R denote the active and reactive partition, respectively.

The diagonal measurement covariance matrix follows the proposed partition, being represented by:

*Phase difference between sending end voltage and receiving end voltage of a transmission line.

$$\mathrm{R}=\begin{bmatrix} R_A & 0 \\ 0 & R_R \end{bmatrix} \tag{8.19}$$

The partition of the Jacobian matrix that conforms to the new arrangement for states and measurement vectors can be represented by:

$$\mathrm{H}=\begin{bmatrix} H_{AA} & H_{AR} \\ H_{RA} & H_{RR} \end{bmatrix} \tag{8.20}$$

where the submatrices are given by the first derivatives of $h(.)$, in terms of θ and V, that is:

$$H_{AA} = \frac{\partial h_A(x)}{\partial \theta} \tag{8.21}$$

$$H_{AR} = \frac{\partial h_A(x)}{\partial V} \tag{8.22}$$

$$H_{RA} = \frac{\partial h_R(x)}{\partial \theta} \tag{8.23}$$

$$H_{RR} = \frac{\partial h_R(x)}{\partial V} \tag{8.24}$$

From (8.9), (8.19), and (8.20), the corresponding partitioned Gain matrix is given by:

$$\mathrm{G} = \begin{bmatrix} G_{AA} & G_{AR} \\ G_{RA} & G_{RR} \end{bmatrix} \tag{8.25}$$

where:

$$G_{AA} = H_{AA}^T(R_A)^{-1}H_{AA} + H_{RA}^T(R_R)^{-1}H_{RA} \tag{8.26}$$

$$G_{AR} = H_{AA}^T(R_A)^{-1}H_{AR} + H_{RA}^T(R_R)^{-1}H_{RR} \tag{8.27}$$

$$G_{RA} = H_{AR}^T(R_A)^{-1}H_{AA} + H_{RR}^T(R_R)^{-1}H_{RA} \tag{8.28}$$

$$G_{RR} = H_{RR}^T(R_R)^{-1}H_{RR} + H_{AR}^T(R_A)^{-1}H_{AR} \tag{8.29}$$

Likewise, the right-hand vector **T** in (8.10) is now expressed by:

$$\mathbf{T} = \begin{bmatrix} T_A \\ T_R \end{bmatrix} \tag{8.30}$$

where:

$$T_A = H_{AA}^T(R_A)^{-1}[z_A - h_A(x)] + H_{AR}^T(R_R)^{-1}[z_R - h_R(x)] \tag{8.31}$$

$$T_R = H_{RR}^T(R_R)^{-1}[z_R - h_R(x)] + H_{RA}^T(R_A)^{-1}[z_A - h_A(x)] \tag{8.32}$$

The fact that the Gain matrix does not significantly change during the convergence process can be explored along with the decoupled techniques to derive fast-decoupled approaches [13]. Applying the decoupling simplifications directly to the Gain matrix or to the Jacobian matrix leads to the two main versions of the fast-decoupled state

estimation [12, 13], model-decoupled and algorithm-decoupled, described in the next subsections.

8.2.3 Model-decoupled state estimator

In the usual range of transmission system operations, relatively small power angle[†] is found. When added to the characteristic high X/R ratios of the transmission lines, low sensitivity of the active (reactive) quantities with respect to the bus voltage magnitudes (phase angles) is observed, which simplifies the state estimation Jacobian matrix, as discussed next.

In the model-decoupled state estimator, the off-diagonal block matrices of the Jacobian matrix (H_{AR} and H_{RA}) are ignored, resulting in the following decoupled matrix:

$$\mathrm{H}^{\mathrm{md}} = \begin{bmatrix} H_{AA} & 0 \\ 0 & H_{RR} \end{bmatrix} \tag{8.33}$$

The above approach clearly implies the approximations in both the Gain matrix and the right-hand side vector of the problem solution. Applying (8.33) in (8.8) and (8.10), the state estimation is now solved by the successive solution of the following decoupled linear systems.

Active subproblem:

$$G_A^{\mathrm{md}} \Delta\theta = T_A^{\mathrm{md}} \tag{8.34}$$

$$\theta^{k+1} = \theta^k + \Delta\theta^k \tag{8.35}$$

where:

$$G_A^{\mathrm{md}} = H_{AA}^T (R_A)^{-1} H_{AA} \tag{8.36}$$

$$T_A^{\mathrm{md}} = H_{AA}^T (R_A)^{-1} [z_A - h_A(\theta^k, V^k)] \tag{8.37}$$

Reactive subproblem:

$$G_R^{\mathrm{md}} \Delta V = T_R^{\mathrm{md}} \tag{8.38}$$

$$V^{(k+1)} = V^k + \Delta V^k \tag{8.39}$$

where:

$$G_R^{\mathrm{md}} = H_{RR}^T (R_R)^{-1} H_{RR} \tag{8.40}$$

$$T_R^{\mathrm{md}} = H_{RR}^T (R_R)^{-1} [z_R - h_R(\theta^{(k+1)}, V^k)] \tag{8.41}$$

[†]Phase difference between sending end voltage and receiving end voltage of a transmission line.

During the entire interactive process, the Gain and Jacobian matrices are kept constant further reducing the computational effort. Besides, ignoring line resistances in submatrix H_{AA} or in submatrix H_{RR} leads to the well-known XB and BX version, respectively [2]. The convergence process ends when the two subproblems satisfy the convergence criterion (the same as that of the coupled version), which may occur in different iterations in each subproblem. The difference in the results when the decoupled method is applied is acceptable as long as the operation and parameter condition are in accordance with the decoupled assumptions discussed above.

Algorithm 1: Model-Decoupled State Estimator

Input: $z_A, z_R, h_A, h_R, R_A, R_R, H_{AA}, H_{RR}, \theta^0, V^0$
Output: Estimated states: θ, V
Compute G_A^{md} and G_R^{md} ;
for $k = k+1$ **do**
  Active iteration:
  Compute T_A^{md} ;
  Solve (8.34) for $\Delta\theta^k$;
  Update θ ;
  Reactive iteration:
  Compute T_R^{md} ;
  Solve (8.38) for ΔV^k ;
  Update V ;
  until: $\Delta\theta^k$ and ΔV^k are larger than predefined tolerance
end

8.2.4 Algorithm-decoupled state estimator

The strong $P\theta$ and QV sensitivities can be exploited directly in the computation of the Gain matrices, given rise to the algorithm-decoupled state estimator.

In the algorithm-decoupled state estimator, the off-diagonal submatrices of the Gain matrix (G_{AR} and G_{RA}) are neglected and a flat start operating condition applied, yielding in the following constant and decoupled Gain matrix:

$$\mathrm{G}^{\mathrm{ad}} = \begin{bmatrix} G_A^{\mathrm{ad}} & 0 \\ 0 & G_R^{\mathrm{ad}} \end{bmatrix} \tag{8.42}$$

The iteration process is composed of the successive solution of the following decoupled linear systems:

$$G_A^{\mathrm{ad}} \Delta\theta = T_A(\theta^k, V^k) \tag{8.43}$$

$$\theta^{k+1} = \theta^k + \Delta\theta \tag{8.44}$$

$$G_R^{\mathrm{ad}} \Delta V = T_R(\theta^{k+1}, V^k) \tag{8.45}$$

$$V^{(k+1)} = V^k + \Delta V^k \tag{8.46}$$

where:

$$G_A^{\text{ad}} = H_{P\theta}^T (R_A)^{-1} H_{P\theta} \tag{8.47}$$

$$G_R^{\text{ad}} = H_{QV}^T (R_R)^{-1} H_{QV}^T \tag{8.48}$$

Alternative versions can be found in the literature regarding the computation of the block-diagonal matrices of the Gain matrix and the right-hand side vector [13].

Different from the model-decoupled version 8.2.3, once the decoupling assumptions are assured, the presented version of the algorithm-decoupled model leads to the same results provided by the coupled version, at the expense of higher computational cost. This is expected since no approximation is introduced in the right-hand side vector (recomputed at each iteration), which limits the effects of the approximation to the converge process only.

Algorithm 2: Algorithm-Decoupled State Estimator

Input: $z_A, z_R, h_A, h_R, R_A, R_R, H_{AA}, H_{AR}, H_{RA}, H_{RR}, \theta^0, V^0$
Output: Estimated states: x_A, x_R
Compute G_A^{ad} and G_R^{ad} ;
for $k = k+1$ **do**
  Active iteration:
  Compute T_A ;
  Solve (8.43) for $\Delta\theta^k$;
  Update θ ;
  Reactive iteration:
  Compute T_R ;
  Solve (8.45) for ΔV^k ;
  Update V ;
  until: $\Delta\theta^k$ and ΔV^k are larger than predefined tolerances
end

8.3 Bus-section level modeling in state estimation

Bus-branch modeling, applied in traditionally steady-state analyses, relays on the topology processor to build a simplified network model, where substation bus-sections connected through closed switch devices are merged to form a single node/bus. This procedure avoids the explicit representation of switching devices and allows a direct association of the basic network matrices, such as the admittance matrix and incidence matrix, with the resulting bus-branch model. Despite the advantages of this simplified model, it imposes the following limitations to state estimation studies: (a) the network connectivity described by bus-section and switch device is lost and the network topology is assumed correct, which may jeopardize the bad data process (by mistaking topology error as gross measurement error); (b) in practice, meter location is given in terms of bus-sections and switches devices,

which means that not all of them can be assigned in the measurement set of the bus-branch model, clearly reducing the redundancy level [10]; (c) if topology error pass undetected through topology processor, bus-branch model is compromised and state estimation will yield incorrect results; and (d) processing topology error using conventional bus-branch model is not always effective.

The GSE arises to tackle the above critical issues. In this approach, the physical level representation of the network is adopted, where the switches and circuit breakers are explicitly represented, deriving the bus-section model [10]. The state vector is extended and a set of additional information is added either in terms of pseudo-measurements or equality constraints, resulting in an enlarged problem [10]. Thanks to the explicit representation of the substations arrangements, the GSE enabled the development of a new series of more efficient algorithms for the topology error processing, such as [14–18]. Further developments have been presented in the literature to cope with the increase in the problem size imposed by the bus-section level representation, such as the zoomed-pack area [14], relevant subnetwork [19] and reduced substation representation [17]. The use of the decoupled technique has also been proposed [20] and can be seen as an important ally to GSE computational time reduction. The fast-decoupled version of the GSE is presented and discussed in the next sections.

8.3.1 Generalized decoupled formulation

The generalized state vector includes the active and reactive power flow through switching branches as new state variables along with the complex bus voltages. As done before in Section 8.2, for decoupling purposes, the active and reactive nature of the state variables are used to form a partitioned extended state vector, that is:

$$\bar{x}_A = \begin{bmatrix} \theta \\ t \end{bmatrix} \tag{8.49}$$

$$\bar{x}_R = \begin{bmatrix} V \\ u \end{bmatrix} \tag{8.50}$$

where θ and V are the vector of phase and magnitude of bus voltage, respectively; t and u are the vector of active and reactive power flow through modeled switching devices, respectively.

The information regarding switching device status is included in the problem formulation as new pseudo-measurements. For a closed device connected between nodes k and m, the voltage drop and angle difference are zero ($V_k - V_m = 0$ and $\theta_k - \theta_m = 0$) and are included in z_o (with index cld). On the other hand, if the device is open, zero active and reactive power flow through the device ($t_{km} = 0$ e $u_{km} = 0$) are assumed (index opd). Following previous nomenclature [15], these equations are referred to as operational pseudo-measurements and will be represented in the extended problem as $z_o(\bar{x}) = 0$.

The extended formulation must also include the zero active and reactive injections at bus-sections that arise from the physical representation of substations. This is done by considering $P_k = 0$ and $Q_k = 0$ for a given zero injection bus-section k.

Finally, bus-section level representation shall envisage the common occurrence of network islanding, when a bus reference angle must be defined for each island. This information is also included as additional data under the form $\theta_i = 0$ for each reference bus/bus-section i. These new sets of information are collectively referred to as structural pseudo-measurements equations, represented by $z_s(\bar{x}) = 0$. Isolated nodes/subsections may be excluded to reduce the problem formulation.

In the decoupled approach, the extended measurement vector $\bar{z}$, as well as its corresponding vector of nonlinear functions, can be partitioned according to the active and reactive nature of their components, as follows:

$$\bar{z}_A = \begin{bmatrix} z_m^A \\ z_o^A \\ z_s^A \end{bmatrix} \tag{8.51}$$

where:

$$z_m^A = \begin{bmatrix} z_{P_{flow}} \\ z_{P_{inj}} \end{bmatrix} \tag{8.52}$$

$$z_o^A = \begin{bmatrix} z_{\theta_{\text{cld}}} \\ z_{t_{\text{opd}}} \end{bmatrix} \qquad h_o^A = \begin{bmatrix} \theta_{\text{cld}} \\ t_{\text{opd}} \end{bmatrix} \tag{8.53}$$

$$z_s^A = \begin{bmatrix} z_{P_{\text{null}}} \\ z_{\theta_{\text{ref}}} \end{bmatrix} \qquad h_s^A = \begin{bmatrix} P_{\text{null}} \\ \theta_{\text{ref}} \end{bmatrix} \tag{8.54}$$

and

$$\bar{z}^R = \begin{bmatrix} z_m^R \\ z_o^R \\ z_s^R \end{bmatrix} \tag{8.55}$$

where:

$$z_m^R = \begin{bmatrix} z_{Q_{flow}} \\ z_{Q_{inj}} \\ z_V \end{bmatrix} \tag{8.56}$$

$$z_o^R = \begin{bmatrix} z_{V_{\text{cld}}} \\ z_{u_{\text{opd}}} \end{bmatrix} \qquad h_o^R = \begin{bmatrix} V_{\text{cld}} \\ u_{\text{opd}} \end{bmatrix} \tag{8.57}$$

$$z_s^R = \begin{bmatrix} z_{Q_{\text{null}}} \end{bmatrix} \qquad h_s^R = \begin{bmatrix} Q_{\text{null}} \end{bmatrix} \tag{8.58}$$

where the subscripts m, o, and s refer to conventional measures, operational pseudo-measurements, and structural pseudo-measurements, respectively. $h_{\theta_{\text{cld}}}$ and $h_{V_{\text{cld}}}$ are the function vectors composed by the zero angular difference and zero voltage drop across

closed breakers, respectively. $h_{t_{\text{opd}}}$ and $h_{u_{\text{opd}}}$ are the function vectors of zero active and reactive power flow through open breakers, respectively. P_{null} and Q_{null} are the function vectors of active and reactive injections at null injection nodes, respectively.

As the power flow through the switchable devices are defined as state variables, the nonlinear functions that represent the active and reactive power injections at bus k are revised [10, 16], being expressed by:

$$P_k = \sum_{m\in\Omega_k} P_{km}(V_k, V_m, \theta_k, \theta_m) + \sum_{l\in\Gamma_k} t_{kl} \tag{8.59}$$

$$Q_k = -Q_k^{sh}(V_k) + \sum_{m\in\Omega_i} Q_{km}(V_k, V_m, \theta_k, \theta_m) + \sum_{l\in\Gamma_k} u_{kl} \tag{8.60}$$

where, P_k (Q_k) is the active (reactive) power injection at bus k; P_{km} (Q_{km}) is the active (reactive) power flow through conventional branches $k-m$; t_{kl} (u_{kl}) is the active (reactive) power flow through switchable devices $k-l$; Ω_k is the set of buses connected to bus k through conventional branches; and Γ_k is the set of buses connected to bus k through switchable devices.

In line with the $P\theta$ and QV partition of the extended state and measurement vectors, the GSE Jacobian matrix can be expressed as:

$$\overline{H} = \begin{bmatrix} \overline{H}_{AA} & \overline{H}_{AR} \\ \overline{H}_{RA} & \overline{H}_{RR} \end{bmatrix} \tag{8.61}$$

where:

$$\overline{H}_{AA} = \begin{bmatrix} \dfrac{\partial P_{flow}}{\partial \theta} & \dfrac{\partial P_{flow}}{\partial t} \\ \dfrac{\partial P_{inj}}{\partial \theta} & \dfrac{\partial P_{inj}}{\partial t} \\ \dfrac{\partial \theta_{cld}}{\partial \theta} & \dfrac{\partial \theta_{cld}}{\partial t} \\ \dfrac{\partial t_{opd}}{\partial \theta} & \dfrac{\partial t_{opd}}{\partial t} \\ \dfrac{\partial P_{null}}{\partial \theta} & \dfrac{\partial P_{null}}{\partial t} \\ \dfrac{\partial V}{\partial \theta_{ref}} & \dfrac{\partial u}{\partial \theta_{ref}} \end{bmatrix}, \overline{H}_{AR} = \begin{bmatrix} \dfrac{\partial P_{flow}}{\partial V} & \dfrac{\partial P_{flow}}{\partial u} \\ \dfrac{\partial P_{inj}}{\partial V} & \dfrac{\partial P_{inj}}{\partial u} \\ \dfrac{\partial \theta_{cld}}{\partial V} & \dfrac{\partial \theta_{cld}}{\partial u} \\ \dfrac{\partial t_{opd}}{\partial V} & \dfrac{\partial t_{opd}}{\partial u} \\ \dfrac{\partial P_{null}}{\partial V} & \dfrac{\partial P_{null}}{\partial u} \\ \dfrac{\partial \theta_{ref}}{\partial V} & \dfrac{\partial \theta_{ref}}{\partial u} \end{bmatrix}, \tag{8.62}$$

$$\overline{H}_{RA} = \begin{bmatrix} \dfrac{\partial Q_{flow}}{\partial \theta} & \dfrac{\partial Q_{flow}}{\partial t} \\ \dfrac{\partial Q_{inj}}{\partial \theta} & \dfrac{\partial Q_{inj}}{\partial t} \\ \dfrac{\partial V_{mag}}{\partial \theta} & \dfrac{\partial V_{mag}}{\partial t} \\ \dfrac{\partial V_{cld}}{\partial \theta} & \dfrac{\partial V_{cld}}{\partial t} \\ \dfrac{\partial u_{opd}}{\partial \theta} & \dfrac{\partial u_{opd}}{\partial t} \\ \dfrac{\partial Q_{null}}{\partial \theta} & \dfrac{\partial Q_{null}}{\partial t} \end{bmatrix}, \overline{H}_{RR} = \begin{bmatrix} \dfrac{\partial Q_{flow}}{\partial V} & \dfrac{\partial Q_{flow}}{\partial u} \\ \dfrac{\partial Q_{inj}}{\partial V} & \dfrac{\partial Q_{inj}}{\partial u} \\ \dfrac{\partial V_{mag}}{\partial V} & \dfrac{\partial V_{mag}}{\partial u} \\ \dfrac{\partial V_{cld}}{\partial V} & \dfrac{\partial V_{cld}}{\partial u} \\ \dfrac{\partial u_{opd}}{\partial V} & \dfrac{\partial u_{opd}}{\partial u} \\ \dfrac{\partial Q_{null}}{\partial V} & \dfrac{\partial Q_{null}}{\partial u} \end{bmatrix}$$

The operational equations related to switchable devices are linear with respect to the extended state vector so that the corresponding blocks of the Jacobian matrix are merely composed by "0" and "1", resulting in:

$$\overline{H}_{AA} = \begin{bmatrix} \frac{\partial P_{flow}}{\partial \theta} & 0 \\ \frac{\partial P_{inj}}{\partial \theta} & 0;\pm 1 \\ 0;\pm 1 & 0 \\ 0;\pm 1 & 0 \\ \frac{\partial P_{null}}{\partial \theta} & 0;\pm 1 \\ 0;1 & 0 \end{bmatrix}, \overline{H}_{AR} = \begin{bmatrix} \frac{\partial P_{flow}}{\partial V} & 0 \\ \frac{\partial P_{inj}}{\partial V} & 0 \\ 0 & 0 \\ 0 & 0 \\ \frac{\partial P_{null}}{\partial \theta} & 0 \\ 0 & 0 \end{bmatrix}, \tag{8.63}$$

$$\overline{H}_{RA} = \begin{bmatrix} \frac{\partial Q_{flow}}{\partial \theta} & 0 \\ \frac{\partial Q_{inj}}{\partial \theta} & 0 \\ 0 & 0 \\ 0 & 0 \\ 0 & 0 \\ \frac{\partial Q_{null}}{\partial \theta} & 0 \end{bmatrix}, \overline{H}_{QV} = \begin{bmatrix} \frac{\partial Q_{flow}}{\partial V} & 0 \\ \frac{\partial Q_{inj}}{\partial V} & 0;\pm 1 \\ \frac{\partial V_{mag}}{\partial V} & 0 \\ 0;\pm 1 & 0 \\ 0 & 0;\pm 1 \\ \frac{\partial Q_{null}}{\partial V} & 0;\pm 1 \end{bmatrix}$$

Correspondingly, the extended Gain matrix can be represented as:

$$\overline{G} = \begin{bmatrix} \overline{G}_{AA} & \overline{G}_{AR} \\ \overline{G}_{RA} & \overline{G}_{RR} \end{bmatrix} \tag{8.64}$$

From (8.63), it is clear that the operational pseudo-measurements contribute only (and linearly) with the block diagonal submatrices (H_{AA} and H_{RR}), having no numerical influence over the off-diagonal submatrices H_{AR} and H_{RA} (for which the corresponding elements are null). Structural pseudo-measurements can be grouped along with the conventional power injection measurements, in the case of null power injections, and a vector of reference bus (one for each island) replaces the single reference bus of bus-branch modeling. It can be concluded that the bus-section modeling does not deteriorate the decoupling nature of the Jacobian matrix. On the contrary, it is reinforced in the GSE approach, where bus-section model of the network is adopted.

Therefore, all previously discussed decoupling techniques can be applied to GSE formulation. The model- and algorithm-decoupled versions of the fast-decoupled GSE can be easily derived, and its performance is subject to the same assumptions discussed before.

8.4 *cpu*-based fast-decoupled DSSE

The effectiveness of the $P\theta - QV$ decoupling is subject to high X/R ratios of transmission lines, characteristic naturally assigned to transmission systems (TS). For this reason, traditionally, fast-decoupled approaches were not recommended for DS applications, where low X/R ratios imply in higher sensitivity of the active quantities with respect to the bus-voltage magnitudes and of the reactive quantities regarding the phase angles.

The *cpu* normalization, discussed in Chapter 7, has allowed a pattern shift. By adopting a complex power base, with a predefined base angle, this generalized normalization artificially adjusts the X/R ratio of the DS parameters to the same level as those found in TS, allowing an effective use of the decoupled approaches to DS. When applied in association with the fast-decoupled state estimation, this alternative approach brings the latter well-known effectiveness, robustness, and computational efficiency to meet the needs required to process the active nature, the large dimension, and topologies of the newly raised DS networks.

The *cpu* normalization of the available data and set of measurements enables the fast-decoupled DS state estimation (FD-DSSE). This, in turn, allows the processing of distribution networks that may contain strong insertion of DGs and eventual transition from radial to mixed radial-meshed topology. In addition, fast-decoupled computational performance is an important ally to deal with the large dimension of DS in real-time operation.

The concepts and definitions of the *cpu* technique along with its effectiveness when combined with fast-decoupled power flow are presented in Chapter 7. The particularities of the *cpu* application to the state estimation problem are discussed next.

8.4.1 Data and measurement under cpu *normalization*

The *cpu* normalizes the network data in the same way as conventional *pu* normalization, except that it uses a complex power base (voltage bases are kept real). The computation of the power base angle, base quantities and of the normalized values for branch and bus data, such as series resistance and reactance, shunt susceptances, active, and reactive injections, are described in Chapter 7, subsection 7.3.1. When the decoupled state estimator is intended to be applied to DSs, a new set of input data must be submitted to the complex normalization process: measures and pseudo-measures.

It should be emphasized that, as for power flow studies, when properly applied, *cpu*-based fast-decoupled state estimation provides exactly the same solution for the state variables as those obtained when convectional *pu* is chosen. The difference lies in the *cpu* ability to provide an effective solution for the DSSE via fast-decoupled approaches.

8.4.2 Conventional measurement data in cpu *system*

The active and reactive power injection at bus k in the *cpu* system is given by:

$$\dot{S}_{k_{[cpu]}} = P_{k_{[cpu]}} + jQ_{k_{[cpu]}} = \frac{P_{k_{[W]}} + jQ_{k_{[Var]}}}{S_{\text{base}_{[VA]}} e^{-j\phi_{\text{base}}}} \tag{8.65}$$

Applying Euler's identity, the normalized value of an active and reactive power injection measure at bus k in *cpu* system is computed by:

$$z_{P_{k_{[cpu]}}} = \frac{z_{P_{k_{[W]}}}}{S_{\text{base}_{[VA]}}} cos\phi_{\text{base}} - \frac{z_{Q_{k_{[Var]}}}}{S_{\text{base}_{[VA]}}} sin\phi_{\text{base}} \tag{8.66}$$

$$z_{Q_{k_{[cpu]}}} = \frac{z_{Q_{k_{[Var]}}}}{S_{\text{base}_{[VA]}}} \cos\phi_{\text{base}} + \frac{z_{P_{k_{[W]}}}}{S_{\text{base}_{[VA]}}} \sin\phi_{\text{base}} \tag{8.67}$$

From (8.66) and (8.67), it is clear that, if the power injection measurement is available in conventional *pu* system, the conversion to the *cpu* system is given by:

$$z_{P_{k_{[cpu]}}} = z_{P_{k_{[pu]}}} \cos\phi_{\text{base}} - z_{Q_{k_{[pu]}}} \sin\phi_{\text{base}} \tag{8.68}$$

$$z_{Q_{k_{[cpu]}}} = z_{Q_{k_{[pu]}}} \cos\phi_{\text{base}} + z_{P_{k_{[pu]}}} \sin\phi_{\text{base}} \tag{8.69}$$

Similarly, the power flow measures through branch $k - m$ are converted to the *cpu* system by the following equations:

$$z_{P_{km[cpu]}} = \frac{z_{P_{km[W]}}}{S_{\text{base}_{[VA]}}} \cos\phi_{\text{base}} - \frac{z_{Q_{km[Var]}}}{S_{\text{base}_{[VA]}}} \sin\phi_{\text{base}} \tag{8.70}$$

$$z_{Q_{km[cpu]}} = \frac{z_{Q_{km[Var]}}}{S_{\text{base}_{[VA]}}} \cos\phi_{\text{base}} + \frac{z_{P_{km[W]}}}{S_{\text{base}_{[VA]}}} \sin\phi_{\text{base}} \tag{8.71}$$

The conversion from *pu* to the *cpu* system can be expressed by:

$$z_{P_{km[cpu]}} = z_{P_{km[pu]}} \cos\phi_{\text{base}} - z_{Q_{km[pu]}} \sin\phi_{\text{base}} \tag{8.72}$$

$$z_{Q_{km[cpu]}} = z_{Q_{km[pu]}} \cos\phi_{\text{base}} + z_{P_{km[pu]}} \sin\phi_{\text{base}} \tag{8.73}$$

The presence of phasor unit measurements (PMUs) in the electrical power system provides voltage phasor at its connected bus and current phasor through adjacent transmission lines and transformers (subject to channel availability). The phasor voltage at bus k in *cpu* is the same as in the *pu* system, as discussed before, so it does not need to be converted. The current phasor measurement, however, must be converted to *cpu* system, as follows.

Since the power base is complex, the current base in *cpu* system is also a complex quantity, that is:

$$\mathbf{I}_{\text{base}} = \frac{V_{\text{base}}}{S_{\text{base}} e^{j\phi_{\text{base}}}} = I_{\text{base}} e^{-j\phi_{\text{base}}} \tag{8.74}$$

Thus, the normalization of the PMU current phasor measurement in *cpu* is given by:

$$z^{PMU}_{I_{km[cpu]}} = \frac{z^{PMU}_{I_k m[A]}}{I_{\text{base}} e^{-j\phi_{\text{base}}}} = \frac{I_{km[A]}}{I_{\text{base}}} e^{j(\theta_i + \phi_{\text{base}})} = z^{PMU}_{I_{km[pu]}} e^{j(\theta_i + \phi_{\text{base}})} \tag{8.75}$$

Usually, rectangular form is adopted to incorporate the phasor current measurement in state estimation formulation [21, 22]. In this case, the corresponding real and imaginary values in *cpu* system can be computed by:

$$z^{PMU}_{I_{\text{real}[cpu]}} = \frac{I_{km[\text{real}]}}{I_{\text{base}}}\cos(\theta_i + \phi_{\text{base}}) = z^{PMU}_{I_{\text{real}[pu]}}\cos(\theta_i + \phi_{\text{base}}) \tag{8.76}$$

$$z^{PMU}_{I_{\text{imag}[cpu]}} = \frac{I_{km[\text{Imag}]}}{I_{\text{base}}}\sin(\theta_i + \phi_{\text{base}}) = z^{PMU}_{I_{\text{imag}[pu]}}\sin(\theta_i + \phi_{\text{base}}) \tag{8.77}$$

8.5 Measurement simulator

For SE studies, the measurement simulator is an essential requirement to provide a coherent set of measures, from which new SE methodologies can be tested and evaluated. For this purpose, the power flow analysis results are used to generate the system true state values and a corresponding set of perfect measures. This is a common practice in studies involving TS state estimation [20, 23], where classical power flow methods apply, such as Newton–Raphson and fast-decoupled approach. Random errors are then introduced, emulating the small magnitude intrinsic errors of the measurement process.

The measurement simulator is identically needed in DS state estimation studies. When the *cpu*-based fast-decoupled DS state estimator is chosen, *cpu*-based fast-decoupled power flow, described in Chapter 7, Subsection 7.3.2, can be explored to generate the true state vector and the set of *perfect* measurements composed of the true values of the measured quantities (in *cpu* or *pu* system, as desired).

Equation (8.1), reproduced in (8.78), describes the measurement model as a function of the true values and the measurement errors:

$$z = z_{\text{true}} + \eta \tag{8.78}$$

The true (perfect) measurement vector, z_{true}, is obtained by an exact power flow, as discussed above. The measurement error vector η follows the common assumptions regarding its statistical properties [8], that is, measurement errors are random Gaussian variables with zero mean and standard deviation calculated to reflect the expected accuracy of the meter. Since measurement errors are assumed independent, the covariance matrix, R, is a diagonal matrix, given by:

$$R = \text{diag}(\sigma_1^2, \sigma_2^2, \ldots \sigma_m^2)\,, \tag{8.79}$$

where σ_i is the standard deviation of measurement i and m is the number of measurements.

The computation of the measurements' standard deviation is clearly a relevant issue for the effectiveness of WLS-SE, since it defines the weight of each measurement in the estimation process (8.1), and, therefore, it must properly reflect the quality of the measurement. Usually, they are written as a function of the magnitude of the measured value and full scale of the measuring equipment [24]. The following are some of the main approaches used by industry and measurement simulation studies.

The standard deviation formula adopted by the American Electric Power Company's state estimator for power and voltage measurements is given by [25]:

$$\sigma_{\text{power}} = (6.7 \cdot S_{[VA]} + 1.6 \cdot fe) \cdot 10^{-3} \tag{8.80}$$

$$\sigma_V = (6.7 \cdot |V| + 1.6 \cdot fe) \cdot 10^{-3} \tag{8.81}$$

where fe is the full-scale deflection of the meter, and:

$$S_{[VA]} = \begin{cases} \sqrt{P_{flow}^2 + Q_{flow}^2} \text{ for power flow measurement} \\ \sqrt{P_{inj}^2 + Q_{inj}^2} \text{ for power injection measurement} \end{cases} \tag{8.82}$$

Typical values for $S_{[VA]}$ and $|V|$ can be adopted so that the covariance matrix does not need to be recomputed at each iteration unless a drastic change occurs.

In [8], the standard deviation values for power and voltage measurements are defined as function of the meter's precision class and full-scale deflection, pr and fe, respectively, that is:

$$\sigma_{\text{power}} = pr \cdot fe \tag{8.83}$$

$$\sigma_V = 0.1(pr \cdot fe) \tag{8.84}$$

The full-scale value can be defined in accordance with the system size and the largest magnitude expected for the measured quantity. For voltage magnitude, $fe = 1.1$, for example.

For measurement simulator purposes, the standard deviation of a simulated measurement i, σ_i, can be computed by [20, 23]:

$$\sigma_i = \frac{(pr \cdot z_{\text{true}i})}{3} \tag{8.85}$$

where pr is again the precision class and z_{true_i} is the true value of the measured quantity i, obtained by the exact power flow method.

Finally, the measurement error of a simulated measurement i can be defined by the desired characteristic of the meter and a random (normally distributed) number, α, that is [20, 23]:

$$\eta_i = (3\sigma_i) \cdot \alpha \tag{8.86}$$

It is important to mention that the random errors inserted by the measurement simulator correspond to the smaller magnitude errors, defined as normal noise. This noise is caused by imperfections in measuring instruments, current and potential transformers (TCs and TPs), meter accuracy or even the presentation of the supervisory control and data acquisition system. Extreme errors are filtered out before the state estimation process itself, while gross errors are subject to a more elaborate processing that relies on the redundancy of the measurement plan and the intrinsic capacity of the estimators to detect and identify these errors.

8.6 *cpu*-based real-time distribution system network modeling algorithm

Figure 8.1 illustrates the main steps of a *cpu*-based real-time network modeling for DSs. The network configuration is the first step of the algorithm, where a conventional or a generalized topology processing can be chosen. The conventional topology processing results in the traditional bus-branch network modeling. The

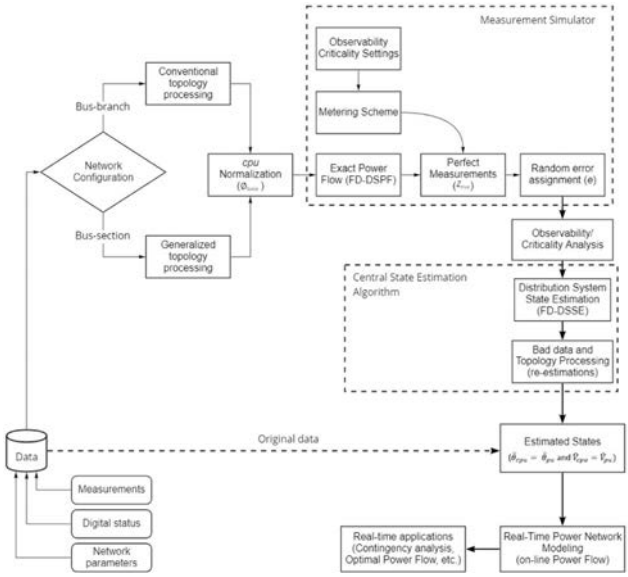

Figure 8.1 cpu-*based fast-decoupled state estimator*

generalized topology processing, in turn, allows the explicit representation of normally open switches in the network model. In this way, maneuvers involving these switches for ring operations or network reconfiguration, commonly required in DS, are automated and easily represented into the network model. It also applies to strategically represent the suspect region (a piece of the network whose bus sections and switches are modeled and solved explicitly) for topology error detection and identification, as commonly applied in advanced TS topology-error/bad-data processing algorithms, such as those proposed in [14–18].

The *cpu* normalization of the original data is the fundamental step to enable a reliable application of the fast-decoupled state estimation to DSs. Equation (7.37) (Chapter 7, subsection 7.3.1.1) is effective in providing a proper power base angle for the *cpu* normalization process, assuring that the well-known high performance and effectiveness of fast-decoupled method is reproduced when applied to *cpu*-normalized DS networks. It should be emphasized that in *cpu* system, the power base magnitude and the real voltage bases are assigned exactly as in the conventional per unit system, as discussed in Chapter 7, subsection 7.3.1.

The following steps of the *cpu*-based real-time network modeling are summarized in Figure 8.1. Measurement simulator is triggered only for the purposes of studies involving the state estimation process. Since the estimated values of bus voltage magnitudes and angles obtained in *cpu* system are exactly the same as those obtained with a conventional *per* (*pu*) system, they can be used along with the original data to provide the real-time model (on-line power flow model) of the monitored distribution network, without the need of *cpu* "deconversion," as illustrated in 8.1.

Finally, it should be noted that a null base angle adoption in the *cpu* normalization step implies in the conventional *pu* normalization [7]. It means that the algorithm in 8.1 consists of a unique tool capable to process TS and DS networks simply by properly calculating the complex power base angle [7, 20].

8.7 Case studies and performance evaluation

To illustrate the application of the *cpu*-based DSSE algorithm depicted in Figure 8.1, the 141-bus distribution test-system whose online diagram is shown in Figure 7.8, Chapter 7, is used. The original data can be found in Matpower [26], which implies in an average X/R ratio of 0.705184. Dashed lines in Figure 7.8, Chapter 7, represent normally open switching devices and are explicitly represented (as described in Section 8.3) by triggering the generalized topology processing. From that on, two topological configurations are simulated: typically radial topology, in which all the switching devices are kept open, and a fully meshed topology, where all devices are closed. Besides, two different levels of DG insertion are considered: the base case, without DG, and a 50% DG insertion, with all even buses with DG (detail in Chapter 7). While a null DG level of insertion and radial topology emulate the typical passive characteristic of DSs, a high level of DG insertion and a fully meshed topology envision the expected evolution of modern active DSs. The extreme cases are designed to illustrate the versatility of the alternative approach described in this chapter.

Measurement schemes are composed by voltage magnitude, active and reactive power injection measurement at all even buses, and active and reactive power flow measurement through all branches. In this way, redundancy is assured and the computational performance is stressed since a high number of measurement need to be processed. The reader can find additional results in Ref. [20], where the performance of the *cpu*-based DSSE algorithm considering distinct redundancy levels involving a real 907-nodes European test-feeder are employed and evaluated.

The data *cpu* normalization step assigns a proper base angle for each DG level. The *cpu* base angle computation follows Ref. [7] (see also Chapter 7 for details and specific values for the employed 141-bus test-system).

Measurement simulation provides the perfect set of measurement z_{true} from an exact power flow, the standard deviations, σ, and meter imprecision error, η, computed for each measurement using (8.85) and (8.86), with $pr = 2\%$.

As regards the accuracy of results (Central State Estimation Algorithm), the estimated state values obtained from each of the following approaches are compared with the true values resulting from the exact power flow calculation from where all measurements have been simulated.

- cpu_{md}: model-decoupled SE
- cpu_{ad}: algorithm-decoupled SE
- cpu_{full}: full SE, without decoupling

Table 8.1 Accuracy of the estimated measurements in DSSE considering radial topology (x10⁻³)

GD	**Voltage magnitude**		**Angle**	
	ε^{max}	$\bar{\varepsilon}$	ε^{max}	$\bar{\varepsilon}$
cpu_{md}	0.3518	0.2960	0.0442	0.0259
cpu_{ad}	0.0474	0.0087	0.0271	0.0552
cpu_{full}	0.0318	0.0042	0.01201	0.0367
no DG	**Voltage magnitude**		**Angle**	
	ε^{max}	$\bar{\varepsilon}$	ε^{max}	$\bar{\varepsilon}$
cpu_{md}	1.1693	1.1036	0.0874	0.0347
cpu_{ad}	0.0112	0.0084	0.0164	0.0083
cpu_{full}	0.0073	0.0030	0.0083	0.0024

The absolute error (ε) and the mean absolute error ($\bar{\varepsilon}$) are the metrics used to evaluate the obtained results, as summarized in Table 8.1. While cpu_{ad} keeps the accuracy of the results within the convergence threshold ($\epsilon = 10^{-3}$), the cpu_{md} imposes (acceptable) approximations, as expected. Different from traditional DSSE, where weekly meshed topologies require elaborate procedures to avoid performance degradation, the cpu_{based} FD-DSSE has seen its performance improve when fully meshed topology is considered, as shown in Table 8.2. This is a relevant feature when the envisioned configuration of modern DS, with a massive insertion of DG, is to be analyzed.

Table 8.3 presents a computational time performance comparison between the model- and the algorithm-decoupled versions with the full approach, cpu_{full} (largest time referred to as t_0). For all cases of the considered test-system, the cpu_{md} and

Table 8.2 Accuracy of the estimated measurements in DSSE considering meshed topology (x10⁻³)

GD	**Voltage magnitude**		**Angle**	
	ε^{max}	$\bar{\varepsilon}$	ε^{max}	$\bar{\varepsilon}$
cpu_{md}	0.4859	0.1700	0.1273	0.1023
cpu_{ad}	0.0340	0.0190	0.0318	0.0251
cpu_{full}	0.0382	0.017	0.0275	0.0179
no DG	**Voltage magnitude**		**Angle**	
	ε^{max}	$\bar{\varepsilon}$	ε^{max}	$\bar{\varepsilon}$
cpu_{md}	1.3758	1.3114	0.0732	0.0467
cpu_{ad}	0.0495	0.0070	0.0521	0.0394
cpu_{full}	0.0260	0.0016	0.0108	0.0062

Table 8.3 Relative computational time

	Radial topology without DGs	**Radial topology with DGs**	**Meshed topology without DGs**	**Meshed topology with GDs**
cpu_{md}	0.59 t_0	0.64 t_0	0.20 t_0	0.23 t_0
cpu_{ad}	0.59 t_0	0.66 t_0	0.23 t_0	0.24 t_0
cpu_{full}	0.86 t_0	t_0	0.61 t_0	0.70 t_0

cpu_{ad} present equivalent performance, always much less time consuming than the cpu_{full} algorithm. It should be emphasized that the difference in computational performance between both decoupled versions, as well as between each of them and the full version, tends to increase as the system size increases. This is the case of real-size distribution feeders/systems, where thousands of buses can be easily reached, and model-decoupled computational performance may be indispensable.

8.8 Final remarks

This chapter describes a *cpu*-based DSSE methodology. The alternative approach uses the *cpu* system to efficiently extend the fast-decoupled approaches, originally developed to TS, so as to accommodate the distribution network characteristics.

It also includes the bus-section model for the network, where strategically located switches/breakers (switchable branches) or suspect regions/substations can be explicitly represented. This allows commonly used maneuvers in DS system be easily handled at the same time that contributes to the topology error processing algorithms.

Enabling the use of decoupling techniques for SD offers a series of advantages involving modern DS, whose advances and needs move toward the characteristics previously exclusive to TS, such as active nature, advanced measurement infrastructure, meshed topology, and so on.

Finally, the decoupled formulation is especially important to reduce the numerical burden associated with the dimension of the DSSE, where a high number of nodes and measurements (a single feeder may contain thousands of buses) needs to be handled in real-time operation.

References

[1] Baran M.E., Kelley A.W. ‘State estimation for real-time monitoring of distribution systems’. *IEEE Transactions on Power Systems*. 1994, vol. 9(3), pp. 1601–9.

[2] Lu C.N., Teng J.H., Liu W.-H.E. ‘Distribution system state estimation’. *IEEE Transactions on Power Systems*. 1995, vol. 10(1), pp. 229–40.

[3] Baran M.E., Kelley A.W. 'A branch-current-based state estimation method for distribution systems'. *IEEE Transactions on Power Systems*. 1995, vol. 10(1), pp. 483–91.
[4] Ghosh A.K., Lubkeman D.L., Downey M.J., Jones R.H. 'Distribution circuit state estimation using a probabilistic approach'. *IEEE Transactions on Power Systems*. 1997, vol. 12(1), pp. 45–51.
[5] Roytelman I., Shahidehpour S.M. 'State estimation for electric power distribution systems in quasi real-time conditions'. *IEEE Transactions on Power Delivery*. 1993, vol. 8(4), pp. 2009–15.
[6] Celik M.K., Liu W.H. 'A practical distribution state calculation algorithm'. *1999 Winter Meeting*; New York, August; 1999. pp. 442–7.
[7] Tortelli O.L., Lourenço E.M., Garcia A.V., Pal B.C. 'Fast decoupled power flow to emerging distribution systems via complex Pu normalization'. *IEEE Transactions on Power Systems*. 2014, vol. 30(3), pp. 1351–8.
[8] Abur A., Exposito A.G. *Power System State Estimation: Theory and Implementation*. 1st edition. New York: CRC Press; 2004.
[9] Schweppe F., Wildes J. 'Power system static-state estimation, part I: Exact model'. *IEEE Transactions on Power Apparatus and Systems*. 1970, vol. PAS-89(1), pp. 120–5.
[10] Monticelli A. *Power System State Estimation: A Generalized Approach*. Boston, MA: Kluwer Academic Publishers; 1999.
[11] Horisberger RJC H.P., Rossier C. 'Fast-decoupled static state-estimator for electric power systems'. *IEEE Transactions on Power Systems*. 1976, vol. PAS-95(1), pp. 208–15.
[12] Monticelli A., Garcia A. 'Fast decoupled state estimators'. *IEEE Transactions on Power Systems*. 1990, vol. 5(2), pp. 556–64.
[13] Garcia A., Monticelli A., Abreu P. 'Fast decoupled state estimation and bad data processing'. *IEEE Transactions on Power Apparatus and Systems*. 1979, vol. PAS-98(5), pp. 1645–52.
[14] Alsac O., Vempati N., Stott B., Monticelli A. 'Generalized state estimation'. *IEEE Transactions on Power Systems*. 1998, vol. 13(3), pp. 1069–75.
[15] Clements K.A., Costa A.S. 'Topology error identification using normalized Lagrange multipliers'. *IEEE Transactions on Power Systems*. 1998, vol. 13(2), pp. 347–53.
[16] Lourenco E.M., SimoesCosta A., Clements K.A. 'Bayesian-based hypothesis testing for topology error identification in generalized state estimation'. *IEEE Transactions on Power Systems*. 2004, vol. 19(2), pp. 1206–15.
[17] Expósito A.G., de la Villa Jaen A. 'Reduced substation models for generalized state estimation'. *IEEE Transactions on Power Systems*. 2001, vol. 16(4), pp. 839–46.
[18] Lourenço E.M., Coelho E.P.R., Pal B.C. 'Topology error and bad data processing in generalized state estimation'. *IEEE Transactions on Power Systems*. 2015, vol. 30(6), pp. 3190–200.
[19] Coelho T.C., Lourenço E.M., Simões Costa A., Costa A.S. 'Anomaly zone determination for topology error processing in power system state estimation'.

Journal of Control, Automation and Electrical Systems. 2013, vol. 24(3), pp. 312–23.

[20] Nogueira E.M., Portelinha R.K., Lourenço E.M., Tortelli O.L., Pal B.C. 'Novel approach to power system state estimation for transmission and distribution systems'. *IET Generation, Transmission & Distribution*. 2019, vol. 13(10), pp. 1970–8.

[21] Phadke A.G., Thorp J., Zhou M. 'Recent developments in state estimation with Phasor measurements'. *Power Systems Conference and Exposition*; 2009. pp. 1–7.

[22] Huang Y.F., Werner S., Gupta V. 'State estimation in eletric power grids: Meeting new challenges presented by the requirements of the future grid'. *IEEE Transactions on Power Systems*. 2012, vol. 29(5), pp. 33–43.

[23] Castillo M.R.M., London J.B.A., Bretas N.G., Lefebvre S., Prevost J., Lambert B. 'Offline detection, identification, and correction of branch parameter errors based on several measurement snapshots'. *IEEE Transactions on Power Systems*. 2010, vol. 26(2), pp. 870–7.

[24] Irving M.R., Owen R.C., Sterling M.J.H. 'Power-system state estimation using linear programming'. *IET Proceedings of the Institution of Electrical Engineers*. 1978, vol. 125(9), pp. 879–85.

[25] Gómez-Expósito A., Conejo A.J., Cañizares C. *Electric Energy Systems: Analysis and Operation*. Boca Raton, FL: CRC Press; 2018.

[26] Khodr H.M., Olsina F.G., Jesus P.M.D.O.-D., Yusta J.M. 'Maximum savings approach for location and sizing of capacitors in distribution systems'. *Electric Power Systems Research*. 2008, vol. 78(7), pp. 1192–203.

This page intentionally left blank

Chapter 9

Bayesian approach for distribution system state estimation

Marco Pau[1], Paolo Attilio Pegoraro[2], Ferdinanda Ponci[1], and Sara Sulis[2]

9.1 Introduction

When dealing with the new Smart Grid scenario, it is clear that the distribution grid will play a fundamental role. Indeed, the most important changes in the electric system will probably concern the distribution network [1], which was traditionally considered mainly a passive infrastructure but, in the last decade, underwent strong transformations, pushed by market liberalisation and technological evolution. Distributed generation (DG) has already become one of the key factors of the new paradigm, and thus distribution grids can no longer be conceived only as a mean to transfer energy from transmission network to the users. Possible bidirectional flows must be considered by every new approach to network management and control, which will rely on the contribution from all the different and fast changing players interfaced with the network.

In this perspective, new typologies of customers and loads are rapidly emerging. Considering, for instance, the electric vehicles, which will have a disruptive effect on the consolidated electric grid management and planning, it appears evident that a higher capacity of the system will be required, and that the complexity will increase constantly in the next years while the transition towards a carbon-free society evolves [2]. Unpredictability and variability of new consumption and generation patterns and the widespread presence of power electronics and storage technologies ask for new control applications.

The prerequisite for an efficient management of the distribution grid is given by the possibility to monitor the operating conditions accurately and frequently. For this reason, distribution system state estimation (DSSE) will play an important role

[1]E.ON Energy Research Center, Institute for Automation of Complex Power Systems, RWTH Aachen University, Aachen, Germany

[2]Department of Electrical and Electronic Engineering, University of Cagliari, Cagliari, Italy

in the design of a future-proof monitoring architecture by providing valuable information to the applications and to automated decision-making.

DSSE is thus receiving greater attention in recent years, in conjunction with the introduction of modern measurement devices, such as distribution-level phasor measurement units (D-PMUs) and smart meters (SMs). DSSE needs to address the peculiarities of distribution systems and the resulting challenges [3]. This requires a great activity on both algorithms and architectures. Algorithms for DSSE have been proposed since the 1990s [4, 5], but only in the last decade the research activity has been boosted [6–8].

Many problems in the definition of DSSE must be addressed. One of the most important is the lack of measurements to fully monitor the network. The accuracy of DSSE is strictly related to amount and quality of available information on voltages, currents, injected or absorbed power, power flows, and so on. Despite the great efforts in proposing new [9] and low-cost devices [10] that are tailored for distribution network needs and that can be installed to upgrade the monitoring infrastructure, it is not possible to foresee that a full, or even redundant, direct monitoring of the quantities of interest in real time will be available in distribution systems in the near future (as it is, instead, for transmission systems).

For this reason, DSSE will rely strongly on the so-called pseudo-measurements. Pseudo-measurements are, from a general perspective, every kind of available information that can be used to integrate real-time measurements from the field. The most typical and important type of pseudo-measurements is represented by data on power consumption or injection at network nodes. Information about power absorption and generation is thus key for designing a DSSE algorithm and typically includes historical and forecast data. Advanced pseudo-measurement models keep into account also non-electrical measurements such as climatic data or weather forecast information, which can have a significant impact on expected power, and thus they require refined techniques and accurate descriptions.

In practice, real-time measurements are few in a distribution system, and pseudo-measurements are the prevailing source of information in DSSE definition, which allows reaching the needed observability of the network and thus solving the estimation task. Pseudo-measurements are thus essential, but they are obviously not as accurate as real-time measurements.

In most common DSSE implementations, all the available data must be associated with their uncertainty so that each value (measured or pseudo-measured) is weighted depending on this accuracy. Pseudo-measurements are, as already mentioned, typically associated with forecast power evaluations based on statistical and historical data. The accuracy of the available data is typically low with respect to a real-time power measurement, and thus the relevance of each pseudo-measurement within the DSSE must be weighted accordingly. For instance, the assumed active power at a specific hour for a specific load is the result of the modelling process, which can involve several quantities (also measurements) and is thus described by a range of possible values that can be quite large, depending on the accuracy of the available information and of the adopted prediction model. The uncertainty of the pseudo-measurements significantly affects the accuracy of DSSE, and thus it is

important to describe the possible power values in a statistical way through an appropriate representation of the confidence intervals and of the associated probabilities.

Pseudo-measurements are used in DSSE design, and their impact on the estimation performance has been analysed recently [11], considering also the source of pseudo-measurement values. In Ref. [12], for instance, aggregation of data recorded by SMs was considered to define meaningful pseudo-measurements. Pseudo-measurements based on an artificial neural network (ANN) load modelling have been proposed [13]. Other methods are also based on ANN to forecast power and define pseudo-measurements starting from previous DSSE results [14]. New applications have also emerged, and thus, according to the characteristics of the involved loads and generators, new pseudo-measurement descriptions need to be introduced. For instance, in Ref. [15], demand-response-enabled loads are considered, and a technique to define pseudo-measurements when dealing with these types of loads has been proposed for DSSE.

Loads and generators (in particular the distributed generators), and their combination, the so-called prosumers, do not have Gaussian distributions, as typically assumed in the weighted least square (WLS) formulations of the DSSE. Their statistical description can be therefore much more complex. In traditional DSSE formulations, only some summarising parameters can be used to grasp the variability of pseudo-measured power. For example, standard deviation (STD) is often used in the WLS formulation. However, a concise representation is intrinsically an approximate representation, and this could result in additional estimation errors for the DSSE output.

Much research has been devoted to the description of loads, which should reflect on pseudo-measurement definition. In Ref. [16], different models were considered to represent load power and, in particular, the normal, the log-normal and the beta distributions were used as possible candidates. Beta distribution was preferred since it has parameters that can be fine-tuned to obtain the target shape. The research in Ref. [17] also shows that beta distribution can be effectively used to represent the behaviour of residential loads. The statistics of absorbed power are clearly indicating non-Gaussian distributions as best suited for pseudo-measurement description. Gaussian mixture models (GMM) have been used to account for complex or multimodal behaviours [18, 19]. Under this framework, data distribution is represented as a weighted sum of Gaussian distributions. This can be interesting, for instance, when both loads and generators are connected to the same node in the network, and the net power balance needs to be modelled.

All the mentioned contributions show how the distribution underlying the pseudo-measurement model can be extremely complex and vary, depending on the considered scenario and the load or DG properties. Thus, the pseudo-measurement, in general, summarises an extremely variegated statistical behaviour, and DSSE requires a flexible framework that allows integrating the available information seamlessly without turning to possibly coarse approximations. DSSE accuracy strongly depends on the uncertainty description of pseudo-measured quantities and, for this reason, it is important to find new techniques to deal with unmonitored nodes and to integrate the available statistics in DSSE in a more complete and accurate way.

In Ref. [20], the proposal is to treat non-Gaussian statistics through transformations that can be performed only when the distribution is analytically known and that allow finding equivalent normal data.

It is important to remind here that also real-time measurements from field instrumentation can have non-Gaussian uncertainty descriptions, which, as will be discussed in the next sections, ask for specific DSSE solutions. Considering all these aspects, in this chapter, a recently proposed method for DSSE based on a Bayesian approach that allows considering every available statistics of the measured and pseudo-measured quantities is presented and discussed [21, 22]. The main idea is to exploit directly the empirically obtained distribution of absorbed or generated power and the available instrument specifications through the application of the Bayes' rule to the estimation process. The objective is to go beyond the simplified description that is typically used for measurements and pseudo-measurements in the WLS formulation (see, e.g., [6]), or in similar methods, and to address the complex conditions that can arise in modern and future networks. Features and potentialities of the method based on this innovative Bayesian approach (Bayesian DSSE) are theoretically introduced and discussed with the help of simulation results based on real-field data.

9.2 Power statistics and pseudo-measurements

One of the most important sources of pseudo-measurements is given by the statistics of power consumption or generation. In the following, some examples are reported and discussed, with the aim to illustrate how probability distributions can be extremely variegated, thus confirming the need for a tool such as the Bayesian DSSE, which allows integrating the available information with all its peculiarities.

In the following, the discussion is based on real-world data available every 15 minutes or every hour, considered for the definition of the power-related statistics. Clearly, many other approaches can be used, but the aim of this section is to highlight the importance of an accurate description, whatever the specific source of what, in the DSSE context, can be called 'prior information'.

Power profiles and power statistics may depend on the network voltage level, on the geographical and topological characteristics, on people behaviour and economic scenario. When considering loads and generators, it is important to keep into account also the non-electrical information, that is, at least, the season, the type of day (working days, weekend days, festivities) and the time of the day.

Focusing on low voltage systems, the SMs, monitoring either the connected load or distributed generator (or both) can be used to gather important information on the power characteristics. Active and reactive power injection or absorption can be obtained both for statistics and for day ahead forecast. Single users clearly show high variability in their consumption and are almost unpredictable, but the statistics of aggregated loads can be better described. Bayesian DSSE can be applied at different levels and thus pseudo-measurement definition and estimation performance depend on the considered scenario.

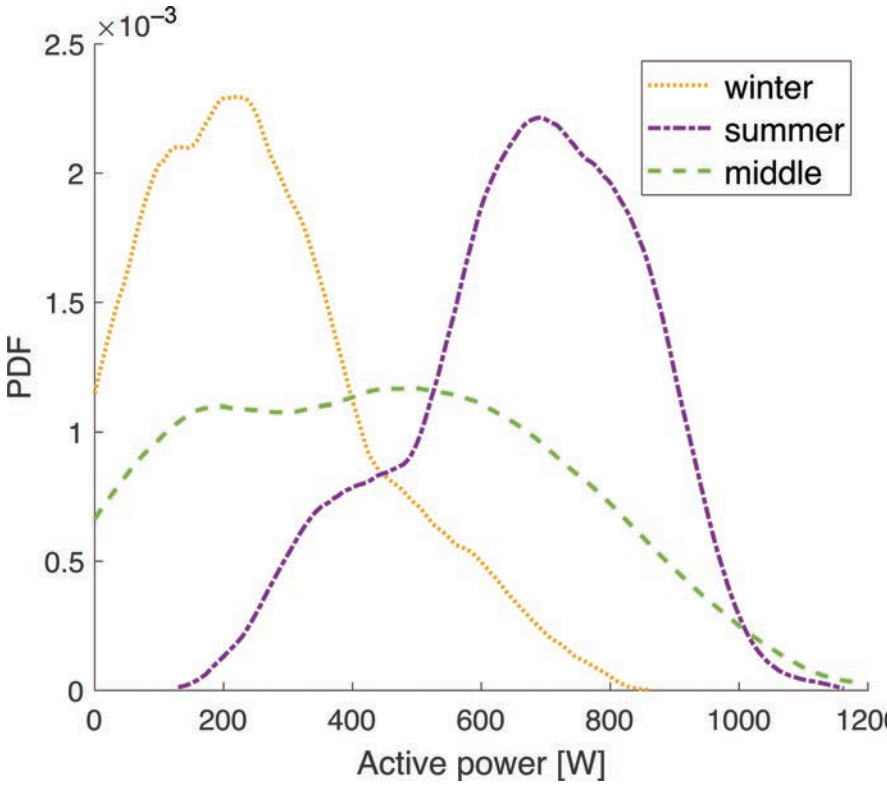

Figure 9.1 Empirical PDF computed from SM data for a small photovoltaic unit

Electrical customers at low voltage typically present power consumption time series that are far from Gaussianity, when considered as random processes, and renewable generation at customer premises also offers a variable and non-Gaussian behaviour. Besides, when dealing with prosumers, the power balance statistics are even more complex, and it is important to keep in mind that emerging applications, such as demand-response, might reshape the probabilistic behaviour. Figure 9.1 shows the non-Gaussian behaviour of active power for a small photovoltaic unit, obtained from the actual data of a customer in Italy recorded by the installed SM. The probability density functions (PDFs), obtained via kernel distribution fitting (Epanechnikov kernel is adopted, for example), refer to the quarter of hour after 13.00 in a day belonging to different seasons. Figure 9.2 shows instead the PDFs of the power balance for the same customer and time of the day during a working day. Negative power indicates absorption, since the convention of injected power is always adopted in this chapter. Even though the figures are related to a specific example, they clearly show why pseudo-measurements must rely on a meaningful statistical description. Every additional information that can help in refining the model and building more informative data should be used as input for the DSSE.

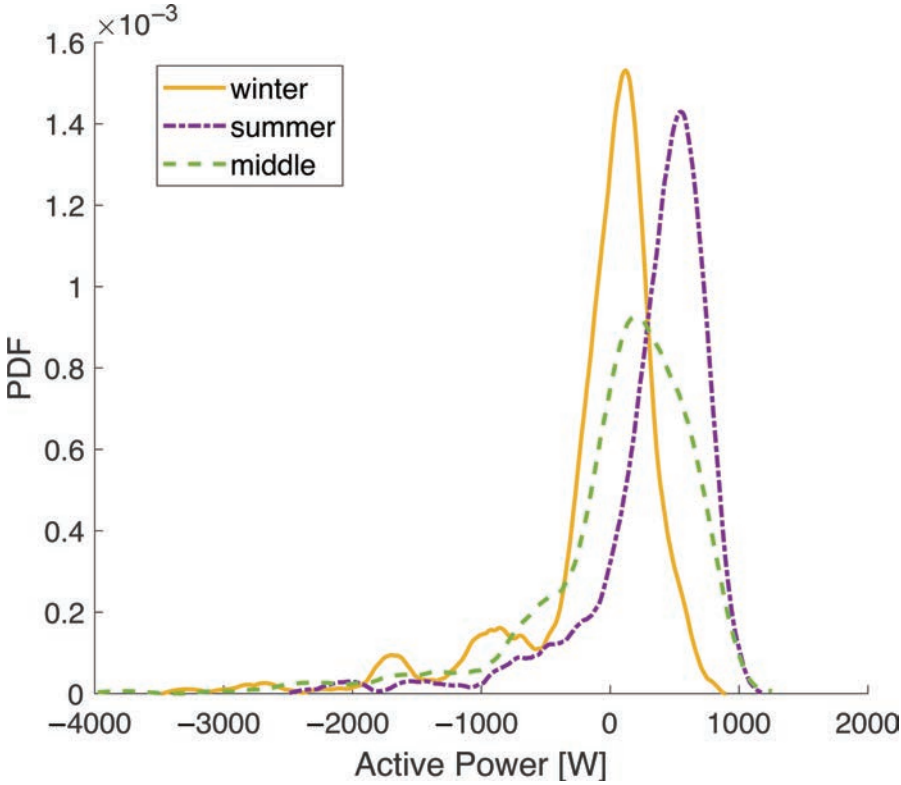

Figure 9.2 Empirical PDF computed from SM data for a prosumer with photovoltaic unit

In the following, medium voltage (MV) grids are instead considered. At this level, the contributions of many customers are aggregated to give a single pseudo-measurement information. This might seem a counterexample for the Bayesian approach application, which will be discussed in the following, since one might expect to achieve Gaussianity through aggregation. However, this is not true in this context since customer behaviours can be extremely variegated and, typically, each aggregated MV load is the result of different load sizes and typologies, such as apartments, schools, as well as commercial and industrial customers. The widespread presence of DG contributes in shaping the statistics of the overall power, which are the main elements of interest in the DSSE formulation at MV level. Level of aggregation and load type prevalence are relevant aspects, and the choice of the correct representation is an important task for the distribution system operator. It is thus easy to understand why a Bayesian approach can give a handful tool for a seamless integration of the available information. Indeed, one of its most important aspects is flexibility, because every kind of data distributions can be accommodated when needed.

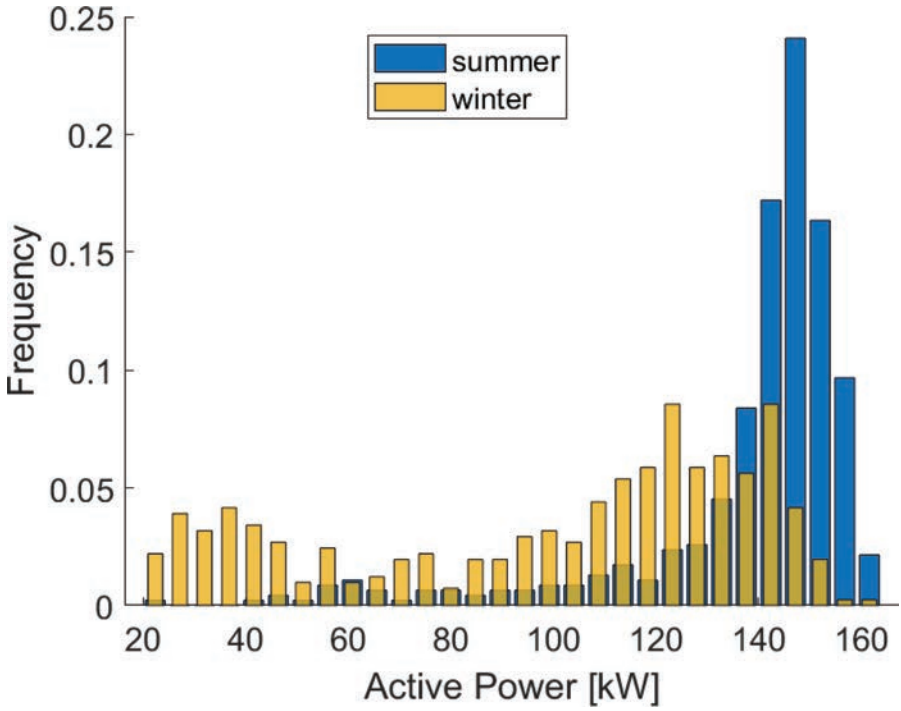

Figure 9.3 Histograms of active power for a 200-kW photovoltaic plant for different seasons

In the following, a few examples of power statistics for both loads and generators at MV are reported to strengthen the above claims through a visual inspection of the probability representations. The PVWatts calculator tool [23], which was designed on the basis of historical irradiance data, allows generating power profiles and comparing different statistics, depending on the hour and the season. For instance, Figure 9.3 shows the histograms of the generated power for a sample photovoltaic plant (size 200 kW) at hour 12.00 during either a summer or a winter day. The histogram counts are normalised so that statistical frequency is reported and reveals a clearly skewed distribution which, depending on the considered season, is more peaked towards the nominal power of the plant. Generated power depends also on the specific hour of the day, as it can be seen from Figure 9.4, where the same power plant production is represented through two histograms associated with different hours: 12.00 and 17.00 during a summer day.

Similar considerations hold also for the load power at MV. Here the examples are drawn from the OpenEI repository [24], considering the state of California, United States. Figure 9.5 clearly shows that also for a hospital the absorbed power can vary greatly depending on the hour, because of the different activities carried out at the hospital, which, from the point of view of the DSSE, is represented as a large load and summarised by its power consumption.

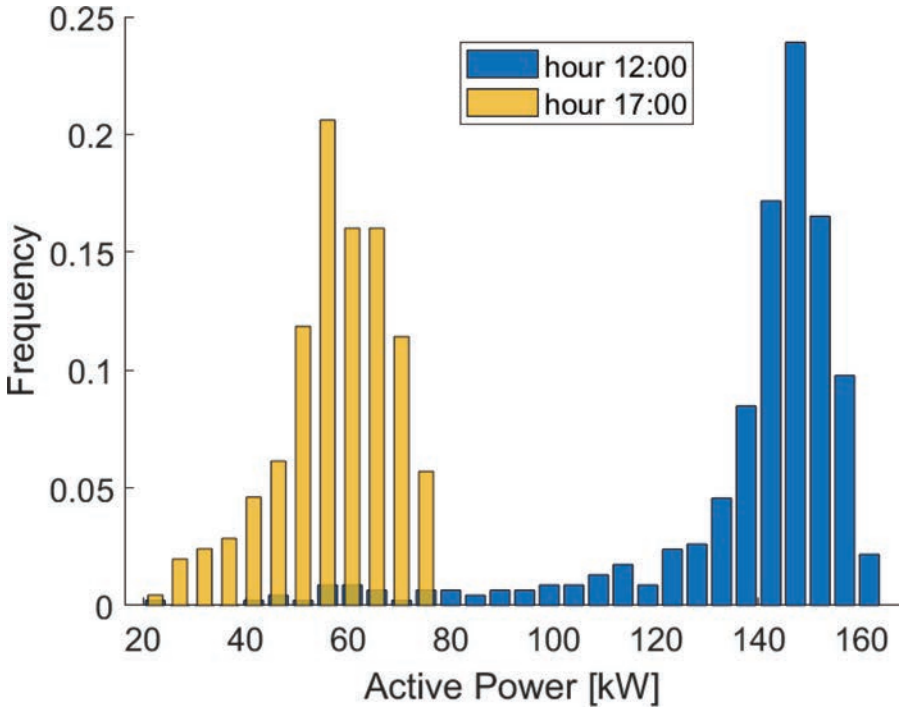

Figure 9.4 Histograms of active power for a 200-kW photovoltaic plant at different hours during summer

The characteristics of the load vary depending also on its peculiarities, because it can represent blocks of flats, supermarkets, shops, schools, and so on, with various levels of aggregation and of DG. Every type of load has its own power absorption pattern, because the underlying activities have different dynamics. Moreover, each activity depends on the hour, day or season in a different manner. For instance, Figure 9.6 shows the active power histograms for a typical primary school during both working days and Sundays. The plots are referred to 10.00 and show the reduced power drawn during weekends.

The above examples, even if partial, show why it is important to consider the most refined available information, that is to use the best available statistics about the considered power. The DSSE must be designed to use the active and reactive power data and must be capable of using all measurement types, which can include both supervisory control and data acquisition (SCADA) measurements and new generation synchronised measurements, which are becoming more and more interesting also for distribution systems [25].

When available, node power measurements can be directly integrated into the method according to the procedure described in Section 9.3.2. The Bayesian approach implicitly assumes that all the measured quantities are referred to the same time instant, which becomes the estimation time instant. If some measurements are either

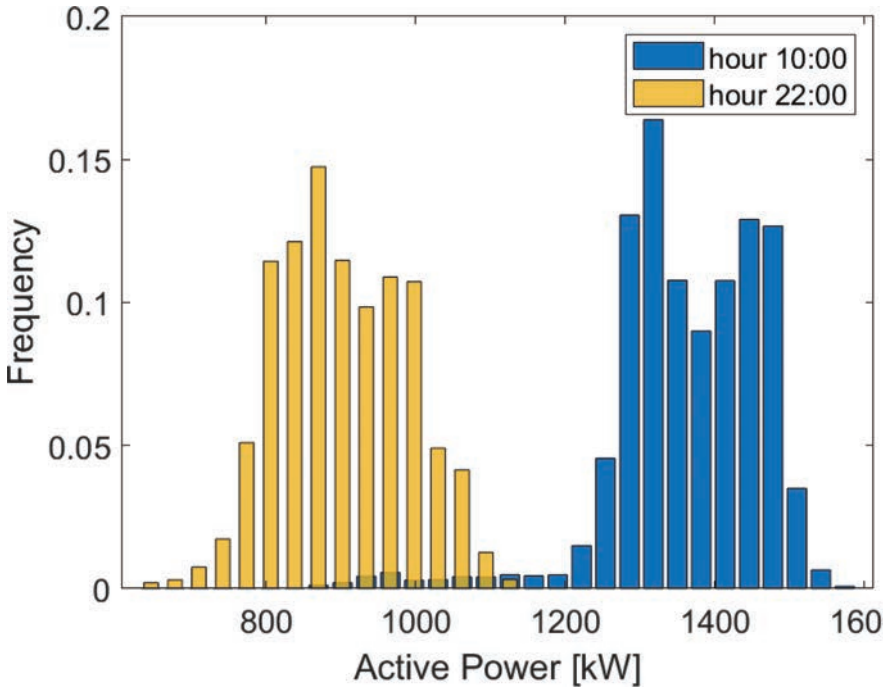

Figure 9.5 *Histograms of active power for a hospital at different hours during mid-season*

non-synchronised (thus lacking any time reference) or belong to a different time window with respect to the others, they must be carefully handled. In fact, different measurement instruments have different synchronisation accuracies and rely on different measurement calculation procedures. A detailed description of instrument features is beyond the scope of this chapter, but it is important to highlight that each digital instrument has not only a different synchronisation degree (when available) but also a different time interval to which the measured value refers. Indeed, each measurement requires a set of samples, i.e., an observation window, and the window duration impacts on both the accuracy and the latency of the measurement process. For this reason, when the measurement timestamp is not available or it is not extremely accurate, the distribution associated with the measurement can be relaxed and modified to keep into account possible time shifts. As it will become clear in the next section, the Bayesian approach perfectly meets this metrological need, because the variable associated with a measurement, a derived measurement or a pseudo-measurement is always treated in the same way, leaving the required flexibility to the uncertainty description.

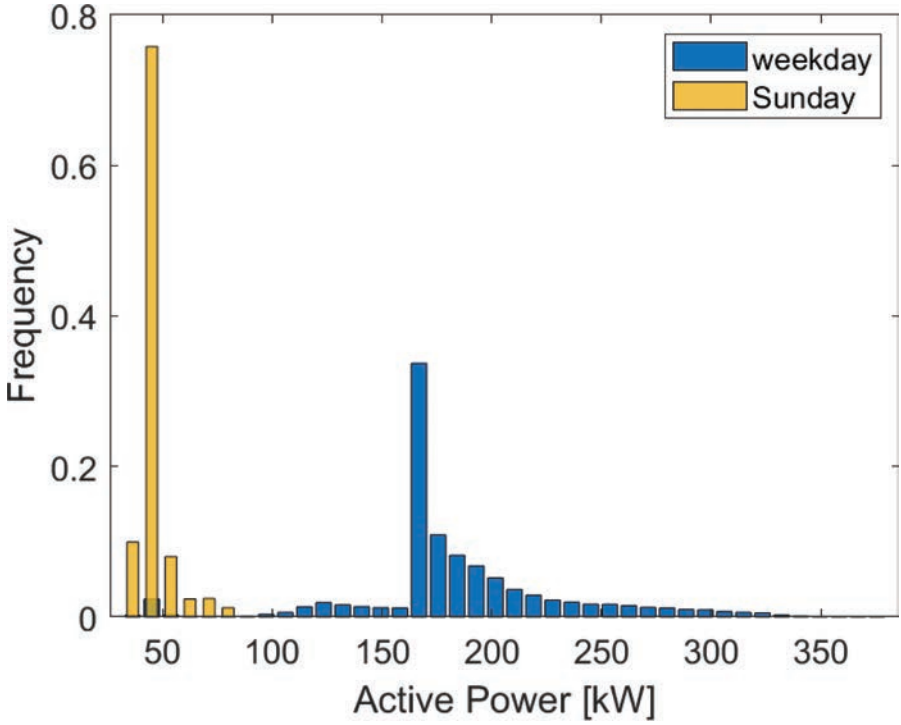

Figure 9.6 Histograms of active power for a typical primary school in different days

9.3 Bayesian approach for state estimation in distribution systems

In this section, the innovative Bayesian DSSE, which leads to a more accurate DSSE algorithm, is presented. First, an introduction to the considered measurement model is reported, so that it becomes clear why the Bayesian approach perfectly fits the inverse estimation problem while describing in an appropriate way all the available information uncertainties, such as those introduced in the previous section.

9.3.1 Measurement model

The basis of every estimation problem is the measurement model, which can be represented as:

$$\mathbf{z} = \mathbf{h}(\mathbf{x}) + \mathbf{e} \tag{9.1}$$

where $\mathbf{z}$ is the vector of the obtained measurements, which should include all the available information, measurements produced by the instruments on the field and pseudo-measurements computed starting from other sources (direct or indirect) of data concerning the network conditions. Vector $\mathbf{x}$ defines the N-dimensional state

vector, including a set of variables that is sufficient to uniquely determine the network operating point. **h** represents the measurement function vector, where the analytical relationships linking state variables to measured values are reported. Finally, **e** is the vector defining, for each measured quantity z_i (subscript i indicates the ith entry of a vector), the difference e_i between the reference model represented by $h_i(\mathbf{x})$ and z_i. The measurement error depends on the characteristics of the used instrumentation for real-time measurements and on the inaccuracy in the predicted values for pseudo-measurements.

Each measurement error e_i and, according to the above model, its associated measurement z_i can be considered as a random quantity, characterised by its PDF $f_{z_i}(\cdot)$, which depends on the probability distribution of the errors preventing an 'exact' knowledge of the actual values*. It is important to highlight that such random model is not equivalent to considering errors as random quantities in repeated measurements, but with a metrological viewpoint that is more coherent with the considered domain (power systems), it can be instead considered as the lack of knowledge associated with the available measurement. The description of such uncertainty is given by the PDF and thus depends on the instrument specifications, on the result of the characterisation process of meters and algorithms and, more in general, on the statistical description of possible errors [26].

Focusing on measurements, the only available information is usually given by instrument datasheets, which typically include only maximum deviations, represented by an accuracy value or by a range. If no further information is available, it is natural to assume that errors are uniformly distributed in the range and thus the PDF of measurement error e_i is:

$$f_{e_i}(a) = \begin{cases} \frac{1}{2\Delta e_i} & \text{when } a \in \left[-\Delta e_i, +\Delta e_i\right] \\ 0 & \text{otherwise} \end{cases} \tag{9.2}$$

where Δe_i is the maximum absolute error and a, from here on, indicates the generic realisation value.

In other circumstances, it is possible to assume Gaussianity. In fact, when the uncertainty specifications are given in terms of expanded uncertainty with a given coverage factor $k = 2$ or 3, this clearly points to normality in the error distribution. Sometimes, the Gaussianity of the errors is explicitly mentioned or it results from the sum of several independent error contributions through central limit theorem. In this case, it is sufficient to know the standard uncertainty associated with the error, i.e., the STD of the corresponding random variable [26], and the PDF is given as follows:

*This is clearly a simplification for illustration purposes only, because no 'true' value exists in measurement.

$$f_{e_i}(a) = \frac{1}{\sqrt{2\pi}\sigma_{e_i}} e^{-\frac{a^2}{2\sigma_{e_i}^2}} \tag{9.3}$$

where σ_{e_i} is the STD of e_i. Considering the model in (9.1) and assuming that $\mathbf{h}(\cdot)$ is deterministic, it is clear that, given the reference state $\mathbf{x}$, measurement z_i can be described by the same PDF as e_i. The only difference is given by the translation quantity $h_i(\mathbf{x})$, which directly impacts on the mean value of the random variable. For this reason, σ_{z_i} is always the same as σ_{e_i}. When considering the Gaussian PDF (9.3), σ_{e_i} is obtained as $\frac{\Delta e_i}{k}$. The deviation Δe_i is typically found in instrument specifications, and k depends on the level of confidence associated with the expanded uncertainty interval.

Considering instead pseudo-measurements, the description can be much more complex. In classical WLS DSSE formulations, not only measurements but also pseudo-measurements are typically assumed to be Gaussian random variables, each load is independent from the others and a large STD value (e.g., corresponding to 30–50% of the nominal load power) is considered as the only parameter to represent the variability. Some research activities have been focused on introducing correlation among pseudo-measurements [27], since it is evident that even forecast algorithms should leverage correlations present in power absorption among different loads or between active and reactive power.

However, as discussed before, these solutions cannot account for the high variability of the absorbed and generated powers, particularly when dealing with new technologies concerning DG, new load types or new management applications such as demand-response.

9.3.2 A Bayes framework for DSSE

In Refs. [21, 22], a novel approach to the estimation of the state is introduced to take advantage of rich statistical models about inputs $\mathbf{z}$. The underlying concept is the following: the state estimate $\hat{\mathbf{x}}$ can be computed through Bayesian estimation, that is by finding the posterior distribution of the state given the data available in $\mathbf{z}$ and their uncertainty description. Differently from the common interpretation of (9.1), it is also possible to separate the contribution of the real-time measurements (included in $\mathbf{z}$) and of prior information about the state variables.

The DSSE is performed through the following:

$$\hat{\mathbf{x}} = \mathbb{E}[\mathbf{x}|\mathbf{z}] = \iint_{\mathrm{A}} \mathbf{a} f_{\mathbf{x}|\mathbf{z}}(\mathbf{a}|\mathbf{z}) d\mathbf{a} \tag{9.4}$$

where the estimated state vector corresponds to the expectation of the posterior PDF. $f_{\mathbf{x}|\mathbf{z}}(\mathbf{a}|\mathbf{z})$ indicates the posterior density function depending on the uncertainty description, and A indicates the domain of integration, that is the domain of state variability. Vector $\mathbf{a}$ is the searching variable covering all possible state values. With a somehow loose notation, in (9.4), $\mathbf{z}$ indicates also the generic condition, for now left undetermined.

According to Bayes' rule, the posterior PDF can be rewritten as:

$$f_{\mathbf{x}|\mathbf{z}}(\mathbf{a}|\mathbf{b}) = \frac{f_{\mathbf{z}|\mathbf{x}}(\mathbf{b}|\mathbf{a}) f_{\mathbf{x}}(\mathbf{a})}{f_{\mathbf{z}}(\mathbf{b})} \tag{9.5}$$

where $f_{\mathbf{z}|\mathbf{x}}(\mathbf{b}|\mathbf{a})$ is the conditional PDF of the measured values (spanned by **b**, which stands for the observed value of **z**) with respect to the state realisation **a**, $f_{\mathbf{x}}(\mathbf{a})$ is the prior PDF of the state and $f_{\mathbf{z}}(\mathbf{b})$ is the overall PDF of the measured values (the so-called evidence value).

Measurements in **z** can include both conventional measurements and synchronised phasor measurements. Conventional measurements are voltage and current magnitudes, active and reactive power flows or injections. Synchronised phasor (synchrophasor) measurements instead include voltage phasors at nodes and current phasors, which can be both node and branch currents, and come from D-PMUs or PMU-like devices. PMUs are synchronised with a common timescale, linked to coordinated universal time (UTC) and obtained through global navigation satellite systems typically [28].

Real-time measurements, both conventional and synchronised, even in a near future scenario, are going to be insufficient for full network observability and thus for DSSE. As mentioned before, pseudo-measurement data are needed to deal with measurement scarcity, and thus it is essential to introduce their statistical description within the model. It is important to highlight that, since predicted power for loads and generators is highly uncertain and variable, the correct probabilistic description can be critical.

The most common approach is to define the statistics from historical data and time series, and thus non-Gaussian behaviour has to be expected, as clearly highlighted by the examples in Section 9.2. The PDF depends on the characteristics of the loads and on the interactions between loads and generators. As discussed above, an MV load can be, for instance, the result of the contributions of several customers, and there are many variables affecting power consumption. It is interesting to notice that the statistical distribution depends on the considered parameters (e.g., hour of the day, type of day, type of prevailing customers) and also on the available knowledge. It is therefore quite different to rely on pure historical data or on SM data for a short-term pseudo-measurement look ahead.

These considerations and the possible non-Gaussian behaviour of measurements again ask for a more complete probabilistic description of the involved quantities. According to the Bayes' approach, a possible model is obtained when considering a state representation in terms of power injections (or absorptions, depending on the convention). A node voltage phasor from a reference node must also be included to define a set of variables sufficient to uniquely define the network state. With this assumption, the state vector can be written as:

$$\mathbf{x} = \begin{bmatrix} V_s \\ \varphi_s \\ \mathbf{P} \\ \mathbf{Q} \end{bmatrix} \tag{9.6}$$

where V_s and φ_s are, respectively, the magnitude and phase angle of the node chosen as a reference (e.g., the slack bus would be a good choice). Vectors **P** and **Q** include the active and reactive power injections of all the nodes where a power contribution is present. Clearly, such powers can be conceived as the input power balance depending on the connected loads or generators.

The presented state definition is meaningful only if at least one PMU is available for real-time monitoring. Without any synchronised device, an absolute definition of the phase angle would not be possible with respect to UTC, and thus the reference voltage phase angle needs to be considered arbitrary (only relative phase definitions can be used) and should not be included in **x** [6]. In addition, when more PMUs are available at different nodes, the use of φ_s is not only possible but also leads to improvements in the estimation of the phase angle profile that allows going beyond PMU accuracy [29].

Once the state is defined, each PDF in (9.5) must be defined, and this is where the approach perfectly fits the measurement and pseudo-measurement uncertainty representation. Function $f_{\mathbf{x}}$ is thus the model of the input statistical description of **P** and **Q**, together with some prior information about reference voltage. Active and reactive powers can be represented by their PDFs, which can be obtained through two different approaches: starting from a given distribution, its parameters can be obtained from data, or the PDF can be obtained empirically using either histograms or empirical distribution fitting.

As for the prior of V_s, it can be chosen, for instance, as a uniform distribution in the a-priori variability range, for instance, 1 ± 0.1 p.u. For φ_s, there are different possible strategies. If the reference bus is equipped with a PMU, the range of variability around the measured value coincides with the expanded uncertainty interval, and thus an uniform PDF can be associated with it. When no PMU measurements are available at the reference node, it is easy to have a guess range along with a uniform distribution around a measured PMU voltage phase angle at another node (possibly a close one), since low phase angle differences usually appear in distribution networks. It is important to highlight that the reference node can be chosen according to the needs.

The conditional PDF $f_{\mathbf{z}|\mathbf{x}}(\mathbf{b}|\mathbf{a})$, which, with a change of perspective can be seen as the likelihood function, is associated with the measurement uncertainty description. Measurements from different on-field devices are typically considered as independent, and thus a Gaussian or uniform PDF can be defined for each measured value, depending on the device specifications. As mentioned before, when only maximum errors are reported in the datasheet, uniform distribution is better suited to the case at hand and thus it is possible to write:

$$f_{\mathbf{z}|\mathbf{x}}(\mathbf{b}|\mathbf{a}) = \prod_{i=1}^{M} f_{z_i|\mathbf{x}}(b_i|\,\mathbf{a}) = \begin{cases} \frac{1}{\prod_{i=1}^{M} 2\Delta e_i}, & \text{when } \mathbf{b} \in \prod_{i=1}^{M} [h_i(\mathbf{a}) - \Delta e_i,\ h_i(\mathbf{a}) + \Delta e \\ 0 \quad , & \text{otherwise} \end{cases} \tag{9.7}$$

where M is the number of measurements.

If Gaussian distributions can be assumed, the conditional PDF is instead:

$$f_{\mathbf{z}|\mathbf{x}}(\mathbf{b}|\mathbf{a}) = \prod_{i=1}^{M} \frac{1}{\sqrt{2\pi}\sigma_{e_i}} e^{-\frac{(b_i - h_i(\mathbf{a}))^2}{2\sigma_{e_i}^2}} \tag{9.8}$$

The above examples are only the two most common approaches, but nothing prevents from using more specific distributions when instrument specifications or other characterisations allow further details to be included. A full discussion about this point is beyond the scope of this chapter, but Section 9.3.3 will give further insight into the PMU case.

The solution of (9.4) is numerical, mainly because of the complex statistics that can be included through $f_{\mathbf{x}}$. It is important to highlight here that the aim is to allow the computation of (9.5). Conditional and prior PDFs are computed based on measured values, thus defining the posterior up to a factor, given by $f_{\mathbf{z}}(\mathbf{b})$. The term $f_{\mathbf{z}}(\mathbf{b})$ is the result of the integration of the numerator in (9.5) and, as will be discussed in the following, it is not necessary to find numerically the expectation in (9.4). This is intuitive, since $f_{\mathbf{z}}$, computed based only on the measured values, does not depend on the state candidate $\mathbf{a}$ and thus should not influence the procedure.

9.3.3 Measurement handling

Conventional measurements are directly handled as described above, through (9.7), (9.8) or a mix of the independent PDFs, depending on the available uncertainty description in the device specifications. If further details or different and specific PDFs are given for some measurements, they can be easily accommodated in a similar way.

Attention must be paid to D-PMU measurements, since the obtained values are magnitudes (rms values) and phase angles of voltage and current synchrophasors. As usual, datasheets can be quite different, but the uncertainty is typically expressed through either maximum relative magnitude errors (as percent values) and maximum phase angle deviations or percent total vector error (TVE). TVE corresponds to the relative vector error between the measured phasor and the reference one.

Considering, as an example, a measured node voltage synchrophasor $\dot{V} = Ve^{j\varphi_V}$ when accuracies of magnitude and phase angle measurements are available, uniform random variables can be used. Maximum magnitude deviation is obtained multiplying V by the maximum percent error while maximum phase angle deviation is already provided. The same holds true for current synchrophasors. Classical WLS

DSSE uses the same measurement accuracy description through STD calculation (σ_{e_i} is equal to the maximum deviation divided by $\sqrt{3}$ when uniform distribution is assumed).

When only TVE specification is known, with the Bayesian approach, it is possible to fit perfectly the uncertainty description. The maximum TVE % ($\text{TVE}_{\max}$) corresponds to a circle centred in the reference phasor and defining possible measurement outcomes. The joint PDF of amplitude and phase angle is thus (for a voltage synchrophasor, but the same holds for a current one):

$$f_{z_V,z_{\varphi_V}|\mathbf{x}}(V,\varphi_v|\mathbf{a}) \begin{cases} \dfrac{1}{\pi(V\cdot \text{TVE}_{\max}/100)^2} & \text{when } |Ve^{j\varphi_v} - \dot{h}_v(\mathbf{a})| \le V\cdot \text{TVE}_{\max}/100 \\ 0 & \text{otherwise} \end{cases} \tag{9.9}$$

where z_V and z_{φ_V} indicate the magnitude and phase angle random variables of the considered synchrophasor measurement, and $\dot{h}_v$ is the complex measurement function linking the synchrophasor to the generic state defined by $\mathbf{a}$.

9.3.4 Prior description

Active and reactive powers (with a sign depending on whether it is generated or absorbed) must be statistically described to be included in the Bayesian model through $f_{\mathbf{x}}$. As mentioned before, both analytical model and empirical distributions can be used to describe loads and generators, or, more generally, their aggregation in a given node.

Active and reactive powers of the same node (indicated as P_n and Q_n for a generic node n) can be correlated, therefore, prior PDFs should consider this aspect. A possible approach is to consider P_n and Q_n altogether through a bivariate PDF f_{P_n,Q_n}. The node power balance can thus be represented without macroscopic approximations. It is also possible to follow another approach, particularly useful when less data are available to extract the statistical description. The statistics of P_n and Q_n correspond to the marginal PDFs, and f_{P_n,Q_n} is defined through the use of a bidimensional copula, which allows keeping correlation into account.

A copula C_n can be associated with the two random variables P_n and Q_n so that the distribution of the copula becomes:

$$F_{C_n}(u_1,u_2) = \mathbb{P}[U_{P_n} \le u_1, U_{Q_n} \le u_2] \tag{9.10}$$

where $U_{P_n} = F_{P_n}(P_n)$ and $U_{Q_n} = F_{Q_n}(Q_n)$ are obtained transforming P_n and Q_n through their cumulative distribution functions F_{P_n} and F_{Q_n}, respectively. U_{P_n} and U_{Q_n} are thus uniform variables in the range $(0, 1)$. The distribution function F_{C_n} is the means to express the correlation between P_n and Q_n. This aspect is theoretically guaranteed by the Sklar's theorem [30], which states that univariate marginal distribution functions together with a copula can represent any joint distributions. Using this approach, it is possible to simplify the pseudo-measurement PDF definition, since active and reactive power PDFs can be derived from data and integrated with the model given by the copula to grasp data correlation. In the particular case of active and reactive power of a node, it is possible to write:

$$f_{P_n,Q_n}(p_n, q_n) = f_{C_n}(F_{P_n}(p_n), F_{Q_n}(q_n)) \cdot f_{P_n}(p_n) \cdot f_{Q_n}(q_n) \tag{9.11}$$

where, for a generic pair of values (p_n, q_n), the PDF is easily expressed through the three components. f_{C_n} is the PDF associated with $(F_{P_n}(p_n), F_{Q_n}(q_n))$, and different models can be adopted. For instance, a Gaussian copula can be very useful under many practical circumstances.

Considering all the aforementioned choices, a possible representation of the complete prior is:

$$f_{\mathbf{x}}(\mathbf{a}) = f_{V_s}(a_1) f_{\varphi_s}(a_2) \prod_{n \in \Lambda} f_{P_n,Q_n}(a_{i(n)}, a_{j(n)}) \tag{9.12}$$

where $i(n)$ and $j(n)$ are the indices of the active and reactive powers of node n within the state vector. The set Λ includes the indices of the considered buses that are interested by loads or generators, and the reference node is not counted among them. It is important to notice that $f_{\varphi_s}(a_2)$ is only present when absolute phase angle is included in the state.

The presented approach is both general and flexible. When zero-injection nodes are considered, it is very simple to use a state vector that includes only unknown quantities and replaces zero powers where needed in the measurement function formulation. This helps in avoiding the possible issues due to the insertion of zero-injection constraints as very accurate pseudo-measurements, as it is often done in conventional WLS-based DSSE, and is very useful, for instance, for MV network where several zero-injection buses may be present.

9.3.5 Numerical computation of the Bayesian DSSE

As mentioned before, the problem (9.4) allows a very good description of the uncertainty of all the involved quantities to be obtained, and it is typically solved through numerical methods. Clearly, the presented approach is independent from the specific estimation procedure, but it is interesting to know that there are techniques that are well suited for Bayesian DSSE solution. One of the most interesting is the Metropolis-Hastings (M-H) algorithm. In brief, M-H method seeks to produce a series of vectors $\mathbf{x}_k$ (a Markov chain), whose statistics correspond to a target distribution Γ. In the Bayesian framework, the target is given by the posterior $f_{\mathbf{x}|\mathbf{z}}$, and thus, once the computed state vectors are collected, the expectation of $\mathbf{x}$ can be calculated via numerical average.

In practice, M-H operates in two steps for each iteration k, starting from an initial guess $\mathbf{x}_0$:

1. First, a new candidate $\mathbf{y}_{k+1}$ is obtained, starting from the previous vector, from a transition PDF $\Pi(\mathbf{y}|\mathbf{x}_k)$. Typically, Π is considered symmetric, that is $\Pi(\mathbf{y}_{k+1}|\mathbf{x}_k) = \Pi(\mathbf{x}_k|\mathbf{y}_{k+1})$.
2. Then, $\mathbf{y}_{k+1}$ is either kept or discarded, based on an acceptance probability:

$$\alpha(\mathbf{y}_{k+1}|\mathbf{x}_k) = \min\left\{1, \frac{\Gamma(\mathbf{y}_{k+1})}{\Gamma(\mathbf{x}_k)}\right\} \tag{9.13}$$

when accepted, it becomes the new point $\mathbf{x}_{k+1}$, otherwise $\mathbf{x}_{k+1} = \mathbf{x}_k$.

It is important to notice that, when $f_{\mathbf{x}|\mathbf{z}}(\mathbf{y}_{k+1}) \geq f_{\mathbf{x}|\mathbf{z}}(\mathbf{x}_k)$, the proposal $\mathbf{y}_{k+1}$ is always accepted. So, when the target PDF is increasing, the point of the series continuously changes, otherwise it changes only with a probability α depending on the relative PDF decrease. In the latter case, acceptance can thus be checked through the extraction of a random value from a uniform distribution in (0, 1) and its comparison with α.

Another essential aspect for DSSE is that only a ratio between posterior PDF values is involved, and thus the denominator in (9.5) (the evidence value $f_{\mathbf{z}}$), which does not depend on the current point $\mathbf{x}_k$, or on the proposal $\mathbf{y}_{k+1}$, but only on measured values, does not need to be computed. Indeed any normalising constant can be neglected.

To make the numerical algorithm more effective and stable, it is useful to exploit logarithms of the involved quantities. When using the prior expression in (9.12), α can be thus computed for each iteration as:

$$\begin{aligned}\log(\alpha(\mathbf{y}_{k+1}|\mathbf{x}_k)) \quad &= \min\left\{1, \sum_{i=1}^{M}\left[\log f_{z_i|\mathbf{x}}(\mathbf{y}_{k+1}) - \log f_{z_i|\mathbf{x}}(\mathbf{x}_k)\right]\right. \\ &+ \log f_{V_s}(V^y_{s,k+1}) - \log f_{V_s}(V_{s,k}) + \log f_{\varphi_s}(\varphi^y_{s,k+1}) - \log f_{\varphi_s}(\varphi_{s,k}) \\ &+ \sum_{n\in\Lambda}\left[\log f_{C_n}(F_{P_n}(p^y_{n,k+1}), F_{Q_n}(q^y_{n,k+1})) - \log f_{C_n}(F_{P_n}(p_{n,k}), F_{Q_n}(q_{n,k}))\right. \\ &+ \left.\left. \log f_{P_n}(p^y_{n,k+1}) - \log f_{P_n}(p_{n,k}) + \log f_{Q_n}(q^y_{n,k+1}) - \log f_{Q_n}(q_{n,k})\right]\right\}\end{aligned} \tag{9.14}$$

where $V_{s,k}$, $\varphi_{s,k}$, $p_{n,k}$, $q_{n,k}$ are the current point values for voltage magnitude, voltage phase angle, active and reactive power at node n, respectively. Superscript y indicates instead the candidate values. Equation (9.14) can be modified accordingly if additional correlations or multivariate priors are considered.

Under a few hypotheses, the computed Markov chain is ergodic and converges to the target posterior distribution. There are many possible ways to customise the M-H algorithm to the specific DSSE problem, by using, for instance, an adaptive Π [21] that changes along the chain to speed up the space exploration.

Then, N_p points belonging to the series $\mathbf{x}_k$ with $k = 1, \ldots, N_p$ are obtained. The state space can be assumed to be covered according to the needed posterior distribution, and thus it is straightforward to find the estimation of (9.4) through:

$$\hat{\mathbf{x}} = \frac{1}{N-k_0+1}\sum_{k=k_0}^{N}\mathbf{x}_k \tag{9.15}$$

where k_0 determines the initial invalid points (burn-in period). The estimated state $\hat{\mathbf{x}}$ is thus a simple average of the available states. The average value is an unbiased estimation of the state vector given the available measurements, their uncertainty description and pseudo-measurements statistics.

It is also possible to compute other statistical indices on the available series realisation. For instance, as will be discussed in the next section, percentiles of the posterior are useful to evaluate also the uncertainty intervals corresponding to given confidence levels, so that a sound estimation of the uncertainty can also be associated with the estimated states.

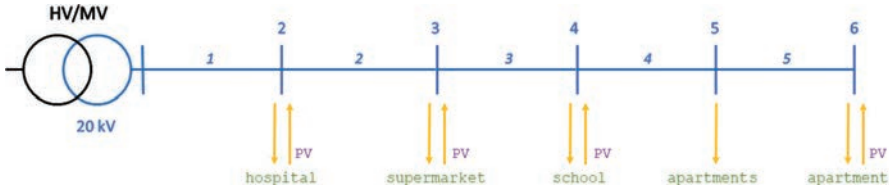

Figure 9.7 Simple MV network used for the tests

9.4 Examples of Bayesian distribution system state estimation

In this section, some examples of the estimation results obtained with the Bayesian DSSE are discussed in order to investigate its properties and the advantages in terms of estimation accuracy and uncertainty description. To make the presentation simple and effective, a small MV network is used, and the simulation results obtained through different tests and configurations are discussed. The network is extremely simple and is composed of six buses along a single feeder. Figure 9.7 reports the topology of the considered MV network along with the node and branch numbers and the indications about what type of loads are involved and where DG is present. Each node presents a combination of loads and generators, chosen as representative of possible realistic conditions for illustrative purposes. The MV side rated voltage is 20 kV and, since the focus is mainly on the description of the loads, the lines have been configured to have all the same length, 0.8 km, and impedance ($0.7031 + j0.141\ \Omega$/km), corresponding to a real cable (OC_AL_50_169 from project Atlantide [31]).

Measurements can have different accuracies depending on their type and on the considered instrument. The measurement system includes all the available measurements and, as mentioned before, their integration into the DSSE depends on their characteristics (possibility to measure absolute phase angle, description of the instrument specifications, etc.). In the following, each measurement is associated with its accuracy, and the accuracy is associated with the assumed distribution. Uniform distribution is considered for all the real-time measurements, and its maximum deviation is equal to the considered accuracy. The maximum deviation is 1% for voltage magnitude and 3% for active and reactive power flow measurements, which are used to monitor specific branches.

The pseudo-measurements and their probability representation are built according to the available data, similar to those described in Section 9.2. From each dataset, the PDF is obtained using a kernel distribution fitting. Other strategies can be adopted, from models matching given distributions to GMM, where a few Gaussian distributions are linearly combined to deal with non-Gaussian behaviours, such as the presence of multiple modes. The chosen method is not particularly important for the Bayesian approach, but, clearly, it can affect the quality of the representation and also the speed of the posterior computation.

It was proven in the literature [29] that voltage measurements have a direct impact on the accuracy of the estimated voltage profile and, even more interesting,

their presence has a global effect, particularly when the network is not heavily loaded and when only highly uncertain pseudo-measurements are available. This means that the improvement on the voltage profile carried by an additional voltage measurement can be felt all across the network, even far away from the measurement point. In addition, the estimation accuracy, to a first approximation, reflects mainly the accuracy and the number of voltage measurements. This effect can be obtained both with synchronised and conventional instruments, but its extent depends on their accuracy. It is thus more interesting to focus on power estimations (power flows or power injections), which are instead significantly affected by pseudo-measurement description quality. These quantities, along with currents, are mainly affected by the accuracy of near pseudo-measurements and of power and current measurements, due to the local effect of information on current estimations [32]. For this reason, in the following, results in terms of estimated node active power are reported, which can be essential for distribution management system applications.

Different results can be obtained with different measurement configurations. Starting with a default measurement system, composed of a single voltage measurement monitoring the MV side in the HV/MV substation, it is possible to verify the behaviour of the Bayesian DSSE with a minimal measurement set. With such a configuration, it is not possible to refine the measurement accuracy of the substation measurement and every power-related quantity is not observed by any real-time measurement, meaning that prior information cannot be enhanced. Figure 9.8 shows the prior PDF relating to the active power of node 6, obtained from the statistics on absorption and generation (hour 10.00 during winter), together with the corresponding posterior obtained by the Bayesian DSSE algorithm. The posterior, like the prior, is computed through kernel fitting from the data, which, in this case, are provided by the M-H algorithm as extractions from a population whose PDF is the target posterior PDF. It is interesting to notice that the two PDFs are almost identical, thus confirming that the default measurement system cannot help in reducing the uncertainty associated with power estimation. The reported graphs also underline how the algorithm is capable of reproducing complex statistical patterns, due to different sources and influence parameters (temperature, irradiation, etc.). In this case, the estimation, which is given by the average of the posterior, cannot but coincide with the reported pseudo-measurement,[†] which is the average of the available power data. Even such simple and somehow expected outcome is emblematic of the role of PDFs in the estimation. In a conventional WLS approach only STD is available, whereas, with Bayesian approach, the full description is preserved for further computations.

When additional instruments are used, an upgraded monitoring system is considered, and the posterior PDFs start to diverge from the corresponding priors, thus confirming that the additional information coming from instruments allows

[†]The pseudo-measurement is indicated with a circle reported on the curve only for readability.

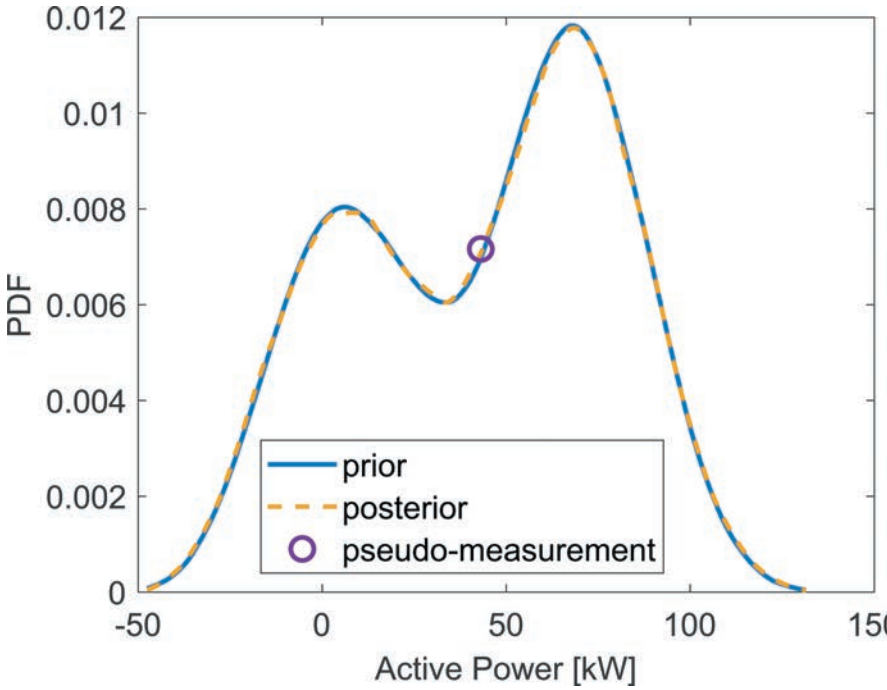

Figure 9.8 *Minimal measurement configuration – prior and posterior PDFs for node 6 active power*

reducing the uncertainty. Two voltage measurements are located at nodes 1 and 5, and two active and reactive power flow measurements are also considered as available at the same measurement point, in particular corresponding to branches 1 and 4. This measurement configuration may correspond to two measurement units placed at the nodes of interest. In this way, the posteriors become narrower and, even though they keep their non-Gaussian character, the shape changes more or less on a case-by-case basis, depending on the proximity, accuracy and type of available measurements. Figures 9.9 and 9.10 report the posterior PDF along with the estimated value obtained as the average of the posterior for the two nodes 4 and 6. Figure 9.9 shows how, thanks mainly to the measured power flows, the posterior shrinks, thus reducing the region of possible active power values. Power measurements have a 3% variability with respect to reference power, and thus they limit possible combinations when performing power estimation. Figure 9.10 is even more explicit, because the estimation of the active power at node 6 relies also on the power flow measured between nodes 4 and 5. In this case, the power drawn by node 5 is not large, thus allowing the effect of real-time measurements to propagate until the feeder end node. Comparing this figure also with Figure 9.8, it is evident that the large prior is reduced to a narrow peak in the new posterior, and the estimated value belongs to this peak. The range of possible values is thus

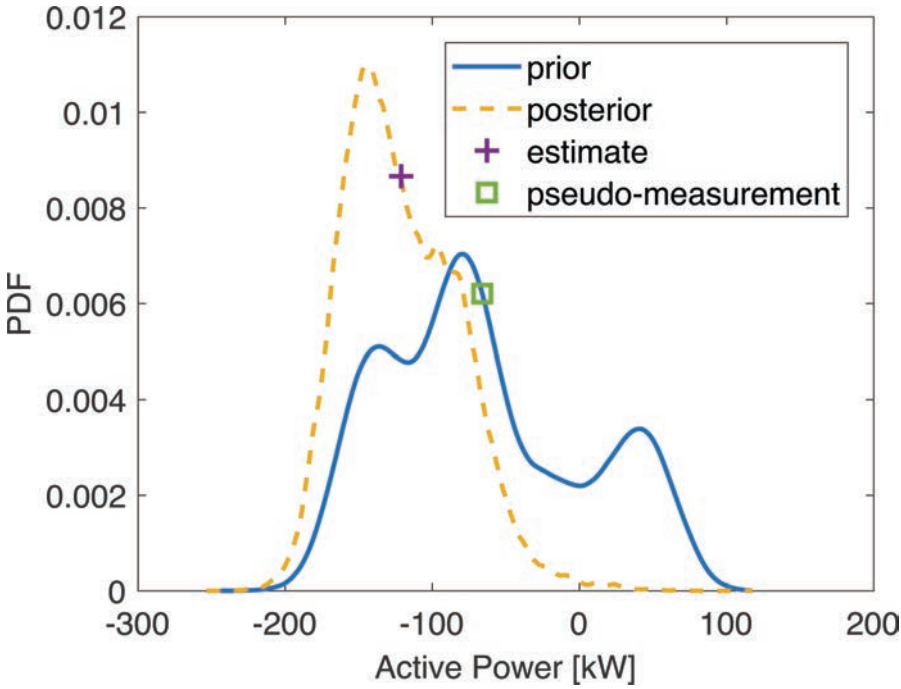

Figure 9.9 Upgraded measurement configuration – node 4 active power estimate, prior and posterior PDFs

much smaller, and the uncertainty associated with the estimated value is noticeably reduced with respect to prior uncertainty.

It is important to highlight that the exact behaviour depends on the specific characteristics of the loads and generators, on the actual operating condition of the network and, as discussed so far, on the monitoring system characteristics. Nevertheless, the considerations drawn from previous examples have general validity and illustrate the peculiarities and the outcomes of the method.

Further looking at the above example, it is possible to highlight that, since the algorithm provides a population of state vectors that is associated with the desired posterior, it is also possible, for each quantity of interest, to obtain other estimations and to compute additional statistics. For instance, the maximum a-posteriori estimate might also be computed, because it corresponds to the maximum in the obtained posteriors. This is not an unbiased estimator, but can be particularly useful with multimodal posteriors.

Even more important, it is possible to give an uncertainty description which is richer and more accurate. The quantiles of the computed posterior or the confidence intervals around the estimated quantity can be provided as additional outputs with minimum effort. The typical output of a traditional WLS estimator is given by the estimated value for each quantity of interest and by the associated STD, which is

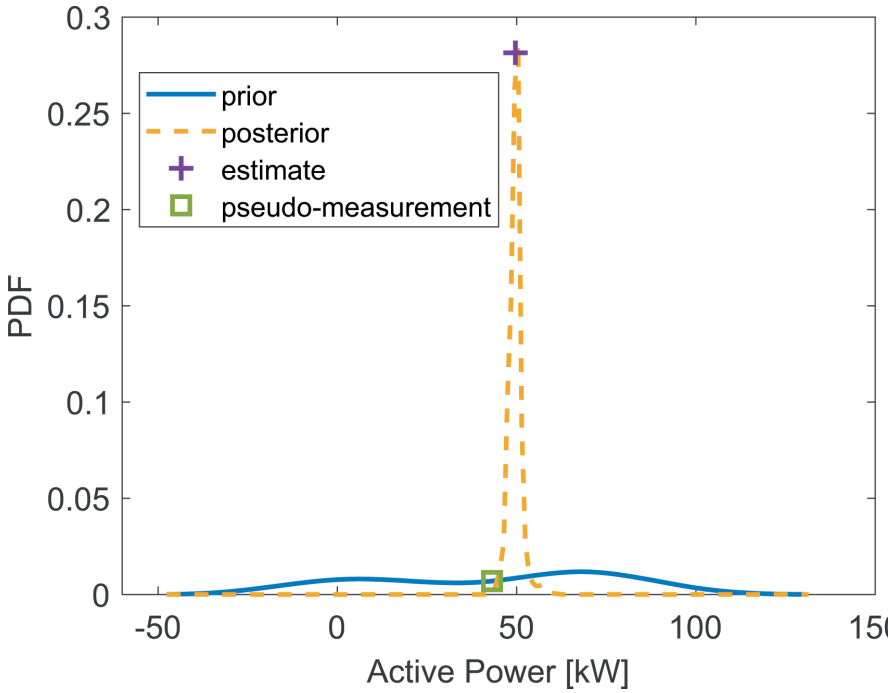

Figure 9.10 *Upgraded measurement configuration – node 6 active power estimate, prior and posterior PDFs*

computed through the estimates covariance matrix. The expanded uncertainty that can be provided to the DSSE user is obtained assuming Gaussian distributions and using thus the coverage factors appropriate for each confidence level. Moreover, the confidence intervals are considered symmetrical around the estimated value. When the posterior is clearly non-Gaussian or highly skewed as those presented in this chapter, such representation is clearly deficient, and Bayesian approach allows to obtain asymmetric and accurate intervals to define the uncertainty of the estimated value. Having a complete probabilistic description of the estimates enables the applications working on the outputs of the DSSE to define new algorithms and new safety margins that keep into account the complex scenario without oversimplifications possibly dangerous or costly.

Figure 9.11 exemplifies the above discussion. The posterior PDF of the active power of node 2 is reported, under the same conditions as before, depicting also the uncertainty associated with the estimated value ('+' symbol). The PDF is filled with two different colours, darker and lighter, to represent the two regions corresponding to the 95% and 99.73% confidence intervals around the estimated power. The limits of such areas are delimited by two pairs of quantiles: the first one corresponds to the probabilities 0.025 and 0.975, while the second one is between 0.00135 and 0.99865. These two areas, as expected, include the reference value, which is the

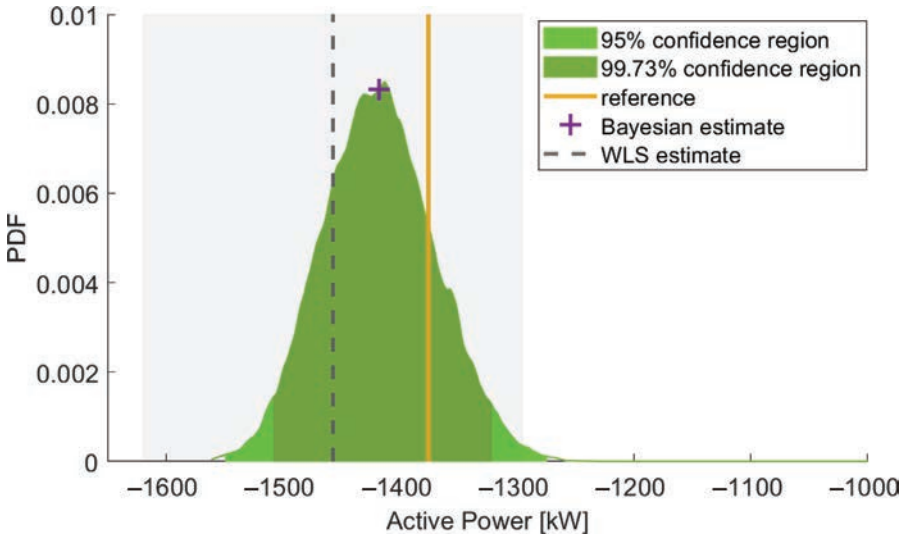

Figure 9.11 Upgraded measurement configuration – comparison between the uncertainty evaluation of the Bayesian and WLS methods

actual value of active power considered during the test. As a term of comparison, the estimate obtained with a WLS DSSE is reported (dashed vertical line) together with its uncertainty. The WLS is the most widespread method for DSSE nowadays, and it is important to recall that it corresponds to the Bayesian approach when the distribution associated with all the measurements and pseudo-measurements is Gaussian. It is important to highlight that the conventional WLS has been modified (see [22]) for the test to consider the full covariance matrix of the measurements and pseudo-measurements, so that a fair comparison is possible. The covariance matrix includes the variances of all the input quantities and the relevant covariances as obtained from the same measurement specifications and available statistical data used for the Bayesian DSSE. In the figure, the expanded uncertainty of WLS estimate is represented with a grey area and corresponds to the 95% confidence interval defined by the estimated STD (from the corresponding entry of the inverse gain matrix [6]) and by the coverage factor 1.96. It is evident that the WLS estimation error is about twice the Bayesian estimation error. In addition, WLS uncertainty greatly overestimates the actual uncertainty and fails to cover the region of interest, whereas large negative values (large absorption) are included. This type of result is general: Bayesian DSSE gives both a better estimation accuracy and a better uncertainty description. The specific impact depends again on the considered network condition and on the monitoring system.

Another interesting confirmation of the capability of the Bayesian DSSE to represent accurately even complex distributions is given in Figure 9.12. The figure gives a meaningful representation of the bivariate posterior obtained for node 4 considering both active and reactive injected powers. The posterior obtained as a result

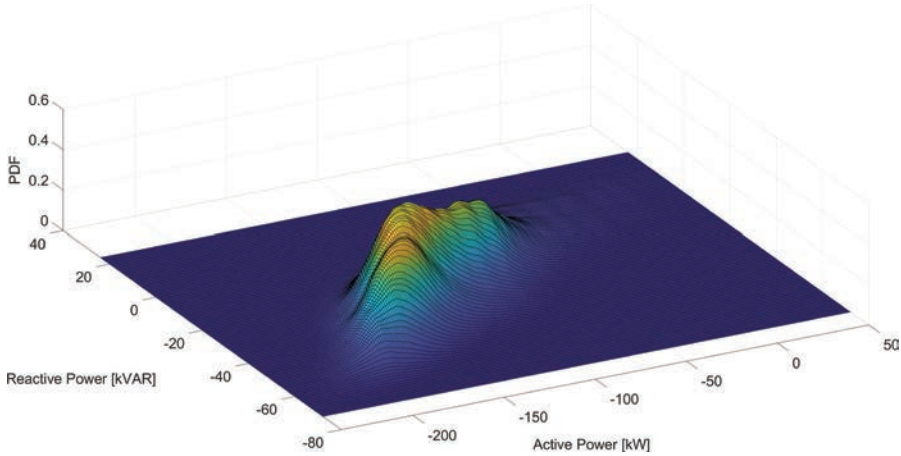

Figure 9.12 Bivariate PDF for active and reactive powers of node 4

of the Bayesian DSSE not only captures the clearly non-Gaussian behaviour of the estimated quantities but also follows the correlations and the specific features in the multidimensional domain of the sought state variables. In fact, the algorithm allows describing the estimated quantities in a comprehensive way, also permitting further computations when needed.

Matching the correlation and the higher order properties of the involved distributions allows including the dependencies (e.g., between active and reactive powers) both in the input and output data. This faithful representation of the actual behaviour helps both in improving the estimation and in speeding up the space exploration, since it is useful in computing a chain of possible states that is more focused in the regions of actual interest.

Similar results can be obtained also using synchronised measurements, for instance, voltage and current synchrophasors. When dealing with synchronised measurements, PMU-like devices, that is instruments with high synchronisation accuracy (in the order of 1 μs) are assumed. Measurements are always treated by including the distributions associated with their specifications. Unlike WLS approach, Bayesian approach thus allows synchrophasor measurements whose accuracy is described in terms of TVE only to be included. As described in Section 9.3.3, the TVE defines a circle in the complex plane and thus, starting, for instance, from the 1% TVE limit only, it is easy to integrate the available magnitude and phase angle measurements as an uniform distribution in the uncertainty region. This allows avoiding the typical approximations of WLS DSSE, such as associating a variance to each measurement when dealing with a phasor either in polar or rectangular coordinates.

9.5 Concluding remarks

In this chapter, an innovative approach to state estimation for distribution systems based on an application of the Bayes' rule and on the integration of all the available information concerning the real-time measurements and the so-called pseudo-measurements has been presented. The underlying idea can be summarised as finding a way to put together all the probabilistic descriptions that are available and need to be transformed in inputs for the state estimator.

The algorithm provides a general framework that is particularly effective when non-Guassian statistics are the best tool to represent the uncertainty behaviour of obtained measurements (conceived as random variables in their accuracy ranges) and of the historical or forecast data on loads and generators connected to the network. Each measurement or pseudo-measurement is thus considered as a random quantity associated with a region of possible values of different probabilities, and the estimates are found by grasping the real behaviour a-posteriori of the quantities of interest.

This approach perfectly fits the needs of a distribution network since data can be variegated. The distribution network cannot be fully monitored because of its complexity and due to cost constraints. Thus a statistical description of the expected power at the nodes and of the DG, also refined with forecasting tools, is the best information to integrate real-time data available from the field and to support state estimation routines. Moreover, each instrument has its own peculiarities, and each manufacturer has its own way of characterising and reporting the accuracy specifications and the information about measurement uncertainty. In addition, a distribution system operator might want to rely on ad-hoc characterisation procedures of the instruments before installation, to provide more appropriate and complete uncertainty description. The Bayesian DSSE encourages these good practices and provides the possibility of a seamless integration.

The Bayesian approach thus, starting from a more detailed description of the inputs, results in a more accurate estimation and, even more important for distribution system management and control applications, in a better description of the uncertainty associated with the estimator outputs. Higher management layers can thus lie on a more accurate picture of the network status and make their decisions in a more informed way.

Clearly, the increased accuracy and flexibility come at the expenses of a higher computational cost with respect to classical estimators (such as WLS and weighted least absolute value estimators), but there are numerical solutions of the Bayesian estimation problem, as that discussed in this chapter, that do not suffer of the dimensionality curse of other Monte Carlo methods and combinatorial approaches. It is also possible, for very large networks, to split the network and introduce multiarea techniques (see, for instance [33]). The interested reader is referred to Chapter 10 in this book for further details. Here it is important to highlight that the Bayesian DSSE is a good candidate for multiarea integration, since, from a given area, it provides good uncertainty descriptions to the other areas and can work on similar data coming from its peer estimators running for different areas.

References

[1] Fan J., Borlase S. 'The evolution of distribution'. *Power and Energy Magazine, IEEE*. 2009, vol. 7(2), pp. 63–8.

[2] Heydt G.T. 'The next generation of power distribution systems'. *IEEE Transactions on Smart Grid*. 2010, vol. 1(3), pp. 225–35.

[3] Della Giustina D., Pau M., Pegoraro P.A., Ponci F., Sulis S. 'Electrical distribution system state estimation: Measurement issues and challenges'. *IEEE Instrumentation & Measurement Magazine*. 2014, vol. 17(6), pp. 36–42.

[4] Baran M.E., Kelley A.W. 'A branch-current-based state estimation method for distribution systems'. *IEEE Transactions on Power Systems*. 1995, vol. 10(1), pp. 483–91.

[5] Lin W.-M., Teng J.-H. 'Distribution fast decoupled state estimation by measurement pairing'. *IEE Proceedings - Generation, Transmission and Distribution*. 1996, vol. 143(1), pp. 43–8.

[6] Pau M., Pegoraro P.A., Sulis S. 'Efficient branch-current-based distribution system state estimation including synchronized measurements'. *IEEE Transactions on Instrumentation and Measurement*. 2013, vol. 62(9), pp. 2419–29.

[7] Haughton D.A., Heydt G.T. 'A linear state estimation formulation for smart distribution systems'. *IEEE Transactions on Power Systems*. 2013, vol. 28(2), pp. 1187–95.

[8] Primadianto A., Lu C.-N. 'A review on distribution system state estimation'. *IEEE Transactions on Power Systems*. 2017, vol. 32(5), pp. 3875–83.

[9] Castello P., Liu J., Muscas C., Pegoraro P.A., Ponci F., Monti A. 'A fast and accurate PMU algorithm for P+M class measurement of synchrophasor and frequency'. *IEEE Transactions on Instrumentation and Measurement*. 2014, vol. 63(12), pp. 2837–45.

[10] Angioni A., Lipari G., Pau M., Ponci F., Monti A. 'A low cost PMU to monitor distribution grids'. *IEEE International Workshop on Applied Measurements for Power Systems*. Liverpool, UK; 2017. pp. 1–6.

[11] Angioni A., Schlösser T., Ponci F., Monti A. 'Impact of pseudo-measurements from new power profiles on state estimation in low-voltage grids'. *IEEE Transactions on Instrumentation and Measurement*. 2016, vol. 65(1), pp. 70–7.

[12] Chen Q., Kaleshi D., Fan Z., Armour S. 'Impact of smart metering data aggregation on distribution system state estimation'. *IEEE transactions on industrial informatics*. 2016, vol. 12(4), pp. 1426–37.

[13] Adinolfi F., D'Agostino F., Morini A., Silvestro F., Saviozzi M. 'Pseudo-measurements modeling using neural network and Fourier decomposition for distribution state estimation'. *IEEE PES Innovative Smart Grid Technologies*. 2014, pp. 1–6.

[14] Carcangiu S., Fanni A., Pegoraro P.A., Sias G., Sulis S. 'Forecasting-aided monitoring for the distribution system state estimation'. *Complexity*. 2020, vol. 2020(Article ID 4281219), pp. 1–15.
[15] Liu J., Singh R., Pal B.C. 'Distribution system state estimation with high penetration of demand response enabled loads'. *IEEE Transactions on Power Systems*. 2021, vol. 36(4), pp. 3093–104.
[16] Ghosh A.K., Lubkeman D.L., Downey M.J., Jones R.H. 'Distribution circuit state estimation using a probabilistic approach'. *IEEE Transactions on Power Systems*. 1997, vol. 12(1), pp. 45–51.
[17] Heunis S.W., Herman R. 'A probabilistic model for residential consumer loads'. *IEEE Transactions on Power Systems*. 2002, vol. 17(3), pp. 621–5.
[18] Singh R., Pal B.C., Jabr R.A. 'Statistical representation of distribution system loads using Gaussian mixture model'. *IEEE Transactions on Power Systems*. 2010, vol. 25(1), pp. 29–37.
[19] Valverde G., Saric A.T., Terzija V. 'Stochastic monitoring of distribution networks including correlated input variables'. *IEEE Transactions on Power Systems*. 2013, vol. 28(1), pp. 246–55.
[20] Mínguez R., Conejo A.J., Hadi A.S. *Non Gaussian State Estimation in Power Systems*. Boston, MA: Birkhäuser; 2008. pp. 141–56.
[21] Angioni A., Pau M., Ponci F., AMPS., *et al.* 'Bayesian distribution system state estimation in presence of non-Gaussian pseudo-measurements'. *2016 IEEE International Workshop on Applied Measurements for Power Systems*; 2016. pp. 1–6.
[22] Pegoraro P.A., Angioni A., Pau M., *et al.* 'Bayesian approach for distribution system state estimation with non-Gaussian uncertainty models'. *IEEE Transactions on Instrumentation and Measurement*. 2017, vol. 66(11), pp. 2957–66.
[23] NREL. *PVWatts Calculator tool* [online]. Available from http://pvwatts.nrel.gov.
[24] *OpenEI open energy information* [online]. Available from http://en.openei.org/datasets/files/961/pub/.
[25] Monti A., Muscas C., Ponci F. *Phasor Measurement Units and Wide Area Monitoring Systems: From the Sensors to the System*. Amstdedam: Elsevier, Academic Press Inc.; 2016.
[26] Joint Committee for Guides in Metrology. 'JCGM 100: Evaluation of Measurement Data - Guide to the Expression of Uncertainty in Measurement'. *JCGM*. 2008.
[27] Muscas C., Pau M., Pegoraro P.A., Sulis S. 'Effects of measurements and pseudomeasurements correlation in distribution system state estimation'. *IEEE Transactions on Instrumentation and Measurement*. 2014, vol. 63(12), pp. 2813–23.
[28] Carta A., Locci N., Muscas C., Pinna F., Sulis S. 'GPS and IEEE 1588 synchronization for the measurement of synchrophasors in electric power systems'. *Computer Standards & Interfaces*. 2011, vol. 33(2), pp. 176–81.

[29] Muscas C., Pau M., Pegoraro P.A., Sulis S. 'Uncertainty of voltage profile in PMU-based distribution system state estimation'. *IEEE Transactions on Instrumentation and Measurement*. 2016, vol. 65(5), pp. 988–98.
[30] Nelsen R.B. *An Introduction to Copulas*. New York: Springer; 1999.
[31] *ATLANTIDE project* [online]. Available from http://www.progettoatlantide.it/.
[32] Pau M., Pegoraro P.A., Monti A., Muscas C., Ponci F., Sulis S. 'Impact of current and power measurements on distribution system state estimation uncertainty'. *IEEE Transactions on Instrumentation and Measurement*. 2019, vol. 68(10), pp. 3992–4002.
[33] Pau M., Ponci F., Monti A., Sulis S., Muscas C., Pegoraro P.A. 'An efficient and accurate solution for distribution system state estimation with multiarea architecture'. *IEEE Transactions on Instrumentation and Measurement*. 2017, vol. 66(5), pp. 910–9.

This page intentionally left blank

Chapter 10

Multiarea state estimation for distribution systems

Julio Augusto Druzina Massignan[1], João Bosco Augusto London Junior[2], Marco Pau[2], and Paolo Attilio Pegoraro[3]

10.1 Introduction

The large scale of real distribution systems makes difficult the development of computational tools for real-time monitoring of these systems. Thus, the decomposition of distribution networks into smaller sub-networks emerges as an alternative for this development, embracing the use of smaller models, instead of a single large-scale model, parallel computing and decentralized processing architectures.

This chapter introduces decomposition methods to perform state estimation in large-scale distribution networks, employing the concepts of multiarea state estimation (MASE). A brief contextualization of scalability and decentralization is presented to emphasize the need of such architectures. Then, the main ideas of MASE are discussed. Two multiarea state estimation algorithms are presented, both make use of specialized methods for distribution system state estimation. However, one based on the traditional approach of the nodal voltage state estimation and the other on current-based model. Finally, numerical examples with both estimators illustrate the accuracy and computational aspects.

10.1.1 Large-scale distribution systems and motivations for MASE

Distribution systems are networks spread into vast areas, usually with hundreds of primary feeders corresponding to thousands of three-phase unbalanced buses. The inclusion of new sensors at the level of the low-voltage (LV) circuits, such as Phasor Measurement units (PMUs) and smart meters, has motivated the development of state estimators considering the whole distribution system, from the high voltage

[1]Department of Electrical and Computing Engineering, School of Engineering of São Carlos, University of São Paulo, São Carlos, São Paulo, Brazil
[2]E.ON Energy Research Center, Institute for Automation of Complex Power Systems, RWTH Aachen University, Aachen, Germany
[3]Department of Electrical and Electronic Engineering, University of Cagliari, Cagliari, Italy

substation through the primary feeders to the LV circuits. Thus, it becomes necessary to extend the network model to the consumer units that are connected to the LV circuits, which may lead to hundreds of thousands of variables. In this sense, the large-scale comprises the number of buses in numerous primary feeders and LV circuits from various substations, which may share interconnections.

Network analysis in distribution systems is typically performed on a feeder basis, naturally separable according to each feeder circuit and voltage level (substation, primary feeders, and LV networks). However, ultimately, operators are given the task of assessing the state of the whole network or automatically taking actions that involve one or more substations. The scale is undoubtedly dependent on the typical structure and region under operation by a single utility. For instance, in Brazil, a utility is responsible for large portions of state-wide areas, encompassing the electrical network of multiple cities. There are also some cases of local cooperatives, with a single city under responsibility, and other countries that typically have a local municipal utility. The scale is different, but even a single town may present several substations and widespread feeders, easily accounting for thousands of nodes.

The orchestration of algorithms that fully exploit computing architectures available at the distribution operation center may benefit the response time of operators and enlarge the scope of automatic applications while dealing with such a large scale of the whole network. Typically, a single application is concentrated in separate computing units in a server to avoid overlapping processes and reduce possible communication traffic that may hamper the overall performance. A basic illustration of a computing server typically available at distribution operation centers is illustrated in Figure 10.1.

Furthermore, modern computing units in those servers present high-performance computing elements available, such as multicore central processing units (CPUs) and accelerators based on graphical processing units. In this sense, MASE appears to be a promising feature to enhance computational performance and provide fast

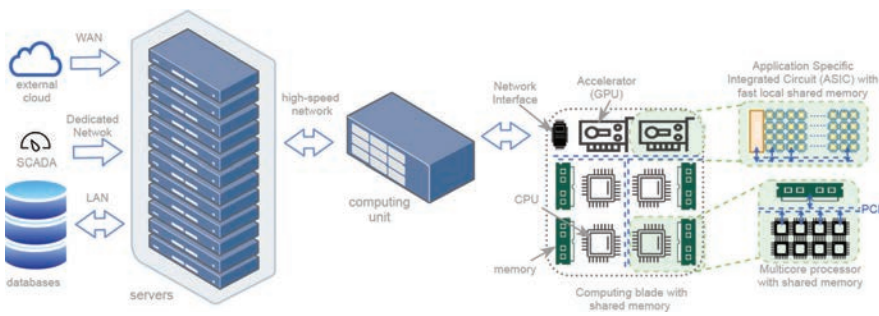

Figure 10.1 *A basic illustration of the computing architecture from modern data processing centers, with high-performance computing elements, such as multiprocessor cores, computing acceleration, and high-speed interconnection*

full network assessment by decomposing the network models and analysis into smaller problems solved in parallel.

Another motivation to pursue decomposition of state estimation into the multiarea formulations is the proposition of decentralized operation of distribution networks. Recent advances in smart grids enable edge computing applications and more embedded intelligence closer to the consumers, for instance, aggregators and microgrids under a joint local controller. In this sense, MASE provides a formulation that naturally captures a distributed monitoring architecture of these multiple agents (and their respective subnetworks). It enables advanced monitoring to be processed closer to the consumers and provides faster decisions, such as harmonizing the dispatch of renewable resources, electric vehicles, and energy storage. These aggregators and microgrids may even exchange information with a central utility operation center, in order to coordinate the decentralized operation. (Figure 10.2).

In such a vast and favorable research field, MASE flourishes as an essential feature for any scalable state estimation implementation at distribution operators [1, 2]. A few drivers of these approaches are enumerated below:

- evaluating scalability and computational requirements, such as bandwidth and communication among processes [3–5];
- employing specialized state estimators for distribution networks, further enhancing the numerical stability and increasing computational performance [6–8];
- more recently, exploring new computational decentralized architectures, unlocking new advances in cloud computing and Internet of Things (IoT) paradigms [9].

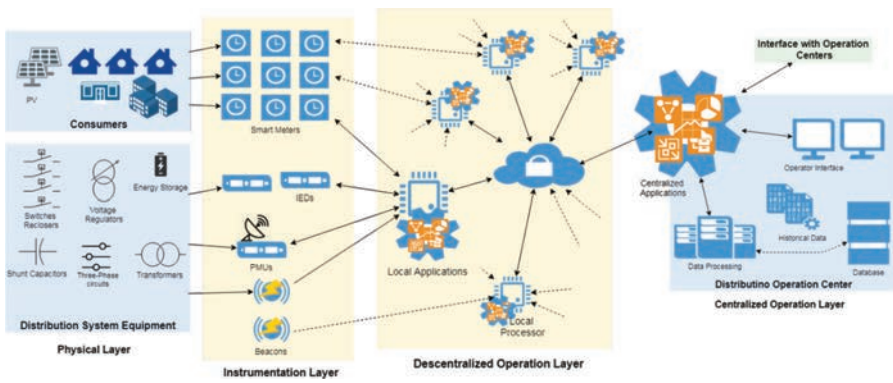

Figure 10.2 Illustration of a decentralized architecture of distribution grid monitoring, operation, and control. Cloud and edge computing are examples that can be exploited along with MASE.

10.2 Multiarea State Estimation

In conventional state estimators, the measured information is processed in a centralized manner. Given the dimension and natural subdivision of a distribution system into different feeders, the MASE approaches are an interesting solution to the scalability problem [1, 2]. Right after the conception of state estimation, in the 1970s, the idea to operate the transmission systems with a decomposition into areas and in a decentralized manner emerged [10]. The main motivation was the presence of different operators for separate regions of the transmission systems. Another motivation was improvements for the computational efficiency of the estimators. This way, throughout the years, several estimators were proposed using the concept of decomposition of the transmission systems into areas [11]. However, very few works dealt with the same problem of scalability regarding distribution systems [1, 2, 6, 8], despite the requirement and importance of the theme.

10.2.1 Terminology, definitions, and classifications of multiarea state estimators

Following the presentation of the formulation of state estimation in power systems, this section presents the main concepts related to MASE. The multiarea state estimator corresponds to the efficient application of state estimation procedures in large-scale power systems, seeking computational performance gains (processing time, memory allocation, and processing capacity), by exploring the fact that measurements are obtained from a wide area spread across the electrical network [11]. The basic approach of such an estimation process consists of the separation of the power systems into subareas, in which a local state estimation (LSE) is formulated for the internal nodes of such subareas and with a special treatment for frontier regions (boundaries of each area). Different architectures of MASE perform the state estimation process separately for each area, and the results refine the estimation of the frontier nodes. This section presents the nomenclature, definitions, classifications, and characteristics proposed for MASE [11]. Such concepts are important to any practical implementation that aims at large-scale applications.

Initially, let's consider a power system comprised of A connected subareas. Let us denote as S_k the set of nodes that belong to the k-th area and S the set of nodes of the whole power system. Initially, it is possible to define

$$S = \bigcup_{k=1}^{A} S_k \tag{10.1}$$

According to the level of overlapping among areas, the MASE can be classified as the following, as illustrated in Figure 10.3:

1. *MASE without overlapping areas*: different areas do not present any nodes or branches in common;
2. *MASE with overlapping nodes*: adjacent areas share a common node in a single level of interconnection (only the nodes at the boundaries);

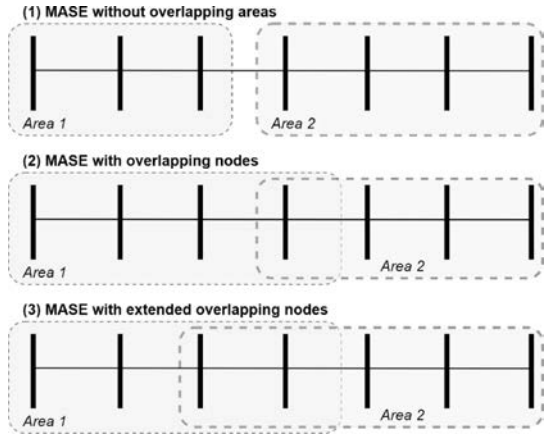

Figure 10.3 Different types of overlapping zones among different areas in MASE

3. *MASE with extended overlapping nodes*: adjacent areas share more than one common node in multiple levels of interconnection (more nodes besides the ones at the boundaries);

Thus, depending on the level of overlapping the state variables vector in each area may be composed of:

- x_{ik}: state variables associated with the internal nodes of each area k;
- x_{bk}: state variables associated with the boundary nodes of each area k;
- x_{nk}: state variables associated with the internal nodes of adjacent areas to the area k (areas with extended overlapping zones).

Besides, the measurement vector can be devised for each area as:

- z_{ik}: internal measurements, that relate internal state variables x_{ik} and boundary state variables x_{bk};
- z_{bk}: boundary measurements, that relate boundary state variables x_{bk}, as well as the state variables of extended overlapping zones x_{nk}.

The measurement model for the centralized state estimation can be rewritten for each area k separately according to the equations below, decomposing internal measurements and boundary measurements [12]:

$$\begin{aligned} z_{ik} &= h_{ik}(x_{ik}, x_{bk}) + \varepsilon_{ik} \qquad k = 1, ..., A \\ z_{bk} &= h_{bk}(x_{bk}, x_{nk}) + \varepsilon_{bk} \qquad k = 1, ..., A \end{aligned} \tag{10.2}$$

From a numerical optimization perspective, the MASE can be seen as a particular application of decomposition techniques [12–14]. With the above measurement model, the state estimation problem can be formulated to minimize the weighted

least squares (WLS) criterion, as previously described. Thereby, the MASE can be formulated as the following constrained optimization problem for the above measurement model [12]:

$$\begin{aligned} \min \quad & J(x) = \frac{1}{2} r_b^T . R_b^{-1} . r_b + \frac{1}{2} \sum_{k=1}^{A} r_{ik}^T . R_{ik}^{-1} . r_{ik} \\ \text{s.a.} \quad & r_b - z_b + h_b(x) = 0 \end{aligned} \tag{10.3}$$

where the subscript b represents the boundary measurements for all subareas of the electrical network with the respective weighting matrix R_b^{-1} (inverse of boundary measurement error covariance matrix), $r_{ik} = z_{ik} - h_{ik}(x_{ik})$ is the internal measurements residual for each area k and respective weighting matrix R_{ik}^{-1}. Although it has been presented as a constrained problem, it can also be written as an unconstrained problem.

The MASE problem consists of separating the above objective function into two parts: one related to the internal measurements (the local estimation process) and the second related to boundary measurements (the coordination process). Different methods have been proposed to solve the MASE problem, as presented in Ref. [11]. They rely on the traditional state estimation WLS criterion at the local estimation process, as well as in the coordination process. Some approaches apply heuristics to simplify the optimality conditions of the problem. Also, there are methods based on equality constraints among adjacent areas that are solved by variations of the Lagrangean method and other nonlinear programming frameworks [14].

Regarding the developed architectures, an important characteristic is a possibility to interchange information among different areas during the MASE process. As a consequence, the architectures are mostly related to the computer architecture implemented. They can be separated into two main categories [11]:

1. **MASE with hierarchical architectures:** a local estimation process is performed in each area independently, followed by a centralized coordination process that synchronizes and coordinates different local estimations;
2. **MASE with distributed architectures:** in this case, there is no centralized coordination, and the local processes are performed considering an exchange of information in neighbor areas. The coordination among areas is usually performed by substituting boundary state variables with the latest estimated values, thus it is a relaxed version of the centralized estimation problem.

Regarding the coordination among local estimations, the hierarchical MASE can be divided into [11]:

- **Coordination at the state estimation level:** local estimators provide the final converged solution from their respective areas to the central coordination. Whenever only on coordination exchange process is performed, this methodology provides suboptimal estimates. However, this approach requires less adaptations to traditional centralized state estimators;

- **Coordination at the iteration level:** local estimators provide information for the centralized coordination step at each iteration of the local convergence process. The estimations are coordinated at each iteration, enabling faster convergence to the optimal solution of the state estimator. This approach requires more adaptations to the core algorithms of traditional centralized state estimators and demands faster communication among local estimators and the central coordinator;
- **Hybrid coordination:** consists of a balanced option among the two previous processes, where at some amount of iterations the local estimations are provided for the central coordinator.

Another important aspect of any MASE is the synchronization among measurements and processes, especially for distributed architectures. Measurement synchronization is important since the updating rate of the Supervisory, Control and Data Acquisition (SCADA) systems may present a large range, and, in some cases, even fail to communicate. This problem can be countered by accepting some level of suboptimality or by improving the communication and redundancy of the SCADA system. Besides, the incorporation of synchronized phasor measurements requires special treatment across the different areas during the estimation process [11]. Regarding the estimation process synchronization, it comprises the updating rate and availability of information among adjacent areas, or among areas and the central coordinator. In general, the central or the decentralized processes use the latest available information from adjacent areas or assume some standby time to receive missing information.

10.2.2 Hierarchical architecture

This section presents the MASE hierarchical architecture comprised of two stages:

1. First stage (local): local solutions are obtained for each area, neglecting totally or partially information and constraints from neighboring areas;
2. Second stage (coordination): coordination of local solutions by a central processor to consider the interaction among different areas, neglected in the first stage.

As previously mentioned, in the first stage, an LSE problem, for each area k, is solved independently according to the respective measurement model of each area:

$$z_{ik} = h_{ik}(x_{ik}, x_{bk}) + \epsilon_{ik} \tag{10.4}$$

The measurement vector, and consequently the nonlinear measurement model $h(.)$, is also composed of considering the boundaries of each area and the approach for decomposing the network. This way, in some cases the boundary measurements can be neglected, due to the lack of information about adjacent areas in the local estimation. Once the local estimation processes converge, the local state variables, x_{ik}, are obtained together with the respective state covariance matrix:

$$Cov(\hat{x}_{ik}) = G_{ik}^{-1} = (H_{ik}^{T} R_{ik}^{-1} H_{ik})^{-1} \tag{10.5}$$

where H_{ik} is the Jacobian matrix of $h_{ik}(x_{ik})$.

The second stage of the hierarchical estimator consists of the coordination process among different local estimations. It depends on the level of overlapping among areas and the amount of available information exchanged with the central processor. The state vector in this coordination stage, denoted by x_c, is composed of the state variables at all boundaries x_{bk} and by a set of coordination variables for the local reference voltage angles, denoted by u_k:

$$x_c = \begin{pmatrix} x_{bk} \\ u_k \end{pmatrix} \qquad k = 1, ..., A \tag{10.6}$$

While the measurement vector includes two components:

$$z_c = \begin{pmatrix} \hat{x}_{bk} \\ z_{bk} \end{pmatrix} \tag{10.7}$$

where $\hat{x}_{bk}$are the local estimates for the boundary state variables x_{bk}, and z_{bk} are the boundary measurements, previously neglected in the local estimation stage. If the decomposition has overlapping nodes, the state vector is composed of the boundary nodes and the extended boundary nodes of the overlapping areas. This later approach often improves the optimality of the solution; however, it relies on a larger exchange of information among areas [15].

Thereby, the measurement model in the coordination stage is composed of a set of nonlinear equations and a complementary set of linear equations:

$$z_{bk} = h_{bk}(x_{bk}, u_k) + e_{z_{bk}} \qquad k = 1, ..., A \tag{10.8}$$

$$\hat{x}_{bk} = x_{bk} - Bu_k + e_{x_{bk}} \tag{10.9}$$

where the elements of the matrix B are equal to zero for the elements referred to as the voltage magnitudes and ones for the elements referred to as the phase angle components.

In the above measurement model, the covariance matrix of the vector of boundary measuremet error $e_{z_{bk}}$ is assumed as known (as for the conventional state estimator) and the covariance matrix of the vector of boundary state variables error $e_{x_{bk}}$ can be obtained previously or by employing the results of the local estimation in the local state covariance matrix $Cov(\hat{x}_{ik})$. The state estimate of the above measurement model is obtained by the WLS method, resulting in the boundary states and the coordination vector for the different areas [15].

Once the coordination stage comprises the exchange of information between each of the local areas and a central processor, the application of hierarchical MASE requires a communication infrastructure between each of the local areas and the central processor. This can also be applied in centralized monitoring, where all measured information is gathered at the same operation center, and the state estimation solution decomposes the network to employ parallel computing and obtain a significant gain in computational performance. Regarding distribution systems, this later goal is very interesting for current monitoring architectures, where the

network model of the primary feeders is already available at the operation center and the challenge is to include several LV secondary networks monitored by advanced metering. Once again, the communication requirements must be taken into account since it can introduce additional latency in the estimation process due to measurement gathering or exchange of boundary information.

10.2.3 Distributed architecture

In the distributed architecture there is an absence of a central processor to perform the coordination stage. In this case, there is a constant exchange of information among adjacent areas to complement and coordinate the local estimates. Each area has a local estimation process, similar to the previously described, with its respective internal measurements. However, the boundary measurements are related to state variables of the adjacent area j, according to:

$$z_{bk} = h_{bk}(x_{ik}, x_{bk}, x_{bj}) + e(z_{bk}) \tag{10.10}$$

The above measurement model is associated with a WLS estimator at each area k, and the state variables of adjacent boundaries x_{bj} are substituted by the latest available estimation $\hat{x}_{bj}$, exchanged among adjacent areas through a communication channel. This approach consists of a relaxation of the original MASE formulation, basically based on a distributed implementation of local estimations. Typically, it may take more iterations to converge than the hierarchical approach since many adjacent communication must be performed among the areas, while in the hierarchical approach, such information is processed altogether [15].

The distributed approach is often associated with widespread local controllers instead of a single operation center. Similar to the hierarchical architecture, the distributed approach relies on a communication infrastructure connecting different areas. It has also been used in transmission systems, where different operators are responsible for different areas of the system. However, the need for integration among different utilities limits the possibility of exchanging information. Regarding distribution systems, such limitation is not often the case since the networks are often under the responsibility of a single utility. However, the growing interest on microgrid architectures, which can operate independently with local controllers, has increased the interest on distributed approaches.

10.3 MASE for distribution systems

10.3.1 Two-step method with branch current estimator

The multiarea estimator that will be presented in this section is a fast two-step approach coordinated at the state estimation level, which can be implemented with a fully distributed architecture. The aim of this approach is to enhance the estimation accuracy achievable through the local estimators while reducing as much as possible the data exchange and communication required for the coordination of the inter-area harmonization process (i.e. the process leading to the refinement of the

local estimation outputs with information coming from different areas). The proposed solution generally provides suboptimal estimation results, but, as it will be shown in Section 10.4.1, in specific cases it is possible to benefit from the topological characteristics of distribution systems and to obtain results very close to those of a centralized estimator running on the whole grid.

The devised approach builds upon some design options that are key for the applicability of the proposed method and some other settings that can be recommended for achieving the best possible estimation results. In particular:

- The grid must be partitioned into areas with minimum overlapping, as this is at the base of the designed harmonization process; as a result, each area shares its boundary nodes with one or more neighboring areas; to maximize the benefits associated with the partition of the state estimation problem, the different areas should possibly have a similar number of nodes;
- Each of the areas in which the grid is partitioned must be observable; pseudo-measurements may be also employed to reach observability, as typically done at the distribution level; having local observability is an essential requirement for applying the presented method and it additionally provides robustness to the multiarea approach since the estimation results obtained locally would be available also in case of problems in the execution of the harmonization step (e.g. due to issues in the communication with the neighboring areas);
- No constraints exist for the placement of the meters, which in principle can be installed at any point of the grid; however, meters measuring the voltage at the boundary nodes and the currents (or powers) of the converging branches allow maximizing the accuracy performance of the proposed approach. This aspect may be also considered for defining the grid partition accordingly;
- While the proposed method could be potentially implemented also with a hierarchical set-up, adopting a distributed architecture is strongly recommended; the reason for this is that a decentralized solution allows not only distributing the processing tasks but also distributing the burden associated with communication (e.g. for the coordination of the harmonization step) and data storage (e.g. for grid data, pseudo-measurements, historical measurements, estimation results).

Given the above settings, the proposed multiarea approach consists of two WLS steps, the first one to carry out local estimations and the second one to refine the estimation results [8]. In particular, the second step allows for improving the first-step results by integrating into the estimation process, for each area, the estimation of the voltages at the shared buses provided by the neighboring areas. As mentioned before, both the first and second steps are based on a WLS formulation. More details on the design of the first and second steps, and on some mathematical considerations relevant to the design of the harmonization process, are provided in the following.

10.3.1.1 First-step design

The first step of the proposed multiarea approach aims at performing local estimations in each area by using locally available measurements. For this purpose, a branch current-based WLS estimator is adopted [16]. This formulation uses branch currents expressed in rectangular coordinates as state variables. In addition, the voltage at an arbitrary reference node is also added to the state vector to have a complete description of the grid state. This gives the possibility to compute all the electrical quantities of the network starting from the estimated variables. Referring, for the sake of simplicity, to an equivalent single-phase formulation (the three-phase model can be easily derived as an extension of the single-phase case), the state vector is expressed as

$$x = [V_{ref,re}, V_{ref,im}, I_{1,re}, ..., I_{n_{br},re}, I_{1,im}, ..., I_{n_{br},im}]^T \tag{10.11}$$

where $V_{ref,re}$ and $V_{ref,im}$ are the real and imaginary parts of the voltage at the chosen reference node, whereas $I_{k,re}$ and $I_{k,im}$ are the currents (the real and imaginary parts, respectively) at the k-th of the n_{br} branches of the grid, for $k = 1, ..., n_{br}$. The expression of the state vector in (10.11) is compliant with the possible presence of PMUs in the measurement system. In case no PMU measurements are available, the phase angle θ_{ref} of the voltage at the reference node must be defined a priori (it is commonly set equal to 0° in the single-phase framework) and the imaginary voltage can be consequently removed from the state vector as it can be automatically derived from the estimation of the other voltage variable.

An iterative WLS algorithm is used for the estimation of the above variables during the local estimation process. The branch current estimator is composed of three main operations, which are performed at each iteration of the WLS procedure.

1. Conversion of power measurements into equivalent current measurements: this is done to linearize the power measurements and to simplify the computation of measurement functions and, thus, of the Jacobian in the WLS; the conversion of each power measurement into the corresponding current phasor measurement is done via the following relationship:

$$I_{re} + jI_{im} = \frac{P \cdot V_{re} + Q \cdot V_{im}}{V^2} + j\frac{P \cdot V_{im} - Q \cdot V_{re}}{V^2} \tag{10.12}$$

   where P and Q are the active and reactive power, respectively, and V, V_{re}, and V_{im} are, respectively, the magnitude, real, and imaginary parts of the voltage at the bus where the power is measured. The adopted convention in the power direction defines the current convention.
2. Solution of the normal equations of the WLS, namely:

$$G \cdot \Delta x = H^T W \cdot [z - h(x)] \tag{10.13}$$

   where z is the vector of input measurements, $h(x)$ is the vector of measurement functions linking measurements to state variables, W is the weighting matrix computed as the inverse of the covariance matrix of the measurement errors, H is the Jacobian of the measurement functions $h(x)$, $G = H^T WH$ is the

so-called gain matrix, and Δx is the updating state vector used to refine the estimation of the state variables at each iteration of the WLS.

3. Voltage computation via a forward sweep: this provides the estimation of all the voltages along the grid, which is necessary for the conversion of power measurements into equivalent currents. The voltage at the i-th bus can be computed through the following equation:

$$V_{i,re} + jV_{i,im} = V_{ref,re} + jV_{ref,im} - \sum_{k \in \Lambda_i} Z_k \cdot (I_{k,re} + jI_{k,im}) \tag{10.14}$$

where Z_k is the impedance of the k-th branch (possibly with its sign changed if the branch current is in opposite direction with respect to the path direction between the reference bus and bus i) and Λ_i is the set of branches in the path between the reference bus and the considered node i.

The iterative WLS procedure stops when a certain convergence criterion is met, which is usually when the infinity norm of the updating state vector is smaller than a chosen threshold. The branch currents and voltages obtained at the last iteration represent hence the final estimates of the first step. Among them, the estimation of the voltages at the boundary nodes has to be transmitted, together with the associated uncertainties, to the neighboring areas for the second-step execution. The last task within the first-step estimation process is thus the computation of the voltage uncertainties. For this purpose, the covariance matrix $R_{\hat{x}}$ of the estimates in the state vector is first computed through the inverse of the gain matrix. Then, the covariance matrix $R_{\hat{V}_{re}\hat{V}_{im}}$ of the voltage estimates is computed by applying the following formula for the propagation of the uncertainties:

$$R_{\hat{V}_{re}\hat{V}_{im}} = H_{V_{re}V_{im}} \cdot R_{\hat{x}} \cdot H_{V_{re}V_{im}}^T \tag{10.15}$$

where $H_{V_{re}V_{im}}$ is the Jacobian of the measurement functions $h_{V_{re}}(x)$ and $h_{V_{im}}(x)$ linking the rectangular bus voltages to the WLS state variables, according to (10.14). Following this process, the standard uncertainty of the boundary bus voltage estimates can be eventually extracted from the covariance matrix $R_{\hat{V}_{re}\hat{V}_{im}}$.

10.3.1.2 Analysis of first-step voltage estimates

The design of the harmonization process performed in the second step of the multi-area estimator stems from the analysis of the voltage estimation results, which is presented in the following. For the sake of simplicity, let us consider a linearized and complex-valued version of the WLS problem where state variables and measurements are expressed with their complex values. In this case, the WLS solution can be written as:

$$G \cdot x = H^T W \cdot z \tag{10.16}$$

Separating, in all the matrices and vectors, the components related to voltages and currents, equation (10.16) can be rewritten as:

$$\begin{bmatrix} G_{V,V} & G_{V,I} \\ G_{I,V} & G_{I,I} \end{bmatrix} \begin{bmatrix} \dot{V}_{ref} \\ \dot{I} \end{bmatrix} = \begin{bmatrix} H_{V,V} & H_{V,I} \\ H_{I,V} & H_{I,I} \end{bmatrix}^T \begin{bmatrix} W_V & 0 \\ 0 & W_I \end{bmatrix} \begin{bmatrix} z_V \\ z_I \end{bmatrix} \tag{10.17}$$

In the above equation, for each matrix, vector, or scalar, the subscripts indicate the quantities with which they are coupled. For the measurement vector **z**, note that the division in voltage and current subvectors takes into account the fact that powers are converted into equivalent current measurements.

Let us focus now on the first of the equation blocks resulting from the relationship in (10.17). From the matrix products it is possible to find:

$$G_{V,V} \cdot \dot{V}_{ref} + G_{V,I} \cdot \dot{I} = H_{V,V}^T \cdot W_V \cdot z_V + H_{I,V}^T \cdot W_I \cdot z_I \tag{10.18}$$

Accordingly, it is possible to express the estimation of the voltage at the reference bus as:

$$\dot{V}_{ref} = G_{V,V}^{-1}(H_{V,V}^T \cdot W_V \cdot z_V + H_{I,V}^T \cdot W_I \cdot z_I - G_{V,I} \cdot \dot{I}) \tag{10.19}$$

Looking at the derivatives in the Jacobian and at the resulting entries in the gain matrix, it is possible to find:

$$G_{V,V} = \sum_{i=1}^{n_V} w_{V_i} \tag{10.20}$$

$$H_{V,V}^T \cdot W_V \cdot z_V = \sum_{i=1}^{n_V} w_{V_i} \cdot z_{V_i} \tag{10.21}$$

$$H_{I,V}^T \cdot W_I \cdot z_I = 0 \tag{10.22}$$

$$G_{V,I} \cdot \dot{I} = \sum_{k=1}^{n_{br}} -Z_k \cdot \dot{I}_k \cdot \sum_{i \in \Psi_k} w_{V_i} = -\sum_{i=1}^{n_V} w_{V_i} \cdot \sum_{k \in \Lambda_i} Z_k \cdot \dot{I}_k \tag{10.23}$$

where n_V is the total number of voltage measurements and Ψ_k is the set of voltage measurements that have the branch k in the path between the reference bus and the node where the voltage is measured.

Given the above results, the estimation of the voltage at the reference bus can be thus expressed as:

$$\dot{V}_{ref} = \frac{\sum_{i=1}^{n_V} w_{V_i} \cdot (z_{V_i} + \sum_{k \in \Lambda_i} Z_k \cdot \dot{I}_k)}{\sum_{i=1}^{n_V} w_{V_i}} \tag{10.24}$$

In (10.24), it can be observed that, for each voltage measurement i, the term between parenthesis at the numerator corresponds to a voltage measurement *shifted* to the reference bus by means of the voltage drops in the branches between the same reference bus and the voltage measurement point. For each voltage measurement i, it is thus possible to define a corresponding voltage measurement shifted to the reference bus as follows:

$$z_{V_i}^* = z_{V_i} + \sum_{k \in \Lambda_i} Z_k \cdot \dot{I}_k \tag{10.25}$$

Substituting these newly defined voltage measurements in the expression (10.24), the estimation of voltage at the reference bus eventually becomes:

$$\dot{V}_{ref} = \frac{\sum_{i=1}^{nV} w_{V_i} \cdot z^*_{V_i}}{\sum_{i=1}^{nV} w_{V_i}} \tag{10.26}$$

Regardless of the impossibility to calculate (10.25) (the current estimates are unknown at the beginning of the estimation process), equation (10.26) shows that a bus voltage estimation is equal to the weighted average of the voltage measurements shifted into this bus. It is worth noting also that this holds for the voltage estimation at any node of the grid since the used branch current estimator model does not put any constraint on the selection of the reference bus.

For the design of the harmonization process, the information about the voltage estimate has to come together with the associated uncertainty. For a weighted average with the aforementioned assumptions on the weights, the resulting variance can be found to be equal to:

$$\sigma^2_{\dot{V}_{ref}} \approx \frac{1}{\sum_{i=1}^{nV} w_{V_i}} \tag{10.27}$$

The result in (10.27) is an approximation of the actual uncertainty of the voltage estimate since it neglects the uncertainty of the current estimates used for computing (10.25). However, this is an acceptable approximation in most of the practical scenarios since the uncertainties associated with the voltage drops are usually very small and almost negligible with respect to the measurement standard uncertainties σ_{V_i} [17].

10.3.1.3 Impact of shared measurements on the harmonization process

To analyze the outcome of integrating the estimation results of different areas, let us now suppose to have a grid divided into n_A areas. Without loss of generality, let us suppose that all the areas share the same bus s and that they all use this shared node as their reference bus. Let us indicate with n_{V_j} the number of voltage measurements that each area j has in buses other than the shared one. The total number of voltage measurements in the grid is thus:

$$n_V = \sum_{j=1}^{n_A} n_{V_j} + n_{V_s} \tag{10.28}$$

where n_{V_s} is either one or zero depending on whether a voltage measurement is present in the bus shared among all the areas or not.

When performing state estimation on the entire grid, equation (10.26) can be used to find the resulting voltage estimation on the reference bus:

$$\dot{V}_s = \frac{n_{V_s} \cdot w_{V_s} \cdot z_{V_s} + \sum_{j=1}^{n_A} \sum_{i=1}^{nV_j} w_{V_{i(j)}} \cdot z^*_{V_{i(j)}}}{n_{V_s} \cdot w_{V_s} + \sum_{j=1}^{n_A} \sum_{i=1}^{nV_j} w_{V_{i(j)}}} \tag{10.29}$$

where $z^*_{V_{i(j)}}$ is the i-th voltage measurement present in area j (shifted to the reference bus). The result in (10.29) is, ideally, the result to be reached also in the distributed version of the state estimation problem. Considering the partition in the n_A areas, always using (10.26), it is possible to compute the following reference bus voltage estimation for each area j:

$$\dot{V}_{s,j} = \frac{n_{V_s} \cdot w_{V_s} \cdot z_{V_s} + \sum_{i=1}^{nV_j} w_{V_{i(j)}} \cdot z^*_{V_{i(j)}}}{n_{V_s} \cdot w_{V_s} + \sum_{i=1}^{nV_j} w_{V_{i(j)}}} \tag{10.30}$$

Comparing (10.29) and (10.30), it is possible to see that the voltage estimated locally in each area j differs from the target one obtained in the full grid estimator since it involves only a subset of the voltage measurements globally available in the grid. Looking at the voltage estimation uncertainties, using (10.27), the variance of the voltage estimated by the full grid estimator is computed as:

$$\sigma^2_{V_s} = \frac{1}{n_{V_s} \cdot w_{V_s} + \sum_{j=1}^{n_A} \sum_{i=1}^{nV_j} w_{V_{i(j)}}} \tag{10.31}$$

whereas the one achievable by the local estimator on the area j is:

$$\sigma^2_{V_{s,j}} = \frac{1}{n_{V_s} \cdot w_{V_s} + \sum_{i=1}^{nV_j} w_{V_{i(j)}}} \tag{10.32}$$

Comparing (10.31) and (10.32), it can be observed that the local estimation process has degradation of the accuracy performance due to the lower number of considered voltage measurements.

Let us now consider a harmonization process, done in a second step, where each area j receives the voltage estimated at the shared bus by the other $n_A - 1$ areas. Given the findings obtained until now, the harmonization step can be designed as a process to update the voltage estimation at the shared bus via a weighted average of the voltages $\dot{V}_{s,j}$ estimated locally. Using the shared bus estimates found in (10.30) as voltage inputs and the inverse of the variance in (10.32) as weight, applying (10.26) eventually leads to:

$$\dot{V}_s = \frac{\sum_{j=1}^{n_A} \sigma^{-2}_{V_{s,j}} \dot{V}_{s,j}}{\sum_{j=1}^{n_A} \sigma^{-2}_{V_{s,j}}} = \frac{n_A \cdot n_{V_s} \cdot w_{V_s} \cdot z_{V_s} + \sum_{j=1}^{n_A} \sum_{i=1}^{nV_j} w_{V_{i(j)}} \cdot z^*_{V_{i(j)}}}{n_A \cdot n_{V_s} \cdot w_{V_s} + \sum_{j=1}^{n_A} \sum_{i=1}^{nV_j} w_{V_{i(j)}}} \tag{10.33}$$

The comparison between (10.33) and the full grid estimation result in (10.29) highlights the impact brought by the possible presence of measurements at the shared bus. When no measurements are available at the shared bus, n_{V_s} is equal to 0; in this case, the results obtained via the harmonization process perfectly match the estimation obtained by a full grid estimator. Instead, when a measurement is present at the shared bus, n_{V_s} is equal to 1; in this case, the shared measurement brings a bias in the final estimation obtained with the harmonization process due to the fact that it is considered n_A times instead of one. This effect, however, can be easily compensated. This can be done by considering as additional input for the weighted

average in (10.33) the shared measurement and by assigning to it a weight equal to $(1 - n_A) \cdot w_{V_S}$.

The example here reported considers a simplified scenario where all the areas have a bus in common that is used as the overlapping bus. However, similar findings can be found also when neighboring areas share different overlapping buses. In this case, to avoid biased estimation results, each area should compensate for the effects of measurements at the shared buses by introducing, as input to the second-step WLS, each of the measurements at the shared bus, with their weight multiplied by a factor equal to $1 - n$ (where n is the number of areas sharing that measurement). It is worth noting that the same strategy can be applied also if more than one voltage measurement is present at a shared bus (in this case, each measurement at a shared bus has to be introduced in the second step with the above-mentioned weight).

10.3.1.4 Second-step design

The second step of the MASE process aims at improving the voltage estimation results by integrating the estimates of neighboring areas. In particular, the second step focuses on the refinement of the voltage estimation since the current estimates do not have much margin for improvement (with respect to the first-step estimation results), above all when measurements are placed into the shared boundary nodes [6]. Its design builds upon the considerations of the voltage estimation results and the impact brought by measurements placed at the shared nodes presented in the previous section. Based on those findings, for each area j, the second step consists of a second WLS that uses as input:

- the reference bus voltage estimated locally at the first step;
- the voltage estimates at the shared nodes provided by the neighboring areas, shifted to the local reference bus by means of (10.25);
- the voltage measurements at the shared nodes, if present, also shifted to the local reference bus by means of (10.25).

The second step to refine the reference bus voltage at area j can, therefore, be written as the following linear WLS:

$$H_2^T \cdot W_2 \cdot H_2 \cdot \dot{V}_{ref}^{(2)} = H_2^T \cdot W_2 \cdot z^{(2)} \tag{10.34}$$

where $\dot{V}_{ref}^{(2)}$ is the voltage at the reference bus computed via this second step, the Jacobian H_2 is, in this case, simply a column vector of ones, whereas the input vector $z^{(2)}$ and the weighting matrix W_2 are:

$$z^{(2)} = [\dot{V}_{ref,j}, \dot{V}^*_{s,\Gamma}, z^*_{V_{S1}}, ..., z^*_{V_{Sn_S}}]^T \tag{10.35}$$

$$W_2 = \begin{bmatrix} w_{V_{ref,j}} & 0 & 0 & \dots & 0 \\ 0 & W_{V_{s,\Gamma}} & 0 & & 0 \\ 0 & 0 & (1-n_{\Gamma_1})\cdot w_{V_{s_1}} & & 0 \\ 0 & 0 & 0 & \ddots & 0 \\ 0 & 0 & 0 & & (1-n_{\Gamma_{n_s}})\cdot w_{V_{s_{n_s}}} \end{bmatrix} \tag{10.36}$$

where $\dot{V}^*_{s,\Gamma}$ is the vector of voltage estimates of the shared bus provided by the set Γ of all the neighboring areas and shifted to the local reference bus; $z^*_{V_{s_k}}$ is the voltage measurement (when present) at the k-th node shared by the considered area j,with n_{Γ_k} neighboring areas, for $k = 1, \dots, n_s$(shifted to the reference bus); $W_{V_{s,\Gamma}}$ is a diagonal submatrix with the weights associated with the voltage estimates received from the neighboring areas; and, finally, $w_{V_{s_k}}$ is the weight associated with the voltage measurement at the shared bus k. Through the application of (10.34), the following second-step voltage estimation can be found:

$$\begin{aligned} \dot{V}^{(2)}_{ref,j} &= \frac{w_{V_{ref,j}}\cdot \dot{V}_{ref,j} + \sum_{l\in\Gamma} w_{V_{s,l}}\cdot \dot{V}^*_{s,l} + \sum_{k=1}^{n_s}(1-n_{\Gamma_k})\cdot n_{V_{s_k}}\cdot w_{V_{s_k}}\cdot z^*_{V_{s_k}}}{w_{V_{ref,j}} + \sum_{l\in\Gamma} w_{V_{s,l}} + \sum_{k=1}^{n_s}(1-n_{\Gamma_k}) n_{V_{s_k}}\cdot w_{V_{s_k}}} \\ &= \frac{\sum_{k=1}^{n_s} n_{V_{s_k}}\cdot w_{V_{s_k}}\cdot z^*_{V_{s_k}} + \sum_{l\in\Gamma}\sum_{i=1}^{nV_l} w_{V_{i(l)}}\cdot z^*_{V_{i(l)}} + \sum_{i=1}^{nV_j} w_{V_{i(j)}}\cdot z^*_{V_{i(j)}}}{\sum_{k=1}^{n_s} n_{V_{s_k}}\cdot w_{V_{s_k}} + \sum_{l\in\Gamma}\sum_{i=1}^{nV_l} w_{V_{i(l)}} + \sum_{i=1}^{nV_j} w_{V_{i(j)}}} \end{aligned} \tag{10.37}$$

where n_s is the number of shared nodes for the considered area. The computed variance of this estimated voltage becomes:

$$\begin{aligned} \sigma^2_{V^{(2)}_{ref,j}} &= \frac{1}{w_{V_{ref,j}} + \sum_{l\in\Gamma} w_{V_{s,l}} + \sum_{k=1}^{n_s}(1-n_{\Gamma_k}) n_{V_{s_k}}\cdot w_{V_{s_k}}} \\ &= \frac{1}{\sum_{k=1}^{n_s} n_{V_{s_k}}\cdot w_{V_{s_k}} + \sum_{l\in\Gamma}\sum_{i=1}^{nV_l} w_{V_{i(l)}} + \sum_{i=1}^{nV_j} w_{V_{i(j)}}} \end{aligned} \tag{10.38}$$

Once the voltage at the reference bus is refined by means of (10.34), the complete profile of the voltages in the considered area can be updated through the forward sweep calculation in (10.14), using the newly estimated voltage at the reference bus and the branch current estimates obtained in the first step of the MASE process. The first-step branch currents and the refined voltage profile obtained through this second step represent thus the final estimation result of this two-step multiarea procedure. Equations (10.37) and (10.38) show that the estimated voltage and resulting uncertainty improve due to the integration of the voltage measurements coming from the neigbouring areas. In general, this methodology does not allow achieving the same results as the estimator running on the full grid since only a subset Γ of the existing areas will be adjacent to the considered area j (therefore, only the benefits associated with the measurements available in those neighboring areas can be introduced). At the same time, however, this procedure allows for improving the results obtained through the first-step local estimation, while entailing only a minimum level of communication and data exchange.

10.3.2 Bayesian inference method with nodal voltage estimator

The Bayesian reasoning for multiarea power system state estimation extends the concept of the state vector as a random variable, in the sense that a set of possible state values may occur in the network given the measured observations and prior knowledge about the system. Estimation then becomes performing inference on the probabilistic model of the posterior distribution instead of seeking a fixed set of state values that yields the maximum likelihood. The proposed Bayesian Spatial Fusion comprises two stages, as a hierarchical approach:

1. Local Estimation Step: an independent estimation step is performed for each area, employing internal latest boundary state variables and extended boundary state variables available;
2. Coordination Step: a central processor gathers boundary information from local estimation and updates them to achieve consensual values among adjacent areas.

In the local estimation step, the proposed spatial fusion extends the probabilistic model for each local area by including a prior distribution for the state variables, as the following:

$$x_{ik} = x_{ik}^{p} + \omega_{ik}^{p} \tag{10.39}$$

$$x_{bk} = x_{bk}^{p} + \omega_{bk}^{p} \tag{10.40}$$

$$x_{nk} = x_{nk}^{p} + \omega_{nk}^{p} \tag{10.41}$$

$$z_{ik} = h_{ik}(x_{ik}, x_{bk}, x_{nk}) + e_i \tag{10.42}$$

where x_{ik}^{p}, x_{bk}^{p}, and x_{nk}^{p} are the expected values of the prior distribution assumed for the internal boundary and extended boundary state variables, along with a random component to represent state variations ω_{ik}^{p}, ω_{bk}^{p}, and ω_{nk}^{p}, respectively. Note that separate priors are given for the internal variables, the boundary variables, and the extended boundary variables, to accommodate a reduced set of information exchange among areas, only the boundary and extended state variables and their priors are exchanged.

Applying the Bayes' Theorem yields the posterior distribution for each local area:

$$f_{X|Z}(x_{ik}, x_{bk}, x_{nk}|z_{ik}) = \frac{f_{Z|X}(z_{ik}|x_{ik}, x_{bk}, x_{nk}) f_X(x_{ik}, x_{bk}, x_{nk})}{f_Z(z_{ik})} \tag{10.43}$$

where $f_{X|Z}(x_{ik}, x_{bk}, x_{nk}|z_{ik})$ is the conditional probability function of the state given the measurements in each local area, $f_{Z|X}(z_{ik}|x_{ik}, x_{bk}, x_{nk})$ is the likelihood function of the local area according to the measurement model, $f_X(x_{ik}, x_{bk}, x_{nk})$ is the prior distribution in the hierarchical model, and $f_Z(z_{ik})$ is the measurements probability of occurrence, a constant value that scales the posterior probability function and is often neglected.

The estimation process in each area is triggered as soon as the respective measurements become available, or if there is an update on the boundary state variables. It updates the state by a maximum a posteriori (MAP) estimation given in (10.44).

The estimation result for the boundary of each area is then used as the prior distribution in the coordination step, a Bayesian hierarchical model [18].

$$\hat{x}_k = \arg\max_x f_{X|Z}(x_{ik}, x_{bk}, x_{nk} \mid z_{ik}) \tag{10.44}$$

In this formulation, both boundary and extended boundary states are updated in the local estimation steps. Such estimation results are then exchanged with a central processor, that performs spatial fusion with the locally estimated boundary variables and boundary measurements neglected in the local stage. The essence of this coordination step is to obtain a probabilistic consensus for the boundary variables among the local areas, searching for coherent values among adjacent areas that are updated in the next local estimation executions as new prior knowledge.

The coordination stage also extends the boundary measurement vector to accommodate a prior distribution for the boundary and extended boundary variables, as the following:

$$x_b = x_{bk}^{p-1} + \omega_{bk}^{p-1} \tag{10.45}$$

$$x_b = x_{nk}^{p-1} + \omega_{nk}^{p-1} \tag{10.46}$$

$$z_b = h_b(x_b) + e_b \tag{10.47}$$

where x_{bk}^{p-1} and x_{nk}^{p-1} are the expected values and associated random characteristics ω_{bk}^{p-1} and ω_{nk}^{p-1} of the prior distribution, for the boundary and extended boundary state variables obtained in the previous local estimation execution ($p-1$), and x_b is the boundary state vector for all areas. Note that the extended boundaries obtained in the local estimations are also included but in this case, modeled as relations regarding the boundary state variables. This introduces the results obtained by adjacent areas in the search for coherent values for the boundary states, as complementary prior information.

The coordination step yields a common boundary state vector for all different areas. Such common boundary values are then exchanged back to the local areas to update their internal state variables using the latest boundary state variables available. Therefore, the coordination step is iterative, in the sense that, in each iteration boundary information keeps being exchanged between local areas as new local updates are provided. The coordinaiton step stops when the boundary state variables update is reduced below a numerical tolerance (the convergence criterion). Figure 10.4 illustrates the probabilistic model employed. Details about the state estimation solution in the local and coordination steps are described in the following subsections.

10.3.2.1 Local estimation step

The local estimation step provides the state vector of each area k composed of $x_k = (x_{ik}, x_{bk}, x_{nk})$. A conjugate-Gaussian prior model is assumed for the state variables, to accommodate prior knowledge while maintaining computational tractability. This assumption is a simplification of the real behavior of the state variables, but fair enough since the multiarea formulation is a decomposition of an original

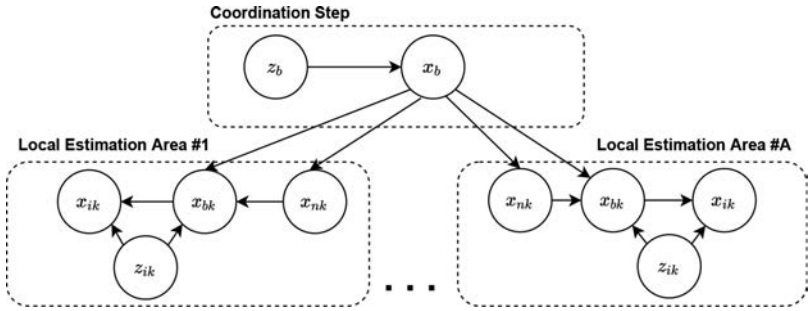

Figure 10.4 Probabilistic representation of the proposed multiarea distribution system state estimation. Prior information is included to complement local observability and also to coordinate the boundary state variables in adjacent areas.

Gaussian process estimation. Besides, the coordination step reduces the effects of such approximations since it updates iteratively the boundary state variables with the latest available information among different areas. The superscript p denotes the iteration of the coordination step that provides the prior information.

$$\textit{Prior}: \quad x_{ik} \sim \mathcal{N}(x_{ik}^p, P_{ik}^p) \tag{10.48}$$

$$x_{bk} \sim \mathcal{N}(x_{bk}^p, P_{bk}^p) \tag{10.49}$$

$$x_{nk} \sim \mathcal{N}(x_{nk}^p, P_{nk}^p) \tag{10.50}$$

$$\textit{Likelihood}: \quad z_{ik} \mid x_{ik}, x_{bk}, x_{nk} \sim \mathcal{N}(h_{ik}(x_{ik}, x_{bk}, x_{nk}), R_{ik}) \tag{10.51}$$

where P_{ik}^p, P_{bk}^p, and P_{nk}^p are the state covariance matrices from the prior knowledge at each area, also updated in the coordination step, and R_{ik} is the measurement covariance matrix for each area.

The prior knowledge in this local estimation can be represented by the following prior state vector and prior state covariance matrix, with each prior expected value and respective covariance from the above model:

$$\begin{aligned} \mathrm{x}_k^p &= [x_{ik}^p \quad x_{bk}^p \quad x_{nk}^p]^T \\ P_k^p &= \begin{pmatrix} P_{ik}^p & 0 & 0 \\ 0 & P_{bk}^p & 0 \\ 0 & 0 & P_{nk}^p \end{pmatrix} \end{aligned} \tag{10.52}$$

By assuming a Gaussian conjugate model for the priors and likelihood function, the following MAP estimation is obtained by the Bayes' Theorem, formulated as an unconstrained minimization problem:

$$\hat{x}_k = \min_x (z_{ik} - h_{ik}(x_k))^T R_{ik}^{-1} (z_{ik} - h_{ik}(x_k)) + (x_k - x_k^p)^T (P_k^p)^{-1} (x_k - x_k^p) \tag{10.53}$$

A nonlinear optimization algorithm, the modified Newton method with a backtracking algorithm for the step length α, provides the local estimates, with an iterative update of the state variables, according to the following equations:

$$\left(H^T R_{ik}^{-1} H + (P_k^p)^{-1}\right) \Delta x_k^{it} = H^T R_{ik}^{-1} (z_{ik} - h_{ik}(x_k^{it}) + (P_k^p)^{-1} (x_k^{it} - x_k^p) \tag{10.54}$$

$$x_k^{it+1} = x_k^{it} + \alpha \Delta x_k^{it} \tag{10.55}$$

where H is the Jacobian matrix of $h_{ik}(x_k)$ evaluated at each iteration it point x_k^{it}. The algorithm is iterative until convergence is met according to a numerical tolerance ($tol = 1.0E^{-5}$), with $|\Delta x_k^{it}|_\infty \leq tol$.

An orthogonal formulation improves numerical conditioning and computational performance in each local estimation step [19, 20], with the following factorization.

$$\begin{pmatrix} (P_k^p)^{-1/2} \\ R_{SL}^{-1/2} H \end{pmatrix} = \mathcal{Q}^T \mathcal{R} \tag{10.56}$$

The iterative solution then becomes:

$$\mathcal{R} \Delta x_k^{it} = \mathcal{Q} \begin{pmatrix} (P_k^p)^{-1/2} (x_k^{it} - x_k^p) \\ R_{ik}^{-1/2} (z_{ik} - h_{ik}(x_k^{it})) \end{pmatrix} \tag{10.57}$$

Besides, exploring the above optimization model yields the advantage of the proposed multiarea method, the ability to include prior knowledge to compensate for the lack of local observability. The demonstration is straightforward by exploring the rank of the matrix being factorized [21]. Thus, if complete prior knowledge is given about the state variables, that is $P_k^p > 0$ and full rank, it is possible to perform separate and independent local estimation steps disregarding the full observability in the decomposition, as shown in (10.58) the posterior covariance will also be full rank and positive definite. It is noteworthy that, if the full network is not observable, then the prior knowledge will be the sole information to provide knowledge about the local state variables. This shows the importance of the coordination step, which updates the boundary information in order to include real-time information from adjacent areas into such nonobservable areas.

$$H^T R_{ik}^{-1} H + (P_k^p)^{-1} > 0 \tag{10.58}$$

After convergence, the boundary and extended boundary state variables are exchanged with the central processor. Both the estimated values and posterior variance are shared with the central coordination, as the following:

$$x_{bk}^p = \hat{x}_{bk} \tag{10.59}$$

$$x_{nk}^p = \hat{x}_{nk} \tag{10.60}$$

$$P_{bk}^p = \left[(H^T R_{ik}^{-1} H + (P_k^p)^{-1})^{-1} \right]_{bk} \tag{10.61}$$

$$P_{nk}^p = \left[(H^T R_{ik}^{-1} H + (P_k^p)^{-1})^{-1} \right]_{nk} \tag{10.62}$$

For the boundary covariance matrices above, only the respective elements (rows and columns) relative to the boundary and extended boundary state variables are considered, represented as a submatrix with the subscripts *bk* and *nk*.

Prior knowledge may be constructed in a noninformative way, such as assigning large variances (low weights) to a standard operational condition (or a flat start situation). It can also be based on informative knowledge, from previous operational conditions, from load calculations, or sampled from typical load behavior, with tuned variances to represent a flexible uncertainty about the state. For this implementation of the Bayesian MASE, a noninformative priorwas assumed based on a flat voltage profile, whose boundary state variables values are updated by the coordination step.

The works in Refs. [21, 22] employ a similar perspective to deal with the measurement at different timestamps, an additional challenge in distribution networks, while here the measurements are assumed aligned in time (as typically employed in state estimation). This is done to evaluate the isolated effects of the decomposition solely.

10.3.2.2 Coordination step

The local estimation step results in the state variables of each area, and values for their own boundaries that are shared along with the central processor. The coordination step processes these local boundaries information in order to provide common and coherent boundary values among adjacent areas.

The solution of the coordination is obtained by employing the remaining boundary measurements along with the boundary and extended boundary state variables estimated in the local areas. The coordination state vector comprises the full set of boundary variables. The goal of this step is to obtain coherent values among adjacent areas that will be exchanged back again to each local area.

As performed in the local areas, the coordination step also employs a conjugate-Gaussian prior model for the boundary state variables. In this case, the state vector comprises $x_b = [x_{b1}, x_{b2}, ..., x_{bA}]^T$, the boundary values among all areas. And the prior knowledge is arranged as the following, using the local estimation results exchanged, from both the boundary and extended boundary obtained in each area:

$$x_{bk}^{p-1} = \begin{bmatrix} x_{b1}^{p-1} & x_{b2}^{p-1} & \dots & x_{bA}^{p-1} \end{bmatrix}^T$$
$$P_{bk}^{p-1} = \begin{pmatrix} P_{b1}^{p-1} & 0 & \dots & 0 \\ 0 & P_{b2}^{p-1} & \dots & 0 \\ \dots & \dots & \dots & \dots \\ 0 & 0 & \dots & P_{bA}^{p-1} \end{pmatrix} \tag{10.63}$$

$$x_{nk}^{p-1} = \begin{bmatrix} x_{n1}^{p-1} & x_{n2}^{p-1} & \dots & x_{nA}^{p-1} \end{bmatrix}^T$$
$$P_{nk}^{p-1} = \begin{pmatrix} P_{n1}^{p-1} & 0 & \dots & 0 \\ 0 & P_{n2}^{p-1} & \dots & 0 \\ \dots & \dots & \dots & \dots \\ 0 & 0 & \dots & P_{nA}^{p-1} \end{pmatrix} \tag{10.64}$$

The coordination step is also comprised of a MAP estimate, given by the following optimization problem:

$$\begin{aligned}\hat{x}_b = \min_x (z_b - h_b(x_b))^T R_b^{-1}(z_b - h_b(x_b)) + (x_b - x_{bk}^{p-1})^T (P_{bk}^{p-1})^{-1}(x_b - x_{bk}^{p-1}) \\ +(x_b - x_{nk}^{p-1})^T (P_{nk}^{p-1})^{-1}(x_b - x_{nk}^{p-1})\end{aligned} \tag{10.65}$$

A nonlinear optimization algorithm, the modified Newton method with a backtracking algorithm for the step length α, then provides the local estimates, with an iterative update of the state variables, according to the following equations:

$$\begin{aligned}\left(H^T R_b^{-1} H + (P_{bk}^{p-1})^{-1} + (P_{nk}^{p-1})^{-1}\right) \Delta x_b^{it} = H^T R_b^{-1}(z_b - h_b(x_b) \\ +(P_{bk}^{p-1})^{-1}(x_b^{it} - x_{bk}^{p-1}) + (P_{nk}^{p-1})^{-1}(x_b^{it} - x_{nk}^{p-1})\end{aligned} \tag{10.66}$$

$$x_k^{it+1} = x_k^{it} + \alpha \Delta x_k^{it} \tag{10.67}$$

In this case, H is the Jacobian matrix of the boundary measurement model $h_b(x_b)$.

If any measurement is left to be processed in the coordination step the above problem becomes linear, only the updated prior knowledge among different areas is considered in the above equations, and the boundary state variables are obtained in a single iteration. This is accomplished by the extended boundary approach, where boundary measurements can be included in each local estimation since the state vector is extended one node deep into adjacent areas.

Another aspect that can be exploited is a hierarchical weighting during the coordination step, increasing the prior weights (reducing the variance) in a *top-down* approach, or from areas that are observable. This way is possible to reinforce the values obtained for the boundary state variables at the first and highest voltage levels when compared with prior values from the medium voltage (MV) levels and then to the secondary voltage levels, that is, from the substation to the LV nodes.

Finally, the boundary state vector is exchanged back to the local estimation steps. Different strategies to trigger the coordination step may also be employed, such as waiting for local convergence or by a predefined number of local iterations. This exchange is performed after local convergence is achieved. Distributed approaches may apply this strategy, by updating boundary variables and performing the coordination step according to communication latency and data volume constraints, but further exploration is required to define the best exchange strategies according to practical constraints (communication bandwidth, refresh rate, data volume, etc.).

10.4 Application examples of MASE for distribution systems

10.4.1 Example I: Two-step multiarea DSSE

In this section, some examples of the results achievable by means of the two-step multiarea state estimator described in Section 10.3.1 will be presented. Tests have been performed in two different distribution grids to underline the performance with different topologies and to highlight the scenarios where the proposed estimator can reach accuracy performance similar to those of a centralized estimator.

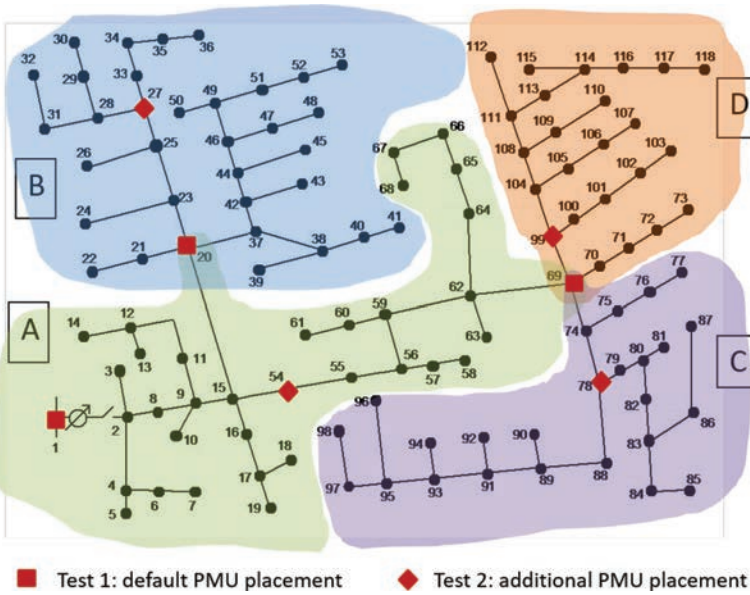

Figure 10.5 IEEE 123-bus distribution grid

10.4.1.1 Tests on IEEE 123-bus grid

The IEEE 123-bus grid is an unbalanced three-phase distribution grid often used to test algorithms in the distribution system scenario [23]. For the purposes of the tests here presented, the grid has been simplified by removing the voltage regulators and the nodes have been renumbered (for the sake of clarity branch indexes correspond to the arrival node index, i.e. the maximum of each pair, decremented by one). The two-step multiarea approach has been tested by partitioning the overall grid in four different areas, as shown in Figure 10.5. All the areas share one node with the neighboring areas thus creating a partition with minimum overlapping.

To evaluate the estimator's performance, a first test has been carried out by considering a minimal measurement configuration composed of PMUs only at the substation (bus 1) and at the overlapping nodes (buses 20 and 69). PMUs are supposed to measure the bus voltage and the currents of all the converging branches. Tests have been performed using the results of a power flow calculation as true reference values, from which measurements are then extracted. For the PMU, as an example, normally distributed errors with an expanded uncertainty (coverage factor 3) equal to 0.7 % and to 0.7 crad have been considered for the magnitude and phase angle measurements, respectively, so that the total vector error is below 1 %. Pseudo-measurements are also used to obtain the observability of the grid. These have been considered to have normally distributed errors with expanded uncertainty (coverage factor 3) equal to 50 %. The results presented in the following compare the accuracy performance of the proposed two-step MASE approach to the performance of the integrated state estimator (ISE) running on the entire grid and to the results given

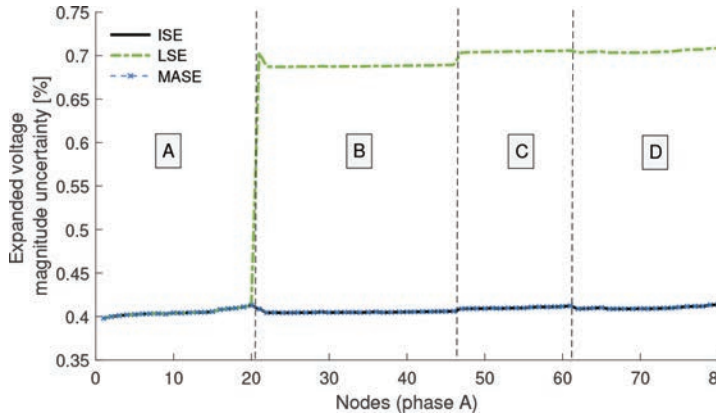

Figure 10.6 Expanded uncertainty of the estimated voltage magnitudes with measurements at the shared nodes

by the LSE at the first step of the MASE approach. The accuracy of the different estimators is evaluated statistically via a Monte Carlo procedure, using simulations with 5 000 iterations. Expanded uncertainty (with coverage factor 3) is used as the performance index. Moreover, the mean estimation error has been also monitored in all the tests, proving the proposed MASE provides unbiased estimation results (since this result holds for all the tests presented in the following, this is not explicitly remarked again for each test).

Figure 10.6 shows the results obtained for the estimation of the voltage magnitude at phase A of the grid (similar considerations hold for all the three phases of the system, therefore, in the following, phase A will be always taken as a reference to discuss the results). The ISE exhibits a quite flat profile of uncertainty of the estimated voltage magnitude, with uncertainty levels lower than the starting uncertainty of the PMU, as it is possible to expect due to the effect brought by the multiple voltage measurements in the grid [17]. It is possible to note also that the obtained level of uncertainty is coherent with the value that can be calculated via (10.27).

When distributing the state estimation process in the created areas, different results are obtained and degradation of the accuracy performance would be experienced if only the local estimators were run. Area A is the only one that does not exhibit any accuracy degradation through the LSE: the reason for this is that this portion of the grid contains all the measurements available in the grid. For the other areas, instead, the LSE provides a clearly worse estimation accuracy. The application of the proposed harmonization procedure at the second step of the MASE is, however, able to refine the estimation results also for these areas. Thanks to the MASE second step, in this scenario, all the areas are able to achieve the same accuracy performance as the ISE. Indeed, thanks to the information provided by the neighboring area A, all the areas can incorporate in their estimation the effects of all the three measurements available in the grid.

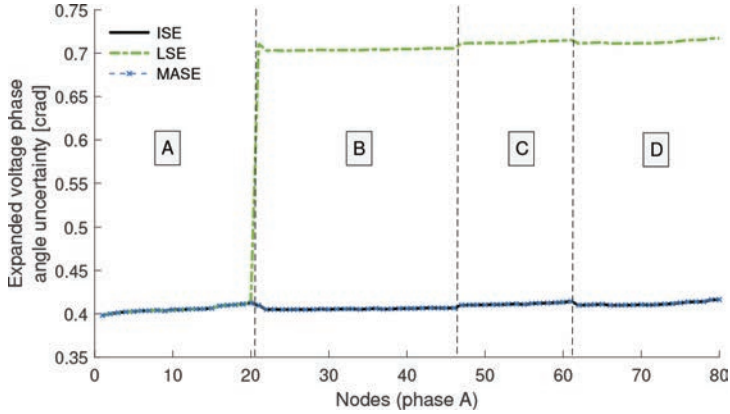

Figure 10.7 Expanded uncertainty of the estimated voltage phase angles with measurements at the shared nodes

Analogous results are obtained also for the estimation of the voltage phase angles, as shown in Figure 10.7. As it can be observed, not only the trends are similar to those seen in Figure 10.6 for the voltage magnitude estimation but also the numerical values of the uncertainty are similar. These levels of uncertainty are coherent with the approximated uncertainty that can be obtained by applying (10.27). The similarity in the numerical values is due to the analogous values of starting uncertainty in the PMU (the assumed expanded uncertainty is 0.7 % for the magnitude measurements and 0.7 crad for the phase angles).

One of the characteristics of the proposed MASE is to focus the second-step harmonization efforts only on the voltage estimation. For the current estimation, the same results obtained in the first step are kept as the final result also after the second step. This choice is justified for two main reasons. First of all, it has been proven that current estimations are mostly affected by measurements of current or power, which, however, only exhibit a local impact [24]. Contrarily to the voltage estimations, where the presence of each voltage measurement has a global effect on the accuracy of all the estimated voltages, the accuracy of the current estimations mainly depends on the accuracy of nearby current and power measurements, if any. Moreover, in the designed scenario, measurements are placed at the shared boundary nodes. The local impact of current measurements leads in this case to almost decouple the estimation of the branch currents of different areas. In other words, measurements available in the neighboring areas have practically no effect on the estimation results of the considered area. These considerations are proven by looking at the results in Figure 10.8. It can be observed in fact that the LSE is already able to achieve the same accuracy performance as the ISE, due to the decoupling effect of the measurements placed at the boundary nodes. Measurements external to each area thus do not bring any significant effect on the estimation of the local branch currents. Such results confirm that it is possible to avoid further processing

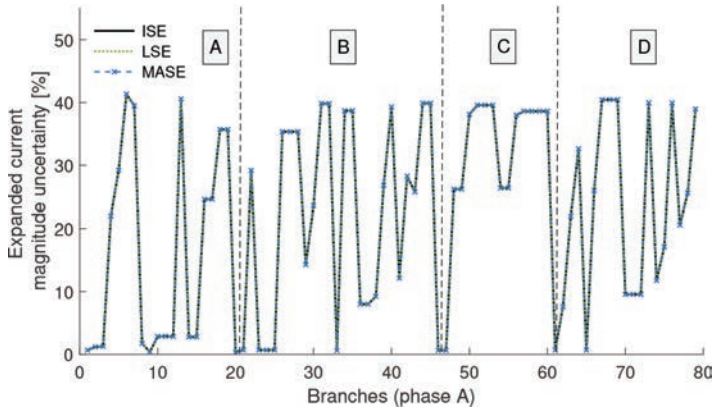

Figure 10.8 Expanded uncertainty of the estimated current magnitudes with measurements at the shared nodes

of the current estimations at the second step of the multiarea process and justify the adopted voltage shifts.

To further analyze the accuracy performance of the proposed MASE, the second series of tests has been performed by considering an upgraded measurement configuration, with additional PMUs placed at nodes 27, 54, 78, and 99. As in the previous case, the additional PMUs measure the bus voltage and the current of all the converging branches. Same uncertainty characteristics have been also considered. Figure 10.9 shows the results of uncertainty for the estimated voltage magnitude. Comparing the results with those previously shown in Figure 10.6, it is first of all possible to notice that the ISE has in this case a lower level of estimation uncertainty. This is clearly an effect of the larger number of voltage measurements

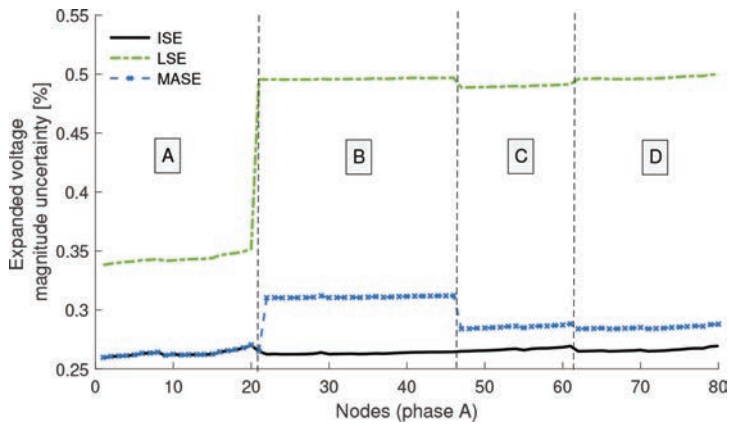

Figure 10.9 Expanded uncertainty of the estimated voltage magnitudes with upgraded measurement configuration

available in the grid, which is also coherent with the results that can be predicted by looking at (10.27).

Also, the LSE results are clearly improved with respect to the previous test scenario. Again, also in this case, the level of uncertainty is related to the number of voltage measurements that each area has locally. In particular, area A has the best LSE voltage estimation accuracy because it contains four voltage measurements (at nodes 1, 20, 54, and 69), whereas areas B, C, and D exhibit similar LSE accuracy performance since they all have two local voltage measurements (at nodes 20 and 27 for area B, at nodes 69 and 78 for area C, and at nodes 69 and 99 for area D).

The application of the second step of the MASE allows appreciating the improvements that can be achieved via the designed voltage harmonization procedure. Recalling the analytical results in (10.37) and (10.38) and the related considerations in Section 10.3.1.4, it is possible to see how the uncertainty of the MASE voltage estimation depends on the number of voltage measurements that can be introduced from the neighboring areas via the harmonization step. In particular, area A is able to reach the same results as the ISE since it is adjacent to all the other areas and, as a result, it can integrate the effects of all the measurements in the grid. Unlike area A, area B is adjacent only to area A and, as a consequence, it can incorporate the beneficial effects of only five voltage measurements (measurements at buses 1, 54, and 69 in addition to those already present locally at buses 20 and 27). Areas C and D can finally benefit from the measurements present in areas A, C, and D, for a total of six voltage measurements. As visible in Figure 10.9, the performance of the estimator in these two areas is indeed similar between them and better than area B. Both, however, are not able to reach the same performance as the ISE since one of the measurements (at bus 27, in area B) cannot be taken into account in the second-step procedure. Results analogous to those just presented are obtained also for voltage phase angle estimations. The same considerations as those reported for the previous test scenario (namely, same results for ISE, LSE, and MASE) are still valid also for the branch current estimations.

10.4.1.2 Tests on typical Italian distribution grid

To complement the results discussed until now, additional tests have been performed using a typical Italian MV distribution grid, as shown in Figure 10.10. This grid is composed of several feeders departing from the primary substation and this represents a topology that can be found quite often in European distribution grids. A logical solution to partition the grid, in this case, is to split it according to the already available division in feeders. The first bus of the grid can be used as an overlapping node and it is, therefore, a bus shared by all the feeders (areas) of the grid. This test case thus reflects perfectly the scenario described in Section 10.3.1.3, where all the areas were supposed to share the same overlapping bus.

Tests have been performed in this scenario considering PMUs placed at nodes 1, 10, 14, 32, 44, 67, 87, 97, and 101. Similar to the previous series of tests, PMUs have been assumed to measure the voltage at the bus and the current at all the converging branches. The uncertainties considered for synchronized phasor magnitude and phase angle measurements are 0.7 % and 0.7 crad, respectively.

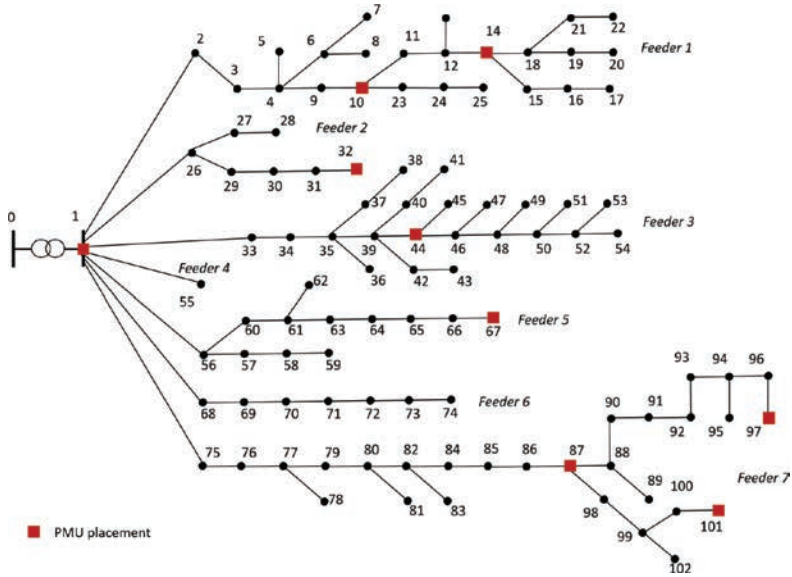

Figure 10.10 Example of Italian distribution grid from Atlantide project

Figure 10.11 shows the results of voltage magnitude expanded uncertainty obtained in this scenario. Similar to the previous test case, the LSE results lead to an important degradation of the accuracy performance. In particular, it is possible to observe that the different feeders exhibit varying levels of uncertainty, which depend on the number of voltage measurements available locally in the feeder. Results are significantly improved when applying the second step of the MASE procedure. Moreover, as visible in Figure 10.11, in this scenario, the MASE is able to

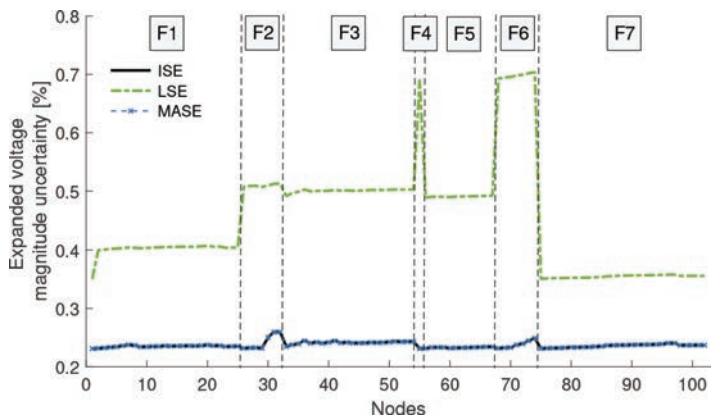

Figure 10.11 Expanded uncertainty of the estimated voltage magnitudes in an Italian distribution grid

reach the same accuracy performance as the ISE. In fact, each feeder sees the other ones as neighboring areas due to the fact that they all share the same overlapping bus. As described in Section 10.3.1.3, this hence allows integrating the beneficial effects of all the voltage measurements of the grid through the MASE second step.

Similar results (not presented here for the sake of brevity) are also obtained for the uncertainty of the voltage phase angle estimates. Overall, this test case, which is based on a topological scenario very common in MV and LV distribution grids, can be thus effectively handled via the proposed MASE approach without compromising the estimation accuracy performance. The proposed MASE hence allows easily distributing the state estimation process among the different feeders and, with this type of distribution grid, it provides accuracy performance comparable to those of the ISE, while requiring only two steps and a limited amount of communication and data exchange.

10.4.2 Example II: Bayesian inference multiarea DSSE

In this section, some examples with the two-step multiarea state estimator described in Section 10.3.2 will be presented. The simulation results illustrate the idea of spatial fusion in a network comprising high-voltage primary feeders and LV circuits. The simulation results also illustrate the impact of computational performance on a large-scale distribution system with more than 260,000 three-phase unbalanced nodes.

10.4.2.1 Performance evaluation

The performance simulations were carried out with the IEEE US LV (IEEE342) test system. It consists of an LV urban network with high reliability composed of spot loads in 408 V and a meshed LV network in 208 V, with a grounded Wye connection. Eight primary feeders in 13.2 kV comprise the MV system in the Delta connection. Finally, the 230/13.2 kV substation with two delta-connected transformers and a small portion of the subtransmission are represented. The network model and reference load flow scenario are available in Ref. [25].

The following metering system was considered during the simulations: high-voltage substation and subtransmission lines with active and reactive power flows and voltage magnitude SCADA measurements in all terminals ; primary network with active and reactive power flow and voltage magnitude SCADA measurement only at the feeder's bay; LV networks with active and reactive power injection and voltage magnitude obtained from smart meters. The full network also presents several virtual measurements representing nodes without loads, that is, nodes with zero active and reactive power injections, with a very low standard deviation (assumed as 1.0 E-7). Table 10.1 presents the amount of measurements considered in each part of the distribution system, where each metering device provides the respective electrical quantities in each phase (phase ABC).

Regarding the area decomposition, a level-based approach was devised in this simulation. This way the 230/13.2 kV substation and subtransmission lines correspond to a particular area; each MV feeder corresponds to a separate area, with eight

Table 10.1 Metering system location and total amount per location in the distribution system (each presenting the respective three-phase information)

Sources of information	Three-phase electrical quantities	Substation	Primary network	LV network
SCADA	Active and reactive power flow	14	8	–
	Active and reactive power injections	1	0	–
	Voltage magnitudes	5	8	–
Virtual measurements	Active and reactive power injection (zero injection)	6	131	68
Smart meters	Active and reactive power injection and voltage magnitude	–	–	104

total areas for the primary network in 13.2 kV; and each spot load in the 408 V LV networks corresponds to an individual area, and the meshed 208 V LV network is divided into four areas. The boundaries of the different areas are defined by the power transformers in the network, with a total of 21 areas. Figures 10.12 and 10.13 present an illustration of the area decomposition in each part of the distribution system.

To demonstrate the solution to the MASE problem with the proposed hierarchical approach, Figure 10.14 presents the estimation error for all state variables of the

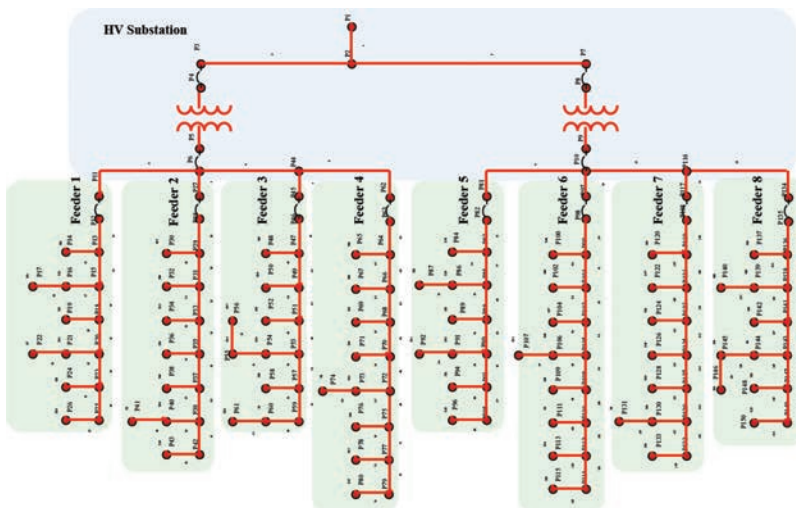

Figure 10.12 Decomposition of the high-voltage substation and MV feeders in the IEEE US LV test feeder [25]

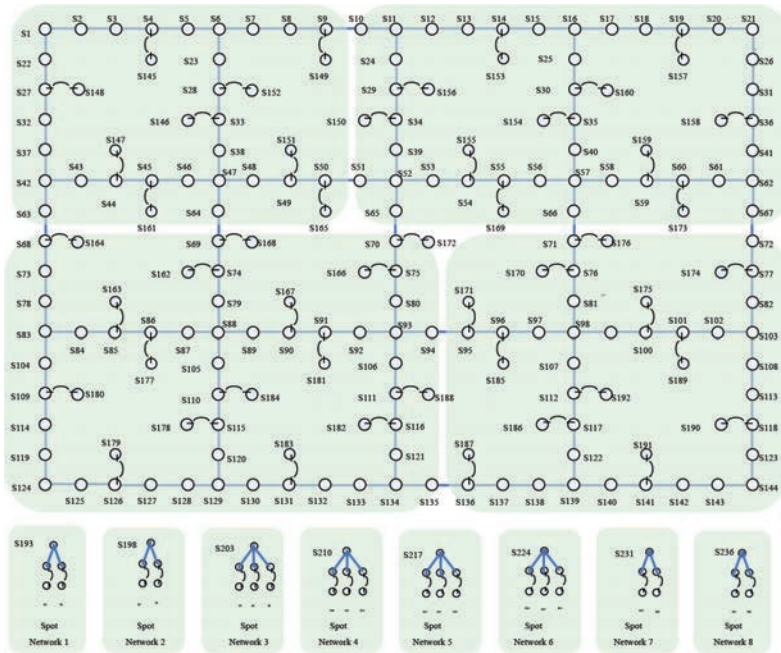

Figure 10.13 Decomposition of the LV circuits in the IEEE US LV test feeder [25]

network (voltage magnitude and phase angle) compared with the estimated results from the centralized approach.

Regarding the accuracy of the estimation process, the hierarchical approach carries an additional bias, reducing its accuracy, due to the fact it does not use all the information at once. This bias consists of a trade-off between accuracy and computational performance to achieve scalability and must be taken into account depending on the requirements for each final application. Still, such level of accuracy is

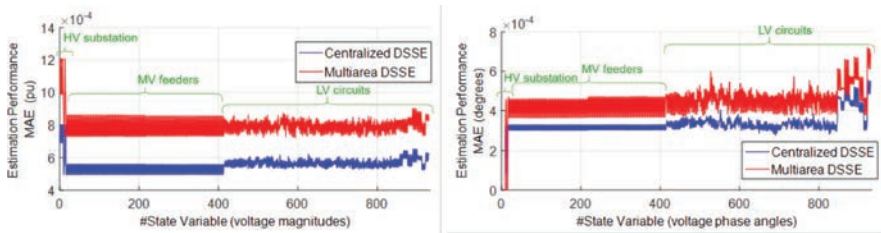

Figure 10.14 Estimation performance for the state variables (voltage magnitude and phase angles) of the IEEE US LV system, with the centralized and the multiarea approaches

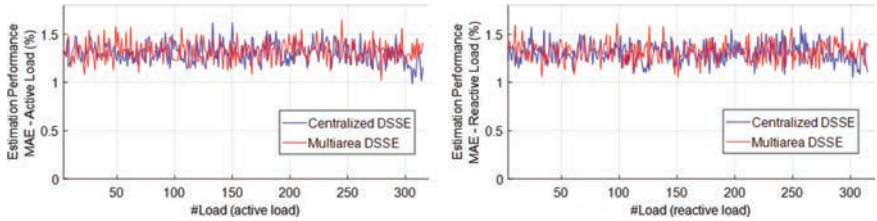

Figure 10.15 *Estimation performance for the power injections (active and reactive loads) of the IEEE US LV system, with the centralized and the multiarea approaches*

adequate for many real-time applications for the distribution system operator (DSO), especially in critical scenarios such as aiding service restoration procedures [26, 27].

Nonetheless, the results demonstrate a feasible solution to perform inference about the state using a probabilistic approach for the decomposition, rather than relying solely on optimization principles. In this sense, the bias also reflects a relation between prior and likelihood in the spatial decomposition. The prior knowledge, in this case, is built in an almost noninformative manner, by only updating the boundaries. Better priors could also help to reduce the effects of such bias. Another important aspect is the fact that the likelihood incorporates nonlinear models, which essentially results in non-Gaussian distributions. Thus, the approximation from the conjugate model may also induce such bias.

The estimation error was also evaluated for the loads at the secondary LV networks (active and reactive power injections) and for the active and reactive power flows at the MV/LV transformers (13.2/0.48 and 13.2/0.208 kV). To clarify the impact of estimated electrical quantities on the network, Figure 10.15 presents the estimation error, mean absolute percentage error, for the loads in all phases and nodes of the system. Figure 10.16 presents the estimation error, mean absolute percentage error, for the MV/LV transformers' power flows.

Both centralized and MASE approach presented similar accuracy for the load estimation, around 1.5% of accuracy, a consonant improvement on the initial assumed precision for the smart meters (5%). A similar result is also observed for

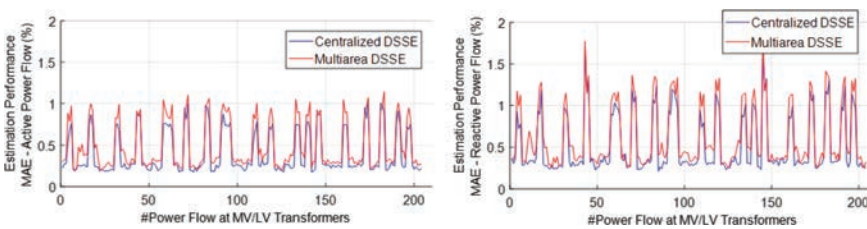

Figure 10.16 *Estimation performance for the active and reactive power flow at the MV/LV transformers of the IEEE US LV system, with the centralized and the multiarea approaches*

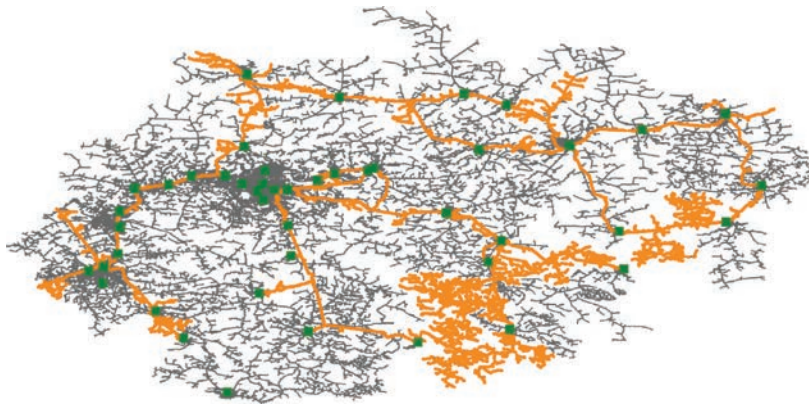

Figure 10.17 Extended large-scale distribution network in Brazil. The distribution networks comprise 35 feeders in 34.5 kV (orange) and 241 feeders in 13.8 kV (gray), in 48 substations (green).

the power transformers but, in this case, with an increase in their relative precision of power flow estimation when compared with the accuracy of the loads. This is essentially related to the fact that the uncertainty of many loads is redundantly considered altogether for the calculation of the power flows on the MV/LV transformers of the meshed network. For the case of spot loads, such accuracy increase is not that expressive since only the uncertainty of a single load monitored by the respective smart meter provides the information regarding the transformers' loading. This is an advantage of properly representing each individual load instead of directly aggregating them as loads in the primary feeders, which may not consider such effect properly depending on the aggregation strategy.

It is noteworthy that the smart meters were allocated only at the consumer units (loads) and that the MV/LV transformers are not monitored by any sensors. Besides, different indicators regarding the operational condition of the network, such as power losses, voltage unbalance, voltage drop, equipment loading, among others, were also estimated with similar precision.

10.4.2.2 Scalability and computational aspects

To evaluate scalability with practically sized distribution networks, the proposed MASE was applied in a real distribution system of a Brazilian utility. The pilot region comprises an extension of 33 cities under the responsibility of a single central operator. The region comprises almost 1 million inhabitants and an area of more than 12 000 km^2 in the south of Brazil, as illustrated in Figure 10.17. The size of the region was chosen to capture the spatial location of both types of feeders since the majority of the 34.5 kV spread across different cities in long urban and rural networks. All feeders are represented according to their unbalanced and asymmetrical characteristics. Box 10.1 illustrates some quantification of this test system under the supervision of a Brazilian utility.

Box 10.1 An example of the large scale in a Brazilian distribution system

The large-scale distribution system state estimation is mainly related to the number of variables rather than the number of measurements, which typically are very few in distribution systems. The amount of measurements is on a growing trend with the deployment of smart meters. However, this will also increase even further the scale since both MV and LV will be a part of the model.

To further illustrate the scale and the asymmetry of distribution networks, a few more details are provided about the network in Figure 10.17 . The distribution system comprises 48 substations, with 35 primary feeders in 34.5 kV and 241 primary feeders in 13.8 kV. The system comprises more than 260,000 nodes. Table 10.2 shows the total length of distribution circuits per phase and voltage level of this system. The 34.5 kV presents a diverse set of connection in this case since it also comprises some rural areas, while the majority of urban areas concentrate on a three-phase MV network. Table 10.3 provides information about the MV/LV distribution transformers and respective phases, another indication of the system asymmetry and load unbalance.

Those values only illustrate the scalability requirement and provide a notion of the network model and computational burden under the responsibility of distribution operators. It is noteworthy that the full system under the responsibility of the utility encompasses an area even greater, with more than 11 million inhabitants, a total area of almost 200,000 km, almost 400 cities, and a total length of more than 200 000 km of distribution circuits. Thereby, the utility must encompass such a scale framework into its energy management systems, spread into its five distribution operation centers.

Initially, Figure 10.18 presents the convergence rate of the local estimations, showing a boxplot of the reduction in the state variable changes in all 276 feeders per iteration. It illustrates a quadratic characteristic of convergence was obtained. This, however, was only possible due to the orthogonal formulation and the sparsity treatment employed. Sparsity treatments and special ordering are also employed to

Table 10.2 Length and asymmetry on MV distribution feeders

Voltage level		Phase A	Phase B	Phase C	Phases AB	Phases BC	Phase CA	Phases ABC
13.8 kV	Total length (km)	0.40	0.12	–	41.62	2 260.83	86.40	6 740.35
	Percentage	0.004	0.001	0.000	0.456	24.763	0.946	73.829
34.5 kV	Total length (km)	314.82	513.64	440.66	–	0.48	5.85	871.37
	Percentage	14.664	23.926	20.526	0.000	0.022	0.272	40.589

Table 10.3 Amount of MV/LV distribution transformers

Voltage level		Phase A	Phase B	Phase C	Phases AB	Phases BC	Phase AC	Phases ABC
13.8 kV	Total length (km)	2	6	5	309	7 160	259	24 467
	Percentage	0.01	0.02	0.02	0.96	22.23	0.80	75.97
34.5 kV	Total length (km)	933	1 433	1 089	0	6	2	605
	Percentage	22.94	35.23	26.77	0.00	0.15	0.05	14.87

support the numerical stability and performance of the orthogonal formulation. The proper treatment of only nonzero elements, less than 5% in all feeders, increases computational performance since less operations are performed to solve the estimation problem and also increases numerical stability since it reduces fill-ins during the factorization process.

Finally, the most important aspect of real-time applications at DSOs is the processing time at such a large scale. Figure 10.19 presents the individual computational time for each local estimation performed. It also presents the total computational time after the coordination step evaluations. As it can be seen, less than 2 seconds (s) are required to perform local estimation. This level of computational performance is in accordance with the real-time requirements of energy management systems. The effects of parallel computing using a shared-memory paradigm with OpenMP were evaluated by increasing the number of parallel threads created (as a reference the i7-9750H processor presents 6 physical processors, with hyper-threading enabled, with a total of 12 concurrent threads). In this case, it is noteworthy that a pure centralized version of the state estimator did not converge with the ill-conditioned and full system at once.

For comparison purposes, a backward/forward sweep method, with a similar implementation of routines and data structures, solves a load flow problem in this large-scale network in about 3 s (while maintaining less than 20 ms per feeder) [28].

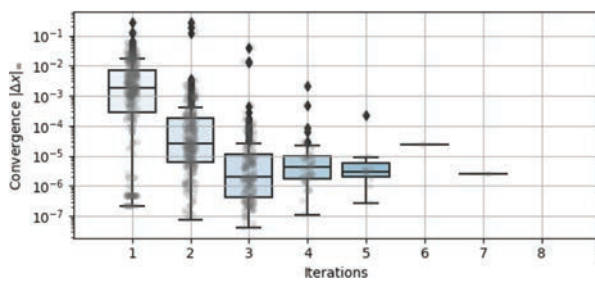

Figure 10.18 Boxplot of iterations per each local estimation among the 276 feeders

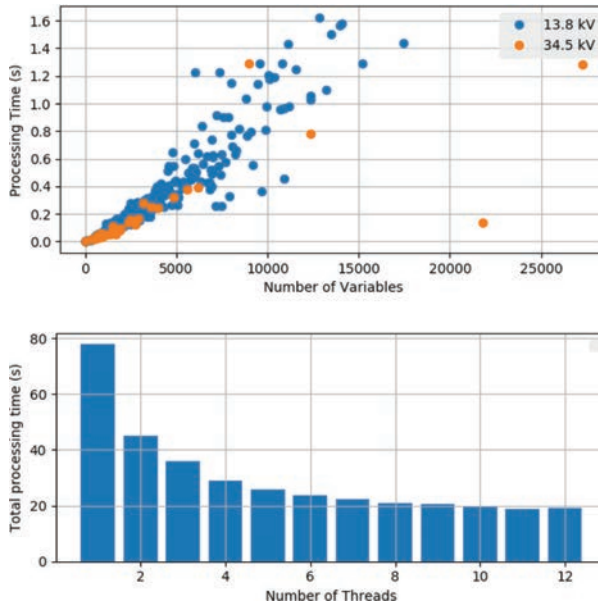

Figure 10.19 *Individual local area is processing time for each of the 276 feeders and total computational time of the spatial fusion MASE using different amount of parallel threads. All feeders and systems are evaluated simultaneously, providing assessment for more than 260,000 three-phase unbalanced nodes in a few seconds.*

It is noteworthy that there is space for enhancements, such as employing optimized general-purpose computing routines, improving memory locality, object-oriented programming, and employing benchmark libraries. Regarding memory allocation, each local area requires a small amount, which tends to grow linearly.

10.5 Concluding remarks

Decomposition techniques are a straightforward method to deal with the entire distribution networks' immense scale beyond the simple feeder basis analysis. The partitioning of a large scale distribution system may be given according to voltage levels, feeder basis, monitored area, control responsibility. Moreover, modeling the mutual effects of subsystems enables achieving an enhanced state estimation with reduced communication and computational cost. It can further support specialized algorithms according to each area and locally available information (such as dynamic and topology co-estimation).

The use of new technologies is also aligned with the issue of scalability and the multiarea perspective. As some examples, we can cite using big data for model

calibration, exploiting new computing architectures such as cloud and edge computing, and enabling new features by higher decentralization and connectivity with the IoT.

Specialized algorithms, such as the branch current estimator, have proven to provide higher performance when dealing with radial networks. Spatial data fusion also appears as a promising approach to tackle vast and wide-area systems, which can be further enhanced by including better quality prior information. There is an accuracy trade-off on such approaches, familiar to any multiarea method, resulting in an optimality gap compared with a centralized approach. The gap can be negligible, given that centralized approaches may be numerically infeasible or even sometimes cannot attain real-time computational requirements.

From a general perspective, multiarea approaches address multiple challenges. Not all might be of interest to every utility but must be taken into account in any scalable, practical implementation:

- *Scalability*: As the complexity of the power grid increases, either due to extending the monitored network to lower voltage levels, to the presence of active distribution systems, or due to adding detailed models of new devices (such as power electronic devices), multiarea approaches remain on the technological pathway since parallel CPUs are available;
- *Privacy*: If individual area operators do not want to exchange measurement or model information with neighbors or the central coordinator, this will not impact the implementation of a system-wide state estimator;
- *Independence of individual area* State Estimators (SEs): It is noted that when implementing hierarchical MASE, individual area SEs can use different methods, i.e. they do not all have to use the WLS approach, any SE method will work and will not impact the overall implementation.

Finally, the incorporation of multiarea techniques has an important numerical facet to be considered since the scale associated with three-phase component models often results in severe ill-conditioning for distribution system analysis. These issues are discussed in other chapters through a more detailed analysis of branch current algorithms, orthogonal methods to improve numerical robustness along with the data fusion, and detailed models of distribution network components.

References

[1] Primadianto A., Lu C.-N. ‘A review on distribution system state estimation’. *IEEE Transactions on Power Systems*. 2017, vol. 32(5), pp. 3875–83.

[2] Ahmad F., Rasool A., Ozsoy E., Sekar R., Sabanovic A., Elitaş M. ‘Distribution system state estimation:A step towards smart grid’. *Renewable and Sustainable Energy Reviews*. 2018, vol. 81(4), pp. 2659–71.

[3] Garcia L.A., Grenard S. ‘Scalable distribution state estimation approach for distribution management systems’. *2nd IEEE PES International Conference*

and Exhibition onInnovative Smart Grid Technologies (ISGT Europe); 248235, Manchester, Inglaterra; 2011. pp. 1–6.

[4] Nusrat N., Irving M., Taylor G. *'Development of distributed state estimation methods to enable smart distribution management systems'*In: *Proceedings of the 2011 IEEE International Symposium on Industrial Electronics, Gdansk, Poland, 27–30 June*; 2011. pp. 1691–6.

[5] Nusrat N., Lopatka P., Irving M.R., Taylor G.A., Salvini S., Wallom D.C.H. 'An overlapping zone-based state estimation method for distribution systems'. *IEEE Transactions on Smart Grid*. 2015, vol. 6(4), pp. 2126–33.

[6] Muscas C., Pau M., Pegoraro P.A., Sulis S., Ponci F., Monti A. 'Multiarea distribution system state estimation'. *IEEE Transactions on Instrumentation and Measurement*. 2015, vol. 64(5), pp. 1140–8.

[7] Angioni A., Shang J., Ponci F., Monti A. 'Real-time monitoring of distribution system based on state estimation'. *IEEE Transactions on Instrumentation and Measurement*. 2016, vol. 65(10), pp. 2234–43.

[8] Pau M., Ponci F., Monti A., Sulis S., Muscas C., Pegoraro P.A. 'An efficient and accurate solution for distribution system state estimation with multiarea architecture'. *IEEE Transactions on Instrumentation and Measurement*. 2017, vol. 66(5), pp. 910–9.

[9] Pau M., Patti E., Barbierato L., *et al.* 'Design and accuracy analysis of multilevel state estimation based on smart metering infrastructure'. *IEEE Transactions on Instrumentation and Measurement*. 2019, vol. 68(11), pp. 4300–12.

[10] Cutsem T., Ribbens-Pavella M. 'Critical survey of hierarchical methods for state estimation of electric power systems'. *IEEE Transactions on Power Apparatus and Systems*. 1983, vol. PAS-102(10), pp. 3415–24.

[11] Gómez-Expósito A., de la Villa Jaén A., Gómez-Quiles C., Rousseaux P., Van Cutsem T. 'A taxonomy of multi-area state estimation methods'. *Electric Power Systems Research*. 2011, vol. 81(4), pp. 1060–9.

[12] Korres G.N. 'A distributed multiarea state estimation'. *IEEE Transactions on Power Systems*. 2011, vol. 26(1), pp. 73–84.

[13] González X., Ramirez J.M., Marmolejo J.A., Caicedo G. 'Methodology for multiarea state estimation solved by a decomposition method'. *Electric Power Systems Research*. 2015, vol. 123(1), pp. 92–9.

[14] Conejo A.J., Castillo E., Minguez R., García-Bertrand R. *Decomposition Techniques in Mathematical Programming: Engineering and Science Applications*. Heidelberg: Springer Science & Business Media; 2006.

[15] Gómez-Exposito A., Abur A., De La Villa Jaén A., Gomez-Quiles C. 'A multilevel state estimation paradigm for smart grids'. *Proceedings of the IEEE*. 2011, vol. 99(6), pp. 952–76.

[16] Pau M., Pegoraro P.A., Sulis S. 'Efficient branch-current-based distribution system state estimation including synchronized measurements'. *IEEE Transactions on Instrumentation and Measurement*. 2013, vol. 62(9), pp. 2419–29.

[17] Muscas C., Pau M., Pegoraro P.A., Sulis S. 'Uncertainty of voltage profile in PMU-Based distribution system state estimation'. *IEEE Transactions on Instrumentation and Measurement*. 2016, vol. 65(5), pp. 988–98.
[18] Congdon P. *Bayesian Statistical Modelling*. vol. 704. Chichester: John Wiley & Sons; 2007.
[19] Davis T.A. 'Algorithm 915, Suitesparse QR: Multifrontal multithreaded rank-revealing sparse QR factorization'. *ACM Transactions on Mathematical Software*. 2011, vol. 38(1), pp. 1–22.
[20] Hebling G.M., Massignan J.A.D., London Junior J.B.A., Camillo M.H.M. 'Sparse and numerically stable implementation of a distribution system state estimation based on multifrontal QR factorization'. *Electric Power Systems Research*. 2020, vol. 189(5), p. 106734.
[21] Massignan J.A.D., London J.B.A., Bessani M., Maciel C.D., Fannucchi R.Z., Miranda V. 'Bayesian inference approach for information fusion in distribution system state estimation'. *IEEE Transactions on Smart Grid*. 2022, vol. 13(1), pp. 526–40.
[22] Massignan J.A.D., London J.B.A., Maciel C.D., Bessani M., Miranda V. 'PMUs and SCADA measurements in power system state estimation through Bayesian inference'. *IEEE Milan PowerTech*; Milan-Italy, 23-27 Jun; 2019. pp. 1–6.
[23] *IEEE Test Feeder Specifications* [online]. 2012. Available from http://ewh.ieee.org/soc/pes/dsacom/testfeeders/.
[24] Pau M., Pegoraro P.A., Monti A., Muscas C., Ponci F., Sulis S. 'Impact of current and power measurements on distribution system state estimation uncertainty'. *IEEE Transactions on Instrumentation and Measurement*. 2019, vol. 68(10), pp. 3992–4002.
[25] IEEE. *IEEE PES Ieee pes distribution systems analysis subcommittee radial test feeders* [online]. 2018. Available from http://sites.ieee.org/pes-testfeeders/.
[26] Camillo M.H.M., Fanucchi R.Z., Romero M.E.V., *et al.* 'Combining exhaustive search and multi-objective evolutionary algorithm for service restoration in large-scale distribution systems'. *Electric Power Systems Research*. 2016, vol. 134(3), pp. 1–8.
[27] Fanucchi R.Z., Bessani M., Camillo M.H.M., *et al.* 'A multi-objective algorithm to determine patrol sequences for out-of-service nodes in power distribution feeders'. *Electric Power Systems Research*. 2021, vol. 196(99), p. 107198.
[28] Massignan J.A.D., Pereira B.R., London J.B.A. 'Load flow calculation with voltage regulators bidirectional mode and distributed generation'. *IEEE Transactions on Power Systems*. 2016, vol. 32(2), pp. 1–1577.

Chapter 11

Including synchronized and non-synchronized measurements with different sample rates in distribution system state estimation

Mohammed Ansar Mohammed Manaz[1], Yu-Jen Lin[2], Shao-Jie Wang[1], João Bosco Augusto London Junior[3], Julio Augusto Druzina Massignan[3], and Chan-Nan Lu[1]

11.1 Introduction

The distribution system (DS) was considered a predictable, collectively managed system that needed little real-time interventions unless under emergency situations. As more distributed energy resources (DER), such as photovoltaics (PV), electric vehicles (EV), and distributed generators, are integrated, and actively participate in demand side management programs, the intermittent bus net-loads would cause power flows and feeder voltage profiles in the distribution network to become more diversified and unpredictable. To maintain the service quality, there is an urgent need for active monitoring of the grid in real-time and intervention by the operator when necessary.

Complex interactions among different functions in modern distribution networks have significantly changed the feeder load profiles, network configuration, and operation practice. To mitigate possible impacts of DER on the network security and power quality, smart grid initiatives have been deployed, which created new sources of data. Data gathered promptly at various information systems from intelligent electronic devices (IEDs), automated feeder switches and voltage regulators, smart inverters of DER and phasor measurement units (PMUs) provide an opportunity to enhance system situation awareness [1–6]. Through active monitoring systems, operators are not just seeking to improve network reliability and efficiency

[1]Department of Electrical Engineering, National Sun Yat-sen University, Kaohsiung, Taiwan
[2]Department of Electrical Engineering, I-Shou University, Kaohsiung, Taiwan
[3]Department of Electrical and Computing Engineering, School of Engineering of São Carlos, University of São Paulo, São Paulo, Brazil

but also maximize utilization of existing assets to accommodate DER integrations without compromising established operational restrictions [7–10].

A distribution system state estimation (DSSE)-based real-time network model is an essential instrument in the control and protection of distribution networks to meet the changes in technology, environment, and commerce. However, due to economic and technical limitations, measurements cannot be independently utilized to estimate the complete DS states. Synergy among all types of sensor data can refine and achieve network models for analyses more promptly when needed. This chapter introduces techniques suitable for DSSE in presence of non-synchronized measurements with different sampling rates.

11.2 Data sources for DSSE

Due to the inherent size and complexity of the DS, data from several sources in distribution management system (DMS) can be exploited to enable DSSE, such as,

1. Equipment connectivity status information from:
    1. automated mapping and facility management (AM/FM) systems
    2. geographic information system (GIS)
    3. outage management systems (OMS)
2. Real-time voltage, current, and power flow measurements from:
    1. distribution automation (DA),
    2. fault detection, isolation and restoration (FDIR) devices,
    3. SCADA systems,
    4. IED
    5. micro-phasor measurement units (μPMU) if any.
3. Customer interval demands and DER output data from customer information system (CIS) and metre data management system (MDMS).

To implement DSSE in the control centre, interface functions are developed to convert 'maps' and attribute data from AM/FM/GIS environment to the operational database structure that supports DSSE and DS analyses. Feeder topology, parameters, and measurements required are gathered by data query tools searching through CIS, OMS(AM/FM/GIS), SCADA databases, and MDMS. To develop an efficient and seamless online model for conducting various operational and business processes, a common information model (CIM) is important to address the data interoperability and facilitate data exchange. Data can be accessed by multiple utility applications through the CIM data layer that includes adapters for converting data into the CIM-compliant data definitions [1, 11].

An advanced DMS utilizes multiple data sources to monitor, control, and coordinate the DS operations. The interactions among various systems and databases enabling the DMS functions are shown in Figure 11.1. Different metering devices and the respective databases are connected via a wide area network, and the

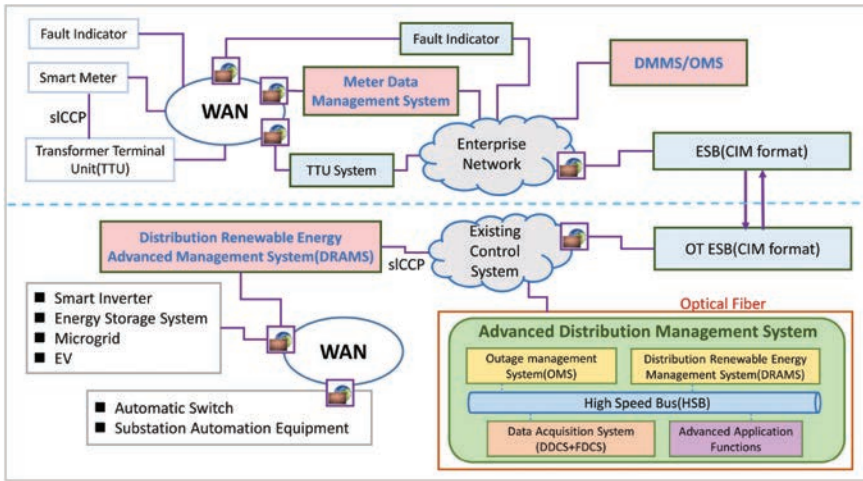

Figure 11.1 Data synergy in a power DS

interactions between different but compatible systems are accomplished using inter-control centre protocol. The higher-level applications such as OMS and distribution mapping management system receive data from MDMS, transformer terminal unit (TTU) system, and fault indicator system databases through the enterprise network. The CIM facilitates the interaction between different management systems/databases through enterprise service bus.

11.2.1 Measurement data used in DSSE

Unlike the transmission network state estimation, a distribution network without simplification contains numerous state variables to be determined. To ensure full observability, large amount of meter data is required; installing enough metering devices is economically and practically infeasible. To overcome this, three types of measurement are incorporated into DSSE: (1) real measurements, (2) pseudo-measurements, and (3) virtual measurements.

11.2.1.1 Real measurements

To perform DSSE, the measurements from Distribution automation system (DAS), SCADA, IED, Advanced Metering Infrastructure (AMI), and μPMU can be used. Table 11.1 shows the data sources and measurement characteristics. For different operation purposes, each data source has its sampling rate: SCADA data are available every few seconds and some are reported by exception, AMI may report measurements once every 15 minutes or inlonger time intervals, and μPMU and IEDs have settable rates of 1–60 messages per second.

Each system may provide different sets of measurements: SCADA data may include bus voltages, branch currents, powers and switch status at a few feeder

Table 11.1 Data sources and measurement characteristics

Sources	Attributes				
	Measurement types	**Sampling rates**	**Data transfer delay**	**Errors**	**Data repository systems**
SCADA	P, Q, I, V magnitude	Status change 15-minute polling	3–30 seconds		ADMS
DAS	P, Q, I, V magnitude	Status change	3–30 seconds		ADMS
TTU	P, Q, I, V magnitude	1 minute	5 minutes	±0.5% (I,V) ±1% (P,Q)	TTU server
DREAMS (renewable inverters)	P, Q, I, V magnitude	Status change 15-minute polling	1–2 minutes		DREAMS server
Smart metres (AMI)	P, Q magnitude	15 minutes	1–2 hours	±0.5%	AMI server
PMU	V phasor, I phasor P, Q, PF, frequency	10–60 sample per second	40 ms	±1%	Control centre
μPMU	P,Q, PF, frequency, V phasor, I phasor	Up to 120 samples each second	20 ms	±0.05% (±0.01 degrees for phase angle)	Control centre

locations, the AMI data include power consumption data at the customer locations, and μPMU can provide magnitude and phase angle of bus voltages and other power measurement data. μPMU installed in the medium and low voltage level of a DS can measure three-phase voltage phasors, current phasors, active power, reactive power, power factor, and frequency. The μPMU can have a sampling rate of up to 120 samples per second. It has an angle accuracy of ±0.01 degrees and amplitude accuracy of ±0.05%.

Smart meters are installed at the low voltage level of a DS. They can measure load profiles, such as root mean square value (RMS) of voltage, current, active power, reactive power, and power factor. In some cases, smart meters can also measure power quality data. The measurement accuracy of smart meters can be within ±0.5%. TTU is a device usually installed at the feeder of distribution transformers. TTU can measure RMS voltage, current, active power, reactive power, and power factor. It can also indicate when an abnormal event happened. The measurement accuracy of voltage and current is ±0.5%, and the measurement accuracy of active and reactive power is ±1%.

11.2.1.2 Pseudo-measurements

Due to insufficient real measurements available, pseudo-measurements are crucial in most DSSE algorithms for complete observability. They are used to replicate bus power injection measurement data represented by Gaussian distributions with mean and standard deviation derived from load research and customer billing data. The pseudo-measurements are determined by considering customer class load curves. If the loads do not follow a Gaussian distribution, the Gaussian mixture model, a combination of several normal distributions, can be used to represent the load probability density function [12].

11.2.1.3 Virtual measurements

Virtual measurements are zero voltage drops in closed switching devices, zero power flows in open switching devices and zero bus injections at switching stations. Although the virtual measurements are highly reliable, assigning high weights to virtual measurements and low weights to pseudo-measurements may cause ill-condition in some DSSE algorithms [13, 14].

11.3 Temporal aspects of DSSE

The power system is a time-varying system, and its state variables exhibit stochastic behaviour that responds to perturbations. In this way, as long as the traditional formulation of state estimation relies on static perspectives and snapshots to model power system behaviour, this is all the state estimation will be able to capture from the measured data, unrelated frames of a real movie. Therefore, it is necessary to

move the formulation of the state estimation from a single snapshot perspective towards time-variant stochastic and dynamic models.

The stochastic model for the state aims at capturing different possible values for the operating condition of the system. A set of state vectors defines this concept, each element related to a respective set of observations at the instant t, during an observation window Δt.

$$x = \{x_o, x_1, ..., x_{t-1}, x_t, x_{t+1}, ..., x_{\Delta t}\} = x_t \mid_{t \in \Delta t}. \tag{11.1}$$

This dynamic and temporal notion of the state variables emerge from different possible values that may occur during a sequence of observations from the measurements. Such different values can be related to intrinsic component behaviour, such as stationary levels, volatility, trends, or to system's transitions. Examples of such transitions can be described as the following [15]:

- Systemic: due to sudden load variations, generation dispatch or controller actions
- Structural: due to contingencies, switching operations, or changes in the network
- Random: due to intermittency or failure
- Induced: due to cyber-attacks or unsupervised switching

In state estimation formulations they are often conceptualized as anomalies, alongside with the possibility of bad data, with the goal of detecting and identifying the presence of drifts on the system or measurement behaviour. For instance, contingencies, changes in the controller settings, stochastic load variation, generation intermittency, may result on different values for the state variables over time.

Regarding DS, some particularities also emerge related to the stochastic behaviour of such systems. Especially, due to the close connection to end consumers that increases the load volatility and the associated uncertainty. For instance, the load behaviour of a distribution feeder, a distribution transformer and a residential consumer present diverse temporal characteristics that impact the system assessment at each level.

Besides, new technologies related to decarbonization goals and the energy transition also change such stochastic behaviour. For instance, (i) distributed generation intermittency may increase sudden drifts on the state, (ii) the increase of EV may increase load volatility, (iii) new energy markets and demand response also can change load behaviour and finally (iv) energy storage devices and advanced controllers, such as from switched capacitors and transformers with on-load tap changers, may also cause abrupt transitions. As pointed in the previous section, the measurements employed by the state estimators also carry different temporal scales, which will be sensitive to different levels and types of temporal events. Altogether, such new and complex environment demands more active monitoring of DS, considering temporal aspects into the estimation, in all levels of the networks, from low-voltage grids to primary feeders and substations, in a dynamic perspective.

11.3.1 Dynamic state estimation concepts and introduction to Kalman filters

In a general perspective, the dynamic behaviour of a power system is represented by a continuous state-space model, which captures differential and algebraic relations among electrical quantities, formulated in (11.2). The analysis of two separate operating conditions results in different approaches for dynamic state estimation (DySE), the quasi-dynamic (or quasi-steady) and the transient analysis [16].

$$\begin{aligned} \dot{y}(t) &= f\left(y(t), x(t), u(t), p\right) \\ 0 &= g\left(y(t), x(t), u(t), p\right) \\ u_{min} \leq\ & u(t) \leq u_{max} \\ y_{min} \leq\ & y(t) \leq y_{max} \\ x_{min} \leq\ & x(t) \leq x_{max} \\ p_{min} \leq\ & p \leq p_{max} \end{aligned}, \tag{11.2}$$

where, $y(t)$ are the dynamic state variables, $x(t)$ are the algebraic state variables, $u(t)$ represent input variables, p is the set of parameters of the power system, $f(\cdot)$ is a non-linear function, which represents the differential equations, that relates the dynamic response of the system, and $g(\cdot)$ is a non-linear function that represents algebraic relations among the variables. All the variables can be associated to bounds, represented by the *min* and *max* subscripts and respective inequalities, that represent physical limitations of the system variables and parameters.

The dissociation of the state vector into dynamic and algebraic state variables follows the idea of the two approaches for DySE. The variables involved are further exemplified in the following:

- Algebraic variables *x:* the variables that describe the electrical network and power flows, such as the nodal voltages and current phasors;
- Dynamic variables *y:* the variables that are related to the dynamic response of components, such as internal variables of generators and loads, and control architectures.
- Input variables *u:* the controlled variables of the system, such as controller setpoints and dispatched resources.
- Parameters *p:* fixed values that characterize different components of the power system, such as lines and transformers parameters.

In practice, a discrete-time state-space model is employed to describe the system behaviour along with its temporal relations, instead of a continuous formulation [16].

The approach focused on the transient behaviour focuses on dynamic variables, and the model in (11.2) can be rewritten as the following discrete, first-order, non-linear, state-space model in each instant k [16]:

$$\begin{aligned} y_k &= f(y_{k-1}, x_{k-1}, u_k, p) + \omega_{k-1} \\ z_k &= h(y_k, x_k, u_k, p) + e_k, \end{aligned} \tag{11.3}$$

where ω_{k-1} is the process noise and e_k is the measurement error, usually assumed as normally distributed random variables, with zero mean and known covariance

Box 11.1 The family of Kalman Filters

The family of Kalman Filters: The linear Kalman Filter was initially proposed in the seminal work of Kalman in the 1960s [18]. Immediately, it became a new standard for control theory, successfully applied in aerospace systems, navigation, robotics, signal processing, power systems and many other scientific and industry applications. It describes a discrete linear system, such as the following state space:

$$\begin{aligned} x_k &= Fx_{k-1} + q_{k-1} \\ z_k &= Hx_k + e_k, \end{aligned} \tag{11.4}$$

where, x_k and x_{k-1} are the state variable at instant k and $k-1$, F is the state transition matrix, z_k is the measurement vector, H is the linear measurement model matrix, q_{k-1} is the process noise and is the measurement noise. The filter algorithm, in its state estimation perspective, comprises a two-step procedure:

Update step: comprises an a priori update of the state vector $x_{k|k-1}$ and associated covariance matrix $P_{k|k-1}$ by the following equations:

$$\begin{aligned} x_{k|k-1} &= F\hat{x}_{k-1} \\ P_{k|k-1} &= FP_{k-1}F^T + Q_{k-1} \end{aligned} \tag{11.5}$$

Estimation step: comprises an a posteriori estimation of the state vector $\hat{x}_k$ and associated covariance matrix P_k by the following equations:

$$\begin{aligned} K_k &= P_{k|k-1}H^T(HP_{k|k-1}H^T + R)^{-1} \\ \hat{x}_k &= x_{k|k-1} + K_k(z_k - Hx_{k|k-1}) \\ P_k &= P_{k|k-1} - K_kHP_{k|k-1}, \end{aligned} \tag{11.6}$$

where K_k is known as the Kalman gain. Different variations of the above basic formulation encompass a predictive and an estimation perspective, but the same fundamental concepts apply.

In the effort of surpassing many of the practical and theoretical challenges, different versions of the Kalman filter were proposed in the context of power systems, such as the linear Kalman filter [19], the extended Kalman filter (EKF) [20], the unscented Kalman filter (UKF) [21], the cubature Kalman filter [22], the ensemble Kalman filter [23], the H-infinite approach [24], polynomial-chaos approach [25], the maximum correntropy Kalman filter [15], adaptive Kalman filters [26], and many others. The literature is vast, and other scientific applications also present interesting contributions for the Kalman filter family.

matrices Q_k and R_k, respectively. The process noise and measurement error capture different sources of noise and error, communication failures, model approximations and discretization errors.

Conversely, the approach focused on the quasi-steady behaviour focuses on the algebraic variables, capturing the stochastic behaviour of the algebraic variables that arises between subsequent operating conditions, x_k and x_{k-1}. In this case, the model can also be written as a discrete, first-order, non-linear, state-space model in each instant k:

$$x_k = f(x_{k-1}, u_k, p) + q_{k-1}$$
$$z_k = h(x_k, u_k, p) + e_k,$$

where q_{k-1} is the process noise that now captures a stochastic characteristic of the algebraic state variables. The intrinsic difference between these two approaches lies mainly on the length of the observation window of interest. A detailed discussion about these models can be further explored in [16, 17].

The approaches for finding the estimated state variables are typically encompassed by the application of the Kalman filter family of state estimators. Box 11.1 presents a brief introduction to the Kalman filter theory, and such concepts will be further explored in the following sections.

11.3.2 Dynamic, forecasting-aided and tracking state estimation

The previous definitions of state space encompass different types of state estimators for power systems, depending on the level, horizon and type of dynamic response of the system being captured (ranging from milliseconds to seconds and minutes). In this context, three main approaches regarding the process equation represent the state space under the perspective of DySE for power systems:

- Tracking state estimation: this formulation assumes the previous instant as a good approximation for the current estimation step, by a direct relation from all state variables from a previous instant with the following. The tracking state estimation consists in the following discrete time-variant non-linear model:

$$x_k = x_{k-1} + q_{k-1}$$
$$z_k = h(x_k) + e_k \tag{11.7}$$

This is the case whenever true steady-state conditions are satisfied, or whenever state variations are assumed small enough. The algorithm leads to fewer modifications in static estimators, while obtaining significant gains in terms of accuracy. However, the approach is very susceptible to abrupt system changes and in the presence of trends, since it is a simplified forecasting model.

- Forecasting-aided state estimation: this formulation introduces a forecasting stage to capture the temporal relations that may arise from algebraic variables in a linear model, employing regression and trends to predict future state variables. The formulation consists of the measurement model and a forecasting model

that relates the system's state at different instants. In this sense, forecasting-aided state estimation is intended to describe 'slow time evolution of the static-state, observed from multiple scans of measurements' [27, 28]. The state-space model can be used with two different goals: to relate the current state to a previous one by the forecasting model or to predict the next state. The first approach can be written as the following discrete time-variant system:

$$\begin{aligned} x_k &= F_{k-1}x_{k-1} + g_{k-1} + q_{k-1} \\ z_k &= h(x_k) + e_k \end{aligned} \tag{11.8}$$

The tracking state estimation is a simplified version of the forecasting-aided state estimation model, assuming an identity matrix as the state transition and neglecting trends. Different methods may be employed for estimating the transition matrix, such as the exponential smoothing, using Holt's method, or different regression models according to learning algorithms. This approach typically captures smooth transitions; however, it is also highly affected by abrupt changes or systemic transition that drastically modify the stochastic behaviour of the system.

- Dynamic state estimation: this formulation entails the internal variables of electrical machines and components, for instance, generator models along with their respective controllers, into the state estimation formulation. Also, the load dynamics may be incorporated in the model. Such variables are also called dynamic state variables y. And also keep the algebraic state variables x of the electric power network (the complex nodal voltages). Thus, it consists of a set of discretized differential-algebraic equations that describe the fast transients along with the interconnected power network in a single estimation formulation:

$$\begin{aligned} y_k &= f(y_{k-1}, x_{k-1}) + \omega_{k-1} \\ z_k &= h(y_k, x_k) + e_k \end{aligned} \tag{11.9}$$

In this case, the solution method is obtained through numerical integration methods such as Runge–Kutta methods and Euler interpolation, or with Kalman filter formulations in the discrete version of the state space. Often the stochastic aspects of the algebraic state variables are omitted in this type of formulation. More details about such type of formulation may be referred in [17].

11.4 Multistages state estimators based on quasi-dynamic techniques

Quasi-DySE techniques are employed when the state variables change exclusively due to slow changes in load/generation. The estimation process involves two stages: state update and state filtering. In the state update stage, the mean value of the state variables is predicted using time evolution model; and in the state filtering stage, the mean value of the state variables is corrected based on new measurements. Given an algebraic state vector **x** comprising of bus voltage magnitudes and angles, and

a measurement vector **z**, the dynamics of the system can be modelled as a discrete time model [16], as in the forecasting-aided state estimation model in (11.8):

$$\mathbf{x}_k = \mathbf{F}_{k-1}\mathbf{x}_{k-1} + \mathbf{g}_{k-1} + \mathbf{q}_{k-1}, \tag{11.10}$$

$$\mathbf{z}_k = \mathbf{h}\left(\mathbf{x}_k\right) + \mathbf{e}_k, \tag{11.11}$$

$$\mathrm{x}_0 \sim (\bar{\mathrm{x}}_0, \mathbf{R}_0),\ \mathbf{q}_{k-1} \sim (0, \mathbf{Q}_{k-1}),\ e_k \sim (0, \mathbf{W}_k) \tag{11.12}$$

where the subscript k denotes the time. Matrix **F** and vector **g** drive the time evolution of the states, $\mathbf{q}_{k-1}$ is a white Gaussian noise vector of the prediction model at time $k-1$. **h** is a non-linear function relating each measurement to state variables. $\mathbf{e}_k$ is a white Gaussian noise vector of the measurements at time k.

State update

The time evolution of the state variables can be modelled based on the past observations. The $\mathbf{F}_{k-1}$ and $\mathbf{g}_{k-1}$ can be computed using Holt's two-parameter linear exponential smoothing technique [21, 29] or using realistic state transition using network equations [30]. Holt's method approximates $\mathbf{F}_{k-1}$ and $\mathbf{g}_{k-1}$ by assigning decreasing weights to past observations (see Box 11.2).

The predicted state vector $\bar{\mathbf{x}}$,

$$\bar{\mathbf{x}}_k = \mathbf{E}[\mathbf{F}_{k-1}\mathbf{x}_{k-1} + \mathbf{g}_{k-1} + \mathbf{q}_{k-1}], \tag{11.19}$$

Box 11.2 Holt's 2-parameter model

Holt developed a model to predict the next sample in a data series $\{y_1, y_2, ..., y_{k-1}, y_k\}$ having a trend. The model is consisted of 3 equations,

$$\text{Forecast equation} : y_{k+1} = a_k + b_k \tag{11.13}$$

$$\text{Level smoothing} : a_k = \alpha y_k + (1-\alpha)(a_{k-1} + b_{k-1}) \tag{11.14}$$

$$\text{Trend smoothing} : b_k = \beta(a_k - a_{k-1}) + (1-\beta)b_{k-1} \tag{11.15}$$

$a_0 = 0, b_0 = 0, \alpha, \beta \in [0, 1]$ are smoothing parameters. Rearranging these equations, we can write,

$$y_{k+1} = F_k y_k + g_k \tag{11.16}$$

where,

$$F_k = \alpha(1+\beta)I \tag{11.17}$$

(I: Identity matrix having same number of rows as y)

$$g_k = (1-\alpha)(1+\beta)(a_{k-1} + b_{k-1}) - \beta\, a_{k-1} + (-\beta)b_{k-1} \tag{11.18}$$

$$\bar{\mathbf{x}}_k = \mathbf{F}_{k-1}\mathbf{E}[\mathbf{x}_{k-1}] + \mathbf{g}_{k-1}, \tag{11.20}$$

$$\bar{\mathbf{x}}_k = \mathbf{F}_{k-1}\hat{\mathbf{x}}_{k-1} + \mathbf{g}_{k-1}, \tag{11.21}$$

$\hat{\mathbf{x}}_{k-1}$ is the filtered state vector at the previous time instant. The a priori state covariance matrix $\mathbf{R}_k^-$ is then updated.

$$\mathbf{R}_k^- = \mathbf{F}_{k-1}\mathbf{R}_{k-1}^-\mathbf{F}_{k-1}^T + \mathbf{Q}_{k-1} \tag{11.22}$$

As new measurement vectors are received, they are compared against the predicted measurements.

$$\bar{\mathbf{z}}_k = \mathbf{E}\left[\mathbf{h}\left(\mathbf{x}_k\right) + \mathbf{e}_k\right] \approx \mathbf{h}\left(\bar{\mathbf{x}}_k\right) \tag{11.23}$$

The innovation (or new knowledge learned from the new measurements) is defined as the difference between the actual and predicted measurement vectors,

$$\nu_k = \mathbf{z}_k - \bar{\mathbf{z}}_k \tag{11.24}$$

And the states filtering is performed to find the corrected state vector $\hat{\mathbf{x}}_k$ such that the sum of weighted squared deviations of the state vector $(\hat{\mathbf{x}}_k - \bar{\mathbf{x}}_k)$ and measurement vector $(\mathbf{z}_k - \bar{\mathbf{z}}_k)$ is minimized. The solution of this optimization is,

$$\hat{\mathbf{x}}_k = \bar{\mathbf{x}}_k + \mathbf{K}_k \nu_k, \tag{11.25}$$

where, the Kalman gain

$$\mathbf{K}_k = \mathbf{R}_k\mathbf{H}_k^T\left[\mathbf{W}_k\right]^{-1}, \tag{11.26}$$

and the a posteriori error covariance matrix

$$\mathbf{R}_k = \left[\left[\mathbf{R}_k^-\right]^{-1} + \mathbf{H}_k^T\left[\mathbf{W}_k\right]^{-1}\mathbf{H}_k\right]^{-1}. \tag{11.27}$$

The measurement Jacobian matrix $\mathbf{H}_k$ is computed in the neighbourhood of the predicted state vector $\bar{\mathbf{x}}_k$ at time k [31]. The EKF DySE procedure is illustrated in Figure 11.2.

State correction in UKF

In the EKF, the a posteriori error covariance matrix and Kalman gain are computed using the Jacobian of the measurement function ***h*** as in (11.6); however, this linearization can introduce some error. In UKF, this approximation is avoided by using the unscented transformation to approximate the mean and error covariance of the measurements (see equation (11.21)).

Incorporating measurements having different sampling rates

Measurements with different sampling rates and delays, as shown in Figure 11.3, can be used for state estimation in DMS. Assuming that the available measurements at 15-minute intervals satisfy the observability condition, a static weighted least square DSSE can be performed to find the system states. However, the measurements received in subsequent time steps may not satisfy full system observability due to the limited number of devices sending measurements at high sampling rates.

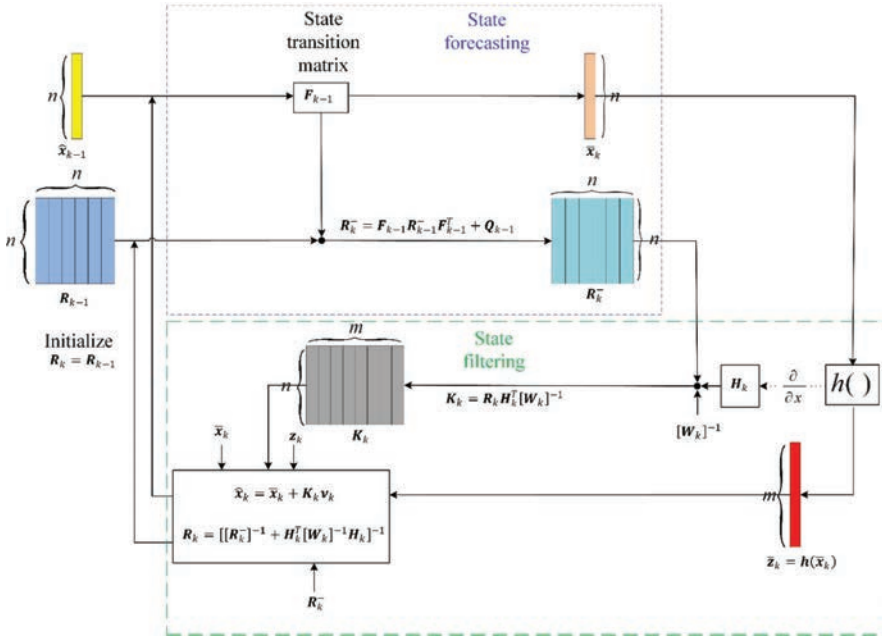

Figure 11.2 EKF DySE procedure

The partial set of measurements received from μPMU or IEDs at different intervals may not guarantee full system observability at the snapshot but useful for state updates. DySE methods can be used to update the system states using the most recent measurements. EKF or UKF algorithms can be adopted in the DySE procedure, as shown in Figure 11.3, to update the system states when only a partial set of measurements is received.

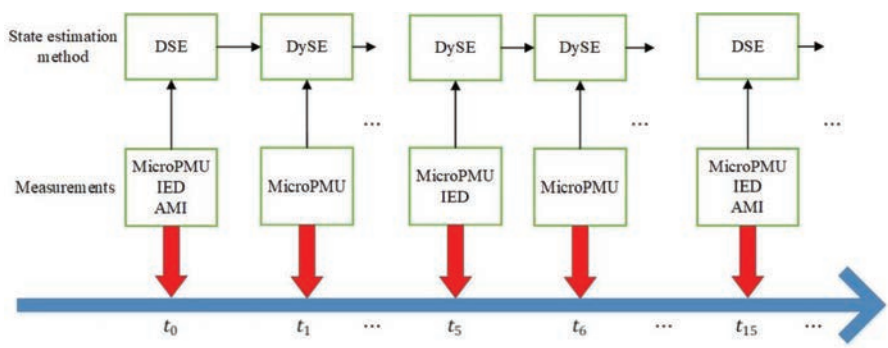

Figure 11.3 Using measurements with different sampling rates for DSSE/DySE

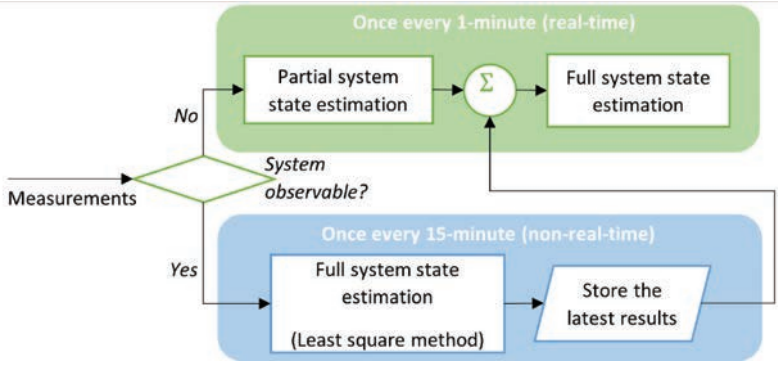

Figure 11.4 Operations of a consensus DSSE using measurements with different sampling times

11.4.1 Limitations of Kalman filter-based methods

Although the quasi-dynamic state-estimation methods provide a direct approach to incorporate the measurements having different sampling rates, some may fail to track system states when sharp net-load intermittency occurs. Hybrid methods using measurements received from real-time measurement units can be adopted to circumvent this issue and trace system states. Compressive sensing and low-rank matrix techniques can circumvent the insufficient real-time measurements available to guarantee complete system observability in previously proposed methods.

11.4.2 Consensus DSSE method

Consensus DSSE methods fuse the limited number of real-time measurements with previous state estimates to update the full system states. For the discussion, here we will consider two groups of measurement devices: (1) real-time measurements and (2) non-real-time measurements. The real-time measurements have a high sampling rate (e.g. once every 1 minute), and the non-real-time measurements have a low sampling rate (e.g. once every 15 minutes). Due to the limited deployment of real-time measurement devices, those measurements alone cannot guarantee the full observability of the system states. A consensus DSSE procedure would accommodate suitable techniques to update the system states using partial measurements and previous DSSE results. The operations of a consensus DSSE are shown in Figure 11.4.

Once every 15 minutes all the measurements will be available to perform a complete system state estimation (assuming that the system is observable using the complete set of measurements); however, in the next minute, only a subset of measurements will be available, which cannot be used directly to perform DSSE. A partial DSSE is performed using the latest measurements and then it is combined with the previous DSSE results to update all system states.

11.4.2.1 DistFlow-based partial DSSE

A partial state estimation procedure based on a linearized DistFlow model is described in the following [32]. By neglecting the line losses and assuming that the phase angle difference between adjacent buses is small, one can approximate the DS power flow equations to a linear set of equations.

$$P_{ij} \approx \sum_{k\in L_j} P_{jk}+p_j \tag{11.28}$$

$$Q_{ij} \approx \sum_{k\in L_j} Q_{jk}+q_j \tag{11.29}$$

$$y_i-y_j \approx r_{ij}P_{ij}+x_{ij}Q_{ij} \tag{11.30}$$

$$\delta_i-\delta_j \approx x_{ij}P_{ij}-r_{ij}Q_{ij} \tag{11.31}$$

where P_{ij} and Q_{ij} are respectively the active and reactive power flow from bus i to bus j; p_j and q_j are the active and reactive power consumption at bus j; r_{ij} and x_{ij} are the resistance and reactance of the line between buses i and j, and δ_i is the voltage magnitude and angle at bus i. $y_i = \frac{1}{2}v_i^2$.

In a radial DS with N number of PQ-buses and a reference bus, using the DistFlow model, the difference between the adjacent bus states can be expressed in a matrix form,

$$d \triangleq \begin{bmatrix} y_1-y_0 \\ \vdots \\ y_N-y_{N-1} \\ \delta_1-\delta_0 \\ \vdots \\ \delta_N-\delta_{N-1} \end{bmatrix} = Z_n S, \tag{11.32}$$

where $S = [p_1,\cdots,p_n, q_1,\cdots,q_n]^T$ is the bus power consumption vector and Z_n is a matrix that depends on the line impedances and bus connectivity [32].

Assume there are M real-time metering devices in a set of critical buses represented by $\Omega_{\mathrm{m}} = \{m_1, m_2, \ldots, m_M\}$, which are the buses where a sudden change in active power is likely. The difference between a real-time measurement $y_{i\in\Omega_m}$ and the reference bus state value y_0 can be expressed as a sum of the difference between each pair of adjacent buses in the path from the reference bus to the bus i, i.e.,

$$y_i - y_0 = (y_i - y_{i-1}) + \cdots + (y_1 - y_0) = \sum_{j\in\{1,\ldots,i\}} (y_j - y_{j-1}). \tag{11.33}$$

Similarly, the difference between each real-time measurement and the reference bus value can be expressed as,

$$d_m = \begin{bmatrix} y_{m_1} - y_0 \\ \vdots \\ y_{m_M} - y_0 \\ \delta_{m_1} - \delta_0 \\ \vdots \\ \delta_{m_M} - \delta_0 \end{bmatrix} = C_m \begin{bmatrix} y_1 - y_0 \\ \vdots \\ y_N - y_{N-1} \\ \delta_1 - \delta_0 \\ \vdots \\ \delta_N - \delta_{N-1} \end{bmatrix} = C_m Z_n \mathrm{S} = Z_m S, \tag{11.34}$$

where C_m is a permutation matrix of dimension $2M \times 2N$. Also notice that for a given distribution network configuration the matrix Z_m is constant.

In (11.34), if only the active power consumption at bus $i \in \Omega_m$ is changed by a small quantity Δp_i,

$$\left[\Delta d_{m_1} \ \ldots \ \Delta d_{m_j} \ \ldots \ \Delta d_{m_i} \ \ldots\right]^T = Z_m \left[0 \ \ldots \ 0 \ \ldots \ \Delta p_i \ \ldots\right]^T \tag{11.35}$$

We get, $\Delta d_{m_j} = z_{ji} \Delta p_i$, $\Delta d_{m_i} = z_{ii} \Delta p_i$, where z_{ji} is the $(j,i)^{th}$ element of Z_m. The sensitivity of each element in Δd_m to change in one of its elements Δd_{m_i} can be given as,

$$\frac{\Delta d_{m_j}}{\Delta d_{m_i}} = \frac{z_{ji}}{z_{ii}} \tag{11.36}$$

Now, assume that a set of real-time and non-real-time measurements is sampled at time $t = t_0$; using these measurements, a static distribution state estimation result is obtained. The real-time measurement devices continue to take measurements once every Δt interval. The problem at hand is to update the system states using the newly obtained measurements at each time instant $t = t_0 + k\Delta t,\ k = \{1, 2, \ldots, K-1\}$ before the time $t = t_1$ when the next set of non-real-time measurements is sampled ($t_1 = t_0 + K\Delta t$). In the following, we will discuss how measurement sensitivities obtained in (11.35) can be used to find the actual power deviations at critical buses where solar PV is installed (assuming that each such bus has a real-time measurement device).

The vector d_m can be obtained using the real-time measurements sampled at $t = t_0$ and $t = t_0 + k\Delta t$, and be denoted $d_m(t_0)$ and $d_m(t_0 + k\Delta t)$. And define the difference between these vectors,

$$\Delta d_m\left(t_0 + k\Delta t\right) = d_m\left(t_0 + k\Delta t\right) - d_m\left(t_0\right) = \begin{bmatrix} y_{m_1}\left(t_0 + k\Delta t\right) - y_0 \\ \vdots \\ y_{m_M}\left(t_0 + k\Delta t\right) - y_0 \\ \delta_{m_1}\left(t_0 + k\Delta t\right) - \delta_0 \\ \vdots \\ \delta_{m_M}\left(t_0 + k\right) - \delta_0 \end{bmatrix} - \begin{bmatrix} y_{m_1}\left(t_0\right) - y_0 \\ \vdots \\ y_{m_M}\left(t_0\right) - y_0 \\ \delta_{m_1}\left(t_0\right) - \delta_0 \\ \vdots \\ \delta_{m_M}\left(t_0\right) - \delta_0 \end{bmatrix}. \tag{11.37}$$

Since the reference values y_0 and δ_0 are fixed, $\Delta d_m\left(t_0+k\Delta t\right)$ represents the measurement change happening at each bus with a real-time measurement device.

$$\Delta d_m\left(t_0+k\Delta t\right)=\begin{bmatrix} y_{m_1}\left(t_0+k\Delta t\right)-y_{m_1}\left(t_0\right) \\ \vdots \\ y_{m_M}\left(t_0+k\Delta t\right)-y_{m_M}\left(t_0\right) \\ \delta_{m_1}\left(t_0+k\Delta t\right)-\delta_{m_1}\left(t_0\right) \\ \vdots \\ \delta_{m_M}\left(t_0+k\right)-\delta_{m_M}\left(t_0\right) \end{bmatrix}=\begin{bmatrix} \Delta y_{m_1}\left(t_0+k\Delta t\right) \\ \vdots \\ \Delta y_{m_M}\left(t_0+k\Delta t\right) \\ \Delta\delta_{m_1}\left(t_0+k\Delta t\right) \\ \vdots \\ \Delta\delta_{m_M}\left(t_0+k\Delta t\right) \end{bmatrix}. \tag{11.38}$$

Now assume that each real-time measurement is represented by an agent. Each agent initially believes that the measurement deviation it is observing (e.g. $\Delta y_{m_i}\left(t_0+k\Delta t\right)$) is caused by a change in active power consumption in that bus only.

$$\Delta\tilde{p}_i\left(t_0+k\Delta t\right)=\frac{\Delta y_{m_i}\left(t_0+k\Delta t\right)}{z_{ii}} \tag{11.39}$$

where $\Delta\tilde{p}_i$ is the active power consumption change apparent at bus based on the deviation of the measured value. The agent can predict (using the sensitivities) how much measurement deviations will be observed in other measurement points due to the presumed active power change in its location.

$$\Delta\tilde{y}_{m_j}=\frac{z_{ji}}{z_{ii}}\Delta y_{m_i}\left(t_0+k\Delta t\right) \tag{11.40}$$

In fact, the measurement deviation at bus *i* could have been collectively caused by the changes in active power consumption at number of other buses,

$$\Delta y_{m_i}\left(t_0+k\Delta t\right)=\left[Z_m\right]_i\begin{bmatrix}\Delta p_{m_1}\\ \vdots \\ \Delta p_{m_M}\end{bmatrix}, \tag{11.41}$$

$\left[Z_m\right]_i$ is a row vector obtained from the *i*th row of Z_m. Hence, by neglecting active power deviations at all other buses (also neglecting reactive power changes at all buses between the interval $[t_0, t_1]$), the measurement deviation at bus *i* can be expressed as,

$$\begin{bmatrix}\Delta y_{m_1}\left(t_0+k\Delta t\right)\\ \vdots \\ \Delta y_{m_M}\left(t_0+k\Delta t\right)\end{bmatrix}=\Delta y_m=Z_m^*\Delta p_m, \tag{11.42}$$

$\Delta p_m=\left[\Delta p_{i\in\Omega_{\mathrm{m}}}\right]\in\mathbb{R}^M$ is the bus power consumption deviation vector. Z_m^* is a $M\times M$ submatrix of Z_m. By solving (11.42), the actual power deviation at the critical buses can be computed. Once the power injections at the critical buses are approximated, they can then be used as measurements in the static DSSE or DySE to find the whole system states.

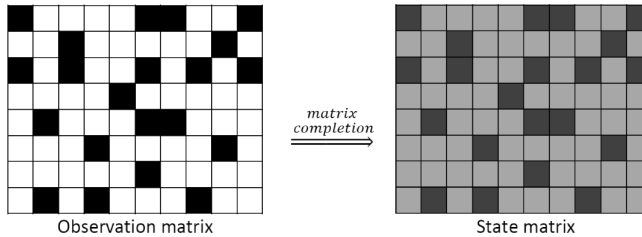

Figure 11.5 Typical structure of an observation matrix and corresponding state matrix

11.4.3 Matrix completion-based system state update with granular measurements

Compressive sensing techniques are widely used in image processing applications where the missing pixels are recovered by exploiting the linear dependency between the adjacent pixels. An image can be considered as an (m x n) matrix where each element represents a pixel. Given such a matrix with some lost pixels, the matrix completion algorithm tries to reconstruct the complete matrix by exploiting the linear dependence of the row space (and column space). The outcome includes the estimates of missing pixels.

The main advantage of matrix completion in DSSE application is that it does not require the measurements to satisfy strict observability conditions like in weighted least square methods, i.e., the use of incorrect pseudo-measurements can be avoided in DSSE. In certain situations, having about 20% of the data in an observation matrix could be enough to reconstruct the whole matrix containing related states and power quantities [33]. This feature makes it a potential method to perform DSSE in low-observable DS [34–36].

To apply this method for DSSE, the first step is to represent the feeder data (states and measurements) as a 2D matrix. Figure 11.5 shows such a matrix, the granular black squares represent the available measurements, the white spaces are unknown variables; the state matrix shown on the right side can be computed using matrix completion techniques. Matrix completion methods estimate the values of the missing variables by exploiting the linear dependency found in the system. Naturally, this problem becomes a search for a matrix solution that has the lowest rank, while satisfying the known measurements. Following standard notation is commonly adopted to describe this problem.

M :Data matrix (m x n)
X :State matrix (m x n)
Ψ : Set of known elements of matrix M. This set contains all the coordinates of the known elements in M. i.e.,$\Psi \subseteq \{1, 2, \ldots, m\} \times \{1, 2, \ldots, n\}$
$P_{\Psi}(\cdot)$: A filtering function.

$$\text{E.g., if } \Psi = \{(1,3),(2,2),(3,1),(3,3)\} \text{ and } \mathrm{M} = \begin{bmatrix} m_{11} & m_{12} & m_{13} \\ m_{21} & m_{22} & m_{23} \\ m_{31} & m_{32} & m_{33} \end{bmatrix}$$

$$\overset{then}{\Longrightarrow} P_{\Psi}(M) = M_{\Psi} = \begin{bmatrix} 0 & 0 & m_{13} \\ 0 & m_{22} & 0 \\ m_{31} & 0 & m_{33} \end{bmatrix},$$

$$\mathrm{X} = \begin{bmatrix} x_{11} & x_{12} & x_{13} \\ x_{21} & x_{22} & x_{23} \\ x_{31} & x_{32} & x_{33} \end{bmatrix} \overset{then}{\Longrightarrow} P_{\Psi}(X) = X_{\Psi} = \begin{bmatrix} 0 & 0 & x_{13} \\ 0 & x_{22} & 0 \\ x_{31} & 0 & x_{33} \end{bmatrix},$$

More formally, the $(i,j)^{th}$ element of the observation matrix,

$$M_{\Psi}(i,j) = \begin{cases} m_{ij} & ;(i,j) \in \Psi \\ 0 & ;\text{otherwise} \end{cases}. \tag{11.43}$$

Given the observation matrix M_{Ψ}, the matrix completion problem is given by,

$$\begin{aligned} &\underset{X \in \mathbb{R}^{m \times n}}{\text{minimize}} && \text{rank}(\mathrm{X}) \\ &\text{subject to} && X_{\psi} = M_{\psi}. \end{aligned} \tag{11.44}$$

Solving this problem is difficult due to two reasons: (1) the rank operator is non-convex and (2) the equality constraint is highly susceptible to noise. This predicament is resolved by choosing an appropriate convex relaxation of the original problem. To this end, the rank operator is replaced by nuclear norm, which is a convex surrogate function for the rank operator (see Box 11.3). And the equality constraint is replaced by inequality to accommodate some mismatch due to noisy measurements. The transformed optimization problem becomes,

$$\begin{aligned} &\underset{X \in \mathbb{R}^{m \times n}}{\text{minimize}} && \|X\|_* \\ &\text{subject to} && \tfrac{1}{2}\sum_{i=1}^{m}\sum_{j=1}^{n}(x_{ij} - m_{ij})^2 \le \delta \end{aligned}, \tag{11.45}$$

where $\delta \ge 0$ is a scalar. Often this problem is expressed in compact form using the Frobenius norm,

$$\begin{aligned} &\underset{X \in \mathbb{R}^{m \times n}}{\text{minimize}} && \|X\|_* \\ &\text{subject to} && \tfrac{1}{2}\|X_{\Psi} - M_{\Psi}\|_F^2 \le \delta \end{aligned}. \tag{11.46}$$

Using convex solvers this optimization problem could be solved efficiently to find a low-rank solution for X such that $X_{\Psi} \approx M_{\Psi}$.

When applying this method for DSSE, the state estimation results can be further improved by incorporating additional constraints that describe the physical laws of

Box 11.3 Some definitions

Nuclear norm of a $m \times n$ matrix A is the sum of its singular values:

$$\|X\|_* = \sum_{i=1}^{\min\{m,n\}} \sigma_i(A).$$

Frobenius norm of a $m \times n$ matrix A is:

$$\|X\|_F = \sqrt{\sum_{i=1}^{m}\sum_{j=1}^{n} \|a_{ij}\|^2}.$$

the power network. Namely, power balance and power flow equations. However, if these constraints are non-linear then the problem becomes non-convex and difficult to solve. Therefore, a linear approximation of the unbalanced three-phase power flow should be adopted in the formulation. The complete problem takes the form,

$$\begin{aligned} \underset{X\in\mathbb{R}^{m\times n}}{\text{minimize}} \quad & \|X\|_* \\ \text{subject to} \quad & \tfrac{1}{2}\|X_\Psi - M_\Psi\|_F^2 \le \delta \\ & \| g(X) \| \le \beta \end{aligned} \tag{11.47}$$

where g(X) is a vector-valued linear function and $\beta \in \mathbb{R}_+^l$ is a vector of appropriate length, which allows for some tolerance in the physics constraints. δ and β shall be specified as inputs or included in the objective function to achieve adequate tolerances.

The matrix completion problem can be solved using standard semi-definite program solvers [36, 37].

11.4.4 Implementations of matrix completion-based DSSE

A matrix completion-based DSSE can be uniquely characterized based on

- selection of data matrix
- linear power flow constraints adopted
- treatment of constraint tolerances as optimization variables/inputs

Data matrix

Branch formulation: The data matrix is structured such that each row represents a power system branch, and each column represents a quantity relevant to that branch. This structure allows us to take advantage of both bus- and branch-related measurements.

For example, data of each branch could include voltage v, complex power s, and current i measurements/variables entries of from-end-bus f and to-end-bus t stored in a row, as shown below.

Branch no.	$\Re(v_f)$	$\Im(v_f)$	$\lvert v_f \rvert$	$\Re(s_f)$	$\Im(s_f)$	$\Re(v_t)$	$\Im(v_t)$	$\lvert v_t \rvert$	$\Re(s_t)$	$\Im(s_t)$	$\Re(i_{ft})$	$\Im(i_{ft})$
1												
2												
⋮												
⋮												

Bus formulation: The data matrix M is structured such that each row represents a bus and each column represents related data associated with that bus. This structure usually results in a smaller data matrix, which can be useful to improve computational efficiency in large systems.

For example, each bus represented by each row.

Bus no.	$\Re(v_b)$	$\Im(v_b)$	$\lvert v_b \rvert$	$\Re(s_b)$	$\Im(s_b)$
1					
2					
⋮					
⋮					

The selection of the data matrix format may depend on the types of measurements available in the system. Depending on the data matrix structure, 'duplication constraints' need to be included where necessary; these are constraints that establish equality between different elements of the data matrix corresponding to the same measurement/state. For example, in the branch formulation, the voltage magnitude of a bus from (in) which multiple branches originate (terminate) may appear in more than one row of the data matrix (in column $|v_f|$ (or $|v_t|$)); the duplication constraints tell the program that the values of these cells must be equal.

Linearized power flow

A linearized DistFlow model is described in the following [34]. By neglecting the line losses and assuming that the phase angle difference between adjacent buses is small, one can approximate the DS power flow equations to a linear set of equations.

$$P_{ij} \approx \sum_{k \in L_j} P_{jk} + p_j, \tag{11.48}$$

$$Q_{ij} \approx \sum_{k \in L_j} Q_{jk} + q_j, \tag{11.49}$$

$$y_i - y_j \approx r_{ij} P_{ij} + x_{ij} Q_{ij}, \tag{11.50}$$

$$\delta_i - \delta_j \approx x_{ij} P_{ij} - r_{ij} Q_{ij}, \tag{11.51}$$

where P_{ij} and Q_{ij} are respectively the active and reactive power flow from bus i to bus j, q_j is the active and reactive power consumption at bus j, x_{ij} is the resistance

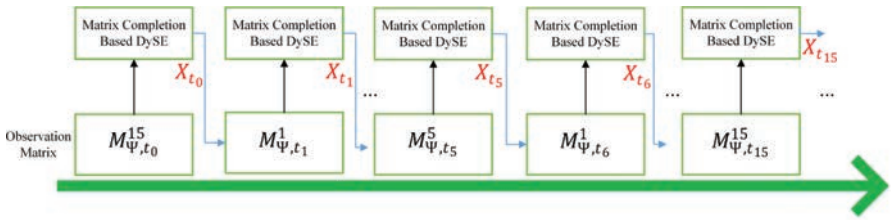

Figure 11.6 Application of matrix completion method using measurements with different sampling time

and reactance of line between buses i and j, and δ_i is the voltage magnitude and angle at bus i. Alternative forms of linearized power flow constraints for DSSE can be found in [36].

Treatment of tolerance as optimization variables

For large enough δ and β, the matrix completion problem will have a feasible solution. To ensure the solutions obtained have tighter tolerance, the augmented objective function can be expressed as,

$$\begin{aligned} \underset{X\in\mathbb{R}^{m\times n}}{\text{minimize}} \quad & \|X\|_* + w_1\delta + w_2\beta^T\beta \\ \text{subject to} \quad & \frac{1}{2}\|X_\psi - M_\psi\|_F^2 \le \delta \\ & \|g(X)\| \le \beta \end{aligned} \tag{11.52}$$

where, $w_1, w_2 > 0$ are weighting parameters.

A DySE procedure using the matrix completion method is shown in Figure 11.6. In this figure, the observation matrix constructed at time t using the measurements sampled every T minutes is denoted $M^T_{\Psi,t}$; the state matrix obtained is denoted X_t. The observation matrix is constructed using the available measurements every 15 minutes; during the subsequent minutes before the next 15-minute interval, the observation matrix is constructed using replacement of available measurement data from previously determined complete matrix X[38, 39].

11.4.5 Numerical results

In this section, we present some state estimation results obtained using EKF, UKF, and matrix completion to demonstrate the salient features and limitations of each method; the results should not be interpreted as a testament to the performance of or as an objective comparison between different techniques. A 39-bus medium voltage distribution test system shown in Figure 11.7 is considered in the simulations. The total net-load of the system is shown in Figure 11.8. The results are presented for a two-and-a-half-hour period from 12.45 p.m. to 3.15 p.m. (as highlighted in Figure 11.8), where the net-load varies significantly due to solar generation intermittency. Table 11.2 shows the locations where the measurements are available.

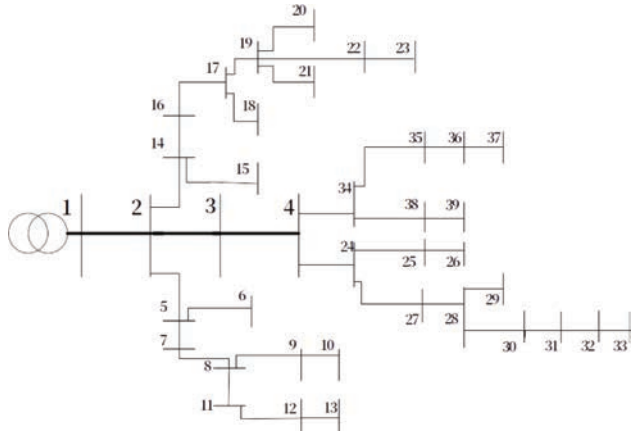

Figure 11.7 39-bus distribution test system

To demonstrate the applications of EKF and UKF, in these simulations, we assume that good static DSSE results are found using the available measurements and pseudo/virtual measurements for every 15 minutes (in practice, running a static DSSE using limited measurements has its hurdles, which we will not discuss further in this chapter). The state prediction is performed using Holt's two-parameter model (see Box 11.2).

Significant voltage variation is observed in Figure 11.9 during the first hour; during the last one-and-a-half hours, the voltage variations are smooth, which is effectively tracked by the state prediction model. However, when there are significant voltage changes, EKF and UKF take multiple times steps to adapt to that change (as can be observed during the initial 1-hour period in Figure 11.9).

Matrix completion method can be applied to each time step, without having to rely on pseudo-measurements. The results in Figure 11.10 show that it can track sudden voltage changes effectively and maintains acceptable performance. The main advantage of the matrix completion method is that it could achieve adequate results

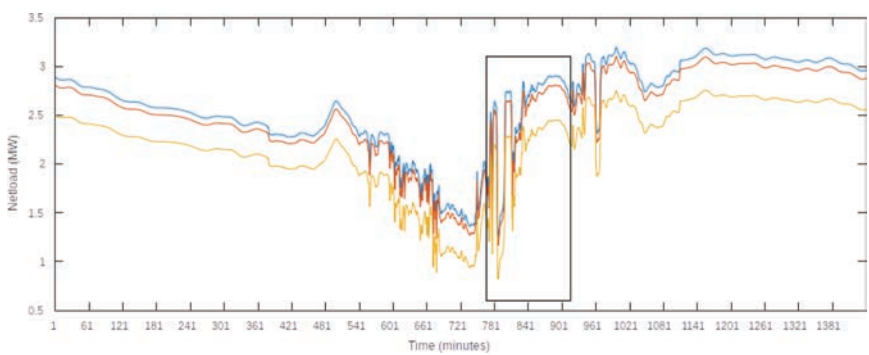

Figure 11.8 One-day netload profile of the test system in each phase a, b, and c

Table 11.2 Measurements available in the test system

Measurement device	Sampling time (min.)	Bus measurements	Line measurements
AMI	15	5,8,14,19,28,31,36,38	–
FTU	5	2,3	2–3,2–14,2–5,3–4
RTU	5	1	1–2
Smart inverter	1	13,23,32,37	–

using only a limited number of measurements. The accuracy of the matrix completion method would improve if more measurements were made available.

11.5 Bayesian information fusion approach for multistage DSSE

A closer look at the measurement vector shows the lack of synchronism among the measurement updating rates (Δt), ranging from a few milliseconds (for PMUs) up to minutes (for smart meters). Thereby, the measurements can be grouped according to their respective sampling and updating rates. Each subset consists of a sampling layer (*SL*), characterized by a similar updating time interval ($\Delta t_{z_i} = \Delta t_{SL}$), as shown in (11.53). In addition, typically each *SL* gathers measurements with similar relative accuracy. This concept of *SL* is illustrated in Figure 11.11. for a typical DS.

$$SL_i := \{z_i \in z \mid \Delta t_{z_i} = \Delta t_{SL_i}\}. \tag{11.53}$$

The challenge consists of treating a vast number of measurements, spread across all parts of a DS, while providing an accurate state vector, denoted as $\hat{x}$. At the same time, dealing with the temporal aspect of each *SL* and maintaining a tractable computational time and numerically stable.

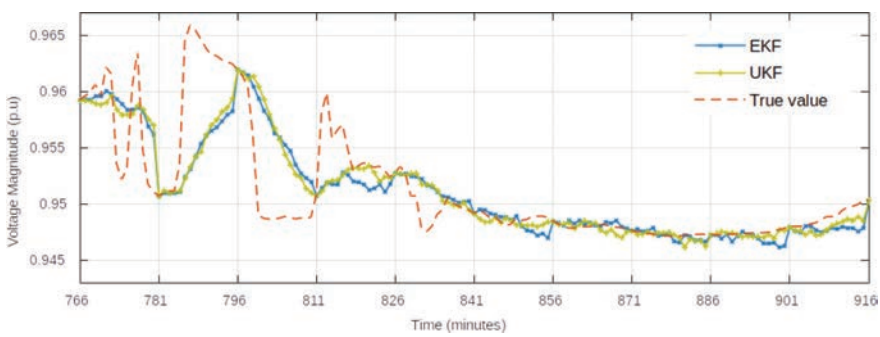

Figure 11.9 State estimation results for voltage magnitude at bus-32 (phase a) using DSSE/DySE method

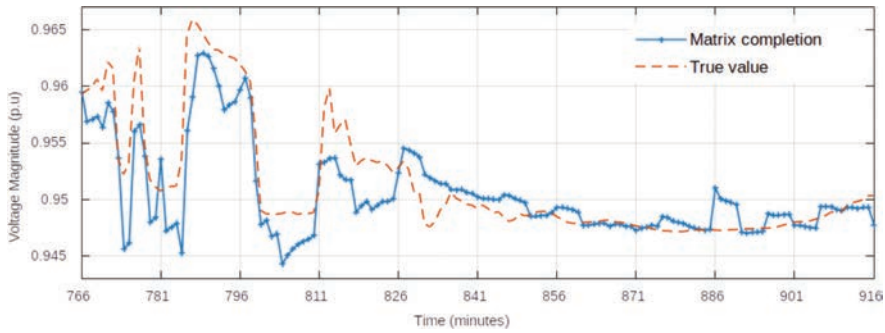

Figure 11.10 *State estimation results for voltage magnitude at bus-32 (phase a) using a matrix completion method*

11.5.1 Bayesian inference concepts and application in DSSE

The Bayesian information fusion consists of a multiple stage state estimation, triggered by each new measurement update from the respective *SL*. The measurement model is decomposed into each separated *SL* [40]. The relation between two layers, and thus between measurements with different synchronization times, is incorporated using a hierarchical model for the state variables as follows:

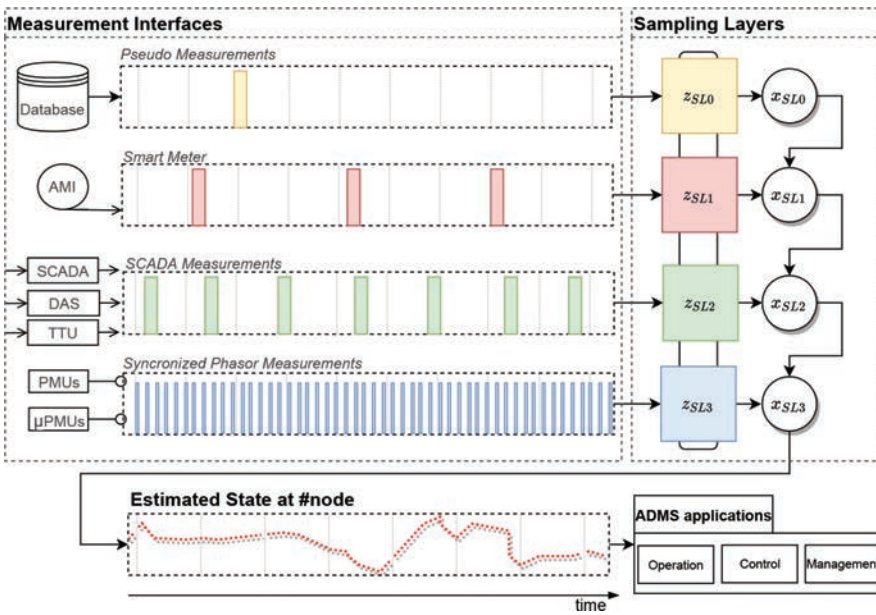

Figure 11.11 SL *concept in the Bayesian information fusion procedure for DSSE*

$$x_{SL} = \hat{x}_{SL-1} + \omega_{SL-1} \tag{11.54}$$

$$z_{SL} = h_{SL}(x_{SL}) + e_{SL} \tag{11.55}$$

where x_{SL} is the state vector at the current SL, $\hat{x}_{SL-1}$ is the estimated value at the previous SL with slower updating rate, z_{SL} is the measurement vector of the respective SL, $h_{SL}(x_{SL})$ is the respective measurement model, e_{SL} is the measurement error vector associated with the measurements in the SL, and ω_{SL} is a random component associated with the uncertainty between the time intervals of two SL.

Such concept entails a probabilistic model for the state vector, encompassing the state of the network as a random variable. Therefore, we can directly apply the concepts used in Bayesian inference, where the estimation problem treats both measurements and states as random variables.

In the Bayesian perspective, each new set of observations of a SL updates the posterior distribution for the state. The likelihood function represents the measurement model and assumed noise characteristic. The prior distribution for the state variables comes from the previous SL posterior distribution, a hierarchical model [41]. Using the Bayes' theorem, we can find the posterior probability function of the state variables as the following conditional probability distribution:

$$f_{X|Z}(x_{SL}|z_{SL}) = \frac{f_{Z|X}(z_{SL}|x_{SL})\, f_X(x_{SL})}{f_Z(z_{SL})} \tag{11.56}$$

where $f_{X|Z}(x_{SL}|z_{SL})$ is the conditional probability function of the state given the measurements in each SL, $f_{Z|X}(z_{SL}|x_{SL})$ is the likelihood function of the SL according to the measurement model, $f_X(x_{SL})$ is the prior distribution in the hierarchical model, and $f_Z(z_{SL})$ is the measurement probability of occurrence, a constant value that scales the posterior probability function and is often neglected.

Estimation is performed in each layer and triggered as soon as the respective measurements become available in the respective layer. A maximum a posteriori (MAP) estimation given in (11.57) updates the state variables, and the result is then used as the prior distribution for the following layers.

$$\hat{x}_{SL} = \arg\max_{x} f_{X|Y}(x_{SL} \mid z_{SL}). \tag{11.57}$$

To provide a fast solution for the state estimation problem, a multivariate Gaussian prior distribution is assumed, as described in (11.58). The likelihood function comes from the typical assumption of a multivariate Gaussian noise associated with the measurement model, as described in (11.59). This maintains a tractable computational for the MAP estimate, an essential aspect for real-time applications. If the measurement model were linear, such as in the case of purely PMUs SL in rectangular coordinates, this approach would provide a closed-form solution for the posterior distribution, a conjugate prior model. Another important aspect of the chosen prior distribution is that it is an informative prior, since it is based on previous knowledge about the model. Non-informative priors may be used; however, it tends to increase the estimator variance.

$$Prior: \qquad x_{SL} \sim \mathcal{N}(\hat{x}_{SL-1}, P_{SL-1}) \tag{11.58}$$

$$\textit{Likelihood}: \qquad z_{SL} \mid x_{SL} \sim \mathcal{N}(h_{SL}(x_{SL}), R_{SL}) \tag{11.59}$$

where P_{SL-1} is the state covariance matrix estimated at the previous *SL* and R_{SL} the measurement covariance matrix of the current *SL*, a sub-matrix of R in the original measurement model.

It is noteworthy the relation and similarity of the Bayesian approach and the Kalman filter for state estimation. In fact, the Kalman filter is a particular case of Bayesian inference, where the error models are assumed as multivariate Gaussian and the state space follows a discrete time Markov process. The conjugate model assumes an approximation of the actual state behaviour, at the vicinity of the results from previous *SL*, instead of any previous instant as employed in the family of Kalman filters [15, 26]. Since it is an informative prior, obtained from the previous *SL*, such approximation tends to follow the system behaviour. However, if an abrupt change occurs, this hypothesis fails and therefore hampers the estimation accuracy.

11.5.2 Posterior inference via orthogonal methods

To overcome the severe ill-conditioning of typical DSs, it is recommended the application of an orthogonal method for solving the posterior estimation. The method consists in first using an orthogonal factorization according to (11.60), obtaining the orthogonal matrix $\mathscr{Q}$ and the upper triangular $\mathscr{R}$.

$$\begin{pmatrix} P_{SL-1}^{-1/2} \\ R_{SL}^{-1/2} H \end{pmatrix} = \mathscr{Q}^T \mathscr{R}. \tag{11.60}$$

With this orthogonal factorization, it is possible to rewrite the iterative equation for the posterior estimation as:

$$\mathscr{R}^T \mathscr{Q} \mathscr{Q}^T \mathscr{R} p^k = \mathscr{R}^T \mathscr{Q} \begin{pmatrix} P_{SL-1}^{-1/2} \hat{x}_{SL-1} \\ R_{SL}^{-1/2} (z_{SL} - h_{SL}(x^k))) \end{pmatrix}. \tag{11.61}$$

Since $\mathscr{Q}\mathscr{Q}^T = I$, where I is the identity matrix, and multiplying both sides by $(\mathscr{R}^T)^{-1}$, we obtain :

$$\mathscr{R} p^k = \mathscr{Q} \begin{pmatrix} P_{SL-1}^{-1/2} (x^k - \hat{x}_{SL-1}) \\ R_{SL}^{-1/2} (z_{SL} - h_{SL}(x^k)) \end{pmatrix}. \tag{11.62}$$

Instead of iterating over the original nonlinear MAP procedure, a better approach is to perform the search for the estimated state with the orthogonal decomposition of the estimation problem at each *SL*. This kind of orthogonal formulation also enables the application on severe ill-conditioned three-phase DSs and in the Bayesian fusion approach [42–45]. Besides, by exploring (11.61) it can be shown that $\mathscr{R}^T \mathscr{R} = P_{SL}^{-1}$. It facilitates the interaction between different *SL*, since $P_{SL}^{-1/2} = \mathscr{R}$. The numerical stability and computational performance can be further enhanced through sparsity treatment and ordering techniques [40, 45].

11.5.3 Bayesian credibility test

The Bayesian approach for DS state estimation previously presented allows the obtaining of a posterior distribution as a multivariate normal distribution. Such distribution can summarize different features, as the MAP estimation of the DS state in (11.57). Another aspect that can be explored from this Bayesian approach is the use of credibility intervals.

The arrival of new PMU measurements at a time instant t induces an update of the probability model. Hence, a comparison between the estimated state $\hat{x}_t$ with the posterior distribution credibility interval, obtained from previous time instants, can be performed. Such test can be used to identify if the constant state transition matrix is correctly representing the system operating condition. Therefore, for a stationary condition, the test will indicate that $\hat{x}_t$ is in accordance with the previous inferred probability distribution. However, for a non-stationary condition, as load ramps or contingencies, the test will indicate a disagreement between $\hat{x}_t$ and previous estimations. The credibility intervals can be defined as the range containing a particular percentage of probable values. That is, the closed interval $[x_{SL}^{-}, x_{SL}^{+}]$ and an associated probability p_{ci}, such that:

$$\int_{x_{SL}^{-}}^{x_{SL}^{+}} f_{X|Y}(x_{SL} \mid z_{SL}) dx_{SL} = p_{ci}. \tag{11.63}$$

This work employs a credibility interval in the vicinity of the MAP estimated state $\hat{x}_{SL}$ of each SL for the ith state variable, using Chebyshev's inequality:

$$\hat{x}_{SL}^{i} - k^{*}\sqrt{P_{SL}^{ii}} \leq x_{SL}^{i} \leq \hat{x}_{SL}^{i} + k^{*}\sqrt{P_{SL}^{ii}}, \tag{11.64}$$

where k^{*} defines the probability level of the credibility interval. For instance, $q = 0.95$, which yields a 95% credibility interval, with $k^{*} = 2$, in a multivariate normal distribution.

Two approaches may define the credibility intervals, providing two level of non-stationary event detection:

1. Credibility test with the latest SL prior distribution: provides a detection of large non-stationary events, in the sense that the estimated state at instant t is far from the one obtained from measurements in a previous SL.
2. Credibility test within the SL posterior distribution: provides a detection of smaller non-stationary events, in the sense that the estimated state at instant t is far from measurements on the same SL at instant $t - 1$.

11.5.4 Numerical results

Simulations with the IEEE 4 nodes test feeder illustrate the numerical aspects of the Bayesian DSSE. A load flow calculation was used to create the reference values for the state variables (x^{lf}) and measurements (z^{lf}). A Monte Carlo simulation by including random noise in the reference load flow values simulates measured

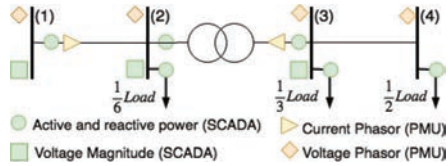

Figure 11.12 IEEE 4 nodes test feeder used to evaluate the proposed Bayesian inference method for including PMUs in DS state estimation

values to perform state estimation [46]. In this illustrative simulation two *SLs* are employed: (1) SCADA *SL* and (2) PMU *SL*.

The noise standard deviation σ_i was obtained using different precision levels for each measurement (in this study, was assumed 2% for active and reactive power measurements from SCADA, 1% for voltage magnitude from SCADA, and 0.1% for voltage and current phasor measurements from PMUs).

To simulate different sampling rates, a first sample from SCADA measurements was considered in the state estimation process, followed by 60 samples from PMUs. Each sample represents a different instant t and the respective measured values. For each instant, a load flow calculation was performed and the measured values are obtained according to the previously explained procedure. Thus, we obtained a sequence of quasi-stationary conditions being monitored by measurements with random noise in our simulations. When using such simulation strategy, based on load flow calculation, the system's dynamics is neglected, such as oscillations during transitory events [47].

Figure 11.12 illustrates the IEEE 4 nodes feeder with SCADA and PMU observable metering systems. The simulation setup employs an unbalanced load scenario with a Grounded Wye–Grounded Wye transformer connection . The load, originally in node 4, was distributed among nodes 2–4 to further represent the PMU non-observable scenario.

11.5.4.1 Performance with SCADA and PMU observable metering systems and fixed loading condition

The first test was performed using SCADA and PMU observable metering systems when the hypothesis of stationary condition is respected. The simulations were performed with fixed nominal loading to represent a stationary condition and to demonstrate the effect of the PMU posterior stage. Two different instants are considered: an initial instant with the acquisition of SCADA measurements and a second instant with the arrival of a PMU sample. The simulations were executed with 300 repetitions, resulting in a calculation of MAE with $n_{trials} = 300$.

To illustrate the effect of the MAP estimation (second stage of the proposed DSSE), Figure 11.13 presents the error histogram for this simulation. As it can be seen, besides the reduction on the MAE indicator, a smaller error variance is also obtained after the execution of MAP based on the PMU *SL*. This is because the

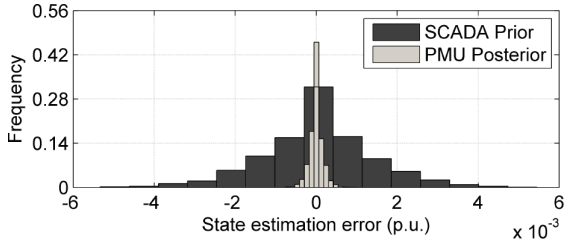

Figure 11.13 Histogram of state estimation error among all state variables for the SCADA prior stage and PMU posterior stage

higher precision assumed for such measurements are naturally considered in the proposed approach through the PMU measurements covariance matrix.

11.5.4.2 Performance with SCADA and PMU observable metering systems and load variation

A second test was performed with the inclusion of a 5% of load variation around the nominal loading. The IEEE 4 nodes feeder with the SCADA and PMU observable metering systems in Figure 11.12 is used again. In this simulation, we considered all the 60 PMU samples. Despite the load variation, this situation is still considered as stationary since the load variation is within a 5% of its nominal value, keeping a constant mean value and variance along the time interval of the PMU samples. This scenario intends to show a more realistic load condition, since there are no guarantees that the loads will keep a fixed value, while the PMU samples are arriving.

The Bayesian DSSE was then compared with a hybrid DSSE, which simultaneously processes both SCADA and PMU measurements in a single stage according to the non-linear measurement model, and with a Kalman filter DSSE that uses recursively the estimated posterior to update the prior belief. An identity matrix for the forecasting model was also used for the Kalman filter DSSE in the tests. Figure 11.14. presents the comparison using the MAE performance metric in both the fixed loading and the 5% of load variation scenarios.

The hybrid approach presented the worst precision, since it assumes both SCADA and PMUs samples represent the same instant. The Kalman filter approach presented a very good estimation for the fixed load scenario, but lost its accuracy for the load variation scenario. This result is expected since Kalman filter has good smoothing properties, and the fixed load value is the smoothest scenario possible. But when load variation was included this premise became false. Furthermore, the proposed Bayesian DSSE presented a similar precision in both scenarios, showing good results in both cases. This is related to the fact that the prior distribution only gives an initial estimate of the state vector and its covariance. Whenever a new PMU sample is gathered, the MAP estimation uses only the values of that sample to update the state vector.

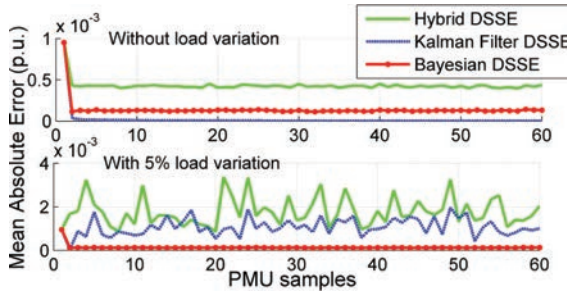

Figure 11.14 *Performance of DSSEs in terms of the mean absolute error in p.u. for each time sample (MAE_t) in the stationary scenarios. In these examples, PMU samples correspond to a sampling rate of 1 per second.*

11.5.4.3 Performance with SCADA observable and PMU non-observable metering systems and non-stationary condition

In this third test, the observable SCADA metering system illustrated in Figure 11.12 was considered. However, in terms of PMU metering system, only the PMU installed at the secondary winding of the transformer was considered (node 3). Therefore, the system is still SCADA observable, but no longer PMU observable, i.e., if only PMUs were considered it would not be possible to perform state estimation for the whole network.

In this test, a large load variation at node 4 (60% increase), only in phase A, was included in the simulation from t = 15 s to t = 20 s, in order to simulate a non-stationary event. In the other instants, the loads were kept within their nominal unbalanced loading with a 5% of variation. For instance, that large load variation could occur when a large load is connected, or due to intermittent distributed generation in the DS.

Figure 11.15 presents the MAE performance index in such scenario. Both Hybrid and Kalman filter approaches had their performance significantly deteriorated during the load temporary event. While the proposed approach had a much smaller influence in its estimation accuracy. To illustrate the state estimation results, Figure 11.16 shows the credibility intervals acquired with the prior and posterior

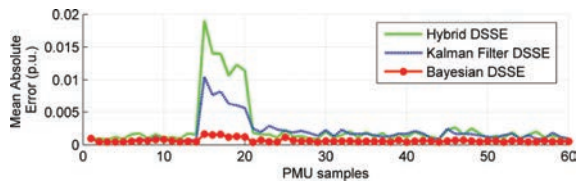

Figure 11.15 *Performance of DSSEs in terms of the mean absolute error in p.u. for each time sample (MAE_t) in the non-stationary scenario*

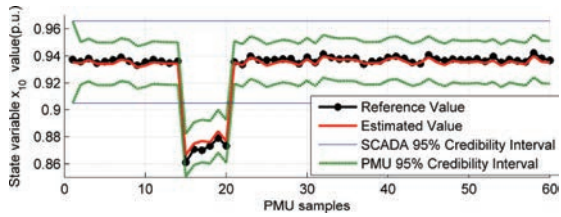

Figure 11.16 *Credibility intervals with SCADA prior and PMU posterior during an event occurrence, for state variable* x_{10}

distribution obtained by the proposed Bayesian DSSE for the real part of the complex voltage at node 4 (state variable x_{10}) at all samples.

Figure 11.17 illustrates the concept of credibility interval in terms of estimated prior and posterior distributions for the state variable x_{10}. The prior distribution and the posterior distribution at $t = 14$ (before the load event) and at $t = 15$ (after the load event) demonstrate the change in the state variable that occurred. While the DS is operating in a stationary condition, all the estimated state values with the PMUs fell inside the prior credibility interval, as it can be seen in the posterior distribution for $t = 14$. When the estimated value obtained in the MAP stage, at $t = 15$, fell outside the prior credibility interval, the previous state is not a good approximation to current state. That is, the system is no longer near the same state when the SCADA measurements were acquired. Since the event was detected with the prior distribution credibility interval, the test indicated a large event occurred.

By dealing with state estimation under the concept of *SL*, it is possible to track if changes of the systems are abrupt or fluctuations near the same state's vicinity. The application of such a promising feature is related to the perspective of autonomous system functionalities based on the state estimator information. Take, for example, the case of PMUs, where the sampling rates can easily achieve a few cycles. Operators cannot track system changes by themselves, and if a separate event detection method is applied, the processing time and latency requirements would be a technical issue to overcome. This integration becomes natural and computationally faster by introducing event detection within the state estimator framework, with very few modifications required.

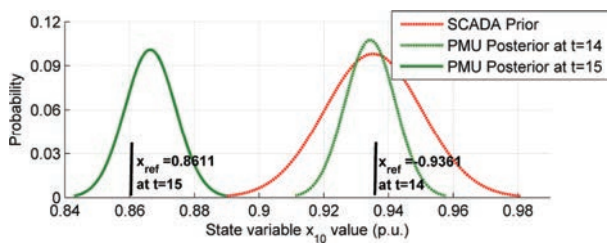

Figure 11.17 *SCADA prior distribution and PMUs posterior distributions, for state variable* x_{10} *at* $t = 14$ *and* $t = 15$

11.6 Applications of DSSE and challenges

DSSE shown in Figure 11.18 exploits data from different sources to provide the initial state/condition for many DMS applications, such as volt/VAR control, capacitor switching, loss minimization, congestion management, conservation voltage reduction (CVR), distribution transformer usage optimization, feeder reconfiguration, service restoration, and demand-side management. DSSE accuracy has a high impact on distribution network operations applications.

The integration of renewables at the distribution level poses operational challenges, such as the occurrence of overvoltages and voltage fluctuations due to output intermittency. DSSE results enable real-time distribution grid monitoring and assist system operators for effective volt/VAR controls to maintain voltage quality and assist reconfiguration under emergency.

A transformer load management system is used by network designers to estimate and examine the historical and current loadings of transformers and to test proposed load situations. The DSSE results can be used in transformer load modelling and management [48]. With more accurate distribution transformer load models, CVR conducted during power shortage periods would be more effective for energy conservation and transformer/feeder loading relief. The deployment of smart metres enhances DSSE accuracy. A consistent DSSE solution provides a guided search of potential irregularity of electricity usage [49] and adjustment of voltage unbalance in the network [50]. When the model does not represent the actual network condition, DSSE could detect, locate, and repair the erroneous information [51, 52]. Moving forward to carbon neutrality society, challenges for DSSE implementation are still open and new monitoring and management solutions are required, such as,

- adaptive and efficient feeder modelling methodologies for future wide-area active distribution network monitoring;

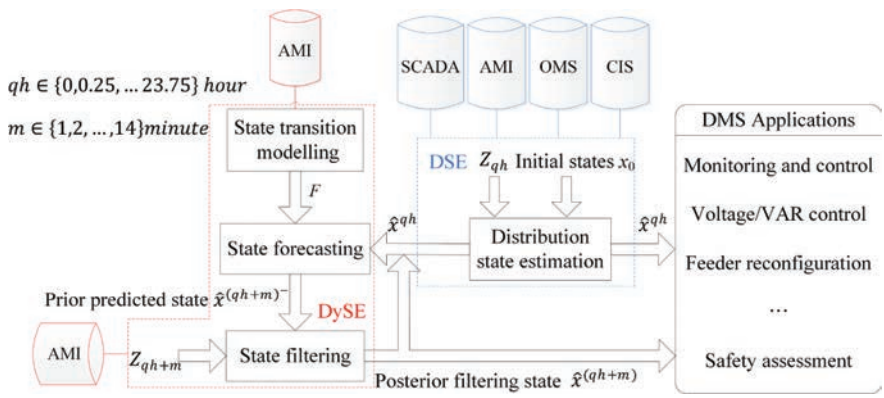

Figure 11.18 Data synergy in a power DS

- data synergy, fusion, and consensus techniques to exploit the large amount of heterogeneous data in the modern control centre and distributed renewable energy management system environment;
- edge computing, big data, and communication techniques to tackle the problem of efficiently collecting and coordinating the measurement results;
- a multi-level state estimation for better interaction among distribution and transmission network operations.

11.7 Concluding remarks

Transition to a sustainable energy future would result in complex and fast aggregated generator and load dynamics, which will lead to operation impacts on distribution networks. The DS monitoring process is made complicated not only because of special network characteristics and low redundancy of measurements but also due to the high number of nodes, the geographical extension of the networks, and the integrations of DER.

Many DSSE algorithms provide efficient procedures to build on-line distribution network models for system operation and planning. To improve the accuracy of online model, the synergy of a large amount of heterogeneous data from different systems with various data formats, unsynchronized polling cycles, communication delay, is crucial. Incorporating high sampling rate data of μPMUs, IEDs, and digital relays with delayed interval data from smart meters will improve overall DSSE accuracy. The use of big data is beneficial for model calibration [53]. Cloud-based IoT platforms [35], CIM [54], and data fusion techniques [55] are valuable for effective measurement data processing and monitoring active system situations.

Micro-grids and automation islands are evolving from a collection of sensor platforms that provide information to regional data centres; to a network of autonomous regions that exchange data among each other in order to optimize certain operational functions. Large intermittent variations of power injections from RES have made it difficult to achieve consistent state estimation results by augmenting pseudo-measurements with unsynchronized measurements having different sampling rates. The DySE techniques based on EKF and UKF had helped avoid relying on pseudo-measurements; however, their performance degrades when faced with sudden changes. Latest developments in sparsity-based techniques, such as matrix completion, have helped to overcome these limitations.

This chapter also presented a three-phase Bayesian inference DSSE based on information fusion and *SL* concepts. . Theoretical arguments and simulations support the interesting features of this approach when dealing with multi-scale instrumentation devices. For instance the multiple scales due to the different sampling rates of Smart Meters, Load Profiles, PMUs and SCADA measurements . It enables the integration of PMU measurements providing estimation with smaller mean errors, even for buses that are not observable by PMU measurements directly. Although formulated assuming stationary operating conditions, the Bayesian Fusion DSSE is

able to detect small and large non-stationary events based on credibility tests, due to an inherent notion of probabilistic characterization of the state variables.

Multi-area State Estimation (MASE) algorithms augmented with small-area SE to form hierarchical DSSE would meet operation requirements. In this respect, a consensus algorithm [56, 57] is an alternative for local control area DSSE that provides intelligence as well as topology, observability, and bad data analyses to local SE. MASE begins with many local SE, communicates their estimates to neighbouring areas continuously, and eventually making all local estimates converge to the centralized state estimation result [58]. Chapter 10 presented a detailed analysis of MASE.

The variations of the voltage values and other indicators can be used in adaptive DSSE to cope with the active nature of the distribution network. An event-triggered approach for sensing, communicating, and information processing is attractive to reduce computation and communication burdens. Using a report-by-exception scheme, the measurement data are sent to perform DSSE at higher rates and the estimation process runs consequently on a finer time scale to achieve a bandwidth-efficient and smart data transmission [59, 60].

References

[1] Gray G.R., Simmins J., Rajappan G., Ravikumar G., Khaparde S.A. 'Making distribution automation work: Smart data is imperative for growth'. *IEEE Power and Energy Magazine*. 2016, vol. 1, pp. 58–67.

[2] Huang S.-C., Lu C.-N., Lo Y.-L. 'Evaluation of AMI and SCADA data synergy for distribution feeder modeling'. *IEEE Transactions on Smart Grid*. 2015, vol. 6(4), pp. 1639–47.

[3] Feng X., Yang F., Peterson W. 'A practical multi-phase distribution state estimation solution incorporating smart meter and sensor data'. *IEEE Power and Energy Society General Meeting*. 2012, pp. 1–6.

[4] Muttaqi T., Baldwin T.L., Chiu S.C. 'Distribution system state estimation with AMI based on load correction method'. *North American Power Symposium (NAPS)*. 2019, pp. 1–6.

[5] Jia Z., Chen J., Liao Y. 'State estimation in distribution system considering effects of AMI data'. *Proceedings of IEEE Southeastcon*. 2013, pp. 1–6.

[6] Samarakoon K., Wu J., Ekanayake J.. *IEEE power and energy Society general meeting*; 2011. pp. 1–6.

[7] Chen T.-H., Chen M.-S., Hwang K.-J., Kotas P., Chebli E.A. 'Distribution system power flow analysis: a rigid approach'. *IEEE Transactions on Power Delivery*. 1991, vol. 6(3), pp. 1146–52.

[8] Teng J.-H. 'Modelling distributed generations in three-phase distribution load flow'. *IET Generation, Transmission & Distribution*. 2008, vol. 2(10), p. 330.

[9] Ranković A., Sarić A.T. 'Modeling of photovoltaic and wind turbine based distributed generation in state estimation'. *15th International Power*

Electronics and Motion Control Conference (EPE/PEMC); 2012. pp. LS2b.2–1–LS2b.2–6.

[10] Shabaninia F., Vaziri M., Vadhva S., Vaziri J. 'A novel state estimation formulation for distribution grids with renewable energy sources'. *2012 IEEE Power and Energy Society General Meeting*; 2012. pp. 1–5.

[11] Primadianto A., Lu C.-N. 'A review on distribution system state estimation'. *IEEE Transactions on Power Systems*. 2017, vol. 32(5), pp. 3875–83.

[12] Singh R., Pal B.C., Jabr R.A. 'Distribution system state estimation through Gaussian mixture model of the load as pseudo-measurement'. *IET Generation, Transmission & Distribution*. 2010, vol. 4(9), pp. 50–9.

[13] Lin W.M., Teng J.H. 'State estimation for distribution systems with zero-injection constraints'. *IEEE Transactions on Power Systems*. 1996, vol. 11(1), pp. 518–24.

[14] Muscas C., Pau M., Pegoraro P.A., Sulis S. 'An efficient method to include equality constraints in branch current distribution system state estimation'. *EURASIP Journal on Advances in Signal Processing*. 2015, vol. 2015(1), pp. 1–11.

[15] Massignan J.A.D., London Jr J., Miranda V. 'Tracking power system state evolution with maximum-correntropy-based extended Kalman filter'. *Journal of Modern Power Systems and Clean Energy*. 2020, vol. 8(4), pp. 616–26.

[16] Zhao J., Qi J., Huang Z., *et al.* 'Power system dynamic state estimation: Motivations, definitions, methodologies, and future work'. *IEEE Transactions on Power Systems*. 2019, vol. 34(4), pp. 3188–98.

[17] Zhao J., Netto M., Huang Z., *et al.* 'Roles of dynamic state estimation in power system modeling, monitoring and operation'. *IEEE Transactions on Power Systems*. 2020, pp. 1–1.

[18] Kalman R.E. 'A new approach to linear filtering and prediction problems'. *Journal of Basic Engineering*. 1960, vol. 82(Series D), pp. 35–45.

[19] Sarri S., Zanni L., Popovic M., Le Boudec J.-Y., Paolone M. 'Performance assessment of linear state estimators using Synchrophasor measurements'. *IEEE Transactions on Instrumentation and Measurement*. 2016, vol. 65(3), pp. 535–48.

[20] Fan L., Wehbe Y. 'Extended Kalman filtering based real-time dynamic state and parameter estimation using PMU data'. *Electric Power Systems Research*. 2013, vol. 103(1), pp. 168–77.

[21] Valverde G., Terzija V. 'Unscented Kalman filter for power system dynamic state estimation'. *IET Generation, Transmission & Distribution*. 2011, vol. 5(8), pp. 29–37.

[22] Sharma A., Srivastava S.C., Chakrabarti S. 'A Cubature Kalman filter based power system dynamic state estimator'. *IEEE Transactions on Instrumentation and Measurement*. 2017, vol. 66(8), pp. 2036–45.

[23] Zhou N., Meng D., Huang Z., Welch G. 'Dynamic state estimation of a synchronous machine using PMU data: a comparative study'. *IEEE Transactions on Smart Grid*. 2015, vol. 6(1), pp. 450–60.

[24] Zhao J. 'Dynamic state estimation with model uncertainties using H_∞ extended Kalman filter'. *IEEE Transactions on Power Systems*. 2018, vol. 33(1), pp. 1099–100.
[25] Xu Y., Mili L., Zhao J. 'A novel polynomial-chaos-based Kalman filter'. *IEEE Signal Processing Letters*. 2019, vol. 26(1), pp. 9–13.
[26] Bretas A.S., Bretas N.G., Massignan J.A.D., London Junior J.B.A. 'Hybrid physics-based adaptive Kalman filter state estimation framework'. *Energies*. 2021, vol. 14(20), p. 6787.
[27] Brown Do Coutto Filho M., de Souza J.C.S. 'Forecasting-aided state estimation—Part I: Panorama'. *IEEE Transactions on Power Systems*. 2009, vol. 24(4), pp. 1667–77.
[28] Brown Do Coutto Filho M., de Souza J.C.S., Freund R.S. 'Forecasting-aided state estimation—Part II: Implementation'. *IEEE Transactions on Power Systems*. 2009, vol. 24(4), pp. 1678–85.
[29] Leite da Silva A.M., Do Coutto Filho M.B., de Queiroz J.F. 'State forecasting in electric power systems'. *IEE Proceedings C Generation, Transmission and Distribution*. 1983, vol. 130(7), pp. 237–44.
[30] Durgaprasad G., Thakur S.S. 'Robust dynamic state estimation of power systems based on M-estimation and realistic modeling of system dynamics'. *IEEE Transactions on Power Systems*. 1998, vol. 13(4), pp. 1331–6.
[31] Lewis F.L., Xie L., Popa D. *Optimal and Robust Estimation: With an Introduction to Stochastic Control Theory*. Boca Raton, FL: CRC Press; 2017.
[32] Dobbe R., Arnold D., Liu S., Callaway D., Tomlin C. 'Real-time distribution grid state estimation with limited sensors and load forecasting'. *ACM/IEEE 7th International Conference on Cyber-Physical Systems (ICCPS)*; Viena, Austria; 2016. pp. 1–10 pp..
[33] Comden J., Colombino M., Bernstein A., Liu Z. 'Sample complexity of power system state estimation using matrix completion'. *IEEE International Conference on Communications, Control, and Computing Technologies for Smart Grids*; Beijing, China; 2019. pp. 1–7 pp..
[34] Liu B., Wu H., Zhang Y., Yang R., Bernstein A. 'Robust matrix completion state estimation in distribution systems'. *IEEE Power Energy Society General Meeting (PESGM)*; Atlanta, USA; 2019. pp. 1–5 pp..
[35] Zhang Y., Bernstein A., Schmitt A., Yang R. 'State estimation in low-observable distribution systems using matrix completion'. *Proceedings of the 52nd Hawaii International Conference on System Sciences*; Maui; 2019. pp. 3552–8.
[36] Donti P.L., Liu Y., Schmitt A.J., Bernstein A., Yang R., Zhang Y. 'Matrix completion for low-observability voltage estimation'. *IEEE Transactions on Smart Grid*. 2020, vol. 11(3), pp. 2520–30.
[37] Candès E.J., Recht B. 'Exact matrix completion via convex optimization'. *Foundations of Computational Mathematics*. 2009, vol. 9(6), pp. 717–72.
[38] Hu J.C., Chen Z.C., Manaz M.A.M., Lu C.N. 'Applicability of matrix completion method for distribution system state estimation'. *Proceedings of 26th SPEEDAM Meeting*; Sorrento, Italy; 2022.

[39] Wang S.J. Measurement fusion by matrix completion for granular recurrent distribution system state estimation[Mater's]Taiwan, National Sun Yat-sen University; 2021.
[40] Massignan J.A.D., London J.B.A., Bessani M., Maciel C.D., Fannucchi R.Z., Miranda V. 'Bayesian inference approach for information fusion in distribution system state estimation'. *IEEE Transactions on Smart Grid*. 2022, vol. 13(1), pp. 526–40.
[41] Congdon P. *Bayesian statistical modelling*. vol. 704. New York: John Wiley & Sons; 2007.
[42] Machado P.A., Azevedo G.P.D., Monticelli A.J. 'A mixed pivoting approach to the factorization of indefinite matrices in power system state estimation'. *IEEE Transactions on Power Systems*. 1991, vol. 6(2), pp. 676–82.
[43] van Amerongen R.A.M. 'On the exact incorporation of virtual measurements on orthogonal-transformation based state-estimation procedures'. *International Journal of Electrical Power & Energy Systems*. 1991, vol. 13(3), pp. 167–74.
[44] Freitas V., Costa A.S., Miranda V. 'Orthogonal method for solving maximum correntropy-based power system state estimation'. *IET Generation, Transmission & Distribution*. 2020, vol. 14(10), pp. 1930–41.
[45] Hebling G.M., Massignan J.A.D., London Junior J.B.A., Camillo M.H.M. 'Sparse and numerically stable implementation of a distribution system state estimation based on multifrontal QR factorization'. *Electric Power Systems Research*. 2020, vol. 189(5) 106734.
[46] Castillo M.R.M., London J.B.A., Bretas N.G., Lefebvre S., Prevost J., Lambert B. 'Offline detection, identification, and correction of branch parameter errors based on several measurement snapshots'. *IEEE Transactions on Power Systems*. 2011, vol. 26(2), pp. 870–7.
[47] Zhao J., Zhang G., Das K., *et al.* 'Power system real-time monitoring by using PMU-based robust state estimation method'. *IEEE Transactions on Smart Grid*. 2016, vol. 7(1), pp. 300–9.
[48] YL L., Huang S.C., CN L. 'Transformational benefits of AMI data in transformer load modeling and management'. *IEEE Transactions on Power Delivery*. 2014, vol. 29(2), pp. 742–50.
[49] YL L., Huang S.C., CN L. 'Non-technical loss detection using smart distribution network measurement data'. *IEEE PES Innovative Smart Grid Technologies*. 2012, pp. 1–5.
[50] Woolley N.C., Milanović J.V. 'Estimating the voltage unbalance factor using distribution system state estimation'. *IEEE PES Innovative Smart Grid Technologies Conference Europe (ISGT Europe)*; Gothenburg, Sweden; 2010. pp. 1–7 pp..
[51] Korres G.N., Manousakis N.M. 'A state estimation algorithm for monitoring topology changes in distribution systems'. *IEEE Power and Energy Society General Meeting*; San Diego, USA; 2012. pp. 1–8 pp..
[52] Baran M.E., Jung J., McDermott T.E. 'Topology error identification using branch current state estimation for distribution systems'. *Transmission*

Distribution Conference Exposition: Asia and Pacific; Seoul, Korea; 2009. pp. 1–4 pp..

[53] Peppanen J., Reno M.J., Broderick R.J., Grijalva S. 'Distribution system model calibration with big data from AMI and PV inverters'. *IEEE Transactions on Smart Grid*. 2016, vol. 7(5), pp. 2497–506.

[54] Magnago F., Zhang L., Nagarkar R. 'Three phase distribution state estimation utilizing common information model'. *IEEE Eindhoven PowerTech*; Eindhoven, Netherlands; 2015. pp. 1–6 pp..

[55] Castanedo F. 'A review of data fusion techniques'. *The Scientific World Journal*. 2013, vol. 2013, pp. 1–19.

[56] Olfati-Saber R., Fax J.A., Murray R.M. 'Consensus and cooperation in Networked multi-agent systems'. *Proceedings of the IEEE*. 2007, vol. 95(1), pp. 215–33.

[57] Kar S., Moura J.M.F. 'Consensus + innovations distributed inference over networks: Cooperation and sensing in networked systems'. *IEEE Signal Processing Magazine*. 2013, vol. 30(3), pp. 99–109.

[58] Xie L., Choi D.-H., Kar S., Poor H.V. 'Fully distributed state estimation for Wide-Area monitoring systems'. *IEEE transactions on smart grid*. 2012, vol. 3, pp. 1154–69.

[59] Pegoraro P.A., Meloni A., Atzori L., Castello P., Sulis S. 'Adaptive PMU-based distribution system state estimation exploiting the cloud-based IoT paradigm'. *IEEE International Instrumentation and Measurement Technology Conference Proceedings*; Taipei, Taiwan; 2016. pp. 1–6 pp..

[60] Liao H., Milanovic J.V. 'Pathway to cost-efficient state estimation of future distribution networks'. *IEEE Power and Energy Society General Meeting (PESGM)*; 2016. pp. 1–5.

This page intentionally left blank

Chapter 12

State estimation for low voltage distribution grids

Andreas Kotsonias[1], Markos Asprou[1], Lenos Hadjidemetriou[1], and Christos Panayiotou[1]

This chapter discusses the subject of distribution system state estimation (DSSE) in low voltage distribution grids (LVDG). In theory, DSSE schemes developed for medium voltage distribution grids (MVDG) are also applicable to LVDGs because of their similar characteristics. However, several limiting factors exist in LVDGs that can severely impact the DSSE performance. First, the measurement infrastructure in LVDGs is lacking with a limited sensor deployment and an absence of communication between the end consumers and the operator. In addition, scarce measurement devices and a slow reporting rate from smart meters with asynchronous measurements render most LVDGs unobservable. Second, there is a lack of reliable and accurate system-related information. This includes information about the topology, parameters and equipment used in any given LVDG which results to a system model with considerable uncertainty. Third, most DSSE methodologies developed for MVDGs are for three-wire networks or four-wire networks with the neutral wire multigrounded. This allows simplifying the problem formulation as the neutral voltage can be approximated to 0 V. In LVDGs, this assumption typically does not hold, and the non-zero neutral voltage has a detrimental impact on the operation of the classical DSSE. These limiting factors along with their impact and mitigation strategies in order to develop adequate DSSE solutions for LVDG are discussed in this chapter.

12.1 The need for DSSE in LVDGs

Traditional distribution grids were designed for unidirectional power that flows from large power generation plants toward the residential, commercial and industrial consumers. Until recently, the operation of the distribution grids was passive with minimal control of power flow. In recent years, the urgent need for a fossil fuel neutral energy

[1]KIOS Research and Innovation Center of Excellence and the Department of Electrical and Computer Engineering, University of Cyprus, Nicosia, Cyprus

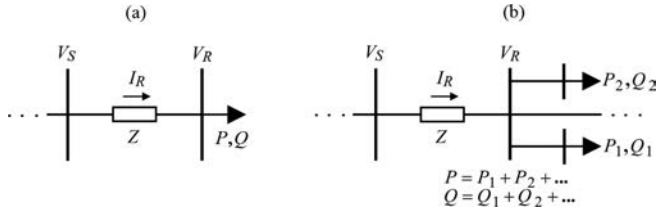

Figure 12.1 Calculation of voltage deviation ΔV *when* V_R *is the voltage (a) at the premises of a consumer or (b) at a system node*

sector has resulted in a significant increase of distributed energy resources (DER) in LVDGs. Photovoltaic (PV) and energy storage systems, the charging of electric vehicles (EVs), and the introduction of demand response schemes are changing the landscape in distribution grids. More specifically, the LVDG is transitioning from a passive grid with simplistic behavior into an active and complex system where a re-evaluation of its classical operation is necessary.

Besides the obvious environmental and economic benefits, the energy transition imposes several challenges to the distribution system operators (DSOs). Studies [1, 2] have shown that a large penetration of PVs and EVs in the LVDG can have detrimental effects on its operation. The most critical effects for the LVDG operation are (1) the effect of DERs and EV charging on the voltage profile, (2) the possible overloading and thermal limit violation of the distribution lines/transformer and (3) the increase of phase unbalance. To better understand how the voltage profile of the LVDG is affected by the increase of PVs and EVs, the voltage deviation ΔV across a distribution line due to the energy consumption/generation of the consumers' needs to be considered,

$$\Delta \dot{V} = \dot{V}_S - \dot{V}_R = Z \cdot \dot{I}_R = \frac{RP+XQ}{V_R} + j\frac{XP-RQ}{V_R} = \Delta V_{re} + j\Delta V_{im} \tag{12.1}$$

where R and X are the resistance and reactance of the distribution line, V_R is the receiving end voltage magnitude that can be either at the premises of a consumer (Figure 12.1.a) or at any system node (Figure 12.1.b), V_S is the voltage magnitude at the sending-end of the distribution line and P/Q is the active/reactive power flow along the considered line. With $\dot{V}_R$ as the reference, the magnitude of the sending end voltage V_R is,

$$V_S = \sqrt{(V_R + \Delta V_{re})^2 + \Delta V_{im}^2} \tag{12.2}$$

Noticing that $\Delta V_{im} \ll (V_R + \Delta V_{re})$ and that ΔV_{re} can be approximated by substituting V_R with V_S, the magnitude of the receiving end V_R can be approximated by [3],

$$V_R \approx V_S - \frac{RP + XQ}{V_S} \tag{12.3}$$

Note that (12.3) assumes a load convention for the receiving end of the distribution line with $P = P_{LOAD} + P_{PV}$ where $P_{LOAD} \in \mathbb{R}^+$ is the consumption of the conventional load and $P_{PV} \in \mathbb{R}^-$ is the local PV power generation. Typically, distribution

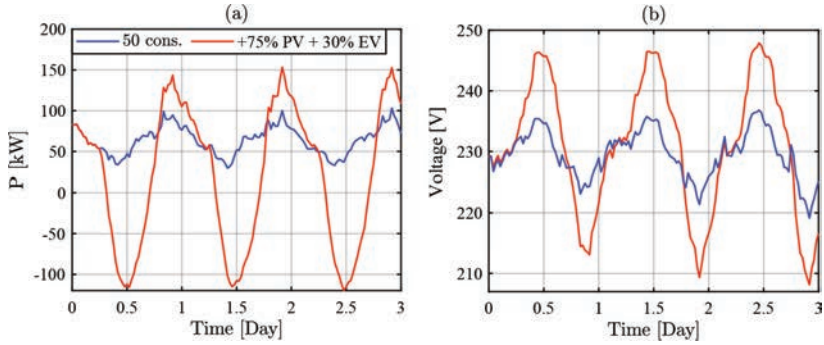

Figure 12.2 Impact of PV and EVs on the (a) load profile and (b) positive sequence voltage profile of a sub-urban residential feeder

lines have a high R/X ratio, compared with transmission lines, and as a result, in addition to the reactive power flow, the active power flow has a significant impact on the voltage profile as well. Therefore, the generation and consumption of active power from PVs and EVs, respectively, have a major influence on the voltage profile of an LVDG.

Figure 12.2 illustrates the impact of a high penetration of PVs and EVs on both the load and voltage profile of a typical residential feeder with 50 consumers. The 75% PV penetration denoted in this figure is in relation to the total energy consumed by the 50 consumers, and the 30% EV penetration corresponds to 15 EV owners. During reverse power flow conditions, where P is negative (local conventional load is lower than the local generated energy by PVs), the voltage across the LVDG increases, as indicated in (12.3) due to reverse power flow. Under intense reverse power flow conditions, the resulting voltage rise can lead to a violation of the admissible limit. On the other hand, the increase in energy demand by EV charging has a similar but conversely effect on the voltage profile. As EVs at LVDGs will be mostly privately owned, users will plug-in their vehicles for charging at their home during the after-work hours, which are the peak hours for the conventional load. Consequently, uncoordinated charging of EVs can increase significantly the forward peak demand, which can lead to severe undervoltage conditions and to the overloading of the distribution transformer. To mitigate their detrimental impacts and to facilitate a high integration of DERs and EVs in LVDGs, an advanced distribution management system (DMS) is necessary [4]. Within the smart grid concept, an advanced DMS is expected to provide a number of services and grid support functionalities to facilitate the modernization of the distribution grid. Local voltage management and global frequency support schemes will be shortly available by utilizing controllable and flexible assets in the distribution grid such as the PV inverters, EV chargers and energy storage systems. In addition, demand-side and congestion management applications are expected to have a critical role in the DMS. Typically, most of the DMS applications and functionalities require at least some

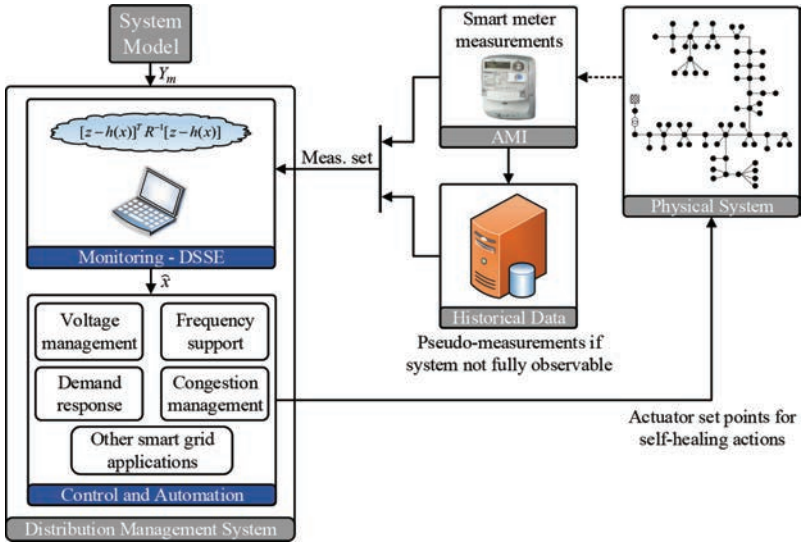

Figure 12.3 An active LVDG with automated management

level of information regarding the operational state of the system in order to take the appropriate control decisions.

In this sense, a successful deployment of DSSE in LVDGs can be a powerful tool in the DSO DMS. It allows for an optimized and cost-effective operation; it can aid in identifying weak grid points where reinforcement may be required to handle the rising energy demand; it can detect network reconfigurations and update the relevant system models; and most importantly, it provides the required data to the control schemes of the DMS for an effective operation. Until recently, the situational awareness in the LVDG has been very limited due to their traditionally passive behavior. As LVDGs become more active, a robust DSSE also becomes a necessity for maintaining the reliable operation of LVDGs. For this purpose, DSOs are investing significant resources in increasing the situational awareness and observability of LVDGs by developing advanced metering infrastructures (AMI). This entails a mass adoption of smart meters to end users where, besides their use for automatic billing of consumers, can be utilized for DSSE purposes. The key role of an AMI system is illustrated in Figure 12.3 where the general structure of the envisioned LVDG is shown. The AMI enables the operation of a DSSE, which in turn provides the necessary information regarding the operational state of the system and drives the online management of the LVDG through advanced DMS functionalities. In this chapter, the DSSE will be further analyzed, providing some insights about their particularities in LVDGs.

12.2 Classical DSSE approach

State estimation (SE) techniques in transmission systems have been widely used over the past decades for monitoring the power system and for increasing the situational awareness of the operators. Technological advancements such as dedicated metering devices with high sampling rates, time-stamped–synchronized measurements (phasor measurement units) and a communication infrastructure with high network bandwidth have enabled the near real-time monitoring of transmission systems. However, because of different characteristics, SE schemes and monitoring concepts developed for transmission systems are, in general, not applicable to the distribution grids. For instance, distribution lines have short lengths and a high R/X ratio which is indicatively 4 to 6 times higher in comparison to the transmission lines. Therefore, any fast decoupled or linear (DC) power flow/SE technique will have a lower performance when applied to LVDGs if the high R/X ratio is not properly accounted for. Note that the DC power flow refers to the simplification of the power flow problem by neglecting the $Q - V$ equations and assuming the voltage magnitudes at 1 pu. Moreover, it can be assumed that transmission systems operate under near phase-balanced conditions. Consequently, most SE methodologies consider only the positive sequence of the voltage and solve the SE problem through a single-phase equivalent. In contrast, distribution grids operate under intense unbalanced conditions where three-phase–coupled SE schemes should be considered.

There are several DSSE schemes that were developed for the MVDG in the literature and can be applied to LVDGs as well. This is because usually MVDGs and LVDGs have similar characteristics such as an unbalance operation, high R/X ratios and limited observability. In order to have a self-explanatory chapter, the well-established weighted least squares (WLS) DSSE scheme and the assumptions made for four-wire LVDGs are presented next.

12.2.1 WLS DSSE

The WLS DSSE [5] is the most widely used SE application in power systems. The measurement vector $\boldsymbol{z} \in \mathbb{R}^m$ is related with the state variables through the nonlinear measurement functions included in vector $\boldsymbol{h} \in \mathbb{R}^m$ as,

$$\boldsymbol{z} = \boldsymbol{h}(\boldsymbol{x}) + \boldsymbol{e} \tag{12.4}$$

where $\boldsymbol{x} \in \mathbb{R}^n$ is the state vector and contains the states of the system, and vector $\boldsymbol{e} \in \mathbb{R}^m$ includes the noise for each measurement. Note that depending on the choice of state variables (typically either the nodal voltages or brunch currents), $\boldsymbol{x}$ can be a complex number instead of real. The WLS SE problem is formulated as an optimization problem where the optimal values of the state vector minimize the summation of the weighted measurement residuals,

$$\hat{\boldsymbol{x}} = \arg\min_{\boldsymbol{x}} \left(\sum_{i=1}^{m} \frac{[z_i - h_i(x)]^2}{w_i} \right) = \arg\min_{\boldsymbol{x}} \boldsymbol{J}(\boldsymbol{x}) \tag{12.5}$$

where $\hat{\boldsymbol{x}}$ is the estimated state vector, w_i is the weight given to the ith measurement and $\boldsymbol{J}(\boldsymbol{x})$ is the objective function of the minimization problem. The weight of each

measurement represents the confidence for its accuracy. Typically, these weights are related to the variance σ_i^2 of the measurement noise associated with the measurement device. The objective function $J(\boldsymbol{x})$ can be written in a matrix format as,

$$J(\boldsymbol{x}) = \left[\boldsymbol{z} - \boldsymbol{h}(\boldsymbol{x})\right]^T \boldsymbol{W} \left[\boldsymbol{z} - \boldsymbol{h}(\boldsymbol{x})\right] \tag{12.6}$$

with the measurement weighting matrix $\boldsymbol{W}$ being equal to the inverse of the measurement error covariance matrix $\boldsymbol{R} \in \mathbb{R}^{m \times m}$, which is formulated as,

$$\boldsymbol{R} = \begin{bmatrix} \sigma_1^2 & \sigma_{1,2} & \cdots & \sigma_{1,m} \\ \sigma_{2,1} & \sigma_2^2 & \cdots & \sigma_{2,m} \\ \vdots & \vdots & \ddots & \vdots \\ \sigma_{m,1} & \sigma_{m,2} & \cdots & \sigma_m^2 \end{bmatrix} \tag{12.7}$$

where $\sigma_{i,j}$ is the covariance of the error between the ith and jth measurements. In conventional approaches it is typically assumed that the noise of each measurement is statistically independent, and therefore $\boldsymbol{R}$ becomes a diagonal matrix. At the minimum value of the objective function $J(\boldsymbol{x})$, the optimality condition is satisfied and therefore $\nabla J(\boldsymbol{x}) = \boldsymbol{0}$,

$$\nabla J(\boldsymbol{x}) = -\boldsymbol{H}^T(\boldsymbol{x}) \boldsymbol{W} [\boldsymbol{z} - \boldsymbol{h}(\boldsymbol{x})] = \boldsymbol{0} \tag{12.8}$$

where $\boldsymbol{H}(\boldsymbol{x}) = [\partial \boldsymbol{h}(\boldsymbol{x}) / \partial \boldsymbol{x}]$ is the Jacobian matrix of $J(\boldsymbol{x})$. Using the Gauss–Newton method, one can obtain the estimated states $\hat{\boldsymbol{x}}$, that is the solution of (12.8) through an iterative procedure as,

$$\begin{aligned} \boldsymbol{x}_{k+1} &= \boldsymbol{x}_k + \Delta \boldsymbol{x}_k \\ \Delta \boldsymbol{x}_k &= \boldsymbol{G}(\boldsymbol{x}_k)^{-1} \boldsymbol{H}(\boldsymbol{x}_k)^T \boldsymbol{W} [\boldsymbol{z} - \boldsymbol{h}(\boldsymbol{x}_k)] \\ \boldsymbol{G}(\boldsymbol{x}_k) &= \boldsymbol{H}(\boldsymbol{x}_k)^T \boldsymbol{W} \boldsymbol{H}(\boldsymbol{x}_k) \end{aligned} \tag{12.9}$$

where $\boldsymbol{G}$ is the gain matrix, and k is the iteration number. Note that before the first iteration the state vector is initialized by considering the voltage phasors at 1 pu and at an angle of $0°, 120°, -120°$ for phase a, b, c, respectively. The iterative process described above is repeated until the update vector $\Delta \boldsymbol{x}_k$ satisfies a convergence criterion, such as its max-norm being less than a predetermined threshold ϵ.

12.2.1.1 Inclusion of virtual measurements

The term *virtual measurements* refers to the information known about the operation of the system with zero uncertainty. This can be the net zero power injection at nodes without any consumers and distributed generation connected, zero power flows in open switching devices, zero voltage drops in closed switching devices, etc. As this information is known without any uncertainty, the associated measurements are assigned high weights in relation to the conventional measurements. To avoid an ill-conditioned system due to the high weights of the virtual measurements, these types of measurements are included in the WLS SE problem as equality constraints [6],

$$\begin{aligned}\hat{\boldsymbol{x}} &= \arg\min_{\boldsymbol{x}} \left[\boldsymbol{z}-\boldsymbol{h}(\boldsymbol{x})\right]^T \boldsymbol{W}\left[\boldsymbol{z}-\boldsymbol{h}(\boldsymbol{x})\right] \\ &\quad s.t \quad \boldsymbol{c}(\boldsymbol{x}) = \boldsymbol{0}\end{aligned} \tag{12.10}$$

$$\begin{aligned}\left\{\hat{\boldsymbol{x}},\ \hat{\boldsymbol{\lambda}}\right\} &= \arg\min_{\boldsymbol{x},\boldsymbol{\lambda}} \left[\boldsymbol{z}-\boldsymbol{h}(\boldsymbol{x})\right]^T \boldsymbol{W}\left[\boldsymbol{z}-\boldsymbol{h}(\boldsymbol{x})\right] + \boldsymbol{\lambda}^T\boldsymbol{c}(\boldsymbol{x}) \\ &= \arg\min_{\boldsymbol{x},\boldsymbol{\lambda}} L(\boldsymbol{x},\boldsymbol{\lambda})\end{aligned} \tag{12.11}$$

where $\boldsymbol{\lambda}$ is the Lagrange multipliers vector. By applying the optimality conditions $\nabla L(\boldsymbol{x},\boldsymbol{\lambda}) = \boldsymbol{0}$,

$$\begin{aligned}\frac{\partial L(\boldsymbol{x},\boldsymbol{\lambda})}{\partial \boldsymbol{x}} &= -\boldsymbol{H}^T(\boldsymbol{x})\boldsymbol{W}[\boldsymbol{z}-\boldsymbol{h}(\boldsymbol{x})] + C(\boldsymbol{x})^T\boldsymbol{\lambda} = \boldsymbol{0} \\ \frac{\partial L(\boldsymbol{x},\boldsymbol{\lambda})}{\partial \boldsymbol{\lambda}} &= c(\boldsymbol{x}) = \boldsymbol{0}\end{aligned} \tag{12.12}$$

where $\boldsymbol{C}(\boldsymbol{x}) = [\partial \boldsymbol{c}(\boldsymbol{x})/\partial \boldsymbol{x}]$. By applying Gauss–Newton method to solve the resulting nonlinear system of equations, the state update step from (12.9) is changed to,

$$\begin{bmatrix}\Delta \boldsymbol{x}_k \\ \boldsymbol{\lambda}_k\end{bmatrix} = \begin{bmatrix}\boldsymbol{H}^T\boldsymbol{W}\boldsymbol{H} & \boldsymbol{C}(\boldsymbol{x}_k)^T \\ \boldsymbol{C}(\boldsymbol{x}_k) & \boldsymbol{0}\end{bmatrix}^{-1} \begin{bmatrix}\boldsymbol{H}^T\boldsymbol{W}[\boldsymbol{z}-\boldsymbol{h}(\boldsymbol{x}_k)] \\ -\boldsymbol{c}(\boldsymbol{x}_k)\end{bmatrix} \tag{12.13}$$

12.2.2 State variables and measurement functions

The available measurements in an LVDG that can be utilized for DSSE applications are typically the active/reactive power injection and voltage magnitude measurements at the premises of the consumers. Therefore, the measurement vector is formulated as $\boldsymbol{z} \in \mathbb{R}^m = \begin{bmatrix}\boldsymbol{P} & \boldsymbol{Q} & \boldsymbol{V}\end{bmatrix}^T$ with $m = 3N_{1\Phi} + 9N_{3\Phi}$, where $N_{1\Phi}$ and $N_{3\Phi}$ are the number of single-phase and three-phase loads in an LVDG, respectively. Depending on the selection of state variables the measurement function vector $\boldsymbol{h}(\boldsymbol{x})$, which relates the state variables to the available measurements, is formulated differently.

One of the most popular choices for state variables is the nodal voltages in either a polar ($\dot{V} = V\sphericalangle\theta$) or in a rectangular ($\dot{V} = V_{re} + jV_{im}$) form. Because of the unbalanced nature of the distribution grid, a coupled three-phase formulation is typically used. This increases the overall complexity as every system node has two state variables per available phase, and the power injection measurements contain cross product terms between phases. In addition, the admittance matrix $\boldsymbol{Y}$ of the system which describes the connectivity of the system nodes, is formulated as,

$$\boldsymbol{Y} = \begin{bmatrix}\boldsymbol{Y}_{11} & \cdots & \boldsymbol{Y}_{1N} \\ \vdots & \cdots & \vdots \\ \boldsymbol{Y}_{N1} & \cdots & \boldsymbol{Y}_{NN}\end{bmatrix} \rightarrow \boldsymbol{Y}_{ij} = \begin{bmatrix}Y_{ij}^{aa} & Y_{ij}^{ab} & Y_{ij}^{ac} \\ Y_{ij}^{ba} & Y_{ij}^{bb} & Y_{ij}^{bc} \\ Y_{ij}^{ca} & Y_{ij}^{cb} & Y_{ij}^{cc}\end{bmatrix} \tag{12.14}$$

with N being the total number of system nodes, $\boldsymbol{Y} \in \mathbb{C}^{3N\times 3N}$, $Y_{ij}^{pm} = G_{ij}^{pm} + jB_{ij}^{pm}$ where $p,m \in \{a,b,c\}$ and B_{ij}^{pm} are the conductance and susceptance, respectively, between phase p at node i and phase m at node j. Note that $\boldsymbol{Y}$ is a symmetrical

matrix where $\boldsymbol{Y}_{ij} = \boldsymbol{Y}_{ji}$ and $Y_{ij}^{pm} = Y_{ij}^{mp}$. The complex power S_i^p generated or consumed in the ith system node and in phase p is derived by,

$$S_i^p = P_i^p + jQ_i^p = \dot{V}_i^p \left(\dot{I}_i^p\right)^* = \dot{V}_i^p \left(\sum_{k=1}^{N}\sum_{m=a}^{c} Y_{ik}^{pm} \dot{V}_k^m\right)^* \tag{12.15}$$

where P_i^p, Q_i^p are the active and reactive power injections, respectively, generated/consumed in phase p at node i and $\dot{I}_i^p$ is the relevant current phasor. Note that $\dot{I}_i^p$ in (12.15) is derived by the nodal equations for the specific node and phase. Considering the voltage in polar format, the complex power injection is given by,

$$\begin{aligned} S_i^p &= V_i^p \sum_{k=1}^{N}\sum_{m=a}^{c} \left(G_{ik}^{pm} - jB_{ik}^{pm}\right) V_k^m \sphericalangle \left(\theta_i^p - \theta_k^m\right) \\ &= V_i^p \sum_{k=1}^{N}\sum_{m=a}^{c} V_k^m \left(G_{ik}^{pm} - jB_{ik}^{pm}\right) \left[cos\left(\theta_{ik}^{pm}\right) + jsin\left(\theta_{ik}^{pm}\right)\right] \end{aligned} \tag{12.16}$$

where $\theta_{ik}^{pm} = \theta_i^p - \theta_k^m$. By taking the real and imaginary parts of (12.16) the measurement functions for active and reactive power injections with the nodal voltages in polar form as state variables are,

$$\begin{aligned} P_i^p &= Re\{S_i^p\} = V_i^p \sum_{k=1}^{N}\sum_{m=a}^{c} V_k^m \left[G_{ik}^{pm} cos\left(\theta_{ik}^{pm}\right) + B_{ik}^{pm} sin\left(\theta_{ik}^{pm}\right)\right] \\ Q_i^p &= Im\{S_i^p\} = V_i^p \sum_{k=1}^{N}\sum_{m=a}^{c} V_k^m \left[G_{ik}^{pm} sin\left(\theta_{ik}^{pm}\right) - B_{ik}^{pm} cos\left(\theta_{ik}^{pm}\right)\right] \end{aligned} \tag{12.17}$$

When the nodal voltages in rectangular form are selected as state variables then, by following a similar procedure, the measurement functions for active and reactive power injections are changed to,

$$\begin{aligned} P_i^p &= \sum_{k=1}^{N}\sum_{m=a}^{c} V_{re,i}^p \left(V_{re,k}^m G_{ik}^{pm} - V_{im,k}^m B_{ik}\right) + V_{im,i}^p \left(V_{im,k}^m G_{ik}^{pm} + V_{re,k}^m B_{ik}\right) \\ Q_i^p &= \sum_{k=1}^{N}\sum_{m=a}^{c} V_{im,i}^p \left(V_{re,k}^m G_{ik}^{pm} - V_{im,k}^m B_{ik}\right) - V_{re,i}^p \left(V_{im,k}^m G_{ik}^{pm} + V_{re,k}^m B_{ik}\right) \end{aligned} \tag{12.18}$$

In (12.19), the structure of the Jacobian matrix is given when the polar form is adopted for the state variables (the nodal voltage phasor). $\boldsymbol{I} \in \mathbb{R}^{M_V \times SV_V}$ and $\boldsymbol{0} \in \mathbb{R}^{M_V \times SV_\theta}$ are the identity and zero matrix, respectively, with M_V being the number of voltage measurements, SV_V the number of state variables related with a voltage magnitude and SV_θ the number of state variables related with a phase angle. Note that the Jacobian matrix under these state variables is state dependent and therefore it is recalculated at every iteration, which increases the overall computational burden. When a small angle difference assumption is made, a linear formulation is possible which yields a direct solution but at a reduced accuracy [7]. For state variables in rectangular format, the Jacobian matrix can become state independent when the power measurements are transformed to equivalent current measurements [8]. The drawback of this formulation is the increased complexity and its limited applicability to only radial networks.

$$\boldsymbol{H}(\boldsymbol{x}) = \begin{bmatrix} \frac{\partial \boldsymbol{P}}{\partial \boldsymbol{V}} & \frac{\partial \boldsymbol{P}}{\partial \boldsymbol{\theta}} \\ \frac{\partial \boldsymbol{Q}}{\partial \boldsymbol{V}} & \frac{\partial \boldsymbol{Q}}{\partial \boldsymbol{\theta}} \\ \frac{\partial \boldsymbol{V}}{\partial \boldsymbol{V}} & \frac{\partial \boldsymbol{V}}{\partial \boldsymbol{\theta}} \end{bmatrix} = \begin{bmatrix} \frac{\partial \boldsymbol{P}}{\partial \boldsymbol{V}} & \frac{\partial \boldsymbol{P}}{\partial \boldsymbol{\theta}} \\ \frac{\partial \boldsymbol{Q}}{\partial \boldsymbol{V}} & \frac{\partial \boldsymbol{Q}}{\partial \boldsymbol{\theta}} \\ \boldsymbol{I} & \boldsymbol{0} \end{bmatrix} \tag{12.19}$$

Another popular choice for state variables is the branch currents [9] in either polar or rectangular form. For simplifying the Jacobian matrix, power measurements are converted to equivalent current measurements through backward and forward voltage substitutions. Comparisons in Ref. [10] have indicated that both selections (node voltages or branch currents) result to a similar estimation accuracy. However, rectangular branch currents when voltage measurements are excluded have better computational performance. When several voltage measurements are considered then rectangular node voltages can exhibit better computational performance. This is due to the additional complexity introduced in the case of the rectangular branch current state variables that consider voltage measurements in the estimation process. In addition, special considerations and efforts are needed in the branch current formulation for slightly meshed grids which result to a decreased estimation accuracy.

12.2.3 Kron's reduction: four wires to three wires

LVDGs are typically four-wire grids where the neutral conductor is required for power supply. Most electricity consumers at the LVDG have a single-phase connection where the neutral conductor is used as the return path of the load current back to the distribution transformer. Most DSSE applications in MVDGs consider the *abc* phases in a three-phase formulation. For such methods to be applicable in LVDGs that are four-wire systems, special considerations are needed. Considering the four-wire line illustrated in Figure 12.4.a, by applying Kirchhoff's voltage law the voltage at the sending end can be expressed as,

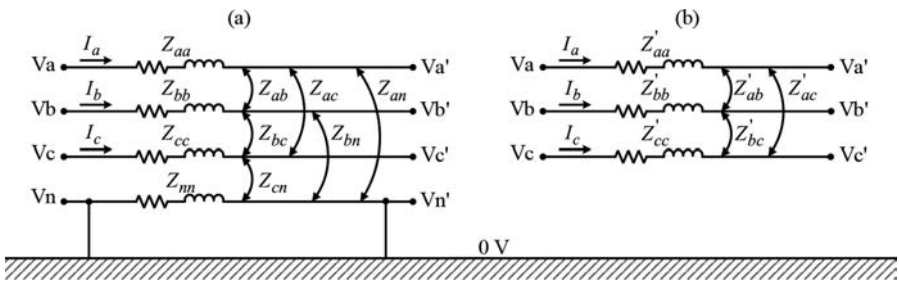

Figure 12.4 (a) Series and mutual impedance of a four-wire line and (b) its three-wire representation through Kron's reduction

$$\begin{bmatrix} \dot{V}_a \\ \dot{V}_b \\ \dot{V}_c \\ \dot{V}_n \end{bmatrix} = \begin{bmatrix} \dot{V}'_a \\ \dot{V}'_b \\ \dot{V}'_c \\ \dot{V}'_n \end{bmatrix} + \begin{bmatrix} Z_{aa} & Z_{ab} & Z_{ac} & Z_{an} \\ Z_{ba} & Z_{bb} & Z_{bc} & Z_{bn} \\ Z_{ca} & Z_{cb} & Z_{cc} & Z_{cn} \\ Z_{na} & Z_{nb} & Z_{nc} & Z_{nn} \end{bmatrix} \begin{bmatrix} \dot{I}_a \\ \dot{I}_b \\ \dot{I}_c \\ \dot{I}_n \end{bmatrix} \tag{12.20}$$

where the diagonal elements of matrix $\boldsymbol{Z}$ correspond to the series impedance of each conductor while the off-diagonal elements correspond to the mutual impedance between them. Equation (12.20) can be written in a partitioned form with the phase and neutral conductors separated as [11],

$$\begin{bmatrix} \boldsymbol{V}_{abc} \\ V_n \end{bmatrix} = \begin{bmatrix} \boldsymbol{V}'_{abc} \\ V'_n \end{bmatrix} + \begin{bmatrix} \boldsymbol{Z}_{abc} & \boldsymbol{Z}_{pn} \\ \boldsymbol{Z}_{np} & Z_{nn} \end{bmatrix} \begin{bmatrix} \boldsymbol{I}_{abc} \\ I_n \end{bmatrix} \tag{12.21}$$

where $\boldsymbol{V}_{abc}$, $\boldsymbol{V}'_{abc}$, $\boldsymbol{I}_{abc}$, $\boldsymbol{Z}_{pn} \in \mathbb{C}^{3\times1}$, $\boldsymbol{Z}_{np} \in \mathbb{C}^{1\times3}$ and $\boldsymbol{Z}_{abc} \in \mathbb{C}^{3\times3}$ include the respective terms from (12.20). By assuming that the neutral wire of the distribution line is multigrounded, or in general that its voltage drop can be approximated to zero, Kron's reduction method can be applied [12]. This allows the reduction of the impedance matrix of each line to a more conventional and compatible 3 × 3 form for three-wire lines, as indicated in Figure 12.4.b. Under these conditions, the neutral current is calculated as,

$$0 = 0 + \boldsymbol{Z}_{np} \cdot \boldsymbol{I}_{abc} + Z_{nn} \cdot I_n \rightarrow I_n = -\frac{\boldsymbol{Z}_{np} \cdot \boldsymbol{I}_{abc}}{Z_{nn}} \tag{12.22}$$

Note that this neutral current is induced by the current flow in the phase conductors due to the coupling between them and is not related with the loading asymmetry. By substituting (12.22) in (12.21) the phase voltages are,

$$\boldsymbol{V}_{abc} = \boldsymbol{V}'_{abc} + \boldsymbol{Z}_{abc} \cdot \boldsymbol{I}_{abc} - \boldsymbol{Z}_{pn} \cdot \frac{\boldsymbol{Z}_{np} \cdot \boldsymbol{I}_{abc}}{Z_{nn}} = \boldsymbol{V}'_{abc} + \boldsymbol{Z}'_{abc} \cdot \boldsymbol{I}_{abc} \tag{12.23}$$

$$\boldsymbol{Z}'_{abc} = \boldsymbol{Z}_{abc} - \frac{\boldsymbol{Z}_{pn} \cdot \boldsymbol{Z}_{np}}{Z_{nn}} \rightarrow Z'_{km} = Z_{km} - \frac{Z_{kn} \cdot Z_{nm}}{Z_{nn}}, \quad k, m = a, b, c \tag{12.24}$$

Equation (12.24) gives the transformation of each term of the original 4 × 4 impedance matrix to its equivalent term of the reduced 3 × 3 impedance matrix, as given in (12.25). In LVDGs, the distribution lines are mainly three-phase four-wire lines or single-phase two-wire lines. Applying (12.24) in a single-phase two-wire line results to a single element which is then written in the desired 3 × 3 format by adding zero rows and columns for the missing phases. An example of this is given in (12.26) for a single-phase two-wire line for phase *a* where the 3 × 3 impedance matrix is generated by adding zeros for the terms related with phases *b* and *c*.

$$\begin{bmatrix} Z_{aa} & Z_{ab} & Z_{ac} & Z_{an} \\ Z_{ba} & Z_{bb} & Z_{bc} & Z_{bn} \\ Z_{ca} & Z_{cb} & Z_{cc} & Z_{cn} \\ Z_{na} & Z_{nb} & Z_{nc} & Z_{nn} \end{bmatrix} \overset{(12.24)}{\rightarrow} \begin{bmatrix} Z'_{aa} & Z'_{ab} & Z'_{ac} \\ Z'_{ba} & Z'_{bb} & Z'_{bc} \\ Z'_{ca} & Z'_{cb} & Z'_{cc} \end{bmatrix} \tag{12.25}$$

$$\begin{bmatrix} Z_{aa} & Z_{an} \\ Z_{na} & Z_{nn} \end{bmatrix} \overset{(12.24)}{\rightarrow} Z'_{aa} \rightarrow \begin{bmatrix} Z'_{aa} & 0 & 0 \\ 0 & 0 & 0 \\ 0 & 0 & 0 \end{bmatrix} \tag{12.26}$$

Having the reduced impedance matrix where the neutral node has been eliminated, essentially any DSSE scheme developed for three-phase three-wire MVDGs can be, in theory, also applied to the LVDG and vice versa. Assuming that the neutral voltage can be approximated to zero, and that through Kron's reduction the resulting system model is accurate then the main limitations for applying DSSE schemes in LVDGs arise from the scarce measurement devices with a slow reporting rate, limited measurement redundancy and the asynchronous smart meter measurements.

12.3 Challenges for DSSE in LVDGs

Several limiting factors exist when applying DSSE schemes in LVDGs. The most important and critical for its reliable operation are (1) the limited sensor deployment which results to the LVDG being an unobservable system with low measurement redundancy, (2) the system model with considerable uncertainty due to the lack of reliable system-related information, (3) the asynchronous smart meter measurements with slow reporting rate and (4) the nonzero neutral voltage which renders Kron's reduction assumption invalid. These challenges, their impact on the DSSE and mitigation strategies for overcoming them are discussed and presented below.

12.3.1 Limited sensing

The SE formulations presented in Section 12.2 are under the assumption that the considered network is observable. That is, the available measurements $\boldsymbol{z}$ define an overdetermined problem that ensures a unique solution for $\boldsymbol{x}$. However, since LVDGs used to have unidirectional power flow and passive behavior, a very limited number of measuring equipment was foreseen besides for customer billing purposes. Consequently, the DSSE problem for LVDGs can be an underdetermined system of equations due to the low system observability.

Over the next few decades, significant resources will go toward the modernization, digitization and automation of the distribution grid in an effort to facilitate the energy transition [13]. A significant percentage of these resources will be spent by DSOs for the development of an AMI to increase the measurement redundancy of LVDGs. In fact, it is estimated that by 2030 the smart meter penetration for electricity in the European Union will reach 92% with an overall investment of 46 billion euro [14]. Besides smart meters, devices such as digital relays, intelligent electronic devices, smart inverters, digital substations and micro-PMUs can also be leveraged to increase the overall system observability. However, despite all these promising technologies, the current situation and infrastructure (and at least for the near future as well) in LVDGs are inadequate and most secondary networks are not fully observable. Even in the rare cases of fully observable LVDGs, the

measurement redundancy is very low. Meaning that even these systems can easily become unobservable when a measurement is lost. This can happen when a meter fails, transmits bad data or there are considerable communication bottlenecks and delays.

Common practice for overcoming this challenge in transmission systems has been the generation of pseudo-measurements for the unobservable nodes. Through the use of pseudo-measurements (load forecast for the unobservable loads) the measurement set is augmented, and the otherwise underdetermined system is solvable with a unique solution. Typically this is achieved with the process of available historical and statistical data along with their spatial/temporal correlation with the unobservable loads. With the introduction of DERs, EV charging, demand response schemes and an active participation of the consumers in the electricity market, their load behavior is increasingly becoming more variable and hence more difficult to be predicted. Consequently, the generation of adequate pseudo-measurements for enabling an LVDG DSSE with reliable results is a difficult task.

The aim of pseudo-measurement generation is to generate forecasts as accurate as possible for the power injections in unobservable loads and define their uncertainty so that they can be incorporated in the DSSE procedure. Until recently, the only available measurements related to the operation of the LVDG have been the bimonthly or quarterly manual readings of the energy consumption of each consumer. However, generating pseudo-measurements with a reasonable uncertainty based on this kind of data is nearly impossible. With the introduction and mass deployment of smart meters, utilities are now automatically and periodically able to collect measurements at much higher frequencies and even on-demand, depending on the limitations of the communication infrastructure. Based on these data, it is now possible to generate pseudo-measurements with satisfactory uncertainty for the unobservable loads within a network.

Several different approaches have been developed for this purpose. Noting the compatibility of the WLS formulation with normal distributions for the measurement error (maximum likelihood estimator), a Gaussian distribution is typically assumed for modeling these loads [15]. By processing the available historical data, standard load profiles (representative load profiles for each type of consumer) are generated where each time value corresponds to the mean value of the Gaussian distribution at the specific time interval. Leveraging spacial-temporal correlation between the available measurement data and the unobservable loads, the calculated mean and variance can be corrected leading to a higher load estimation accuracy. In practice, however, the load behavior rarely can be approximated through a Gaussian PDF, see Figure 12.5. For this reason, in Ref. [16], a Gaussian mixture model (GMM) is proposed to model the arbitrary load distributions. This is achieved through the convex combination of several normal distributions, each with its own mean μ_i, variance σ_i^2 and weight w_i,

$$GMM = w_1 N\left(\mu_1, \sigma_1^2\right) + w_2 N\left(\mu_2, \sigma_2^2\right) + \cdots \tag{12.27}$$

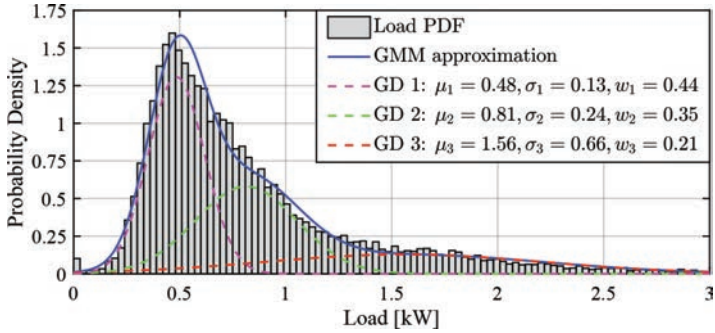

Figure 12.5 Probability distribution of a residential consumer taken from annual half hourly demand measurements and its approximation through a GMM with three Gaussian distribution (GD) components

Besides the probabilistic and statistical approaches for pseudo-measurement generation, recent works employ machine learning methodologies such as neural networks [17] and game theory [18] with promising results but with high computational cost.

12.3.2 Limited system knowledge

The reliability and accuracy of most DSSE schemes are closely related to the system model. The determination of the nodal equations in (12.15) is based on the system's admittance matrix which in turn depends on the topology of the network (connectivity between nodes) and on the line parameters. In the case of the transmission system, it is implicitly assumed that this information is readily available and in some extend this is true. However, in distribution grids and especially in LVDGs, both system topology and line parameters are rarely available. The immense size of these networks and the fact that most of the infrastructure was constructed several decades ago with countless expansions and reconfigurations over the years make the availability of accurate information about the current topology and the equipment used in any distribution grid extremely difficult.

Moreover, the technical databases for such networks, which typically include information about the topology, the line parameters as well as the phase connection of customers may have considerable errors. These errors can be mistakes made during the initial documentation, and/or during its digitization process, erroneous parameters due to aging and fatigue of the equipment or changes made to the physical network over the years that went unregistered (expansion, replacement of equipment to a different type, etc.). The lack of reliable, system related, information for an accurate model increases the difficulty of planning and managing of these networks. Furthermore, it has a highly detrimental impact on the reliability of the DSSE results [19], which is more than important today with the high integration of DERs and EVs.

In this sense, it is important to leverage all available information in an effort to improve the accuracy of the system model before utilizing it in DMS applications. Besides the generation of pseudo-measurements, historical data from the AMI

can also be utilized for this purpose, which highlights the necessity and benefits of investing in the development of this infrastructure. A network topology and configuration processor is typically employed [10] for correcting or generating the network topology. Depending on the level of already known information about the system, different approaches are followed for solving the problem of topology identification. When the general topology of a network is known and its exact energized topology is needed, then the problem is referred to as a system configuration identification problem. Its purpose is to detect changes in the topology of the system, through the utilization of available measurements and update the system model according to the currently energized topology. Such problem is typically solved in a generalized SE [20] approach where the state of circuit breakers is modeled as zero impedance branches, and the power flow through these branches is included as a state variable in $\boldsymbol{x}$. Moreover, additional equality constraints are introduced that referred to the operational constraints of the circuit breakers. These include zero voltage drops and zero angle deviations in closed switches and zero power flows in open ones. Alternative solutions to this problem utilize probabilistic approaches to determine which topology from all possible configurations is most probable based on the available measurements. For instance, in Ref. [21], various network configurations are stored to form a model bank. Then, WLS estimators are executed in parallel for each topology under the same set of measurements. Based on the estimator results, the probability of each model being energized is determined in a recursive Bayesian approach, and the model with the highest probability is selected as the true topology of the system.

When the operators do not have a general sense or knowledge of a system's topology, then the problem is referred to as a topology learning problem. The aim is to utilize the available measurements from the AMI and the limited information that may be known for the system to discover the topology and parameters of a specific network. Several data-driven algorithms have been proposed in the literature with different assumptions, considerations, available measurements and prior information for solving this problem. Commonly, these algorithms are based on graph theory such as in Ref. [22] where the graph-theoretic interpretation of principal component analysis is utilized with energy readings from smart meters to identify the overall network topology. The problem of topology learning and line parameter estimation is solved in a joint framework in Refs. [23,24], where the solution approaches are based on a maximum likelihood estimator and linear regression, respectively. It must be noted that all approaches for system identification, topology learning and line parameter estimation require an adequate measuring infrastructure such that the considered system is fully observable.

12.3.3 Slow reporting rate – asynchronous measurements

A significant limitation of smart meters in regard to their utilization for DSSE purposes is their slow reporting rate and asynchronous measurements. The general size of LVDGs is enormous with hundreds of consumers connected per secondary substation, of which a significant number may also have distributed generation.

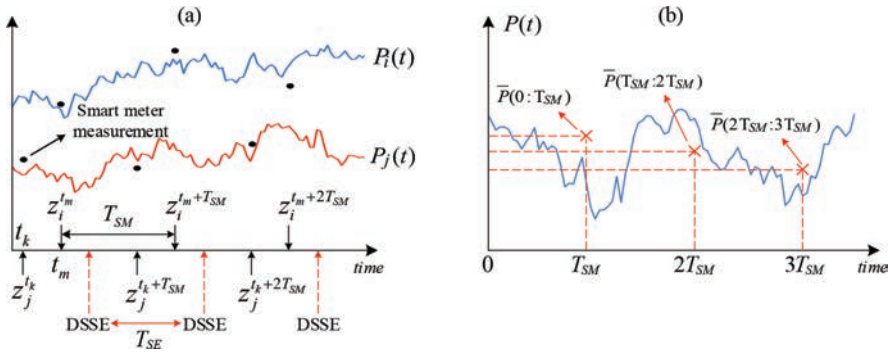

Figure 12.6 Illustration of (a) asynchronous and (b) energy (average power) measurements from smart meters

Consequently, a significant amount of data needs to be transmitted from smart meters to data concentrators, via a neighborhood area network, and then to the control center, via a wide area network. The limitations on the bandwidth and throughput of a conventional communication infrastructure, such as those that are based on power line communication (PLC) or general packet radio service (GPRS) technology, prohibit the high reporting rate of the smart meters as it will result to severe bottlenecks, latency and data losses. To avoid these issues the reporting rate of smart meters is typically low, once every 15–30 minutes, and because of the limited bandwidth each smart meter transmits its measurements to the data concentrator at different time instances. Therefore, due to these limitations, a snapshot of the entire network is not available. Instead, a measurement set for DSSE applications can consist of measurements from significantly different time instances raging from a few seconds to several minutes, that is, $\boldsymbol{z}$ consists of measurements with large time skewness.

An example of asynchronous smart meter measurements is illustrated in Figure 12.6.a. In this example, the active power consumption P_i and P_j are measured by two smart meters every T_{SM} (smart meter reporting rate), and a DSSE is executed every T_{SE}. A measurement of P_i is taken at time instance t_m (denoted as $z_i^{t_m}$) and then again after T_{SM} ($z_i^{t_m+T_{SM}}$), similarly for P_j but with a measurement taken at time instance t_k instead. It can be seen that when the DSSE will be executed, it is possible that the measurement vector $\boldsymbol{z}$ will have measurements that were last sampled a few seconds ago while some other measurements may have not been updated for several minutes (up to T_{SM}). Naturally, during the blind interval (time between measurements) of each smart meter, the measured quantities continuously change and can be significantly different when a DSSE is executed in relation with their latest measurement. In the case of a WLS-based DSSE, weights to each measurement are assigned that are related to the accuracy of each measurement. Typically, these weights are determined by the accuracy of each meter as it is assumed that all measurements are from the same snapshot, and therefore the only source of error is the quality of the considered meter. When the DSSE is executed, the state of P_i can be written as,

$$P_i(t) = z_i^{t_k} + \Delta P_i(t - t_k) + e_i^{t_k} \tag{12.28}$$

where $z_i^{t_k}$ is the latest available measurement for P_i, $\Delta P_i(t - t_k)$ is the variation of P_i since it was last measured at t_k and $e_i^{t_k}$ is the intrinsic error of the smart meter when it sampled the $z_i^{t_k}$ measurement. From this expression, it is evident that due to the considerable blind interval there is an additional source of uncertainty behind each measurement corresponding to its variation since it was last measured. This raises the question of what weights should be given to each measurement. Assuming that all smart meters in an LVDG are identical and of the same accuracy class, under the conventional WLS DSSE approach all measurements of the same type will have equal weights. This means that a measurement that was just updated will have same weight and impact on the DSSE results as a measurement that was updated several minutes ago. Consequently, the DSSE results under this approach may have considerable errors, depending on the variation of each measured quantity in relation to their respective latest available measurements.

Another limitation of smart meters is that they only transmit the average value over the considered resolution window, although they take frequent measurements. The main internal component of a smart meter relevant to this aspect is the metrology module. This module is responsible for sampling the voltage and current signals at specific intervals to determine their RMS values, with typically 1–5 Hz update frequency [25]. The processing unit within the metrology module then calculates various relevant quantities such as the active/reactive power consumption and power factor. The measured voltage and current RMS values as well as the calculated power consumption are stored locally in the meter's memory block. Depending on the specified meter resolution, all measurements acquired during the resolution window are averaged, and the result is the measurement that the smart meter will transmit for the specific time window. As an example, if a smart meter updates locally at 1 Hz and its resolution is specified at 15 minutes, then the measurements that the smart meter will transmit for each 15-minute interval is the average value of 900 samples. As illustrated in Figure 12.6.b, the transmitted average value $\bar{P}$ at the end of each resolution window T_{SM} can be significantly different than the instantaneous value. In addition, by only transmitting the average value a lot of information is lost where overloading and overvoltage/undervoltage conditions are hidden and remain undetected. Figure 12.7 illustrates smart meter measurements under different resolution windows. The instantaneous values $P(t)$ have a 1 s resolution and are taken from Ref. [26], while the smart meter measurements are determined by the average values of $P(t)$ over the considered window. This figure shows how important information is lost when the smart meters have a slow reporting rate. Only when the resolution window is below 10 minutes all peak values of the load are sufficiently captured.

12.3.4 Nonzero neutral voltage

Kron developed the method for node elimination [12] for a system of equations of the form $\boldsymbol{Ax} = \boldsymbol{b}$, with vector $\boldsymbol{b}$ having a zero element in the nth row. The zero

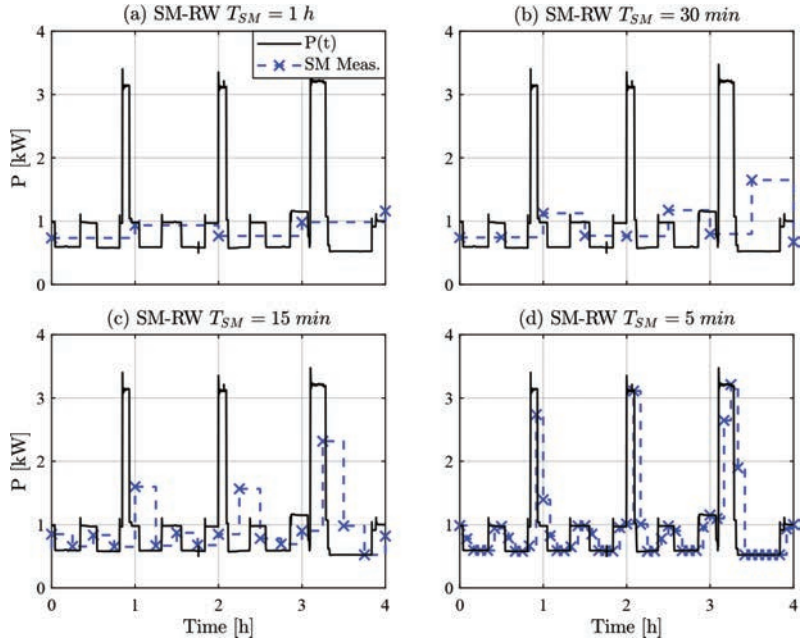

Figure 12.7 Smart Meter (SM) measurements under different Resolution Windows (RW)

element in vector $\boldsymbol{b}$ allows to eliminate the nth row and nth column, as it was illustrated in Section 12.2.3. Let $\boldsymbol{A} \in \mathbb{C}^{n\times n}$ and $\boldsymbol{x}, \boldsymbol{b} \in \mathbb{C}^{n}$, the system of equations under these conditions is,

$$\begin{bmatrix} a_{1,1} & \cdots & a_{1,n-1} & a_{1,n} \\ \vdots & \ddots & \vdots & \vdots \\ a_{n-1,1} & \cdots & a_{n-1,n-1} & a_{n-1,n} \\ a_{n,1} & \cdots & a_{n,n-1} & a_{nn} \end{bmatrix} \begin{bmatrix} x_1 \\ \vdots \\ x_{n-1} \\ x_n \end{bmatrix} = \begin{bmatrix} b_1 \\ \vdots \\ b_{n-1} \\ 0 \end{bmatrix} \tag{12.29}$$

The application of Kron's reduction method allows the reduction of the size of the system equations to $n-1$ with $\boldsymbol{A} \in \mathbb{C}^{n-1\times n-1}$ and $\boldsymbol{x}, \boldsymbol{b} \in \mathbb{C}^{n-1}$. In the case of four-wire LVDGs, the Kron's reduction method allows the elimination of the row and column related to the neutral conductor. This reduces the impedance matrix to the more DSSE compatible form of 3×3. This is under the assumption, however, that the neutral voltage can be approximated to zero. When this holds true, then the application of Kron's reduction method yields an accurate system representation through the three-wire model.

In LVDGs, the most commonly used earthing systems that energy utilities provide are the TT, TN-S and TN-C-S earthing schemes [27], as illustrated in Figure 12.8. To examine what is the possible voltage drop across the neutral

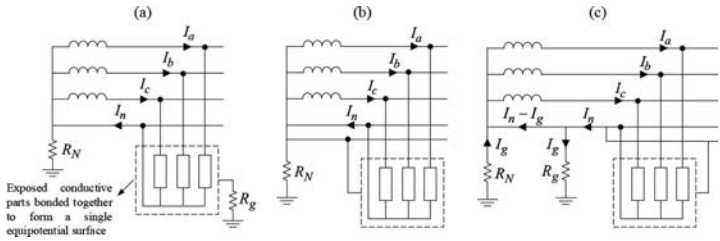

Figure 12.8 (a) TT, (b) TN-S and (c) TN-C-S earthing schemes

conductor, first the operation and influence of these earthing schemes must be taken into consideration. In LVDGs, the neutral conductor is needed for power supply as it provides the main return path of single-phase loads. It is also acting as a return path for the asymmetrical load and triplen harmonic current back to the distribution transformer. The winding configuration of the distribution transformer is in most cases D-Y_n with the neutral grounded at the substation through an electrode R_N. It should be notated that while the neutral conductor has an operational role in distribution grids, the purpose of the earthing system is to provide a close loop return path for fault currents. Its design must ensure that fault currents are sufficiently large to trip the protection mechanisms in the designated time but also small enough to limit the risk of fire.

In the TT and TN-S schemes, the earthing system is separated from the neutral conductor, and the return path of fault currents is established through a local earth electrode R_g at the consumer's premises or through a separated conductor, respectively. Therefore, the operation of these systems is identical regarding the neutral current and the subsequent voltage drop. To save the cost of having an extra conductor, in the TN-C-S scheme the utility provides a common neutral and protective conductor up to the premises of an installation. At the main electrical board, the two conductors are separated with no physical links between them within the installation. As the neutral and protective conductors are common in the supply side, any neutral voltage drop propagates through the protective conductor to the bonded exposed conductive surfaces. To limit the danger of perceived shocks by step voltages, the utilities install auxiliary earth electrodes along their supply lines at specified intervals. The additional earth electrodes provide a parallel path for the neutral current to travel to the distribution transformer via the earth to reduce its voltage drop. The magnitude of the diverted neutral current I_g and its impact on the neutral voltage depends on the resistance of the parallel paths. Considering that in most LVDGs, the surface area of the neutral conductor is typically 100 mm^2, and that it is constructed by aluminium, its resistance can be as low as 0.3 Ω/km. This indicates that to have any significant diverted neutral current the total resistance of the closed loop through the earth must be very low.

In Figure 12.9.a, the neutral voltage at the end of the IEEE European LV feeder is illustrated under the TT, TN-S and TN-C-S earthing schemes. For the TN-C-S scheme, two different values for the total impedance of the closed loop

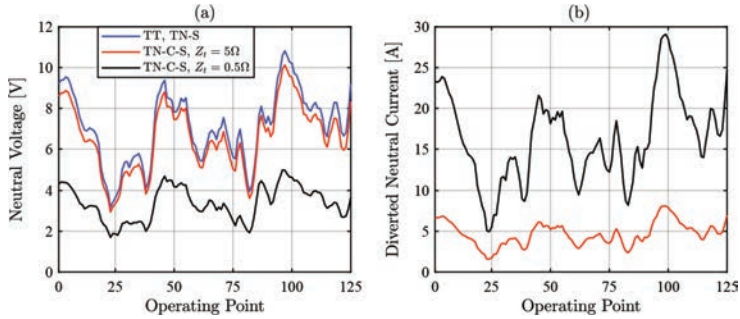

Figure 12.9 (a) Neutral voltage at the end of a feeder (b) diverted neutral current through the auxiliary earth electrodes

through the earth are considered, and an auxiliary earth electrode is placed at intervals of 100 m. Additionally, Figure 12.9.b shows the diverted neutral current that reaches the distribution transformer via the earth. Based on this figure, it can be concluded that for the extra electrodes in TN-C-S to have a significant impact, a very low earth loop impedance is needed. In practice, having an impedance less than 1 Ω is difficult, especially in urban systems where a direct access to earth may not be accessible. In cases that the earth loop impedance is several Ohms, then essentially TN-C-S has similar operation with the other two earthing schemes, in regard to the operation of the neutral conductor under normal conditions. It must be noted that the degree of the voltage drop observed across the neutral conductor is directly related with the loading conditions. Under balanced conditions, this voltage drop becomes insignificant; however, LVDGs are characterized by their unbalanced nature and rarely operate without a significant load asymmetry.

For DSSE applications, a nonzero neutral voltage has two main detrimental impacts. First, it raises the question of system model accuracy through the application of Kron's reduction as it requires the assumption that the neutral voltage can be approximated to zero. Second, the voltage measurements utilized in the DSSE by smart meters are expressed in a different and variable reference as they are phase-to-neutral voltage measurements. Near the distribution transformer, the reference for these measurements can be considered the ground as the neutral voltage is low near the supply electrode. However, measurements taken by smart meters that are far from the transformer have as reference the local neutral voltage which is affected by the changing loading conditions. As a result these measurements might provide a misleading picture of the network's operating condition.

In Table 12.1, the average two-norm $\left(\|\Delta V\|_2^{avg}\right)$, average max-norm $\left(\|\Delta V\|_\infty^{avg}\right)$ and the highest $\left(\|\Delta V\|_\infty^{max}\right)$ estimation error of the WLS DSSE scheme with node voltages as state variables are listed when it is applied in different types of LVDGs. These errors are calculated as,

Table 12.1 Estimation errors of the WLS DSSE scheme

System type	$\|\Delta V\|_2^{avg}$ $[10^{-2}p.u.]$	$\|\Delta V\|_\infty^{avg}$ $[10^{-2}p.u.]$	$\|\Delta V\|_\infty^{max}$ $[10^{-2}p.u.]$	V_N^{avg} [V]	Feeder length (km)
Urban-TT	0.6	1.2	1.7	2.9	0.3
Suburban-TT	1.5	2.4	3.5	6.1	0.6
Rural-TT	1.7	3.0	4.8	9.3	1.2
Rural-TN-C-S, $R_g = 0\ \Omega$	0.2	0.4	0.7	≈0	1.2

$$\begin{aligned} \|\Delta V\|_2^{avg} &= \frac{1}{R \cdot N_V} \sum_{i=1}^{R} \sqrt{\sum_{j=1}^{N_V} \left| \widehat{V}_j^i - V_j^i \right|^2} \\ \|\Delta V\|_\infty^{avg} &= \frac{1}{R} \sum_{i=1}^{R} \max_{1 \le j \le N_V} \left\{ \left| \widehat{V}_j^i - V_j^i \right| \right\} \end{aligned} \tag{12.30}$$

where R is the total number of DSSE runs at different operating points, N_V is the total number of states related to voltage magnitudes, $\widehat{V}_j^i$ is the estimation of the jth state at the ith run and V_j^i is the true value of this state. This table also includes the average neutral voltage at the end of each feeder as well as its total length. It can be seen that as the average neutral voltage of the LVDG increases, the accuracy of the monitoring scheme reduces. This is because of the inaccurate system model that is derived through Kron's reduction and the phase-to-neutral voltage measurements. To highlight the impact of the neutral voltage, the last row in Table 12.1 illustrates the case that the earthing system in the rural LVDG is TN-C-S with ideal auxiliary earth electrodes. This consideration reduces the neutral voltage to approximately 0 V, and therefore the assumption made by Kron's reduction is true. Consequently, the WLS DSSE under these conditions has a very high accuracy. This clearly illustrates the detrimental impact of the nonzero neutral voltage to the DSSE performance.

12.4 Enhancing DSSE

In the previous section, important factors that influence negatively the performance of the DSSE when applied to LVDGs were presented and some mitigation strategies discussed. The limited sensing and limited system knowledge challenges are, in general, addressed and resolved before the execution of the DSSE with the purpose to improve the measurement set and system model. On the other hand, the asynchronous smart meter measurements and the nonzero neutral voltage influence the internal operation of the DSSE. Consequently, modifications must be made to the DSSE in order to address these challenges and enhance its operation by taking into account these particularities of the LVDG. The modifications made to the DSSE to (1) address the asynchronous smart meter measurements by utilizing available historical data and (2) address the nonzero neutral voltage is presented below.

12.4.1 Addressing asynchronous measurements using historical data

As it was discussed in Section 12.3.3, the measurement vector $\boldsymbol{z}$ of a DSSE application based on smart meters typically includes measurements from different snapshots (time instances). In the following context, the term *updated* measurements refers to measurements in $\boldsymbol{z}$ that were just updated while the term *out-of-date* (OD) measurements refers to measurements in $\boldsymbol{z}$ that have not been updated in the current time instance that a DSSE will be executed. As indicated by (12.28), an OD measurement has two sources of error, the intrinsic uncertainty of the meter and the variation of the measured quantity during the blind interval. In Ref. [28], it is proposed to model this additional source of uncertainty as a random variable which its properties are studied by utilizing available historical measurements. Following these considerations, the total error of the ith measurement is written as,

$$e_i = e_{SM,i} + e_{OD,i} \tag{12.31}$$

where $e_{SM,i}$ is the error introduced by the imperfection of the considered meter and $e_{OD,i}$ the error by the variation during the blind interval t_{LU}, with t_{LU} denoting the time that has passed since the last update.

The authors in Ref. [28] performed extensive studies to identify the statistical properties of the load variation between consecutive smart meter measurements. For this purpose, the authors utilize historical measurements that consist of 15-minute active/reactive power readings at a distribution transformer for 1 month. Their reasoning is that if the load variation between consecutive measurements is proven to follow a normal distribution, then the total error e_i can be modeled as the summation of two normally distributed random variables and therefore it is also normally distributed with a known mean and variance as,

$$\begin{aligned} & e_{SM,i} \sim N\left(0, \sigma_{SM,i}^2\right), \quad e_{OD,i} \sim N\left(\mu_{OD,i}, \sigma_{OD,i}^2\right) \\ & \xrightarrow{(12.31)} \; e_i \sim N\left(\mu_{OD,i}, \sigma_{SM,i}^2 + \sigma_{OD,i}^2\right) = N\left(\mu_{OD,i}, \sigma_{t,i}^2\right) \end{aligned} \tag{12.32}$$

where $\sigma_{SM,i}$ is associated with the accuracy of the considered meter and $\mu_{OD,i}$, $\sigma_{OD,i}$ are the mean and standard deviation of the load variation between consecutive measurements at a specific time during the day, for example, between 16.00 and 16.15. For verifying if the OD variation can be considered as a normally distributed random variable, the load variation between consecutive measurements from the historical data is calculated for all smart meter update intervals $t_{T_{SM}}$, with $t_{T_{SM}} \in \left[1, 2, \cdots \frac{24 \cdot 60}{T_{SM}}\right]$. For example, considering a 15-minute update interval for the smart meters ($T_{SM} = 15$), in a day there are in total 96 updating instances with $\sigma_{SM,i}$. If the number of days that historical data is available is equal to d, then for each of the 96 updating instances and its corresponding load variation within a single day there will be d datapoints that can be used for verifying its distribution. For a better understanding, a graphical illustration is shown in Figure 12.10 of how the historical data are processed to generate the data points of each updating instance, which are then used for verifying the distribution of the load variation during each updating interval.

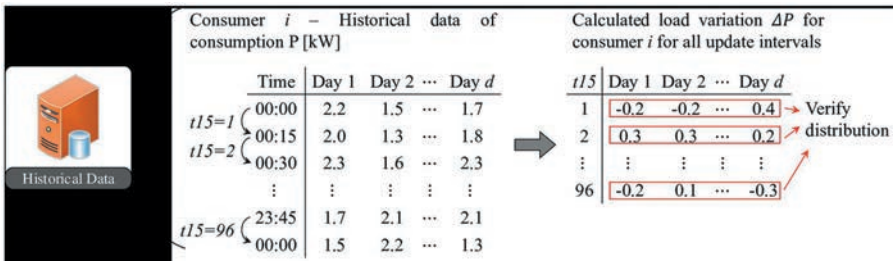

Figure 12.10 Process of historical data to derive the load variation for each update interval for verifying its distribution for the i*th consumer*

To verify if indeed the load variation between any consecutive measurements follows a normal distribution, the d data points of each updating interval are used in normality fitness tests. Specifically, the Anderson–Darling [29] and Shapiro–Wilk [30] fitness tests are employed for this purpose. Based on the results of these tests, the authors in Ref. [28] conclude that both the active and reactive power variation between all consecutive updating intervals within a day can be considered as normally distributed. Note that the load variation in each updating interval and for each smart meter is modeled individually as a normal distribution with a mean and variance computed from the historical data.

The calculated mean and variance of the load variation are values that correspond to the end of the updating interval, just before the new measurement arrives and $t_{LU} \approx T_{SM}$. Within the blind interval and before the new measurement arrives, it is assumed that the load variation (mean and variance) varies linearly over time and therefore their values at any point during the blind interval can be calculated as,

$$\mu_{OD}(t_{LU}) = \frac{t_{LU}}{T_{SM}} \mu_{OD}^{{}^{t}T_{SM}}, \quad \sigma_{OD}^{2}(t_{LU}) = \frac{t_{LU}}{T_{SM}} \left(\sigma_{OD}^{{}^{t}T_{SM}}\right)^{2} \tag{12.33}$$

where $\mu_{OD}^{{}^{t}T_{SM}}$ and $\sigma_{OD}^{{}^{t}T_{SM}}$ are the mean and standard deviation of the load variation for a specific updating interval. Note that at the end of each reporting cycle and when a new measurement arrives, t_{LU} resets to zero and therefore both the mean and variance of the load variation are zero and the error in (12.31) consists of only the meter's uncertainty, denoting an updated measurement. In any other case, the measurement is OD and by using (12.33) the load variation can be adjusted for any point during the smart meter's blind interval.

Before executing the DSSE process (every T_{SE} minutes with $T_{SE} \prec T_{SM}$), equation (12.33) must be evaluated for all OD measurements so that the weight matrix $\boldsymbol{W}$ is updated accordingly with the new values of the error's variance. In addition, from (12.32) it can be seen that the mean value of the error of an OD measurement is not zero. Consider that the true value of an OD measurement at instance t is,

$$P_i(t) = z_{OD,i} - e_i = h_i(\boldsymbol{x}) \tag{12.34}$$

Therefore, an OD measurement is modeled as,

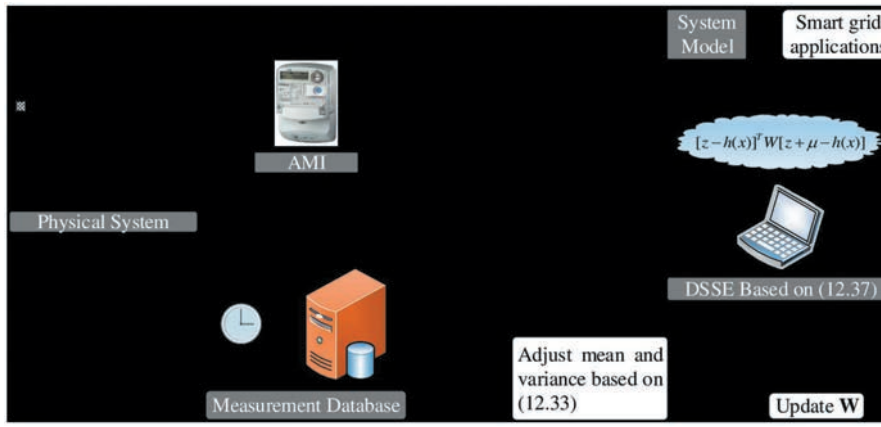

Figure 12.11 *Main steps of the DSSE approach to address the asynchronous smart meter measurements based on the utilization of historical data*

$$z_{OD,i} = h_i(\boldsymbol{x}) + e_i \tag{12.35}$$

Consequently, the PDF of such measurement is modified accordingly to include the impact of the load variation,

$$PDF(z_{OD,i}) = \frac{1}{\sqrt{2\pi}\sigma_{t,i}} e^{-\frac{1}{2}\left(\frac{z_i+\mu_{OD,i}-h_i(x)}{\sigma_{t,i}}\right)^2} \tag{12.36}$$

where $\sigma_{t,i}^2$ is the total variance of the error, as indicated in (12.32). Under these considerations, the update step $\Delta\boldsymbol{x}$ of the state vector $\boldsymbol{x}$ during the WLS DSSE process changes from (12.9) to,

$$\Delta\boldsymbol{x}_k = \boldsymbol{G}(\boldsymbol{x}_k)^{-1}\boldsymbol{H}(\boldsymbol{x}_k)^T\boldsymbol{W}[\boldsymbol{z} + \boldsymbol{\mu}_{OD} - \boldsymbol{h}(\boldsymbol{x}_k)] \tag{12.37}$$

where $\boldsymbol{\mu}_{OD}$ is a vector containing the mean value of the load variation of the OD measurements for the current updating interval. From the above expression, it can be seen that the mean value of the load variation is acting as a corrective operator to the OD measurement to bring it toward the statistically probable behavior for each individual load during a specific updating interval, derived by the process of historical data. In Figure 12.11, the main steps and general structure of this DSSE method are illustrated for a better understanding of its operation. The described DSSE scheme in Ref. [28] is tested by utilizing distribution test systems. It is assumed that each smart meter during a 15-minute interval sends updated measurements at different instances, and the modified WLS DSSE is executed every 200 seconds. Extensive studies and Monte Carlo simulations have shown that the modification of the mean and variance of the measurement error according to the time that has past since a measurement was last sampled results to a higher estimation accuracy. Specifically, it is shown that an improvement of 14–15% is achieved in relation to the traditional

DSSE scheme, which assumes all measurements to be synchronized, with limited additional computational burden.

However, there are several limitations with this approach. First, historical data with sufficient days and resolution for all consumers in a network are needed for statistically evaluating their behavior and load variation during updating instances. For consumers in LVDGs, this kind of information is most of the time not available or the historical measurements are of very low resolution. Second, the load variation between updating intervals in Ref. [28] has been proven to follow a normal distribution for an aggregated load. For consumers in LVDGs, this conclusion may not be valid as it is entirely dependent on the consumption patterns, preferences and general habits of each individual consumer. Finally, it is assumed that the variation between consecutive measurements is linear with time. In reality, this is not guaranteed and is an extra source of uncertainty which, without fast-reporting smart meters, is not possible to know from only 15-minute measurements. In general, addressing the asynchronicity of smart meters with low measurement frequency is a challenging task. Until an advanced and decentralized communication-management-automation infrastructure becomes the norm in LVDGs to allow faster smart meter reporting capabilities, additional research efforts are needed to improve the DSSE operation under asynchronous smart meter measurements.

12.4.2 Addressing the nonzero neutral voltage

In Section 12.3.4, the impact of a nonzero neutral voltage on the performance of a nodal voltage WLS DSSE was discussed and investigated for different types of LVDGs. It was seen that the application of Kron's reduction to simplify the admittance matrix of each line to the more conventional and compatible format of 3×3 is not applicable to such networks. Moreover, as voltage measurements are an important aspect of the DSSE procedure, the nonzero neutral voltage creates also the issue of voltage measurements with different references which give a misleading picture of the network's condition. Instead of the conventional approach, the following modifications can be made to the WLS DSSE to improve its operation under a nonzero neutral voltage [31].

12.4.2.1 Four-phase system

The use of Kron's reduction must be avoided, and the whole 4×4 admittance matrix must be used which includes the fourth wire for the neutral. Therefore, the system is modeled as a four-phase system (*abcn*) and each four-wire node has eight state variables while each two-wire node (single-phase–connected consumers) has four state variables. Assuming polar node voltages as state variables,

$$\begin{aligned} \boldsymbol{x}_{abcn} &= \left(\theta_a, \theta_b, \theta_c, \theta_n, V_a, V_b, V_c, V_n\right) \\ \boldsymbol{x}_{pn} &= \left(\theta_p, \theta_n, V_p, V_n\right) \end{aligned} \tag{12.38}$$

where $p \in \{a, b, c\}$ is the supply phase of single-phase–connected consumers. Note that since the neutral is included as a separate phase in the DSSE process it increases the number of state variables and consequently the complexity and computational

burden are also increased. However, considering that a DSSE is typically executed every few minutes depending on the updating frequency of smart meters, the extra computational burden is insignificant.

12.4.2.2 Measurement functions and Jacobian matrix

As it is mentioned above, the voltage measurements provided by smart meters are in fact phase-to-neutral voltage measurements. In the traditional DSSE scheme with polar node voltages, the state variables of the voltage magnitude can be directly related with their corresponding measurements. For a phase-to-neutral voltage measurement, its measurement function must be modified to include the state of the neutral voltage,

$$\begin{aligned} V_i^{pn} &= \left| V_i^p \angle\theta_i^p - V_i^n \angle\theta_i^n \right| \\ &= \sqrt{\left[V_i^p cos\left(\theta_i^p\right) - V_i^n cos\left(\theta_i^n\right)\right]^2 + \left[V_i^p sin\left(\theta_i^p\right) - V_i^n sin\left(\theta_i^n\right)\right]^2} \\ &= \sqrt{\left(V_i^p\right)^2 + \left(V_i^n\right)^2 - 2V_i^p V_i^n cos\left(\theta_i^p - \theta_i^n\right)} \end{aligned} \tag{12.39}$$

where V_i^{pn} is a phase-to-neutral voltage measurement between phase p and neutral at the ith system node and V_i^p, V_i^n, θ_i^p and θ_i^n are the respective phase-to-ground and neutral-to-ground voltage magnitudes and phase angles. Equation (12.39) shows that the measurement function that relates voltage measurements with state variables consists of four state variables instead of just one as in the traditional DSSE approach. Each phase-to-neutral measurement is related with the state variables that represent the voltage magnitude and phase angle of the corresponding supply phase and the neutral at the system node that the measurement was taken. By taking the partial derivatives of (12.39) in respect to the state variables, the relevant elements of the Jacobian matrix are calculated as,

$$\frac{\partial V_i^{pn}}{\partial V_j^m} = \begin{cases} \dfrac{V_j^m - V_i^n cos\left(\theta_j^m - \theta_i^n\right)}{h_V(\boldsymbol{x})}, & j = i,\ m = p \\ \dfrac{V_j^m - V_i^p cos\left(\theta_i^p - \theta_j^m\right)}{h_V(\boldsymbol{x})}, & j = i,\ m = n \\ 0, & otherwise \end{cases} \tag{12.40}$$

$$\frac{\partial V_i^{pn}}{\partial \theta_j^m} = \begin{cases} \dfrac{V_j^m V_i^n sin\left(\theta_j^m - \theta_i^n\right)}{h_V(\boldsymbol{x})}, & j = i,\ m = p \\ -\dfrac{V_i^p V_j^m sin\left(\theta_i^p - \theta_j^m\right)}{h_V(\boldsymbol{x})}, & j = i,\ m = n \\ 0, & otherwise \end{cases} \tag{12.41}$$

where $h_v(\boldsymbol{x})$ corresponds to (12.39). Note that the relevant Jacobian elements of the traditional DSSE formulation are equal to one for the voltage magnitude partial derivatives when $j = i,\ m = p$ and zero otherwise, as it can be seen from (12.19).

12.4.2.3 Generation of virtual measurements

A drawback of applying the Gauss–Newton method for solving the set of nonlinear functions (12.8), derived by the minimization problem of the WLS method, is the potential convergence issues due to poor initialization of the state variables. Normally this is not a concern as the actual operating conditions are not far from the initialization point at nominal values. The inclusion of neutral voltage with an initialization at 0 V however introduces a new complexity as its operating state is highly fluctuating and volatile which can lead to convergence issues. To mitigate potential issue, virtual measurements are constructed for the neutral voltage by exploiting the available power measurements in a modified forward-backward voltage Sweep (FBS) method [32] that includes the neutral voltage. Note that several studies conducted in Ref. [33] have shown that the configuration of the neutral conductor affects the convergence of the FBS method when multiple solutions exist due to the neutral voltage. The solution that the FBS method converges is determined by the initialization of the neutral voltage. In Ref. [32], it is shown that for the TT earthing scheme FBS converges to the same solution regardless of the initialization of the neutral voltage. Once the modified FBS converges, the information regarding the magnitude V^n and phase angle θ^n of the neutral voltage is included in the measurement vector $\boldsymbol{z}$,

$$\boldsymbol{z} = \begin{bmatrix} \boldsymbol{P} & \boldsymbol{Q} & \boldsymbol{V}^{pn} & \boldsymbol{V}^{n} & \boldsymbol{\theta}^{n} \end{bmatrix}^T \tag{12.42}$$

where $\boldsymbol{V}^n$ and $\boldsymbol{\theta}^n$ are vectors that include the virtual measurements for the neutral voltage magnitude and phase angle, respectively. Consequently the Jacobian matrix is now given in (12.43),

$$\boldsymbol{H}(\boldsymbol{x}) = \begin{bmatrix} \frac{\partial \boldsymbol{P}}{\partial \boldsymbol{V}} & \frac{\partial \boldsymbol{Q}}{\partial \boldsymbol{V}} & \frac{\partial \boldsymbol{V}^{pn}}{\partial \boldsymbol{V}} & \frac{\partial \boldsymbol{V}^{n}}{\partial \boldsymbol{V}} & \boldsymbol{0} \\ \frac{\partial \boldsymbol{P}}{\partial \boldsymbol{\theta}} & \frac{\partial \boldsymbol{Q}}{\partial \boldsymbol{\theta}} & \frac{\partial \boldsymbol{V}^{pn}}{\partial \boldsymbol{\theta}} & \boldsymbol{0} & \frac{\partial \boldsymbol{\theta}^{n}}{\partial \boldsymbol{\theta}} \end{bmatrix}^T \tag{12.43}$$

The statistical properties of the error associated with the virtual measurements of neutral voltage should be verified in order to comply with the assumption of the WLS DSSE that the measurement error follows a normal distribution. For this purpose the modified FBS method is applied to the suburban LVDG, as illustrated in Figure 12.12.a. Power measurements are constructed for the residential loads with an assumed error of 1% for the active power and 2% for the reactive power. In total, 3 000 Monte Carlo trials are conducted where for each trial the error of the virtual measurements is computed by comparing it to its true value (result of FBS without error in the power measurements). The error of the power measurements is generated as,

$$z_m = z_{true} + FS \cdot N\left(0, \sigma_{P,Q}^2\right) \tag{12.44}$$

where FS is the full-scale meter reading and z_{true} is the selected operating point of the active/reactive power of a load. Having 3 000 data points for each error (V^n, θ^n) and for each system node (the considered system has in total 72 nodes, excluding the MV grid node and the second node in which the neutral is grounded), the fitness tests

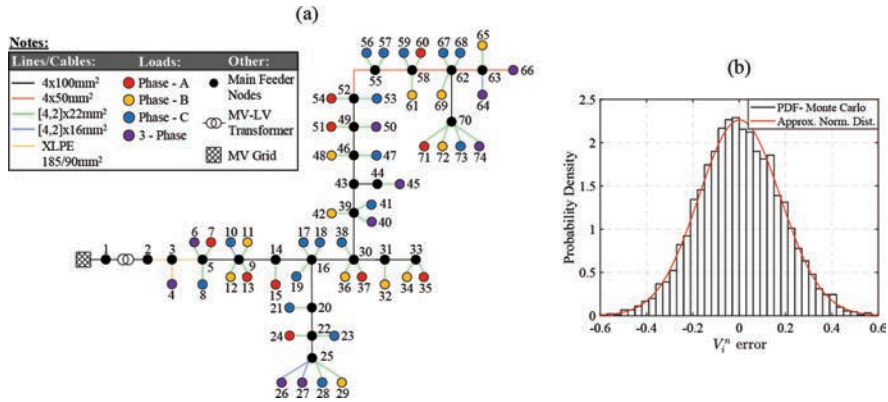

Figure 12.12 *(a) LVDG used for calculating the error of virtual measurements and (b) the calculated PDF of a single measurement error*

introduced in Section 12.4.1 are applied. From the resulting 144 indices denoting their fitness to a normal distribution it is concluded that indeed, the error of the virtual measurement does follow a normal distribution and can be incorporated in the WLS DSSE scheme. Figure 12.12.b shows the PDF of the error of a random virtual measurement as calculated by the 3 000 Monte Carlo trials and its approximation through a normal distribution.

12.4.2.4 Weights for virtual measurements

Assuming that the four-wire line illustrated in Figure 12.4 is ungrounded, the neutral voltage on the receiving end based on (12.20) is equal to,

$$\dot{V}^n = \dot{V}'_N - z_{na}\dot{I}_a - z_{nb}\dot{I}_b - z_{nc}\dot{I}_c - z_{nn}\dot{I}_n \tag{12.45}$$

By substituting the neutral current as the summation of the phase currents and by assuming that the mutual impedance terms of (12.20) are identical and equal to z_m to simplify the problem, equation (12.45) is simplified to,

$$\dot{V}^n = \dot{V}'_N - z_T\dot{I}_{abc} = \dot{V}'_N - \dot{V}_L \tag{12.46}$$

with $z_T = z_{nn} + z_m$ and $\dot{V}_L = z_T\dot{I}_{abc}$ the voltage drop over a branch due to the current flow. For a radial distribution grid, the phase currents flowing through any given branch are determined by the downstream loads,

$$\dot{I}_{abc} = \sum_{i=K}\left[\left(\frac{P_a^i + jQ_a^i}{\dot{V}_a^i}\right)^* + \left(\frac{P_b^i + jQ_b^i}{\dot{V}_b^i}\right)^* + \left(\frac{P_c^i + jQ_c^i}{\dot{V}_c^i}\right)^*\right] \tag{12.47}$$

where K is a set containing all downstream loads in relation with a specific branch. For simplicity, the voltage is assumed to be equal to its nominal value and by taking as reference the MV side of the D-Y_n distribution transformer and accounting for the phase shift it introduces, they are equal to,

$$\begin{aligned}\dot{V}_a &= V_{nominal} \lhd -30° = 0.87 - j0.5 = e - jd \\ \dot{V}_b &= V_{nominal} \lhd -150° = -0.87 - j0.5 = -e - jd \\ \dot{V}_c &= V_{nominal} \lhd 90° = j1 = jg\end{aligned} \tag{12.48}$$

with $V_{nominal} = 1pu$. Having made this assumption, the V_L term in (12.46) can now be written as,

$$\begin{aligned}\dot{V}_L \quad &= Z_L \sum_{i=K} \left(eP^i_a - dQ^i_a - eP^i_b - dQ^i_b + gQ^i_c\right) \\ &+j\left(eQ^i_b + gP^i_c - dP^i_b - eQ^i_a - dP^i_a\right) = R + jX\end{aligned} \tag{12.49}$$

where $Z_L = z_T/V^2_{nominal}$. The calculation of the weights for each virtual measurement is conducted in forward sweep approach. Starting at the distribution transformer in which the neutral is grounded and moving downstream the neutral voltage can be calculated as,

$$\begin{aligned}\dot{V}^2_n &= 0 - \dot{V}^2_L = a_2 + jb_2 \\ \dot{V}^3_n &= \dot{V}^2_n - \dot{V}^3_L = a_2 - R_3 + j(b_2 - X_3) = a_3 + jb_3 \\ &\vdots \\ \dot{V}^i_n &= \dot{V}^{i-1}_n - \dot{V}^i_L = a_{i-1} - R_i + j(b_{i-1} - X_i) = a_i + jb_i\end{aligned} \tag{12.50}$$

From (12.49) to (12.50), it can be seen that the real (a_i) and imaginary (b_i) part of the neutral voltage at any system node are functions of several power measurements. Therefore, the uncertainty of these terms can be calculated using the theory of uncertainty propagation. As an example and for simplicity, assume that downstream of node 2 there are only two single-phase loads connected, denoted as i and j. Then, based on (12.45)–(12.49), the real and imaginary terms of $\dot{V}^2_n$ are functions of four variables,

$$\begin{aligned}a_2 &\rightarrow f_a\left(P_i,\ P_j,\ Q_i,\ Q_j\right) \\ b_2 &\rightarrow f_b\left(P_i,\ P_j,\ Q_i,\ Q_j\right)\end{aligned} \tag{12.51}$$

Accordingly, if the error of these four erroneous variables is uncorrelated then the uncertainty of the real part can be calculated as,

$$\sigma_{a_2} = \sqrt{\sum_x \left(\frac{\partial f_a}{\partial x}\right)^2 \boldsymbol{\sigma}^2_x} \tag{12.52}$$

where $\boldsymbol{x} = \left[P_i, P_j, Q_i, Q_j\right]$. The uncertainty of the imaginary part σ_{b_2} is calculated on the same manner. The virtual measurements of each system node are calculated as,

$$\begin{aligned}V^i_n &= \sqrt{a^2_i + b^2_i} \ \rightarrow f_{V_n}\left(a_i, b_i\right) \\ \theta^i_n &= tan^{-1}\left(\frac{b_i}{a_i}\right) = tan^{-1}\left(k\right) \rightarrow f_{\theta_n}\left(a_i, b_i\right)\end{aligned} \tag{12.53}$$

As both types of virtual measurements are functions of the real and imaginary part of the neutral voltage, by applying (12.52) again their uncertainty is equal to,

$$\begin{aligned}\sigma_{V_n^i} &= \sqrt{\left(\frac{a_i}{V_n^i}\right)^2 \sigma_{a_i}^2 + \left(\frac{b_i}{V_n^i}\right)^2 \sigma_{b_i}^2} \\ \sigma_{\theta_n^i} &= \frac{|k|}{1+k^2}\sqrt{\left(\frac{\sigma_{a_i}}{a_i}\right)^2 + \left(\frac{\sigma_{b_i}}{b_i}\right)^2}\end{aligned} \tag{12.54}$$

For nodal voltage in rectangular coordinates as state variables (12.53)–(12.54) are not applied. In this case, the virtual measurements and their uncertainty are equal to,

$$\begin{aligned}V_{n,re}^i = a_i \;\rightarrow\; \sigma_{n,re}^i = \sigma_{a_i} \\ V_{n,im}^i = b_i \;\rightarrow\; \sigma_{n,im}^i = \sigma_{b_i}\end{aligned} \tag{12.55}$$

12.4.2.5 Case studies

To validate the modifications made to the traditional WLS DSSE to account for the nonzero neutral voltage, the LVDG illustrated in Figure 12.12(a) is used. Measurements from smart meters are utilized to construct the load profile of each consumer within this network with a total of 125 different operating points. Based on these profiles, a load flow analysis is executed to generate the true state of the system for all operating points. Then, based on the accuracy of the considered smart meters, the measurements that are used in the DSSE procedure are constructed using (12.44). The true state of the system is used to compute the two-norm and max-norm estimation error of the enhanced WLS DSSE scheme. Assuming smart meters of accuracy class 1 for measurements of active power and voltage, and class 2 for reactive power, these estimation errors are illustrated in Figure 12.13(a) and 12.13.b. Note that in this figure, C_N refers to the traditional WLS DSSE scheme, N_W to the modified, as presented in Section 12.4.2, and C_{N^+} to the traditional but with an ideal TN-C-S earthing scheme. The results of C_{N^+} represent the maximum accuracy that the traditional WLS DSSE scheme can achieve, under the considered smart meter accuracy class, as the assumption of a neutral voltage close to 0 V holds true. In addition, Figure 12.13.c–12.13.f illustrates the resulting estimation of the voltage profile at the end-of-feeder (EoF) for C_N and N_W. The modifications introduced to the traditional WLS DSSE scheme impact positively the performance of the DSSE scheme since the accuracy of the estimator is very close to C_{N^+}, regardless of the operating conditions. In contrast, the accuracy of C_N is highly degraded in relation to the C_{N^+} and N_W as the operating conditions affect its performance. This is because of the nonzero neutral voltage which its magnitude depends on the constantly changing load asymmetry. In operating points with low load asymmetry, the neutral voltage is also low which results to an acceptable performance from C_N. In occasions with high load asymmetry, the resulting neutral voltage has a significantly detrimental impact on C_N, as discussed previously. Furthermore, the modifications made to the traditional WLS DSSE scheme allow for an accurate estimation of the neutral voltage.

Another important aspect of the modifications made to the traditional WLS DSSE is its convergence characteristics. As already mentioned, the inclusion of the

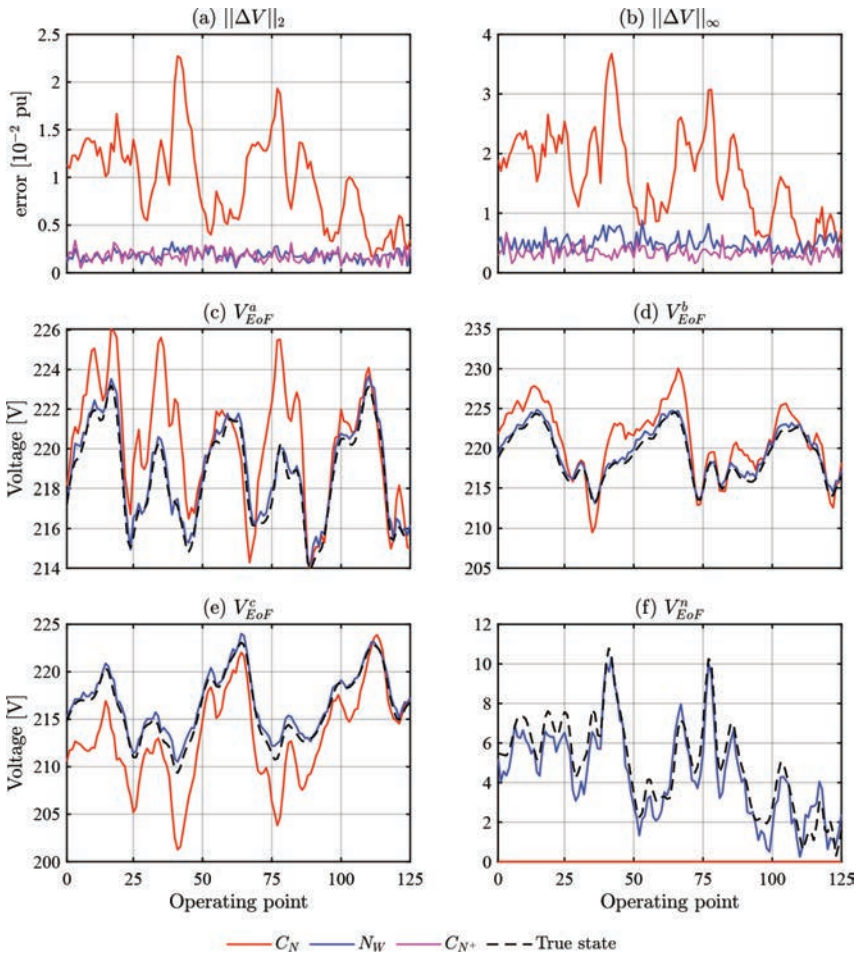

Figure 12.13 *(a) Two-norm and (b) max-norm estimation errors, (c)–(e) voltage profile estimation of phases abc and (f) estimation of neutral voltage at the end-of-feeder (EoF)*

neutral voltage in the estimation process can have a detrimental impact on the convergence of the WLS DSSE method due to a poor initialization point. Figure 12.14 shows the impact of the virtual measurements for the neutral voltage on the estimator's convergence. In this figure, the number of iterations needed as well as the minimum threshold setting e required to converge in less than 30 iterations is illustrated for 25 different operating points. If the estimator in any of the operating points fails to converge within 30 iterations even with a threshold setting of 0.1 pu, then it can be concluded that the estimator failed to converge. Any further increase of the threshold setting under this circumstance will lead to unreliable results even if the estimator manages to converge. Observing Figure 12.14(a), it can be seen that in 7 out of the

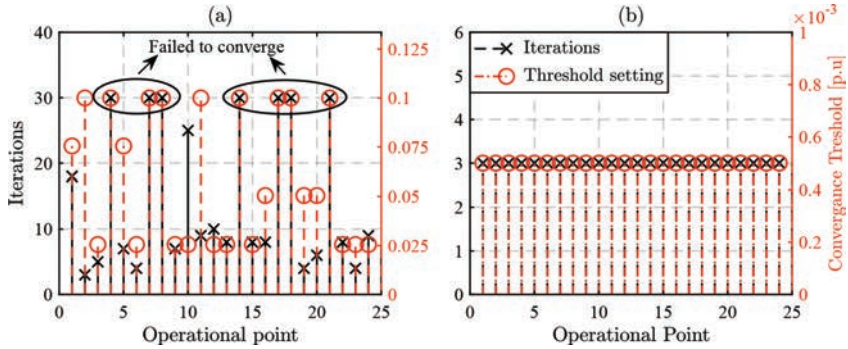

Figure 12.14 Convergence of WLS DSSE scheme when neutral is included: (a) without and (b) with the inclusion of virtual measurements

25 operating points the estimator failed to converge when the virtual measurements are not included. In addition, a relatively high threshold setting is required for the estimator to achieve convergence in the remaining operating points and the number of iterations needed is highly variable. In contrast, when the virtual measurements are included, see Figure 12.14(b), the WLS DSSE becomes significantly more stable and convergence is achieved in all operating points under the minimum e considered ($5 \cdot 10^{-4}$ pu) and within three iterations.

12.5 Future directions

12.5.1 State estimation for the whole distribution grid

Commonly, the utilization of smart meters for DSSE purposes is only considered for one part of the distribution grid, either for the primary (MVDG) or secondary (LVDG) grid. To fully exploit the capabilities and measurements of smart meters at end users, a common framework and formulation of the DSSE application for the whole distribution grid are needed. By coordinating the monitoring schemes of the primary and secondary distribution grid in a hierarchical multilevel DSSE approach, it is possible to fully monitor the distribution grid solely based on smart metering data [34].

Normally, a data concentrator receives measurements from a set of smart meters that are in downstream nodes, assuming a radial network, with several concentrators across an LVDG. By exploiting their computational capabilities, a local SE can be executed which will yield the power injection and voltage at the system node that a specific concentrator is placed. Once all concentrators in an LVDG has generated these measurements, a reduced SE procedure can be executed in the second level to compute the state of the overall LVDG. The output of the reduced LVDG SE procedure includes the information of the power injections and voltage at the distribution transformer. In the third level, this information can be used in the DSSE application of the primary distribution grid. If the primary distribution grid transfers power to

LVDGs in which all end users have a smart meter, then no additional measurement equipment is needed for its monitoring. This allows the utilization of smart meters for enabling the monitoring of the whole distribution grid and thus can increase their investment profitability. However, to support this framework, an adequate communication infrastructure is needed to handle and process the resulting data exchange demands between the various levels and also to allow high reporting rates for the smart meters.

12.5.2 Leveraging information from PV and EV inverters

A lack of sufficient measurement redundancy and a DSSE based solely on asynchronous and delayed smart meter measurements can limit the capabilities and performance of monitoring schemes in LVDGs. In primary distribution grids, devices such as micro-PMUs, intelligent electronic devices, digital relays and voltage regulators can be leveraged to increase observability and measurement redundancy with high frequency data. In contrast, downstream of a secondary substation and within the LVDG the available devices with such capabilities are very limited and are mainly the power inverters of DERs and EV charging stations.

With the increasing share of prosumers and EVs in LVDGs, inverters are becoming more common and are an obvious choice for enhancing the operation of the DSSE. For their internal control, inverters are equipped with local sensors that sample the grid voltage and grid current at a high frequency. The new generation of smart inverters has also two-way communication capabilities that allow to receive commands remotely and to transmit information through the Internet of Things technology. This gives the opportunity to incorporate the high frequency inverter sensor data into the AMI and consequently to the DSSE process. To reduce the communication and computation burdens, an event triggered approach can be followed where an inverter shares its sensor data when it detects sudden and significant voltage variations. Then, the OD smart meter measurements can be adjusted accordingly or on-demand updated measurements can be issued to selective smart meters. Regardless of their exact utilization, the incorporation of high frequency sensor data from inverters to augment the smart metering data will have a positive impact on the DSSE for LVDGs.

12.5.3 Validation in a real-time hardware-in-the-loop framework

As distribution grids transition from their traditionally passive behavior into more complex and active systems, advanced monitoring and control schemes tailored for these systems will become a necessity. Their reliable and robust operation will be vital for the success of the smart grid concept and for facilitating the energy transition. In this direction, it is important that monitoring and control schemes for the management of distribution grids are tested and validated in as realistic as possible conditions. For achieving this, extensive investigations of these schemes in a real-time hardware-in-the-loop framework are needed.

A general structure of such framework is illustrated in Figure 12.15. A digital twin of a considered distribution grid is uploaded in a real-time simulator. Based

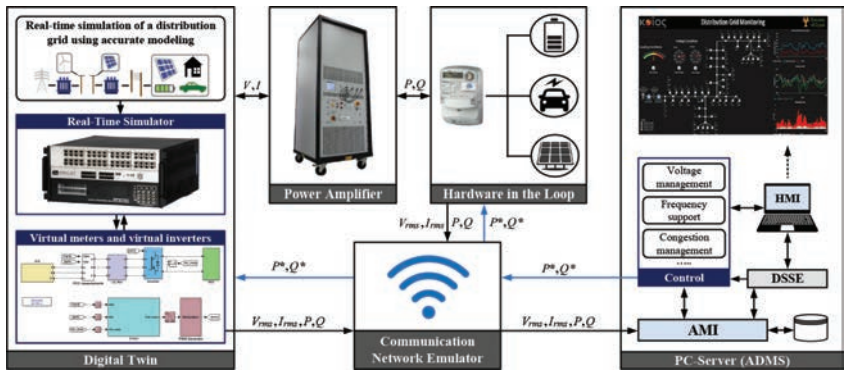

Figure 12.15 Framework for real-time hardware-in-the-loop validation of monitoring and control schemes for active distribution grids

on the modeling approach, a digital twin in a real-time simulator can be the most realistic representation of the actual physical system. An equipment, asset or even a whole node of the digital twin can be replaced with representative hardware through a power amplifier. Note that when the considered hardware can create reverse power flows, such as in the case of a PV emulator or an energy storage system, the power amplifier should be able to operate in all four quadrants. By incorporating relevant hardware in these investigations, it allows to examine their limitations and the additional complexities that they introduce. These limitations and complexities are usually hidden and overlooked when considering only the software side of the problem, and their impact on the operation of the grid management system should be evaluated. In addition, a communication network emulator allows for a realistic representation of the communication infrastructure with adjustable and reconfigurable settings depending on the considered investigations. For example, the impact of the packet loss rate, noise on measurements, bad data and data loss, latency to emulate the physical distance between different assets, adjustable bandwidth restrictions and different communication technologies can be investigated on the operation of both the software and hardware components of the system. Having the various monitoring and control schemes tested and validated in this kind of realistic environment their applicability and technology readiness level are increased. This also acts as proof of concept and can ease their in-field deployment.

12.6 Concluding remarks

This chapter has discussed the concept of DSSE in LVDGs. The classical WLS approach for grid monitoring has been presented with the additional considerations for four-wire grids. Challenges emerging from the measuring infrastructure, limited system knowledge and the nonzero neutral voltage have also been discussed and their impact on the DSSE performance analyzed. Modifications to the classical

DSSE scheme have also been presented in order to enhance its operation under asynchronous measurements and under a nonzero neutral voltage.

For addressing the asynchronous smart meter measurements, historical data are needed for determining the statistical properties of the load variation. The presented method increases the accuracy of the estimation results but the assumptions required are not guaranteed in LVDGs. Consequently, more research efforts are needed for improving the operation of the DSSE in LVDGs under asynchronous smart meter measurements. In addition, the impact of the nonzero neutral voltage on the traditional WLS DSSE scheme has been investigated. It was seen that rural systems are affected more in relation with urban and suburban systems. This is because for the same amount of load asymmetry a higher neutral voltage is induced in rural systems due to their overall higher grid impedance. The detrimental impact of the nonzero neutral voltage has also been addressed with several modifications to the WLS DSSE which enhance considerably its operation.

Moving toward the smart grid concept, the role of the LVDG in the power system will be more significant. A revaluation of its classical operation is needed, and a modernization of its infrastructure is becoming a necessity. As the number of flexible and controllable assets introduced to the LVDG grows, an advanced DMS is vital to maintain its secure operation. In this sense, the DSSE will be an integral part of the envisioned LVDG as it will be the key driver of its online and automated management. Therefore, DSOs must invest sufficient resources to build and prepare the necessary infrastructure to support and enable a reliable DSSE operation.

References

[1] Tonkoski R., Turcotte D., El-Fouly T.H.M. 'Impact of high PV penetration on voltage profiles in residential neighborhoods'. *IEEE Transactions on Sustainable Energy*. 2012, vol. 3(3), pp. 518–27.

[2] Veldman E., Verzijlbergh R.A. 'Distribution grid impacts of smart electric vehicle charging from different perspectives'. *IEEE Transactions on Smart Grid*. 2015, vol. 6(1), pp. 333–42.

[3] Zeraati M., Hamedani Golshan M.E., Guerrero J.M. 'Distributed control of battery energy storage systems for voltage regulation in distribution networks with high pv penetration'. *IEEE Transactions on Smart Grid*. 2018, vol. 9(4), pp. 3582–93.

[4] Sakis Meliopoulos A.P., Cokkinides G., Huang R., *et al.* 'Smart grid technologies for autonomous operation and control'. *IEEE Transactions on Smart Grid*. 2011, vol. 2(1), pp. 1–10.

[5] Monticelli A. *State Estimation in Electric Power Systems: A Generalized Approach*. New York: Springer; 1999.

[6] Teng J., Lin W. 'State estimation for distribution systems with zero-injection constraints'. *IEEE Transactions on Power Systems*. 1996, vol. 11(1), pp. 518–24.

[7] Haughton D.A., Heydt G.T. 'A linear state estimation formulation for smart distribution systems'. *IEEE Transactions on Power Systems*. 2013, vol. 28(2), pp. 1187–95.
[8] Lu C.N., Tang H., Liu W. 'Distribution system state estimation'. *IEEE Transactions on Power Systems*. 1995, vol. 10(1), pp. 229–40.
[9] Baran M.E., Kelley A.W. 'A branch-current-based state estimation method for distribution systems'. *IEEE Transactions on Power Systems*. 1995, vol. 10(1), pp. 483–91.
[10] Dehghanpour K., Wang Z., Wang J., Yuan Y., Bu F. 'A survey on state estimation techniques and challenges in smart distribution systems'. *IEEE Transactions on Smart Grid*. 2019, vol. 10(2), pp. 2312–22.
[11] Kersting W.H. *Distribution System Modeling and Analysis*. 4th ed. Boca Raton, FL: CRC Press; 2018.
[12] Kron G. 'Tensorial analysis of integrated transmission systems Part I. The six basic reference frames'. *Transactions of the American Institute of Electrical Engineers*. 1951, vol. 70(2), pp. 1239–48.
[13] Monitor-Deloitte. *Connecting the dots: Distribution grid investment to power the energy transition* [online]. 2021. Available from https://www.eurelectric.org/connecting-the-dots.
[14] Directorate-General for Energy (European Commission), Tractebel Impact. *Benchmarking smart metering deployment in the EU-28 [online]*. 2020. Available from https://op.europa.eu/en/publication-detail/-/publication/b397ef73-698f-11ea-b735-01aa75ed71a1.
[15] Nguyen D.T. 'Modeling load uncertainty in distribution network monitoring'. *IEEE Transactions on Power Systems*. 2015, vol. 30(5), pp. 2321–8.
[16] Singh R., Pal B.C., Jabr R.A. 'Statistical representation of distribution system loads using Gaussian mixture model'. *IEEE Transactions on Power Systems*. 2010, vol. 25(1), pp. 29–37.
[17] Ding N., Benoit C., Foggia G., Besanger Y., Wurtz F. '*Neural network-based model design for short-term load forecast in distribution systems*'. *IEEE Transactions on Power Systems*. 2016, vol. 31(1), pp. 72–81.
[18] Dehghanpour K., Yuan Y., Wang Z., Bu F. 'A game-theoretic data-driven approach for pseudo-measurement generation in distribution system state estimation'. *IEEE Transactions on Smart Grid*. 2019, vol. 10(6), pp. 5942–51.
[19] Kuhar U., Pantoš M., Kosec G., Svigelj A. 'The impact of model and measurement uncertainties on a state estimation in three-phase distribution networks'. *IEEE Transactions on Smart Grid*. 2019, vol. 10(3), pp. 3301–10.
[20] Lourenço E.M., Coelho E.P.R., Pal B.C. 'Topology error and bad data processing in generalized state estimation'. *IEEE Transactions on Power Systems*. 2015, vol. 30(6), pp. 3190–200.
[21] Singh R., Manitsas E., Pal B.C., Strbac G. 'A recursive Bayesian approach for identification of network configuration changes in distribution system state estimation'. *IEEE Transactions on Power Systems*. 2010, vol. 25(3), pp. 1329–36.

[22] Pappu S.J., Bhatt N., Pasumarthy R., Rajeswaran A. 'Identifying topology of low voltage distribution networks based on smart meter data'. *IEEE Transactions on Smart Grid*. 2018, vol. 9(5), pp. 5113–22.
[23] Yu J., Weng Y., Rajagopal R. 'PaToPa: A data-driven parameter and topology joint estimation framework in distribution grids'. *IEEE Transactions on Power Systems*. 2018, vol. 33(4), pp. 4335–47.
[24] Cunha V.C., Freitas W., Trindade F.C.L., Santoso S. 'Automated determination of topology and line parameters in low voltage systems using smart meters measurements'. *IEEE Transactions on Smart Grid*. 2020, vol. 11(6), pp. 5028–38.
[25] Barai G.R., Krishnan S., Venkatesh B. 'Smart metering and functionalities of smart meters in smart grid: A review'. *Proceedings of the 2015 IEEE Electrical Power and Energy Conference*; London, Canada; 2015. pp. 26–8.
[26] Pecan Street Data Port [Database on the Internet]. 2021. Available from https://www.pecanstreet.org/dataport.
[27] International Electrotechnical Commission. *Electrical Installations of Buildings*. IEC 60364-1; 2005.
[28] Alimardani A., Therrien F., Atanackovic D., Jatskevich J., Vaahedi E. 'Distribution system state estimation based on nonsynchronized smart meters'. *IEEE Transactions on Smart Grid*. 2015, vol. 6(6), pp. 2919–28.
[29] Anderson T.W., Darling D.A. 'A test of goodness of fit'. *Journal of the American Statistical Association*. 1954, vol. 49(268), pp. 765–9.
[30] Shapiro S.S., Wilk M.B. 'An analysis of variance test for normality (complete samples)'. *Biometrika*. 1965, vol. 52(3), pp. 591–611.
[31] Kotsonias A., Asprou M., Hadjidemetriou L., Kyriakides E. 'State estimation for distribution grids with a single point Grounded neutral conductor'. *IEEE Transactions on Instrumentation and Measurement*. 2021, vol. 69(10), pp. 1-9–8177.
[32] Kotsonias A., Hadjidemetriou L., Kyriakides E. 'Power flow for a four-wire radial low voltage distribution grid with a single point grounded neutral'. *Proceedings of the IEEE ISGT*; Bucharest, Romania, 29 Sept–2 Oct 2019; 2019.
[33] de Araujo L.R., Penido D.R.R., Carneiro S., Pereira J.L.R. 'A study of neutral conductors and grounding impacts on the load-flow solutions of unbalanced distribution systems'. *IEEE Transactions on Power Systems*. 2016, vol. 31(5), pp. 3684–92.
[34] Pau M., Patti E., Barbierato L., *et al.* 'Design and accuracy analysis of multilevel state estimation based on smart Metering infrastructure'. *IEEE Transactions on Instrumentation and Measurement*. 2019, vol. 68(11), pp. 4300–12.

Chapter 13

Conclusions

Elizete Maria Lourenço[1] and João Bosco Augusto London Junior[2]

This book has covered various practical and theoretical aspects of the Distribution System State Estimation (DSSE) process, which is currently one of the engineering topics of greatest interest to researchers, public agents, and industry. In recent years, DSSE has become an essential application in advanced distribution management systems, an inevitable process for the implementation of several features envisioned by the smart grid concept.

In this chapter, a historical context is initially provided to show how the interest in developing DSSE algorithms unfolded, highlighting the challenges encountered by the pioneers and the techniques developed. A summary of the alternative modeling and different approaches for DSSE covered in the book is presented in the sequel, and their main features to meet the needs of the emerging active Distribution Systems (DSs) nominated. The chapter ends with the presentation of future research directions expected for DSSE in the coming years.

13.1 Historical context

After the remarkable works of Schweppe et al. in the late 1960s and early 1970s, which outlined the main concepts and the general nature of the power system state estimation problem and solution, the estimation process has evolved and become well established for the transmission system segment of the power system. Conversely, research focusing on DSSE only started in the early 1990s, mainly because of the historic passive behavior of DSs, in which power flows are unidirectional and easily manageable. As a consequence of such characteristics, DSs were not thoroughly monitored by real-time measurements. Their operating condition was mostly

[1]Department of Electrical Engineering, Federal University of Paraná, Paraná, Brazil
[2]Department of Electrical and Computing Engineering, School of Engineering of São Carlos, University of São Paulo, São Paulo, Brazil

determined through statistical characterization of their loads, usually performed by a process called load aggregation.*

The historic passive behavior of DSs has changed in the past few decades, stimulated by the development of smart grid features, which promise many new functions, such as distribution automation, demand-responsive loads, and increased integration of distributed energy resources. From then on, DSs have become highly complex systems, increasingly requiring the implementation of the DSSE process.

In contrast to the transmission systems, DSs pose additional complexities and challenges for the development and implementation of DSSE algorithms, such as (i) greater model complexity due to phase asymmetry diversity (single-, two-, and three-phase circuit), more types of connections in a greater diversity of equipment (delta/wye, lagging/leading, grounded/ungrounded), and a greater variety of types of unbalanced load connections (delta/wye with voltage-dependence); (ii) lower number of available real-time measurements, bringing new challenges to the estimation process; (iii) low X/R (reactance/resistance) ratio of transmission lines; and (iv) greater dimension of the DS networks and, consequently, of the corresponding state estimation problem (a single feeder can have tens of thousands of electrical nodes in medium voltage and hundreds of thousands when considering the low-voltage circuits for a medium-size city). Because of those complexities and challenges, state estimators developed for transmission systems cannot be applied directly to DSs. Therefore, despite the consolidated position of the weighted least squares (WLS) state estimator for transmission systems, those specific characteristics of DSs result in ill-conditioning of the coefficient matrix obtained with the WLS estimator. This has driven significant efforts toward developing specialized algorithms to perform DSSE capable of dealing with specific features of DSs. Apart from that, detailed three-phase network models for DSs steady-state analysis ensure adequate accuracy and adherence in the DSSE results, which further extend model complexity and numerical sensitivity. In contrast, positive sequence models are enough for transmission networks applications.

As a result of the lack of real-time measurements, DSSE tools based on power flow calculations were proposed. This kind of estimator, generally referred to as load estimator, integrates the real-time measurements during the power flow iteration process, resulting in two main stages performed in different time frames. The first stage, referred to as off-line load estimation, is performed off-line via a load aggregation process, i.e., without the need for real-time updated information. The second stage, named real-time load estimation, provides adjustments based on the real-time values of Supervisory Control and Data Acquisition (SCADA) measurements. The main limitation of load estimation techniques is their inability to handle measurements with errors, as well as multiple and conflicting measurements.

Over the years, the expectation of an increase in the number of real-time measurements available in DSs has boosted the development of advanced algorithms

*The load aggregation or load allocation process is based on customer monthly energy consumption, customer classification, e.g., residential, commercial, and industrial, and typical load profiles for each customer class.

to perform DSSE capable of taking advantage of redundant measurements. Among them, two algorithms are the most cited: the Branch Current State Estimator and the Admittance Matrix-Based State Estimator. In order to speed up the process and treat the particularities of DSs (previously mentioned), those algorithms rely on simplifications and approximations of the measurement and network model, which makes it difficult to generalize their results. Alternative WLS formulations emerged to circumvent the intrinsic ill-conditioning of the classical WLS coefficient/gain matrix without using any approximation or simplification of the measurement and network model.

13.2 Alternative modeling and approaches for DSSE

Although the early specialized DSSE algorithms already overcame the critical issues related to particularities of DSs, such as improving convergence and introducing three-phase unbalanced network models, many challenges still prevail.

One of these challenges is the large scale of DSs, comprising electrical networks spread across vast areas, usually with hundreds of primary feeders corresponding to thousands of three-phase unbalanced buses. The inclusion of new sensors at the level of the low-voltage circuits further requires an extension of the network models until the consumer units, which may lead to hundreds of thousands of variables. In this sense, the large scale comprises the number of buses in numerous feeders from various substations, which may share interconnections. To solve the issue of scalability and maintaining accuracy, in some areas referred to as dimensionality curse, DSSE algorithms employing the concepts of Multiarea State Estimation have been proposed for achieving computational performance and scalability.

Furthermore, the numerical sensitivity involved in the solution of the DSSE problem requires an alternative perspective from the algorithms and common assumptions of data preprocessing involved in DSs. This issue is highlighted by employing a new numerical complex basis to perform steady-state analysis, namely complex per unit (*cpu*) normalization. Apart from tackling the inherent ill-conditioning caused by the parameters associated with DS equipment, extending the notion of the *cpu* method to DSSE enables decoupling voltage and phase angle in the measurement model and the Jacobian matrix. With this, all the well-known advantages and high computational efficiency of the established fast-decoupled method are made possible to deal with the new characteristics and large dimensions of DSs. Undoubtedly, faster algorithms with stable numerical properties and the ability to handle radial and meshed topologies are promising and desirable features for real-time applications in modern DSs.

Another challenge of the early specialized DSSE algorithms is the treatment of the temporal aspect of the measurements in the DSSE process. The conventional static-state estimation essentially disregards any temporal aspect, mixing information from asynchronous updates and different sampling rates in the same measurement vector. The integration of different sources of information in modern DSs for state estimation can provide knowledge about the grid's condition at sampling rates

of milliseconds (in case of Phasor Measurement Units), seconds (in case of SCADA measurements), or up to minutes (in case of smart meters and typical load profiles). Therefore, DSSE-dedicated algorithms to adequately address the multiscale measurements have been proposed. The approaches enable evaluating distinct events, such as fast transients and slow trends and their respective effects on the power grid. Among them, those based on Kalman filter theory and one based on Bayesian inference have presented promising results.

From a more fundamental perspective, the quest for better probabilistic models is also an important direction sparkling in DSs, where the basic assumption of Gaussian noise is courageously challenged in recent works. The adherence of a parametric noise model, fairly assumed for well-calibrated instrumentation, is far from the reality of pseudomeasurements, load profiles, and unsynchronized measurements. In this sense, Bayesian approaches provide a numerical framework to include such probabilistic notion. By extending the reasoning from a purely Gaussian process to a more generic family of distributions, the state estimation enables improving accuracy as well as enhancing its predictive capability. Closed solution and iterative methods within this framework become a luxury, and numerical integration and sampling methods play an essential role in this perspective, thus, fully capturing the probabilistic nature of the emerging DS.

Finally, smart meters certainly are the driving engine behind the new data sources in distribution networks, which urges for a spotlight on low-voltage circuits, the location where such meters are effectively installed. These low-voltage levels of DSs are extremely relevant as they capture the direct effect of dispersed energy resources. These effects are becoming more expressive as domestic photovoltaics are installed on a massive scale, as significant changes in the behavior of loads and appliances are pursued due to demand response, and as energy storage and electric vehicle resources are used to support the grid.

13.3 Future perspectives for the evolution of the DSSE process

The state estimation way forward is definitely toward encrusting the data processing as a protagonist of inside advanced distribution management systems. However, the "above and beyond" elevate state estimation as an active process in the power grid digitalization.

It is an inevitable evolution that, at the distribution level, control centers will be fully equipped with high-level functions, with grounds on some form of state estimation. After all, this evolution is both a logical and necessary step: the complexity of modern DSs, encompassing massive distributed generation, smart grid operation, electric mobility, together with frequent system reconfiguration and reliability concerns, requires such enhancement.

In fact, while the transmission systems become more and more stressed, with the injection of power from renewable sources, the reality emerges that a substantial percentage of such resources are growingly attached to the DS. However, to safely operate the bulk power grid, Transmission System Operators (TSOs) need

in present days to rely on flexibility, given the uncertainties pervading the forecasted operation. Nevertheless, many flexibility tools (such as embedded in supply contracts with provisions for demand-side management or combined heat-power generation at industrial facilities or PV, or wind generation) are available or manageable by Distribution System Operators but not accessible to TSOs. In this sense, assessing the level of model resolution and the representation of subtransmission/distribution networks is a promising direction, which promotes end-to-end power system awareness across generation, transmission, and distribution (multilevel monitoring).

This new reality driven by the deployment of smart grids and dispersed renewable generation requires a tacit accommodation of volatility and risk in the DS real-time operation. In this sense, probabilistic methods provide an extended notion of a single and deterministic state vector toward more generic information about the power system state, where stochastic behavior and risk analysis go side by side with decision-making in operational centers. Nonparametric noise characteristics, increased statistical robustness, the inclusion of state-space models, harmonization with statistical learning, pruning neural networks with physical models, and advanced inference concepts will pave the road in this direction of a probabilistic notion for state estimation. The result is layering data-driven concepts on top of the highly detailed electrical models of distribution networks. In this sense, ensuring numerical stability is also a flourishing field for practical implementation of state estimation. Both scalability and convergence are tackled while maintaining model adherence without loss of precision.

In terms of computational performance, it is necessary to reinforce that DSSE tools require high-performance computing. Decentralized efforts combined with some centralized software packages are the present-day computational scenario. However, novel computational architectures with cloud-based computation and data hyperconvergence and increased connectivity open the space for further real-time monitoring applications. For instance, this interaction is essential for any peer-to-peer market that aims at more actionable features of dispersed generation to support grid resilience, using state estimation as a doorway of advanced spot markets at the distribution level.

13.4 Final remarks

The book content demonstrates that the domain of the state estimation process, in general, is conceptually and mathematically deep and computationally demanding. However, from its early days up to the beginning of this century, little has changed in its basic concepts, except for a natural evolution in computation and telecommunication hardware as well as algorithmic improvements. Conversely, in the past few years, we have witnessed a renewed interest in the proposition of new formulations due to technological advances, especially in the development of the smart grid technology that has been concentrated in DSs.

Given the above, for the state estimation process to assume a vital role in DSs, as it does in transmission systems, much technical and scientific work will still be needed in the coming years.

Index

Active power 11, 48, 53, 95, 102, 112, 210, 213, 217, 218, 224–225, 229, 232, 283
Admittance matrix-based load flow (AMBLF) 109, 110, 112–113
  algorithm 118–119
  execution 124–130
  general modelling 116–118
  generation buses 115–116
  load buses 114
  overview 112–113
  reference bus 115
  state variables 113–114
Admittance matrix based power flow 126
Admittance matrix based state estimator (AMBSE) 137–138
  algorithm 137, 151–152, 154–156
  basics 138–140
  case 152–158
  equivalent measurements 140
    converting power measurements 140–141
    modelling voltage measurements 141–142
    variances 142–143
  Jacobian matrix 146–148
  reference bus 143–145
  state variables 140
  WLS solution 145–146
Advanced distribution management system (ADMS) 41, 54, 61
Advanced metering infrastructure (AMI) head-end system 51–53
Aggregation process 91
Algorithm-decoupled state estimator 192–193
AMBLF. *See* Admittance matrix-based load flow (AMBLF)
AMBSE. *See* Admittance matrix based state estimator (AMBSE)
Anderson-Darling fitness test 340
Artificial neural network (ANN) 211
Asynchronous measurements 332–334
Automatic model generation 47–48
Automation 38–39

Backup data center (BDC) 54, 55
Backward/forward sweep (BFS) load flow 119–120
  backward/forward power flow algorithm 121–123
  basic aspects 120
  case studies 123
    admittance matrix-based load flow (AMBLF) execution 124–126
    BFSLF execution 130–132
    branch current-based load flow (BCBLF) execution 126–130
    data preparation 124
  general modelling 120–121
Backward-forward sweep (BFS) methods 164
Backward sweep 130
Battery energy storage system (BESS) 97–99
Bayesian approach 212, 234
  distribution system state estimation (DSSE) 209–212
    active power 224–225
    examples 227–233
    framework 220–223

measurement handling 223–224
measurement model 218–220
numerical computation 225–227
power statistics 212–218
pseudo-measurements 212–218
reactive power 224–225
Bayesian credibility test 306
Bayesian inference method
with nodal voltage estimator 256–261
Bayesian information fusion approach 302–303
application 303–305
Bayesian credibility test 306
bayesian inference concepts 303–305
for multistage distribution system state estimation 302–303
numerical results 306–310
posterior inference via orthogonal methods 305
Bayesian spatial fusion 256
BCBLF. *See* Branch current-based load flow (BCBLF)
BCBSE. *See* Branch current-based state estimator (BCBSE)
Bidirectional control 89
Branch current-based load flow (BCBLF) 109, 110, 112–113
algorithm 118–119
execution 130–132
general modelling 116–118
generation buses 115–116
load buses 114
overview 112–113
reference bus 115
state variables 113–114
Branch current-based state estimator (BCBSE) 137–138, 138–146
algorithm 137, 152, 156–158
basics 138–140
case 152–158
equivalent measurements 140
converting power measurements 140–141
modelling voltage measurements 141–142
variances 142–143
Jacobian matrix 148–151
reference bus 143–145
state variables 140
WLS solution 145–146
Branch current flow 130, 131
Branch formulation 298–299
Brazilian distribution system monitoring 6
141-bus distribution feeder 176–181
39-bus distribution test system 301
Bus formulation 299
Bus-section level modeling 193–197
Bus voltages 129

Carson method 78–81
Carson's equations 78
Classical distribution system state estimation approach 323
Kron's reduction 327–329
measurement functions 325–327
state variables 325–327
WLS DSSE 323–325
Co-generation control 89
Common information model (CIM) 280
Complex current flows 149–150
Complex current injections 149
Compressive sensing techniques 296
Conditional probability distribution 304
Conjugate-Gaussian prior model 257
Consensus DSSE method 292–296
Consumption self-regulation 49
Conventional weighted least-squares state estimation 186–189
Convergence test 12
Corona effect 79
Coulomb's law 79
cpu-based fast-decoupled DSSE 198–200
cpu-based fast-decoupled power flow
cpu-based power flow algorithm 172, 173
normalization 169–173, 181

cpu-based real-time distribution system network modeling algorithm 201–205
Current-based three-phase power flow
  basics 110–111
  bus types 111
  load modelling 112
  specified quantities 111
  state variables 111
Current flows, magnitude of 149
Cyber-security 58

Decoupled formulation 189–191
Delta-connected load 90
Discrete-time state-space model 285
DistFlow-based partial DSSE 292–296
Distributed energy resources (DER) 279
Distributed flexible alternation current transmission systems (D-FACTS) 100
Distributed generation (DG) 93–97, 163–164, 209, 234
Distribution management system (DMS) 280, 321
Distribution network (DN) 29–30
  characteristics and possibilities 32–39
  industrial-grade products 56–57
Distribution operation centers (DOCs) 6
Distribution power utilities (DPUs) 29
Distribution system
  asymmetrical nature 69–72
  overview 68
  physical component models
    distributed generation 93–97
    distribution lines 76–77
    electric vehicles 99–100
    energy storage 97–99
    loads 89–92
    power transformers 81–84
    shunt capacitors 92–93
    shunt reactors 92–93
    static compensators (D-FACTS) 100–102
    voltage regulators 84–89
  state estimation 67–69
  three-phase two-port models (*see* Three-phase two-port models)
  unbalanced nature 69–72
Distribution system state estimation (DSSE) 29–31, 185, 355
  alternative modeling and approaches 357–358
  applications 311–312
  Bayesian information fusion approach 302–303
    application 303–305
    Bayesian credibility test 306
    bayesian inference concepts 303–305
    numerical results 306–310
    posterior inference via orthogonal methods 305
  challenges 311–312
  consensus 292–296
  data sources 280–281
    measurement data 281–283
    Pseudo-measurements 283
    real measurements 281–283
    virtual measurements 283
  DistFlow-based partial DSSE 292–296
  in distribution network (DN)
    problem settings 32–43
  dynamic state estimation 287–288
    concepts 285–287
  forecasting-aided state estimation 287–288
  future perspectives 358–359
  historical context 355–357
  Kalman filters 285–287
    limitations 292
  low voltage distribution grids (LVDG) 319–322
    with automated management 322
    challenges 329–338
    enhancement 338–349
    future directions 349–351

matrix completion-based system implementations 298–300
state update with granular measurements 296–298
multistages state estimators
based on quasi-dynamic techniques 288–292
numerical results 300–302
real-time network model 280
temporal aspects 283–284
tracking state estimation 287–288
Distribution-level phasor measurement units (D-PMUs) 210, 221, 223
Distribution transformers 15
Dynamic state estimation 288

Earthing schemes 335–337
Electric vehicles 99–100
inverters 350
Energy storage 97–99
Equivalent voltages 150
Estimation error 269–271
Exponential model 89

Faraday's law of electromagnetic induction 78
Fast-decoupled approach 167–169
Fast-decoupled distribution system state estimation (FD-DSSE) 198
Fast-decoupled power flow (FDPF) method 164
convergence 174–176
cpu-based fast-decoupled power flow
cpu-based power flow algorithm 172, 173
normalization 169–173, 181
Newton-Raphson power flow (NRPF) 164
fast-decoupled approach 167–169
formulation 165–167
power flow analysis 164–165
Fast-decoupled weighted least-squares state estimation (WLS-SE) 186
algorithm-decoupled state estimator 192–193
conventional weighted least-squares state estimation 186–189
decoupled formulation 189–191
model-decoupled state estimator 191–192
Flexible alternation current transmission systems (FACTS) 100
Forecasting-aided state estimation 287–288
Forward control 88
Forward sweep 131

Gain matrix 139, 188, 190
Gaussian mixture models (GMM) 211
Gauss-Newton method 145
Generalized decoupled formulation 194–197
Generation buses 115–116
Geographic information system (GIS) 52
Granular measurements 296–298

Holt's 2-parameter model 289, 301

IEEE 4 nodes test feeder 85–86
IEEE 123-bus grid 262–266
IEEE123 nodes test feeder 94–95
IEEE test feeders 103
Industrial-grade DSE products 43–44
groups 32–43
practical implementation
problems 45–56
requests 44–45
In-field verification 14–17

Jacobian matrix 117–118
admittance matrix-based load flow (AMBLF) 125

of admittance matrix based state estimator (AMBSE) 146–148
branch current-based load flow (BCBLF) 127–128
of branch current-based state estimator (BCBSE) 148–151
weighted least-squares state estimation (WLS-SE) 187

Kalman filters
introduction to 285–287
limitations 292
Kalman gain 286
Kirchhoff's current law (KCL) 146
Kron reduction technique 81, 85, 327–329

Large-scale distribution network, in Brazil 272–273
Linearized power flow 299–300
Line drop compensation (LDC) 87
Load aggregation 6, 10, 356
Load buses 114
Load estimation 10–11
Local automation 48–49
Locked forward control 88
Locked reverse control 88–89
Low voltage distribution grids (LVDG) 319
with automated management 322
distribution system state estimation (DSSE) 319–322
challenges 329–338
enhancement 338–349
future directions 349–351

Main data center (MDC) 54, 55
MASE. *See* Multiarea state estimation (MASE)
Matrix completion method 301
Matrix completion-based system implementations 298–300
state update with granular measurements 296–298
Maximum a posteriori (MAP) estimation 256–257, 304
Mean estimation error 263
Measurement areas (MAs) 8, 11–13
Measurement simulator 200–201
Medium voltage (MV) grids 214
Meter data management (MDM) 52, 53
Metropolis-Hastings (M-H) algorithm 225
Micro-phasor measurement unit (μ−PMU) 57, 140–142, 148, 281, 283, 291
Model-decoupled state estimator 191–192
Multiarea state estimation (MASE) 239
algorithms 313
classifications 242–245
definitions 242–245
distributed architecture 247
for distribution systems
Bayesian inference method with nodal voltage estimator 256–261
Bayesian inference multiarea DSSE 268–275
two-step method with branch current estimator 247–255
two-step multiarea DSSE 261–268
hierarchical architecture 245–247
large-scale distribution systems and motivations 239–241
terminology 242–245
Multilevel voltage analyses 172–174
Multistages state estimators
based on quasi-dynamic techniques 288–292

Network analysis 240
Newton-Raphson method (NRLF) 109–110, 138

Newton-Raphson power flow (NRPF) 164
  fast-decoupled approach 167–169
  formulation 165–167
  power flow analysis 164–165
Nodal current injection 130, 131
Nodal system conductance matrix 146–147
Nodal system susceptance matrix 146–147
Nodal voltage estimator
  Bayesian inference method with 256–261
Node-depth encoding (NDE) 8, 11
Node power measurements 216
Nonzero neutral voltage 334–338
  case 347–349
  four-phase system 342–343
  Jacobian matrix 343
  measurement functions 343
  virtual measurement
    generation 344–345
    weights 345–347

Open-delta/open-delta (OD/OD) transformer 83
Open-wye/open-delta (OY/OD) transformer 83
Optimization variables 300
Out-of-date (OD) measurement 339, 340

Performance index 187
Phasor measurement unit (PMU) 57, 58, 71, 77, 199, 221–223, 239, 249, 262–266, 279, 304, 306–310, 312
Photovoltaic (PV) inverters 350
Plug-in electric vehicles (PEV) 99–100
Polar coordinates 74–76
Power base angle 171–172
Power electronics 95
Power factor control 93
Power flow analysis
  distributed generation (DG) 164
  Newton-Raphson power flow (NRPF) 164–165
Power statistics 212–218
Power system computational analysis 102
Power transformers 81–84
Probability density functions (PDFs) 213, 231
Proximity effect 78
Pseudo-measurements 21, 91, 211, 212–218, 283, 330
PVWatts calculator tool 215

Quantitative indicators 38
Quasi-dynamic techniques
  multistages state estimators based on 288–292

Reactive power 91, 224–225
Real-time hardware-in-the-loop framework 350–351
Real-time load estimator 9, 11–14
Real-time load forecasting 22–24
Real-time monitoring tool (RTMT) COPEL 5–14
  application
    in distribution system state estimation 20–21
    in-field verification 14–17
    for real-time load forecasting 22–24
    in service restoration 17–20
  Brazilian distribution system monitoring 6
  flowchart 7
  implementation 6–7
    data preprocessing 7–9
    real-time load modeling 9–14
Rectangular coordinates 76–77
Reference bus 115, 143–145, 148, 151

Service restoration software (SRS) 5, 15, 17, 19, 22, 25
Service restoration 17–20
Shapiro-Wilk fitness test 340
Shunt capacitors 92–93
Shunt reactors 92–93
Single-phase transformers 83
Skin effect 78
Smart grid 1
  concept 31, 39, 102, 163, 321, 350, 352, 355
  distribution network (DN) 30, 31
  networks 29
Smart meters (SMs) 25, 38, 53, 57, 71, 90, 91, 136, 210, 239, 268, 269, 271, 272, 273, 283, 312, 319, 322, 329, 330, 332–335, 337–343, 347, 349, 350, 352, 358
Solid-state voltage generator static compensators 101
State of charge (SOC) estimation methods 97–98
State variables 70, 128–130, 132
State variables vector 126–127, 130
Static compensators 100–102
Static synchronous compensator (STATCOM) 101
Static VAR compensator (SVC) 101
Supervisory control and data acquisition (SCADA) measurements 8, 15, 21, 26, 44, 53, 216, 245
Synchronous series compensator (SSSC) 101

Telecommunications infrastructure 39
Three-phase two-port models 72–73
  admittance model 73–74
  polar coordinates 74–76
  power flow equations 73
  rectangular coordinates 76–77
Three-winding three-phase transformers 84
Thyristor-controlled series compensator (TCSC) 101
Time control 93
Total vector error (TVE) 223–224, 233
Tracking state estimation 287
Transformer load management system 311
Transformer terminal unit (TTU) system 283
Transmission networks 35
  consumption and production in 37
Transmission network state estimation (TSE)
  vs. distribution state estimation (DSE) 40–43
Two-bus test system 174–176
Typical Italian distribution grid 266–268

Universal power flow controller (UPFC) 101–102
Unscented Kalman filter (UKF) 286, 290

Variable reactance static compensators 100–101
Vehicle-to-grid (V2G) strategies 99
Virtual measurements 283
Virtual measurements 324–325
Voltage control 93
Voltage magnitude SCADA measurements 268
Voltage regulators 84–89
Weighted least square (WLS) estimator 230, 232, 233

Weighted least square (WLS)
  distribution system state estimation (DSSE) 323–325
  estimation error 232
  formulations 211
Whole distribution grid 349–350

ZIP model 90

Power Distribution System State Estimation

State estimation is a key function for real-time operation and control of electrical power systems since its role is to provide a complete, coherent, and reliable network real-time model used to set up other real-time operation and control functions. In recent years it has extended its applications to monitoring active distribution networks with distributed energy resources. The inputs of a conventional state estimator are a redundant collection of real-time measurement, load and production forecasts and a mathematical model that relates these measurements to the complex nodal voltages, which are taken as the state variables of the system. The goal of state estimation is to adjust models so that they are closer to observed values and deliver better forecasts. In power systems, this is key to maintaining power quality and operating generation and storage units well.

This book, written by international authors from industry and universities, systematically addresses state estimation in power distribution systems. Chapters convey techniques for distribution system state estimation, such as classical methods, three-phase network modelling, power flow calculation, fast decoupled approaches and their new application via complex per unit normalization, the Bayesian method, and multiarea state estimation. Also, synchronized and non-synchronized measurements with different sample rates, real-time monitoring, and practical experiences of distribution state estimation are covered.

Researchers involved with electrical power and electrical distribution systems, professionals working in utilities, advanced students and PhD students will find this work essential reading.

About the Editors

Elizete Maria Lourenço is a professor at the Electrical Engineering Department of the Federal University of Paraná, Brazil.

João Bosco Augusto London Junior is a professor at the Electrical and Computer Engineering Department of the EESC-University of São Paulo, Brazil.

ISBN 978-1-83953-201-6

The Institution of Engineering and Technology
theiet.org
978-1-83953-201-6